Pradeep L. Menezes
Pradeep K. Rohatgi
Emad Omrani *Editors*

Self-Lubricating Composites

Second Edition

MATERIALS.SPRINGER.COM

Springer

Self-Lubricating Composites

Pradeep L. Menezes • Pradeep K. Rohatgi • Emad Omrani
Editors

Self-Lubricating Composites

Second Edition

With 188 Figures and 15 Tables

Springer

Editors
Pradeep L. Menezes
Department of Mechanical Engineering
University of Nevada
Reno, NV, USA

Pradeep K. Rohatgi
Department of Materials Science and Engineering
University of Wisconsin-Milwaukee
Milwaukee, WI, USA

Emad Omrani
Department of Materials Science and Engineering
University of Wisconsin-Milwaukee
Milwaukee, WI, USA

ISBN 978-3-662-64242-9 ISBN 978-3-662-64243-6 (eBook)
https://doi.org/10.1007/978-3-662-64243-6

This Springer imprint is published by the registered company Springer-Verlag GmbH, DE part of Springer Nature.
The registered company address is: Heidelberger Platz 3, 14197 Berlin, Germany

Preface

Solid lubricant materials have become a necessity for present engineering innovation in the field of aerospace, automobile, and bioimplants. Solid lubricating materials have been replacing liquid lubricants due to their superior stability at extreme conditions such as high temperature and high pressure. Understanding of lubrication mechanism for various solid lubricant materials has been the key factor for their reliable application. This book emphasizes on various solid lubricant materials, their application in the form of a coating, self-lubricating composites, and as an additive in oil.

Chapter ▶ 1 details the fundamentals of solid surfaces, contact mechanism, and fundamentals of solid lubricants. The application and mechanism of solid lubricant as the coating material is emphasized to control the tribological properties. Further, various solid lubricant materials are discussed as the chemistry of solid lubricants play an important role in the formation of a lubricating film (tribo-film) during sliding. Along with coating, various other applications of solid lubricant materials are highlighted.

Chapter ▶ 2 presents the application of solid lubricant materials in metal matrix composites, which includes material selection, processing techniques, and tribological performance. The tribological performance is explained through the third body approach as well as the parent materials, where the mechanical, structural, and chemical interactions between the matrix and reinforcement play a key role. Based on the current status of metal matrix composites, this chapter also emphasizes the development of new materials and new processing techniques for further improving the tribological properties.

Graphite is one of the promising reinforcements for self-lubricating composites, and the formation of in situ 2D graphite in composites is the latest development in the field of self-lubricating composites. Detailed processing, characterization, and characterization of in situ–generated turbostratic 2D graphite are described in Chap. ▶ 3. The superior lubrication performance of in situ 2D graphite is also compared with other forms of graphite.

Chapter ▶ 4 describes various self-lubricating polymer matrix composites for both types of the polymers, such as thermoplastics and thermosets. Polymer matrix has been used with multiphase reinforcement materials, such as fibers and textiles for strength, and solid lubricant materials for lubricating properties. A detailed

description of lubrication mechanism, various factors affecting polymer composites, and tribological applications of polymer composites, followed by nanostructured self-lubricating polymer composites, are presented in Chap. ▶ 5. The current state of the art on lubricant nanomaterials is presented, which gives a deep insight to readers about the interaction between filler and matrix materials, modern technologies, and hybrid nanostructures to achieve high-demanding tribological applications.

Chapter ▶ 6 deals with the polymeric solid lubricant transfer film. The transfer film is essential for lower friction and wear rates, and measurement of these transfer films has been the critical part to control tribological performance. This chapter focuses on recent advances in the characterization of polymeric transfer film, which include topographical, adhesive, mechanical, and chemical properties.

Chapter ▶ 7 focuses on the synthesis of self-lubricating alumina matrix composites. Here, mainly three categories of solid lubricants are discussed: soft material, lamellar solids, and other materials (oxides, sulfates, etc.) used in alumina matrix. In addition to single solid lubricant material in alumina matrix, combination of multiple solid lubricants and second hard phase are discussed, which exhibit enhanced tribological and mechanical properties. Also, the formation of in situ solid lubricant phases in the alumina matrix has been highlighted.

Chapter ▶ 8 addresses the self-lubricating ceramic matrix composites that signify the applicability of ceramic composites at extreme environmental conditions due to their high-temperature resistance and chemical inertness. This chapter presents the processing mechanism for two new types of self-lubricating ceramic composites, which are functionally graded materials and core-shell structured composite powders in ceramic matrix. The mechanical and tribological properties of these new composites are also compared with traditional self-lubricating composites.

In the field of tribology, surface engineering plays an important role in controlling the friction and wear phenomena. The significance of surface engineering in self-lubricating alumina matrix composites is shown in Chap. ▶ 9. This chapter brings out the relationship between surface microstructure and properties (mechanical and tribological) in the presence of 3D self-lubricating materials.

The ubiquitous negative effects of different materials on ecosystems are outlined in Chap. ▶ 10, along with the recent efforts to develop eco-friendly lubricant materials. This chapter provides a deep environmental analysis of self-lubricating composites, which gives a clear picture of environmental benefits by using self-lubricating composites, such as aluminum/graphite composites.

Chapter ▶ 11 focuses on various theories and available models on self-lubricating materials for molecular dynamics (MD) simulation. This chapter provides a basic understanding of MD simulation and also the need of MD simulation for self-lubricating composites. This chapter is aimed to improve the understanding of the lubrication mechanism on the molecular level using available models.

This book is intended to provide basic understating as well as knowledge on the recent development in the field of self-lubricating materials to professionals as well as university students. We have added an extensive list of results from different concerning fields, such as are mechanical, chemical, materials and manufacturing, and environmental safety. Professionals connected with the development and

applications of self-lubricating materials will find this book very useful in understanding multidisciplinary knowledge. We have also added an extensive list of references at the end of each chapter, which makes this book an excellent source of references in the field of self-lubricating composites.

Comprehensive knowledge of self-lubricating materials through this book has been possible with the collective efforts of various research groups around the world.

Contents

About the Editors

Pradeep L. Menezes (corresponding author) is an associate professor in the Department of Mechanical Engineering at the University of Nevada, Reno, Nevada. Before joining this university, he worked as an adjunct assistant professor at the University of Wisconsin–Milwaukee (UWM), Wisconsin, and as a research assistant professor at the University of Pittsburgh, Pennsylvania. Dr. Menezes's productive research career has produced more than 120 peer-reviewed journal publications (citations more than 5000, h-index–34), 30 book chapters, and 4 books related to tribology.

Pradeep K. Rohatgi is a UWM Distinguished Professor. He has coedited and coauthored 12 books and more than 400 scientific papers and has 19 US patents. He is considered as a world leader in composites and materials policy for the developing world. He has served on committees of the governments of the USA and India in the areas of materials, especially those related to automotive sector, to promote collaboration. His research includes advanced manufacture of lightweight, energy-absorbing, self-lubricating, and self-healing materials and components, including micro- and nano-composites and syntactic foams. He is the founder chief technology officer (CTO) of Intelligent Composites, LLC, Milwaukee, Wisconsin.

Emad Omrani is a process engineer at Intel Corporation. He was a graduate student of Dr. Rohatgi at the UWM. He has coauthored 2 book chapters and over 10 peer-reviewed scientific papers. At UWM, Dr. Menezes collaborated with Dr. Rohatgi and Dr. Omrani in the areas of tribology and self-lubricating materials and published several research papers on the tribology of self-lubricating materials. Dr. Menezes and Dr. Rohatgi are well-known tribologists and self-lubricating materials scientists. These editors are therefore well known and well connected in this field to put forth an excellent book on this topic.

Contributors

P. Ajay Kumar Department of Materials Science Engineering, University of Wisconsin-Milwaukee, Milwaukee, WI, USA

Department of Mechanical Engineering, Indian Institute of Technology, Tirupati, Andhra Pradesh, India

Ali Bakhshinejad University of Wisconsin-Milwaukee, Milwaukee, WI, USA

Mohammad Hasan Balali Department of Industrial and Manufacturing Engineering, College of Engineering & Applied Science, University of Wisconsin-Milwaukee, Milwaukee, WI, USA

Cristiano Binder Laboratório de Materiais, Departamento de Engenharia Mecânica, Universidade Federal de Santa Catarina, Florianópolis, SC, Brazil

David Burris Department of Mechanical Engineering, University of Delaware, Newark, DE, USA

Richard R. Chromik Department of Mining and Materials Engineering, McGill University, Montreal, QC, Canada

Jose Daniel Biasoli de Mello Laboratório de Materiais, Departamento de Engenharia Mecânica, Universidade Federal de Santa Catarina, Florianópolis, SC, Brazil

Roshan M D'Souza University of Wisconsin-Milwaukee, Milwaukee, WI, USA

Hengzhong Fan State Key Laboratory of Solid Lubrication, Lanzhou Institute of Chemical Physics, Chinese Academy of Sciences, Lanzhou, China

University of Chinese Academy of Sciences, Beijing, China

Yuan Fang State Key Laboratory of Solid Lubrication, Lanzhou Institute of Chemical Physics, Chinese Academy of Sciences, Lanzhou, China

Diana Haidar Department of Mechanical Engineering, University of Delaware, Newark, DE, USA

Litian Hu State Key Laboratory of Solid Lubrication, Lanzhou Institute of Chemical Physics, Chinese Academy of Sciences, Lanzhou, China

Ashish K. Kasar Mechanical Engineering Department, University of Nevada, Reno, NV, USA

Chang-Soo Kim University of Wisconsin-Milwaukee, Milwaukee, WI, USA

Aloisio Nelmo Klein Laboratório de Materiais, Departamento de Engenharia Mecânica, Universidade Federal de Santa Catarina, Florianópolis, SC, Brazil

Pradeep L. Menezes Department of Mechanical Engineering, University of Nevada, Reno, NV, USA

Marjan Nezafati University of Wisconsin-Milwaukee, Milwaukee, WI, USA

Narjes Nouri Lubar School of Business, University of Wisconsin-Milwaukee, Milwaukee, WI, USA

Emad Omrani Department of Materials Science and Engineering, University of Wisconsin-Milwaukee, Milwaukee, WI, USA

Wilkistar Otieno Industrial and Manufacturing Engineering Department, University of Wisconsin-Milwaukee, Milwaukee, WI, USA

Sonia Maria Hickel Probst Laboratório de Materiais, Departamento de Engenharia Mecânica, Universidade Federal de Santa Catarina, Florianópolis, SC, Brazil

Pradeep Rohatgi Department of Materials Science and Engineering, University of Wisconsin-Milwaukee, Milwaukee, WI, USA

Junjie Song State Key Laboratory of Solid Lubrication, Lanzhou Institute of Chemical Physics, Chinese Academy of Sciences, Lanzhou, China

University of Chinese Academy of Sciences, Beijing, China

Andrea Sorrentino Institute for Polymers, Composites and Biomaterials (IPCB), National Research Council (CNR), Lecco, Italy

V. Vishnu Namboodiri National Institute of Construction Management and Research (NICMAR), Hyderabad, Telangana, India

Guangyong Wu School of Mechanical Engineering, Shandong University, Jinan, China

Guangchun Xiao School of Mechanical and Automotive Engineering, Qilu University of Technology, Jinan, China

Key Laboratory of Advanced Manufacturing and Measurement and Control Technology for Light Industry in Universities of Shandong, Qilu University of Technology, Jinan, China

Chonghai Xu School of Mechanical Engineering, Shandong University, Jinan, China

School of Mechanical and Automotive Engineering, Qilu University of Technology, Jinan, China

Key Laboratory of Advanced Manufacturing and Measurement and Control Technology for Light Industry in Universities of Shandong, Qilu University of Technology, Jinan, China

Jiaxin Ye Institute of Tribology, Hefei University of Technology, Hefei, China

Mingdong Yi School of Mechanical and Automotive Engineering, Qilu University of Technology, Jinan, China

Key Laboratory of Advanced Manufacturing and Measurement and Control Technology for Light Industry in Universities of Shandong, Qilu University of Technology, Jinan, China

Yinyin Zhang Department of Mining and Materials Engineering, McGill University, Montreal, QC, Canada

Yongsheng Zhang State Key Laboratory of Solid Lubrication, Lanzhou Institute of Chemical Physics, Chinese Academy of Sciences, Lanzhou, China

Solid Lubricants: Classification, Properties, and Applications

1

P. Ajay Kumar, V. Vishnu Namboodiri, Emad Omrani, Pradeep Rohatgi, and Pradeep L. Menezes

Contents

P. Ajay Kumar (✉)
Department of Materials Science Engineering, University of Wisconsin-Milwaukee, Milwaukee, WI, USA

Department of Mechanical Engineering, Indian Institute of Technology, Tirupati, Andhra Pradesh, India
e-mail: Kumar38@uwm.edu; drajaykumarp@iittp.ac.in

V. Vishnu Namboodiri
National Institute of Construction Management and Research (NICMAR), Hyderabad, Telangana, India

E. Omrani · P. Rohatgi
Department of Materials Science and Engineering, University of Wisconsin-Milwaukee, Milwaukee, WI, USA

P. L. Menezes
Department of Mechanical Engineering, University of Nevada, Reno, NV, USA

P. L. Menezes et al. (eds.), *Self-Lubricating Composites*,
https://doi.org/10.1007/978-3-662-64243-6_1

Abstract

The extreme environmental applications of solid lubricants attained a greater interest to the researchers and product designers. This chapter deals with the processes, mechanisms, properties, and materials for solid lubricants and its real-time applications are established. Reliable and wear-resistive solid lubricants developments are carried out with a synergy between solid lubricant and substrate bearing material for a specific application. It can be applied as either in the form of coatings in substrate surfaces or as dispersed/reinforced particles in self-lubricating composites. Frictional and wear contacts exhibit the formation of a transfer film or tribofilm. The synergic influences of environment and chemical reactions resulting in varying chemical, crystallographic textural, and microstructural behavior can be observed for bulk coated wear surfaces. This inferred that the tribological performance of solid lubricants may vary according to various environment. The non-Amontonian frictional behaviors are recognizable in solid lubricants with decreasing frictional coefficients with increasing contact stress. The sliding between transfer film and worn coating influences the lower friction value at the interfacial regions. In connection to this, various strategies are discussed in this chapter for the design of novel coatings that can be adapted to various environments.

1.1 Introduction

The friction coefficient and wear are considered as most important entities related to the lubrication studies. The past solid lubricants studies revealed the superior low frictional coefficient and high wear life behaviors even under severe loading condition. Conventional lubricants like oils and greases are not considered as a good candidate for conditions like high temperature environment, thus as an alternative the solid lubricants can be effectively utilized for such applications. Poor performance of liquid lubricants is one of the challenges in the early space applications; the inception of the solid lubricants opened a wide range of specific space applications with superior performance (lower frictional coefficient and high wear life). The advancement in additive manufacturing enabled the usage of solid lubricants in various forms to enhance the tribological performances. The synthesis of anti-seize paste and antifriction coatings in greases and oils are few of them [1]. The powdered form of these solid lubricants can be dispersed in asperity peaks and pits of frictional surface. This enables a boundary lubrication effect, resulting in improved tribological parameters at extreme environments. The bearings and gears are fabricated with metallic materials. Tabor [2] illustrated atomic contacts in surface interactions of two flat surfaces. A long-ranged Van der Waals forces influence the formation of initial bonds in the contact interfaces, which forms strong metallic bonds as the separation distance progresses to interatomic distances [2]. Similar and dissimilar metallic bonding studies were established by mutual solubility approach in which mutually soluble pairs show strong adhesive bonding that indicates high friction and insoluble pairs show weak adhesive bonds that indicate low friction [3]. A first kind of generalized material compatibility chart was developed by Rabinowicz [4] which

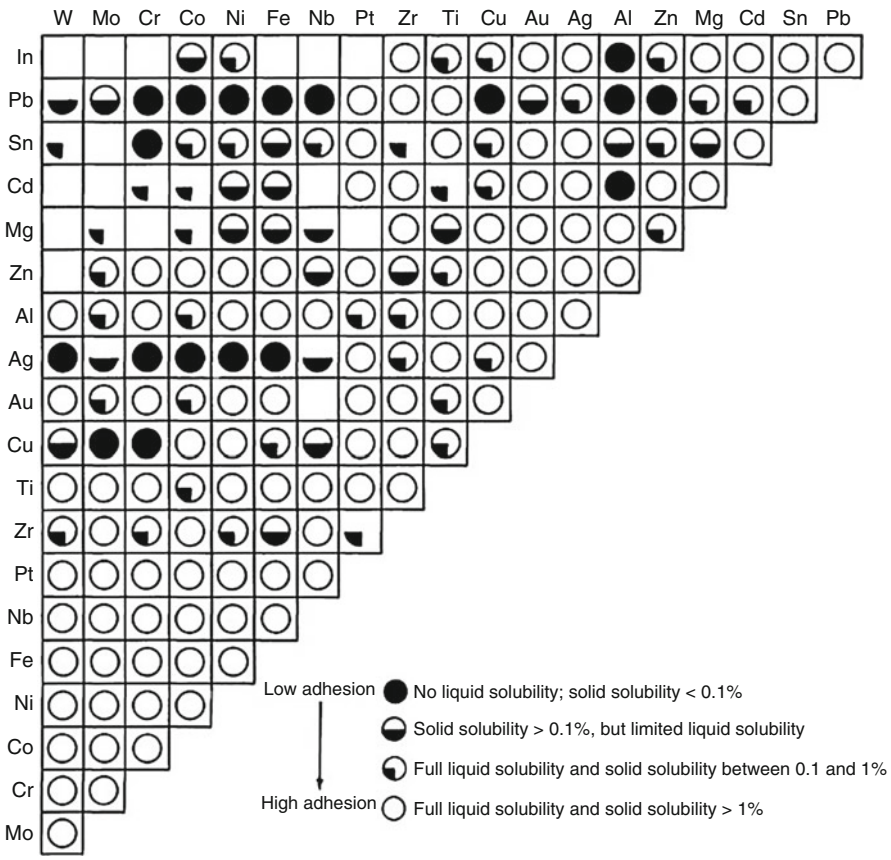

Fig. 1.1 Metal combinations compatibility chart [4]

is formulated based on equilibrium binary phase diagram (Fig. 1.1). The chart indicates the adhesion and friction are decreased for various coupled interactions from same material interaction to metal-nonmetal interactions. This theory is considered as general rule for tribo pairs but not exclusively used for material designs. The mechanical and physical properties of the materials are considered as the design bottlenecks for the tribological material designs. Mitigation of wear and friction can be achieved through the formation of shear-accommodating layer or liquid thin film at contact interfaces. Conventional lubricants especially liquid lubricants are not considered for the high vacuum and temperature environment due to the volatile nature of lubricant. Thus, a nonvolatile lubricant with superior tribological performance is of greater need that enabled the evolution of solid lubricants and coatings. The graphite can be considered as a good example of naturally occurring solid lubricant materials. The modern coating technologies like physical, chemical, and plasma-enhanced chemical vapor deposition methods achieved greater developments. DLC (diamond-like carbon), TMD (transition metal dichalcogenides), and polymeric composite coatings are considered as common solid lubricant materials.

Various spectroscopic analytical techniques were used to analyze the fundamental synthesis-structural tribological relationships. XPS and FIB microscopes are few of them. This chapter deals with the nature of solid surfaces, contact mechanisms, and contact area for solid lubricant. Also, further fundamental mechanisms involved in solid lubrications in relationship with tribochemistry, tribofilms, and contact load are discussed in later. The friction contacts and its loading conditions have significant role in the evolution of surface and subsurface microstructure. Boundary films in solid lubricants exhibit a steady thickness which is uninfluential for process parameters (like sliding speed and applied loads) and temperature. The establishment of solid lubricants can be as fillers in self-lubricating composites or as direct surface coating. The solid lubricant's under-tribological contacts reported a typical formation and transfer of a tribofilm from surface to counterface. The performance responses of solid lubricants may vary according to the environment parameters and chemical reactions throughout the material contact surfaces.

This chapter aims a consolidation in selection, applications, features, advancement, and performance in solid lubrication and coatings.

1.2 Surfaces and Contact Area

Surface mechanisms and its peculiarities are of greater influence in the material properties. The surfaces are comprised with various layers, and in-depth understandings revealed the information on asperities (peaks and pits) even in polished surfaces, which infer that no surfaces exhibit as pure flat surfaces (Fig. 1.2a). The

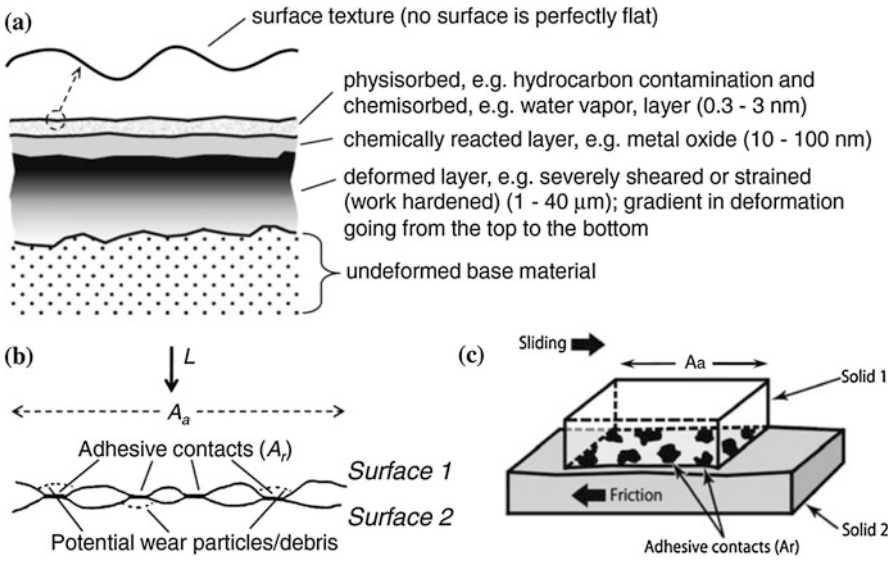

Fig. 1.2 (**a**) Various subsurface layers, (**b**) features of adhesive contact, (**c**) mechanisms of generations of wear particles and transfer films [10]

contact areas can be demonstrated as apparent area (A_a) and real area (A_r) and the asperity level was in the order of 10^{-2} to 10^{-6} for real areas of contact, which is significantly smaller as compared with the apparent area (Fig. 1.2b, c). The estimation of A_r in the surface interfaces is very difficult with conventional experimental routes, thus optically transparent bodies are to be considered for better understandings. Also, the A_r is a function of properties of material, loading conditions, and surface topographical features. To achieve low adhesion, the magnitude of A_r should be minimized which infers the minimal degree of interactions. When apparent contact stresses are elastic in nature, at the tip of the asperities the localized stresses exceed the elastic limit leading to localized plastic deformations. Thus, adhesion can be an entity of plastic deformation of asperities, which significantly affect the magnitude and overall deformation nature [5, 6]. A contact mechanism theory for a rough surface under static loading conditions was developed by Greenwood and Williamson in which a shift from elastic to plastic contact was established [7]. According to their theory, following assumptions were made: the tips of asperities are spherical in shape with radius of curvature (R_s) which follows random or Gaussian distribution. The shape of Gaussian distribution is uninfluential since vertically large asperities take part in the surface interactions.

According to [7], plasticity index (Ψ) expression is as follows:

$$\Psi = \frac{E^*}{H}\sqrt{\frac{\sigma_s}{R_s}} \tag{1.1}$$

The hardness of the soft material (H), standard deviation (σ_s) of peak heights ($\sigma_s^2 = \sigma_1^2 + \sigma_2^2$), and composite peak radius (R_s) and the expression is ($1/R_s = 1/R_1 + 1/R_2$). E^* is the Young's modulus (in composite or reduced form), mean Hertzian contact pressure (P_H) and the expression is as follows,

$$\frac{1}{E^*} = \frac{1-\nu_1^2}{E_1} + \frac{1-\nu_2^2}{E_2} \tag{1.2}$$

where, $E_{1,2}$ is the modulus of elasticity, and $\nu_{1,2}$ is the Poisson's ratio for respective contact material 1 and 2. In Eq. 1.1 the square root term relates the mean slope of the surface (from profilometer). The plasticity index (Ψ) indicates the state of deformations (elastic/plastic behavior) of a rough surface. If $\Psi < 0.61$, elastic deformation dominates; and if $\Psi > 1$, it indicates significant plastic deformation. Further, from [7] the A_r for elastic contacts by Eq. 1.3 relates to Eq. 1.1.

$$\frac{A_r}{A_a} \cong \frac{3.2\,P_H}{E^*\left(\sigma_s/R_s\right)^{1/2}}. \tag{1.3}$$

where A_r is the plastic contacts (Ψ based calculation) and the expression is as follows:

$$\frac{A_r}{A_a} \cong \frac{P_H}{H} \tag{1.4}$$

The plasticity index model developed by Greenwood and Williamson encouraged the subsequent development in plasticity index studies by [8, 9]. The plasticity index is a key indicator for the minimizing adhesive forces by reducing A_r and increasing H and E, and this can be a potential entity for overall friction studies. Introduction of frictional forces increased complexity in various levels like contact mechanics modeling of sliding contact surface.

In addition, with static contact stress, a dynamic contact stresses were originated below the interfaces. The dynamic stresses in the interface are comprised with maximum shear stresses (τ) and different principle stresses (σ_x, σ_z). During the transition from static to dynamic, a compressive stress field was found ahead of the counterbody, and on the other hand stress fields behind are tensile in nature. Apart from the friction, the complexity of contact mechanisms modeling for coated surfaces increased due to the introduction of coating substrate interface. Furthermore, it is important to ensure the coating-substrate integrity from any deformations.

Figure 1.2a illustrates the surface zones having various physiochemical properties that differ from bulk. Significant microstructural changes can be observed in the subsurface regions of frictional adhesive contact surfaces. In metal to metal contacts, in initial run itself the native oxide layer can be deteriorated and subsequently resulting an undesirable metal-metal contacts. The aluminum against steel ball interactions show the transfer of aluminum to the hard steel ball (Fig. 1.3) during the ball on disk tribo test, and this may be due to adhesive friction and wear process mechanisms (Fig. 1.2c). The reduction of friction in aluminum-steel interface is due to the low interfacial shear strength. Thus, aluminum will flow and the resulting material adheres to the counterface of the hard surface, resulting in no need of any external fluid and solid lubricants. Al and Fe (steel) demonstrated a solid solubility >1% (Fig. 1.1). Furthermore, the high adhesion shows good agreement with significant adhesive transfer (Fig. 1.3).

1.3 Fundamentals of Solid Lubrication

From [9], in Eq. 1.5 the frictional coefficient (μ) is the ratio of friction force (F) and normal force (L), and further the friction force is expressed as the product of real contact area (A_r) and shear strength of lubricant material (τ). Figure 1.4 illustrates the sliding mechanisms and its features of a hemispeherical ball against a substrate.

$$\mu = \frac{F}{L} = \frac{A_r.\tau}{L} = \frac{\tau}{P_H} = \frac{\tau_o}{P_H} + \alpha \tag{1.5}$$

Also, this can be expressed in the form of ratio between interfacial shear strength (τ_o) to the mean Hertzian contact pressure (P_H) and pressure dependence shear strength (α). According to the principle, a low friction coefficient can be observed for a hard material with a soft skin and subsequently increasing P_H (low A) was also observed. Figure 1.5a illustrates Bowden and Tabor's concept for a soft versus hard metal contacts. Figure 1.5b illustrates the validated model by Bowden and Tabor for usage of thin film indium metal against harder steel substrate as a solid lubricant. The

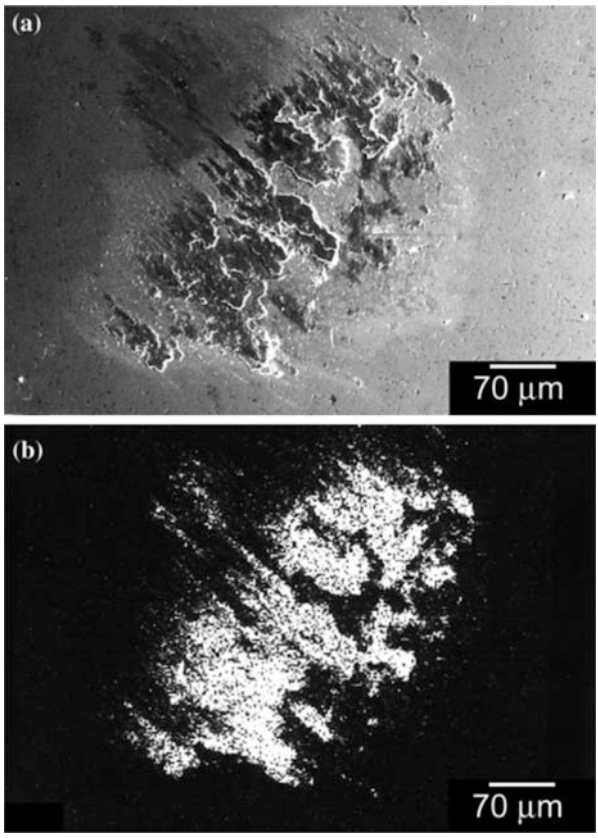

Fig. 1.3 (**a**) Al-steel ball mark observed through SEM image, and (**b**) its corresponding X-ray dot map of Al [10]

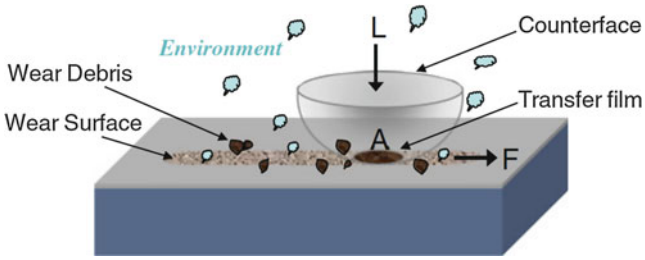

Fig. 1.4 Illustration and details of a hemispherical ball sliding against substrate which is coated with solid lubricant [10]

coefficient of friction for unlubricated steel and mineral oil–based lubricated steel exhibits good agreement with the Amonton's first law of friction. In the case of indium film the contact surfaces of steel show the coefficient of friction decreases with increase in normal load and this phenomenon is due to small increase in real contact area according to increase in the load. This resulted moderately in increase in

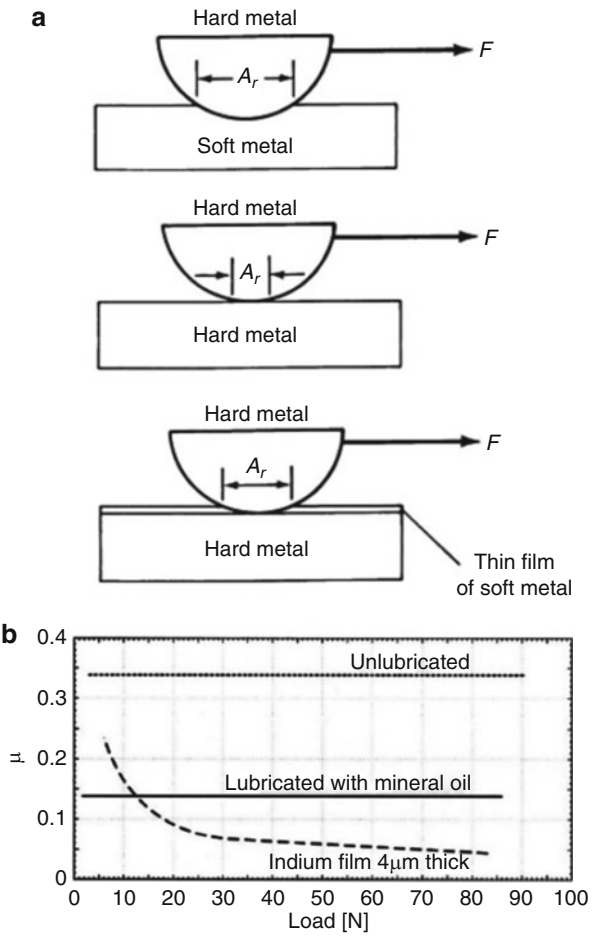

Fig. 1.5 (**a**) Frictional force relationship with metal substrate hardness under various configurations. (**b**) Friction coefficient versus normal load for steel–indium sliding contacts [11]

friction force when normal load progresses. These behaviors eventually increase the coefficient of friction (Eq. 1.5).

The above behavior can be postulated by a sphere-on-flat contact mechanism, which is so-called Hertzian elastic contact model.

The coefficient of friction expression is as follows:

$$\mu = \tau_o.\pi\left(\frac{3R}{4E^*}\right)^{2/3} L^{-1/3} + \alpha \tag{1.6}$$

where R is the sphere radius.

Hertzian contacts is predicted as:

$$\mu \propto L^{-1/3} \tag{1.7}$$

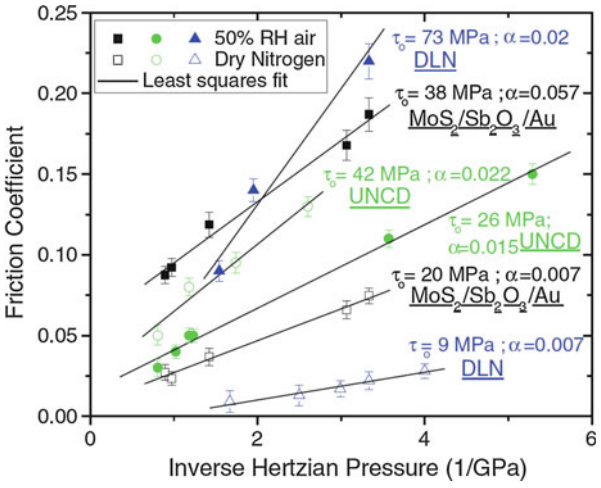

Fig. 1.6 Sliding friction coefficients versus inverse mean Hertzian pressure (linear regression fitted) to Eq. 1.6 for various solid lubricant coatings [10]

For indium film the elastic nature of contact deformations will decrease the coefficient of friction as normal load progresses. Figure 1.6 shows the established the evidence for low frictional behavior for various solid lubricant coatings through experimental validation. In addition, the pressure in thin and soft coatings is supported by the substrate. For a given normal load, contact area decreases with increase in substrate elastic modulus and hardness values. These inferences are good agreement with earlier Greenwood and Williamson model (Eqs. 1.3 and 1.4). In Bowden and Tabor's concept, in general to achieve low friction one must design a contact interface with elastically stiff and hard substrate surface with less contact area. In this the role of coatings can be defined to accommodate the shear and reduce the junction strength up to the moment the substrate starts to yield and plastically deforms. Some divergences in Bowden and Tabor's analysis for Hertzian contacts were observed for lightly loaded contact conditions. In the microscopic load ranges, some of the solid coatings (like MoS_2, Au-MoS_2, and Ti-MoS_2) and nanocomposite (diamond-like nanocomposite [DLN]) do not follow $\mu \propto L^{-1/3}$ behavior [12–14].

The tribological studies [15–17] revealed that the transfer film in the contact interface covers the contact area, thus it prevents a direct contact between sliding surfaces. The tribological performances, especially low friction and higher wear life, will depend on the specialties of the tribofilms. Although the coefficient of friction depends on transfer films, friction coefficient increases with absence of transfer film and vice versa. Also, the absence of transfer film may damage the contact surface in a greater way, and on the other hand the self-retrieval of transfer film brings it to the normal state. As a broad view it can be stated that it is not necessary to show low inherent shear strength in reduction of friction for solid lubricants. Thus, low shear strength of materials cannot take into consideration Hertzian behavior (Eq. 1.6) and wear life. Transfer films have important role in the solid lubricant to their superior performance. Some exception for this can be seen for the materials without having

transfer films, like ultra-nanocrystalline diamond (UNCD) and the near frictionless carbon (NFC). A detailed view is presented in later sections. The various types of films are solid, gas, thin, and fluid films. Some of the examples of solid films are nanotubes, nano-onions, other nanoparticles (C, BN, MoS_2, and WS_2), and diamond and diamond-like carbon coatings [18].

Apart from the adhesive friction and wear mechanisms, the abrasive mechanisms are also quite important to understand the contact mechanisms in a detailed fashion. Abrasion can be simply relating to plowing action. When a hard material slides against a soft material, an asperity to asperity contacts emerged, resulting in formation of permanent groves in soft materials due to the cutting/plowing action that can be called as abrasive action. The terminology of two- and three-body abrasion is very important to understand. The fixed abrasion or two-body abrasion is one in which the particle is attached to any one of the contacting surfaces. In three-body abrasion the particles in loose form accommodate between the two-contact surface. This has severe influence in the performances of the contact surfaces.

It can be noted that the performance parameters like friction and wear are not just influenced by mechanical and physical properties but their environmental conditions are also important entities to take into consideration. In general, solid lubricant materials, environmental conditions, applied loads, counterface material properties, sliding speeds, etc. are important in the establishment of their tribological performance. On the other hand the influences of environmental conditions are of greater impact in the performance of solid lubricants. Thus, designing solid lubricants must be based on the applications and their working environments.

1.4 Solid Lubricant Coatings

The solid lubricants are primarily used in specific applications in which conventional lubricants performances are dormant (e.g., high vacuum, aerospace, extreme speed and loading conditions, and low or high temperature) having extreme environmental conditions. The development of solid lubricants attained remarkable evolution within past few decades. The advancements in aerospace, astronomy, and specific areas where environment has significant influences reduced the usage of conventional lubricants due to their poor performance; in this context the evolution of solid lubricants made the path as an alternative to conventional lubricants. Also, the volatile debris generated by conventional liquid and greases in severe environmental conditions reduced the importance of low emission and environmental impacts are of greater concerns in modern times. This catalyzed the usage of solid lubricants in many applications having severe environmental conditions for superior tribological performances.

The past studies revealed the low coefficient of friction and high wear life of solid lubricants in various conditions. In fact, there are some deficiencies observed in the solid lubrication mechanisms. As of now no single solid lubricants are able to demonstrate both low friction and wear resistance for a wide application. In addition, limited lifetime, oxidation, aging, and difficulty in replenishment are few of them

Table 1.1 Deficiencies of solid lubricant films [18]

Deficiencies	Elimination strategies
Adhesive property	Improvement of Interface mechanisms
Frictional coefficient variation	Removal mechanisms for wear debris and its control
Tribological reactiveness	Influences of temperature and environments
Complex deposition procedures	Reduction of costs
Low thermal conductivity	Mechanisms to remove heat
Defined wear life	Difficulty of restoration

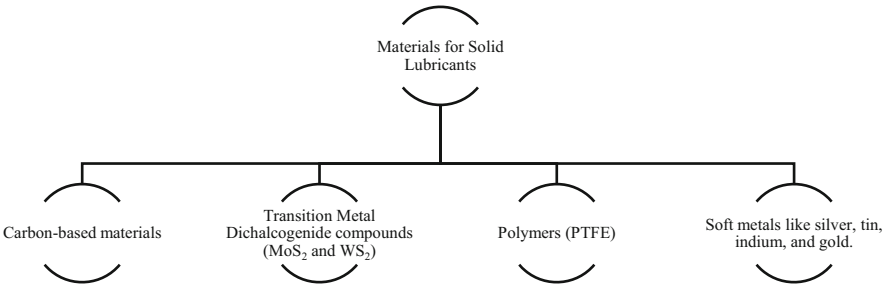

Fig. 1.7 Material classifications for solid lubricants

(specifically for certain lamellar solid lubricants). The deficiencies and probable elimination modes are demonstrated in Table 1.1.

It can be noted that a wide range of solid lubricants are available and they can be utilized as follows:

- Surface modification by fabricating lubricant coating films
- Dispersion of solid lubricant as composite coatings
- Infusion of solid lubricant particles in MMC
- Addition of solid lubricant powder in contact area
- Lubricating oils or greases through additive manufacturing

1.5 Classification of Solid Lubricants

A wide range of solid lubricant material classifications are illustrated in Fig. 1.7.

Most of the solid lubricants are capable of synthesizing a thin film coating except PTFE and their composites. These thin film coatings are useful for applications in magnetic hard drives, seals, and bearings. Single-phase materials and multi-phase composites can be derived for the solid lubricant coatings.

- **Inorganic Lubricants: With Lamellar Structure**

The crystal lattice of lamellar structured materials is comprised of several thin parallel layers having hexagonal rings. The atoms in the plane were bonded with

strong covalent bonding and planes have bonded each other with weak Van der Waals forces. These parallel layers allow sliding movements and due to the weak bonding between the parallel layers establishes the low shear strength and lubrication properties of the materials. Common lamellar structured solid lubricants are graphite, boron nitride (BN), and molybdenum disulfide (MoS_2).

- **Oxide**

  Some examples of oxides are ZnO, B_2O_3, and MoO_2.

- **Soft Metals**

Soft metals like lead (Pb), tin (Sn), bismuth (Bi), indium (In), cadmium (Cd), and silver (Ag) show lubrication properties due to their high plasticity and low shear strength. The soft materials can be used in various forms like the pure form, as coatings in bearings (especially for automobile applications), and in metal matrix composites (especially in Al- and Cu-based composites). Vapor deposition, thermal spraying, and electroplating methods are adopted in fabrication of coatings with soft materials. In the case of composites, casting processes are adopted.

- **Organic Lubricants with Chain Structure of the Polymeric Molecules**

The examples of organic lubricants are polychlorofluoroethylene and polytetrafluoroethylene (PTFE). These materials have long polymer chain molecules parallel to each other and also have weak molecule bonding and helping in sliding properties at lower shear stress regimes. But strength of the molecule across the chain is found to be high due to the strong atomic bonding. These materials are used as coatings on substrate surfaces. The applications in bearings and sleeves are few of them.

- **Graphite**

Graphite is a carbon-based solid lubricant which occurred naturally in the earth, in which carbon atoms are arranged in hexagonal structure. An amorphous class of carbon is the diamond-like carbon (DLC). DLCs are widely used as a solid lubricant in the form of coatings, commonly coined as DLC coatings. These DLC coatings offer greater tribological performances and first ever successful synthesis of DLC coatings was established by [19, 20]. The solid lubricity properties of diamond having nanocrystalline grains was observed in certain operating conditions. Figure 1.8a shows graphite is a layered solid with a hexagonal lattice [21]. The presence of a strong covalent bonding was observed between atoms in the layered basal planes. A weak Van der Waals force is observed in between basal planes and eventually exhibits low surface energies and small adhesion between the planes. Furthermore, the influences of environments, typically the presence of oxygen and water vapor, catalyzed the interlamellar shearing of graphite crystals [22, 23]. Buckley [24] performed studies related to influence of environments in tribological

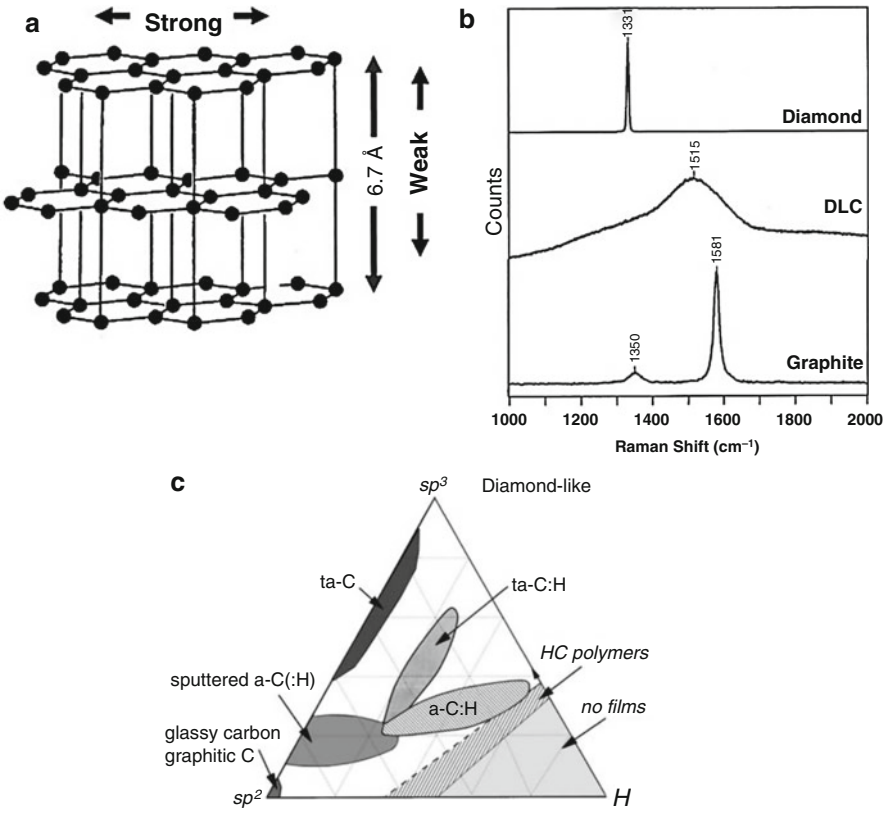

Fig. 1.8 (**a**) Lamellar crystal structure of graphite. (**b**) Raman spectral data for various solid lubricants [30]. (**c**) Bonding ternary phase diagram for amorphous carbon–hydrogen alloys [32]

parameters. Clean metallic surface was in sliding contact with pyrolytic graphite under ultrahigh vacuum environment and observed no adhesive material transfer which results in a low coefficient of friction and showed good agreement with earlier results [24]. High friction coefficient behavior was observed due to adhesive material transfer from metal to graphite surface, in which sliding is in chemically more active prismatic planes. Furthermore, a damaged basal plane increases adhesion due to increase in the edge site energy of lamellae and bonds strongly to other edge sites. The low friction can be achieved in the above case through neutralizing the edge sites by adsorption of water or other condensed vapors [21, 25]. In general, the solid lubricant routed with graphite required moisture/adsorbed gases in the contact interfaces (>100 ppm) for lubrication, otherwise the performance will be inferior. For clarity, the graphite solid lubricants observed poor tribological performance in high altitude, as well as dry and high vacuum conditions [26, 27]. The recent literature indicates that for graphite the interlamellar weaknesses are resulted due to chemisorption or intercalation of vapor molecules near to the surface [28]. The various graphite structures like single crystal, polycrystalline, and highly ordered

pyrolytic graphite (HOPG) can be visualized through Raman spectroscopy. Thus, Raman spectroscopy is a vital tool in microstructural studies [29]. Figure 1.8b shows Raman spectrum for microcrystalline graphite [30]. The spectral data for graphite indicates the presence of G and D peaks observed near 1581 cm^{-1} and 1350 cm^{-1}, respectively. The information of graphite lattice disorders are influencing the D peak intensities and the changes in structure will influence the G peak. Thus, structural changes during the sliding contact could be established through the Raman spectroscopy method. Furthermore, the applications of graphite as solid lubricant emerged as in various forms, such as self-lubricating composites and resin-bonded coatings are few of them.

- **Diamond-Like Carbon (DLC)**

The DLC are of high hardness and offers low frictions [31–33]. This is an exception as compared with the Bowden and Tabor's concept in which the graphite-like materials offer low friction and wear resistance without significant high hardness values like DLCs. During initial developments, DLCs pointed to some of the deficiencies which are related to high residual compressive stress that resulted delamination and they are not mechanically tough. To overcome these deficiencies DLCs are commercially doped with metals and lightweight elements. A typical example is hydrogenated DLCs (a-C:H) that are doped with hydrogen (~10–15 at%). Furthermore, the elements like silicon, silicon dioxide, and nitrogen and metals like chromium, tungsten, and titanium are also used in commercial doping in DLCs. The Raman spectral data for DLC coatings produced by most deposition techniques observed the G peak at 1500 cm^{-1} and 1560 cm^{-1} and small intensity of D peak was also observed at ~1350 cm^{-1} (see Fig. 1.8b) [30]. These G and D peaks provide insight into the structural disorder of these amorphous coatings. The hydrogen content and the presence of sp^2 and sp^3 bondings are observed from the ternary phase diagram (see Fig. 1.8c) [32]. The ternary phase diagram (Fig. 1.8c) represents significant informations that are scattered in three different regions. The H-free amorphous carbon (a-C) was designated to first region along the left axis. The glassy carbon is sp^2 a-C which was synthesized through evaporation or through pyrolysis of hydrocarbon polymers (not considered as DLC) that are first of three main coating types. The a-C having higher sp^3 content, but without H, which is typically routed by sputtering, (considered as DLC) are second type of them. DLC with increased sp^3 contents can be routed through unbalanced magnetron sputtering technique also. The tetrahedral amorphous carbon or ta-C are the last type of a-C coating at higher sp^3 content, which are fabricated through various deposition methods [34]. The hydrogen content in the coating can be in a wide range of ~10–50 at.% [35–37]. The ECR or ICP sources (able to generate very-high-density plasmas) can be used to fabricate tetrahedral amorphous hydrogenated carbon or ta-C: Hin the presence of hydrogen these are last kind of the coatings [38]. The coefficient of friction values for DLC coatings are influenced by testing conditions such as sliding velocity, counterface material, temperature and contact stress, and hydrogen content and the chemical bonding. The friction coefficient values can be

observed in the range of 0.01–0.5. Furthermore, hydrogen-free DLC coatings demonstrated low frictional coefficients (~0.1) for longer durations in humid air condition. Near frictionless carbon (NFC) is another class of DLC coatings. These near frictionless carbon can achieve lowest coefficients of friction ($\mu \sim 0.005$) in a sliding contact (self-mated) regime [39]. The near frictionless carbon also has a dormant behavior in adherent transfer films on the sliding counterface to resulting superior tribological behaviors. The hydrogenated carbon atoms passivating the contacting surfaces are the influencer for super low frictional behavior [33, 40]. Diamond-like carbon also often exhibits the non-Amontonian behavior (see Eq. 1.6) and for a DLN coating (Fig. 1.6) [41].

Single DLC material for both dry and humid environment with superior low friction coefficient is a challenging task to fabricate. The tribological performance of DLN coatings was found superior and the structure consists of two amorphous interpenetrating networks (which are a-C:H and a-Si-O).

A coating residual stress value of ~0.5 GPa and enhanced adhesion observed due to the graphitic carbon growth prevention in high temperatures is due to mutual stabilization of amorphous interpenetrating networks. $(CH_{0.15})_{0.7}(SiO_{0.3})_{0.3}$ are typical DLN composition which may exhibit small variation. Figure 1.9a illustrates the Raman spectral data for DLN coating [41]. The D and G peaks indicate the amorphous structure characteristics were also observed for DLC as similar to DLN. The transfer films on Si_3N_4 counterfaces under dry nitrogen and humid air conditions were established with Raman spectral analysis and also compared with DLN coatings. The results show the narrowing and increasing Raman shift peaks which indicate the transformations to a more nanometer-scale domain-sized graphitic structure. Also, these transformations were documented further for thermal treatment and frictional rubbing also [30, 40, 42, 43]. Furthermore, a thicker transfer film formed in air than in dry conditions was observed [15, 43]. In near surface differences in transfer film tribochemical products, the Raman spectroscopy analyses are found to be insensitive. Time-of-flight secondary ion mass spectroscopy (ToF–SIMS) was used for analysis of chemical mapping of the transfer films. The results observed a difference in the tribochemistry of the transfer films. Hydrogenated carbon-containing species exhibit very low frictional coefficient ($\mu \sim 0.02$) and interfacial shear strengths in dry nitrogen. In another hand, friction coefficients ($\mu \sim 0.2$) in humid air are observed for silicon and silicon oxide species. These specialties lead the DLN's capabilities to adapt in both dry and humid environments applications, eventually coined as one of the environment-friendly low-friction coating. The interfacial tribochemistry and the shear strength of pressure-induced transfer film will help to understand the chemical–mechanical mechanisms involved for the tribological performances in various environments. Thus, rigorous analysis is to be established to processing, structure, and synergies of properties in solid lubricant fabrications.

- **Molybdenum Disulfide (MoS_2)**

MoS_2 consists of lamellar structure, which can be easily sheared in the direction of motion. The usage of MoS_2 in wet environment will impact the dormant

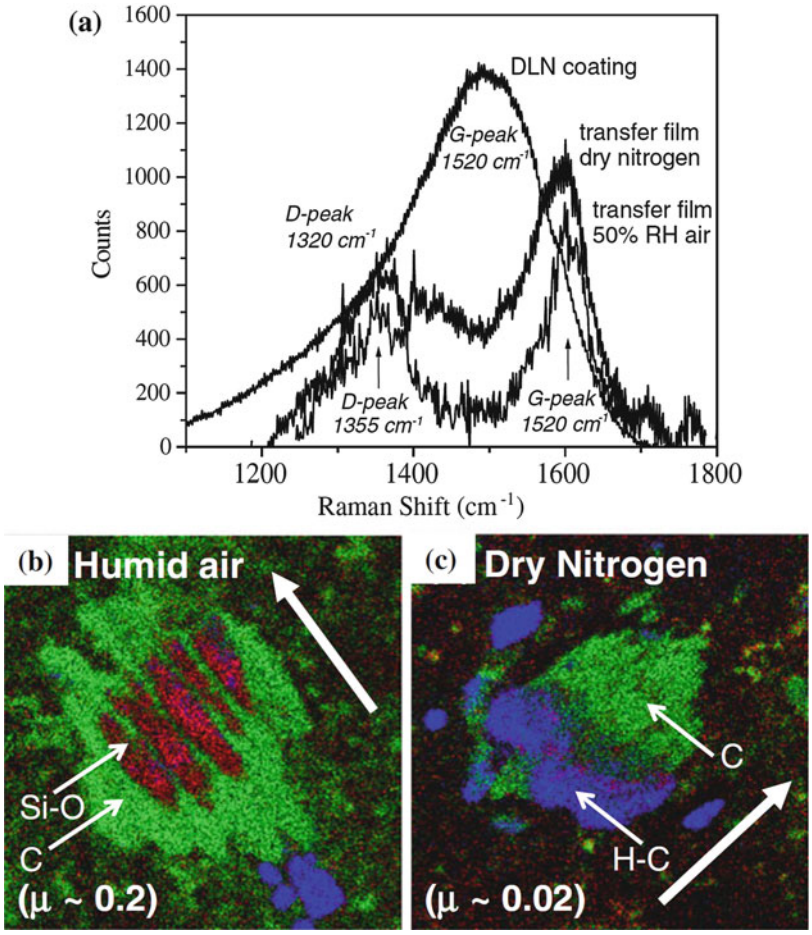

Fig. 1.9 (**a**) Raman spectral data of unworn DLN coating and transfer films. Time of flight on the counterfaces which generated in (**b**) and (**c**) for various conditions [41]

performance like increase in friction, and this may be due to the moisture. But, it has many advantages also. Few of them are presented here, such as high load-bearing capabilities, extended temperature ranges, and low friction at high loads. It is a material found within the granite and extracted through mining and highly required refinement to achieve purity, and thus can be used as lubricants. The performance of MoS_2 lubricants often exceed than graphite especially in vacuum environment where graphite lubricants cannot be used. The oxidation influences are high beyond 300 °C for MoS_2. Large particles resulted in excessive wear by abrasion mechanisms which caused by impurities in the MoS_2, and small particles resulted in accelerated oxidation.

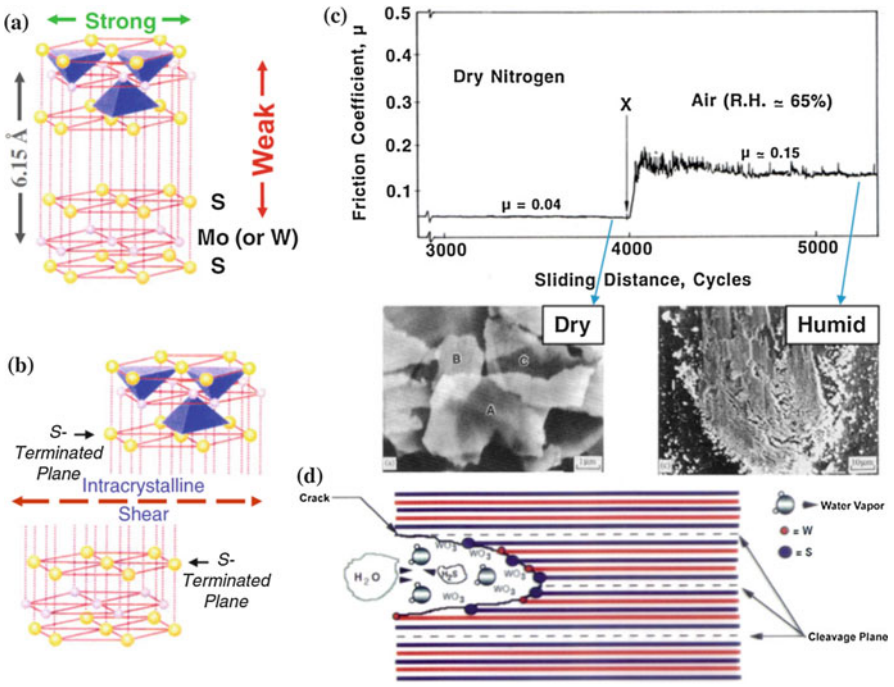

Fig. 1.10 (**a**) Mo (or W) disulfide's lamellar crystal structure. (**b**) Shows the weak Van der Waals forces resulting to interlamellar mechanical weakness. (**c**) Transition in friction coefficient in various environment. (**d**) WS_2 oxidizes and loses its ability to lubricate in humid air conditions [48, 49]

- **Transition Metal Dichalcogenide (TMD) Compounds and Adaptive Nanocomposites**

MoS_2 and WS_2 are considered as the part of TMD family of solid lubricants which have wide range of applications. The intermechanical weakness catalyzed the lubricating behavior. Like graphite the MoS_2 also has a hexagonal crystal structure (Fig. 1.10a) [21, 44].

The MoS_2(S–Mo–S) sandwich has covalent bonding and also weak Van der Waals forces. The basal planes slide over another intracrystalline slip due to a shearing force (Fig. 1.10b). This establishes transfer film formation on the counterface. The development of a transfer film in sliding interface and formation of (0002) basal planes are the mechanisms involved in low interfacial shear in TMD [45]. In general, MoS_2 and WS_2 coatings exhibit low frictional coefficients ($\leq$0.05). Furthermore, these exhibit high wear life under certain environmental conditions such as vacuum and dry inert gas. Also, a dormant behavior was observed in water vapor environment in oxidation. An increase in the frictional coefficient was observed in a humid environment as compared to dry inert gas and vacuum environments; this may be due to the formation

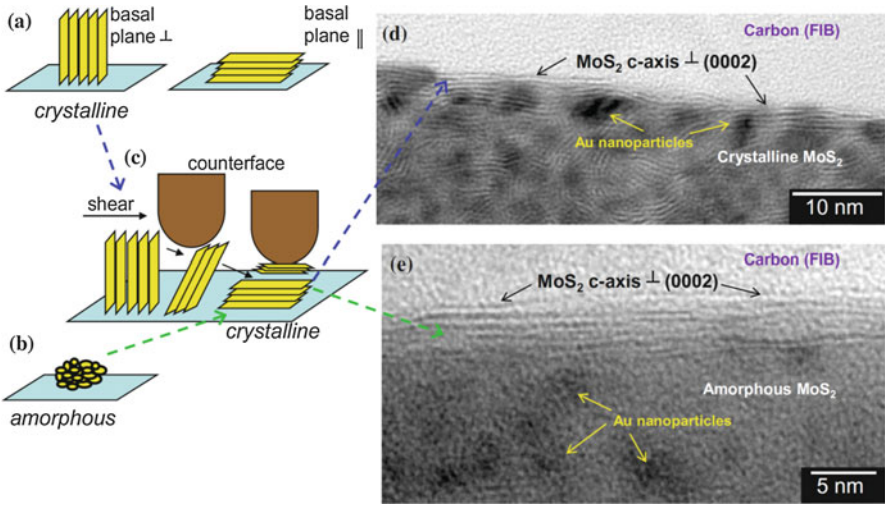

Fig. 1.11 (**a**) Schematic of two crystallographic growth textures. (**b**) Schematic of amorphous structure. (**c**) Shearing of basal plane during the interaction for both (**a**) and (**d**), (**d** and **e**) TEM images inside the wear track of MoS_2/Au coating, and amorphous MoS_2/Sb_2O_3/Au coating [10]

of tribooxidation products [21, 46–50]. Figure 1.10c illustrates frictional behavior of WS_2 coating in various environmental conditions [49, 50]. X-ray photoelectron and laser Raman spectroscopies used for studies related to the transfer films and wear scars observed the oxidation of WS_2 to WO_3 during sliding in air (Fig. 1.10d) [50, 51]. For transition metals in metal-doped DLC coatings, same oxidation tribochemical reaction was observed [17, 52].

In MoS_2 and WS_2, it is not necessary to coat both surfaces for achieving low friction because the transfer film will be formed on the counterface.The stress due to the friction can induce crystallinity into MoS_2-based coatings [53–55]. A structural evolution process at the time of friction in two mode was represented in Fig. 1.11a, b.

From Fig. 1.12, the wear factor of pure MoS_2 in dry nitrogen decreased in comparison with wear rate in air. It can be noted that these coatings were failed to retain up to 10,000 cycles. Furthermore, a significant wear factor improvement can be observed for the composite coatings like MoS_2/Sb_2O_3/Au in regime of dry N_2 and air (with 50% relative humidity). It can be noted that environment has significant influence over performance.

The influences of temperature can be one of the critical factors for the tribological performance of the coatings and the research indicates that TMD alone does not perform low friction and wear. This may be due to formation of oxidation products. Furthermore, WS_2 is thermally stable at ~400 °C, but MoS_2 begins to oxidize above ~300 °C [46, 47]. The significant performance of composite coatings in high temperature friction and wear is of greater interest in the development. In addition, TMDs, such as diselenides and ditellurides of molybdenum and tungsten have not proven to be good solid lubricants. It can be seen that there is a high need for a

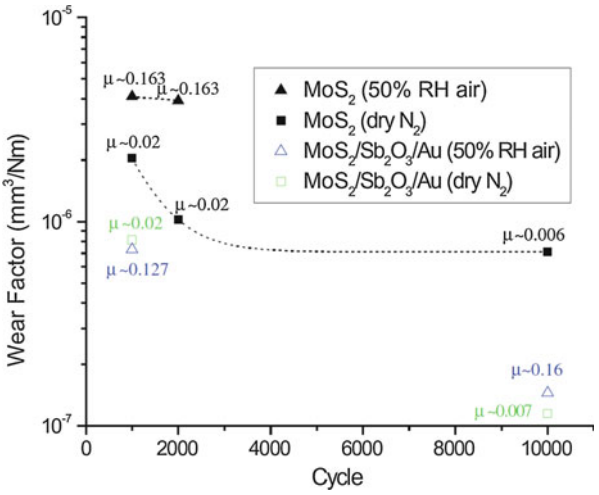

Fig. 1.12 Wear factor values for various combinations in MoS_2 [54]

reliable solid lubricant coating which environmentally also can self-adapt to various environments [54, 56].

Even the targeted objective is superior tribological performance, one of the challenges in the exposure to variable environment. A typical example related to the satellite coatings is exposed to various environment well before the targeted environment, especially humid conditions. So, there is a need of multiphase, nanocomposite materials known as adaptive lubricants and chameleon coatings [56] since TMDs, graphite, UNCD, and DLC cannot provide solid lubrication by themselves under variable humid conditions.

In addition, several metal or oxide dopants (Ti, Al, Ni, Au, Pb, PbO, and Sb_2O_3) in MoS_2 have been established for these humid applications which offer better performance. Increased coating density, hardness, and oxidation resistance are few of them [55, 57, 58], as shown in Figs. 1.6, 1.11, and 1.12, and other doped MoS_2 [59, 60] and WS_2 [61, 62]. The coatings gained a greater acceptance as robust coatings for commercial uses. Table 1.2 summarizes some of these characteristics.

- **Polytetrafluoroethylene (PTFE)**

Synthetic-type polymer which has carbon and fluorine atoms can be called as PTFE. A low surface tension property enabled to be called as highest slippery manmade material. Thus, following performances can be exhibited. They are: low frictional coefficient at lower loads and good chemical resistance, which exhibits lowest frictional coefficient about 0.04 with a limited operating range of 260 °C [63], which is furthermore used as additive material in the lubricants.

- **Boron Nitride**

Typical example for aceramic powder lubricant is boron nitride and its most important property is its high temperature resistance of 1200 °C. High thermal

Table 1.2 Solid lubricants and their characteristics [18]

Solid lubricant	Characteristics
MoS_2	Low coefficient of friction in vacuum and atmosphere conditions High thermal stability up to 1373 K in vacuum environment; however, this range was limited to 623–673 K in air Influence of absorbed water vapor and oxidizing environment are insignificant to the frictional responses Greater loading capacity Hexagonal crystal structure with the intrinsic property of easy shear MoS_2 is effective in vacuum where graphite is not
Graphite	Graphite has a low coefficient of friction Very high thermal stability (2273 K and above) Hexagonal crystal structure with the intrinsic property of easy shear Relies on adsorbed moisture or water vapors to achieve low friction Dry environments applications are found limited, particularly in vacuum Amount of water vapor adsorbed may have significant influences in frictional responses. If the amount of water vapor absorbed is less, the friction coefficient was found to be increased Practical application at high temperatures is limited to a range of 773–873 K because of oxidation High temperature applications are limited and addition of inorganic compounds improves the temperature withstanding ranges
PTFE[a]	Exhibits low coefficient of friction in vacuum and atmosphere; this is because of a lack of chemical reactivity Insignificant behavior to adsorbed vapors or moisture It possesses low surface energy and does not have a layered structure Temperatures range from 173 to 523 K Low load-carrying capacity and durability Low thermal conductivity of PTFE prevents heat dissipation, which causes premature failure due to melting and restricts the usage of low-speed sliding applications where MoS2 is not satisfactory. PTFE displays one of the lowest static and dynamic friction coefficients down to 0.04. Operating temperatures are limited to approximately 523 K

[a]Polytetrafluoroethylene

conductivity properties of boron enabled its usages in various specific applications. The hexagonal chemical structures offer lubricating properties; however, cubic structures are more abrasive [64].

1.6 Requirements to Solid Lubricants Properties

Typical required properties for solid lubricants are low shear strength, high compression strength, and good adhesion. The low shear strength will help in low coefficient of friction. The high compression strength will enable the lubricant to

withstand at higher loads. The good adhesion property will help to provide presence of lubricant on the surface even at high shear stress. The first two properties possess anisotropic materials like graphite, molybdenum disulphide, or boron nitride having lamellar crystal structure.

1.6.1 Characterization of Solid Lubricants

Following are the various advantages and disadvantages of solid lubricants:
Advantages:

- High loadsworking ability
- Greater thermal stability
- Various specific applications

Disadvantages:

- Lower tribological performances in consideration with hydrodynamic regime
- The lubrication film has low stability

1.6.2 Typical Applications of Solid Lubricants

- When conventional lubricants are inadequate the solid lubricants are useful especially for reciprocating motion, for example, in gear and chain lubrication mechanisms. Also, prevent from various corrosion mechanisms.
- Substitutes for chemically active lubricants additives.
- Extreme temperature and oxidizing environmental conditions.
- High loading capabilities (Figs. 1.13, 1.14, and 1.15).

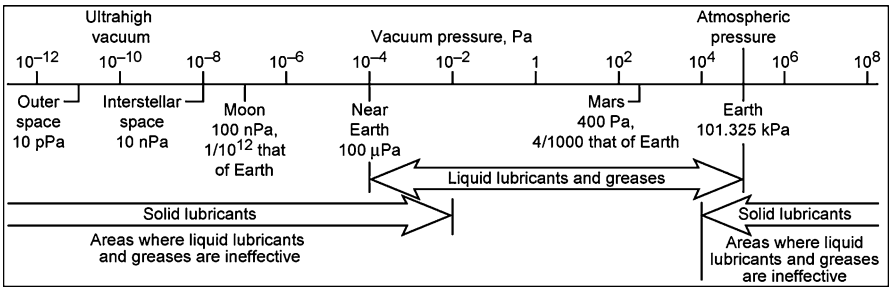

Fig. 1.13 Lubricant applications in vacuum environments [18]

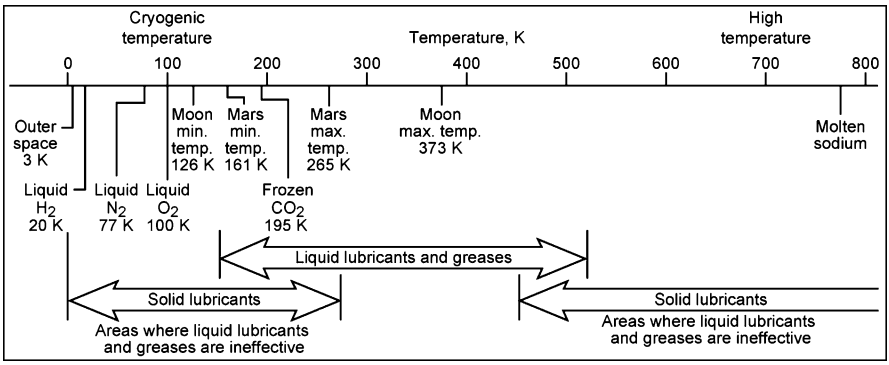

Fig. 1.14 Lubricant applications in cryogenic and high-temperature environments [18]

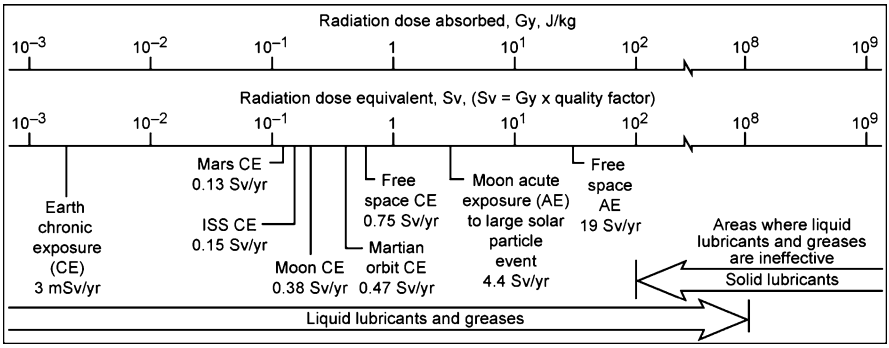

Fig. 1.15 Lubricant applications in radiation environments [18]

1.7 Solid Lubricant in Additive Oils

The usage of nano-particulate solid lubricant in a base oil forms additive oils with greater tribological performances and found superior tribological properties. The mechanisms of nanoparticle additives are as follows: (1) ball effect [65, 66]; (2) tribochemical reactions [67–69]; and (3) adsorption film theory [70]. Dispersion of solid lubricant powders in oil occurs also one way [71–75]. The solid lubricants, such as MoS_2also, can be dispersed in oil which offers significant tribological performances [71, 72, 76]. The graphite existed on the rubbing surfaces stably and formed composition film with the oil-soluble additives [77]. The particle sizes of lubricant and concentrations have vital role in the wear rates. Larger the particles exhibit larger wear and small particles at larger loading conditions exhibit a low wear rates [74]. The addition of solid lubricant to mineral oil offers significant tribological performance. The performances are depending on the types of additives in oils, particle hardness, and size of the solid lubricant particles [74, 75].

Lovell et al. studied green lubricant (environmentally friendly) combinations by homogeneously mixing nano- (20 nm), submicrometer-(600 nm average size), and

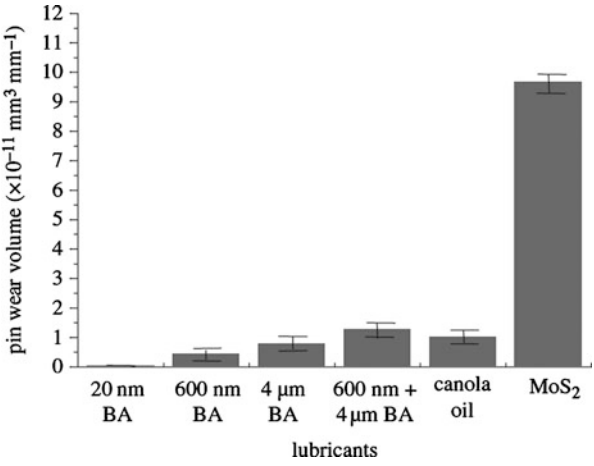

Fig. 1.16 Wear rate variations when the Cu pins slid against Al discs in the presence of various additives [78]

micrometer-scale (4 mm average size) boric acid powder additives with canola oil in a vortex generator and found that the nanoscale (20 nm) particle boric acid additive lubricants significantly outperformed all of the other lubricants with respect to tribological performance (Fig. 1.16) [78].

Reeves et al. investigated tribological performance of a mixed canola oil–based lubricant with boron nitride particles. Significant improvement of tribological performances (reduced friction by 40% and wear by 70%) was observed with addition of boron nitride nanoparticles as compared with micron- and submicron-sized particles in canola oil (Figs. 1.17 and 1.18), and this may be due to the ability to provide better coalesce in the asperity valleys for nanoparticles [79].

Omrani et al. studied the tribological properties of Al-16Si-5Ni-5 graphite composite and showed significant tribological properties under limited lubricated conditions. This may be due to the presence of graphite particles in the composites which act as solid lubricant (Fig. 1.19) [80, 81]. Furthermore, these composite lubricants can be used as a substitute in automobile applications. The various forms of carbon-based solid lubricants used in coatings, lubricants, and composites for tribological applications are recently demonstrated by various researchers [82–91].

Recently, Charoo and Hanie conducted experiments on SAE 20 W50 with various nanoparticles such as hexagonal boron nitride (h-BN), tungsten disulphide (WS2), and graphite. The EN8 steel disk and AISI 52100 steel ball considered as the tribo-pair for the friction and wear tests. It was observed that hexagonal boron nitride (h-BN) outperformed than other combinations (Fig. 1.20). However, the friction coefficient was observed to increase with increase in sliding distance [92]. The tribological performance of addition of fullerene soot in mineral oil combinations was studied by Yunusov et al. It was observed that the addition of fullerene soot helps to reduce the frictional force [93]. Further, the influence of ZnO nanoparticles in diesel oil was investigated by Mousavi and Zeinali Heris. It was observed that the thermophysical and tribological properties are improved due to the addition of ZnO [94].

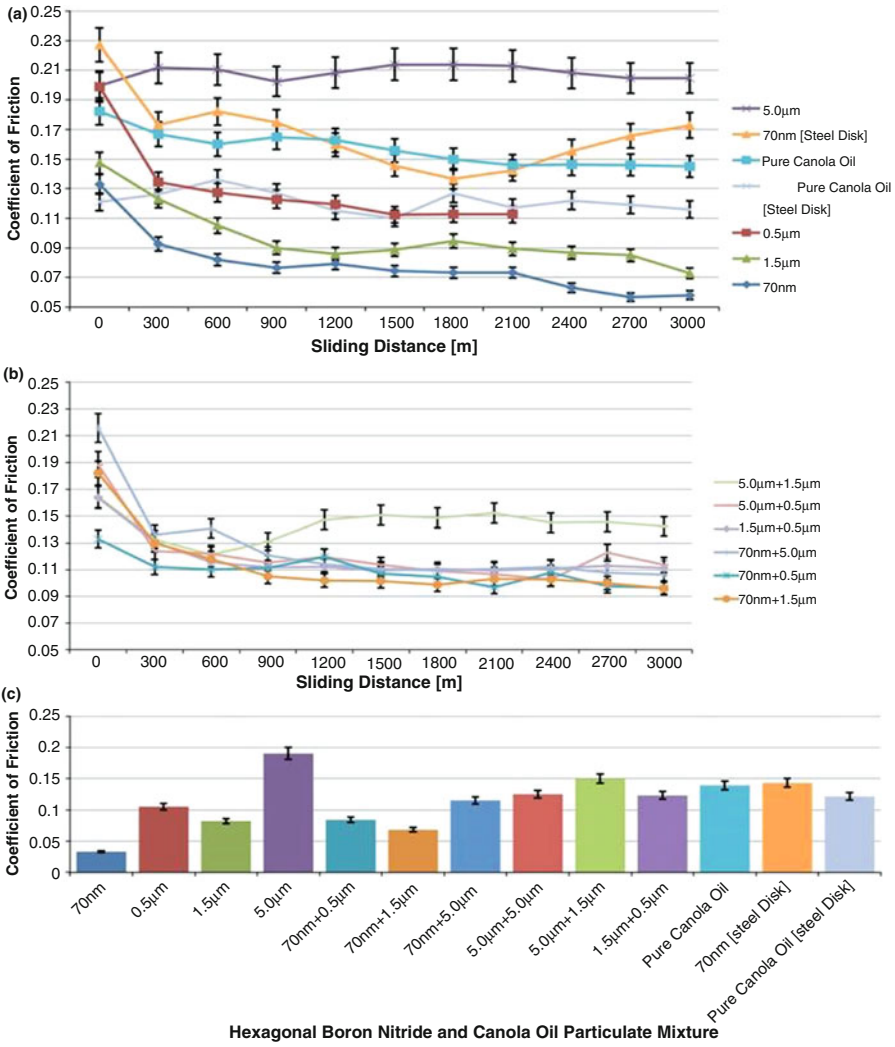

Fig. 1.17 Variation of frictional coefficient for (**a**) single-particle-sized particulate mixtures, (**b**) for multiple particle sized, and (**c**) for various particulate mixtures [79]

1.8 Conclusions

Solid lubricants are good candidate for specific application where conventional lubricant performance is dormant. Some of the examples for solid lubricants are diamond and DLC films, lamellar solids, and lubricious oxides. Current trend in line

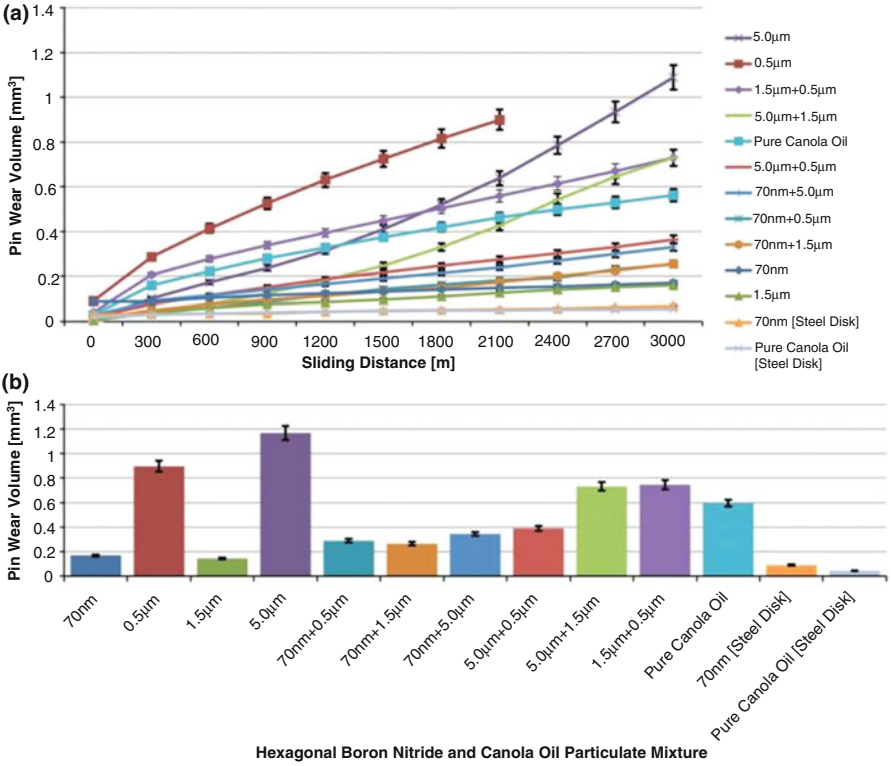

Fig. 1.18 Pin wear volume vs sliding distance for (**a**) particulate mixtures, (**b**) for various particulate mixtures [79]

to an environment-friendly lubricant nourishes the solid lubricant research and developments. Thin solid films are widely considered in the sliding regimes. Various deposition methods like PVD and CVD are good candidates for solid lubricant coatings in various substrate surfaces (like metals and ceramics), which offer strong bondings and greater adaptability to serve applications. The solid lubricant coatings that adapt to the changing condition of tribological applications are called as adaptive or chameleon type. Solid lubricants developed through smart engineering routes offer better tribological performances. For high temperatures applications, most layered solid lubricant is ineffective, except lubricious oxides and fluorides. Novel adaptive solid lubricant and some of the polymers have capabilities in wide temperature ranges. Polymers are suitable due to its greater physical, economical, and mechanical peculiarities. The demand of these solid lubricants is expectedly high. This may be due to the performance of these solid lubricants in some specific applications and in some severe environmental conditions.

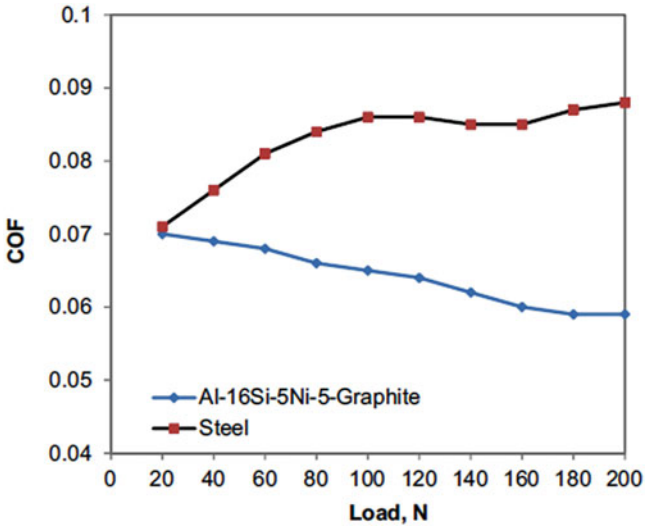

Fig. 1.19 Variation of mean COF versus load for steel and Al-16Si-5Ni-5 graphite composite under fully lubricated regime [80]

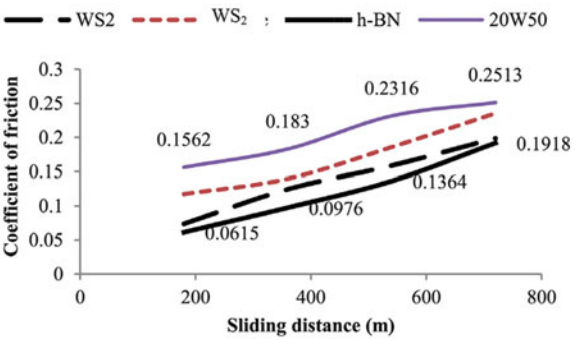

Fig. 1.20 Comparison of coefficient of friction for various nanoparticles in SAE 20W50

References

1. Rohatgi, P.K., Menezes, P.L., Lovell, M.R., Kailas, S.V.: Addition of solid lubricants to metal matrices and liquid lubricants to improve tribological performance. In: 2014 ASIATRIB, Agra
2. Tabor, D.: J. Lubr. Technol. **103**, 169 (1981)
3. Rabinowicz, E.: Friction and Wear of Materials, 3rd edn, p. 34. Wiley, New York (1995)
4. Rabinowicz, E.: ASLE Trans. **14**, 198 (1971)
5. Gao, G.T., Mikulski, P.T., Harrison, J.A.: J. Am. Chem. Soc. **124**, 7202 (2002)
6. Johnson, K.L.: Contact Mechanics. Cambridge University Press, Cambridge (1985)
7. Larsen-Basse, J.: ASM Handbook. Friction, Lubrication, and Wear Technology, vol. 18, p. 30. ASM International (1992)
8. Greenwood, J.A., Williamson, J.B.P.: Proc. R. Soc. Lond. A. **295**, 300 (1966)

9. Whitehouse, D.J., Archard, J.F.: Proc. R. Soc. Lond. **A316**, 97 (1970)
10. Scharf, T.W., Prasad, S.V.: Solid lubricants: a review. J. Mater. Sci. **48**, 511–531 (2013). https://doi.org/10.1007/s10853-012-7038-2
11. Bower, A.F., Johnson, K.L.: J. Mech. Phys. Solids. **34**, 471 (1989)
12. Bowden, F.P., Tabor, D.: The Friction and Lubrication of Solids, pp. 112–120. Clarendon Press, Oxford (1986)
13. Stoyanov, P., Chromik, R.R., Goldbaum, D., Lince, J.R., Zhang, X.: Tribol. Lett. **40**, 199 (2010)
14. Stoyanov, P., Strauss, H.W., Chromik, R.R.: Wear. **274–275**, 149 (2012)
15. Chromik, R.R., Wahl, K.J.: World Tribology Congress III, pp. 829–830. American Society of Mechanical Engineers, New York (2005)
16. Singer, I.L., Dvorak, S.D., Wahl, K.J., Scharf, T.W.: J. Vac. Sci. Technol. A. **21**, S232 (2003)
17. Wahl, K.J., Sawyer, W.G.: MRS Bull. **33**, 1159 (2008)
18. Miyoshi, K.: Solid lubricants, and coatings for extreme environments: state-of-the-art survey. NASA/TM—2007-214668
19. Strauss, H.W., Chromik, R.R., Hassani, S., Klemberg-Sapieha, J.E.: Wear. **272**, 133 (2011)
20. Schmellenmeier, H.: Exp. Tech. Phys. **1**, 49 (1953)
21. Eisenberg, S., Chabot, R.: J. Appl. Phys. **42**, 2953 (1971)
22. Braithwaite, E.R.: Solid Lubricants and Surfaces, p. 139. Clarendon Press, Oxford (1964)
23. Deacon, R.F., Goodman, J.F.: Proc. R. Soc. Lond. A. **243**, 464 (1958)
24. Roselman, I.C., Tabor, D.: J. Phys. D. **9**, 2517 (1976)
25. Buckley, D.H.: Surface Effects in Adhesion, Friction, Wear and Lubrication. Elsevier, Amsterdam (1981)
26. Skinner, J., Gane, N., Tabor, D.: Nature. **232**, 195 (1971)
27. Savage, R.H.: J. Appl. Phys. **19**, 1 (1948)
28. Ramadanoff, D., Glass, S.W.: Trans. Am. Inst. Electr. Eng. **63**, 825 (1944)
29. Yen, B.K., Schwickert, B.E., Toney, M.F.: Appl. Phys. Lett. **84**, 4702 (2004)
30. Robertson, J.: Adv. Phys. **35**, 317 (1986)
31. Tallant, D.R., Parmeter, J.E., Siegal, M.P., Simpson, R.L.: Diam. Relat. Mater. **4**, 191 (1995)
32. Erdemir, A., Donnet, C. (eds.): Tribology of Diamond-like Carbon Films: Fundamentals and Applications. Springer, New York (2008)
33. Robertson, J.: Mater. Sci. Eng. R. **37**, 129 (2002)
34. Grill, A.: Wear. **168**, 143 (1993)
35. Erdemir, A., Donnet, C.: J. Phys. D. Appl. Phys. **39**, R311 (2006)
36. Koidl, P., Wagner, C., Dischler, B., Wagner, J., Ramsteiner, M.: Mater. Sci. Forum. **52**, 41 (1990)
37. Tamor, M.A., Vassell, W.C., Carduner, K.R.: Appl. Phys. Lett. **58**, 592 (1991)
38. Donnet, C., Fontaine, J., Lefevre, F., Grill, A., Patel, V., Jahnes, C.: J. Appl. Phys. **85**, 3264 (1999)
39. Weiler, M., Sattel, S., Giessen, T., Jung, K., Ehrhardt, H., Veerasamy, V.S., Robertson, J.: Phys. Rev. B. **53**, 1594 (1996)
40. Erdemir, A., Eryilmaz, O.L., Fenske, G.: J. Vac. Sci. Technol. A. **18**, 1987 (2000)
41. Erdemir, A.: Proc. Inst. Mech. Eng. J. **216**, 387 (2002)
42. Scharf, T.W., Ohlhausen, J.A., Tallant, D.R., Prasad, S.V.: J. Appl. Phys. **101**, 0635211 (2007)
43. Donnet, C.: Surf. Coat. Technol. **100–101**, 180 (1998)
44. Scharf, T.W., Singer, I.L.: Tribol. Lett. **14**, 137 (2003)
45. Prasad, S.V., Zabinski, J.S.: Nature. **387**, 761 (1997)
46. Singer, I.L.: In: Singer, I.L., Pollock, H.M. (eds.) Fundamentals of Friction: Macroscopic and Microscopic Processes, p. 237. Kluwer, Dordrecht (1992)
47. Brainard, W.A.: NASA TN D5141 (1969)
48. Sliney, H.E.: Tribol. Int. **15**, 303 (1982)
49. Prasad, S.V., Zabinski, J.S.: J. Mater. Sci. Lett. **12**, 1413 (1993)
50. Prasad, S.V., Zabinski, J.S., McDevitt, N.T.: Tribol. Trans. **38**, 57 (1995)
51. Zabinski, J.S., Donley, M.S., Prasad, S.V., McDevitt, N.K.: J. Mater. Sci. **29**, 4834 (1994). https://doi.org/10.1007/BF00356530

52. Chromik, R.R., Strauss, H.W., Scharf, T.W.: J. Manag. **64**, 35 (2012)
53. Muratore, C., Bultman, J.E., Aouadi, S.M., Voevodin, A.A.: Wear. **270**, 140 (2011)
54. Wahl, K.J., Dunn, D.N., Singer, I.L.: Wear. **230**, 175 (1999)
55. Scharf, T.W., Kotula, P.G., Prasad, S.V.: Acta Mater. **58**, 4100 (2010)
56. Hu, J.J., Wheeler, R., Zabinski, J.S., Shade, P.A., Shiveley, A., Voevodin, A.A.: Tribol. Lett. **32**, 49 (2008)
57. Muratore, C., Voevodin, A.A.: Annu. Rev. Mater. Res. **39**, 297 (2009)
58. Hilton, R., Fleischauer, P.D.: Surf. Coat. Technol. **54–55**, 435 (1992)
59. Zabinski, J.S., Donley, M.S., Walck, S.D., Schneider, T.R., McDevitt, N.T.: Tribol. Trans. **38**, 894 (1995)
60. Teer, D.G.: Wear. **251**, 1068 (2001)
61. Fox, V.C., Renevier, N., Teer, D.G., Hampshire, J., Rigato, V.: Surf. Coat. Technol. **116–119**, 492 (1999)
62. Scharf, T.W., Prasad, S.V., Dugger, M.T., Kotula, P.G., Goeke, R.S., Grubbs, R.K.: Acta Mater. **54**, 4731 (2006)
63. Konovalova, O., Suchanek, J.: Significance of polymer nanocomposites in triboengineering systems. In: Proceedings of the 4th International Conference NANOCON 2012, Ostrava: TANGER, spol.sr.o (2012). ISBN 978-80-87294-35-2
64. Jagatheeshwaran, M.S.: A study on the friction and wear behavior of electroless nip composite coating with the addition of sea shell and nano zno particles. Introduction to Sea Shell Particles and Electroless Composite Coating Process. (2018) https://shodhganga.inflibnet.ac.in/bitstream/10603/298422/7/07_chapter1.pdf
65. Tarasov, S., Kolubaev, A., Belyaev, S., Lerner, M., Tepper, F.: Study of friction reduction by nanocopper additive to motor oil. Wear. **252**, 63–69 (2002)
66. Tao, X., Zhao, J., Kang, X., Xue, Q.: Study on the tribological properties of ultradispersed diamond containing soot as an oil additive. Tribol. Trans. **40**(1), 178–182 (1997)
67. Dong, J.X., Hu, Z.S.: A study of the anti-wear and friction-reducing properties of the lubricant additive, nanometer zinc borate. Tribol. Int. **31**(5), 219–223 (1998)
68. Liu, W., Chen, S.: An investigation of the tribological behaviour of surface-modified ZnS nanoparticles in liquid paraffin. Wear. **238**, 120–124 (2000)
69. Chen, S., Liu, W., Laigui, Y.: Preparation of DDP-coated PbS nanoparticles and investigation of the antiwear ability of the prepared nanoparticales as additive in liquid paraffin. Wear. **218**, 153–158 (1998)
70. Xue, Q., Liu, W., Zhang, Z.: Friction and wear properties of a surface-modified TiO_2 nanoparicle as an additive in liquid paraffin. Wear. **213**, 29–32 (1997)
71. Gansheimer, J., Holinski, R.: Molybdenum disulfide in oils and greases under boundary conditions. ASME J. Lubr. Technol. **95**, 242–248 (1973)
72. Wo, H., Kunhong, H., Xianguo, H.: Tribological properties of MoS_2 nanoparticles as additive in a machine oil. Tribology. **24**(1), 33–37 (2004)
73. Bartz, W.J.: Solid lubricant additive-effect of concentration and other additives on antiwear performance. Wear. **17**, 421–432 (1971)
74. Bartz, W.J.: Some investigation on the influence of particle size on the lubrication effectiveness of molybdenum disulfide. ASLE Trans. **15**, 207–215 (1972)
75. Bartz, W.J., Oppelt, J.: Lubricating effectiveness of oil-soluble additives and molybdenum disulfide dispersed in mineral oil. Lubr. Eng. **36**(10), 579–585 (1980)
76. Cusano, C., Sliney, H.E.: Dynamics of solid dispersions in oil during the lubrication of point contacts. Part I. Graphite. ASEM Trans. **25**(2), 183–189 (1982)
77. Chu, S., Jin, Z., Xue, Q.: Study of the interaction between natural flake graphite and oil soluble additives. Tribology. **17**(4), 340–347 (1997)
78. Lovell, M.R., Kabir, M.A., Menezes, P.L., Iii, C.F.H.: Influence of boric acid additive size on green lubricant performance. Philos. Trans. R. Soc. A. **368**, 4851–4868 (2010)

79. Reeves, C.J., Menezes, P.L., Lovell, M.R., Jen, T.-C.: The size effect of boron nitride particles on the tribological performance of biolubricants for energy conservation and sustainability. Tribol. Lett. **51**, 437–452 (2013)
80. Omrani, E., Moghadam, A.D., Algazzar, M., Menezes, P.L., Rohatgi, P.K.: Effect of graphite particles on improving tribological properties Al-16Si-5Ni-5 graphite self-lubricating composite under fully flooded and starved lubrication conditions for transportation applications. Int. J. Adv. Manuf. Technol. **87**, 929–939 (2016)
81. Omrani, E., Reeves, C., Menezes, P.L., Rohatgi, P.K.: Tribological properties of micro- and nano-sized solid lubricant (graphite and graphene) as lubricant oil additives. In: 2015 STLE Tribology Frontiers Conference, Denver, 25–27 October 2015
82. Shiwen, W., Tian, S., Menezes, P.L., Xiong, G.: Carbon solid lubricants: role of different dimensions. Int. J. Adv. Manuf. Technol. **107**(9), 3875–3895 (2020)
83. Siddaiah, A., Kumar, P., Henderson, A., Misra, M., Menezes, P.L.: Surface energy and tribology of electrodeposited Ni and Ni-graphene coating on steel. Lubricants. **7**(10), 87:1–15 (2019)
84. Omrani, E., Menezes, P.L., Rohatgi, P.K.: Effect of micro- and nano-sized carbonous solid lubricants as oil additives in nanofluid on tribological properties. Lubricants. **7**(3), 25:1–13 (2019)
85. Siddaiah, A., Kasar, A.K., Manoj, A., Menezes, P.L.: Influence of environmental friendly multiphase lubricants on the friction and transfer layer formation during sliding against textured surfaces. J. Clean. Prod. **209**, 1245–1251 (2019)
86. Kasar, A.K., Xiong, G., Menezes, P.L.: Graphene-reinforced metal and polymer matrix composites. JOM. **70**(6), 829–836 (2018)
87. Kasar, A.K., Menezes, P.L.: Synthesis and recent advances in tribological applications of graphene. Int. J. Adv. Manuf. Technol. **87**(9–12), 3999–4019 (2018)
88. Nazir, M.H., Khan, Z.A., Saeed, A., Siddaiah, A., Menezes, P.L.: Synergistic wear-corrosion analysis and modelling of nanocomposite coatings. Tribol. Int. **121**, 30–44 (2018)
89. Reeves, C.J., Menezes, P.L.: Evaluation of boron nitride particles on the tribological performance of avocado and canola oil for energy conservation and sustainability. Int. J. Adv. Manuf. Technol. **89**(9–12), 3475–3486 (2017)
90. Bogatov, A., Yashin, M., Viljus, M., Menezes, P.L., Podgursky, V.: Comparative analysis of two methods for evaluating wear rate of nanocrystalline diamond films. Key Eng. Mater. **721**, 345–350 (2017)
91. Yashin, M., Baroninš, J., Menezes, P.L., Viljus, M., Raadik, T., Bogatov, A., Antonov, M., Podgursky, V.: Wear rate of nanocrystalline diamond coating under high temperature sliding conditions. Solid State Phenom. **267**, 219–223 (2017)
92. Charoo, M.S., Hanief, M.: Improving the tribological characteristics of a lubricating oil by nano sized additives. Mater. Today Proc. **28**, 1205–1209 (2020)
93. Yunusov, F.A., Breki, A.D., Vasilyeva, E.S., Tolochko, O.V.: The influence of nano additives on tribological properties of lubricant oil. Mater. Today Proc. (2020). https://doi.org/10.1016/j.matpr.2020.01.447
94. Mousavi, S.B., Zeinali Heris, S.: Experimental investigation of ZnO nanoparticles effects on thermophysical and tribological properties of diesel oil. Int. J. Hydrog. Energy. (2020). https://doi.org/10.1016/j.ijhydene.2020.05.259

Tribology of Self-Lubricating Metal Matrix Composites

2

Yinyin Zhang and Richard R. Chromik

Contents

Y. Zhang · R. R. Chromik (✉)
Department of Mining and Materials Engineering, McGill University, Montreal, QC, Canada

P. L. Menezes et al. (eds.), *Self-Lubricating Composites*,
https://doi.org/10.1007/978-3-662-64243-6_2

Abstract

Self-lubricating metal matrix composites (SLMMCs) are a class of materials that have potential to help engineers meet the demands of global initiatives for green manufacturing and sustainability. While SLMMCs have existed for many decades with traditional lubricant materials like graphite and other lamellar solids, such as MoS_2, WS_2, h-BN and CaF_2, BaF_2, scientists have recently incorporated nanostructured versions of the materials (e.g., carbon nanotubes and graphene). At the same time, new manufacturing and processing techniques have come online, such as additive manufacturing techniques that may provide significant innovation for SLMMCs. In this chapter, the current state of SLMMC research is reviewed, including materials, processing methods, and tribological performance. Processing and property relationships are described, such as influence of testing parameters and content of solid lubricants on friction and wear. Improvements in tribological behavior, as much as possible, are interpreted through third-body approach, which emphasizes materials phenomena at the sliding interface – including mechanical, structural, and chemical changes to the parent materials. Based on the review of SLMMCs and their tribology, recommendations for future research are made that emphasize the use of new materials, new processing routes, and research approaches that seek to reveal more completely the mechanisms by which these materials form tribofilms that are effective at lowering friction and reducing wear.

2.1 Introduction

Modern technology has placed materials into increasingly demanding and harsh environments. To meet the needs of next-generation applications, scientists and engineers are tasked with designing new materials with sufficient life cycle and reliability. Higher forces, temperatures, and exposure to environmental corrosion and mechanical wear lead to the need for various design strategies involving increased mechanical properties both in the bulk and at the surface. One such strategy that can be used for both surface and bulk enhancement of properties is use of composite materials.

Composite materials make use of more than one material class with one acting as the matrix and the other as a reinforcing component. Historically, composites have been used for thousands of years, with the very first examples being mud and straw composites used for housing in Egypt and Mesopotamia (circa 1500 BC) [1]. Modern engineering composites can be found nearly everywhere in our daily life, with the most common variety being polymer matrix composites (PMC) used, for example, as bicycle frames, hockey sticks, and airframe materials. More often than not, modern composites are designed from a mechanical properties perspective, where the matrix alone does not have adequate strength and/or stiffness for the design requirements. The reinforcing component, which in the PMC example is often a glass or ceramic material, enhances mechanical properties by a load transfer or load-sharing mechanism. Alongside the development of PMCs, scientists and engineers developed metal-matrix composites (MMCs). Technologies to fabricate MMCs were

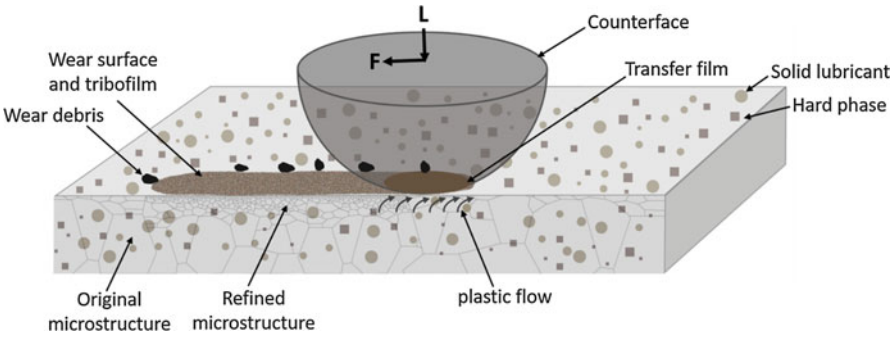

Fig. 2.1 A schematic of a bulk SLMMC that are under service. Solid lubricant–related tribofilms and, in some cases, transfer films are formed. Sliding usually generates refined microstructure on the subsurface of the wear track, and the plastic flow, shown as arrows underneath the counterface, promotes solid lubricant particles squeezing out to replenish the tribofilm and the transfer film

developed in the 1970s with increasing adoption of these materials in various applications in the following decades [2, 3]. Reinforcing components in MMCs can take the form of hard materials such as ceramics or glasses, but may also be materials for enhancement of the surface properties, known as solid lubricants.

Composite materials are often employed for tribological applications, where wear resistance and control of friction are important. Self-lubricating metal matrix composites (SLMMCs) may be in the form of bulk composites [4, 5], thick coatings or claddings [6], or thin nanocomposite coatings [7, 8]. Figure 2.1 depicts the scenarios of a bulk SLMMC that contains solid lubricants to modify friction and hard phases to support load and reduce wear. Common hard ceramic phases are Al_2O_3 and SiC and common solid lubricants are graphite (Gr), MoS_2, h-BN, and many others. The latter impart "self-lubricating" (sometimes "auto-lubricating") properties to the MMC by the formation of lubricating tribofilms and, in some cases, transfer films at the contact that can be regenerated during in-service wear of the component. Here, tribofilm refers to a surface modified layer on the material being tested and transfer films refer to a modified layer attached to the counterface (as depicted in Fig. 2.1). SLMMCs are an important class of materials for future green manufacturing and engineering sustainability. Use of SLMMCs reduces the need for oil lubrication and reduces friction and thus the energy consumption in the systems where they are used. They can also mitigate wear and increase the lifetime of components.

2.2 Selected Tribology Concepts for Metals, Solid Lubricants, and SLMMCs

2.2.1 Third Bodies for Metals and Solid Lubricants

When two surfaces are brought together to form a sliding contact, mechanical and chemical interactions lead to the formation of what tribologists commonly refer to as "third bodies" [9, 10]. The characteristics of third bodies are dictated by the

parent materials (the two "first bodies" sliding against one another), the ambient environment and parameters such as load and sliding velocity. Once the third bodies form, their behavior in the tribological system often has a significant role in determining the friction and wear performance. As shown in Fig. 2.1, transfer films may form on the ball (i.e., "countersurface" or "counterface" material) due to adhesive wear processes. Tribofilms may form on the test material of interest. They may be due to mechanical and chemical modification of the parent material but may also be due to redeposition of transfer film material to the worn surface. Wear debris is third body material that leaves the contact and no longer participates in the sliding process. There are many other names given to third bodies in the open literature, including but not limited to mechanically mixed layers (MML), tribologically transformed structures (TTS), tribomaterial, transfer layer, fragmented layer, highly deformed layer, glaze layer, white-etching layer, and nanocrystal layer [11]. MML is a common terminology in metals tribology where work-hardened, nanocrystalline, and other transformed microstructures are found at the surface [12]. TTS is a terminology used to describe nascent materials that are about to leave the first body to become part of the third bodies in the contact [13, 14]. For this chapter, we restrict discussion to "transfer films," "tribofilms," and "wear debris" – three distinct types of third bodies as labeled in Fig. 2.1.

For decades, third bodies were studied primarily by ex situ methods, where after a laboratory scale test the first bodies were separated and the nature of these materials was examined with a variety of material characterization techniques [15]. More recently, scientists developed in situ methods that are capable of directly examining third bodies during the wear test. These techniques and the history of their development were recently reviewed by Chromik et al. [16] and Wahl and Sawyer [17]. Here we mention these techniques as they were key in demonstrating the importance of examining third body "processes" or third body "flows" and the concept of velocity accommodation [18]. This is especially true for solid lubricants [19–24], such as MoS_2 and DLC. More recently, the techniques have been used to study metals tribology [25–29], which also demonstrated the importance of third bodies in determining the performance of metals in sliding contact. The manner in which third bodies modify how velocity is accommodated between two surfaces in relative motion was described by Berthier et al., where 20 velocity accommodation mechanisms (sometimes "modes") were defined or identified based on experimental evidence [18, 30].

For the context of SLMMCs, understanding of third bodies and their formation is crucial. These materials are designed specifically to form and replenish tribofilms from the self-lubricating fillers within their matrix. The effectiveness of this process and the mechanisms by which it occurs are not always fully explored in the literature. In fact, it is only until recently that in situ tribology techniques have been applied to composite materials for nanocomposite PVD coatings [8] and MMCs [28, 29, 31]. Researchers have, however, used ex situ methods to investigate tribofilm formation on SLMMCs which have demonstrated their importance and role in lubrication and enhancement of the tribological properties [32–36]. It is also true that the nature of self-lubrication for an SLMMC is related to the same processes that occur for solid lubricant applied as coatings. However, the source flow of lubricating material is

potentially much less for an SLMMC and the third bodies that form, and their flows are expected to be substantially altered. As such it is worthwhile to have a short review of what is expected for self-lubrication when solid lubricants are applied as blanket films.

2.2.2 Solid Lubricants

Solid lubricants are a class of materials that provide a lower friction in comparison to standard tribological couples found in engineering systems, where the vast majority are metal-metal or metal-alloy type contacts [15, 37, 38]. The most popular solution is the use of oil lubrication, but in cases where this is not possible (e.g., space applications, open system), one may resort to the use of solid lubrication. The most common solid lubricants are lamellar type solids, such as Gr and a set of metal dichalcogenides (e.g., MoS_2, WS_2). However, there are many others [15] and it is also the case that soft metals (e.g., Pb, In, Au) are considered solid lubricants at elevated temperatures. All solid lubricants typically have a narrow range of effectiveness in term of environmental conditions such as temperature, humidity, and ambient pressure.

The mechanisms by which solid lubricants provide low friction are always a topic of debate. However, scientists do agree on the basic concept of an interfacial shear strength. Figure 2.2 shows schematically the concept of modifying the friction by an interfacial film with lower shear strength than the bulk solid to which it is applied. Velocity is accommodated by the solid lubricant, which could be in the form of a coating or a tribofilm formed from a SLMMC. The velocity accommodation mode (VAM) can be: (i) interfacial sliding between a transfer film and tribofilm; (ii) the counterface material and the tribofilm (absent of transfer film); (iii) interfilm shearing of the transfer film, tribofilm, or both; or (iv) interfacial sliding between the counterface and wear track (absence of tribofilm and transfer film). For a blanket

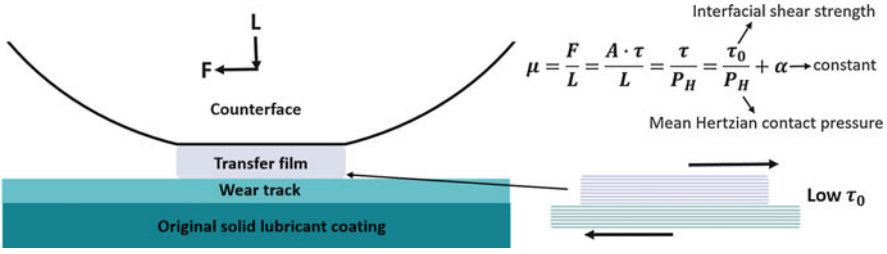

Fig. 2.2 A schematic of interfacial sliding along transfer film and wear track interface and how solid lubricants modify the friction by an interfacial film with low interfacial shear strength. The above expression for the friction coefficient is based on the classical theory of Bowden and Tabor, where friction force can be expressed as a product of real contact area (A) and shear strength of the lubricant material (τ). τ_0 is the interfacial shear strength, a "velocity accommodation parameter" which is a property of the interface, and α is the lowest attainable friction coefficient for a given friction couple [16, 38, 39]

coating of solid lubricants, the most common VAMs are (i) and (iii). For SLMMCs, where there is incomplete coverage of the wear track, all four can occur, but (ii) and (iv) are most common. Interfacial sliding of counterface versus the tribofilm is the mechanism of lubrication for SLMMCs. In the absence of solid lubricant in the tribofilm, interfacial sliding leads to higher friction, and adhesive and/or plowing wear, which provides a mechanism to release more solid lubricant materials from the subsurface of the SLMMCs.

For lubrication by carbonaceous species, there is extensive literature on diamond-like carbon coatings, which was recently summarized in [40, 41]. Carbonaceous films are quite common and also from other species such as oils, varnishes, and greases, as pointed out by Hoffman and Marks [42]. Historically, tribologists explained the lubricating effect from diamond-like carbon coatings as a "graphitization" process by which the initially amorphous coating formed tribofilms that transformed to Gr due to the temperatures and/or pressures induced by the sliding [43, 44]. Work by Scharf and Singer demonstrated the importance of formation of transfer films for a specific Si doped DLC [19, 21]. However, it is not the case that all DLC coatings behave the same way and in some cases one observes that transfer films are less important and tribofilms on the worn surface dominate the process [45]. Sometimes it is even the case that the dominant mechanism determining friction is near surface passivation state of the DLC. Recent computational simulations by Pastewka et al. [46] demonstrated that it is not always a graphitic structure that provides low friction. Sometimes it is sufficient to form sp^2 hybridized carbon from the sp^2/sp^3 matrix of the DLC coating. They also concluded that a passivation process was important for realizing low friction. Experimental observations of superlubricity in some DLC coating support these observations, where the surface termination is highly important for realizing the ultralow friction [47]. Other carbon species, such as graphene (G) or carbon nanotubes (CNTs), have been added as surface layers and resulted in lowered friction an improved tribological performance. Work by Berman et al. [48–51] has demonstrated outstanding lubricating effects by deposition of G onto metallic surfaces.

Coatings made from MoS_2 and WS_2 have been applied for many decades as solid lubricants, having been developed in the early days of the development of space technology [52]. This lamellar solid is most effective for low friction in vacuum or in the absence of humidity. Ambient conditions lead to a rise in friction and more rapid removal of the coating. The mechanism of the effect of humidity is debated in the literature, with some researchers showing evidence of the formation of Mo-oxides [53] and others demonstrating that friction between pristine MoO_3/MoS_2 interfaces is extremely small along the channel direction, which is formed by S atoms at the sliding surface, even smaller than that of MoS_2. The friction rise is due to the high energy barrier of MoO_3 (001) interlayer sliding that leads to an increase in the shear strength [54, 55]. The formation of transfer films is critical for the performance of these materials [8, 56, 57]. Recent work by Hoffman and Marks [58] demonstrated the mechanism for transfer film formation. It is also the case that even after wearing through an MoS_2 coating, low friction can persist by the presence of tribofilms and recirculation of MoS_2 debris back into the tribosystem [59]. Recent work by Lince

et al. demonstrated that other Mo-S compounds that have green manufacturing processes have promise to be as effective as MoS_2 [60]. Similar to carbon materials, MoS_2 and WS_2 have seen an evolution of their structure to make two-dimensional structure (e.g., like G) and nanoparticles/nanotubes [7, 61]. These materials have the possibility to be placed on surfaces for lubrication or added as filler materials in SLMMCs.

2.2.3 Incorporation of Solid Lubricants in MMCs

There is a long history of incorporation of solid lubricant materials into metal matrices. Graphite inclusions are the most extensively studied, with Rohatgi and coworkers carrying out much of the early work on Al-Gr composites fabricated by casting routes [2, 62–66]. Researchers have also incorporated MoS_2, WS_2, and h-BN into metals by powder metallurgy or other techniques [67–69]. Since the early years of manufacture of SLMMCs, which was primarily with casting and powder metallurgy methods, there have been significant advances in both alternative processing technologies and the materials themselves (e.g., Gr replaced by CNTs or G). In the end, regardless of processing route or material system, the fabrication of any SLMMC has a few key goals in mind. Firstly, the solid lubricant should be dispersed as homogeneously as possible and be unmodified by the processing. The actual volume fraction of the solid lubricant included is often a function of the application itself. This is because as the volume fraction of the solid lubricant increases, there is inevitably a detriment to the bulk mechanical properties. Often there may be some benefit to mechanical properties at low volume fractions, but at higher concentrations, the solid lubricant will result in softening. Thus, the second main goal is finding a balance of the lubricant content. Ideally, one requires a sufficient amount that there can be a sustainable lubricating tribofilm at the material's surface throughout its lifetime, but not so much lubricant that there is an unacceptable debit in mechanical properties. This is why one often finds SLMMCs that also include hard phases. The load-supporting nature of hard inclusions helps to overcome the debit in mechanical properties introduced by the solid lubricant. Many of the newly developed processing routes also seek to incorporate higher content of lubricant with better maintainability of mechanical properties. The remainder of this chapter will address the tribology of carbon-based and MoS_2/h-BN/WS_2/CaF_2/BaF_2 SLMMCs with special attention to the role of third bodies in determining the performance of these materials.

2.3 Synthesis of SLMMCs

Historically, Gr has been incorporated in metal matrices for many decades. This is especially true for Al and its alloys, where these materials have found applications as bearing surfaces, fan bushings and pistons and liners of internal combustion engines [4]. These materials can be fabricated in a relatively low-cost casting process [65, 70–73], infiltration techniques [63], or by powder metallurgy routes [74, 75]. More recently, newer processing methods have been developed including friction

Table 2.1 Summary of some fabrication methods for SLMMCs containing Gr, CNTs, or G

Carbon species	Fabrication method	Matrix materials	References
Gr	Stir casting	Al or Al alloy	[65, 70–73]
	Infiltration	Al or Al alloy	[63]
	Powder metallurgy	Al or Al alloy	[74, 75]
	Friction stir welding	Al or Al alloy	[76–82]
	Microwave sintering	Cu	[95]
CNTs	Powder metallurgy	Cu, Al	[99–101]
	Friction stir welding	Al or Al alloy	[76]
	Microwave sintering	Cu	[96]
	Cold spray	Cu, Al	[86–91, 102]
	Laser AM technique	Ni	[98, 103]
	Infiltration	Al	[104]
G	Sintering (spark plasma, semisolid, or laser)	Ni_3Al, Al alloy, Ti	[105–107]
	Powder metallurgy	Al	[108]
	Friction stir welding	Al or Al alloy	[76]

stir techniques [76–82], electrodeposition [83–85], thermal spray, cold spray [86–94], microwave sintering [95–97], and laser melting/additive manufacturing methods [98]. Some of these fabrication methods are more directed as fabrication of coatings (i.e., electrodeposition and thermal spray), while the remainder are directed at fabricating a bulk material. Cold spray is capable of producing coatings and also can be used as an additive manufacturing method to create near-net shape bulk parts. The manufacturing methods and materials for carbon-based lubricants were summarized in Table 2.1 according to the most recent literature, while Table 2.2 listed the most recent main techniques used for synthesis of MoS_2-, h-BN-, WS_2-, CaF_2-/BaF_2-SLMMCs. One may notice that manufacturing methods have a significant influence on material selection, microstructure of the matrix, stability of the solid lubricant reinforcement(s), as well as bonding mechanism between the matrix and the reinforcement(s). Powder metallurgy has been applied to a wide range of matrix materials such as Cu, Mg, steel, and Ni base alloy. Plasma spray and laser cladding can be used to fabricate superalloy–based composites because of high temperatures they are able to achieve. However, cold spray, due to its bonding mechanism (discussed in details later), while has been widely used for ductile metals deposition, is still under development for manufacturing superalloy coatings [119].

2.3.1 Powder Metallurgy

Powder metallurgy basically includes three steps: mixing, compacting, and sintering of mixtures consisting of matrix and reinforcement powders [64]. The current primary problems and challenges regarding fabrication of SLMMCs using powder

Table 2.2 Summary of most recent main synthesis of SLMMCs containing MoS_2, WS_2, h-BN, CaF_2, and BaF_2

Technique of synthesis	Processing temperature (°C) or material state	Matrix material	Solid lubricant(s)	Reference
Powder metallurgy	1200	Ni base alloy	Ag + h-BN	[109]
Powder metallurgy	600 and 1200	SS316L	h-BN, MoS_2	[36]
Powder metallurgy	530	Mg-TiC	MoS_2	[110]
Powder metallurgy	800	Cu-Sn	MoS_2	[111]
Plasma spray	Semi-liquid	NiCr-Cr_3C_2	h-BN	[112]
Plasma spray	Semi-liquid	WC-Co-Cu	MoS_2	[113]
Laser cladding	Liquid	Ni base alloy	WS_2	[114]
Laser cladding	Liquid	Co base alloy-TiC	CaF_2	[115]
Cold spray	Solid	Cu	MoS_2	[32, 116]
Cold spray	Solid	Ni	h-BN	[117, 118]

metallurgy are decomposition of solid lubricants due to high processing temperature, high porosity and poor bonding strength of the matrix and reinforcement(s), and manufacturing of self-lubricating MMCs for high temperature applications.

Decomposition of solid lubricants occurs because sintering temperatures are higher than oxidation or dissociation temperatures of commonly used solid lubricants, as shown in Table 2.3 [38, 120, 121]. For Cu-MoS_2 composites, sintering temperature above 780 °C causes decomposition of MoS_2 and formation of a brittle phase $CuMo_2S_3$ that is detrimental to tribological behavior [111, 122]. Figure 2.3 exhibits typical microstructure of SS316L-15 vol.% MoS_2 composite fabricated by powder metallurgy [36]. During sintering (1200 °C), MoS_2 phase was replaced by iron sulfide due to decomposition of MoS_2 and interaction with 316L. As the newly formed sulfides are not as lubricious as MoS_2 [123], some strategies have been employed to improve maintenance of solid lubricants. Adding alloying elements, i.e., phosphorus (admixed and pre-alloyed) and molybdenum (admixed), into steel matrix delayed, yet did not avoid, MoS_2 decomposition and reaction [123]. Moreover, h-BN or metal-coated h-BN was used to withstand high sintering temperature because of its high thermal and chemical stability [36, 124, 125]. However, due to the low wettability and poor sinterability, incorporation of h-BN into metal matrix led to slight decrease in mechanical property, i.e., hardness [36, 124–126]. Other solid lubricants exhibiting higher oxidation resistance could be potentially applied to stand high sintering temperatures.

Porosity and bonding strength between metal matrix and solid lubricant reinforcements are important material properties that have to take into account. Inadequate bonding occurs when sintering temperature is below melting point of

Table 2.3 Oxidation or decomposition temperatures of selected solid lubricants

	Gr	MoS_2	WS_2	h-BN	(Ca, Ba)F_2
Oxidation/°C	325	370	539	>700	~600

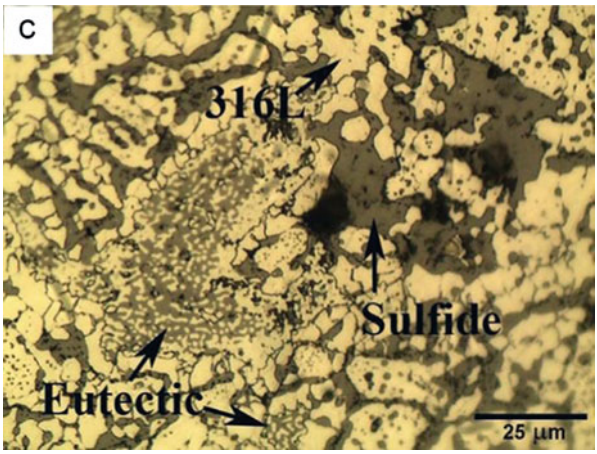

Fig. 2.3 An optical micrograph of cross section of SS316L-15 vol.% MoS_2 composite fabricated by powder metallurgy. Reprinted from [36], with permission from Elsevier

metals. In order to improve it, hot pressing, which performed sintering under a high pressure, and spark plasma sintering, which produced a high heating rate (up to 100 °C/min), were used to effectively decrease porosity and improve bonding strength [64, 127]. Glow discharge sintering is a relatively new technique that uses abnormal glow discharge plasma to generate a rapid and accurate heating process and reduce porosity [128]. Finally, post-treatment such as extrusion improved density and hardness of Cu-Sn-MoS_2 composites [123].

2.3.2 Laser Surface Cladding (LSC)

Due to a recent reduction in cost of laser equipment, researchers have devoted efforts on research and development on laser cladding process [129]. During LSC, an alloy or a composite layer is fused onto the surface under a coherent and high intensity laser beam irradiation [129]. The melt pool temperature can achieve as high as 2000 °C by using extremely high power density [129]. Critical processing parameters include mixing of the feedstock powders, heating rates, convection, diffusion, and cooling rates [129]. A significant difference between LSC and other coating techniques is its strong bond between coating and substrates due to the fact that substrate is partially melted into melt pool and participate in coating development. Therefore, there is no significant interface visible between the substrate and coating. For fabrication of self-lubricating MMCs, LSC has recently been employed to produce superalloy–based composites for high temperature applications [33, 114]. A major problem of LSC applied to solid lubricants is decomposition and

vaporization during the high temperature laser processing. It has been observed that MoS_2 dissociated and interacted with matrix materials in the melting pool [130, 131]. Xu et al. fabricated Ni-TiC-MoS_2 composite on 1045 low carbon steel using laser cladding. MoS_2 was found to be decomposed to Mo and S, resulting in the formation of $Ni_{2.5}Mo_6S_{6.7}$, intermetallic $Mo_{0.84}Ni_{0.16}$, and binary element sulfides (Ni_3S_4, NiS_2, Ni_3S_2, NiS) [130]. Generally, there are two methods to improve the decomposition. First of all, solid lubricants having higher oxidation resistance and melting points such as h-BN, WS_2, CaF_2, and BaF_2 have been observed to have a higher recovery in the final composites [33, 115, 127, 132–134]. Moreover, feedstock pretreatments such as encapsulation solid lubricants with metal by high energy milling or electroless plating reduced effectively decomposition and vaporization of solid lubricants [132, 135–137].

2.3.3 Thermal Spray

In this method, melting or semi-melting metal particles are co-sprayed with solid lubricants. Ni base alloys and WC-Co have recently been sprayed with MoS_2, h-BN, as well as (Ca, Ba)F_2 [112, 113, 139–142]. Figure 2.4 shows typical gas temperature and particle velocity of thermal spray techniques and cold spray [138]. The biggest challenge of the current thermal spray techniques is to prevent solid lubricant from decomposition and interaction to the matrix material during high temperature processing. Metal-coated solid lubricant prepared by ball milling or hydrogen reduction followed by alloying method helped to retain MoS_2 and h-BN in the composite coating [112, 113]. However, due to poor wettability of h-BN with melt metals, real interparticle contact surface and bonding strength decreased with h-BN, and 10 wt% of h-BN was found to destroy the continuity of Ni_3Al matrix [142]. Detonation gun spray, due to its relatively lower heat input and higher particle speed, could potentially minimize MoS_2 decomposition [140].

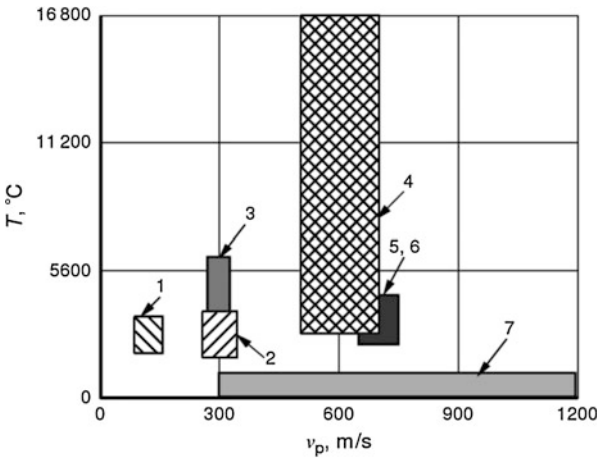

Fig. 2.4 Diagram of jet temperatures (T) and particle velocities (*v*p) used in thermal spray and cold spray methods. *1* low velocity gas plasma; *2* high velocity gas plasma; *3* electric arc; *4* plasma; *5*, *6* detonation and high velocity oxy-fuel (HVOF); and *7* cold spray. Reprinted from [138], with permission from Elsevier

2.3.4 Friction Stir Processing (FSP)

Friction stir processing (FSP) is a solid state process aiming to modify microstructures of a single or multiple workpieces and to fabricate MMCs [81, 143]. A specially designed rotating pin is inserted into the material with a proper tilt angle, and moving along the designed path. Rotation of the pin stirs the metallic surface and generate friction and plastic deformation heat, leading to a mix of the surface material (i.e., coated powder) and the metallic matrix [76, 81]. The mix then flows to the back of the pin, where it is extruded and forged behind the tool, and eventually consolidates and cools down under hydrostatic pressure conditions [81]. FSP is an excellent method to fabricate MMCs showing well-dispersed solid lubricant and/or ceramic reinforcements and improved mechanical properties [76–82]. Gr, G, CNTs, and MoS_2 have been incorporated into aluminum alloy by FSP and these composites exhibited improved mechanical property and tribological performance [76–82, 144]. Hybrid composites including solid lubricant and ceramics such as SiC and Al_2O_3 have been developed successfully by FSP on aluminum alloy surface [76–82, 144]. However, FSP has been mainly applied for aluminum MMCs so far. New applications of FSP to other metallic materials are under development [81].

2.3.5 Cold Spray

Cold spray, or cold gas-dynamic spray, is a solid state deposition process by exposing a suitable substrate to a high velocity (300–1200 m/s) jet of particles, which are generally metals or blends of metals and other materials [119, 146, 147]. The powders are accelerated by a high pressure gas jet through a de Laval nozzle [119, 146, 147]. Upon impact, the metallic particles that achieve a critical velocity undergo adiabatic shear instability, leading to metallurgical bonding, and consequently buildup of a coating [146–148]. The impact phenomenon and comparison with a wide range of other types of impact is summarized in Fig. 2.5, that points out the cold spray deposition possibly occurs within a typical particle size range of 5–150 μm at an impact velocity of 300–1200 m/s, which forms the cold spray regime [145]. Low temperature and high speed deposition make it very attractive for oxidation and heat sensitive materials and to fabricate high density composites [138, 149]. Even though cold spray has been discovered early in 1980s and successfully used for metals and metal-ceramic composites, its application to SLMMCs has just begun [146, 147, 150]. Currently, there are two main research groups including Penn State University and McGill University that have investigated cold sprayability of solid lubricants with metals. Figure 2.6 shows an optical micrograph of cold sprayed Cu-MoS_2 composite using admixed Cu and MoS_2. MoS_2 was distributed along Cu particles, and it was demonstrated that under the optimized spraying condition, average MoS_2 content in the composite was around 2–3 wt%, lower than those fabricated by some of the other techniques, e.g., around

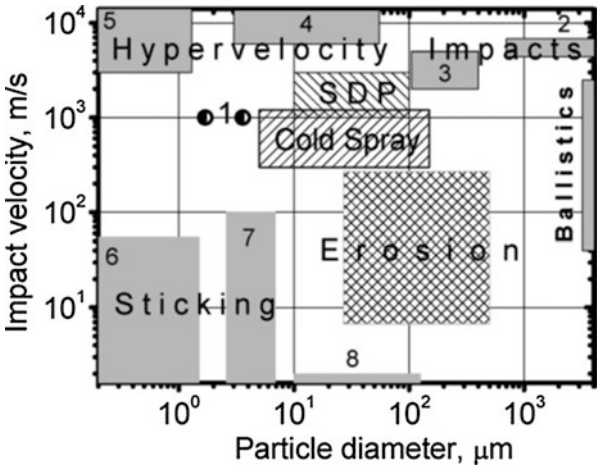

Fig. 2.5 Influence of impact velocity and particle size on material interaction upon impact of ductile metals or alloys with plane solid surfaces. Regions characteristic of impact phenomena are shown: *1*: no adhesion; *2, 3, 4,* and *5*: hypervelocity impacts; *6* and *7*: low-velocity impact; *8*: rebound; *SDP* super-deep penetration. Reprinted from [145], with permission from Elsevier Masson SAS. All rights reserved

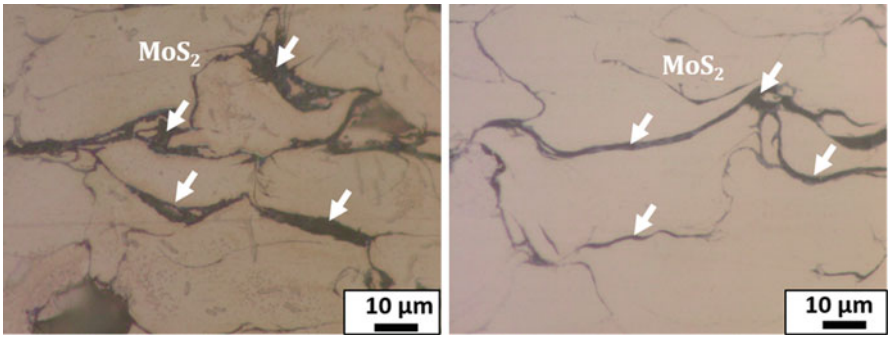

Fig. 2.6 Typical optical micrographs of cold sprayed Cu-MoS_2 composite using admixed Cu and MoS_2. Reprinted from [116], with permission from Springer

30 wt% MoS_2 can be achieved by powder metallurgy [32, 116, 133]. Deposition mechanism of Cu and MoS_2 composite during cold spray was proposed by Zhang et al. [116]. Presence of MoS_2 hindered extensive adiabatic shear instability of Cu occurring, leading to inadequate bonding between Cu particles, and therefore reduced mechanical property e.g., hardness of the composite [116]. Adding ceramic phase, e.g., WC to form hybrid composite Cu-MoS_2-WC could potentially improve mechanical property. Moreover, Ni-coated h-BN was fabricated by electroless process and used as feedstock to develop Ni-matrix h-BN composite. The size of solid lubricant core was found to play an important role on recovery of solid lubricant and bonding between particles. Nano-h-BN (100 nm) encapsulated with Ni helped to achieve around 10 vol.% h-BN retained in the composite [118, 151]. However, they observed 1 vol.% h-BN composite produced the best combination of friction and wear behavior [118, 151]. More extensive observation on bonding mechanism of the solid lubricant and metal particles, as well as its influence on tribological performance, is required.

2.4 Metal-Graphite, CNTs, Graphene SLMMCs

2.4.1 Advances in Materials (Gr → CNTs → G)

An aspect of the carbon-based SLMMCs that has changed over the years is the nature of the carbon species that is impregnated into the composite. In the early days, researchers were limited to Gr flakes as the only commercially available material. With the invention of carbon nanotubes in the 1980s followed by graphene in 2000s, there is now the possibility of including other forms of carbon in place of Gr flakes. The tribology of composites with carbon nanotubes is well researched, having been studied nearly since their invention with a recent review article published on the topic by Moghadam et al. [152]. Research on graphene-containing composites have only recently been demonstrated and carried out [82, 102, 107, 108, 153–156]. Limited information on the tribology of these materials has been published [76, 84, 85, 157–159]. However, for all of these additions, the intention is still that the carbon species will develop a tribofilm on the surface upon sliding.

2.4.2 Tribological Behavior of SLMMCs Containing Graphite, CNTs, and Graphene

The tribological behavior of Gr, CNTs, and G containing SLMMCs has been the subject of recent reviews by Omrani, Moghadam, and coworkers [4, 5, 152, 160]. Some general trends of friction and wear with material and test parameter for MMCs containing Gr are well understood, especially for Al matrices. With increasing Gr content in the composite, there is a reduction in friction coefficient. Figure 2.7a presents friction results versus Gr content for two separate studies by Akhlaghi et al. [161, 162]. Variation in the friction among the studies is related to changes in applied load and sliding velocity, but in general there is a consistent trend to lower friction with increasing Gr content. The trend is observed for the vast majority of literature on Al-Gr MMCs regardless of their method of manufacture. Similarly, for wear of the composite (see Fig. 2.7b), there is a decrease in wear with increase in the Gr content for a set of studies by Ravindran et al. and Suresha et al. [163, 164]. It should be noted that this trend is not always respected. That is, many authors have reported that as the Gr content is increased, eventually wear will increase. There is some optimum content of Gr to obtain both low friction and wear, above which wear will increase even if the low friction is maintained. This is generally related to a reduction in the mechanical properties of the composite with the increased Gr content, which can lend itself to enhance mechanical properties at low inclusion content but with large content, leads to a softening of the composite. In general, the effect can be more pronounced for composites produced by powder metallurgy as compared to those prepared by stir casting. Liu et al. prepared stir cast Al-50%Gr composites and saw a relatively good performance for both friction and wear [63]. However, for composites produced by powder metallurgy, Akhlaghi et al. observed an increasing trend in wear with increasing Gr content [4, 75].

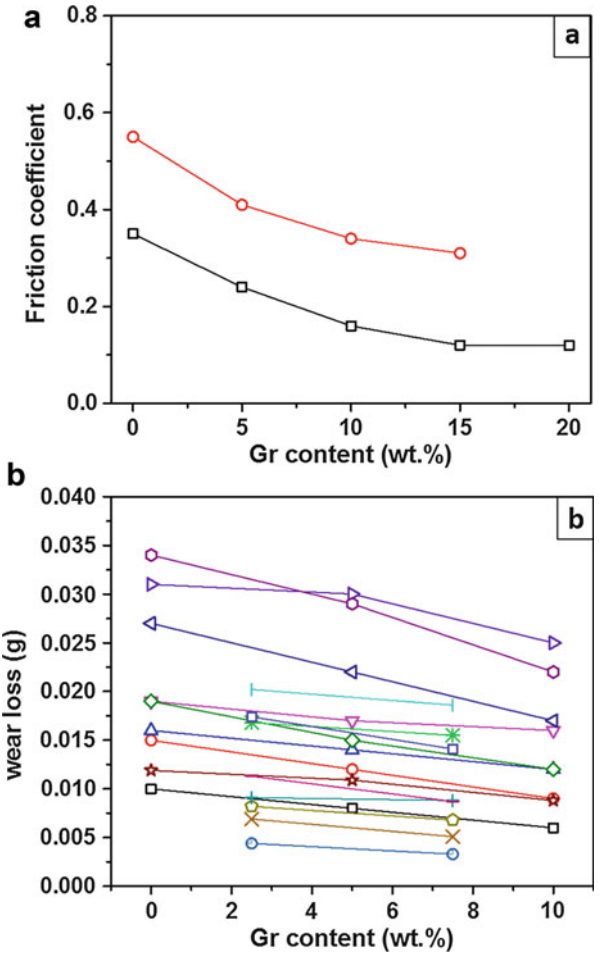

Fig. 2.7 The trends of (**a**) friction [161, 162] and (**b**) wear loss [163, 164] with Gr content in Al SLMMCs

To overcome this trend, they included SiC reinforcements to enhance the mechanical properties of the composite. This is a common strategy that can maintain acceptable wear rates at higher Gr concentrations.

More recently, researchers have mixed CNTs and G into MMCs. The remarkable mechanical properties of CNTs and friction properties of G led naturally to the research question of whether these carbonaceous reinforcements would lead to even better self-lubricating properties than Gr. Zhou et al. [104] studied the tribology of CNT in Al-Mg MMCs. Figure 2.8 demonstrated the reduction in friction and wear they observed with CNT. Similar reductions were also observed by Choi et al. on a CNT-Al composite [165]. One aspect of the inclusion of CNTs that is often not fully explored by all researchers is the state of the CNTs post-processing. Poirier et al. studied Al-CNT composites made by a mechanical milling process and discovered that nearly all of the CNTs were destroyed and had reacted to form carbides with the

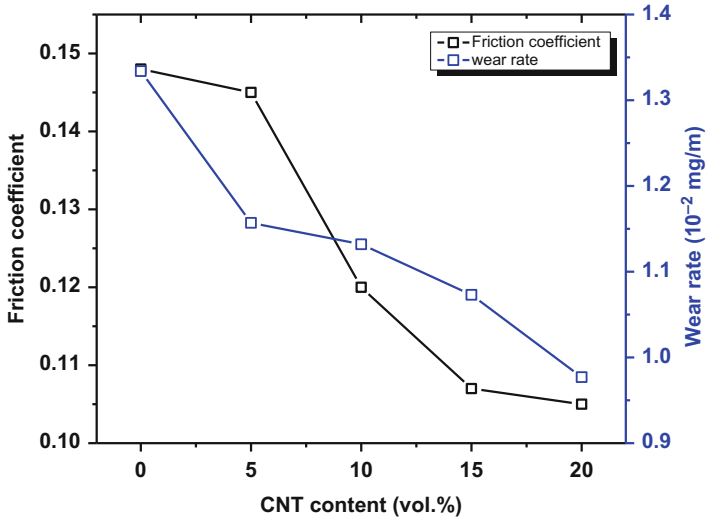

Fig. 2.8 Trends with CNT content in an Al composite made by powder metallurgy methods [104]

Al matrix [166]. Depending on the aggressiveness of the processing steps taken to create the composites, one may find retention of CNT as a distinct phase in the microstructure or instead the formation of carbides. Both Zhou et al. [104] and Choi et al. [165] showed evidence with transmission electron microscopy that nanotubes were retained in their composite in an unreacted state.

Only recently have researchers studied the inclusion of G in MMCs [76, 84, 108, 158, 167]. Ghazaly et al. [108] studied the tribology of Al-G composites and discovered the wear performance was not significantly improved. On the other hand, research on Ni-G composites showed a reduction in both friction and wear of the composite with an increase in G content [84]. Sometimes it is difficult to ascertain the effectiveness of a new materials due to differences in processing, matrix material, and test parameters. As such, it is very difficult at these early stages of G-based SLMMCs to determine whether the form of the carbon introduced in the composite affects significantly the tribological performance. However, a recent paper by Maurya et al. [76] provides a side-by-side comparison of Gr, CNT, and G reinforcements in a friction stir processed Al alloy. In Fig. 2.9, the friction trends they observed are presented. Gr and CNT additions had a similar reduction in the friction coefficient to about 0.4, while G lowered the friction to around 0.25. For the wear of the composite, they observed that all reinforcements reduced wear compared to the friction stir alloy without carbon additions. There was also a trend in wear depending on the carbon species, where G reduces the wear most followed by CNT and the least effective being Gr. While the authors conducted ex situ analysis of their wear scars, the precise mechanism of the differences in the performance of the three carbonaceous species was not identified. Future research on carbon-containing SLMMCs should certainly focus on more side-by-side comparisons between Gr, CNTs, and G.

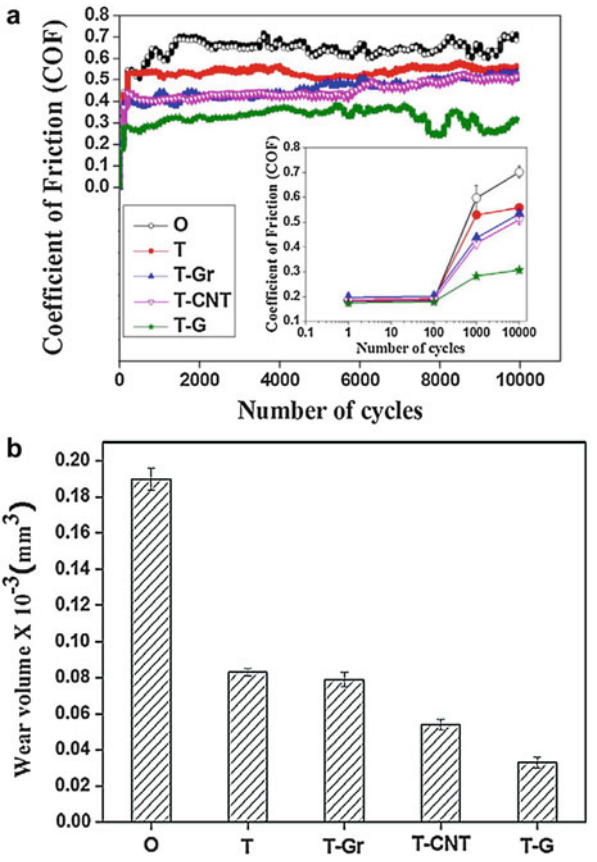

Fig. 2.9 Friction and wear trends with Gr, CNTs, and G composites made with Al6061 alloy with friction stir processing. Reprinted from [76], with permission from Elsevier

2.4.3 Tribofilms Observed for SLMMCs Containing Graphite, CNTs, or Graphene

Examination of worn surfaces after tribology testing can help to determine the wear mechanisms. In the case of SLMMCs, the comparisons between the composite and a pure version of the matrix material can explain the effectiveness of the solid lubricant in reducing friction and wear. Figure 2.10 are secondary electron images of worn surfaces on Al7075/Gr composites with increasing Gr concentration [168]. With no Gr, there is evidence of adhesive wear and plastic deformation on the worn surface. As Gr is introduced to the composite, evidence of this wear mechanism is reduced and instead a smoother worn surface with grooved features is observed. Many authors have explored the characteristics of the graphitic tribofilms formed on Al-Gr composites [63, 161, 163, 169–173]. General trends observed are that with increased Gr content in the composite, there is an enhancement of the tribofilm coverage of the surface that correlates with the reduction in friction. Interestingly, there is a significant lack of observation of the counterface materials in tribological

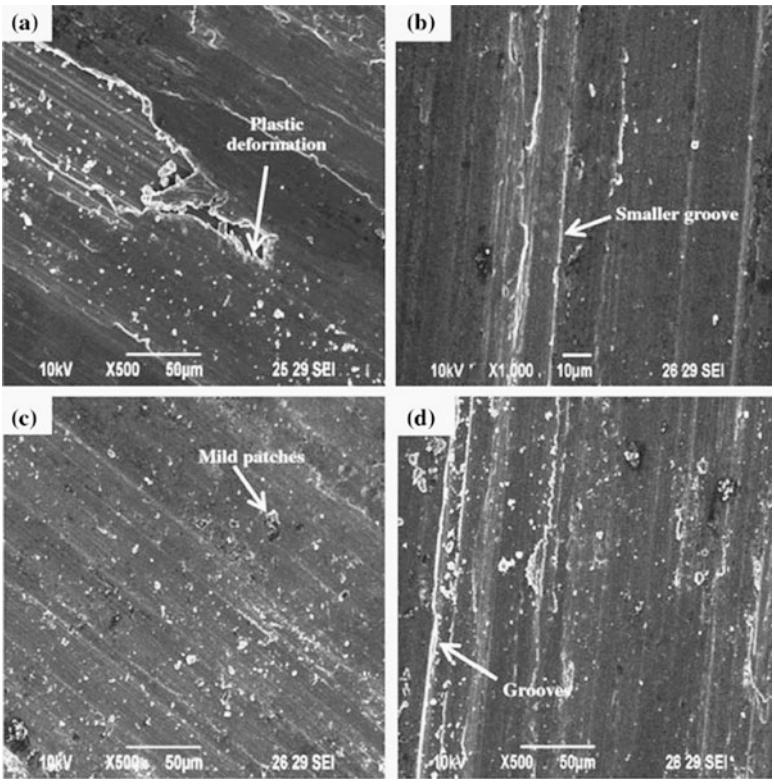

Fig. 2.10 Worn surfaces for an Al-Gr composites (**b**–**d**) with increasing Gr content, compared to the matrix alloy (**a**). Reprinted from [168], with permission from Elsevier

studies of these materials. Without information on transfer films, it makes it problematic to fully understand the third body flows and the mechanisms for replenishment of the graphitic tribofilm. Authors theorize that the replenishment comes from the subsurface of the composite, but tribofilms can also be replenished by recirculation flows between the counterface and wear track.

Similar trends in the appearance of the wear track morphology are also observed for CNT composites (see Fig. 2.11). As Zhou et al. [104] increased the CNT content in their composites, they observed a smoother wear surface. For only 5% CNT content, the wear track was rough and there was evidence of ploughed materials. For 10% and 20% addition of CNTs, the worn surface became smoother, with less evidence of ploughing. This was accompanied by reduction in friction and wear, as was presented above.

Carbon nanotubes can also be incorporated into a composite with cold spray methods. Bakshi et al. [89], using a composite powder, created Al-CNT composites and studied their tribology with a scratch tester. As can be seen in Fig. 2.12, the total wear volume of the scratch was decreased for all normal loads by the introduction of

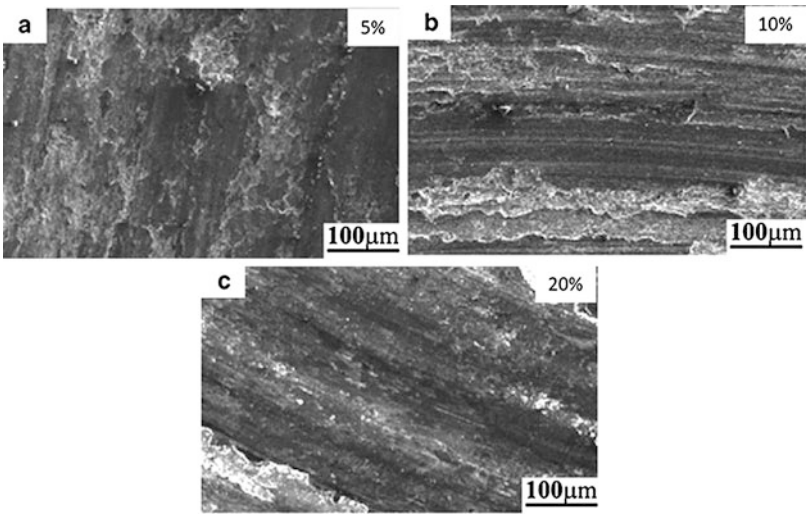

Fig. 2.11 Typical tribofilms observed for Al-CNT composites containing (**a**) 5%, (**b**) 10%, and (**c**) 20% CNTs made by powder metallurgy methods. Reprinted from [104], with permission from Elsevier

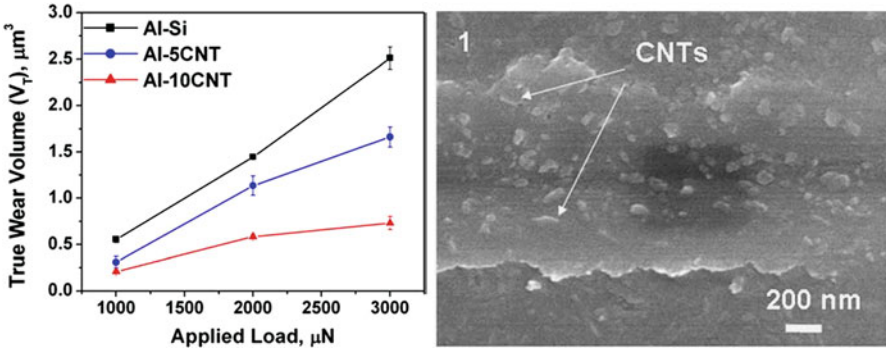

Fig. 2.12 Scratch testing wear results for an Al-CNT composite made by cold spray and corresponding observation of the worn surface with CNTs. Reprinted from [89], with permission from Elsevier

CNTs. The scratch track observed by SEM was found to have CNTs on the surface, which may have aided in the composite to resist wear during the scratch experiment.

Wear tracks can also be examined in cross sections, which can often give significant additional information on the exact nature of the material transformations in the tribofilms. These can be done as mechanical cross sections [169] but more recently can also be examined with focused ion beam (FIB) cross sectioning [98, 174, 175]. Figure 2.13 is an example of a mechanical cross-section of a wear track created on an Al alloy composite with 10% SiC and 4% Gr. In this study by Riahi

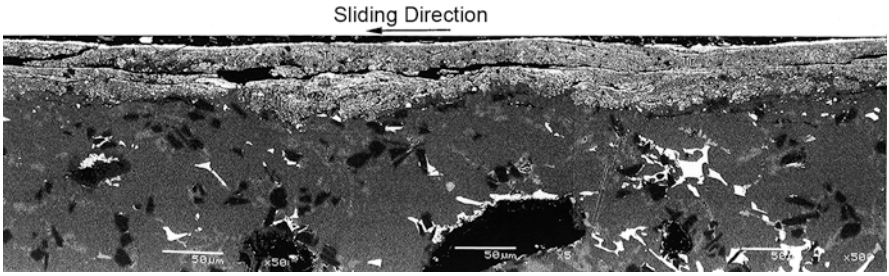

Fig. 2.13 Tribolayer observed on Al-10%SiC-5%Gr composite run against a steel-bearing material. The tribolayer in this case is primarily iron oxide with Al_3Ni and SiC particulates. Reprinted from [169], with permission from Elsevier

and Alpas [169], the composite was run in a block-on-ring test with a bearing steel, a tribo-test that more closely replicates the contact conditions the composite would encounter in service. Rather than high coverage of a carbonaceous tribofilm, the authors found that a thick tribofilm is formed that is composed of a mixture of iron and aluminum oxides, fractured SiC and intermetallic Ni_3Al, which is from the base alloy. Graphite did exist in these tribofilms, but clearly the mechanisms for lubrication and wear of this alloy are significantly more complicated than one can determine from observation of top-down wear track morphology, as was reviewed above.

Use of FIB microscopy in recent years allowed for high resolution observation of the cross section of worn surfaces and also provided the utility of being able to prepare TEM foils when desired. Use of these methods can better reveal the mechanisms for lubrication in SLMMCs. Figure 2.14 are cross sections prepared by FIB from a wear track on a Ni-3Ti-20C composite that was manufactured by laser additive manufacturing methods [98]. Each view is a region within the near surface of the wear track. Once can clearly observe an MML and distinct C tribofilm at the surface of all images. Also, striking is the observation of the mechanism of combined plastic deformation near surface and "wicking" of the carbon within the composite towards the surface to become part of the tribofilm. This observation is particularly interesting as the carbon can be brought to the surface without significant wear occurring but instead by simply the plastic deformation.

2.5 Metal-MoS_2, WS_2, h-BN, CaF_2, and BaF_2 SLMMCs

2.5.1 Tribological Behavior of SLMMCs Containing MoS_2, WS_2, h-BN, CaF_2, and BaF_2

Figures 2.15 and 2.16 summarized coefficient of friction observed in a number of different metal matrices of Cu, steel, Ni, and Ni-based alloy reinforced with MoS_2 and h-BN, respectively. The composites were fabricated by different manufacturing

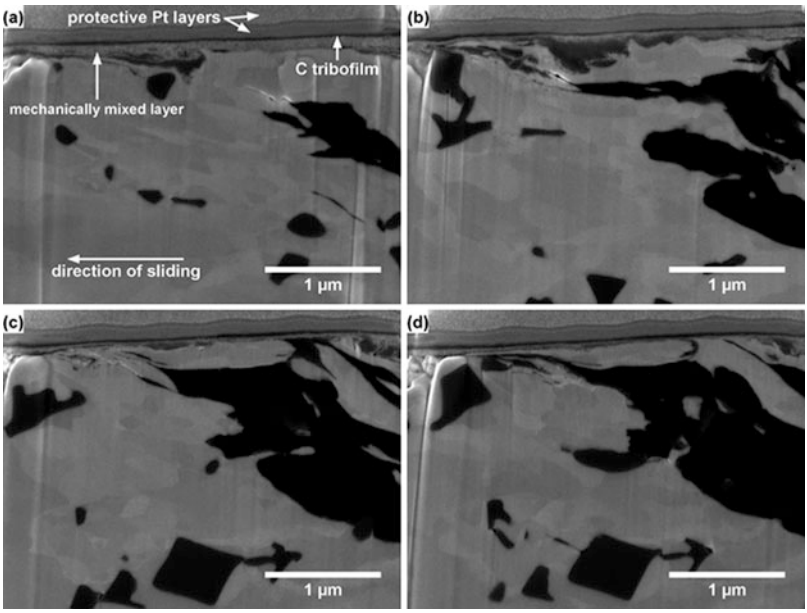

Fig. 2.14 Example of tribofilm formation in a Ni-3Ti-20C composite made by laser additive manufacturing methods. Reprinted from [98], with permission from Springer

methods such as powder metallurgy [34, 35, 122, 176], thermal spray [112, 142], cold spray [32], and laser cladding [132]. The tests were carried out with different tribometer configurations, mainly pin-on-disk and ball-on-plate, different normal loads, sliding speeds, and different counterface materials, e.g., different types of steels, Si_3N_4, alumina. Even though it is difficult to compare the absolute values due to the above variables, all the composites show some common trends. First of all, their coefficient of friction decreased with increasing solid lubricant content and then tended to keep constant or, in some cases, increased slightly. Early research carried out by Tsuya et al. demonstrated that in cold pressed Cu-MoS_2 composites, a minimum friction was reached at a MoS_2 concentration of 7–10% and remained fairly constant up to a concentration of close to 90% [179]. Similar trend was also observed in Gr reinforced SLMMCs by other researchers [64]. However, for the majority of the composites listed in Figs. 2.15 and 2.16, the lowest friction coefficient was around 0.4 or even higher. That is much higher than that sliding against blanket films of solid lubricants fabricated by physical vapor deposition and chemical vapor deposition, indicating metal matrix at the contact plays an important role. The effect of metal matrix component on friction coefficient has been analyzed theoretically by Rohatgi et al. [64]. The friction of an SLMMC can be written as

$$f = \left(1 - A_f\right) f_m + A_f f_f \tag{2.1}$$

Matrix	Cu	Cu	Ni-20Cr+W+Fe+C	Ni-20Cr+W+Al+Ti	316L
	◻	▷ ⬡	△ ○	▽	◁ ◇
Normal load (N)	5	40, 80	5	5	PV=1.1, 1.8
Sliding speed (m/s)	0.002	0.15	0.8	0.8	

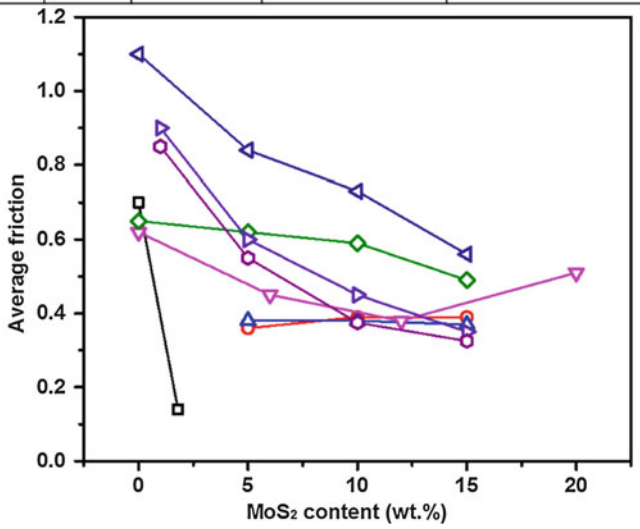

Fig. 2.15 Variation of average friction with content of MoS_2 for composites with different matrix materials and corresponding brief tribology testing parameters [32, 34, 35, 122, 176]

where A_f is fraction of lubricating tribofilm in the contact, f_f, f_m are friction coefficients of the lubricating tribofilm and matrix, respectively. Therefore, the coefficient of friction of composites may vary between f_m and f_f depending on solid lubricant content and ability of development and stability of lubricating film over sliding.

WS_2, BaF_2, and CaF_2 have been used as high temperature solid lubricants and incorporated with metals, e.g., Ni and Ni alloy using powder metallurgy techniques, plasma spray, and laser cladding. The coefficient of friction reduced significantly with even a small amount of solid lubricant in the composites, and this effect was even more pronounced at elevated temperatures [33, 114, 121, 135, 141]. The same trend was observed in wear rates. In general, BaF_2 and CaF_2 exhibit excellent wear resistance at a broad temperature range between room temperature and 1000 °C [112, 121], while WS_2 shows the lowest wear rate at 300 °C [33]. Strong matrix, combined with sulfides and fluorides, sometimes oxides formed at high temperature, are responsible for low friction and high wear resistance at high temperatures [121, 133]. It is worth to note that as the materials have to experience high temperature during fabrication, decomposition of solid lubricants are inevitable, even completely decomposed under some circumstances [114, 135]. However, some high temperature products, e.g., $CaCrO_4$ and $CaMoO_4$ (CaF_2 added

Matrix	Ni_3Al+Ag	Ni_3Al	Ni-20Cr+W+Mo+Al+Ti	Ni-20Cr+W+Mo+Al+Ti+Ag	NiCr+Cr_3C_2	Ni	Ni
	□	◇	△	▽	◁	○	▷
Normal load (N)	5	4.9	20	100	9.8	100	50
Sliding speed (m/s)	0.132	0.188	1	0.5	0.188	0.226	-

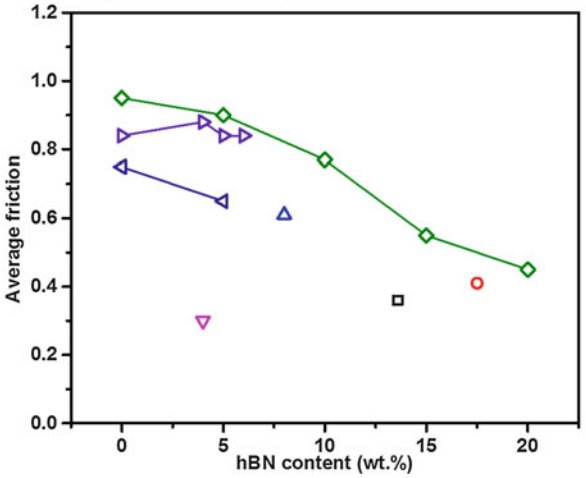

Fig. 2.16 Variation of average friction with content of h-BN for composites with different matrix materials and corresponding brief tribology testing parameters [109, 112, 118, 132, 142, 177, 178]

to Ni_3Al matrix), are lubricious and lead to improved tribological behavior at elevated temperatures [133].

Figure 2.17 shows wear rate evolution with solid lubricant content for composites with various matrix materials and fabricated by different manufacturing processes. Again, even though the absolute values cannot be compared because of different testing conditions and insufficient characterization on the composites, the general trends of wear rate with solid lubricant concentration are revealed. In Fig. 2.17a, the wear rates decreased more rapidly with increasing only a small amount of solid lubricants, and then tended to keep constant with further increase in MoS_2 or h-BN. However, as observed in the Gr SLMMCs, there was an opposite trend where wear rates increased with solid lubricant after a certain amount, as seen in Fig. 2.17b, c. Cold sprayed Cu-MoS_2 composites using admixed feedstock show continuous increase in wear track depth with increase in MoS_2 content (Fig. 2.17c right). The increase in wear rates was mainly due to degraded mechanical property induced by poor bonding strength between solid lubricant and metal matrix [32, 64, 116, 142]. In order to improve wear resistance, adding hard phase like ceramics to increase load-bearing capacity of the matrix was an effective method [3, 95, 130, 164]. Moreover, in the case of powder metallurgy route, increasing sintering temperature to get adequate bonding strength and low porosity was able to reduce significantly wear rate at higher h-BN content, as shown in Fig. 2.17b [126]. Post-plastic deformation, e.g., extrusion, was also able to decrease porosity effectively

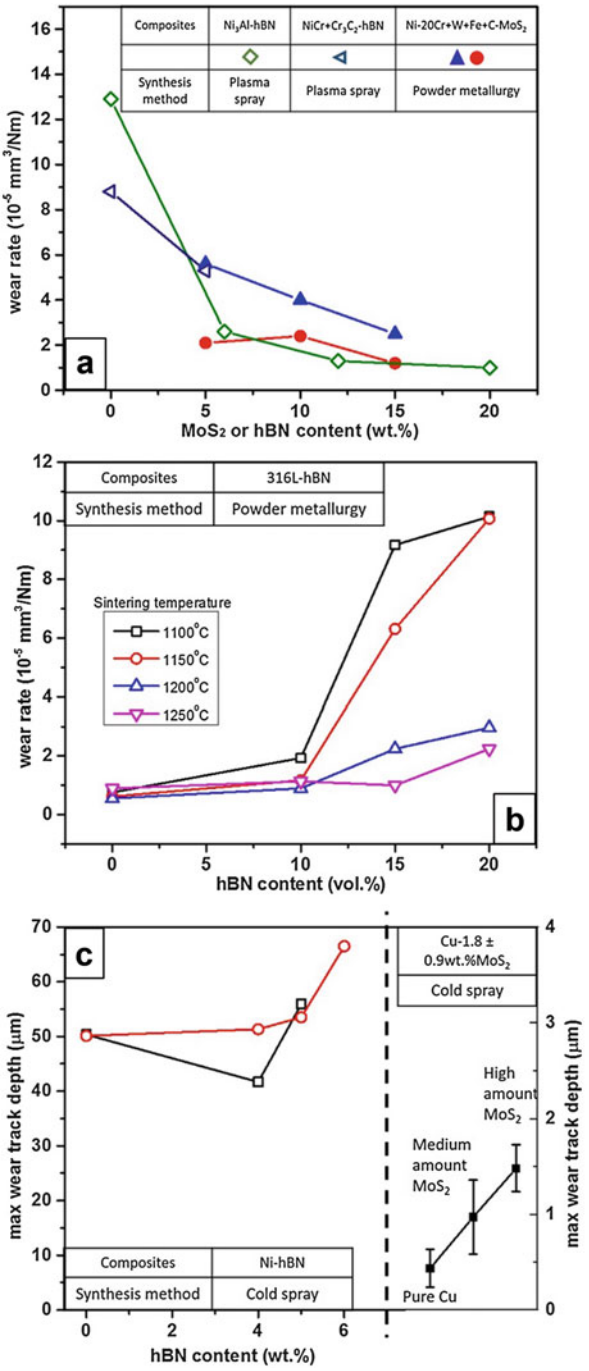

Fig. 2.17 Variation of wear rates with MoS_2 or h-BN content for composites with different metal matrix materials and various synthesis methods. (**a**) Wear rates of Ni alloys reinforced by MoS_2 or h-BN fabricated by plasma spray or powder metallurgy [35, 112, 142], (**b**) wear rates of 316L-h-BN composites developed using different sintering temperatures [125], and (**c**) wear rates of cold sprayed Ni-h-BN (left) [118] and Cu-MoS_2 (right) [32] composites

and therefore improve wear resistance [180]. As described in the Sect. 2.4.2, the transition point based on solid lubricant content above which wear rate starts climbing varies with manufacturing routes. In general, composites made by the liquid methods such as laser cladding and plasma spraying exhibit higher transition point than those fabricated by semisolid and solid methods, e.g., powder metallurgy and cold spray. As shown in Fig. 2.17a, c, plasma sprayed Ni_3Al-h-BN composites showed continuous decrease in wear rate up to 20 wt% h-BN, while for cold sprayed Ni-h-BN composites, wear rate started increasing at around 5 wt% h-BN.

Except for materials, there are some testing parameters that affect wear rate evolution and they are normal load and sliding speed. The influence of those two factors on friction and wear of SLMMCs have been studied extensively and well summarized by Omrani et al. and Rohatgi et al. [4, 5, 64, 181].

2.5.2 Third Bodies Observed for SLMMCs Containing MoS_2, WS_2, h-BN, CaF_2, and BaF_2

As described in Sect. 2.2.1, friction and wear mechanisms are conventionally examined by observation of sliding contact, i.e., worn surfaces using ex situ methods. Even though the design of SLMMCs, as shown in Fig. 2.1, is to form a full solid lubricating film on the wear track or contact, the role of metal matrix has to be taken into account. In general, for metal-metal contact, incorporation of solid lubricants reduced adhesive wear to some extent depending on the solid lubricant concentration and the testing condition [34, 122]. For Cu-MoS_2 composites sliding against Cu, powdery particles of solid lubricant, not a full film, in the contact were responsible for reduced friction and adhesion and was the main wear mechanism [122]. Mahathanabodee et al. [36, 125] proposed a wear model for a 316L-h-BN and a 316L-h-BN-MoS_2 composites sliding against high-chromium steel counterfaces. They observed adhesive wear, abrasive wear, oxidation, formation of a compact layer, as well as delamination. The compact layer consisting of metal, sulfides, h-BN, and oxide helped to reduce friction and wear. However, this layer tended to be detached and caused delamination due to cyclic loading over sliding. WS_2 is used as a high temperature solid lubricant, and the mechanism of improving tribological behavior is presented in Fig. 2.18 [33]. Without WS_2, large pits were found at 300 °C wear track, therefore abrasive and adhesive wear played a role. However, for NiCr/Cr_3C_2/WS_2 coating, WS_2 and newly formed CrS generated transfer films in the contact, leading to a smoother wear track and lower friction coefficient. Moreover, as degradation of mechanical property at 300 °C was minor due to presence of Cr_7C_3, laser clad NiCr/Cr_3C_2/WS_2 composite coating exhibited a good combination of friction and wear at 300 °C. In addition, ceramic phase additives alter wear mechanism of self-lubricating composites as well. Xu et al. [130] reported adhesion, delamination, and plastic deformation were the main wear mechanisms in a Ni-MoS_2 composite, while incorporation of TiC helped to generate a smoother worn surface and eliminated adhesive wear. Although wear mechanisms seem to be identified

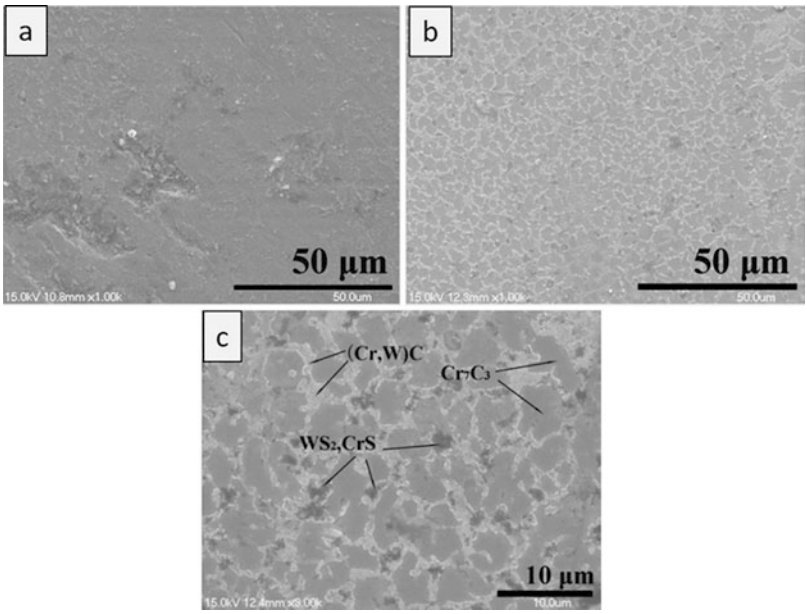

Fig. 2.18 Wear tracks of (**a**) laser clad NiCr/Cr_3C_2 coating and (**b**, **c**) laser clad NiCr/Cr_3C_2/WS_2 coating at 300 °C. Reprinted from [33], with permission from Elsevier

through observation of worn surfaces by ex situ approach, more detailed information on dynamics of third bodies in the contact, e.g., initiation of tribofilms and transfer films, as well as their evolution, is helpful to better understand friction and wear behavior. That is the design purpose of in situ tribometry, as discussed in the Sect. 2.2.1. A combination of ex situ and in situ method has been applied on cold sprayed Cu-MoS_2 composites, and the results will be presented in the remainder of this section.

Zhang et al. [32] reported recently that when Cu-1.8 wt% MoS_2 composite rubbing against alumina, how MoS_2 smeared out forming discontinuous tribofilms, and their evolution with sliding. Spatial friction was extracted to link local coverage of MoS_2 tribofilms. As shown in Fig. 2.19, at 100 cycles, MoS_2 was smeared out and formed MoS_2-rich patches in the wear track. The local friction distribution combined with chemical analysis demonstrated that higher MoS_2 content zones generated lower local friction. The MoS_2 patches were expanded and tended to distribute more homogenously as sliding continued (see MoS_2 distribution of the 1000 cycle wear track in Fig. 2.20). Inside the patches, MoS_2 was found to be powdery and mixed with Cu_2O and/or Cu (Figs. 2.19d, 2.20d, and 2.21e). The mechanism for low friction in a metal-MoS_2 composite was expected to be different from that found in blanket films of MoS_2 made by physical vapor deposition (PVD) or similar methods, which was discussed in Sect. 2.2.2 [59, 182, 183]. The main feature of these latter coatings was to form transfer films on the counterfaces, which led to MoS_2 sliding versus MoS_2 and friction coefficients in the range of 0.02–0.06

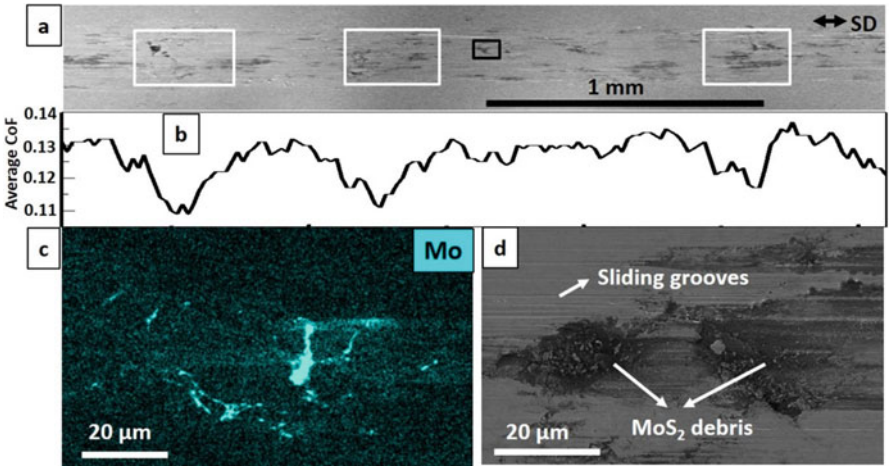

Fig. 2.19 Top-down view of the Cu-MoS_2 wear track after a 100 cycle test. (**a**) Overall morphology; (**b**) spatial friction along the wear track at the 100th cycle; (**c**) an EDX map of the black rectangle in (**a**); (**d**) a closer view of the wear track morphology. Reprinted from [32], with permission from Springer

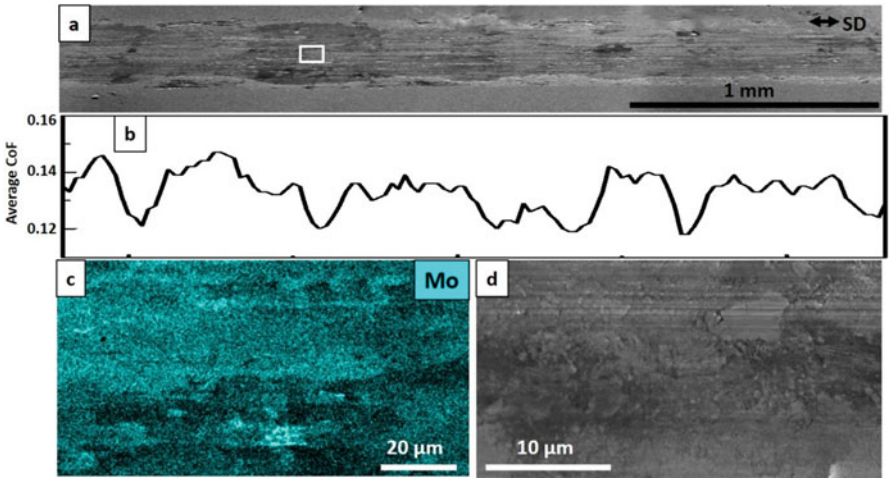

Fig. 2.20 Top-down view of the Cu-MoS_2 wear track after a 1000 cycle test. (**a**) Overall morphology; (**b**) spatial friction along the wear track at the 100th cycle; (**c**) an EDX map of the black rectangle in (**a**); (**d**) a closer view of the wear track morphology. Reprinted from [32], with permission from Springer

in dry air at similar test conditions to those performed here [59]. Thus, while there is a significant friction reduction due to the presence of MoS_2, the mechanisms for this reduction were modified due to the presence of the Cu. The first noticeable difference was the lack of a transfer film observed at 100 and 1000 cycle tests (Fig. 2.21a, b).

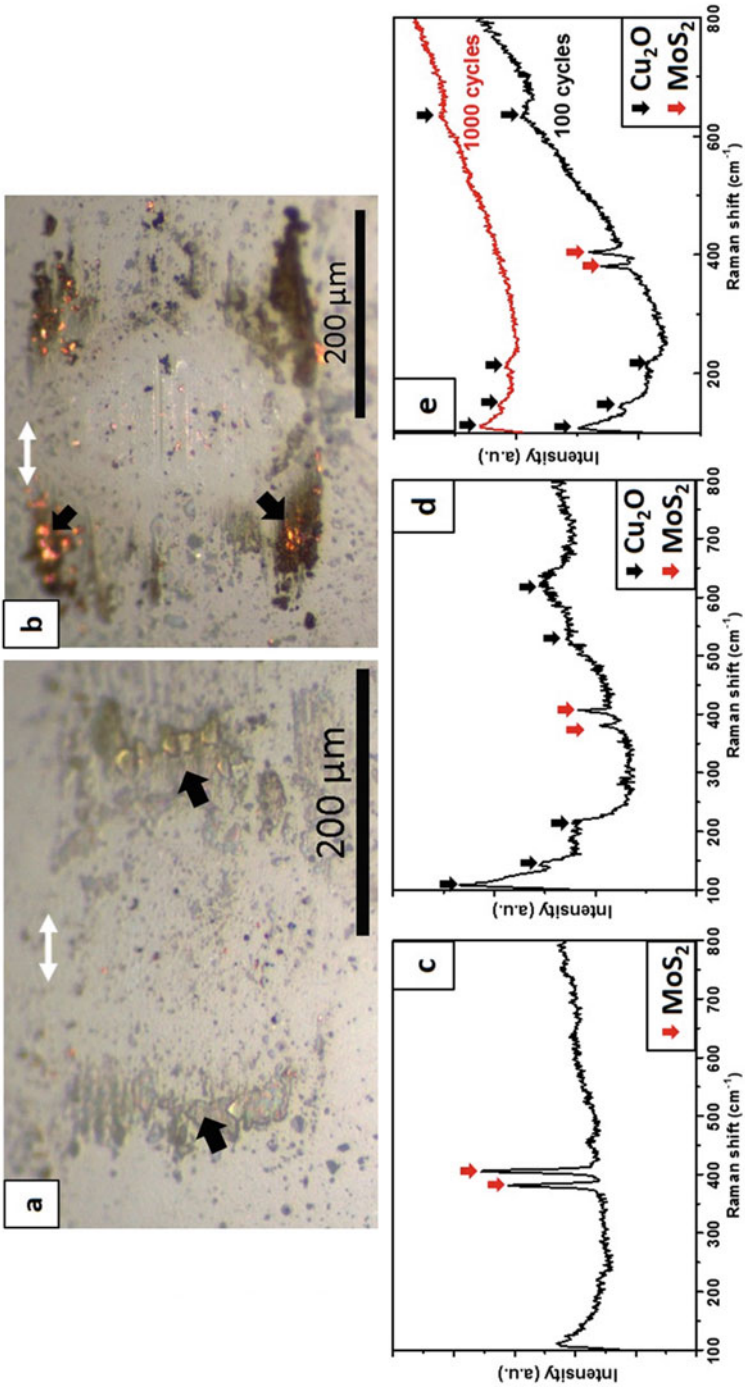

Fig. 2.21 Micrographs of the counterfaces mating with the Cu-MoS_2 coating after (**a**) 100 cycles and (**b**) 1000 cycles. Transferred patches and/or debris were found outside the contact, indicated as black arrows. Their Raman spectra were shown in (**c**) and (**d**), respectively. (**e**) Raman spectra taken from the wear tracks. White arrows indicate sliding direction. Reprinted from [32], with permission from Springer

With only 1.8 wt% MoS_2 in the coating, any transfer films that did form were readily removed and redeposited onto the wear track. This was due to the interactions of MoS_2 with the wear track, which was primarily Cu – a very different contact condition compared to sliding on a PVD coating with a constant source of MoS_2. With the interactions of the metal, the transfer films were unstable and continuously removed, ultimately resulting in MoS_2 patches on the wear track that were expanded over sliding (Figs. 2.19d and 2.20d).

The VAM within MoS_2-rich tribofilms was also explored briefly in this study [32]. Using the two-term friction model that is commonly employed to combine two velocity accommodation modes with an assumption that interaction between the friction mechanisms is negligible [39], the total friction can be written as

$$\mu = \mu_{int} + \mu_{fracture} \tag{2.2}$$

where μ_{int} is friction from interfacial sliding and $\mu_{fracture}$ is the friction from fracture. Dvorak et al. [8, 56, 57] proposed a similar model for taking account of two friction mechanisms in MoS_2. For Cu-1.8 wt% MoS_2, the low MoS_2 content in the coating and the absence of a persistent MoS_2 transfer film on the counterface indicate that interfacial sliding between MoS_2 and MoS_2 did not occur to any great extent. The process by which the transfer films were removed and deposited back to the wear track as powdery MoS_2 was primarily related to the fracture of MoS_2. So the velocity difference was mostly accommodated by fracturing of MoS_2 third bodies. Therefore, $\mu_{int} \cong 0$, and $\mu \cong \mu_{fracture}$. Uemura et al. [184] demonstrated that fracture dominated friction was three to four times higher than interfacial sliding (i.e., $\mu_{fracture} \cong 3.5*\mu_{int}$). Also, Dvorak et al. [8, 56, 57] showed that the friction induced by interfacial sliding in dry air (i.e., $\mu \cong \mu_{int}$) under a wide range of contact pressure (0.41–1.39 GPa) was below 0.05. Thus, based on the results of Uemura and Dvorak, an estimate of fracture-induced friction indicated it should be roughly 0.18 or below. This estimate was in a good agreement with the present study, where the friction of the high MoS_2 zones was 0.11–0.12. This analysis helped to understand how low friction can be observed with MoS_2 through a primarily fracture-based process instead of interfacial shearing. However, the elevated friction compared to an interfacial sliding mechanism must also partly be due to the occurrence of some metallic friction, evidenced by sliding grooves at the zones with little/no MoS_2 (Fig. 2.19d) and oxidation (Fig. 2.21e).

Cross-sectional microstructures of the wear tracks exhibit influence of solid lubricants on tribologically modified microstructure and therefore permit a better understanding of tribological behavior of SLMMCs. As shown in Fig. 2.22, in the Cu-MoS_2 wear track, sliding induced a cohesive mechanically mixed layer (MML) with fine cracks and a shallow dynamic recrystallized (DRX) layer 3–5 μm deep, where a decrease in defect density was observed but no significant grain growth. However, for the Cu wear track, sliding introduced large cracks within the MML. The DRX layer penetrated into the coating as deep as 10–30 μm and substantial grain growth was found in the DRX layer. The minor changes in subsurface microstructure and phase transformation in the Cu-MoS_2 wear track compared to Cu wear track

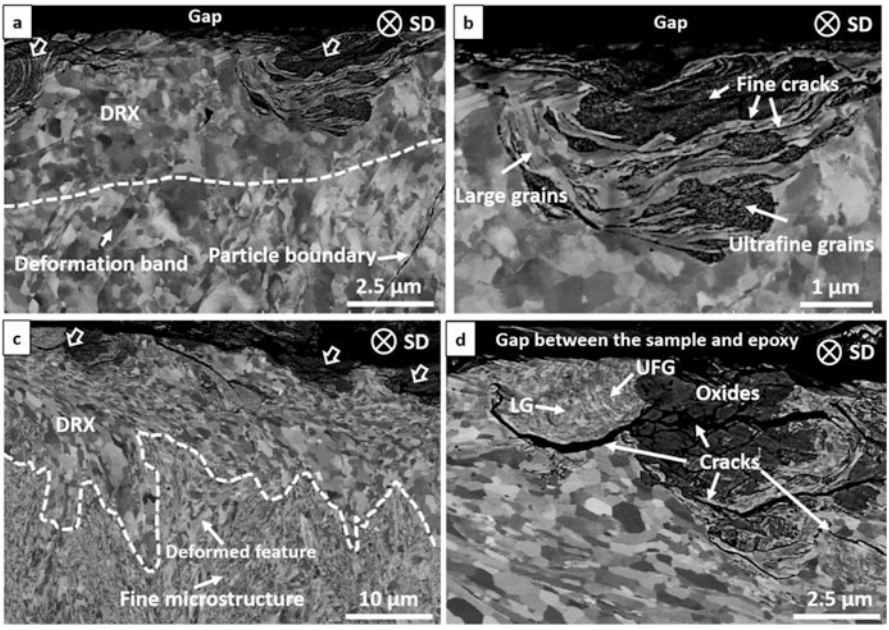

Fig. 2.22 (**a**) Micrograph of cross section of the Cu-MoS_2 wear track after a 3000 cycle test. The hollow arrows denote MML, and the dashed line the border of the sliding-induced microstructure and as-sprayed microstructure. (**b**) A closer view of the sliding-induced microstructure. (**c**) Micrograph of cross section of the Cu wear track after a 3000 cycle test. The hollow arrows denote MML, the dashed line the border of the sliding-induced microstructure and the as-sprayed microstructure. (**d**) A closer view of the sliding-induced microstructure. SD indicates sliding direction. Reprinted from [32], with permission from Springer

probably resulted from a much minder stress field generated underneath the Cu-MoS_2 wear tracks [32, 185–187]. There is a chance that frictional heating might play a role on the microstructural modification [188].

As discussed in Sect. 2.2.1, for SLMMCs, even though traditional ex situ techniques have been used extensively to observe third body behaviors, e.g., formation and evolution of lubricating tribofilms and transfer films, the effectiveness of replenishment process and the mechanisms have not been fully understood. In situ tribology technique is capable of capturing third body "processes" over the whole testing, which provides generation and dynamics of lubricating films at the contact. Here we present formation of MoS_2 tribofilms and transfer films at the very beginning and how they were depleted with sliding. More details on in situ tribometer setup can be found in [16] and sliding wear testing parameters in [32]. As shown in Fig. 2.23, once sliding commenced, patchy MoS_2 transfer film was formed. Where and how much of the transfer film can be generated largely depent on local MoS_2 content. The transfer films were then deposited onto the wear track when rubbing against pure Cu, and were consumed completely eventually, as shown in Fig. 2.23b–d. This process continued with sliding. At 20 cycles (see Fig. 2.24a),

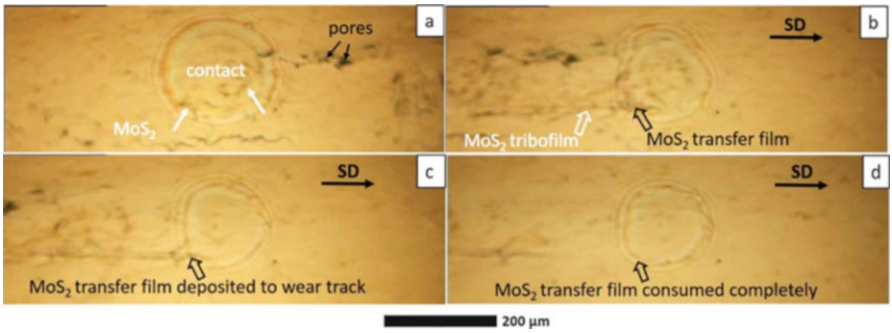

Fig. 2.23 In situ micrographs of Cu-MoS_2 composite during the first half cycle. (**a**) Right before sliding, followed by (**b**–**d**) where sliding commenced. SD indicates sliding direction. (Mining and Materials Engineering, McGill University, Montreal, Canada)

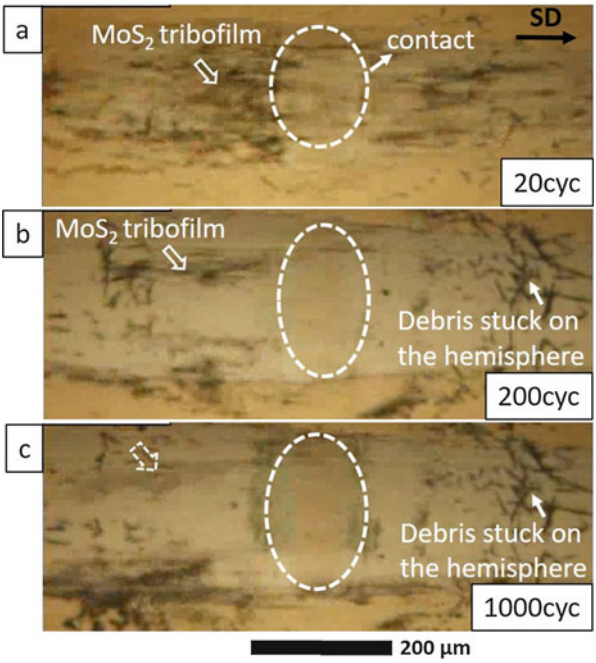

Fig. 2.24 In situ micrographs of Cu-MoS_2 composite at (**a**) 20 cycles, (**b**) 200 cycles, and (**c**) 1000 cycles. The same spot was taken to investigate evolution of the lubricating film. Dashed lines of ellipses indicate contact, while the arrow with dashed lines denotes the MoS_2 tribofilm become barely visible through optical microscope. (Mining and Materials Engineering, McGill University, Montreal, Canada)

more MoS_2 tribofilms were developed, indicating MoS_2 was expanded more extensively and in the meantime MoS_2 was replenished as wearing through the top surface. The MoS_2 tribofilms were then depleted gradually as seen in Fig. 2.24b, c. They could become wear debris deposited onto the counterface or outside the wear track. It is worth noting that even though only a few visible patchy MoS_2 tribofilms over the majority of sliding, the presence of MoS_2 eliminated metal oxidation comparing to the pure Cu case (not shown). These results are consistent with wear

track morphology observation by ex situ techniques (Fig. 2.22). Even though higher resolution micrographs and in situ chemical/phase composition analysis, e.g., in situ Raman spectroscopy, are required to better understand third body generation and evolution over sliding, we believe combination of ex situ and in situ methods are able to reveal third body behavior of SLMMCs more comprehensively.

2.6 Applications, Challenges, and Future Directions

SLMMCs remain an important class of engineering materials, especially considering global initiatives for green manufacturing and increased sustainability in engineering design. These materials find applications in aerospace, automotive, marine, and other sectors where tribological contacts are made that require low friction, such as bearings, bushings, and piston liners. Many different metal matrices have been studied (e.g., Cu, Mg, Al, Ni, Ti, and their alloys) with a range of solid lubricants (e.g., Gr, CNTs, G, MoS_2, WS_2, h-BN, and others). One also finds SLMMCs manufactured by a wide range of methods that have been reviewed here, from the mature stir casting method for Al alloys with Gr to the more recent techniques of cold spray, friction stir processing, and laser additive manufacturing methods. Thus, there is a significant body of scientific literature and knowledge base for SLMMCs. However, based on this review, we have identified some areas of future research that could make significant impact on understanding of the lubrication mechanisms for SLMMCs and also the development of SLMMCs with optimized properties.

The basic understanding of the lubrication mechanisms of SLMMCs consists of tribofilm formation, which is the formation of a surface layer that consists of lubricating material that reduce the fraction of metal-to-metal junctions in the sliding contact. However, as shown in this review the structure of a tribofilm can be considerably more complex than this. In the work of Riahi and Alpas [169], they observed a tribofilm that was composed of many components with a small fraction of the graphite lubricant. Researchers should devote more efforts on describing the exact nature of the tribofilms for SLMMCs as their formation is key for the function of the composite, but the mechanism and the nature of their formation are not always fully elucidated.

Generally, third body flows and lubrication mechanisms for SLMMCs deviate significantly from blanket films of solid lubricants. For blanket films, there is a large volume fraction of solid lubricant available; the VAM is solid lubricant vs. solid lubricant or interfacial shearing of the solid lubricant, as depicted in Fig. 2.2. For SLMMCs, the total volume fraction of lubricant is lower. Often one finds that transfer films do not persist in the sliding contact, as was shown by in situ tribometry above in the work of Zhang et al. (McGill University). Any transfer film material formed generally flows back to the wear track in recirculation flow or out of the contact as debris. This means the mechanisms observed by Mogonye et al. [98] are more important. An understanding of the replenishment mechanisms for the tribofilms from the near surface solid lubricant particles would be key in better design of SLMMCs. The flow of solid lubricant materials toward the surface can naturally occur by wear or

by plastic deformation, but the process must have a dependence on the fabrication methods of the composite, lubricant content and morphology, and the microstructure of the matrix itself. Researchers have already described these as being key variables for the performance of the composites, but these links are not as strong as they could be without more detailed information on the mechanisms of near surface lubricant flow, tribofilm formation and structure, and the recirculation flow of lubricants.

SLMMCs have an opportunity to undergo a significant revolution in both materials and processing/manufacturing. In terms of materials, researchers are actively exploring incorporation of newer forms, often nanostructured, of popular lubricants. Recent excitement on graphene and before that CNTs have translated to their use in SLMMCs. Similarly, 2D versions of MoS_2 are becoming readily available and can be utilized for making SLMMCs. Challenges of course remain for these materials. Researchers must focus as best they can on side-by-side comparisons [76] between these newer materials and traditional forms of the lubricants. Otherwise, the understanding of performance differences becomes lost in the cloud of tribological test parameters. Also, it is critical that the lubricants be examined with electron microscopy and other spectroscopic methods to quantify the state of the lubricant in the SLMMC postprocessing.

On the manufacturing side, new processing routes provide new possibilities for SLMMCs. In particular additive manufacturing provides a new vista. While most additive manufacturing researchers are focused on making bulk parts from metals and alloys, there is a real possibility for using these techniques to tailor the properties for SLMMCs, including but not limited to a more precise control of the lubricant content and morphology in the composite. However, many of these techniques are laser based, and challenges on control of lubricant state in the composite would be a key issue. Similarly, cold spray, which is currently a method primarily focused on metals and coatings, has the potential to become an additive manufacturing method utilized for SLMMCs. Even though cold spray eliminates or avoids decomposition of the solid lubricants that is inevitable for most of the other manufacturing processes, challenges for this technique are precise control of powder delivery systems and development of optimized feedstocks that are suitable for cold spray. The feedstocks can be conceivably modified to composite powders using dryer spraying technique, metal-coated solid lubricant powders made by deposition or ball milling, and even combination of them, i.e., metal-coated composite powders. These pretreatments could improve cold sprayability of the materials according to deposition mechanism described in Sect. 2.3.5. Moreover, due to poor sprayability of solid lubricants, in situ formation of solid lubricants during post spraying treatment, e.g., heat treatment, could avoid spraying solid lubricant directly. This could promote a new route to fabricate SLMMCs using cold spray. In addition, several alternatives of conventional lamellar solid lubricants are some oxides, e.g., TiO_2, and soft metals, e.g., Sn, which could be used as solid lubricants at elevated temperature. In fact, TiO_2 ceramic coating has been sprayed by high pressure cold spray system and low pressure cold spray system [189, 190]. Even though there are some challenges, cold spray provides an interesting opportunity to develop a next generation of SLMMCs.

References

1. Daniel, I.M., Ishai, O.: Engineering Mechanics of Composite Materials. Oxford University Press, New York (1994)
2. Prasad, S., Asthana, R.: Aluminum metal-matrix composites for automotive applications: tribological considerations. Tribol. Lett. **17**(3), 445–453 (2004)
3. Miracle, D.B.: Metal matrix composites – from science to technological significance. Compos. Sci. Technol. **65**(15–16), 2526–2540 (2005)
4. Omrani, E., et al.: Influences of graphite reinforcement on the tribological properties of self-lubricating aluminum matrix composites for green tribology, sustainability, and energy efficiency – a review. Int. J. Adv. Manuf. Technol. **83**(1–4), 325–346 (2016)
5. Omrani, E., et al.: New emerging self-lubricating metal matrix composites for tribological applications. In: Davim, P.J. (ed.) Ecotribology: Research Developments, pp. 63–103. Springer International Publishing, Cham (2016)
6. Dellacorte, C., Fellenstein, J.A.: The effect of compositional tailoring on the thermal expansion and tribological properties of PS300: a solid lubricant composite coating. Tribol. Trans. **40**(4), 639–642 (1997)
7. Zhang, X., et al.: Carbon nanotube-MoS_2 composites as solid lubricants. ACS Appl. Mater. Interfaces. **1**(3), 735–739 (2009)
8. Chromik, R.R., et al.: In situ tribometry of solid lubricant nanocomposite coatings. Wear. **262** (9–10), 1239–1252 (2007)
9. Godet, M.: The third-body approach: a mechanical view of wear. Wear. **100**(1), 437–452 (1984)
10. Godet, M.: Third-bodies in tribology. Wear. **136**(1), 29–45 (1990)
11. Rigney, D.A., Karthikeyan, S.: The evolution of tribomaterial during sliding: a brief introduction. Tribol. Lett. **39**(1), 3–7 (2010)
12. Biswas, S.K.: Wear of metals: a material approach. In: Stachowiak, G.W. (ed.) Wear: Materials, Mechanisms and Practice, pp. 21–36. Wiley, West Sussex (2005)
13. Descartes, S., Busquet, M., Berthier, Y.: An attempt to produce ex situ TTS to understand their mechanical formation conditions – the case of an ultra high purity iron. Wear. **271**(9–10), 1833–1841 (2011)
14. Tumbajoy-Spinel, D., et al.: Assessment of mechanical property gradients after impact-based surface treatment: application to pure α-iron. Mater. Sci. Eng. A. **667**, 189–198 (2016)
15. Singer, I.L.: Solid lubrication processes. In: Singer, I.L., Pollock, H.M. (eds.) Fundamentals of Friction, pp. 237–261. Kluwer, Dordrecht (1992)
16. Chromik, R., Strauss, H., Scharf, T.: Materials phenomena revealed by in situ tribometry. JOM. **64**(1), 35–43 (2012)
17. Wahl, K.J., Sawyer, W.G.: Observing interfacial sliding processes in solid – solid contacts. MRS Bull. **33**(12), 1159–1167 (2008)
18. Berthier, Y., Godet, M., Brendle, M.: Velocity accommodation in friction. Tribol. Trans. **32**(4), 490–496 (1989)
19. Scharf, T.W., Singer, I.L.: Role of third bodies in friction behavior of diamond-like nanocomposite coatings studied by in situ tribometry. Tribol. Trans. **45**(3), 363–371 (2002)
20. Scharf, T.W., Singer, I.L.: Quantification of the thickness of carbon transfer films using Raman tribometry. Tribol. Lett. **14**, 137–146 (2003)
21. Scharf, T.W., Singer, I.L.: Monitoring transfer films and friction instabilities with in situ Raman tribometry. Tribol. Lett. **14**, 3–8 (2003)
22. Scharf, T.W., Singer, I.L.: Role of the transfer film on the friction and wear of metal carbide reinforced amorphous carbon coatings during run-in. Tribol. Lett. **36**(1), 43–53 (2009)
23. Strauss, H.W., et al.: In situ tribology of nanocomposite Ti-Si-C-H coatings prepared by PE-CVD. Wear. **272**, 133–148 (2011)
24. Wahl, K.J., Chromik, R.R., Lee, G.Y.: Quantitative in situ measurement of transfer film thickness by a Newton's rings method. Wear. **264**(7–8), 731–736 (2008)

25. Shockley, J.M., et al.: The influence of Al_2O_3 particle morphology on the coating formation and dry sliding wear behavior of cold sprayed Al-Al_2O_3 composites. Surf. Coat. Technol. **270**, 324–333 (2015)
26. Sriraman, K.R., et al.: Tribological behavior of electrodeposited Zn, Zn-Ni, Cd and Cd-Ti coatings on low carbon steel substrates. Tribol. Int. **56**, 107–120 (2012)
27. Stoyanov, P., et al.: Combining in situ and online approaches to monitor interfacial processes in lubricated sliding contacts. MRS Commun. 6(3), 301–308 (2016)
28. Shockley, J.M., et al.: Third body behavior during dry sliding of cold-sprayed Al-Al_2O_3 composites: in situ tribometry and microanalysis. Tribol. Lett. **54**(2), 191–206 (2014)
29. Shockley, J.M., et al.: In situ tribometry of cold-sprayed Al-Al_2O_3 composite coatings. Surf. Coat. Technol. **215**, 350–356 (2013)
30. Berthier, Y.: Experimental evidence for friction and wear modelling. Wear. **139**(1), 77–92 (1990)
31. Alidokht, S.A., et al.: Role of third-bodies in friction and wear of cold-sprayed Ti and Ti-TiC composite coatings. Tribol. Lett. 65, 114 (2017)
32. Zhang, Y., et al.: Tribological behavior of a cold-sprayed Cu–MoS_2 composite coating during dry sliding wear. Tribol. Lett. **62**(1), 1–12 (2016)
33. Yang, M.-S., et al.: Microstructure and wear behaviors of laser clad NiCr/Cr_3C_2–WS_2 high temperature self-lubricating wear-resistant composite coating. Appl. Surf. Sci. **258**(8), 3757–3762 (2012)
34. Raadnui, S., Mahathanabodee, S., Tongsri, R.: Tribological behaviour of sintered 316L stainless steel impregnated with MoS_2 plain bearing. Wear. **265**(3), 546–553 (2008)
35. Li, J.L., Xiong, D.S.: Tribological properties of nickel-based self-lubricating composite at elevated temperature and counterface material selection. Wear. **265**(3), 533–539 (2008)
36. Mahathanabodee, S., et al.: Dry sliding wear behavior of SS316L composites containing h-BN and MoS_2 solid lubricants. Wear. **316**(1), 37–48 (2014)
37. Scharf, T.W.: Low friction coatings. In: Bruce, R. (ed.) Handbook of Lubrication and Tribology. CRC Press, Boca Raton (2012)
38. Scharf, T.W., Prasad, S.V.: Solid lubricants: a review. J. Mater. Sci. **48**(2), 511–531 (2012)
39. Bowden, F.P., Tabor, D.: The Friction and Lubrication of Solids, vol. 1. Oxford University Press, New York (2001)
40. Erdemir, A., Fontaine, J., Donnet, C.: An overview of superlubricity in diamond-like carbon films. In: Donnet, C., Erdemir, A. (eds.) Tribology of Diamond-Like Carbon Films: Fundamentals and Applications, pp. 237–262. Springer US, Boston (2008)
41. Fontaine, J., Donnet, C., Erdemir, A.: Fundamentals of the tribology of DLC coatings. In: Donnet, C., Erdemir, A. (eds.) Tribology of Diamond-Like Carbon Films: Fundamentals and Applications, pp. 139–154. Springer US, Boston (2008)
42. Hoffman, E.E., Marks, L.D.: Graphitic carbon films across systems. Tribol. Lett. **63**(3), 32 (2016)
43. Liu, Y., Erdemir, A., Meletis, E.I.: An investigation of the relationship between graphitization and frictional behavior of DLC coatings. Surf. Coat. Technol. **86**, 564–568 (1996)
44. Liu, Y., Erdemir, A., Meletis, E.I.: A study of the wear mechanism of diamond-like carbon films. Surf. Coat. Technol. **82**(1), 48–56 (1996)
45. Fontaine, J., et al.: Tribological behaviour of metal-DLC nanocomposite coatings: the critical role of tribofilm build-up. In: World Tribology Congress 2009 – Proceedings (Kyoto, Japan) (2009)
46. Pastewka, L., Moser, S., Moseler, M.: Atomistic insights into the running-in, lubrication, and failure of hydrogenated diamond-like carbon coatings. Tribol. Lett. **39**(1), 49–61 (2010)
47. Al-Azizi, A.A., et al.: Surface structure of hydrogenated diamond-like carbon: origin of run-in behavior prior to superlubricious interfacial shear. Langmuir. **31**(5), 1711–1721 (2015)
48. Berman, D., et al.: Macroscale superlubricity enabled by graphene nanoscroll formation. Science. **348**(6239), 1118–1122 (2015)
49. Berman, D., et al.: Nanoscale friction properties of graphene and graphene oxide. Diam. Relat. Mater. **54**(1), 91–96 (2015)

50. Berman, D., et al.: Extraordinary macroscale wear resistance of one atom thick graphene layer. Adv. Funct. Mater. **24**(42), 6640–6646 (2014)
51. Berman, D., Erdemir, A., Sumant, A.V.: Few layer graphene to reduce wear and friction on sliding steel surfaces. Carbon. **54**, 454–459 (2013)
52. Spalvins, T.: Lubrication with sputtered MoS_2 films: principles, operation, and limitations. J. Mater. Eng. Perform. **1**(3), 347–351 (1992)
53. McDevitt, N.T., Donley, M.S., Zabinski, J.S.: Utilization of Raman spectroscopy in tribochemistry studies. Wear. **166**(1), 65–72 (1993)
54. Liang, T., et al.: First-principles determination of static potential energy surfaces for atomic friction in MoS_2 and MoO_3. Phys. Rev. B Condens. Matter Mater. Phys. **77**(10), 104105 (2008)
55. Liang, T., et al.: Energetics of oxidation in MoS_2 nanoparticles by density functional theory. J. Phys. Chem. C. **115**(21), 10606–10616 (2011)
56. Dvorak, S.D., Wahl, K.J., Singer, I.L.: In situ analysis of third body contributions to sliding friction of a Pb-Mo-S coating in dry and humid air. Tribol. Lett. **28**(3), 263–274 (2007)
57. Wahl, K.J., Belin, M., Singer, I.L.: A triboscopic investigation of the wear and friction of MoS_2 in a reciprocating sliding contact. Wear. **214**(2), 212–220 (1998)
58. Hoffman, E.E., Marks, L.D.: Soft interface fracture transfer in nanoscale MoS_2. Tribol. Lett. **64**(1), 1 (2016)
59. Wahl, K.J., Singer, I.L.: Quantification of a lubricant transfer process that enhances the sliding life of a MoS_2 coating. Tribol. Lett. **1**(1), 59–66 (1995)
60. Lince, J.R., et al.: Tribochemistry of MoS_3 nanoparticle coatings. Tribol. Lett. **53**(3), 543–554 (2014)
61. Spear, J.C., Ewers, B.W., Batteas, J.D.: 2D-nanomaterials for controlling friction and wear at interfaces. Nano Today. **10**(3), 301–314 (2015)
62. Rohatgi, P.K.: Metal matrix composites. Def. Sci. J. **43**(4), 323 (1993)
63. Liu, Y., Rohatgi, P.K., Ray, S.: Tribological characteristics of aluminum-50 vol pct graphite composite. Metall. Trans. A. **24**(1), 151–159 (1993)
64. Rohatgi, P.K., Ray, S., Liu, Y.: Tribological properties of metal matrix-graphite particle composites. Int. Mater. Rev. **37**, 129 (1992)
65. Rohatgi, P.K., et al.: A surface-analytical study of tribodeformed aluminum alloy 319-10 vol. % graphite particle composite. Mater. Sci. Eng. A. **123**(2), 213–218 (1990)
66. Jha, A., et al.: Aluminium alloy-solid lubricant talc particle composites. J. Mater. Sci. **21**(10), 3681–3685 (1986)
67. Bowden, F., Shooter, K.: Frictional behaviour of plastics impregnated with molybdenum disulphide. Res. Appl. Ind. **3**, 384 (1950)
68. Lancaster, J.: Composite self-lubricating bearing materials. Proc. Inst. Mech. Eng. **182**(1), 33–54 (1967)
69. Prasad, S., Mecklenburg, K.R.: Self-lubricating aluminum metal-matrix composites dispersed with tungsten disulfide and silicon carbide. Lubr. Eng. **50**(7), 511 (1994)
70. Das, S., Prasad, S.V., Ramachandran, T.R.: Tribology of Al-Si alloy-graphite composites: triboinduced graphite films and the role of silicon morphology. Mater. Sci. Eng. A. **138**(1), 123–132 (1991)
71. Das, S., Prasad, S.V., Ramachandran, T.R.: Microstructure and wear of cast (Al-Si alloy)-graphite composites. Wear. **133**(1), 173–187 (1989)
72. Gibson, P.R., Clegg, A.J., Das, A.A.: Wear of cast Al-Si alloys containing graphite. Wear. **95** (2), 193–198 (1984)
73. Biswas, S.K., Bai, B.N.P.: Dry wear of Al-graphite particle composites. Wear. **68**(3), 347–358 (1981)
74. Jha, A.K., Prasad, S.V., Upadhyaya, G.S.: Sintered 6061 aluminium alloy – solid lubricant particle composites: sliding wear and mechanisms of lubrication. Wear. **133**(1), 163–172 (1989)

75. Akhlaghi, F., Mahdavi, S.: Effect of the SiC content on the tribological properties of hybrid Al/Gr/SiC composites processed by in situ powder metallurgy (IPM) method. Adv. Mater. Res. **264–265**, 1878–1886 (2011)
76. Maurya, R., et al.: Effect of carbonaceous reinforcements on the mechanical and tribological properties of friction stir processed Al6061 alloy. Mater. Des. **98**, 155–166 (2016)
77. Sarmadi, H., Kokabi, A., Reihani, S.S.: Friction and wear performance of copper–graphite surface composites fabricated by friction stir processing (FSP). Wear. **304**(1), 1–12 (2013)
78. Soleymani, S., Abdollah-Zadeh, A., Alidokht, S.: Microstructural and tribological properties of Al5083 based surface hybrid composite produced by friction stir processing. Wear. **278**, 41–47 (2012)
79. Dolatkhah, A., et al.: Investigating effects of process parameters on microstructural and mechanical properties of Al5052/SiC metal matrix composite fabricated via friction stir processing. Mater. Des. **37**, 458–464 (2012)
80. Alidokht, S.A., et al.: Microstructure and tribological performance of an aluminium alloy based hybrid composite produced by friction stir processing. Mater. Des. **32**(5), 2727–2733 (2011)
81. Gan, Y., Solomon, D., Reinbolt, M.: Friction stir processing of particle reinforced composite materials. Materials. **3**(1), 329 (2010)
82. Chen, L.-Y., et al.: Novel nanoprocessing route for bulk graphene nanoplatelets reinforced metal matrix nanocomposites. Scr. Mater. **67**(1), 29–32 (2012)
83. Nickchi, T., Ghorbani, M.: Pulsed electrodeposition and characterization of bronze-graphite composite coatings. Surf. Coat. Technol. **203**(20), 3037–3043 (2009)
84. Algul, H., et al.: The effect of graphene content and sliding speed on the wear mechanism of nickel-graphene nanocomposites. Appl. Surf. Sci. **359**, 340–348 (2015)
85. Uysal, M., et al.: Structural and sliding wear properties of Ag/Graphene/WC hybrid nanocomposites produced by electroless co-deposition. J. Alloys Compd. **654**, 185–195 (2016)
86. Pialago, E.J.T., Kwon, O.K., Park, C.W.: Cold spray deposition of mechanically alloyed ternary Cu–CNT–SiC composite powders. Ceram. Int. **41**(5), 6764–6775 (2015)
87. Pialago, E.J.T., Park, C.W.: Cold spray deposition characteristics of mechanically alloyed Cu-CNT composite powders. Appl. Surf. Sci. **308**, 63–74 (2014)
88. Cho, S., et al.: Multi-walled carbon nanotube-reinforced copper nanocomposite coating fabricated by low-pressure cold spray process. Surf. Coat. Technol. **206**(16), 3488–3494 (2012)
89. Bakshi, S.R., et al.: Nanoscratch behavior of carbon nanotube reinforced aluminum coatings. Thin Solid Films. **518**(6), 1703–1711 (2010)
90. Bakshi, S.R., et al.: Deformation and damage mechanisms of multiwalled carbon nanotubes under high-velocity impact. Scr. Mater. **59**(5), 499–502 (2008)
91. Bakshi, S.R., et al.: Carbon nanotube reinforced aluminum composite coating via cold spraying. Surf. Coat. Technol. **202**(21), 5162–5169 (2008)
92. Chen, Y., Bakshi, S.R., Agarwal, A.: Correlation between nanoindentation and nanoscratch properties of carbon nanotube reinforced aluminum composite coatings. Surf. Coat. Technol. **204**(16), 2709–2715 (2010)
93. Pialago, E.J.T., et al.: Ternary Cu–CNT–AlN composite coatings consolidated by cold spray deposition of mechanically alloyed powders. J. Alloys Compd. **650**, 199–209 (2015)
94. Pialago, E.J.T., Kwon, O.K., Park, C.W.: Nucleate boiling heat transfer of R134a on cold sprayed CNT–Cu composite coatings. Appl. Therm. Eng. **56**(1), 112–119 (2013)
95. Rajkumar, K., Aravindan, S.: Tribological performance of microwave sintered copper–TiC–graphite hybrid composites. Tribol. Int. **44**(4), 347–358 (2011)
96. Rajkumar, K., Aravindan, S.: Tribological studies on microwave sintered copper–carbon nanotube composites. Wear. **270**(9), 613–621 (2011)
97. Rajkumar, K., Aravindan, S.: Tribological behavior of microwave processed copper–nanographite composites. Tribol. Int. **57**, 282–296 (2013)

98. Mogonye, J.E., et al.: Solid/self-lubrication mechanisms of an additively manufactured Ni–Ti–C metal matrix composite. Tribol. Lett. **64**(3), 37 (2016)
99. Esawi, A.M.K., et al.: Fabrication and properties of dispersed carbon nanotube–aluminum composites. Mater. Sci. Eng. A. **508**(1–2), 167–173 (2009)
100. Kim, K.T., Cha, S.I., Hong, S.H.: Hardness and wear resistance of carbon nanotube reinforced Cu matrix nanocomposites. Mater. Sci. Eng. A. **449–451**, 46–50 (2007)
101. Dong, S.R., Tu, J.P., Zhang, X.B.: An investigation of the sliding wear behavior of Cu-matrix composite reinforced by carbon nanotubes. Mater. Sci. Eng. A. **313**(1–2), 83–87 (2001)
102. Tjong, S.C.: Recent progress in the development and properties of novel metal matrix nanocomposites reinforced with carbon nanotubes and graphene nanosheets. Mater. Sci. Eng. R. Rep. **74**(10), 281–350 (2013)
103. Scharf, T., et al.: Self-lubricating carbon nanotube reinforced nickel matrix composites. J. Appl. Phys. **106**(1), 013508 (2009)
104. Zhou, S.-m., et al.: Fabrication and tribological properties of carbon nanotubes reinforced Al composites prepared by pressureless infiltration technique. Compos. A Appl. Sci. Manuf. **38** (2), 301–306 (2007)
105. Hu, Z., et al.: Laser sintered single layer graphene oxide reinforced titanium matrix nanocomposites. Compos. Part B Eng. **93**, 352–359 (2016)
106. Zhai, W., et al.: Investigation of mechanical and tribological behaviors of multilayer graphene reinforced Ni_3Al matrix composites. Compos. Part B Eng. **70**, 149–155 (2015)
107. Bastwros, M., et al.: Effect of ball milling on graphene reinforced Al6061 composite fabricated by semi-solid sintering. Compos. Part B Eng. **60**, 111–118 (2014)
108. Ghazaly A., Seif B., Salem H.G.: Mechanical and Tribological Properties of AA2124-Graphene Self Lubricating Nanocomposite. In: Sadler B.A. (ed.) Light Metals 2013. The Minerals, Metals & Materials Series. Springer, Cham (2013)
109. Tyagi, R., et al.: Elevated temperature tribological behavior of Ni based composites containing nano-silver and hBN. Wear. **269**(11), 884–890 (2010)
110. Selvakumar, N., Narayanasamy, P.: Optimization and effect of weight fraction of MoS_2 on the tribological behaviour of Mg-TiC-MoS_2 hybrid composites. Tribol. Trans. **59**(4), 733–747 (2016)
111. Kato, H., et al.: Wear and mechanical properties of sintered copper–tin composites containing graphite or molybdenum disulfide. Wear. **255**(1), 573–578 (2003)
112. Du, L., et al.: Preparation and wear performance of NiCr/Cr_3C_2–NiCr/hBN plasma sprayed composite coating. Surf. Coat. Technol. **205**(12), 3722–3728 (2011)
113. Yuan, J., et al.: Fabrication and evaluation of atmospheric plasma spraying WC–Co–Cu–MoS_2 composite coatings. J. Alloys Compd. **509**(5), 2576–2581 (2011)
114. Liu, X.-B., et al.: Development and characterization of laser clad high temperature self-lubricating wear resistant composite coatings on Ti–6Al–4V alloy. Mater. Des. **55**, 404–409 (2014)
115. Yan, H., et al.: Laser cladding of Co-based alloy/TiC/CaF_2 self-lubricating composite coatings on copper for continuous casting mold. Surf. Coat. Technol. **232**, 362–369 (2013)
116. Zhang, Y., et al.: Cold-sprayed Cu-MoS_2 and its fretting wear behavior. J. Therm. Spray Technol. **25**(3), 473–482 (2016)
117. Neshastehriz, M., et al.: On the bonding mechanism in cold spray of deformable hex-BN-Ni clusters. J. Therm. Spray Technol. **25**(5), 982–991 (2016)
118. Smid, I., et al.: Cold-sprayed Ni-hBN self-lubricating coatings. Tribol. Trans. **55**(5), 599–605 (2012)
119. Moridi, A., et al.: Cold spray coating: review of material systems and future perspectives. Surf. Eng. **30**(6), 369–395 (2014)
120. Hou, X., et al.: Preparation and properties of hexagonal boron nitride fibers used as high temperature membrane filter. Mater. Res. Bull. **49**, 39–43 (2014)
121. Bi, Q., S. Zhu, and W. Liu, High Temperature Self-Lubricating Materials. In: Pihtili H. (ed.) Tribology in Engineering, pp.109–134. InTech, Rijeka (2013)

122. Kovalchenko, A., Fushchich, O., Danyluk, S.: The tribological properties and mechanism of wear of Cu-based sintered powder materials containing molybdenum disulfide and molybdenum diselenite under unlubricated sliding against copper. Wear. **290**, 106–123 (2012)
123. Furlan, K.P., et al.: Influence of alloying elements on the sintering thermodynamics, microstructure and properties of Fe–MoS_2 composites. J. Alloys Compd. **652**, 450–458 (2015)
124. Mahathanabodee, S., et al.: Comparative studies on wear behaviour of sintered 316L stainless steels loaded with h-BN and MoS_2. Adv. Mater. Res. **747**, 307 (2013). Trans Tech Publ
125. Mahathanabodee, S., et al.: Effects of hexagonal boron nitride and sintering temperature on mechanical and tribological properties of SS316L/h-BN composites. Mater. Des. **46**, 588–597 (2013)
126. Mahathanabodee, S., et al.: Effect of h-BN content on the sintering of SS316L/h-BN composites. Adv. Mater. Res. **410**, 216–219 (2012)
127. Shi, X., et al.: Tribological behavior of Ni_3Al matrix self-lubricating composites containing WS_2, Ag and hBN tested from room temperature to 800 °C. Mater. Des. **55**, 75–84 (2014)
128. Cardenas, A., et al.: Effect of glow discharge sintering in the properties of a composite material fabricated by powder metallurgy. J. Phys. Conf. Ser. **687**(1), p. 012025 (2016)
129. Quazi, M., et al.: A review to the laser cladding of self-lubricating composite coatings. Lasers Manuf. Mater. Process. **3**(2), 67–99 (2016)
130. Xu, J., Liu, W., Zhong, M.: Microstructure and dry sliding wear behavior of MoS_2/TiC/Ni composite coatings prepared by laser cladding. Surf. Coat. Technol. **200**(14–15), 4227–4232 (2006)
131. Lei, Y., et al.: Microstructure and phase transformations in laser clad CrxSy/Ni coating on H13 steel. Opt. Lasers Eng. **66**, 181–186 (2015)
132. Zhang, S., et al.: Friction and wear behavior of laser cladding Ni/hBN self-lubricating composite coating. Mater. Sci. Eng. A. **491**(1), 47–54 (2008)
133. Zhu, S., et al.: Ni_3Al matrix high temperature self-lubricating composites. Tribol. Int. **44**(4), 445–453 (2011)
134. Liu, X.-B., et al.: Effects of temperature and normal load on tribological behavior of nickel-based high temperature self-lubricating wear-resistant composite coating. Compos. Part B Eng. **53**, 347–354 (2013)
135. Wang, A., et al.: Ni-based alloy/submicron WS_2 self-lubricating composite coating synthesized by Nd: YAG laser cladding. Mater. Sci. Eng. A. **475**(1), 312–318 (2008)
136. Liu, X.-B., et al.: Microstructure and wear behavior of γ/Al_4C_3/TiC/CaF_2 composite coating on γ-TiAl intermetallic alloy prepared by Nd:YAG laser cladding. Appl. Surf. Sci. **255**(11), 5662–5668 (2009)
137. Liu, W.-G., et al.: Development and characterization of composite Ni–Cr–C–CaF_2 laser cladding on γ-TiAl intermetallic alloy. J. Alloys Compd. **470**(1), L25–L28 (2009)
138. Papyrin, A.: 2 – The development of the cold spray process A2. In: Champagne, V.K. (ed.) The Cold Spray Materials Deposition Process, pp. 11–42. Woodhead Publishing, Cambridge, England (2007)
139. Du, H., et al.: Structure, mechanical and sliding wear properties of WC–Co/MoS_2–Ni coatings by detonation gun spray. Mater. Sci. Eng. A. **445**, 122–134 (2007)
140. Du, H., et al.: Fabrication and evaluation of D-gun sprayed WC–Co coating with self-lubricating property. Tribol. Lett. **23**(3), 261–266 (2006)
141. Du, L., et al.: Effect of NiCr clad BaF_2·CaF_2 addition on wear performance of plasma sprayed chromium carbide-nichrome coating. J. Therm. Spray Technol. **19**(3), 551–557 (2010)
142. Du, L., et al.: Preparation and characterization of plasma sprayed Ni_3Al–hBN composite coating. Surf. Coat. Technol. **205**(7), 2419–2424 (2010)
143. Sahraeinejad, S., et al.: Fabrication of metal matrix composites by friction stir processing with different particles and processing parameters. Mater. Sci. Eng. A. **626**, 505–513 (2015)
144. Aruri, D., et al.: Wear and mechanical properties of 6061-T6 aluminum alloy surface hybrid composites [(SiC + Gr) and (SiC + Al_2O_3)] fabricated by friction stir processing. J. Mater. Res. Technol. **2**(4), 362–369 (2013)

145. Klinkov, S.V., Kosarev, V.F., Rein, M.: Cold spray deposition: significance of particle impact phenomena. Aerosp. Sci. Technol. **9**(7), 582–591 (2005)
146. Champagne, V.K.: 1 – Introduction. In: The Cold Spray Materials Deposition Process, pp. 1–7. Woodhead Publishing, Cambridge, England (2007)
147. Papyrin, A.N.: Preface. In: Cold Spray Technology, pp. x–xii. Elsevier, Oxford (2007)
148. Assadi, H., et al.: Bonding mechanism in cold gas spraying. Acta Mater. **51**(15), 4379–4394 (2003)
149. Papyrin, A., et al.: Chapter 1 – Discovery of the cold spray phenomenon and its basic features. In: Cold Spray Technology, pp. 1–32. Elsevier, Oxford (2007)
150. Botef, I., Villafuerte, J.: Overview. In: Villafuerte, J. (ed.) Modern Cold Spray: Materials, Process, and Applications, pp. 1–29. Springer International Publishing, Cham (2015)
151. Stark, L., et al.: Self-lubricating cold-sprayed coatings utilizing microscale nickel-encapsulated hexagonal boron nitride. Tribol. Trans. **55**(5), 624–630 (2012)
152. Moghadam, A.D., et al.: Mechanical and tribological properties of self-lubricating metal matrix nanocomposites reinforced by carbon nanotubes (CNTs) and graphene – a review. Compos. Part B Eng. **77**, 402–420 (2015)
153. Wang, J., et al.: Reinforcement with graphene nanosheets in aluminum matrix composites. Scr. Mater. **66**(8), 594–597 (2012)
154. Bartolucci, S.F., et al.: Graphene–aluminum nanocomposites. Mater. Sci. Eng. A. **528**(27), 7933–7937 (2011)
155. Stankovich, S., et al.: Graphene-based composite materials. Nature. **442**(7100), 282–286 (2006)
156. Rafiee, M.A., et al.: Enhanced mechanical properties of nanocomposites at low graphene content. ACS Nano. **3**(12), 3884–3890 (2009)
157. Xue, B., et al.: Microstructure and functional mechanism of friction layer in Ni_3Al matrix composites with graphene nanoplatelets. J. Mater. Eng. Perform. **25**(10), 4126–4133 (2016)
158. Chmielewski, M., et al.: Tribological behaviour of copper-graphene composite materials. Key Eng. Mater. **674**, 219–224 (2016)
159. Chen, F., et al.: Effects of graphene content on the microstructure and properties of copper matrix composites. Carbon. **96**, 836–842 (2016)
160. Moghadam, A.D., et al.: Functional metal matrix composites: self-lubricating, self-healing, and nanocomposites-an outlook. JOM. **66**(6), 872–881 (2014)
161. Akhlaghi, F., Zare-Bidaki, A.: Influence of graphite content on the dry sliding and oil impregnated sliding wear behavior of Al2024–graphite composites produced by in situ powder metallurgy method. Wear. **266**(1–2), 37–45 (2009)
162. Akhlaghi, F., Pelaseyyed, S.A.: Characterization of aluminum/graphite particulate composites synthesized using a novel method termed "in-situ powder metallurgy". Mater. Sci. Eng. A. **385** (1–2), 258–266 (2004)
163. Ravindran, P., et al.: Investigation of microstructure and mechanical properties of aluminum hybrid nano-composites with the additions of solid lubricant. Mater. Des. **51**, 448–456 (2013)
164. Suresha, S., Sridhara, B.K.: Wear characteristics of hybrid aluminium matrix composites reinforced with graphite and silicon carbide particulates. Compos. Sci. Technol. **70**(11), 1652–1659 (2010)
165. Choi, H.J., Lee, S.M., Bae, D.H.: Wear characteristic of aluminum-based composites containing multi-walled carbon nanotubes. Wear. **270**(1–2), 12–18 (2010)
166. Poirier, D., Gauvin, R., Drew, R.A.L.: Structural characterization of a mechanically milled carbon nanotube/aluminum mixture. Compos. A Appl. Sci. Manuf. **40**(9), 1482–1489 (2009)
167. Venkatesan, S., Anthony Xavior, M.: Investigation of aluminum (Al7050) metal matrix composites reinforced with graphene nanoparticles using stir casting process. Int. J. Appl. Eng. Res. **10**(15), 35778–35783 (2015)
168. Baradeswaran, A., Perumal, A.E.: Wear and mechanical characteristics of Al 7075/graphite composites. Compos. Part B Eng. **56**, 472–476 (2014)

169. Riahi, A.R., Alpas, A.T.: The role of tribo-layers on the sliding wear behavior of graphitic aluminum matrix composites. Wear. **251**(1–12), 1396–1407 (2001)
170. Basavarajappa, S., et al.: Influence of sliding speed on the dry sliding wear behaviour and the subsurface deformation on hybrid metal matrix composite. Wear. **262**(7), 1007–1012 (2007)
171. Guo, M.L.T., Tsao, C.Y.A.: Tribological behavior of self-lubricating aluminium/SiC/graphite hybrid composites synthesized by the semi-solid powder-densification method. Compos. Sci. Technol. **60**(1), 65–74 (2000)
172. Ravindran, P., et al.: Tribological behaviour of powder metallurgy-processed aluminium hybrid composites with the addition of graphite solid lubricant. Ceram. Int. **39**(2), 1169–1182 (2013)
173. Shanmughasundaram, P., Subramanian, R.: Wear behaviour of eutectic Al-Si alloy-graphite composites fabricated by combined modified two-stage stir casting and squeeze casting methods. Adv. Mater. Sci. Eng. **2013**, 8 (2013)
174. Goldbaum, D., et al.: Tribological behavior of TiN and Ti (Si,C)N coatings on cold sprayed Ti substrates. Surf. Coat. Technol. **291**, 264–275 (2016)
175. Li, J., et al.: FIB and TEM characterization of subsurfaces of an Al–Si alloy (A390) subjected to sliding wear. Mater. Sci. Eng. A. **421**(1–2), 317–327 (2006)
176. Li, J.L., Xiong, D.S., Huo, M.F.: Friction and wear properties of Ni–Cr–W–Al–Ti–MoS_2 at elevated temperatures and self-consumption phenomena. Wear. **265**(3), 566–575 (2008)
177. Zhang, S., et al.: Preparation and characterization of reactively sintered Ni_3Al–hBN–Ag composite coating on Ni-based superalloy. J. Alloys Compd. **473**(1), 462–466 (2009)
178. Tyagi, R., Xiong, D., Li, J.: Effect of load and sliding speed on friction and wear behavior of silver/h-BN containing Ni-base P/M composites. Wear. **270**(7), 423–430 (2011)
179. Tsuya, Y., Umeda, K., Kitamura, M.: Optimum concentration of solid lubricant in compact. Lubr. Eng. **32**(8), 402–407 (1976)
180. Kumar, P.S., Manisekar, K., Vettivel, S.C.: Effect of extrusion on the microstructure and tribological behavior of copper-tin composites containing MoS_2. Tribol. Trans. **59**(6), 1016–1030 (2016)
181. Rohatgi, P.K., et al.: Tribology of metal matrix composites. In: Menezes, L.P., et al. (eds.) Tribology for Scientists and Engineers: From Basics to Advanced Concepts, pp. 233–268. Springer, New York (2013)
182. Lince, J.R.: Tribology of co-sputtered nanocomposite Au/MoS_2 solid lubricant films over a wide contact stress range. Tribol. Lett. **17**(3), 419–428 (2004)
183. Stoyanov, P., Strauss, H.W., Chromik, R.R.: Scaling effects between micro-and macro-tribology for a Ti–MoS_2 coating. Wear. **274**, 149–161 (2012)
184. Uemura, M., et al.: Effect of friction mechanisms on friction coefficient of MoS_2 in an ultrahigh vacuum. Lubr. Eng. **43**(12), 937–942 (1987)
185. Rupert, T.J., Schuh, C.A.: Sliding wear of nanocrystalline Ni–W: structural evolution and the apparent breakdown of Archard scaling. Acta Mater. **58**(12), 4137–4148 (2010)
186. Rupert, T., et al.: Experimental observations of stress-driven grain boundary migration. Science. **326**(5960), 1686–1690 (2009)
187. Hamilton, G.M.: Explicit equations for the stresses beneath a sliding spherical contact. Proc. Inst. Mech. Eng. C J. Mech. Eng. Sci. **197**(1), 53–59 (1983)
188. Yao, B., Han, Z., Lu, K.: Dry sliding tribological properties and subsurface structure of nanostructured copper at liquid nitrogen temperature. Wear. **301**(1), 608–614 (2013)
189. Kliemann, J.-O., et al.: Formation of cold-sprayed ceramic titanium dioxide layers on metal surfaces. J. Therm. Spray Technol. **20**(1–2), 292–298 (2011)
190. Yamada, M., et al.: Cold spraying of TiO_2 photocatalyst coating with nitrogen process gas. J. Therm. Spray Technol. **19**(6), 1218–1223 (2010)

3 In Situ Generated Turbostratic 2D Graphite: A New Way to Obtain High-Performance Self-Lubricating Iron-Based Composites

Jose Daniel Biasoli de Mello, Cristiano Binder, Sonia Maria Hickel Probst, and Aloisio Nelmo Klein

Contents

Abstract

The production of self-lubricating composites containing second phase particles is one of the most promising choices for controlling friction and wear in energy efficient modern systems. Initially, we present a new microstructural model/processing route able to produce a homogeneous dispersion of in situ generated, discrete, solid lubricant particles in the volume of sintered composites. The high mechanical and tribological performances of the composites are a result of the combination of matrix mechanical properties and structural parameters, such as the degree of continuity of the metallic matrix, the nature, the amount, and the lubricant particle size and shape which determine the mean free path between

J. D. B. de Mello (✉) · C. Binder · S. M. H. Probst · A. N. Klein
Laboratório de Materiais, Departamento de Engenharia Mecânica, Universidade Federal de Santa Catarina, Florianópolis, SC, Brazil
e-mail: ltm-demello@ufu.br

P. L. Menezes et al. (eds.), *Self-Lubricating Composites*,
https://doi.org/10.1007/978-3-662-64243-6_3

solid lubricant particles and the active area covered by each lubricant particles. This new route was achieved by in situ formation of graphite nodules due to the dissociation of a precursor (SiC particles) mixed with metallic matrix powders during the feedstock preparation. Thermal debinding and sintering were performed in a single thermal cycle using a plasma-assisted debinding and sintering (PADS) process. Nodules of graphite (size $\leq$20 μm) presenting a nanostructured stacking of graphite foils with thickness of a few nanometers were obtained. Micro-Raman spectroscopy indicated that the graphite nodules are composed of a so-called turbostratic 2D graphite which has highly misaligned graphene planes separated by large interlamellae distance. The large interplanar distance and misalignment among the graphene foils has been confirmed by transmission electron microscopy and is, probably, the origin of the remarkably low dry friction coefficient (0.06). The effects of precursor content (0 to 5 wt% SiC) and of sintering temperature (1100 °C, 1150 °C and 1200 °C) on tribolayer durability and average friction coefficient in the lubricious regime ($\mu < 0.2$) are presented and discussed. In addition, the effect of the metallic matrix composition (Fe-C; Fe-C-Ni; Fe-C-Ni-Mo) is presented. Friction coefficient decreased and durability drastically increased with the amount of graphite formed during sintering, whereas friction coefficient was little affected by sintering temperature. However, the durability of the tribolayer was greatly increased when lower sintering temperatures were used. The addition of alloying elements considerably reduced wear rate and friction of specimens and counter-bodies. Friction coefficient values as low as 0.04 were obtained for the Fe-C-Ni-Mo composites. We also analyzed the effect of precursor content and of sintering temperature on the tribological behavior under constant normal load sliding tests. Again, the presence of graphite nodules significantly reduced the friction coefficients and wear rates, whereas the sintering temperature hardly affected these parameters. The results were compared with those caused by other forms of graphite (nodules in nodular cast iron and powder graphite) and were discussed in terms of the crystalline structure of the analyzed graphite using micro-Raman spectroscopy. Chemical analyses of the wear scars using scanning electron microscopy (SEM – EDX) and Auger electron spectroscopy (AES) showed a tribolayer that was composed predominantly of carbon and oxygen. This tribolayer is removed and restored during sliding and is continuously replenished with graphite. Finally, the strong effect of surface finishing is presented and discussed.

3.1 Introduction

The crucial need for more energy efficient mechanical systems exacted the change in the severity of the tribological contacts, increasing operational failure for traditional designs. In this context, the tribology of critical contacts and possible new contact materials are under intense research investigation [1–3]. Furthermore, the interfaces in contact in these modern systems must be able to withstand severe operating

conditions caused by the tendency of using smaller clearances and increased speeds to achieve higher efficiency [4]. In addition, the state of lubrication in many components is unknown and usually operates in the boundary and mixed lubrication regimes [5].

In particular, solid lubrication and solid lubricants are one of the most promising choices for controlling friction and wear in energy efficient modern systems. A combination of solid and liquid lubrication is also feasible and may have a beneficial synergistic effect on the friction and wear performance of sliding surfaces, in particular in the elasto-hydrodynamic regime of lubrication [6].

Several inorganic materials (e.g., transition-metal, graphite, hexagonal boron nitride, boric acid) can provide excellent lubrication [7–10]. Most of these solids owe their lubricity to a lamellar or layered crystal structure. A few others (e.g., soft metals, polytetrafluoroethylene, polyimide, certain oxides and rare-earth fluorides, diamond and diamond-like carbons (DLC), fullerenes) can also provide lubrication although they do not have a layered crystal structure [8–10].

In spite of considerable research development, through more than 2000 published papers during the past 25 years, there exists no single solid lubricant that can provide both low friction and low wear over broad operational conditions [11]. In order to achieve a combination of high wear resistance, high load support, and low friction coefficient, a multifunctional production process combining purpose-oriented phases can be applied [12, 13].

The increasingly multifunctional needs and more stringent operating conditions envisioned for future mechanical systems will certainly make solid tribological materials and advanced coatings far more important. [14].

To meet the increasing tribological needs of these advanced systems, researchers are constantly exploring new materials and developing novel coatings. As a result, great strides have been made in recent years in the fabrication and diverse utilization of new tribomaterials and coatings that are capable of satisfying the multifunctional needs of more advanced mechanical systems [14].

Accordingly to Erdemir [15], solid lubricants can be applied to a tribological surface in a variety of forms. The oldest and simplest method is to sprinkle, rub, or burnish the fine powders of solid lubricants. Certain solid lubricants have been blended in an aerosol carrier and sprayed directly onto the surfaces to be lubricated. Solid lubricant powders can be strongly bonded to a surface by appropriate adhesives and epoxy resins to provide longer wear life [12]. Powders and nano-particles made of solid lubricants have been mixed with oils and greases to achieve improved lubrication under extreme pressure and high temperature conditions [16–21]. In most modern applications, thin films of solid lubricants, generally deposited onto surfaces by advanced vacuum deposition processes, are preferred to powders or bonded forms. In this case, the durability of the lubricious effect is limited due to the finite lubricant film thickness. To increase durability of these films, a self-replenishment or resupply mechanism is needed but is very difficult to obtain [15].

In this context the production of self-lubrication composites containing second phase particles incorporated into the volume of the material appears to be a

promising solution [11, 22, 23]. Indeed, self-lubricating composites have been available for a long time and are used rather extensively by industry to combat friction and wear in a variety of sliding, rolling, and rotating bearing applications [15].

Composite self-lubricating components have been used for several decades in household and office light equipments such as printers, electric shavers, drills, blenders, and others. The most used metallic matrices materials are copper, ferrous, and Niguel alloys. Compounds like MoS_2, WS_2, $MoSe_2$, NbS_2, $TaSe_2$, $MoTe_2$, h-BN, low melting metals like Ag, Sn and Pb, graphite and polytetrafluorethylene (PTFE) are the most used as solid lubricants [11, 23–25]. The majority of the composites developed contain a high percentage of solid lubricant particles (15–40%) in order to obtain a low friction coefficient. This results in a largely discontinuous metallic matrix that exhibits poor mechanical properties.

The production of new high-performance self-lubricating composites containing second phase particles incorporated into a continuous matrix and having a low friction coefficient combined with high mechanical strength and wear resistance appears to be a promising solution for controlling friction and wear in energy efficient modern systems and points to an engineered microstructure.

3.2 Microstructural Model

The high mechanical and tribological performance is a consequence of the combination of matrix mechanical properties and structural parameters such as the degree of continuity of the metallic matrix, the shape, amount, and the size of solid lubricant particles and the resulting mean free path between them. In addition, it is clear that the development of high-quality composites demands improved mechanical resistance.

Figure 3.1 presents a schematic drawing of the ideal microstructure of a self-lubricating composite. The microstructure must consist of a continuous matrix containing regularly dispersed solid lubricant particles and take into account the mean free path between them and the active area to be covered by each one of them.

The solid lubricant dispersed in the volume of the composite material should be a completely discontinuous phase and many aspects such as the content of solid lubricant [26]; the size and size distribution of solid lubricant particles [27, 28] and the mean free path between the solid lubricant particles [29] have to be considered for microstructural optimization of the composite. To further minimize the interruption of the metallic matrix, the amount of the dispersed solid lubricant must be kept as low as possible. In this context, in addition to the traditional characteristics of the metallic matrix and of the solid lubricant powder particles such as type, amount, and shape, special attention must be paid to the relative size of particles (d_m/d_{sl}) since this parameter has a great influence on the degree of continuity of the matrix which, in turn, as already said, is determinant in the mechanical and tribological behavior of the composite. In fact, as illustrated in Fig. 3.1b, insoluble particles much smaller than those of the matrix tend to be located in the

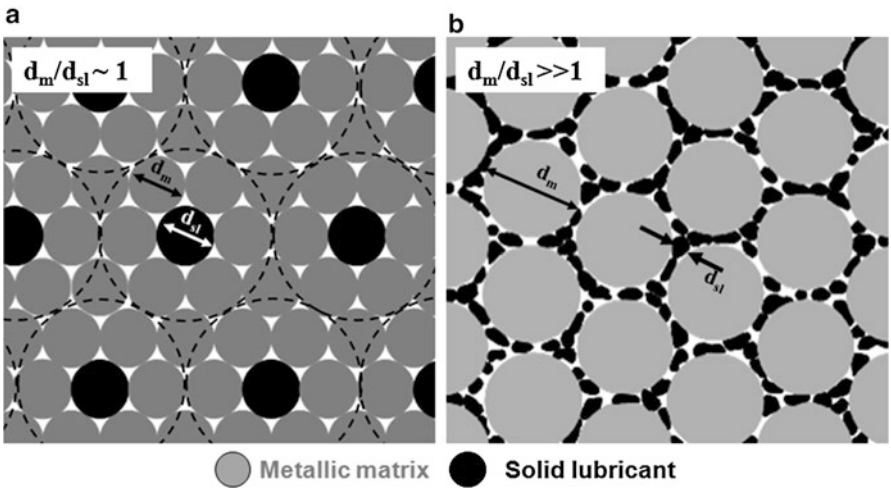

Fig. 3.1 Microstructural model (schematic). (**a**) Desirable distribution of the solid lubricant particles in the volume of the matrix and the corresponding area to be lubricated by each particle. (**b**) Continuity of the matrix

interstices occupying almost the entire interface between the metallic particles with a strong tendency to be the continuous phase which does not happen when they have equivalent sizes, Fig. 3.1a.

The metallic matrix which is the continuous phase that gives strength to the composite must be hard and tough enough to avoid the occurrence of micro-plastic deformation by friction and wear. The mass flow that occurs by plastic deformation may gradually cover the solid lubricant reservoirs and block the self-replenishment or resupply of solid lubricant to the interface. Further, it is important that the metallic matrix does not chemically react with the solid lubricant phase.

There are several possible manufacturing routes for producing such composites, in polymeric, metallic, or even ceramic matrices [30–32]. For the particle reinforced metallic matrix composites the methods to synthesize them are generally classified into (1) solid state processing, (2) liquid state processing, and (3) vapor deposition [33]. The most frequently used metallic matrix materials are copper [34], nickel [35], and ferrous alloys [36, 37]. Powder metallurgy techniques are especially suitable for the production of such composites.

3.3 Powder Metallurgy

For the development of metal-matrix composites, powder metallurgy (PM), widely used in industry, is a competitive and attractive technique because of its low cost when applied to large-volume production and because of its great versatility due to the suitability of the technique for tailoring the microstructure according to the

requirements imposed by a given application. In addition, PM processes are very advantageous for developing complex shape parts or even small-size components, which have been increasingly required due to the miniaturization of modern mechanical systems.

The high porosity of sintered components leads to reduced mechanical strength and load capacity when compared with fully dense materials. However, they have the potential to store lubricant that can be released during the use of the component [38, 39]. Also, the pores could eventually play an important role in the removal of wear debris from the sliding interfaces, as suggested by some authors [40]. Therefore, powder metallurgists are continuously searching for new alternatives and mechanisms to improve mechanical resistance and load support. In this sense, several processing parameters must be strictly controlled such as temperature and time of sintering, compression method, and techniques for the dispersion of the solid lubricant particles in the volume of the composite. Sintering is the most important step in the production of the composite. The variables in sintering are atmosphere, heating rate, temperature, dwelling time, and cooling rate. The sintering temperature should be lower than the decomposition temperature of solid lubricant. Reactions among the matrix, alloying elements and solid lubricant, which result in loss of solid lubricant, should also be avoided.

Special attention should be devoted to the compression technique. Several compaction techniques, like uniaxial die pressing, extruding, rolling, 3D prototyping, and powder injection molding, must be considered depending on the geometry and properties desired for the composite material. Uniaxial mechanical pressing, due to its low manufacturing costs, is still the most traditional processing route. It also produces the closest tolerances in the finished parts, thus nearly eliminating post-sintering operations such as machining [41]. However, depending on the configuration (single or double action), this technique presents gradients of porosity that may eventually be very high [42–44].

Recently [45], we presented a potential alternative for improving the mechanical strength of self-lubricating sintered composites: the use of the double pressing/double sintering (DPDS) technique [46] originally developed by Hoeganaes [47] and used in the automotive industry. The goal of this method is to increase the density of composites by twofold pressing. According to German [48], reductions of 2–3% in porosity would result in up to a 20% increase in mechanical strength. Although more expensive, MIM has the advantage of flexibility of the processing parameters, which allows the production of very small parts presenting high geometric complexity, refined microstructure, and elevated final density [49]. That is not feasible with the current uniaxial die cold pressing process. For the case of self-lubricating composites, the metal injection molding method is particularly indicated due to the small powder size which induces more homogeneous tribolayers covering the whole interface, Fig. 3.1a.

Roughly speaking, in MIM process, metal powders are premixed with polymeric binders. The mixture is heated and forced under pressure into a die cavity, where it cools and is subsequently ejected. The polymer is then removed (debinding stage) and the component sintered to the required density, Fig. 3.2.

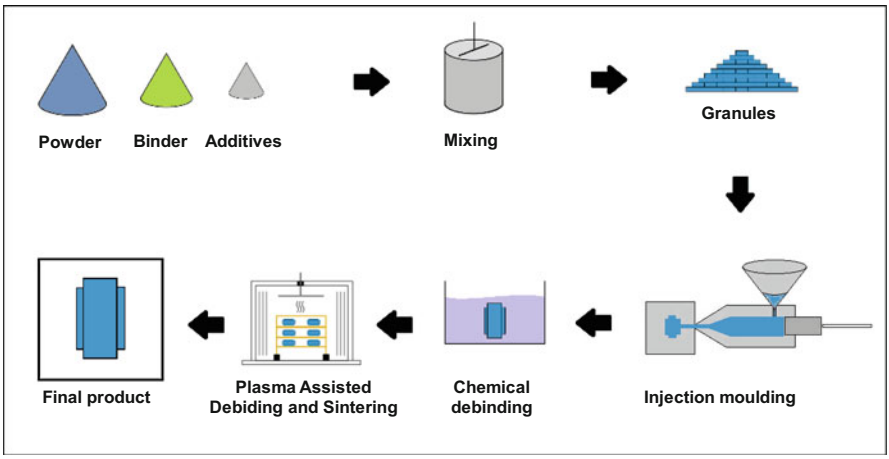

Fig. 3.2 Metal injection mold processing route

The debinding stage, during which polymer is removed, can greatly influence the mechanical properties of the sintered component [49, 50]. In our case, the debinding was carried out in a stepwise process: chemical debinding was followed by plasma-assisted thermal debinding. The chemical step consisted of the dissolution in hexane of the low molecular weight components of the binder system, forming an open pore network within the injected parts.

The thermal debinding, as well as the sintering, was performed in a single thermal cycle (plasma-assisted debinding and sintering – PADS) [50]. In summary, its advantages are short processing time (debinding and sintering in about 10 h versus 90 h for the thermochemical classical processes) and no binder residues after debinding. This process allows sintering in a single cycle and eliminates a cleaning procedure after every cycle. In the plasma-assisted debinding process, the polymer macromolecules are dissociated by bombardment of energetic electrons (inelastic collision) resulting in hydrocarbon radicals (C_xH_y) whose recombination is prevented by the presence of atomic hydrogen present in the hydrogen plasma, Fig. 3.3b. The reaction of atomic hydrogen with hydrocarbon radicals results in hydrocarbon gas that is removed from the reactor chamber via the vacuum pump.

The plasma reactor, developed in [51], was specially designed for the PADS process and described in [50–52] allows the control of the processing temperatures and the heating rates independently of the plasma parameters. The vacuum chamber, shown schematically in Fig. 3.3a, contains electrodes for the generation of plasma DC and electrical heaters for heating control. The samples were set on ceramic plates supported by the structure of the anode and were initially processed in floating potential plasma. Abnormal hydrogen glow discharge was then generated and the power supply voltage was biased to the cathode during the isothermal sintering.

As already pointed out (Fig. 3.1a), the ideal microstructure of a self-lubricating composite must consist of a continuous matrix containing regularly dispersed solid

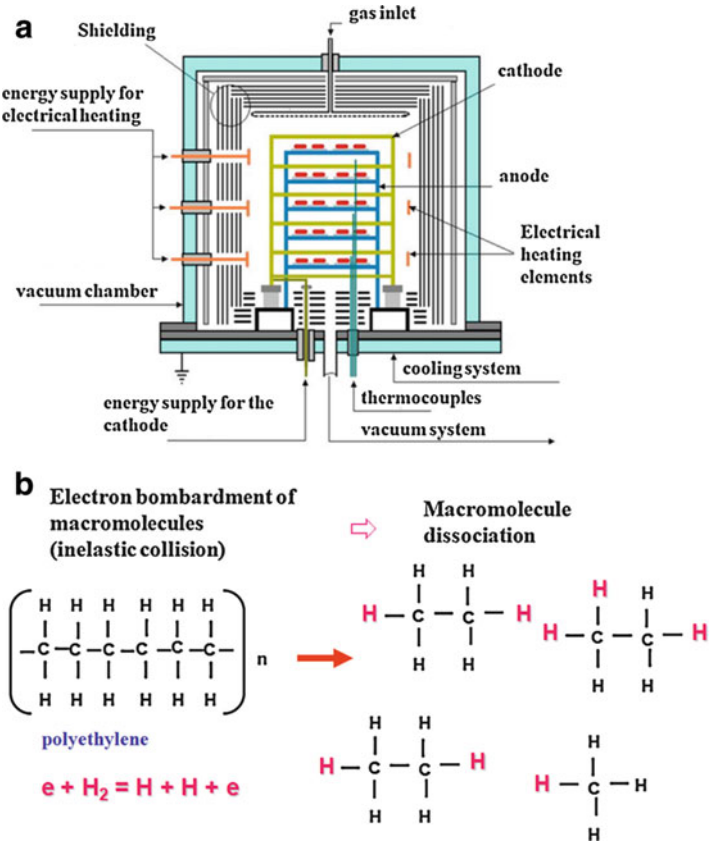

Fig. 3.3 Plasma-assisted debinding and sintering process. (**a**) Hybrid reactor [50]. (**b**) Macromolecule dissociation principle

lubricant particles. Unfortunately, such an ideal distribution of the solid lubricant particles is not obtained simply by blending metallic and solid lubricant powders.

In order to produce a self-lubricating sintered composite, there are basically two ways of dispersing the solid lubricant particles in the volume of the metal matrix [53, 54]:

(i) Mixing the solid lubricant particles with matrix powders
(ii) "In situ" generation of the solid lubricant particles during the sintering by dissociation of a precursor mixed to the powders of the metallic matrix

In the first method, where the composite is obtained by mixing the metallic matrix powders with the solid lubricant particles, the shear stresses that occur during mixing and compacting spread the solid lubricant by shearing between the powder particles of the metal matrix. This leads to an undesirable arrangement in which the solid lubricant covers the metallic particles to a large extent [55]. The presence of these

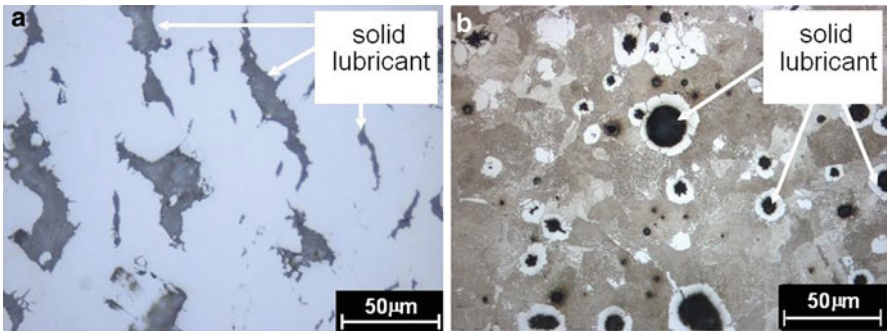

Fig. 3.4 Solid lubricant particles dispersion. (**a**) Mixing of powders prior to compaction. (**b**) In situ generated by decomposition of a precursor

layers of insoluble solid lubricant hampers the formation of contacts between the particles during sintering. This results in a metallic matrix with a high degree of discontinuity, Fig. 3.4a, and leads to a composite material with reduced mechanical strength.

There are two possibilities to overcome these difficulties. The first one is to rearrange the solid lubricant phase in discrete agglomerates by the capillary action of a liquid phase. The liquid phase spreads and penetrates the interfaces between the metal and the lubricant, thus pushing the solid lubricant and rearranging it in agglomerates. The second one is to produce the solid lubricant phase in situ during sintering by decomposition or dissociation of a precursor, giving rise to a more continuous and sound matrix, Fig. 3.4b.

Preliminary studies evidenced that the in situ generation of the solid lubricant phase particles during the sintering by the dissociation of a precursor was the most promising production route.

3.4 In Situ Generated Graphite

Silicon carbide (SiC), molybdenum carbide (Mo_2C), chromium carbide (Cr_3C_2), etc., are potential precursors to generate graphite nodules in ferrous matrix [56, 57]. Among them, those inducing the stabilization of the body-centered cubic phase of iron (α-Fe) are the most indicated in order to produce iron-based self-lubricating composites. SiC is particularly appropriate since it features a high carbon content, and silicon is a strong alpha phase stabilizer in addition to being one of the most effective hardening elements of ferrite [58].

Figure 3.5 shows typical aspects of the microstructure of the composites.

The reference alloy (Fe + 0.6 C + 4 Ni) presented a microstructure constituted of perlite (P) + ferrite (α), Fig. 3.5a, whereas the addition of SiC to the feedstock powder induced the formation of graphite nodules. The graphite nodules (G) are always surrounded by ferrite (α) rings, Fig. 3.5b.

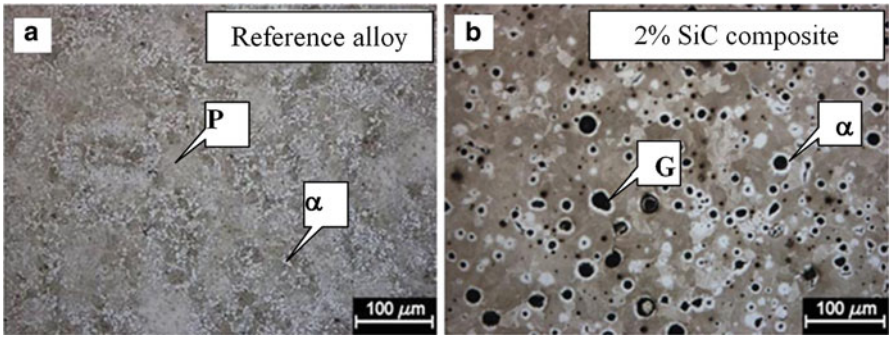

Fig. 3.5 Typical aspects of the microstructure. (**a**) Reference alloy (matrix alloy – Fe-0.6%C-4% Ni). (**b**) 2 wt% SiC composite. Sintering temperature 1150 °C

The evolution of the microstructure depends on precursor (SiC) content, sintering parameters (temperature, time, and atmosphere), and the previous composition (other alloying elements) of the ferrous matrix. [53]. For example, the presence of carbon in the matrix prior to the startup of SiC dissociation reduces the dissolution of the carbon originated from the dissociation of SiC and increases the size and the amount of the graphite nodules formed [36, 59]. The presence of Ni, a strong stabilizer of the face-centered cubic phase of iron (γ-phase) of the iron matrix, positively influences the morphology of the graphite nodules [36].

Such microstructure formation was expected from thermodynamic considerations as evidenced by the Ellingham diagram presented in Fig. 3.6a and its evolution depends on sintering time and temperature, as well as on the amount of SiC added to the ferrous matrix. This is well described in a recent paper [53].

Roughly, during the sintering, at the initial stage of the dissociation of the SiC particles, silicon and carbon atoms diffused into the ferrous matrix, Fig. 3.6b. However, the continuous enrichment of the ferrous matrix with Si around the former silicon carbide particles leads to stabilization of the body-centered cubic structure of the ferrous matrix (ferrite) in which the solubility for the carbon atoms is very low (solubility $\leq$0,022 wt%), [60], drastically reducing the dissolution of graphite. The dissolution of silicon, in contrast, is maintained [60]. As a consequence ferrite rings are formed around the former SiC particles, Fig. 3.7a [53, 54, 61].

The remaining carbon forms graphite nodules (size $\leq$20 μm), Fig. 3.7b which present a nanostructured stacking of graphite layers a few tenths of nanometers thick, Fig. 3.7c, d. The evolution of such microstructure depended on the amount of SiC, as well as on sintering temperature and time and is fully described in a recent paper [59]. The precipitation of graphite nodules started at temperatures higher than 1100 °C. At this temperature the precipitation is important for times superior to 1 h as evidenced by XRD analysis [61].

Finally, Fig. 3.8 presents line profiles of C and Si throughout a graphite nodule and a ferrite ring evidencing the low solubility of carbon in the ferrite and the depletion of silicon in the former SiC particle.

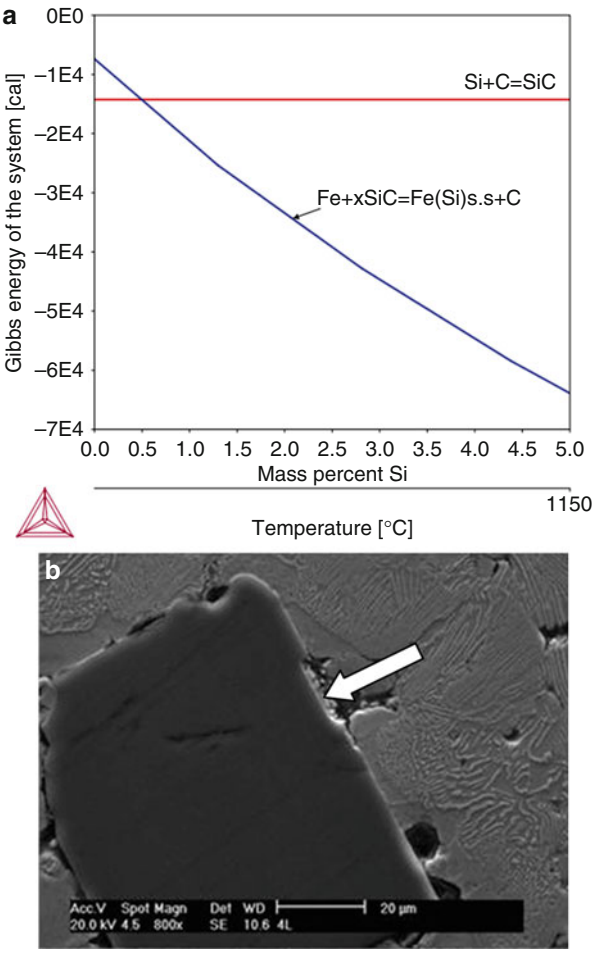

Fig. 3.6 Thermodynamic equilibrium. (**a**) Ellingham diagram. (**b**) Initial stage of SiC dissociation, SEM

The nodules are composed mostly of carbon, whereas the ferrite ring around the nodule has an almost constant high concentration of silicon, and the carbon concentration is greatly reduced. Outside the ferrite ring, the silicon concentration decreases, and the carbon concentration in the matrix increases. This interface is the separation between the ferritic (α-Fe) phase and pearlitic (γ-Fe) regions, thus confirming the formation of the carbon nodules by the SiC dissociation and the formation of a diffusion barrier due to α-Fe phase stabilization by silicon.

3.5 Tribological Characterization

The tribological behavior was evaluated using two types of experiments schematized in Fig. 3.9:

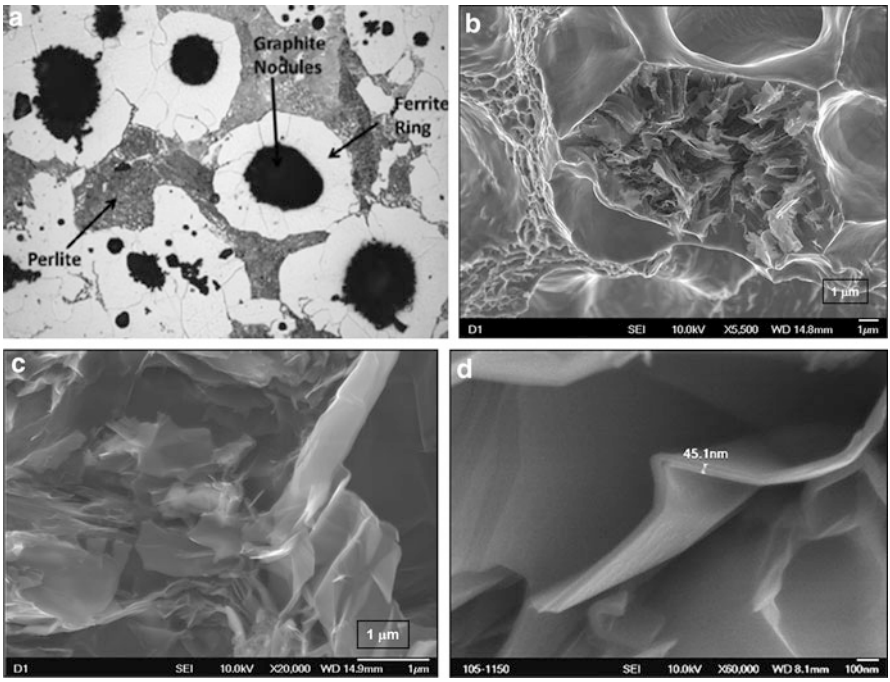

Fig. 3.7 Typical aspects of the microstructure. Composite Fe-0.6C-4 Ni-2 SiC. (**a**) Ferrite ring. (**b**–**c**) Graphite nodule (fractography). (**d**) Graphite layer

(a) Reciprocating sliding tests were conducted at constant normal load to access the friction coefficient and wear rates of specimens and counter-bodies.
(b) Reciprocating sliding tests were carried out in an incremental loading mode. In this case, by increasing the normal load in increments of 7 N at 10 min. intervals, the scuffing resistance was determined. The scuffing resistance was defined as the work (N m) at which the value of the friction coefficient first rose above 0.20 (lubricity effect) [12].

In both kind of experiments, a hard steel AISI 52100 ball (diameter 5 or 10 mm) was fixed on a pivoted arm and rested against the specimen surface under constant stroke (5 mm) and frequency (2 Hz). The tests were conducted under controlled relative humidity (50%) and temperature (22 ± 4 °C).

Wear scars were analyzed by using SEM-EDX as well as FEG-SEM, micro-Raman spectroscopy, Auger electron spectroscopy, and laser interferometry.

3.6 Mechanical Properties

The evolution of the mechanical properties with precursor content and sintering temperature is illustrated in Fig. 3.10.

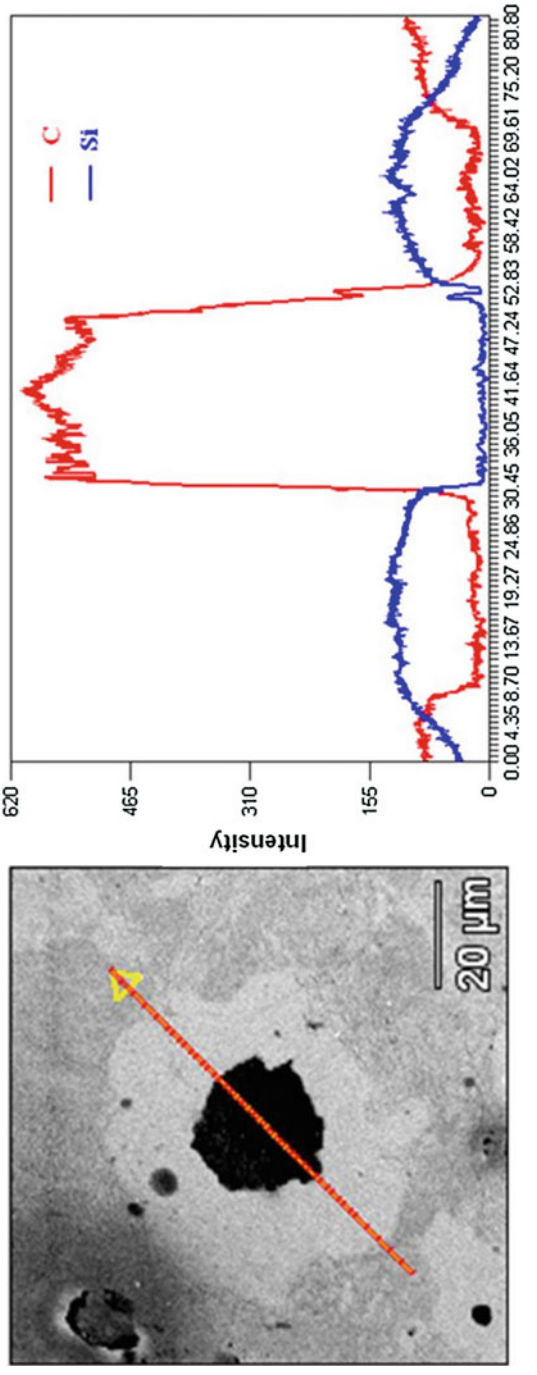

Fig. 3.8 Line profile showing the concentration of silicon and carbon along the graphite nodule and the surrounding metal matrix

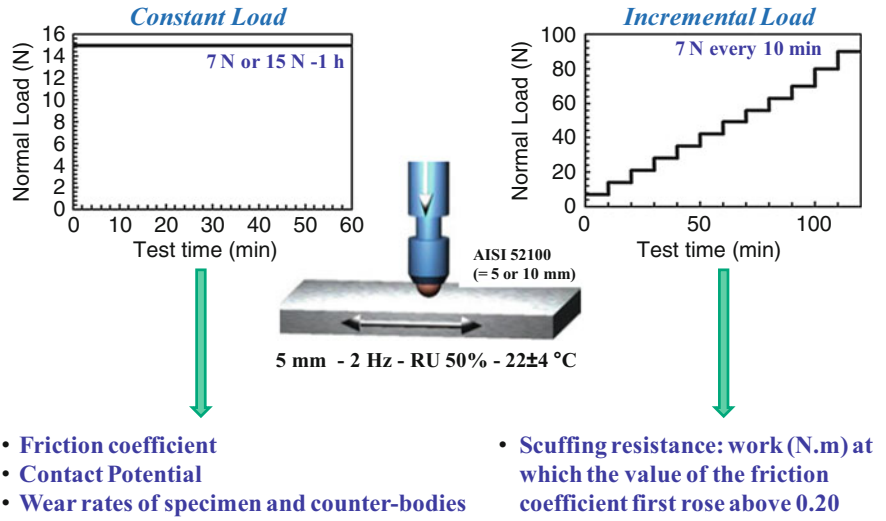

Fig. 3.9 Tribological characterization

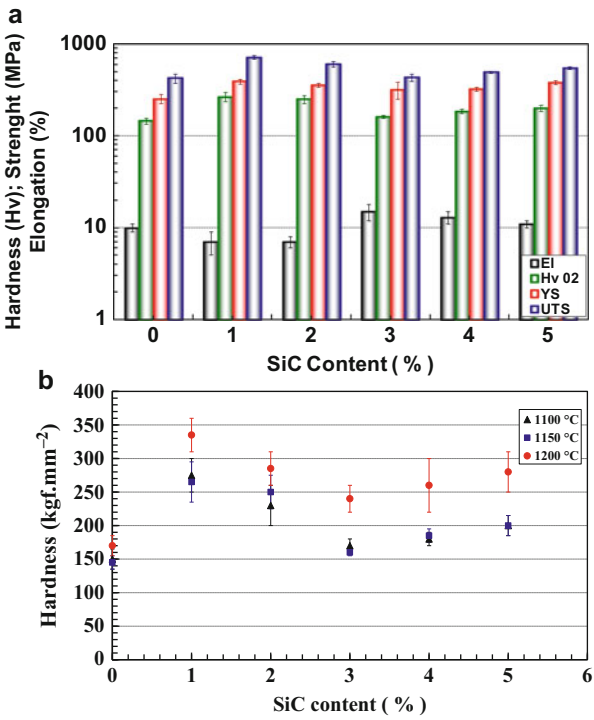

Fig. 3.10 Typical evolution of the mechanical properties. (**a**) Effect of SiC content on mechanical properties for composites sintered 1150 °C. (**b**) Influence of SiC content and sintering temperature on hardness

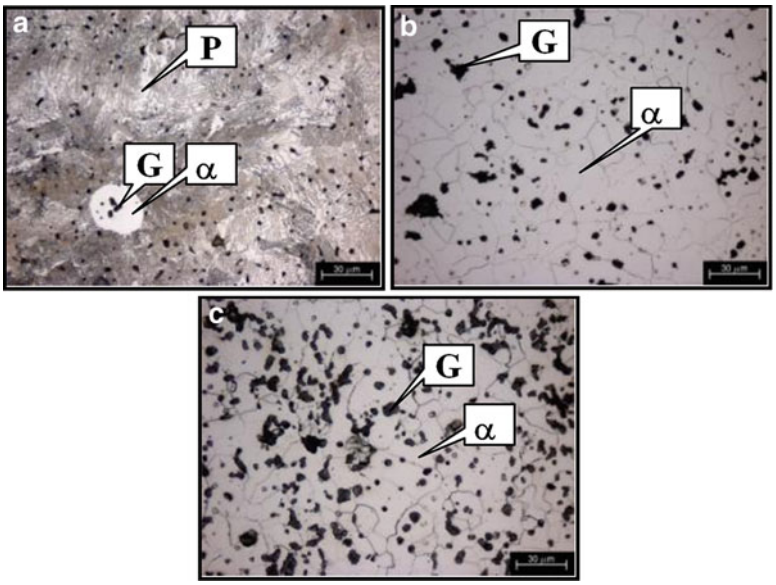

Fig. 3.11 Typical microstructures. Sintering temperature 1150 °C. (**a**) 1% SiC; (**b**) 3% SiC; (**c**) 5% SiC

The addition of SiC induced a quite complex evolution of the mechanical properties, Fig. 3.10a. There is a sharp increase up to a maximum for additions of 1% SiC. Then the hardness decreased to a minimum at 3% SiC and afterwards gradually increased. The strength of the composites follows the same behavior whereas, of course, the elongation behaved in the opposite sense.

In terms of hardness, Fig. 3.10b, the dissociation of SiC particles produced harder composites than those of the metallic matrix alone. There is a sharp increase up to a maximum for additions of 1% SiC. Then the hardness decreased to a minimum at 3% SiC and afterwards gradually increased. Indeed, for composites presenting 3% SiC the metallic matrix is mainly constituted of ferrite (α), Fig. 3.11b, whereas for smaller SiC contents the microstructure presents a certain amount of perlite (P), Fig. 3.11a. For higher SiC amounts, Fig. 3.11c, it is reasonable to suppose that the great availability of silicon induces a larger hardening of the matrix (ferrite).

The mechanical properties of the composites are a compromise between the two different effects of the dissolution of the SiC particles [53, 61]:

(i) An increase in the mechanical resistance caused by the strengthening of the metallic matrix due to the dissolution of Si
(ii) A decrease in the mechanical resistance as a consequence of the formation of graphite nodules during the sintering process, which decreases the degree of continuity of the metallic matrix.

Silicon is known to be one of the most efficient promoters of the hardening of ferrous matrix by the formation of substitutional solid solution [62, 63].

On the other hand, the sintering temperature produced a strong effect on the mechanical properties as illustrated by hardness, Fig. 3.10b. The high sintering temperature produced harder (up to 50%) composites whereas the variation from 1100 °C to 1150 °C produced almost no effect. The higher values presented by the samples sintered at 1200 °C are supposed to be mainly due to the higher degree of the homogeneity of the composites (in particular the distribution of Si and pearlitic regions in the matrix) sintered in this higher temperature. However, for composites with 4% and 5% SiC sintered at 1200 °C, values of yield and tensile stress decrease, which was related to the formation or "line structures" reducing matrix continuity and affecting the material properties [59].

3.7 Tribological Behavior

3.7.1 Introduction

In this section, the tribological behavior of self-lubricating composites produced taking advantage of the powder injection molding process, the recently introduced plasma-assisted debinding and sintering (PADS) process, and the in situ formation solid lubricant particles is presented and discussed. In this case, we obtained the in situ formation of graphite nodules in the volume of the sintered composites during sintering simply by dissociation of particles of silicon carbide (SiC) mixed to the metallic matrix powders prior to the compaction.

Recent studies concluded that a transfer film is found on the sliding surfaces [53]. The formation of such a film on the sliding interfaces seems to be the key for achieving low friction and long wear life in most solid-lubricated surfaces [13]. It was found that, initially, transfer films were not present but were formed as a result of surface wear and subsurface deformation. These films are continuously replenished by embedded graphite particles dispersed in the matrix [64].

The effects of precursor content (0 to 5 wt% SiC) and of sintering temperature (1100 °C, 1150 °C and 1200 °C) on tribolayer durability, average friction coefficient in the lubricious regime ($\mu < 0.2$), and wear rate of the specimens and counter-bodies are presented and discussed. In addition, the effect of the metallic matrix composition (Fe-C; Fe-C-Ni; Fe-C-Ni-Mo) and surface finishing are also presented. Special emphasis is given to the protective tribolayer.

3.7.2 Materials

Sintered composites with different chemical compositions were produced by mixing carbonyl iron powder (Carbonyl BASF grade OM) with elemental powder of the alloying elements. The carbonyl iron used had a particle size of 7.8 μm and

contained 0.8% carbon. Different contents of silicon carbide (Cobral) powder (1%, 2%, 3%, 4%, and 5% SiC) having particle size of 10 μm were added to the carbonyl iron powder. The feedstock for injection was prepared in a Haake Sigma mixer (180 °C, 70 rpm, 90 min) using 8% of an organic binder system containing paraffin wax, polypropylene, stearic acid (surfactant), ethylene vinyl acetate copolymer (EVA), and amide wax.

Samples with the appropriate geometry for performing tensile and tribological tests were injected (injection pressure of 100 MPa) using an Arbourg 320S injection molding machine. The debinding was performed in two steps: a chemical debinding followed by plasma-assisted thermal debinding. The thermal debinding, as well as the sintering, was performed in a single thermal cycle in a plasma reactor, i.e., using the plasma-assisted debinding and sintering (PADS).

A hydrogen abnormal glow discharge was generated at a pressure of 133 Pa (1 Torr) and the gas flow was adjusted to $3.33.10^{-6}$ m^3 s^{-1} (200 sccm). The power supply voltage biased to the cathode was fixed at 500 V. A heating rate of 0.7 °C/min was fixed up to 500 °C for the plasma-assisted thermal debinding step. Then, the heating rate was increased to 5 °C/min up to the sintering temperature. The isothermal sintering was processed at 1100 °C, 1150 °C, and 1200 °C for 60 min.

In order to analyze the effect of the metallic matrix, three compositions of sintered composites (Fe–Si–C, Fe–Si–C–Ni, and Fe–Si–C–Ni–Mo) were also produced. The same iron powder was used (Carbonyl BASF grade OM). The alloying elements Ni and Mo were mixed to the feedstock in the form of elemental Ni (Vale Inco Type 123) and elemental Mo (H.C. Starck Type) powder. Silicon was added in the form of 3 wt% silicon carbide powder (Cobral) aiming at its dissociation during sintering. The same processing route was used but just one sintering temperature and time (Ts = 1150 °C- 60 min) were used.

3.7.3 Tribological Evaluation

3.7.3.1 Incremental Load Tests (Scuffing Resistance)

Typical results are shown in Fig. 3.12.

All results present similar behavior. There is a transient associated with the onset of contact between specimen and counter-body at the beginning of tests before a high lubricity steady state is reached. The reasons for the difference in the evolution of the friction coefficient within the transient period are not yet well understood and will not be treated in the present chapter. However, it is reasonable to suppose that the stabilization of the friction coefficient is related to the generation of a protective tribolayer, where the transient corresponds to the kinetics of formation of the layer. As long as the formation rate of the tribolayer is different from the degradation rate, friction coefficient will vary. Once this formation rate is equal to or greater than the degradation rate, a steady state is reached.

All specimens behaved in a similar manner in the lubricious regime. However, low SiC content composites (e.g., 1% SiC) presented higher friction coefficient which gradually increases with the sliding distance associated with a shorter and

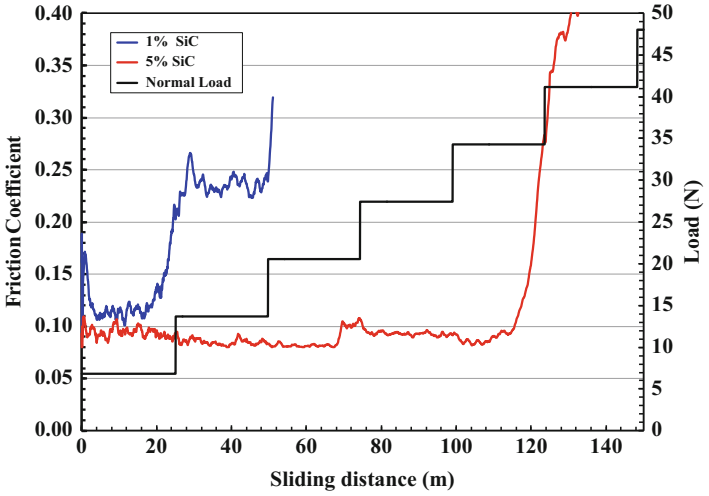

Fig. 3.12 Typical evolution of friction coefficient with sliding distance and applied normal load

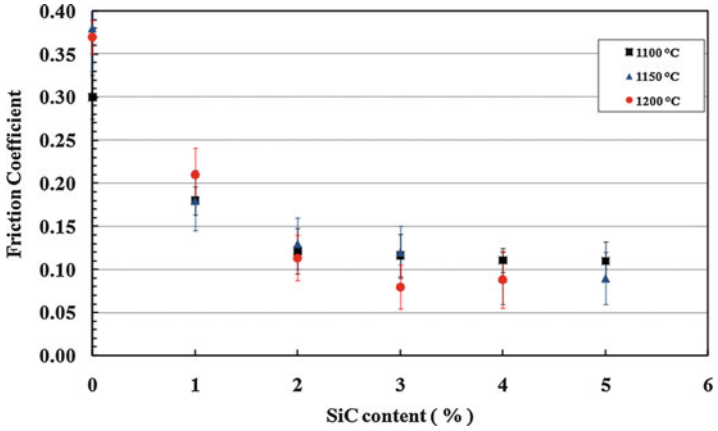

Fig. 3.13 Effect of SiC content and of sintering temperature on the average friction coefficient during the lubricious regime

almost equivalent scuffing resistance, whereas the high SiC content (e.g., 5% SiC) composites exhibited lower friction coefficients coupled with much longer period in the lubricious regime signalized by a rapid increase in the friction coefficient. The friction coefficient values for each test were computed by averaging the lubricious steady-state values.

The influence of the precursor content and of the sintering temperature on the friction coefficient behavior is synthesized in Fig. 3.13.

Independently of the sintering temperature, increasing the precursor content and, as a consequence, the number of graphite nodules produced a reduction of the

average friction coefficient. In general, the reduction was substantial, up to 3% SiC. For higher values of SiC content, the friction coefficient was almost constant. It is reasonable to suppose that graphite foils are removed from the in situ generated graphite nodules and remain at the interface thus contributing to the formation of a protective tribolayer. Due to the small size of the powders, the mean free path between graphite nodules is also small and the complete "coverage" of the surface between nodules is easily reached. As a consequence, the number of graphite foils generated in composites containing more than 3% of SiC is sufficient to produce the protective layer and low friction coefficients. Additionally, there is almost no effect of the sintering temperature on the average friction coefficient.

A comparison between Figs. 3.10 and 3.13 shows that there is, definitely, no correlation associating the friction coefficient with mechanical properties of the composites.

Figure 3.14 presents typical aspects of the wear scars. The test was interrupted at the normal load of 14 N which is within the lubricious regime ($\mu < 0.2$).

At low magnifications, Fig. 3.14a, the wear scar appears quite homogeneous. It presents flat and smooth regions where contact with the counter-body occurred. It seems that there is a protective layer on the active interface (brown/gray areas, confirmed, by using back scattered electrons, to be composed of elements presenting low atomic number). It is reasonable to suppose that graphite foils are removed from the in situ generated graphite nodules and remain at the interface (Fig. 3.14b) thus contributing to the formation of the protective tribolayer. Due to the small size of the powders, the mean free path between graphite nodules is also small and the complete "coverage" of the surface between nodules is easily reached. As a consequence, the number of graphite foils generated in composites containing more than 3% of SiC is sufficient to produce the protective layer and low friction coefficients thus explaining the saturation of the friction coefficient variation with precursor content, Fig. 3.13.

On the other hand, since the tribolayers also degrade under the action of the sliding (Fig. 3.14c).

Figure 3.14d presents a typical Raman spectra obtained in the central region of the wear scar. It clearly presents a widened G band (associated with the sp^2 hybridization) and a D band (associated with crystallinity disorder). The widening of the bands, the ID/IG ratio, and the size of the graphite crystallites are, accordingly to literature [61, 65–68], clear evidence of disorder in the material. They are also a strong indication of the presence of the so-called turbostratic 2D graphite which presents longer interlamellae distances among the graphene foils when compared to the highly oriented 3D graphite coupled with a strong misalignment of the graphene foils. Moreover, the analysis of the second-order band G′ confirms the greater contribution of the 2D graphite to the formation of the D band.

The increase in distance may induce low interaction between these atomic planes and is, probably, the origin of the low friction coefficient [69].

To further understand this point, a few other types of graphite were analyzed under the same tribological configuration: They are graphite nodules in a nodular cast iron, and the contact was submerged in graphite in powder. The matrix alloy (graphite-free – Fe 0.6 wt% C) was also tested as a reference.

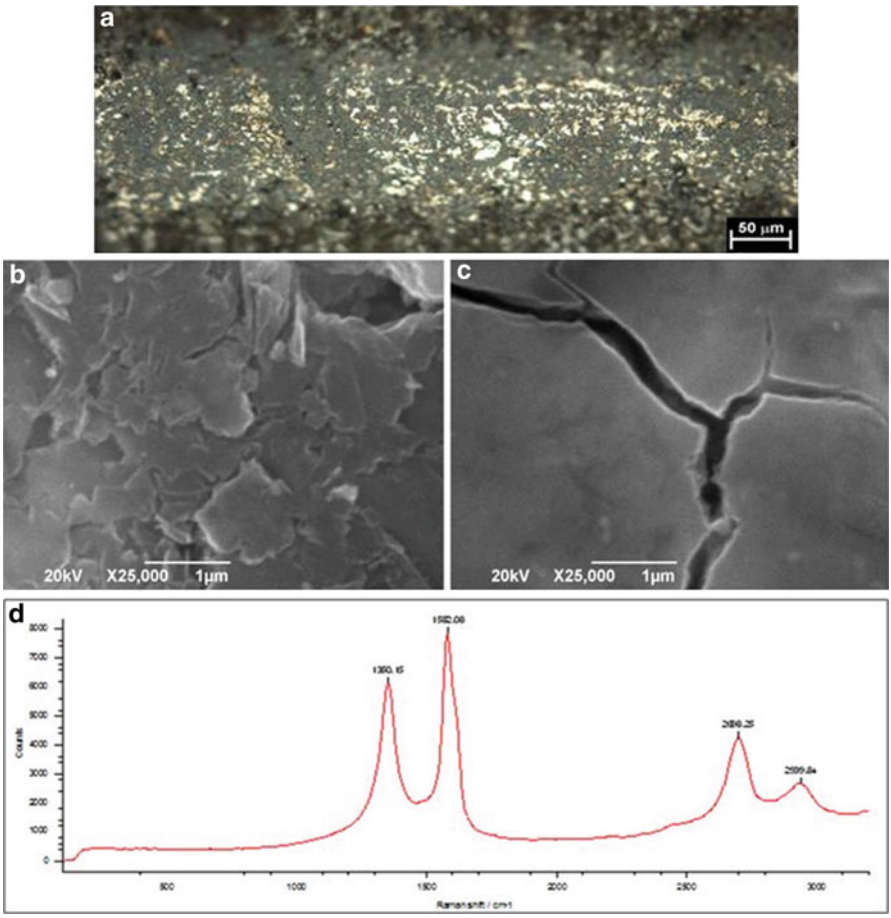

Fig. 3.14 Typical wear scars produced in the lubricious regime ($\mu < 0.2$). Fe + 0.6C + 5SiC. (**a**) General aspect, optical microscopy; (**b**, **c**) FEG-SEM; (**d**) Raman spectra

Figure 3.15 shows the average friction coefficient (steady state) of different materials.

The reference alloy presented the highest friction coefficient. The presence of graphite (nodules in nodular cast iron and graphite in powder) strongly reduced the friction coefficient (170% and 290%, respectively). The addition of 3 wt% SiC further reduced the friction coefficient (530%) and induced a remarkably low value (0.06).

Figure 3.16 presents the typical Raman spectra of different graphite types.

They clearly show a G band at approximately 1580 cm^{-1}. The spectrum of the graphite nodules produced by the SiC decomposition (Fig. 3.16a) clearly presents a D and a D′ band both associated with crystallinity disorder. The analysis of the spectra shows many evidence (the widening of the bands, the I_D/I_G ratio, the size of

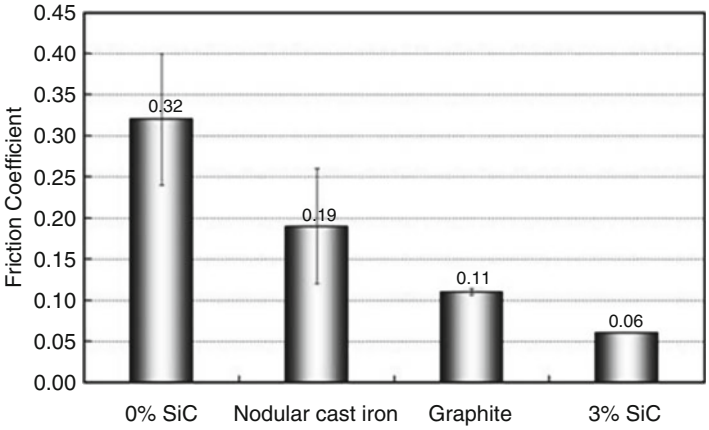

Fig. 3.15 Effect of graphite type on friction coefficient

the graphite crystallites, and the shape of the second-order G′ band) of the presence of the so called turbostratic graphite (2D graphite). Moreover, the analysis of the second-order G′ band (very sensitive to the stacking order of the graphene sheets along the c axis [70, 71]) confirms the greater contribution of 2D graphite to the formation of the D band. Graphite associated with graphite powders, Fig. 3.16b, and nodular cast iron, Fig. 3.16c, is characterized as 3D graphite and is highly aligned according to the literature [65–67].

According to the literature [61–68, 72], the widening of the bands, the ID/IG ratio (widely used for characterizing the defect quantity in graphitic materials) [70–73] and the size of the graphite crystallites (La) are clear evidence of disorder in the graphite nodules in the composite Fe-0.6 wt% C + 3 wt% SiC. They also strongly indicate the presence of the so-called turbostratic 2D graphite, which has highly misaligned graphene planes separated by larges paces. A recent paper presents the main aspects of the 2D turbostratic graphite including a comprehensive analysis of the Raman spectra of the different graphite types [72] clearly evidencing that major contribution to the G′ band stems from graphite 2D, not from 3D graphite.

Transmission electron microscopy, Fig. 3.17, confirmed the large interplanar distance, Fig. 3.17b ($\geq$3.499 Å against 3354 Å for the high aligned 3D graphite), among the graphene foils and the misorientation of the graphene foils, inset in Fig. 3.17c.

Figure 3.17a, b show bright field images of graphite sheets obtained from the graphite nodules of a Fe +0.6C + 3SiC composite and the corresponding SAED. Figure 3.17c presents high-resolution (HRTEM) image with fringes representing individual carbon layers and the SAED pattern (inset) taken from this region. Moreover, the increased interlayer spacing could be correlated to the stacking fault disorder, inherent of turbostratic graphite [74, 75].

These large spaces associated with the misalignment among the graphene planes drastically decreased the interaction among the planes, which results in a low shear

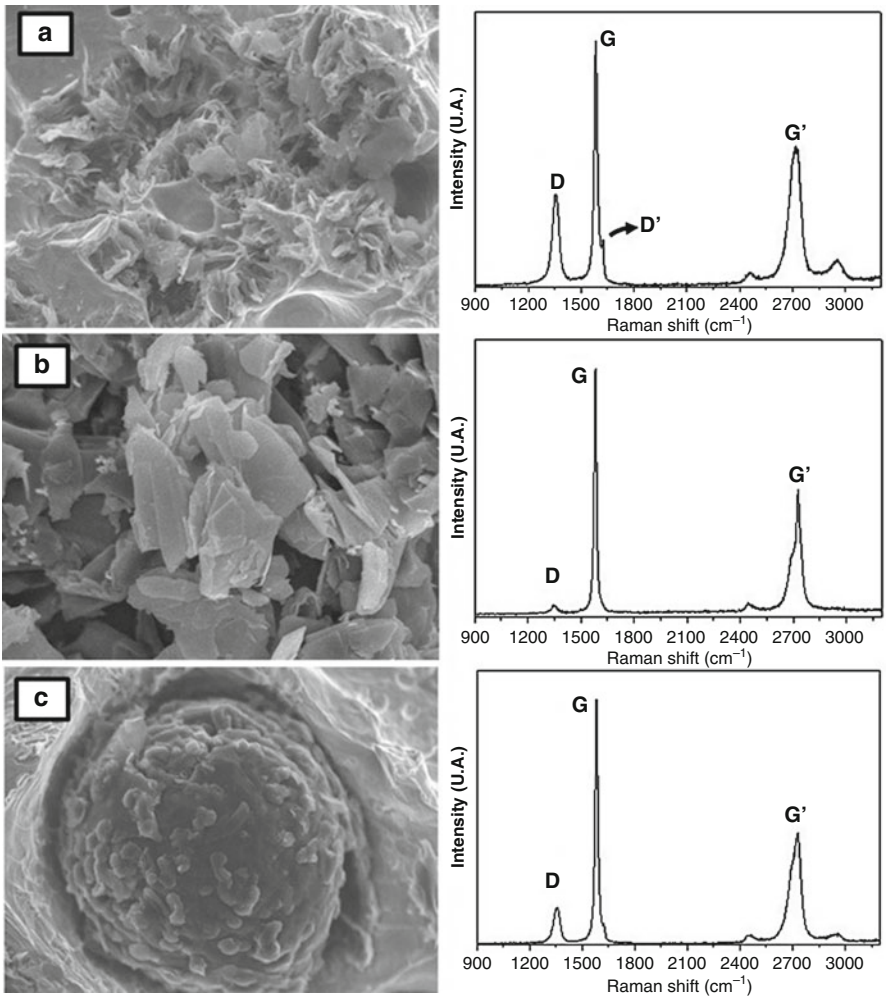

Fig. 3.16 Typical Raman spectra. (**a**) Graphite nodule obtained via SiC dissociation, (**b**) graphite in powder, (**c**) graphite nodule in nodular cast iron [72]

strength. Thus, it is reasonable to suppose that during the reciprocating sliding, the graphite planes easily shear and maintain a constantly lubricated contact interface.

There is almost no effect of the sintering temperature on the lubricious average friction coefficient. On the contrary, the sintering temperature strongly influences scuffing resistance, Fig. 3.18. The low sintering temperature induces significantly higher scuffing resistance (5×).

For the extreme sintering temperatures, increasing SiC content up to 2% induced a strong increase in scuffing resistance and then it remained almost constant, Fig. 3.18. In this case, the saturation effect is reached at 2% of SiC indicating that the self-replenishment provided by the graphite nodules is already active at this

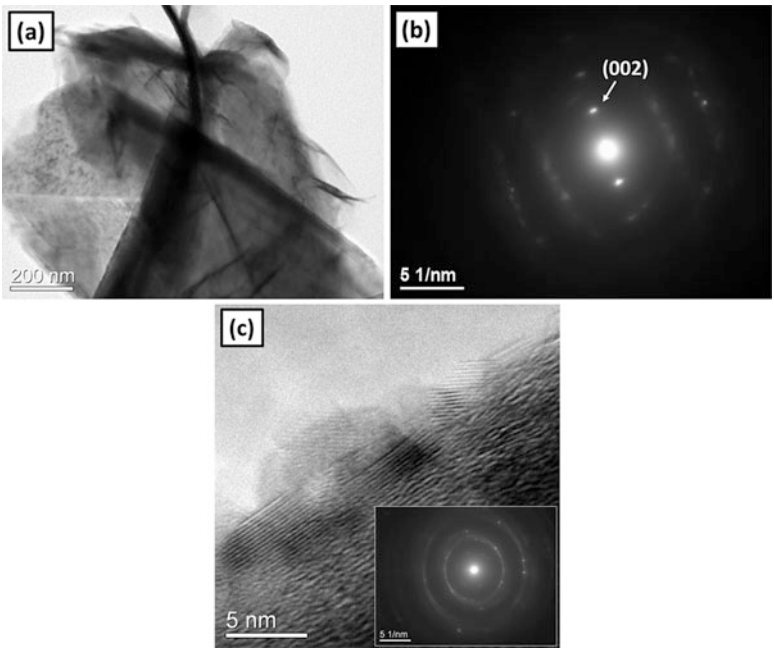

Fig. 3.17 (**a**) Bright field TEM micrograph, (**b**) the corresponding SAED pattern, and (**c**) high-resolution TEM image of graphite sheets obtained from graphite nodules for a Fe + 0.6C + 3SiC sample. The inset in (**c**) shows a typical SAED pattern recorded from this region (graphite sheets) [72]

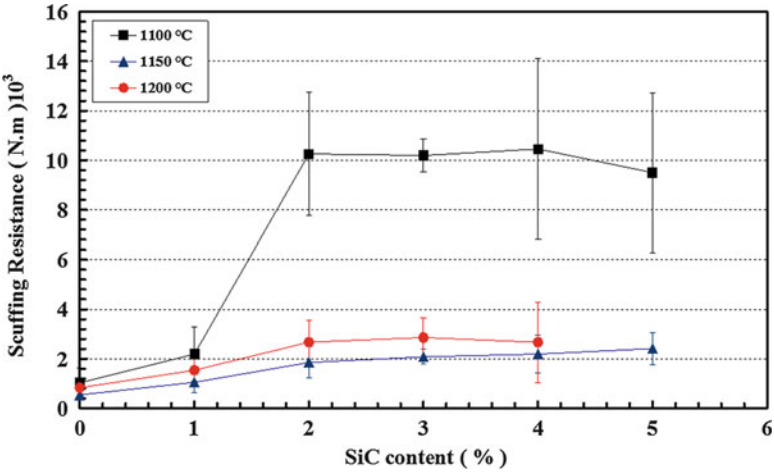

Fig. 3.18 Effect of SiC content and of sintering temperature on scuffing resistance

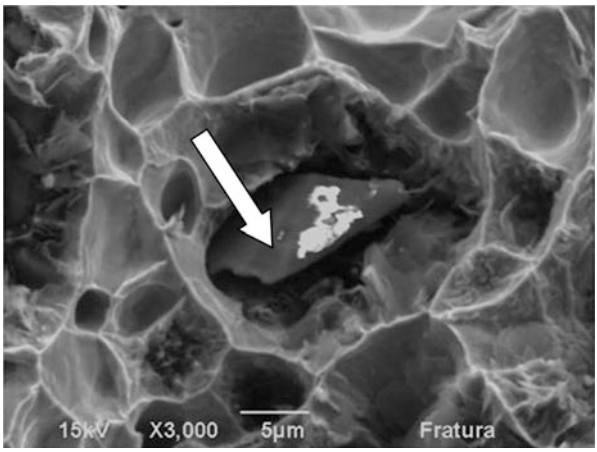

Fig. 3.19 Typical undissociated SiC particle. Fe + 0.6C + 3SiC, 1100 °C, 60 min

lower value. However, for the intermediate sintering temperature there is an almost monotonous increase of scuffing resistance after this threshold is reached.

Again, there is definitely no correlation associating the scuffing resistance with mechanical properties of the composites. In order to further understand why the low sintering temperature induced higher scuffing resistance, Fig. 3.18, the samples sintered at 1100 °C were cryogenically fractured and then the surfaces were analyzed using SEM. A typical aspect of the graphite nodules present in Fe + 0.6C + 3SiC composite is illustrated in Fig. 3.19.

The white arrow points to a partially dissolved SiC particle. EDS point analysis showed that there is, probably, a ring of ferrite around the nodule since the chemical composition was higher than 2.1 wt% Si.

Taking into account that the metallic matrix is continuous, it is reasonable to suppose that the solid lubricant, or its precursor, does not contribute to the mechanical resistance of the composite as already illustrated and discussed in the hardness/SiC content relationship. However, the presence of undissociated particles of SiC may produce a greater load-bearing capacity and the protection of the matrix/tribolayer, thus inducing higher scuffing resistance.

3.7.3.2 Constant Load Tests

Effect of Precursor Content and Sintering Temperature

In this section, the effect of the sintering temperature (1100 °C, 1150 °C, and 1200 °C) and SiC content (0–5 wt%) on the tribological behavior (friction coefficients and wear rates of specimens and counter bodies) is presented and discussed.

In all cases, the evolution of the friction coefficient with time exhibited a transient state at the beginning of the tests; then, a steady state with similar fluctuations from the start to the end of the test was attained, Fig. 3.30. The evolution of the average steady-state fiction coefficient with precursor content and sintering temperature is presented in Fig. 3.20.

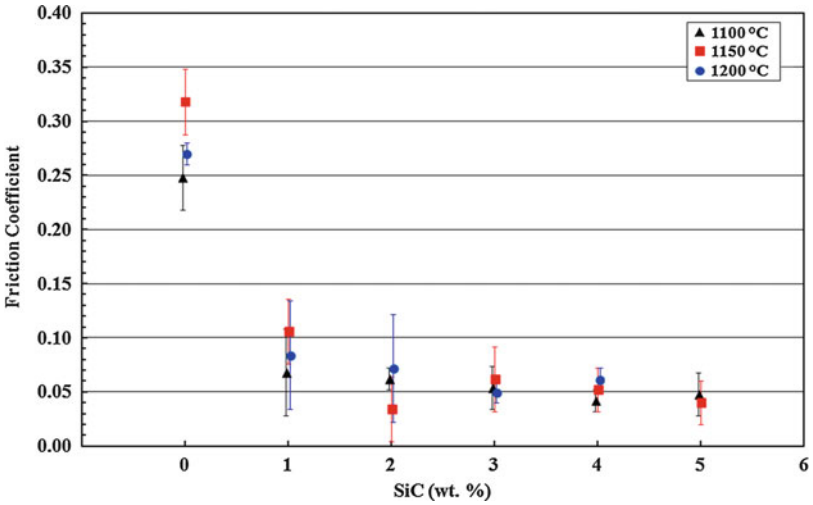

Fig. 3.20 Effect of the silicon carbide content and sintering temperature on the steady-state friction coefficient. *The x values were slightly shifted* (±0.02) *to the left and to the right in order to separate overlapping symbols*

Independently of the sintering temperature, an increase of the precursor content, which increased the number of 2D turbostratic graphite nodules, reduced the average friction coefficient. In general, the reduction was substantial (up to 3 wt% SiC).

For higher SiC contents, the friction coefficient was almost constant. It is also noticeable that the friction coefficient was hardly affected by the sintering temperature. All composites showed a considerably smaller friction coefficient (one order of magnitude) than the matrix alloys (carbide-free alloys). Again, there is, definitely, no correlation associating the friction coefficient with the mechanical properties of the composites and the outstanding tribological behavior may be attributed to the presence of the so-called turbostratic 2D graphite.

Figure 3.21a shows the effect of the silicon carbide content and sintering temperature on the wear rate of the specimens.

The addition of SiC, which creates 2D turbostratic graphite nodules, clearly enhances the tribological behavior. The matrix alloy showed a considerably higher (one order of magnitude higher) wear rate than the composites. When the SiC content increased, there was a decrease to a minimum at 3 wt% SiC; then, the wear rate gradually increased. The wear rate of the counter-bodies had an equivalent behavior. It is also noticeable that despite the higher hardness, the counter bodies had a much higher wear rate than the specimens (one order of magnitude), Fig. 3.21b.

There is a complex competition among different phenomena:

(i) During the silicon carbide dissociation, the matrix hardened because of the Si diffusion, which increased the strength of the composite. However, the mechanical strength decreased because graphite nodules and pores (4–12% [59])

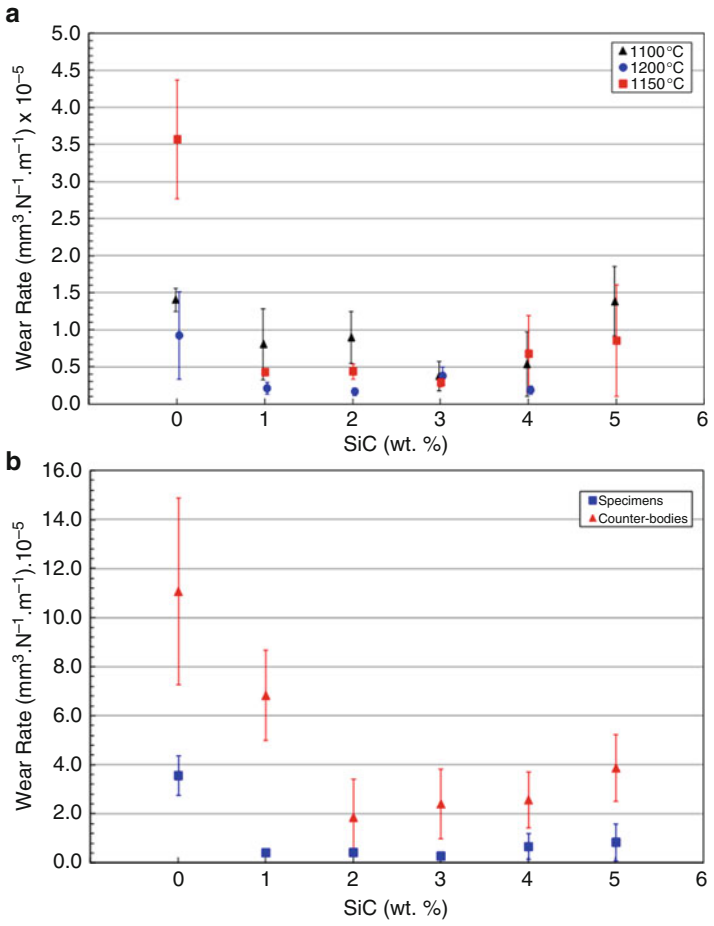

Fig. 3.21 Wear rate. (**a**) Effect of the SiC content and sintering temperature on the wear rate of the specimens. *The x values were slightly shifted* (±0.02) *to the left and to the right in order to separate overlapping symbols*). (**b**) Evolution of the wear rate of the specimens (sintering temperature = 1150 °C) and counter-bodies as a function of the SiC content

formed during the sintering process, which decreased the degree of continuity of the metallic matrix [69].

(ii) The graphite nodules formed a protective tribolayer at the interface, which led to the better tribological behavior of the composites.

Composites with SiC amounts exceeding 4 wt% featured an increased wear rate, which may be associated with a decreased mechanical strength due to the large amount of pores/graphite nodules (large discontinuity of the matrix) [59], as illustrated in Fig. 3.11b, c. In this case, the graphite nodules decreased the hardness and increased wear despite the presence of a rich carbon-based protective layer in the contact interface, which is responsible for the low friction coefficient (Fig. 3.20).

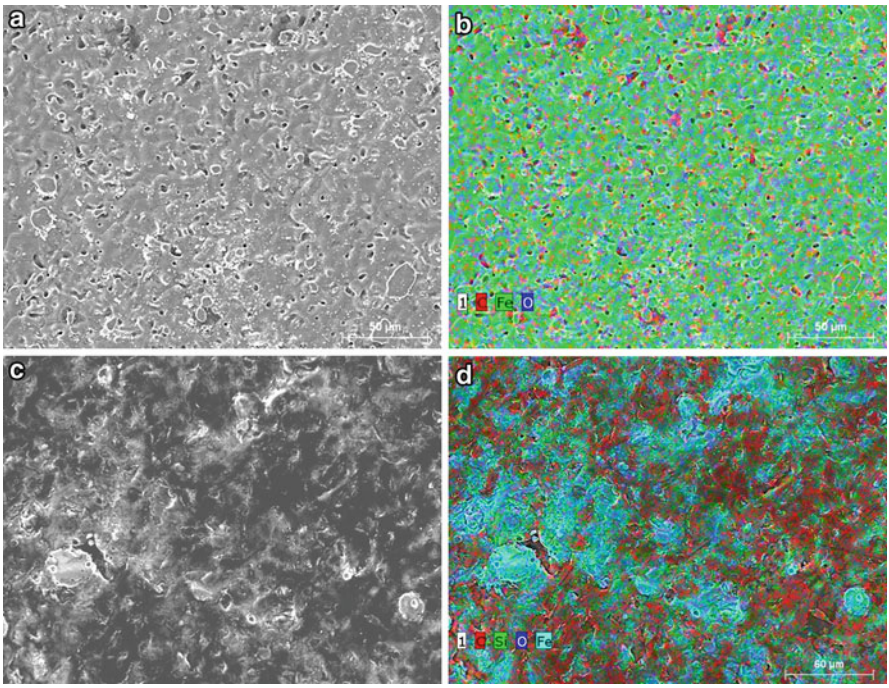

Fig. 3.22 Typical SEM images and elemental mapping of specimen surfaces before the tests. (**a**, **b**) Matrix alloy (Fe-0.6 wt% C); (**c**, **d**) composite Fe-0.6 wt% C + 3 wt% SiC

Figure 3.22 shows the typical SEM and elemental mapping images of the specimen surfaces before the tests. It is noticeable that the matrix alloy exhibited a slightly higher porosity. Moreover, the use of SiC as a precursor for the graphite nodules was notably efficient. In fact, the elemental mapping images clearly show large amounts of carbon (red regions) well distributed on the composites surfaces.

Figure 3.23 shows typical aspects of the surfaces after the tests and illustrates the wear mechanisms that acted on the specimens and counter-bodies. For the matrix alloy (Fig. 3.23a), the wear marks have smoother surfaces where third-body "islands" (arrow) are observed. Moreover, third-body islands are also visible in notably smooth and even counter-body worn surface, which are indicated with an arrow in Fig. 3.23b. The EDX analysis of these regions [76] shows that they are rich in oxygen.

Surprisingly, unlike the observation in the reference sample, composites with graphite nodules in the microstructure (3 and 5 wt% SiC) show strong evidence of plastic deformation, Fig. 3.23c, which is characterized by the presence of grooves parallel to the sliding direction, which indicates abrasive wear as the dominant wear mechanism. This aspect is even more evident in the wear marks of the counter-bodies, Fig. 3.23d.

A great quantity of wear debris was observed on the wear marks. Figure 3.24 shows the general aspect, morphology, and dimensions of the produced particles.

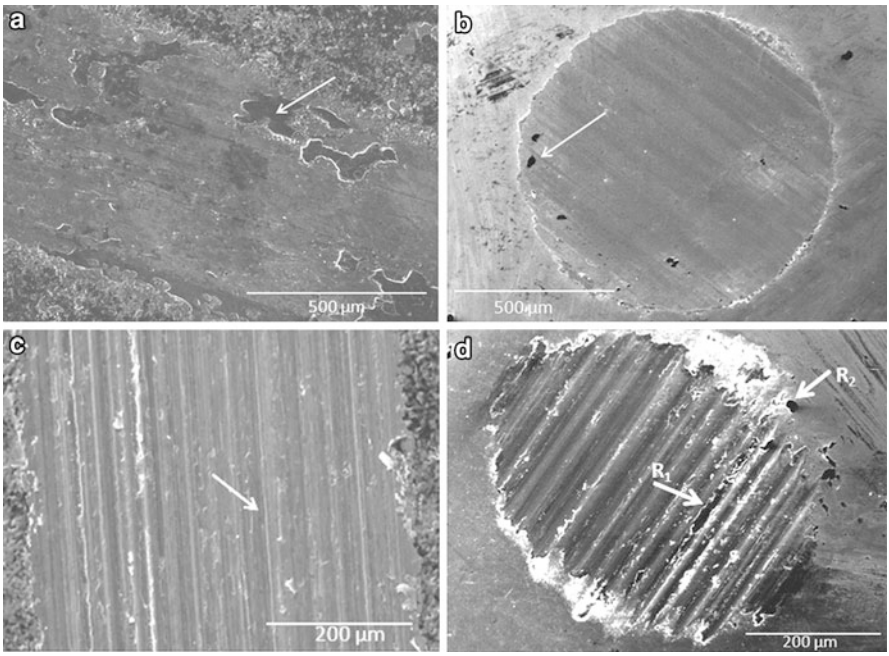

Fig. 3.23 Typical wear mechanisms. (**a**) Matrix alloy, specimen; (**b**) matrix alloy, counter-body; (**c**) 3 wt% SiC composite, specimen; (**d**) 3 wt% SiC composite, counter-body

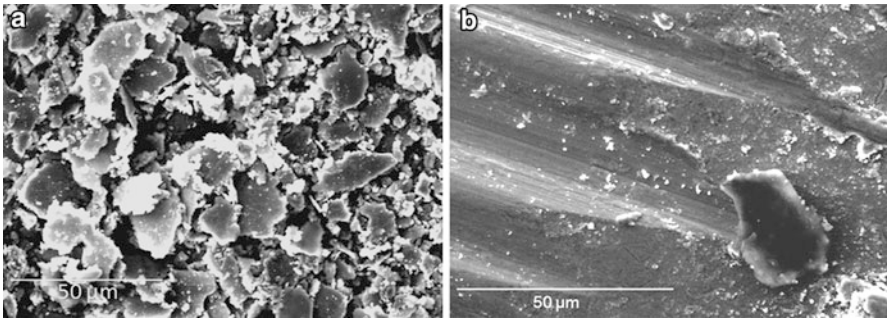

Fig. 3.24 Wear debris. (**a**) General aspect; (**b**) producing abrasion on the counter-body. Composite Fe-C- 3 wt% SiC

They consist primarily of carbon and oxygen, as evidenced by EDX. It is reasonable to assume that these particles actively operate in the abrasion process, as clearly shown in Fig. 3.24b.

The chemical composition analysis using EDX [76] in the regions indicated with arrows in Fig. 3.23 shows the presence of oxygen and an important carbon content in the wear mark of the samples. Even if the strong abrasion apparently does not allow for tribolayer formation, a significant amount of carbon (approximately 20 wt%) was

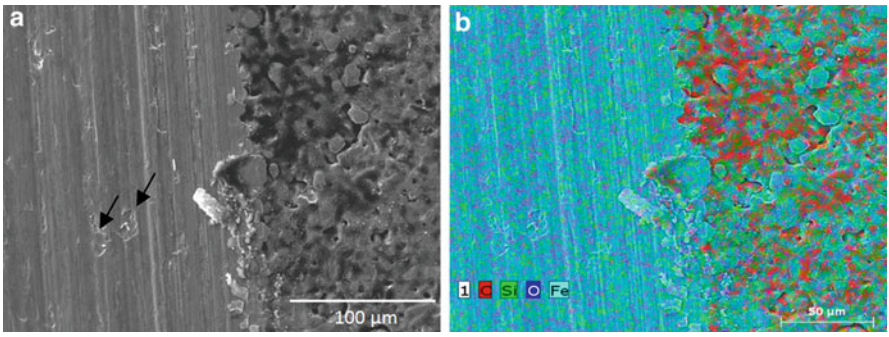

Fig. 3.25 Wear scar. (**a**) Typical aspect at the boundary; (**b**) X-ray map obtained using EDS. Composite Fe-C- 3 wt% SiC

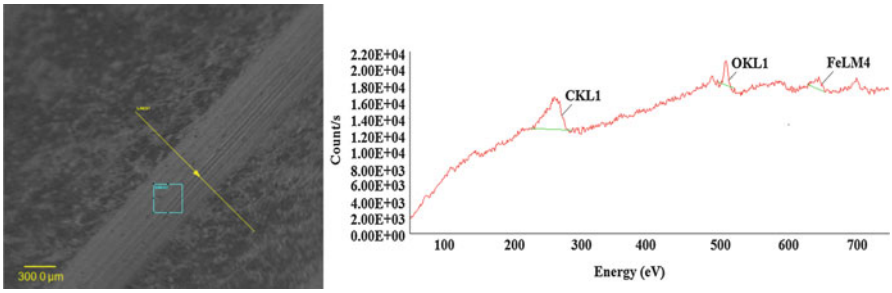

Fig. 3.26 Typical AES analysis. Fe-C- 3 wt% SiC composite

found in the wear mark of the counter-body (regions R_1 and R_2, Fig. 3.23d), which proves the existence of a carbon-rich material.

A high magnification analysis (Fig. 3.25a) shows a tenuous tribolayer that is fractured at various points.

By associating this image with the map of elements obtained using EDX (Fig. 3.25b), it is possible to verify that the contact is fuelled by carbon from the graphite nodules. Furthermore, oxygen is observed (dark blue region), which was expected because the tribological tests were performed in air.

To further understand this point, the wear scar of the 3 wt% SiC composite was analyzed using Auger electron spectroscopy (AES), Fig. 3.26.

Analyses in the wear scar confirmed that the tribolayer, which was formed during sliding, was composed of oxygen and predominantly carbon. In contrast, a similar analysis performed on the wear marks of the reference sample (matrix alloy) [76] showed the predominance of oxygen in the worn surface, which indicates the presence of oxides in the tribolayer.

To further understand the formation and degradation of the tribolayer, using the 3 wt% SiC composite as specimens, sliding tests were conducted and interrupted at predefined moments, corresponding to 100, 1000, and 2000 cycles.

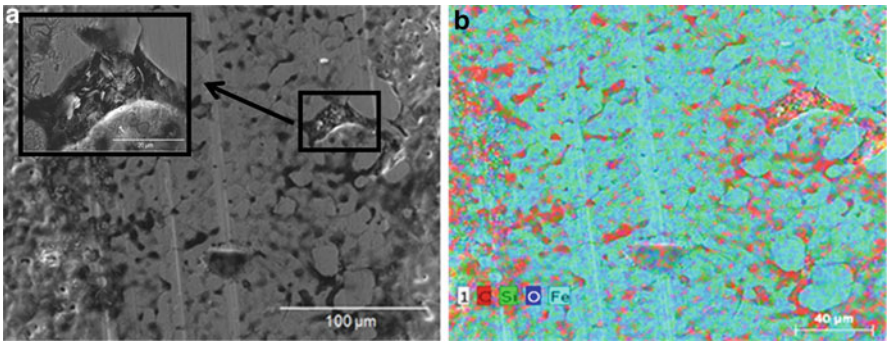

Fig. 3.27 Wear scar after 100 cycles: (**a**) SEM images and (**b**) elemental analyses

Figure 3.27 shows the typical aspects of the wear scar after 100 cycles.

The pores in the samples were filled with lamellar structures, as shown in the high-magnification inset in Fig. 3.27a. The elemental map shows that this material is rich in carbon, which was confirmed using the EDX analysis (~31 wt% C). It is reasonable to suppose that the graphite foils are removed from the in situ-generated graphite nodules and remain at the interface, which contributes to the formation of the protective tribolayer interface.

However, despite the presence of a few scratches, the surface of the counter-body had a large amount of carbon (~30 wt%), which indicates material transfer during the test and the early formation of a graphite-rich tribolayer at the contact interface, which maintained the region lubricated and reduced the coefficient of friction at the end of 100 sliding cycles.

The main features associated with longer test times (1000 and 2000 cycles) were pore closure and tribolayer degradation. Figure 3.28 illustrates the typical aspects of the wear scars after 1000 cycles.

The strong plastic deformation that led to the pore closure at the center of the wear scar was evidently associated with the tribolayer spalling. Additionally, EDS chemical analyses showed the presence of carbon and oxygen. Furthermore, the oxidation processes associated with tribochemical reactions contributed to the formation of oxide regions on the counter-body surface.

Effect of Surface Finishing

In this section, the influence of surface finishing (as sintered and polished) on the tribological behavior of MIM self-lubricating composites sintered at 1150 °C with (3 and 5% wt%) and without SiC additions is presented. The tribological behavior was analyzed using linear reciprocating sliding tests (constant load of 7 N, 60 min duration). Polishing of the specimens was performed manually with sand paper #1200, #2400, and #4000 in a polishing machine with automatic controls of time and rotation, for 10 min and 150 rpm. After polishing, the surface topography was characterized.

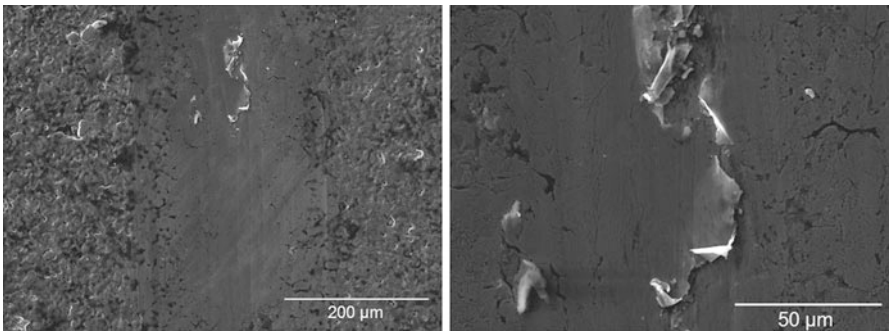

Fig. 3.28 Wear scar after 1000 cycles

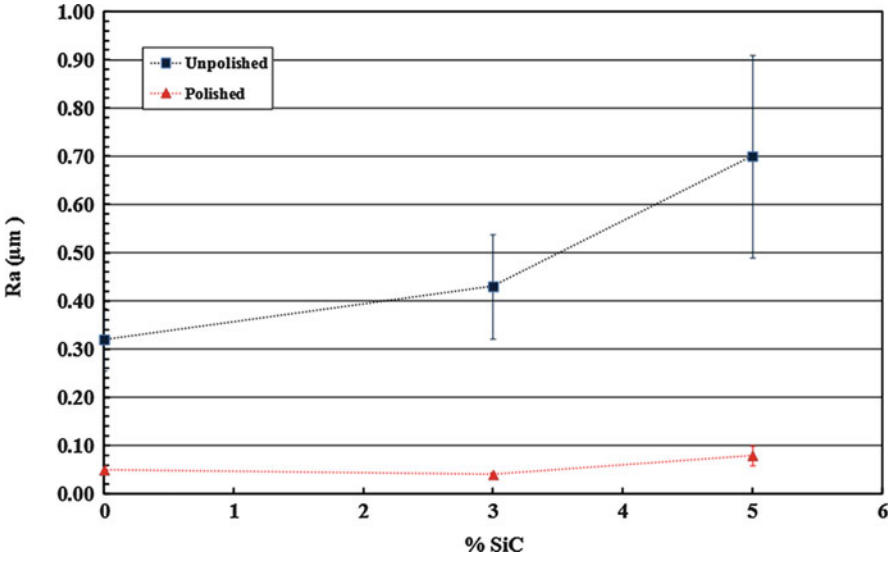

Fig. 3.29 Average surface roughness according to SiC content before and after polishing

The effect of SiC content on surface topography before and after polishing is illustrated in Fig. 3.29.

The mean surface roughness of unpolished samples increases significantly when the SiC content increases. Such behavior can be observed also for polished samples, but in a more subtle way. As already mentioned, the reference alloy presented a microstructure constituted of perlite + ferrite whereas the addition of SiC induces the formation of 2D turbostratic graphite nodules which in turn induced increased surface roughness. Thus, higher SiC contents increase the quantity of graphite nodules and, therefore, increase surface roughness. After polishing, a significant reduction of the average values of Ra is observed when compared with the values obtained for the unpolished samples.

Typical aspects of the surfaces before and after polishing are presented in Fig. 3.30.

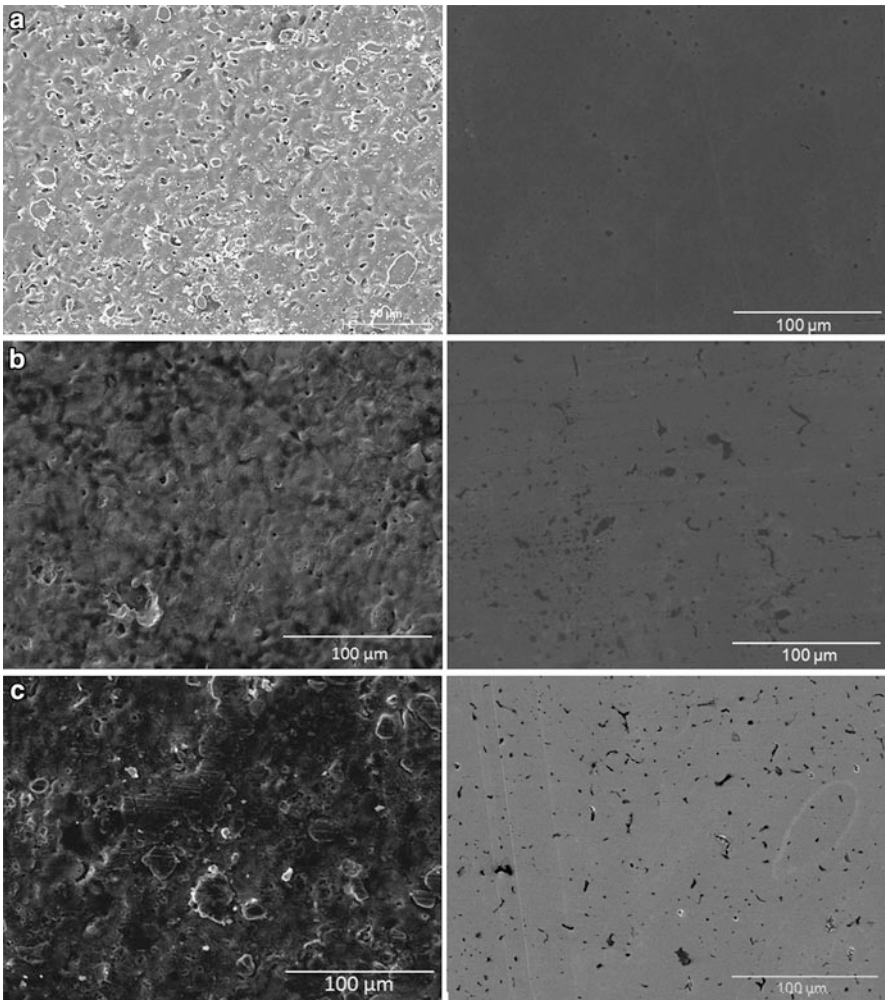

Fig. 3.30 Typical surfaces of unpolished surfaces (left) and polished (right) specimens. (**a**) 0 wt% SiC; (**b**) 3 wt% SiC and (**d**) 5 wt% SiC

It is clearly observed that after polishing the surfaces are smoother and feature dark regions constituted of graphite nodules and pores. From now on, these dark regions will be called lubricant reservoirs. Due to limitations of the technique used for image analysis already reported in the literature [59, 61], it was not possible to distinguish between pores and graphite nodules. The dark regions were previously identified as turbostratic 2D graphite. Compared with the polished surface of the reference sample (0 wt% SiC), the polished surfaces of specimens containing 3 and 5 wt% SiC presented increasing amounts of dark regions (pores + graphite nodules) evenly distributed on the surface.

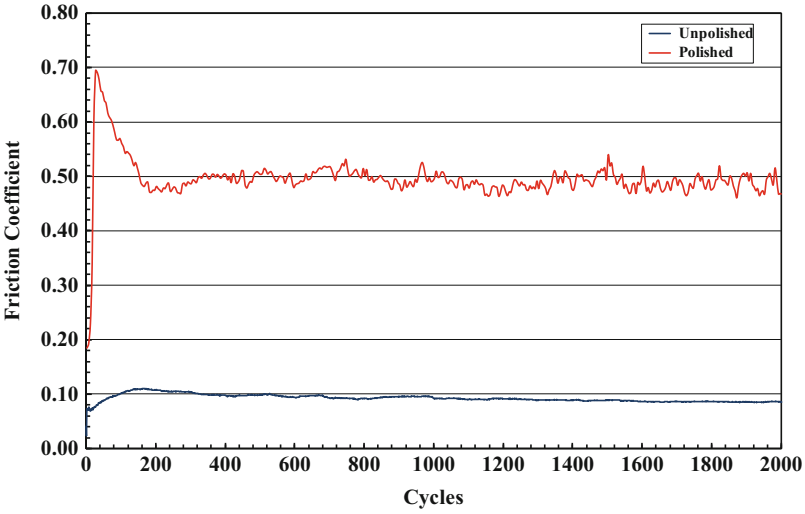

Fig. 3.31 Typical evolution of friction coefficient with number of cycles. 3 wt% SiC

Figure 3.31 shows how the evolution of the friction coefficient during the test duration is influenced by surface finishing.

All results present similar behavior. There is a transient associated with the onset of contact between specimen and counter-body at the beginning of tests before a steady state is reached. For the unpolished specimens, friction coefficient showed a rapid increase and stayed nearly constant during the rest of the test, i.e., a steady state was reached. For the polished specimens, after a rapid initial increase, friction coefficient starts to gradually decrease to a lower steady-state value.

As already discussed the reasons for the difference in the evolution of the friction coefficient within the transient period will not be treated in the present chapter. However, it is reasonable to suppose that the stabilization of the friction coefficient is related to the generation of a protective tribolayer, where the transient corresponds to the kinetics of formation of the layer. The values of the friction coefficient for each test were computed by averaging the steady-state values. The results are summarized in Fig. 3.32.

Increasing the precursor content and, as a consequence, the number of turbostratic 2D graphite nodules produced a reduction of the average friction coefficient. In general, the reduction was substantial, up to 3% SiC. For higher values of SiC content, the friction coefficient was almost constant. As already stated, the graphite foils are removed from the in situ-generated graphite nodules and remain at the interface thus contributing to the formation of the protective tribolayer.

Additionally, it is observed that the friction coefficient is strongly influenced by surface finish. Polished specimens exhibit significantly higher friction coefficients ($\mu > 0.4$) suggesting that the 2D turbostratic graphite nodules do not actively participate in the tribolayer formation. In fact, multielemental X-ray maps obtained

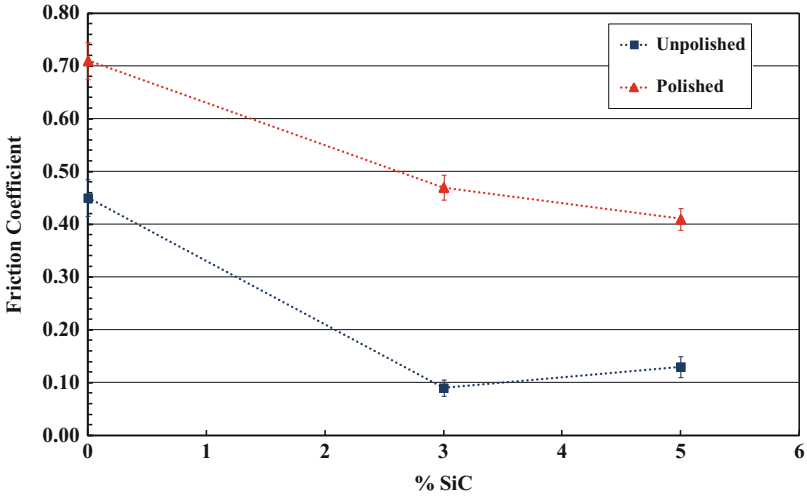

Fig. 3.32 Steady-state friction coefficient

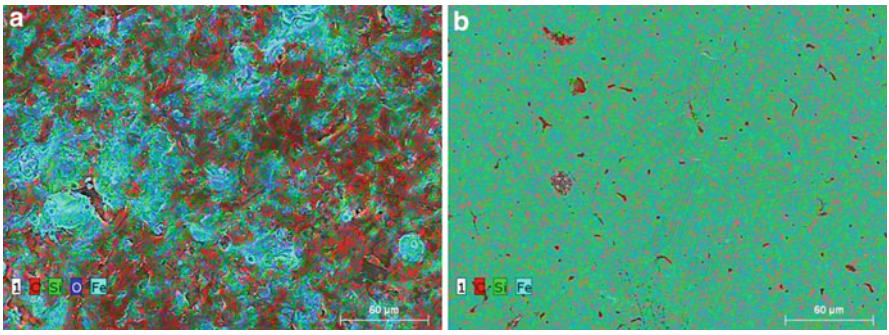

Fig. 3.33 Multielemental X-ray map obtained by EDS. Composite Fe-0.6% C-3% SiC. (**a**) Unpolished. (**b**) Polished

by EDS (Fig. 3.33), in which the red color is associated with carbon, clearly show a large decrease in the amount of graphite nodules for the polished surface.

Besides significantly reducing the surface roughness, as illustrated in Figs. 3.29 and 3.30, polishing also affected the availability of solid lubricant reservoirs in the active sliding interface. It is well known the paramount role played by pores (in our case pores + solid lubricant reservoirs) in the tribological behavior of sintered materials [39, 78].

In addition to a reduction in strength and, as a consequence, in load bearing capacity, the presence of porosity alone might influence the wear mechanisms acting on the surfaces of powder metallurgy parts in a number of ways. In particular, open pores in the active interface are reported to act as foci for the generation and trapping

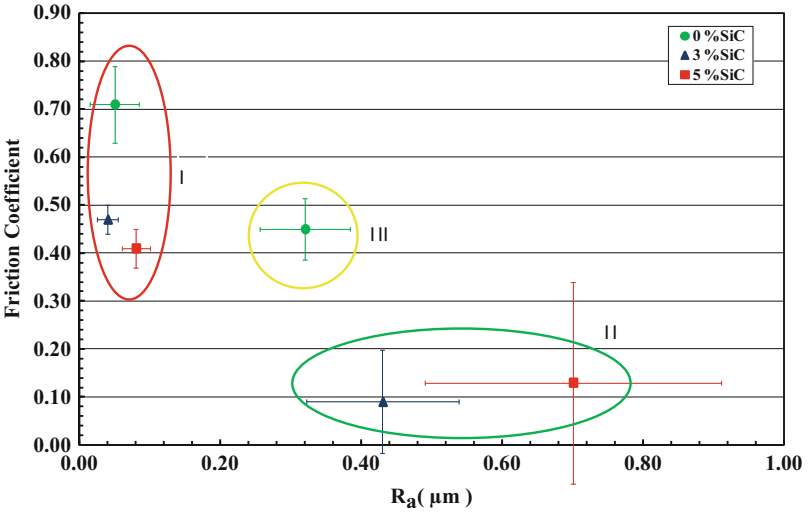

Fig. 3.34 Friction coefficient in function of surface roughness and SiC content

of wear debris during sliding wear [77]. If the reservoirs remain active (open), there will be a continuous self-replenishment of solid lubricants to the contact area and, as a consequence, the maintenance of a protective tribolayer [45]. The plastic deformation imposed by polishing induces the closure of pore + solid lubricants reservoirs, which significantly reduces the lubricant supply into the active interface. This justifies the high friction coefficient presented by the polished composites. Without a doubt, the closure of the reservoirs is an important factor in increasing friction coefficient of the composites containing SiC. On the other hand, it would not justify the increased friction coefficient also observed for the reference composites alloys (without SiC) since they do not contain graphite nodules. In this case, it is reasonable to suppose that the variation in friction coefficient is mainly due to changes in surface topography during polishing.

In addition, friction coefficient decreased when the amount of precursor (SiC) increased for both surface finishing routes. The reference specimen (0% SiC) presented a mean friction coefficient significantly higher than those of the samples containing 3% and 5% SiC. It is remarkable the positive influence of turbostratic 2D graphite nodules on the tribological behavior of these composites. For the case of the unpolished specimens, the addition of 3% SiC induced a remarkable 80% reduction in friction coefficient.

There is a compromise between surface topography and solid lubricant availability in the active interface. Figure 3.34 shows the average friction coefficient as a function of roughness. Three regions are highlighted in Fig. 3.34: The first region (I) consists of the polished samples (0%, 3%, and 5% SiC); the second region (II) is associated with unpolished samples containing 2D turbostratic graphite nodules (3% and 5% SiC), and finally, the third region (III) concerns the unpolished reference alloy (0% SiC).

The polished samples, regardless of the chemical composition, showed higher friction coefficients and obviously low roughness when compared with the unpolished ones. On the other hand, the unpolished composites (region II) presented higher roughness associated with lower friction coefficient. Also noteworthy is the unpolished reference alloy behavior (region III): It presents intermediate values for both roughness and friction coefficient, suggesting the already mentioned compromise between surface topography and solid lubricant availability in the active interface suggesting that the presence of 2D turbostratic graphite nodules affects the surface topography of the samples and has a great influence on the dynamics of the formation of protective tribolayers, and consequently on wear mechanisms [69, 78]. In fact, the polished samples, regardless of the chemical composition, presented very low values of reduced valley height (Rv) (0.1–0.18 μm) when compared with the unpolished ones (0.67–1.51 μm). Since Rv is related to the distribution of valleys or pores in a surface [79], this evidences the closure of pores + solid lubricant reservoirs during polishing.

According to Keller et al. the difference in surface topography has an important impact on wear mechanisms and building up of tribolayers [79]. A rough surface, i.e., small real contact area or high real contact pressure, leads to higher friction coefficients and wear [79]. However, despite being considerably rougher than the polished specimens, the unpolished specimens presented significantly lower friction coefficients, pointing to an important participation of the turbostratic graphite nodules in the lubrication process. It appears that during sliding, due to the high contact pressure, the formation of the protective tribolayer occurs rapidly in the initial cycles, preventing direct metal-metal contact, and thus maintaining low friction coefficients. If the reservoirs remain active (open), there will be a continuous self-replenishment of solid lubricants to the contact area and, as a consequence, the maintenance of a protective tribolayer as illustrated in Fig. 3.35 which shows a kind of self-healing feature of the tribolayer. Whenever the normal force is increased (black curve) there is a partial destruction of the tribolayer as indicated by the sharp decrease in electrical potential of the contact. Immediately, the tribolayer is reestablished as clearly indicated by the rapid increase in electrical potential of the contact.

Figure 3.36 presents the influence of the precursor content and of the specimen surface finish on the wear rates of the specimens and their respective counter-bodies.

The influence of surface finish was marginal for the reference alloys (0% SiC). However, for the composites (3% and 5% SiC), the unpolished specimens exhibited significantly lower wear rates compared to the polished samples, Fig. 3.36a.

The counter-bodies (Fig. 3.36b) presented much higher wear rates when siding against the polished surfaces, being this even more significant for the reference alloy (0% SiC). The absence of graphite nodules associated with the smooth surface topography of the reference samples promoted an increased wear of the specimen and respective counter-bodies. Polishing, besides modifying the surface topography of the sample, promoted the closure of the pores and of the graphite reservoirs as already described. This resulted in increased friction coefficient and wear rates for both sides of the tribo pair.

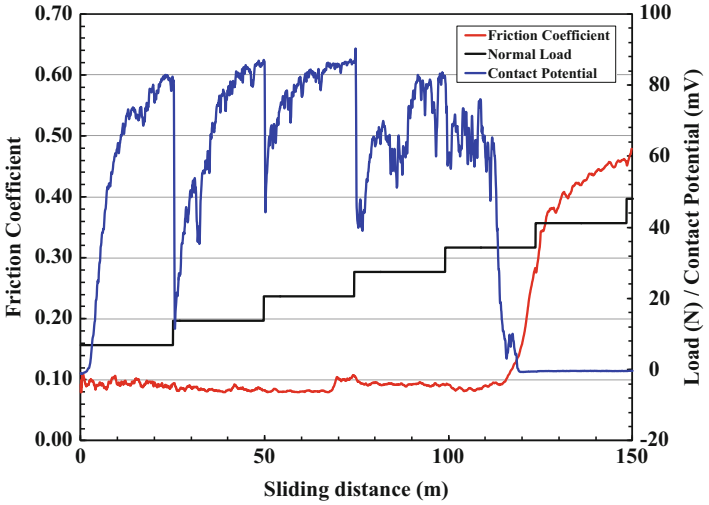

Fig. 3.35 Self-healing of the tribolayer

Typical aspects of the wear scars of specimens and counter-bodies associated with polished specimens are shown in Fig. 3.37. In both cases, there are clear indications of abrasive wear. For the reference alloy, analysis by EDX in selected areas indicated a strong presence of oxygen in the active interface of both specimens (30%) and counter-bodies (14%), a clear evidence of oxidative wear [76].

Abrasive wear evidence is even more visible in wear scars associated with specimens rich in 2D turbostratic graphite, Fig. 3.38.

Moreover, EDX analysis indicated the presence of a protective tribolayer in the wear scars of both specimen and counter-body, as indicated by the higher amounts of carbon (specimen: 9%; counter-body: 14%) in relation to the reference alloy.

Again, a great quantity of wear debris was observed on the wear marks. Elemental analysis by EDX of the wear debris [76] showed that the debris generated for the reference alloy have higher oxygen content than the debris produced by the composites containing 2D turbostratic graphite nodules which, in turn, are richer in carbon. During sliding in air, oxygen reacts at the contact interface giving rise to a tribolayer that forms and breaks down cyclically. For the reference alloys, the rupture of this tribolayer gives rise to wear debris consisting mainly of iron and oxygen. The debris originated from the composites, in addition to iron and oxygen, also present, as expected, a significant amount of carbon, since the graphite nodules actively participate in lubrication of the contact interface, thereby justifying the low friction coefficients and wear rates measured for the unpolished samples.

Effect of the Metallic Matrix

Apart from contributing to the formation and degradation of the tribolayer, the microstructure of the metallic matrix always has large influence on the tribological

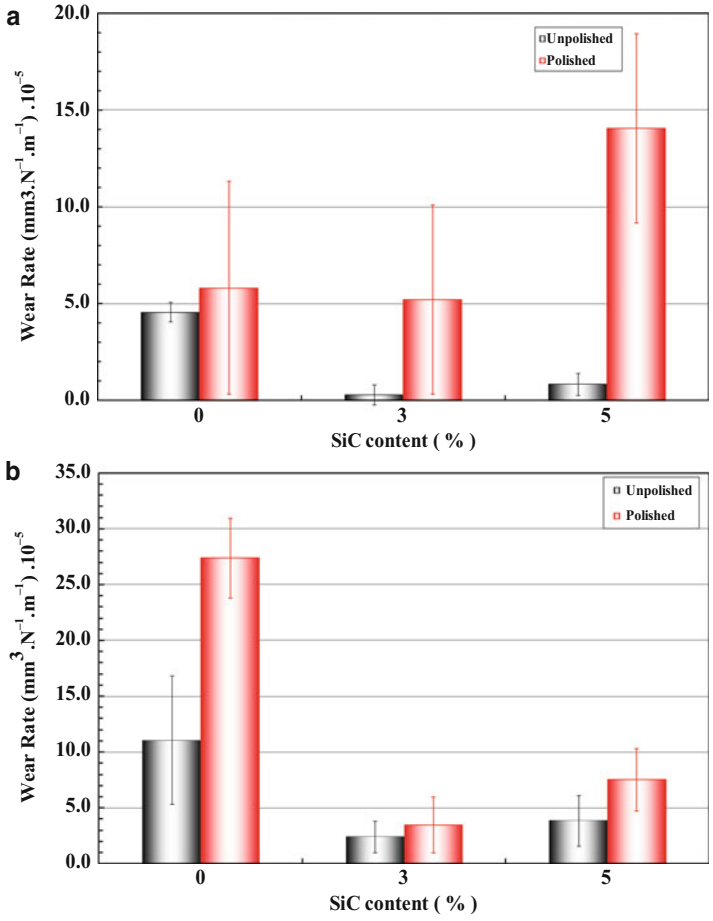

Fig. 3.36 Wear rate. (**a**) Specimens. (**b**) Counter-bodies

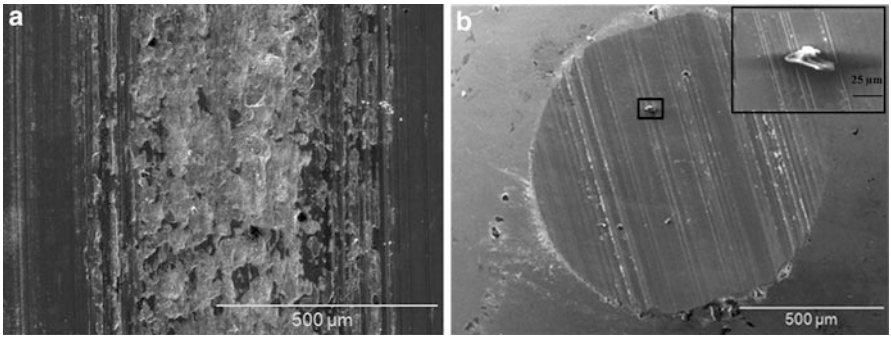

Fig. 3.37 Typical aspects of the wear scars. Reference alloy (0% SiC) (**a**) polished specimen. (**b**) Counter-body

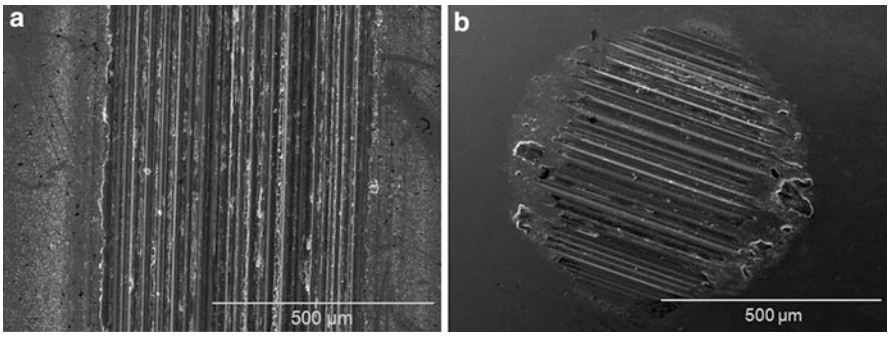

Fig. 3.38 Typical aspects of the wear scars. 3% SiC composite (**a**) polished specimen. (**b**) Counterbody

behavior of any material. According to Zum Gahr [80], when considering wear, the best tribological behavior of a metallic material is reached by combining the most appropriate combination of strength, ductility, and fracture toughness.

In this section, the effect of the metallic matrix composition on the formed microstructural constituents, as well as their effect on the tribomechanical behavior of plasma-assisted debinded and sintered MIM self-lubricating composites is presented and discussed. Three different metal matrices containing embedded 2D turbostratic graphite nodules were obtained by adding alloying elements (Ni and Ni + Mo) to the initial composition of the Fe-C-SiC composite.

Figure 3.39 illustrates the typical microstructures of the studied composites.

All composites were prepared by mixing 3% SiC to the feedstock and were sintered at 1150 °C for 1 h. All three microstructures have in common the presence of graphite nodules (arrows), induced by the addition of SiC to the feedstock powder, whereas for the present imposed conditions, the metallic matrix varies from ferrite to martensite. Addition of Nickel did not substantially change the microstructural constituents (ferrite + small fractions of perlite), Fig. 3.39b, but it seems that the graphite nodules are a little larger and in greater quantities than in the standard Fe-C-composites. For the Ni + Mo containing composite, the metallurgical constituents changed from ferrite/perlite to martensite even under the low cooling rates imposed by the PADS reactor (7 °C/min). The addition of these elements probably dislocated the TTT curve of this steel, favoring the formation of martensite [81].

Figure 3.40 summarizes the mechanical properties of the composites.

They were evaluated by measuring the micro-hardness of the metallic matrix and the tensile resistance of the composite (elongation, yield strength, and ultimate strength). It is possible to observe that even with the presence of solid lubricant nodules in the metallic matrices, the level of resistance for the composites is very high. This occurs because the nodules of graphite are very small (less than 20 µm) and they are homogeneously dispersed throughout the ferrous matrix thus preserving the matrix continuity.

As expected, the addition of alloying elements produced a strong effect on the hardness and mechanical strength of the matrices. Nickel increases the resistance of

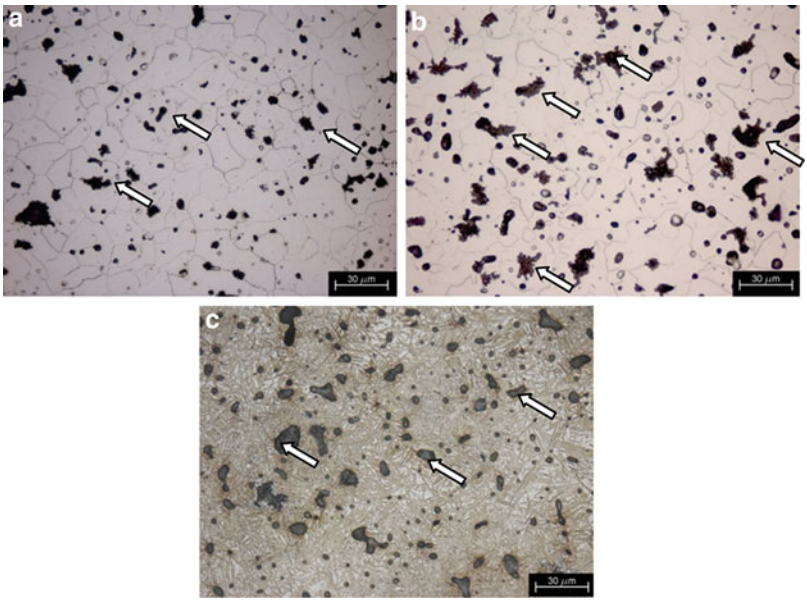

Fig. 3.39 Typical microstructure of self-lubricating composites produced by adding 3% SiC. (**a**) Fe + 0.6%C. (**b**) Fe + 0.6%C + 4.0%Ni. (**c**) Fe + 0.6%C + 4.0%Ni + 1.0%Mo

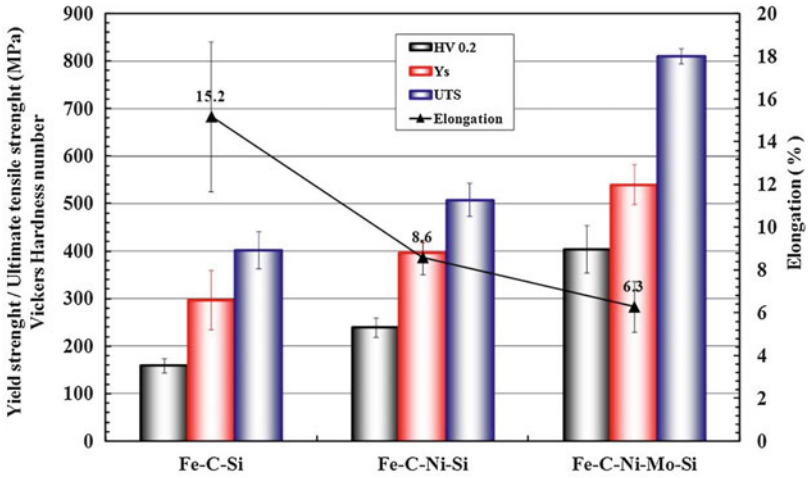

Fig. 3.40 Mechanical properties

the composites by solid solution and partially reduces its ductility in relation to the standard Fe-C composite. The combination of Ni + Mo induces a large increase in mechanical resistance because it changes the metallurgical microstructure from ferrite/perlite to martensite. As explained earlier, the martensite transformation

occurs for the Fe-C-Ni-Mo even under low cooling rates. As expected, the elongation behaved in a contrary manner.

It is worth noting that UTS values as high as 1000 MPa were reported for the Ni + Mo containing composite when sintered at 1200 °C [61]. A possible factor for such an increase in mechanical properties was the higher homogenization obtained at higher temperatures. It is very well known that the diffusion rates are enhanced with temperature. Furthermore, at 1200 °C, liquid phase sintering may occur, thus producing a better chemical homogenization and densification.

It might also be interesting to point out that the UTS of self-lubricating composites available on the market do not normally exceed 300 MPa. This is a result of the large discontinuity of the metallic matrix produced by the addition of up to 40% of large solid lubricant particles which are necessary to keep friction at low levels.

The friction coefficient of the reference composite (Fe-C) gradually increases with the sliding distance until, at about 100 m, it evolves in a more uniform and constant way. For the composites containing nickel and molybdenum, the friction coefficient evolves in a more stable way from the beginning of the test. Although presenting a significantly lower average value, the evolution alternates low and high intensities periods. Furthermore, a higher oscillation of the contact potential was verified, indicating instability of the insulating tribolayer. The Ni-containing composites presented a similar evolution at values in between those of the reference composite and that of the Ni-Mo composites [82].

The effect of metallic matrix composition on the steady-state friction coefficient is presented in Fig. 3.41.

The reference composite, Fe-C, presented the highest friction coefficient (0.11). The addition of alloying elements considerably reduced the friction coefficient (45% reduction for the Ni composites) and values as low as 0.04 (65% reduction) for the Fe-C-Ni-Mo composites. This remarkably low value may be considered superlubricity in the real world.

Figure 3.42 illustrates the general appearance of the wear scars produced in both specimens and counter-bodies.

Wear scars associated with the specimens presented different widths and the general appearance of the wear marks also varied. The wear volume was reduced by the introduction of the alloying elements. Inside the wear scar there is a clear evidence of abrasive wear, as evidenced by the presence of multiple parallel scratches. The intensity and number of scratches varied according to the material. The wear loss of the counter-bodies (AISI 52100 steel ball) presented the same behavior as the specimens. The wear rate of specimens and counter-bodies is summarized in Fig. 3.43.

The lowest wear rate value determined was 8.29×10^{-6} mm^3 N^{-1} m^{-1} for the Fe-C-Ni-Mo composites whereas the highest wear rate was measured for the reference composite (Fe-C), 34.5×10^{-6} mm^3 N^{-1} m^{-1}. This corresponded to a 420% reduction. For the nickel composites (14.5×10^{-6} mm^3 N^{-1} m^{-1}), the reduction was 240% in relation to the reference composite. In all cases, the wear rate of the ball was almost identical [(9.47; 19.31 and 37.22) $\times 10^{-6}$ mm^3 N^{-1} m^{-1}, respectively] which induced the same order of magnitude in wear reduction.

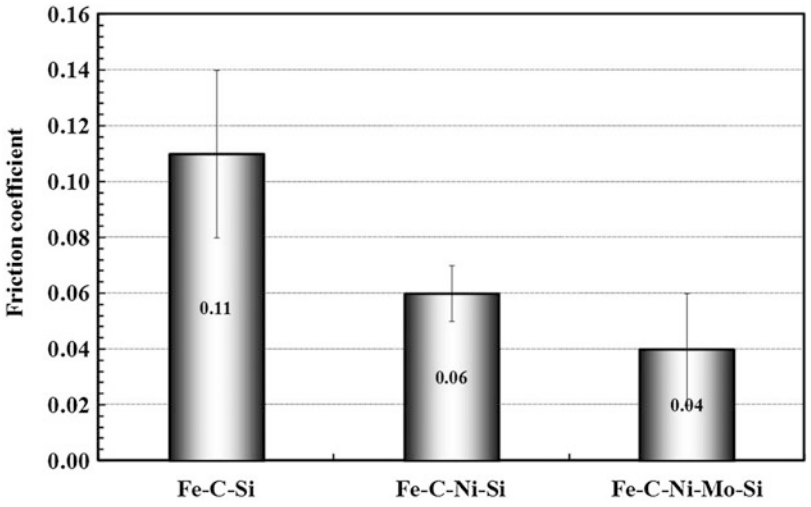

Fig. 3.41 Steady-state friction coefficient

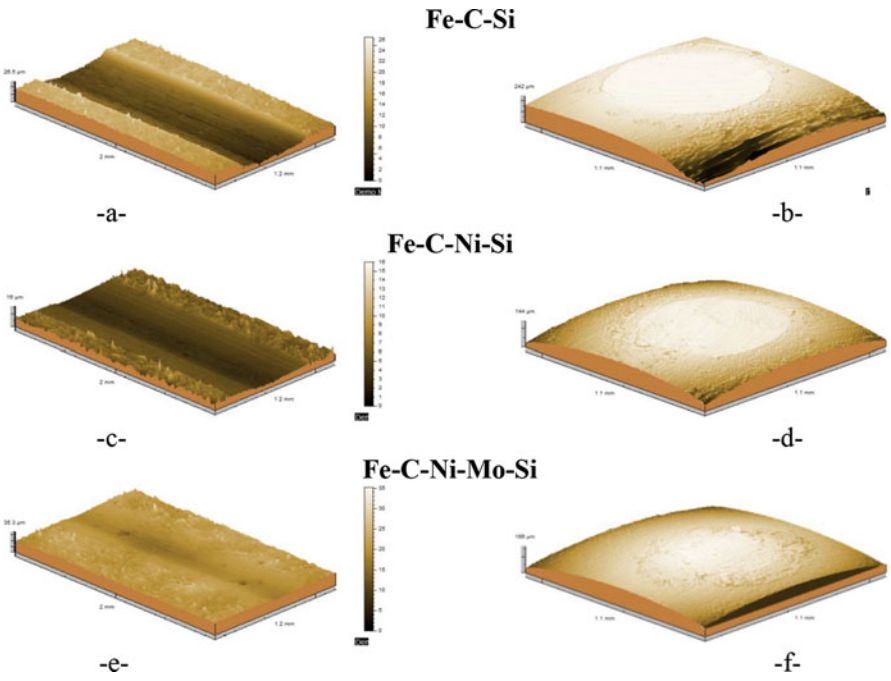

Fig. 3.42 Typical aspects of the wear scars obtained by laser interferometry. Composite Fe-C-Si, (**a**) specimen, (**b**) counter-body. Composite Fe-C-Ni-Si, (**c**) specimen, (**d**) counter-body. Composite Fe-C-Ni-Mo-Si, (**e**) specimen, (**f**) counter-body

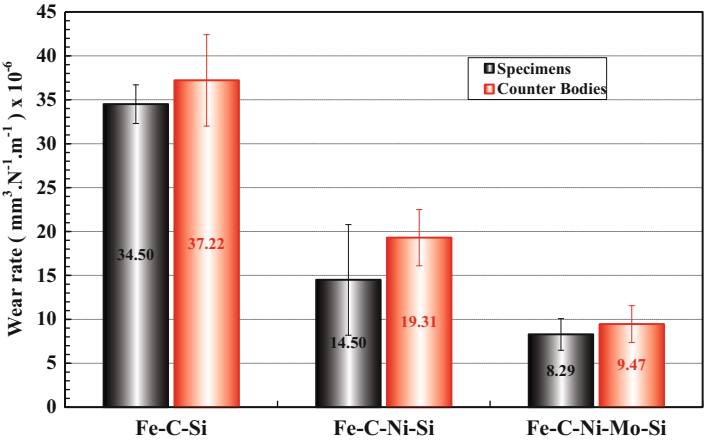

Fig. 3.43 Wear rate of the self-lubricating composite and AISI 52100 steel ball

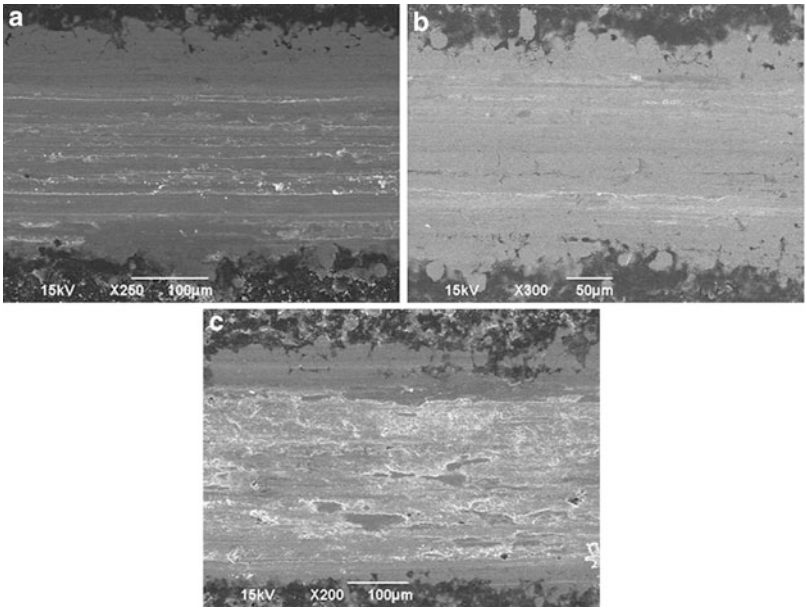

Fig. 3.44 General appearance of the wear scars. (**a**) Fe-C. (**b**) Fe-C-Ni. (**c**) Fe-C-Ni-Mo

Figure 3.44 illustrates the general appearance of the wear scars produced.

Wear mechanisms acting on the reference composite and on the nickel-containing composite are quite similar: Abrasive wear is present as indicated by the fine scratches in the sliding direction. The intensity and number of scratches varies according to the material. The shallow, thinner, and less numerous scratches are present in Fe-C-Ni specimens. They are probably caused by the abundant hard,

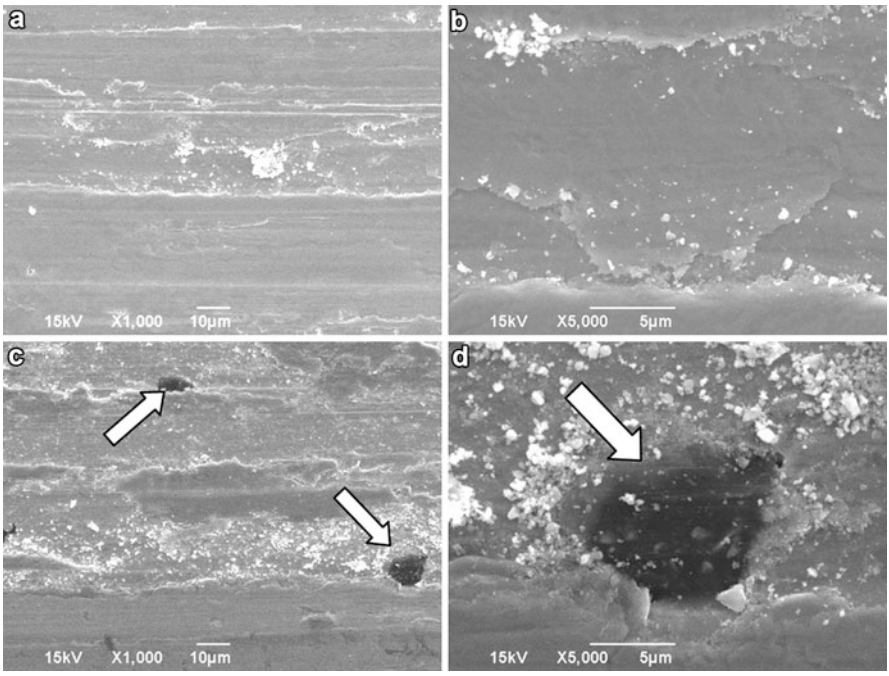

Fig. 3.45 Selected appearance of the wear scars. (**a**, **b**) Fe-C-Si composite. (**c**, **d**) Fe-C-Ni-Mo-Si composite

oxidized wear debris generated at the interface. On the other hand, for the nickel-molybdenum composite the tribological conditions produced smoother surfaces where third-body "islands" were observed.

This behavior might be linked to the resistance of the metallic matrix to plastic deformation and consequently, to the sealing of lubricant reservoirs, Fig. 3.45.

For the higher friction coefficient and wear rate specimens (Fe-C composites, Fig. 3.45a, b), the intense plastic deformation produces the complete closure of the solid lubricant reservoirs, whereas for the lower friction coefficient and wear rates (Fe-C-Ni-Mo composites, Fig. 3.45c, d), the solid lubricant reservoirs remains open and active (white arrow).

If the solid lubricant particles do not reach the surface, the self-replenishment mechanism of the tribofilm is partially restrained and the friction coefficient remains relatively high.

In order to further understand the effect of the metallic matrix on the tribolayer (and, as a consequence, on the tribological behavior), the wear scars present on the specimens and counter-bodies were analyzed by micro-Raman spectroscopy. Figure 3.46 synthesizes these results.

Again, only the borderline results are presented: Fe-C samples (higher friction coefficient and wear rates) and Fe-C-Ni-Mo composites (lower friction coefficient and wear rates).

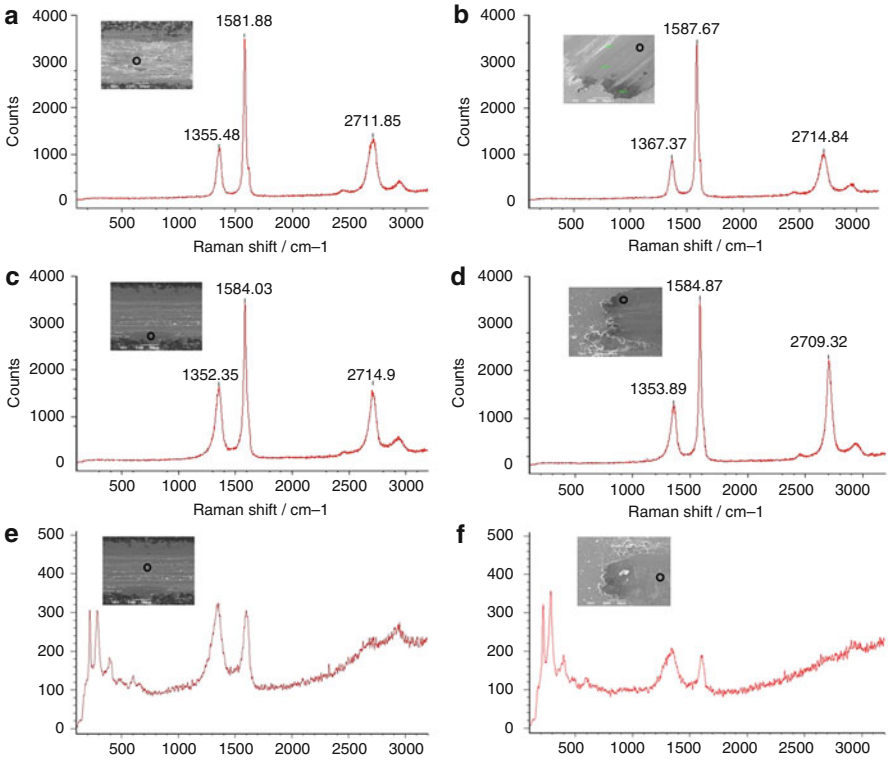

Fig. 3.46 Typical Raman spectra. (**a**) Fe-C-Ni-Mo specimen. (**b**) Fe-C-Ni-Mo counter-body. (**c**) Fe-C specimen, border of the scar. (**d**) Fe-C counter-body, border of the scar. (**e**) Fe-C specimen, center of the scar. (**f**) Fe-C counter-body, center of the scar

Figure 3.46a, b present the dominant spectra found in the wear scar of the Fe-C-Ni-Mo composite. All spectra clearly show the presence of the so-called turbostratic 2D graphite as evidenced by the typically widened G band and the presence of a D band which is associated with crystallinity disorder. The measured widening of the bands, the ID/IG ratio, the size of the graphite crystallites, and the analysis of the second-order band G′ also confirm the disorder in the material. It is also noticeable that the spectra of tribolayers presented in the wear scars of the specimens or in the counter-bodies are almost identical and indicate the beneficial presence of the turbostratic 2D graphite on both sides of the tribo pair.

On the contrary, the spectra found in the wear track of the reference composite changed according to their position in the wear scar. Spectra similar to those found in the previous case were measured near the border of the wear scars, Fig. 3.46c, d whereas those found in the center of the scar were a little different, Fig. 3.46e, f. Despite presenting lower intensities of the 2D graphite characteristic bands and a certain amount of fluorescence, the spectra also presented other smaller bands at lower frequencies. The origin of these bands was attributed [13] to the formation of

Table 3.1 Relevant properties

Property		MIM + PADS + In situ
Scuffing resistance [N m]		8000
Friction coefficient		0.04
Wear rate $[mm^3\ N^{-1}\ m^{-1}] \cdot 10^{-6}$	Specimen	8.28
	Counter-body	9.47
Ultimate tensile strength [Mpa]		500
Elongation [%]		6.3

iron oxide by tribochemical reaction caused by the surrounding atmosphere and is, probably, a consequence of the high energy availability associated with high friction coefficients. The positions of the bands in the range of 225–650 cm^{-1} match fairly well those observed for iron oxide phases [83].

The bands at 290, 408, 497, and 607 cm^{-1} indicated the presence of hematite Fe_2O_3 whereas the band at 667 cm^{-1} was assigned to magnetite Fe_3O_4 [84–86]. It is reasonable to suppose that the presence of iron oxides associated with the smaller intensities of the graphitic phase is likely to induce inferior tribological performance.

3.8 Concluding Remarks

We introduced a new microstructural model/processing route (metal injection molding followed by a single thermal cycle using a plasma-assisted debinding and sintering process and in situ formation of graphite nodules due to the dissociation of a precursor (SiC particles)). The results clearly show the great tailoring ability of the proposed microstructural model/processing routes applied to the development of innovative, low-cost, self-lubricating composites presenting low friction coefficient associated with high mechanical strength and wear resistance. Moreover, the optimized processing parameters produced outstanding new iron-based self- lubricating composites as illustrated in Table 3.1.

References

1. Cannaday, M.L., Polycarpou, A.A.: Tribology of unfilled and filled polymeric surfaces in refrigerant environment for compressor application. Tribol. Lett. **19**, 249–262 (2005)
2. Demas, N.G., Polycarpou, A.A.: Tribological investigation of cast iron air-conditioning compressor surfaces in CO_2 refrigerant. Tribol. Lett. **22**(3), 271–278 (2006)
3. Lee, Y.Z., Oh, S.D.: Friction and wear of the rotary compressor vane–roller surfaces for several sliding conditions. Wear. **255**, 1168–1173 (2003)
4. Solzak, T.A., Polycarpou, A.A.: Tribology of WC/C coatings for use in oil-less piston-type compressors. Surf. Coat. Technol. **201**, 4260–4265 (2006)
5. Pergande, S.R., Polycarpou, A.A., Conry, T.F.: Nanomechanical properties of aluminum 390-T6 rough surfaces undergoing tribological testing. J. Tribol. Trans. ASME. **126**, 573–582 (2004)

6. Oliveira Jr., M.M., Hammes, G., Binder, C., Klein, A.N., de Mello, J.D.B.: Solid lubrication in fluid film lubrication. Lubrication Science. **30**, 102–115 (2018)
7. Lancaster, J.K.: Solid lubricants. In: Booser, E.R. (ed.) CRC Handbook of Lubrication: Theory and Practice of Tribology Theory and design, vol. II, pp. 269–290 (1). CRC Press, Boca Raton (1984)
8. Sliney, H.E.: Solid lubricant materials for high temperatures: a review. Tribol. Int. **15**, 293–302 (1982)
9. Lansdown, A.R. Molybdenum disulphide lubrication. In: Dowson, D. (Ed.) Tribology series, vol. 35. Elsevier, Amsterdam (1999)
10. Brookes, C.A., Brookes, E.J.: Diamond on perspective. A review of mechanical properties of natural diamond. Diamond Relat. Mater. **1**, 13–17 (1991)
11. Donnet, C., Erdemir, A.: Historical developments and new trends in tribological and solid lubricant coatings. Surf. Coat. Technol. **180/181**, 76–84 (2004)
12. De Mello, J.D.B., Binder, R.: A methodology to determine surface durability in multifunctional coatings applied to soft substrates. Tribol. Int. **39**, 769–773 (2006)
13. De Mello, J.D.B., Binder, R., Demas, N.G., Polycarpou, A.A.: Effect of the actual environment present in hermetic compressors on the tribological behaviour of a Si rich multifunctional DLC coating. Wear. **267**, 907–915 (2009)
14. Bhushan, B. (ed.): Modern Tribology Handbook, vol. II. CRC Press, Boca Raton (2001)
15. Erdemir, A.: In: Bhushan, B. (ed.) Modern Tribology Handbook, vol. II, pp. 787–825. CRC Press, Boca Raton (2001)
16. Kimura, Y., Wakabayashi, T., Okada, K., Wada, T., Nishikawa, H.: Boron nitride as a lubricant additive. Wear. **232**, 199–206 (1999)
17. Erdemir, A.: Review of engineered tribological interfaces for improved boundary lubrication. Tribol. Int. **38**(3), 249–256 (2005)
18. Rapoport, L., Feldman, Y., Homyonfer, M., Cohen, H., Sloan, J., Hutchison, J.L., Tenne, R.: Inorganic fullerene-like material as additives to lubricants: structure-function relationship. Wear. **225–229**, 975–982 (1999)
19. Joly-Pottuz, L., Dassenoy, F., Belin, M., Vacher, B., Martin, J.M., Fleischer, N.: Ultralow-friction and wear properties of IF-WS_2 under boundary lubrication. Tribol. Lett. **18**(4), 477–485 (2005)
20. Tontini, G., Semione, G.D.L., Bernardi, C., Binder, R., de Mello, J.D.B., Drago, V.: Synthesis of nanostructured flower-like MoS_2 and its friction properties as additive in lubricating oils. Indust. Lubr. Tribol. **68**(6), 658–664 (2016)
21. Pacheco, F.G., Oliveira Jr, M.M., Santos, A.P., Costa, H.L., de Mello, J.D. B., Furtado, C.A.: Tribological evaluation of carbon nanotubes as additives in palm biolubricants. Submitted to Lubricants (2017)
22. Pauleau, Y., Thièry, F.: Deposition and characterization of nanostructured metalycarbon composite films. Surf. Coat. Technol. **180–181**, 313–322 (2004)
23. Erdemir, A.: Review of engineered tribological interfaces for improved boundary lubrication. Tribol. Int. **38**, 249–256 (2005)
24. Kato, H., Takama, M., Iwai, Y., Washida, K., Sasaki, Y.: Wear and mechanical properties of sintered copper–tin composites containing graphite or molybdenum disulfide. Wear. **255**, 573–578 (2003)
25. Dangsheng, X.: Lubrication behaviour of Ni–Cr-based alloys containing MoS_2 at high temperature. Wear. **251**, 1094–1099 (2001)
26. Huang, C., Du, L., Zhang, W.: Effects of solid lubricant content on the microstructure and properties of NiCr/Cr_3C_2–BaF_2·CaF_2 composite coatings. J. Alloys Compd. **479**, 777–784 (2009)
27. Zhu, S., Bi, Q., Yang, J., Liu, W., Xue, Q.: Effect of particle size on tribological behaviour of Ni_3Al matrix high temperature self-lubricating composites. Tribol. Int. **44**, 1800–1809 (2011)
28. Reeves, C.J., Menezes, P.L., Lovell, M.R., Jen, T.C.: The influence of surface roughness and particulate size on the tribological performance of bio-based multi-functional hybrid lubricants. Tribol. Int. **88**, 40–55 (2015)

29. Zhang, D., Lin, P., Dong, G., Zen, Q.: Mechanical and tribological properties of self-lubricating laminated composites with flexible design. Mater. Des. **50**, 830–838 (2013)
30. Burris, D.L., Sawyer, W.G.: A low friction and ultra-low wear rate PEEK/PTFE composite. Wear. **261**, 410–418 (2006)
31. Ouyang, J.H.: Microstructure and tribological properties of $ZrO_2(Y_2O_3)$ matrix composites doped with different solid lubricants from room temperature to 800 °C. Wear. **267**, 1353–1360 (2009)
32. Chen, B., Bi, Q., Yang, J., Xia, Y., Hao, J.: Tribological properties of solid lubricants (graphite, h-BN) for Cu-based P/M friction composites. Tribol. Int. **41**, 1145–1152 (2008)
33. Moghadam, A.D., Omrani, E., Menezes, P.L., Rohatgi, P.K.: Mechanical and tribological properties of self-lubricating metal matrix nanocomposites reinforced by carbon nanotubes (CNTs) and graphene: a review. Compos. Part B Eng. **77**, 402–420 (2015)
34. Tsuya, Y., Shimura, H., Umeda, K.: A study of the properties of copper and copper- tin base self-lubricating composites. Wear. **22**, 143–162 (1972)
35. Liu, E.R., Wang, W., Gao, Y., Jia, J.: Tribological properties of Ni-based self-lubricating composites with addition of silver and molybdenum disulfide. Tribol. Int. **57**, 235–241 (2013)
36. Binder, C., Hammes, G., Schroeder, R.M., Klein, A.N., de Mello, J.D.B., Binder, R.: 'Fine tuned' steels point the way to focused future. Met. Powder Rep. **65**, 29–37 (2010)
37. Mahathanabodee, S., Palathai, T., Raadnui, S., Tongsri, R., Sombatsompop, N.: Effects of hexagonal boron nitride and sintering temperature on mechanical and tribological properties of SS316L/h-BN composites. Mater. Des. **46**, 588–597 (2013)
38. de Mello, J.D.B., Binder, R., Klein, A.N., Hutchings, I.M.: Effect of compaction pressure and powder grade on microstructure and hardness of steam oxidised sintered iron. Powder Metall. **44**, 53–61 (2001)
39. de Mello, J.D.B., Hutchings, I.M.: Effect of processing parameters on the surface durability of steam-oxidized sintered iron. Wear. **250**, 435–448 (2001)
40. Ahn, H.S., Kim, J.Y., Lim, D.S.: Tribological behaviour of plasma-sprayed zirconia. Wear. **203**, 77–87 (1997)
41. PM Design Center of Metal Powder Industries Federation: Conventional Powdered Metal Components, 17 p (2012)
42. Tamura, S., Aizawa, T., Mitzuno, T., Kihara, J.: Steel powder compaction analysis. Int. J. Powder Metall. **34**, 50–59 (1998)
43. Al-Qureshi, H.A., Galiotto, A., Klein, A.N.: On the mechanics of cold die compaction for powder metallurgy. J. Mater. Process. Technol. **166**, 135–143 (2005)
44. Pavanati, H.C., Maliska, A.M., Klein, A.N., Muzart, J.L.R.: Comparative study of porosity and pores morphology of unalloyed iron sintered in furnace and plasma reactor. Mater. Res. **10**(1), 87–93 (2007)
45. Hammes, G., Schroeder, R.M., Binder, C., Klein, A.N., de Mello, J.D.B.: Effect of double pressing/double sintering on the sliding wear of self-lubricating sintered composites. Tribol. Int. **70**, 119–127 (2014)
46. Milligan, D., et al.: Materials properties of heat treated double pressed/sintered P/M steels in comparison to warm compacted/sinterhardened materials. In: PM^2TEC Advances in Powder Metallurgy and Particulate Materials, vol. 4, pp. 130–137 (2002)
47. James, B., et al.: Optimized double press-double sinter powder metallurgy method. US Patent 5,080,712, 1992
48. German, R.M.: Powder Metallurgy and Particulate Materials Processing, 1st edn, p. 528. Metal Powder Industries Federation, Princeton (2005)
49. German, R.M.: Powder Injection Molding, p. 521. Metal Powder Industries Federation, Princeton (1990)
50. Machado, R., Ristow, Jr., W., Klein, A.N., Muzart, J.L.R., et al.: Industrial plasma reactor for plasma assisted thermal debinding of powder injection molded parts. US Patent US7,718,919B2, PCT (WO 2006012718) and INPI (PI-0403536-4), 2010

51. Wendhausen, P.A.P., Fusao, D., Klein, A.N., Muzart, J.L.R., et al.: Plasma assisted debinding and sintering: process and equipment. In: Proceeding of the Powder Metallurgy World Congress & Exhibition, EURO PM2004, Vienna, vol. 4, pp. 37–142 (2004)
52. Klein, A.N., Muzart, J.L.R, et al.: Process for removal of binders from parts produced by powder injection moulding. US Patent US 6,579,493 B1, 2003
53. Klein, A.N., Binder, C., Hammes, G., de Mello, J.D.B., Ristow, W., Binder, R.: Self lubricating sintered steels with high mechanical resistance obtained via in situ formation of solid lubricant particles during sintering. In: Proceedings of EURO PM2009, vol. 1, pp. 191–196 (2009)
54. Binder, R., Klein, A.N., Binder, C., Hammes, G., Parucker, M.L., Ristow Jr., W.: Composicao metalurgica de materiais particulados, produto sinterizado autolubrificante e processo de obtencao de produtos sinterizados autolubrificantes. Patent application, PI 0803956-9, INPI, Brazil, 2008
55. Binder R., Binder, C., Ristow Jr., W., Klein, A.N.: Composition of particulate materials for forming self-lubricating products in sintered steels, product in self- lubricating sintered steel and process for obtaining self-lubricating products in sintered steel, PI0805606-Brazil; US 20110286873A1-USA; International Number: WO 2010/069020 A2-Europe; CN102497948A-China; JP 2012-512320-Japan; 10-2011-0110179-South Korea; SG 172168 A1-Singapore, TW 201034773 A1-Taiwan 2008
56. Lancaster, J.K.: Solid lubricants. In: Booser, E.R. (ed.) CRC Handbook of Lubrication, Theory and Practice of Tribology Theory and design, vol. II. CRC Press, Boca Raton (1984)
57. Xua, J., Zhang, R., Chena, P., Shena, D., Yea, X., Ge, S.: Mechanism of formation and electrochemical performance of carbide-derived carbons obtained from different carbides. Carbon. **64**, 444–455 (2013)
58. Totten, G. (ed.): Steel Heat Treatment: Metallurgy and Technologies, p. 191. CRC Press, Boca Raton (2007)
59. Binder, C., Bendo, T., Pereira, R. V., Hammes, G., de Mello, J.D.B, Klein, A.N.: Influence of the SiC content and sintering temperature on the microstructure, mechanical properties and friction behaviour of sintered self-lubricating composites. Powder Metallurgy. **59**, 1–10 (2016). https://doi.org/10.1080/00325899.2016.1250036
60. Callister Jr., W.D.: Fundamentals of Materials Science and Engineering, p. 552. Wiley, New York (2001)
61. Binder, C.: Desenvolvimento de novos tipos de aços sinterizados autolubrificantes a seco com elevada resistência mecânica aliada a baixo coeficiente de atrito via moldagem de pós por injeção. Ph.D. Thesis, Federal University of Santa Catarina, Brazil, 178 p. In Portuguese (2009)
62. ASM: ASM Handbook, Volume 1: Properties and Selection: Irons, Steels, and High-Performance Alloys, vol. 1. ASM International, Materials Park. 1063 p (1990)
63. Thelning, K.E: Steels and its heat treatment, 2nd edn. Butterworths, London. 450 p (1984)
64. Rohatgi, P.K., Ray, S., Liu, Y.: Tribological properties of metal matrix graphite particle composites. Int. Mater. Rev. **37**, 129–149 (1992)
65. Matthews, M.J., Pimenta, M.A., Dresselhaus, G., Dresselhaus, M.S., Endo, M.: Origin of dispersive effects of the Raman D-band in disordered carbon materials. Phys. Rev. B. **59**, R6585 (1999)
66. Cançado, L.G., Pimenta, M.A., Saito, R., et al.: Stokes and anti-stokes double resonance Raman scattering in two-dimensional graphite. Phys. Rev. B. **66**, 035415 (2002)
67. Ferrari, A.C., Meyer, V., Scardaci, C., et al.: Raman spectrum of graphene and graphene layers. Phys. Rev. Lett. **97**, 187401 (2006)
68. Ferrari, A.C.: Raman spectroscopy of graphene and graphite: disorder, electron–phonon coupling, doping and non adiabatic effects. Solid State Commun. **143**, 47–57 (2007)
69. de Mello, J.D.B., Binder, C., Binder, R., Klein, A.N.: Effect of precursor content and sintering temperature on the scuffing resistance of sintered self-lubricating steel. Wear. **271**, 1862–1867 (2011)
70. Ferrari, A.C., Robertson, J.: Interpretation of Raman spectra of disordered and amorphous carbon. Phys. Rev. B. **61**, 14095–14107 (2000)

71. Lespade, P., Marchand, A., Couzi, M., Cruege, F.: Caracterisation de materiaux carbones par microspectrometrie Raman. Carbon. **22**, 375–385 (1984)
72. Binder, C., Bendo, T., Hammes, G., Neves, G.O., de Mello, J.D.B, Klein, A.N., Binder, R.: Structure and properties of in situ generated 2D turbostratic graphite nodules. Carbon. **124**, 685–692 (2017)
73. Pimenta, M.A., Dresselhaus, G., Dresselhaus, M.S., Cançado, L.G., Jorio, A., Saito, R.: Studying disorder in graphite-based systems by Raman spectroscopy. Phys. Chem. Chem. Phys. **9**, 1276–1291 (2007)
74. Le Roux, H.: An electron diffraction analysis of turbostratic graphite in cemented carbides. Acta Metall. **33**, 309–315 (1985)
75. Karthik, C., Kane, J., Butt, D.P., Windes, W.E., Ubic, R.: Microstructural characterization of next generation nuclear graphites. Microsc. Microanal. **18**, 272–278 (2012)
76. Campos, K.R.: Caracterização tribológica da lubrificação sólida. Ph.D. Thesis, Universidade Federal de Uberlândia, Brazil, 2012, 162 p. In Portuguese (2012)
77. Lim, S.C., Brunton, J.H.: The unlubricated wear of sintered iron. Wear. **113**, 371–382 (1986)
78. Campos, K.R., Kapsa, P., Binder, C., Binder, R., Klein, A.N., de Mello, J.D.B.: Tribological evaluation of self-lubricating sintered steels. Wear. **332–333**, 932–940 (2015)
79. Keller, J., Fridrici, V., Kapsa, P.H., Huard, J.F.: Surface topography and tribology of cast iron in boundary lubrication. Tribol. Int. **42**, 1011–1018 (2009)
80. Zum Gahr, K.H.: Microstructure and Wear of Materials Tribolology Series, vol. 10. Elsevier, Amsterdam (1987.) 560 pp
81. Babu, S.S.: Acicular ferrite and bainite in steels. Ph.D. Thesis, University of Cambridge, UK (1992)
82. de Mello, J.D.B., Binder, C., Hammes, G., Klein, A.N.: Effect of the metallic matrix on the sliding wear of plasma assisted debinded and sintered MIM self-lubricating steel. Wear. **301**, 648–655 (2013)
83. Beattie, I.R., Gibson, T.R.J.: J. Chem. Soc. A. **6**, 980 (1970)
84. Oh, S.J., Cook, D.C., Townsend, H.E.: Characterization of iron oxides commonly formed as corrosion product on steel. Hyperfine Interact. **112**, 59–65 (1998)
85. Crockett, R.M., Derendinger, M.P., Hug, P.L., Roos, S.: Wear and electrical resistance on diesel lubricated surfaces undergoing reciprocating sliding. Tribol. Lett. **16**, 187–194 (2004)
86. Ouyang, M., Hiraoka, H.: Structure and magnetic properties of iron oxide films deposited by excimer laser ablation of a metal-containing polymer. Mater. Res. Bull. **32**, 1099–1107 (1997)

Self-Lubricating Polymer Composites: Mechanisms, Properties, and Applications

4

P. Ajay Kumar, V. Vishnu Namboodiri, Emad Omrani, Pradeep Rohatgi, and Pradeep L. Menezes

Contents

P. Ajay Kumar (✉)
Department of Materials Science Engineering, University of Wisconsin-Milwaukee, Milwaukee, WI, USA

Department of Mechanical Engineering, Indian Institute of Technology, Tirupati, Andhra Pradesh, India
e-mail: Kumar38@uwm.edu; drajaykumarp@iittp.ac.in

V. Vishnu Namboodiri
National Institute of Construction Management and Research (NICMAR), Hyderabad, Telangana, India

E. Omrani · P. Rohatgi
Department of Materials Science and Engineering, University of Wisconsin-Milwaukee, Milwaukee, WI, USA

P. L. Menezes
Department of Mechanical Engineering, University of Nevada, Reno, Reno, NV, USA

P. L. Menezes et al. (eds.), *Self-Lubricating Composites*,
https://doi.org/10.1007/978-3-662-64243-6_4

Abstract

The tribological parameters in sliding/rolling mechanism have significant role in overall performance of the materials. To design a material that offers low friction and wear, the material must have specific mechanical and physical properties. In this context the lubrication has important role and it is known that lubrication can reduce the undesired parameters during sliding/rolling. There are certain limitations in the usages of liquid lubricants such as high and low temperatures, extreme load, and speed environments. This raised the requirement of a lubricant in a solid form and coined as solid lubricant. In a situation where no external lubrication is possible, there is a need of lubricant that performs by itself which is called as self-lubricant, and the widely used self-lubricants are polymer based. This chapter provides insight into self-lubricating polymer composites, structural features, mechanisms, factors influencing tribological properties, and applications of polymer composites.

4.1 Introduction

Liquid lubricants cannot be utilized for specific applications like very low, severe temperatures and liquid contaminations. In these cases, solid lubricants are a good candidate in its performances. There are various usage routes that are available such as vapor deposition, applied as film on substrates and also by surface burnish. Over the years, it is witnessed that the solid lubricants with various reinforcements, recent emerging material, carbonous materials, can act as self-lubricating composites. These composite materials offer superior thermal, mechanical, and self-lubricating properties [1, 2]. In the past decades, the research world witnessed significant improvements in the development of reinforcement in aluminum alloys along with the development of polymer composites, typically with graphite in the matrix, and these composites exhibited superior self-lubricant properties for a wide range of materials [3–8]. Furthermore, the significant tribological improvements are observed for the composites which are reinforced with solid lubricant rather than the composites reinforced with ceramic. The micron ranged graphite particles are considered for the fabrication of composites which exhibit better tribological, mechanical, and self-lubricating properties [9–17].

The natural fiber reinforcement in a polymer matrix demonstrated superior tribological performance, greater economic viability, and greater adaptability toward specific environments [18]. The graphene nanoplatelets reinforced nanocomposites exhibited superior tribological and self-lubricating properties [19]. The self-lubricating composites can be used as alternatives for toxic petroleum-based lubricants. Furthermore, these offer greater impact in the reduction of emissions to the environment and also in the reduction of energy dissipations which improve the energy efficiencies [14, 20].

Self-lubricating composites consist of a reinforced matrix of solid lubricant additives and various other constituents and are well suitable for rolling element bearing. Furthermore, commonly used solid lubricant materials are graphite, molybdenum disulfide, layer lattice compounds, and polytetrafluoroethylene (PTFE). The performances of graphite in space applications are dormant since it requires humid/absorbed vapor environment to exhibit good performance. On the other hand, molybdenum disulfide exhibits greater performance for these applications. Some of the disadvantages of molybdenum disulfide are: (1) shortened life when long sliding in air environment, and (2) the formation of molybdenum oxide can the performance.

PTFE exhibits significant performance in both vapor and vacuum environments. The cold flow under loading conditions is one of the disadvantages of the PTFE. To eliminate this, one has to add suitable binding material. The past research indicates that very limited polymer-based self-lubricants were fabricated. Recent studies revealed that some of the polyimide polymers are capable for superior performance in vacuum environments [21]. A rigorous research is required in these areas since polymer-based lubricants have vast potential. This chapter is intended to understand the tribological properties and environmental influences on the properties of these polymer-based solid lubricants for various applications. Furthermore, various polymers, its fillers, and routes for polymer composites especially for a sliding environment will be discussed. The usages and challenges of polymers and polymer-based composites for space applications as a solid lubricant will also be discussed.

4.2 Structural Features of Polymer

The polymer molecular studies are important to understand the mechanisms involved in the physical properties, and in current scenario most of the polymer-based lubricants are organic based. Very large molecules with carbon atoms are the main component in the organic polymers. The formation of the polymer is by recurring of monomer units and the polymerization conditions influence the growth of the polymer which can be achieved to a molecular weight of several millions. The length of the chain influences the mechanical behavior of the polymers.

Polymers can be classified as thermoplastics and thermosets. The cross-linking capabilities are dormant to the thermoplastics while thermosets are highly cross-linked. In addition, another classification can be noted as amorphous or crystalline. Even in well-crystallized polymers, existence of amorphous regions is existed and vice versa and may affect physical properties. For instance the physical properties of polymer some models are required to demonstrate and presented here. Random coil, fringed micelle, folded or extended chain, and molecular domain are significant models to understand the mechanisms of physical properties. The folded chain model is considered as the much appreciated model than the others. In addition, the existence of complex aggregates of molecules, called spherulites, is the base for folded chain model. XRD studies revealed that the spherulites are comprised of plate like uniform thick lamellae. Further, the SEM and XRD studies also confirmed that

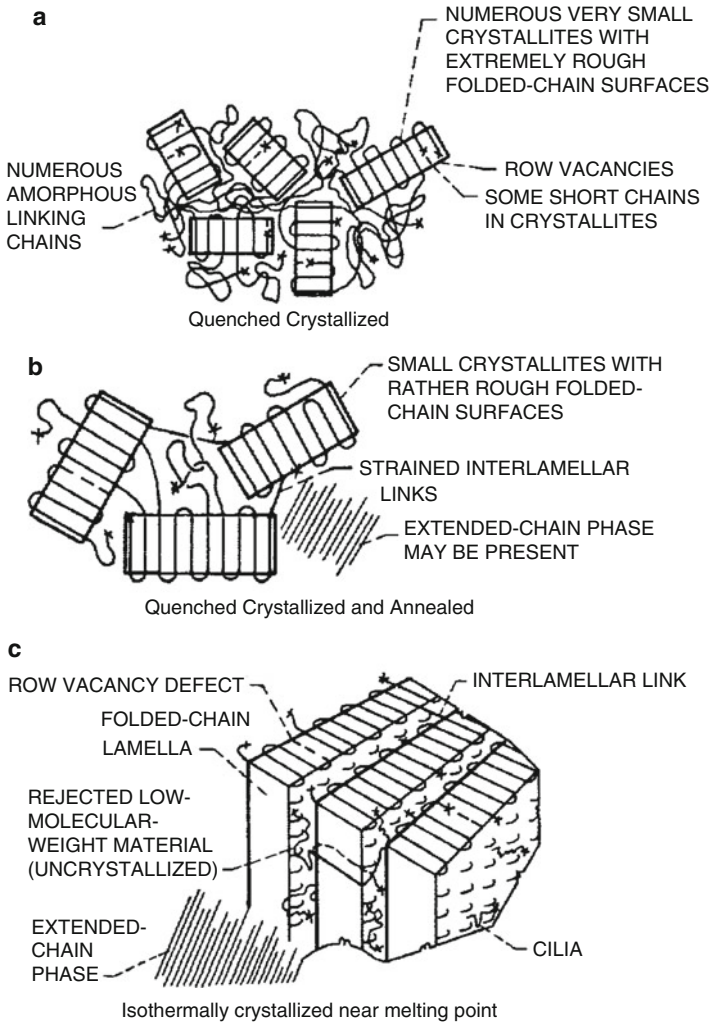

Fig. 4.1 (**a**–**c**) Shows fine structure of a polymer prepared under various conditions [22]. (**a**) Quenched crystallized. (**b**) Quenched crystallized and annealed. (**c**) Isothermally crystallized near melting point

lamellae consist of folded chains which are perpendicular to lamellae surface and are thus called as folded chain. Figure 4.1 illustrates a crystallized polymer for various crystallization conditions. Furthermore, all models also exhibited [22]. The distance between the folds determines extended (>200 nm) or fully extended (no presents of folds) chain crystal.

Melt by regulating crystallization, annealing, and mechanical stress are the routes to the formation of extended chain crystals. The mechanical stress method exhibits the chain unfolding features and two models have been proposed [23]. In the first

model, plastic deformation influences the chain unfolding in the applied force direction. In second model, shearing deformation influences the chains gradually to become tilted by twisting and slipping in along the direction of force. In general, the low friction and wear properties are exhibited in exteneded chain structure.

4.3 Polymer Composites: Self-Lubricating

The addition of various materials to polymers is carried out to improve the load-carrying capacity, tribological performances, and thermal conductivity. The load-carrying capacities can be improved by adding the fibers as reinforcement materials to the polymer and together they form the polymer composites. Also, additives used to improve the tribological properties may reduce the load-carrying capacities (may have easy slip planes). Thus, thorough considerations and understandings are required to meet both requirements. This can be achieved by reinforcement of fibers and lubricating additives, or combination of non-lubricating and lubricating fibers. Small pieces of fibers can be dispersed in the matrix. Improvement in the thermal conductivity of the polymer composite can be achieved by dispersing thermally conductive materials in the matrix. In general, combinations of polymers and various additives can be used [24]. As discussed in an earlier section, the usage of polymer composites for specific applications requires understanding and the possible polymer composites in space applications are PTFE/glass fiber, PTFE/glass fiber/MoS_2, Polyimide/MoS_2 and PTFE/Woven glass fiber/resin as bearings, gears, and cages.

4.4 Lubrication and Wear Mechanisms of Polymer Composites

The success of the solid lubricant determined by the level of holding the stress formed due to the loading and tangential friction stresses for polymer-based composites. If not, they may experience plastic deformations, brittle fracture evolutions, high wear, and even catastrophic failures. In some cases, it is observed that rapid wear sustains until the polymer supports the progressive increase in the contact area. Also, dynamic stress highly influences the wear mechanisms. A lower dynamic stress is beneficial to exhibit a mild wear behavior. These infer that stress plays vital role in the performance of self-lubricating polymer-based composites. In general, while designing these types of lubricants an account of stress must also be considered with greater attention for better performances.

The synergy between polymer and additives is important in terms of their tribological properties and their working environments even when they are having significant load-bearing capacity [25]. A shear layer development in the mating surfaces will support the improved properties for designing better lubricants. This layer reduces the adhesive and abrasive action in the sliding surfaces and stresses in the polymer surfaces. Also, a thin layer will be adequate to exhibit these improved properties. Some polymer materials have self-forming ability of shear layer.

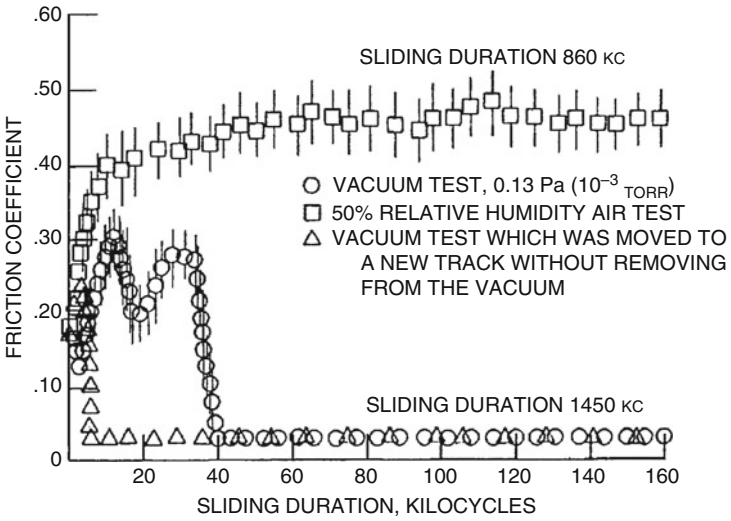

Fig. 4.2 The friction responses of a commercially available polyimide in various environments [27]

The extended chain mode of PTFE chain in the surface reduces shear and results in low friction [26]. Furthermore, bulk PTFE may not have good load-bearing capacity. In these conditions, the usage of PTFE as reinforcement in body and as coatings or films is the preferred way to achieve greater life.

In vacuum and air environments, some polyimides form thin shear layer at the surfaces [21, 27].

The tribological performance (friction and wear) of the polyimides are superior in nature for various environmental conditions like vacuum and high temperature. Furthermore, one of the reasons behind performance is the formation of extended chain molecule [27]. The load-bearing capacities of these polyimides are greater as compared with PTFE and also exhibit low friction. This infers that in some special cases like space applications, the additives are not required to reinforce. On the other hand, the tendency to absorb water and the subsequent increase in the friction are the challenges in the development and applications of polyimides. Thus, removal of water vapor and water vapor layer is important while using polyimides for a specific application.

The friction coefficients of polyimides in various environmental conditions are illustrated in Fig. 4.2; the result shows an increase in the coefficient of friction in air with 50% humidity conditions, whereas the coefficient of friction decreases in the vacuum conditions [27].

Ultra-high-molecular-weight-polyethylene (UHMWPE) polymers offer greater load-bearing capabilities. On the other hand, this polymer has poor temperature withstanding capabilities, and this infers that these polymers may have good performance in low temperature conditions.

The quality of the shear layer formed determines lubrication performance of the composites. This shear layer has significant role in maintaining the performance.

Thus, quality and reliability are important in bonding to the polymer surface and this can be called in a short way as "flowing into itself." The layer movement without failure during sliding determines the sustainability of the lubrication performance. Furthermore, the factors influencing the layer must be analyzed thoroughly especially the fatigue. The formation and specialties of transfer films are important in the wear behavior. A thin film offers good wear performance, while thick film promotes the adhesive forces, resulting in severe wear.

4.5 Lubricating Mechanisms: Transfer Film of Polymer Composites

The shear layer and its mechanisms play important role in various aspects as stated in the earlier section. It can be noted that the shear emerges within shear layer on the bulk surface, transfer film on counter surface, or it can occur in between the both. The mechanism involved in the performance of ball bearing uses a double transfer lubricating film as shown in Fig. 4.3.

The influence of load in an ambient air environment on the double transfer of PTFE (Rulon-A and 5% MoS_2) composite was studied by [29] on testing apparatus (Fig. 4.4). The result indicated that as increase in load leads to slight decrease in the roughness of the wear track. In addition, at the mean stress level of 1.38 GPa the transfer film was insufficient to prevent roughening of the surfaces (Fig. 4.5). These indicate the importance of the limiting stress for the effective transfer film at ambient air atmosphere. The double transfer lubrication regime can be successfully used in higher load conditions only. Thus, it can be a potential candidate for the various space applications.

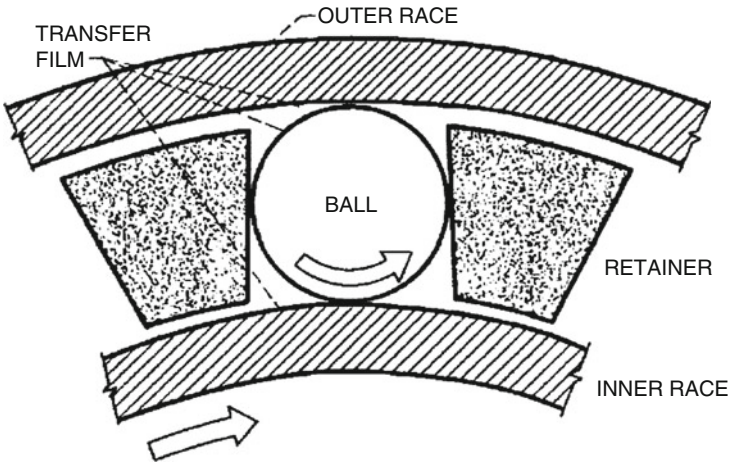

Fig. 4.3 Ball bearing film transfer mechanism [28]

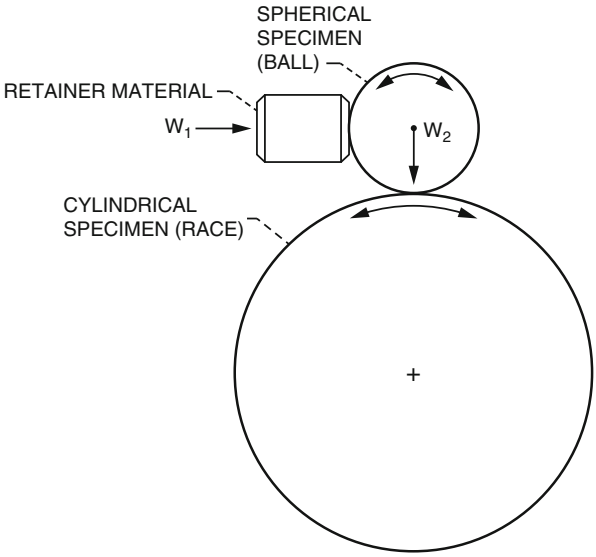

Fig. 4.4 Transfer analysis equipment [29]

4.6 Factors Influencing Polymer Composite Wear and Transfer

This section deals with the factors that affect the performance of polymer composites.

4.6.1 Load/Stress

As stated in an earlier section, it is clear that the polymer film and its wear behaviors are highly influenced by the load and stress [30]. The mild wear was exhibited on low loads and severe wear was exhibited at high loads. The formation of shear layer and its delamination features and thin transfer film results in the mild wear behavior. The formation of brittle fracture or severe plastic deformations results in severe wear. In addition, polyamide-bonded graphite fluoride film of 0.0025 cm thickness exhibits the mild wear and severe wear regime specialties as stated above [31]. A linear progress of wear rate was observed in mild wear regime and an exponential progress was observed in severe wear regime.

4.6.2 Contact Area

The contact stress and its effects in the transfer film are important entities on the performance of polymer-based composites. The contact stress is deducted from the contact area. Thus, in a case where the load cannot be reduced further, another alternative is to increase the contact areas which will helps to reduce the contact

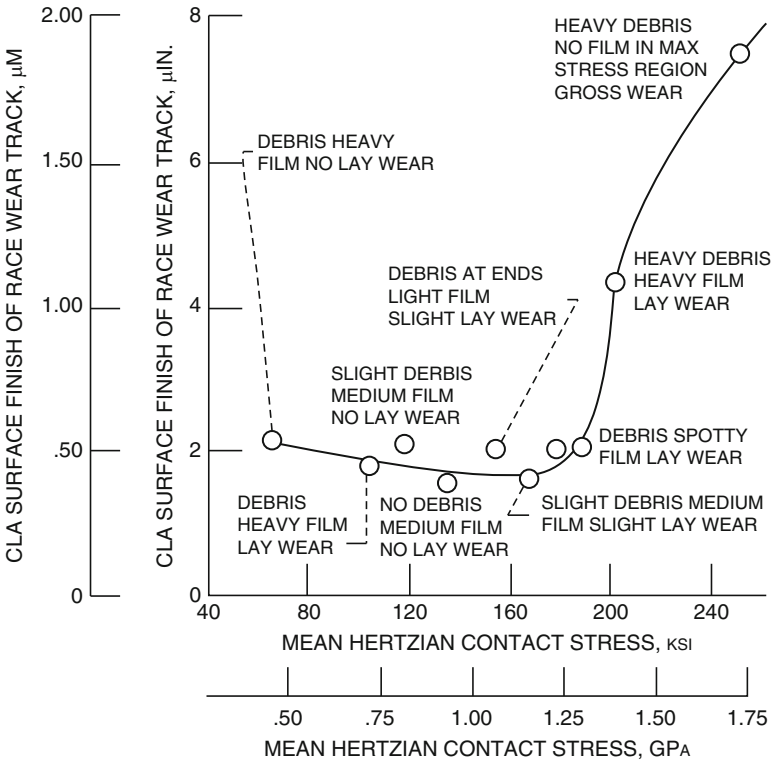

Fig. 4.5 Surface finish of race wear track Vs mean Hertzian contact stress (lubricated with a Rulon-a + 5%MoS_2 transfer film) [29]

stress and the resulting mild wear [30]. Figure 4.6 illustrates the variation of wear rates for polyimide-bonded graphite fluoride film. The formation of transfer film was influenced by the contact areas. The increased contact area and the lower stress lead to poor tribological performance. This is due to the formation of ridges and this increases the localized stress and adhesion. This infers that the contact area plays an important role in the optimum designing of the lubricant.

4.6.3 Sliding Speed

The sliding speed influences the generation of heat due to friction at higher speed. This affects the performance of the additives in the composite matrix. Also, in some cases this frictional heat will help in many ways such as removal of water vapor, influences the molecular relaxation in the polymer molecule, and thus improves its mobility. Furthermore, the sliding speed influences the wear debris size and wear. However, the performance of wear mechanisms is highly influenced by properties of shear film and transfer film. The high sliding speed restricts the reorientation of

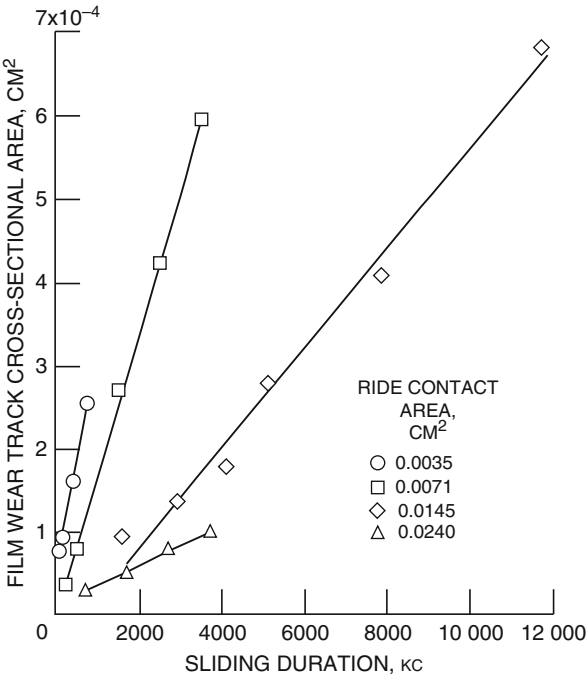

Fig. 4.6 Polyimide-bonded graphite fluoride film wear rate Vs sliding duration for a constant load sliding [32]

molecular chains and thus results in the high wear particles and high wear. In addition, the process parameters like sliding speed optimization are important in the design to exhibit superior performances.

4.6.4 Environment

The lubricants like graphite and molybdenum disulfide are highly influenced by the environmental conditions. These lubricants are in two extremes; the graphite exhibits good lubrication performance in absorbed gas or vapor atmosphere, whereas the molybdenum disulfide exhibits better performance in the absence of absorbed gas or vapor atmosphere. In addition, the polymer composites are also highly influenced by the environment during sliding. This phenomenon is due to the additives that are sensitive to the environment. All of these lubricants the PFTE exhibit superior performance in various environmental conditions. The polymer having free hydrogen is highly influenced by the environmental conditions like absorbed vapor and water vapor regimes. The poor mobility of the molecules in the polymer is highly influenced by the presence of water and restricts formation of thin surface layers. In general, polyimides demonstrate better performance in vacuum conditions [27].

4.6.5 Counter Surface Topography

The tribological performance of polymer composites is highly dependent on the counter face material and its specialties. If the counterface is too rough, it restricts the formation of shear and transfer film and thus affects the important tribological properties. Figure 4.7 illustrates the effect of the surface roughness of counter surface for various materials like stainless steel, etc. and Fig. 4.8 illustrates the effect of the surface roughness graphite-fiber-reinforced polyimide composites sliding against different materials. It can be noted that Pyrex glass offers lowest possible frictional coefficient. However, highest frictional coefficient was observed on SS 301 [32]. The results show that at lower roughness counter surfaces exhibit lower wear rates.

Furthermore, the low root mean square (RMS) value and center line average (CLA) value of roughness not always indicates the smoothness of the surface. The over polishing may deteriorate the softer materials and form the hard material in the counterface surface which results in severe abrasion in polymer surface. Especially this behavior can be seen for overpolished 440C HT Stainless Steels against a polymer surface. In initial sliding the surface finish and material type have a dormant influence on the coefficient of friction. As sliding distance progress surface finish and material type influence the coefficient of friction significantly. The Pyrex glass has the smoothest surface and has ability to form extremely thin transfer films for the best performance.

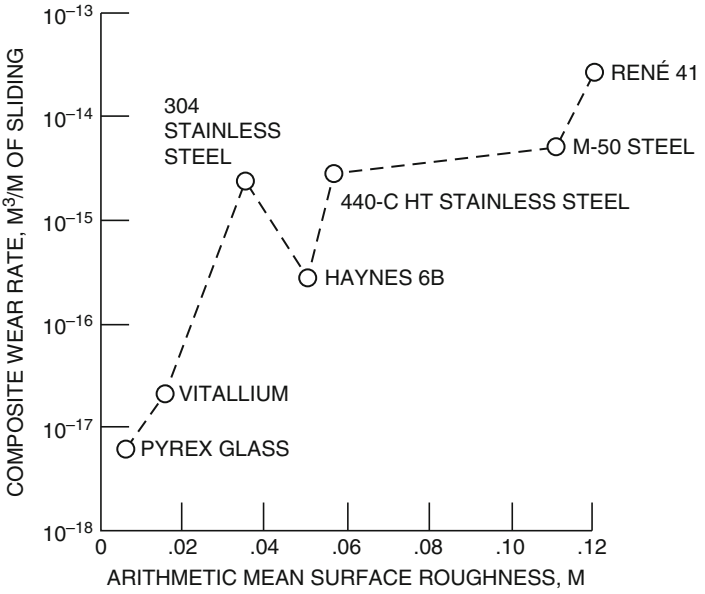

Fig. 4.7 Composite pin wear rate vs arithmetic mean surface roughness for various materials [32]

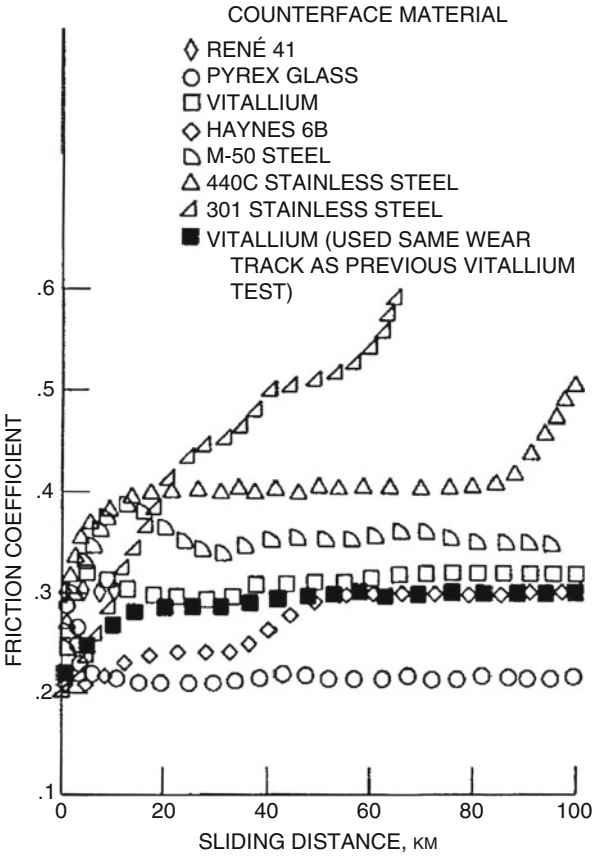

Fig. 4.8 Friction coefficient in 50% relative humidity air at 25 °C [32]

4.6.6 Cleanliness

The surface cleanliness is one of the factors to be considered with greater attention. A dirty surface may exhibit an abrasive action and resulting poor tribological performances. Figure 4.9 illustrates the embedded small hard particles into an UHMWPE polymer solid which acts like an abrasive particle and wore a grove in 440C stainless steel counterface [30].

4.6.7 Temperature and Molecular Relaxation

As discussed earlier, the interrelationship between temperature and molecular relaxation is important for the performance of the composite. The movement of chain, or can be called as mobility, depends on certain temperature. This can be above or below the transition temperature which results in high mobility and low mobility,

Fig. 4.9 Surface profile of the sliding contact areas [30]

respectively. In general, the tribological performances of the polymer composites are highly dependent on temperature and subsequent influence on the molecular mobilities. Also, the limited molecular movement will reduce the formation of thin shear layer. Torsional braid analysis (TBA) method is good candidate for analysis of relaxation temperatures [33]. Fusaro [23] conducted studies to understand the synergy of molecular relaxation by TBA method. Polyimide (PI 4701) was considered for the studies and the results demonstrated TBA peaks. The highest peak correlated to glass transition temperature (α-peak). Furthermore, highest peak compared with coefficient of friction shows significant change and another correlated to B-H20 peak (due to absorbed water vapor). From Fig. 4.10, if polyimide is heated to 500 °C in a dry argon environment, it increases the glass transition temperature to 500 °C which offers low coefficient of friction in the range of 300–500 °C. In addition, a low coefficient of friction can be achieved even at 50 °C and the absorbed water vapor should be removed from the polyimide surface as shown in Fig. 4.10a, b.

The molecular relaxation in PTFE-based composite also exhibited couple of relaxations well below the ambient temperatures but not exceptional as they are at or above ambient temperature (~25 °C). Furthermore, the restriction of molecular mobility of PTFE chain for a specific region results in the low coefficient of friction. Also, the additives in the polymer composites influence the lubrication properties. Furthermore, some polymers exhibit an independent behavior to the temperature for their tribological performance.

4.7 Tribological Applications of Polymer Composites

4.7.1 Gears

The gears made of polymer composites are currently being used in light load and space applications which require high precision. These gears run against the SS or Al alloys. The stiffness and hardness with low coefficient of friction are required for these gears. Furthermore, the major challenge in the gear design is the accommodation of physical properties and tribological performance for a specific application. Also, it can be noted that this scenario limits the common polymer usages for various applications. Polyimides, polyamides (nylons), polyamide-imides, and polyacetals

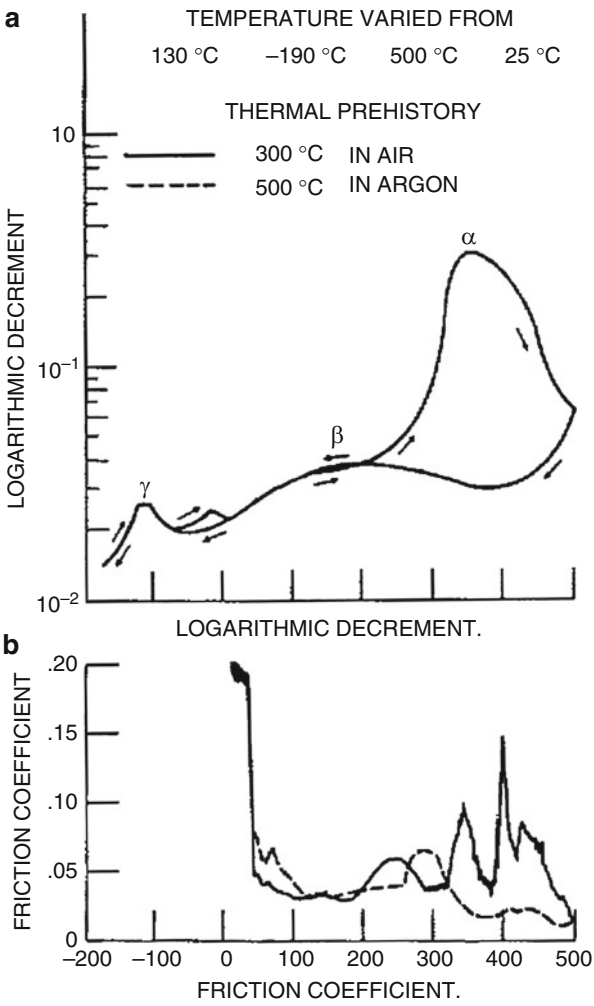

Fig. 4.10 (**a**) Logarithmic decrement comparison and (**b**) the friction coefficient variations for a polyimide film in various temperature regime [23]

are various polymers that can be used for specific applications along with PTFE. In the reinforcement, the fiber glass and MoS_2 are also considered to provide the low coefficient of friction. In addition, in some cases the polyimide with MoS_2 powder additive are being used in the space applications. This offers greater flexibility in the manufacturing and machining regimes to produce fine pitch gears. High-pressure laminate of cotton fabric and a phenolic polymer also can be utilized for the fabrication of gears with greater benefits but offers difficulty in precise manufacturing and machining process [34]. The tribological performance of certain plastic gears was established by Steven [34]. Table 4.1 illustrates the tribological performance of various types of plastic gears.

Table 4.1 Tribological response of plastic gears [34]

Test	Materials		Tooth load, N/mm	Pinion speed, rpm	Lubricant	Total pinion revs	Tooth flank wear rate, mm depth per encounter	
	Pinion	Wheels					Pinion	Wheels
1	Carbon fibre inpoly-acetal	Stain-less steel	[a]21 (60)	50	Dry	5×10^4	1×10^{-7}	Zero
2	↓	↓	21	50	Dry	3×10^5	7×10^{-8}	↓
3			21	50	↓	5×10^5	7×10^{-8}	
4			21	100		7×10^5	2×10^{-8}	
5			21	200		16×10^5	5×10^{-9}	
6			21	500		30×10^5	5×10^{-9}	
7			21	1000		60×10^5	5×10^{-9}	
8			7(35)	1000		30×10^5	[b]3.5×10^{-9}	
9			3(23)	1000		30×10^5	[b]2×10^{-9}	
10	↓	↓	1(13)	1000	↓	30×10^5	[b]1×10^{-9}	↓
11	Vespel SP31	Stain-less steel	21 (50)	50	Dry	5×10^4	1×10^{-8}	Zero
12	↓	↓	21	50	↓	3×10^5	7×10^{-9}	↓
13			↓	50		5×10^5	7×10^{-9}	
14				100		7×10^5	9×10^{-9}	
15				200		16×10^5	6×10^{-9}	
16				500		30×10^5	5×10^{-9}	
17				1000		60×10^5	4×10^{-9}	
18			7(30)	1000		30×10^5	3×10^{-9}	
19			3(20)	1000		30×10^5	2×10^{-9}	
20	↓	↓	1(10)	1000	↓	30×10^5	1×10^{-9}	↓
21	Vespel SP8	Stain-less steel	7	200	Dry	1×10^5	4×10^{-8}	Zero
22	↓	↓	↓	200	Dry	40×10^5	4×10^{-9}	↓
23				200	BP110	1×10^5	8×10^{-8}	
24	↓	↓	↓	200	BP110	40×10^5	4×10^{-9}	↓

[a]Tooth contact stress in N/mm^2

[b]Steady state wear rate after running-in wear completed

Polyimide and polyacetals gears running against materials like SS, Ti, or Al for low loads exhibited superior tribological performance which was studied by European Space Tribology Lab (ESTL). In comparison, with polyimide and polyacetals, the polyimide dominates in the low wear rate even the polyacetals reinforced with carbon fiber with a maximum load of 10 N/mm tooth width.

PTFE + MoS_2 + glass fibers-based polymer composite has been studied by Vest [36] and used as retainer material for oscillating bearings. The results show that the usage of this composite performed in a significant way even after 1×10^6 cycles of testing. In addition, even after 7.6×10^7 cycles at 100 rpm the bearings are in good conditions at 7 N. Furthermore, the loading of the bearing also influences the generation of wear debris. High wear debris is observed in the unidirectional test having loading value of 23 N. This implies the poor performance in the higher loads.

PTFE-MoS_2 polymer composite as a cage material which is used in gimbal ball bearings was studied by Christy [35] who observed the potential usage since they produce uniform transfer films.

The ESA demonstrated potential usage capabilities of PTFE/glass fibers/MoS_2 composite for various bearing applications [37]. They observed that the composite exhibits superior performances, which is limited to maximum Hertzian contact stress of 1200 MN/m^2 at 20 °C. Also, they demonstrated the composite without MoS_2 and claimed that there are a lot of advantages for the usage of MoS_2 as an additive in the matrix. Some of the advantages are prevention of tick transfer which results in better performance.

The torque results of various lubricants like sputtered MoS_2, ion-plated lead, and PTFE composite cage show that the sputtered MoS_2 bearing failed (b/w 0.7 to $3.6x10^6$) in certain revolutions with low torque noise. In the case of ion-plated lead and PTFE composite cage, both performed in a similar manner, but greater torque noise was observed in the ion-plated lead cage [37]. A comparison of torque properties was established for above PTFE polymer composites with various cases by Roberts [38] (Fig. 4.11). The results indicate that sputtered MoS_2 film has significant torque performances.

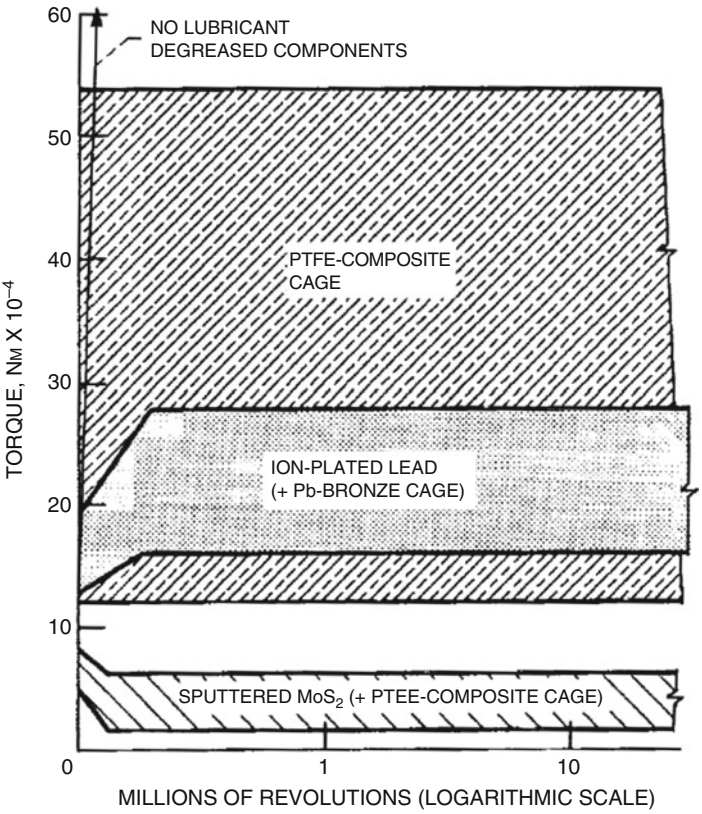

Fig. 4.11 Mean torque bands from repeated tests of solid lubricated ball bearing (ED20: 40 N preload) preload pairs in vacuum conditions [38]

4.7.2 Cryogenic Ball Bearings

The cryogenic technologies are backbone of the space missions. In which contains various electrical instruments, devices which required to be working in a cryogenic temperature [39]. Apart from the instruments and devices, it is quite important to the mechanical components and its performance in the cryogenic temperatures for various space vessels. Some of the examples are high speed turbo pumps and cryogenic engines which require bearings that are capable to produce significant performances in various harsh cryogenic environments where conventional bearings cannot adopt. In this situation the importance of solid lubricants arises.

NASA established notable research works related to the development of the self-lubricating composite materials and its usages are bearings for cryogenic environments [28, 40–45]. The turbopumps consist of several ball bearings which require thorough design considerations for better performance. For this, one has to give importance to ball race material, self-lubricating cage material, cage with superior physical and mechanical properties, and several design factors to reduce the internal heat generation.

PTFE are considered as the best lubricant for these cryogenic applications. On the other hand, PTFE offers poor strength; cold flow and poor thermal conductivity are some of the challenges. In the case of heat generation, the PTFE dominates the performances. This opens up the research opportunities to reinforce the PTFE with other additives to improve the performances in various aspects. In connection to this, an early PTFE composite formulation and its features are illustrated in Table 4.2 as bearings which serve in extreme conditions.

To study the formation and specialties transfer film form cages to bearing inner race was established through profile tracing technique. Figure 4.12 illustrates surface profile for a specific composite cage of inner-race groove of a bearing with a laminated-glass cloth with PTFE binder cage material having shaft speed, 20,000 rpm; thrust load, 200 pounds; coolant, in a hydrogen gas environment [28].

Table 4.2 Properties of PTFE formulated composite bearing cages [28]

Bearing designation	Cage material	Composition, wt%	Cage construction
A	Laminated-glass cloth with PTFE binder	38% glass cloth laminates with 62% PTFE binder	One-piece body with riveted aluminum side plates
B			
C	Glass-fiber-molybdenum disulfide filled PTFE	15% glass fibers, 5% molybdenum disulfide, 80% PTFE	One piece body with no external support
D			
E	Glass-fiber-filled PTFE	15–20% glass fibers, balance PTFE	One-piece body with one-piece riveted aluminum shroud
F			
G	Bronze-filled PTFE	30% bronze powder, 70% PTFE	One-piece body with no external support
H			

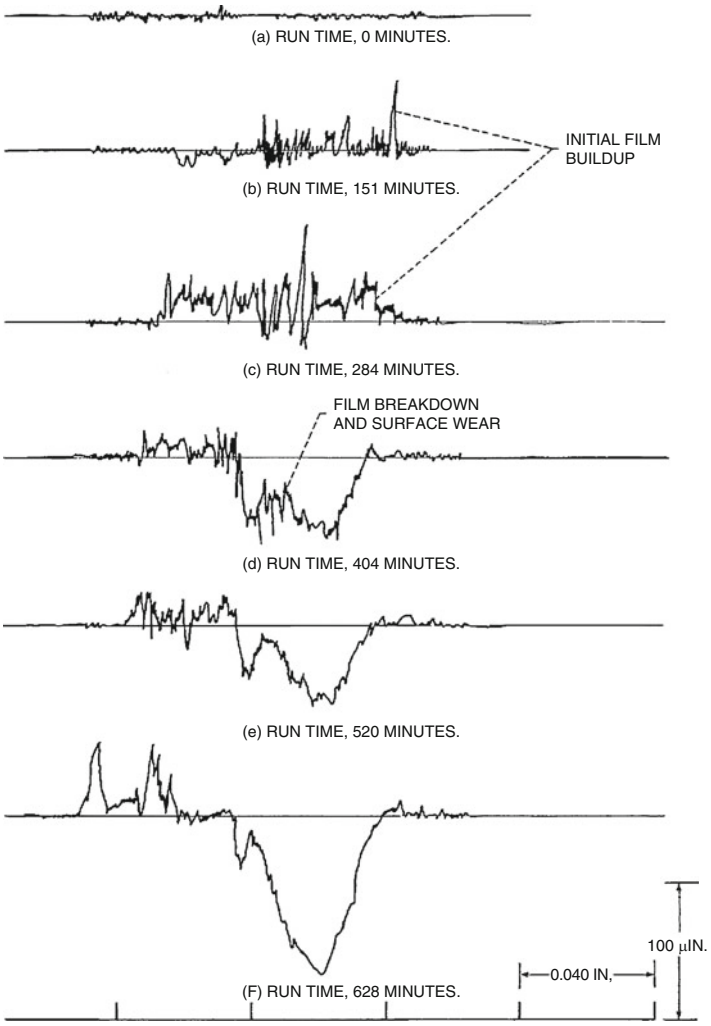

Fig. 4.12 Progressive profile traces of inner-race groove of bearing a with a laminated-glass cloth with PTFE binder cage material [28]

A considerable deposition film was observed after 284 min in the inner race along with scratches formed by abrasive action of glass-fibers in the cage material. This trend breaks down as continuous running progress and finally results in an increase in the wear. After 10 h the bearing progress to a failure. This may be due to the breakdown of the film and subsequent increase in the abrasive action (Fig. 4.13) which indicates alternate layers of glass cloth and PTFE in which soft PTFE worn in a short period of time and then exposed to the glass fiber and eventually fragmented and submerged into the transferred PTFE film. This catalyzed the abrasive action which soon influences the breakdown of the transfer film and increases the wear rates.

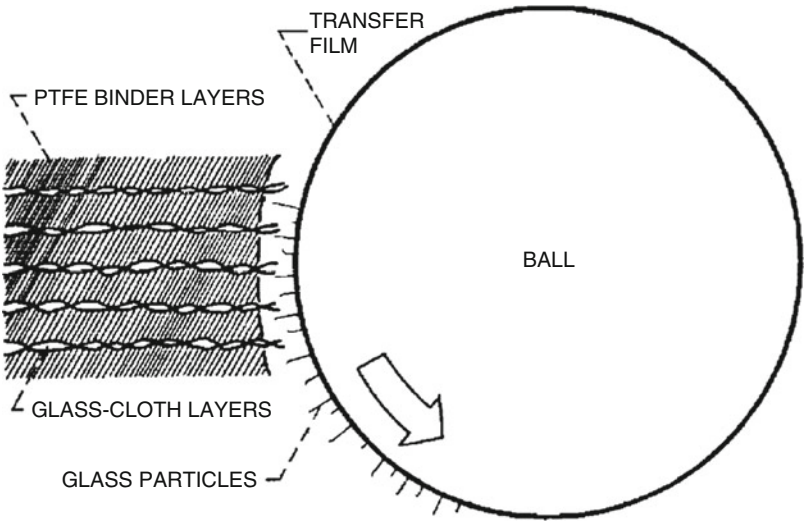

Fig. 4.13 Progress of PTFE binder retainer wear of ball bearing [28]

In general, PTFE composites exhibit better lubrication performance but limited to a period of 10 hrs. Figure 4.14 illustrates the percentage weight loss for all four types of PTFE and the results show that all four have significantly low weight loss. Among those the bronze cage exhibited maximum than the others.

The performance of PTFE composite retainer material was experimentally evaluated by Cunningham and Anderson [43]. The radial load varies from 450 to 2700 N with a speed up to 30,000 rpm. This test has been done in 40-mm-bore ball bearings. The results show that laminated glass cloth-PTFE binder provides better wear resistance among the three PTFE composites (Fig. 4.15). Also, these materials showed better performance in liquid hydrogen pumps rather than in liquid oxygen pumps. In liquid oxygen pumps the laminated glass cloth-PTFE as a cage material exhibits excessive wear and is to be reconsidered for space shuttle main engine applications [46, 47].

4.7.3 Pin Joint Applications

The pin joints are used to establish the articulated motions. The reliability of these joints is to be improved carefully. One such study was conducted by Zhu et al. [48]. The PEEK and its composites (reinforced with 30 wt% carbon fiber, 30 wt% glass fiber, and 10 wt% carbon fiber, 10 wt% graphite and 10 wt% PTFE) were considered for their studies. Figure 4.16 shows the variation of coefficient of friction for different materials. It was observed that for lower and higher loads the composite C (10 wt% carbon fiber, 10 wt% graphite, and 10 wt% PTFE reinforced with PEEK) shows better performance than PEEK and other composites. However, the

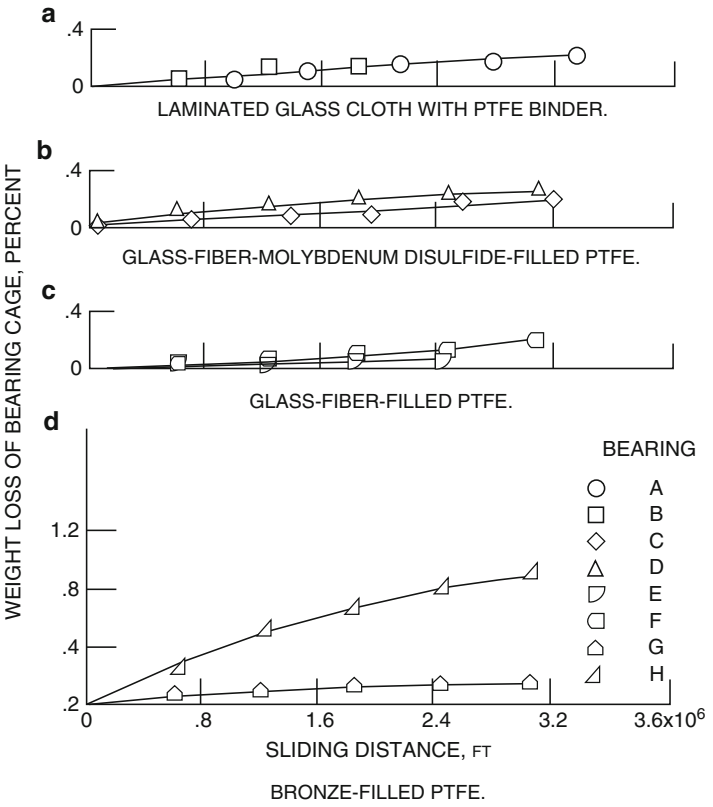

Fig. 4.14 Bearing cage weight loss versus sliding at specific condition for (**a**) laminated glass cloth-PTFE binder, (**b**) glass-fiber-molybdenum disulfide filled PTFE, (**c**) glass-fiber-filled PTFE, and (**d**) bronze-filled PTFE [28]

coefficient of friction for composite B (30 wt% glass fiber) was observed to be increased as the normal load increases.

Recently, PEEK composites utilized as bush materials for articulating revolute pin joints were investigated by Zhu et al. [49]. It was observed that the PEEK-based composite material formulated by PTFE, graphite, and carbon fiber shows better performance than other composites.

4.8 Concluding Remarks

An overview of self-lubricating polymer composites was demonstrated with information related to their influencing factors, tribological properties, and film transfers. Furthermore, environmental conditions also have significant role in tribological properties. Especially a distinct performance was observed in air and vacuum environments. The extreme testing resulted in a good understanding of the influences

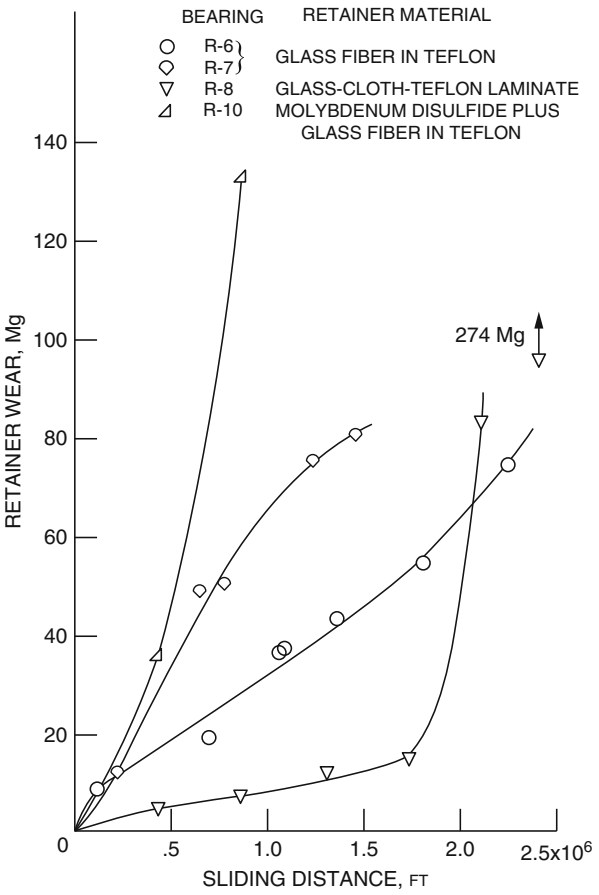

Fig. 4.15 Bearing cage weight loss as a function of sliding distance at specific conditions [45]

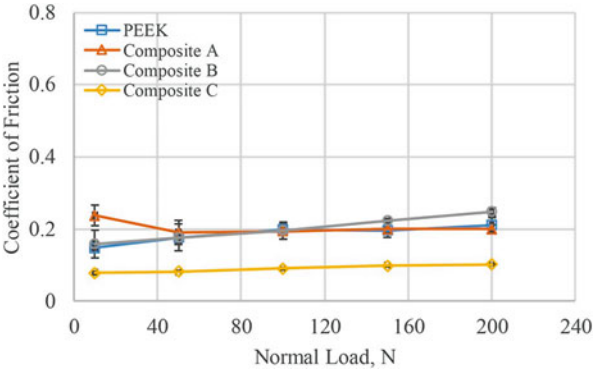

Fig. 4.16 Variation of coefficient of friction vs normal load for various materials [48]

of various parameters. It is noted that the behavior of the solid lubricants may vary for different conditions. The performances of end use devices in real time also may exhibit variable performances as compared with a controlled testing condition. Rigorous and extended research is required to understand the behavior of polymer composites in various environments for a specific application. It is important to extract the superior properties of various polymers and polymer composites for wide range of applications, which are still in a progressive path, and there are special factors that significantly influence the performance of the designed components, especially the transfer film mechanisms and its features, loading, and environmental conditions. A good self-lubricating polymer composite must have significant tribological, mechanical, and thermal properties.

References

1. Moghadam, A.D., Omrani, E., Menezes, P.L., Rohatgi, P.K.: Mechanical and tribological properties of self-lubricating metal matrix nanocomposites reinforced by carbon nanotubes (CNTs) and graphene: a review. Compos. Part B Eng. **77**, 402–420 (2015)
2. Dorri-Moghadam, A., Schultz, B.F., Ferguson, J., Omrani, E., Rohatgi, P.K., Gupta, N.: Functional metal matrix composites: self-lubricating, self-healing, and nanocomposites-an outlook. JOM. **66**(6), 872–881 (2014)
3. Baradeswaran, A., Perumal, E.: Wear and mechanical characteristics of Al 7075/graphite composites. Compos. Part B. **56**, 472–476 (2014)
4. Baradeswaran, A., Perumal, A.E.: Study on mechanical and wear properties of Al 7075/Al_2O_3/graphite hybrid composites. Compos. Part B. **56**, 464–471 (2014)
5. Iacob, G., Ghica, V.G., Buzatu, M., Buzatu, T., Petrescu, M.I.: Studies on wear rate and microhardness of the Al/Al_2O_3/Gr hybrid composites produced via powder metallurgy. Compos. Part B Eng. **69**, 603–611 (2015)
6. Liu, X.-B., Liu, H.-Q., Liu, Y.-F., He, X.-M., Sun, C.-F., Wang, M.-D., et al.: Effects of temperature and normal load on tribological behavior of nickel-based high temperature self-lubricating wear-resistant composite coating. Compos. Part B Eng. **53**, 347–354 (2013)
7. Rohatgi, P.K., Tabandeh-Khorshid, M., Omrani, E., Lovell, M.R., Menezes, P.L.: Tribology of metal matrix composites. In: Tribology for Scientists and Engineers, pp. 233–268. Springer, Berlin (2013)
8. Kestursatya, M., Kim, J., Rohatgi, P.: Wear performance of copper-graphite composite and a leaded copper alloy. Mater. Sci. Eng. A. **339**(1), 150–158 (2003)
9. Liu, Y., Rohatgi, P., Ray, S.: Tribological characteristics of aluminum-50 vol% graphite composite. Metall. Trans. A. **24**(1), 151–159 (1993)
10. Rohatgi, P., Ray, S., Liu, Y.: Tribological properties of metal matrix-graphite particle composites. Int. Mater. Rev. **37**(1), 129–152 (1992)
11. Liu, Y., Lim, S., Ray, S., Rohatgi, P.: Friction and wear of aluminium-graphite composites: the smearing process of graphite during sliding. Wear. **159**(2), 201–205 (1992)
12. Krishnan, B., Raman, N., Narayanaswamy, K., Rohatgi, P.: Performance of an Al_2Si-graphite particle composite piston in a diesel engine. Wear. **60**(1), 205–215 (1980)
13. Badia F, Rohatgi P. Dispersion of graphite particles in aluminum castings through injection of the melt. 1969
14. Menezes, P.L., Rohatgi, P.K., Lovell, M.R.: Self-lubricating behavior of graphite reinforced metal matrix composites. In: Green Tribology, pp. 445–480. Springer, Berlin (2012)
15. Menezes, P.L., Reeves, C.J., Rohatgi, P.K., Lovell, M.R.: Self-lubricating behavior of graphite-reinforced composites. In: Tribology for Scientists and Engineers, pp. 341–389. Springer, Berlin (2013)

16. Menezes, P.L., Rohatgi, P.K., Lovell, M.R.: Self-lubricating behavior of graphite reinforced metal matrix composites. In: Green Tribology Biomimetics, Energy Conservation and Sustainability, pp. 445–480. Springer, Berlin (2012)
17. Omrani, E., Menezes, P.L., Rohatgi, P.K.: State of the art on tribological behavior of polymer matrix composites reinforced with natural fibers in the green materials world. Int. J. Eng. Sci. Technol. **19**, 717–736 (2016)
18. Tabandeh-Khorshid, M., Omrani, E., Menezes, P.L., Rohatgi, P.K.: Tribological performance of self-lubricating aluminum matrix nanocomposites: role of graphene nanoplatelets. Int. J. Eng. Sci. Technol. **19**, 463–469 (2016)
19. Omrani, E., Moghadam, A.D., Menezes, P.L., Rohatgi, P.K.: Influences of graphite reinforcement on the tribological properties of self-lubricating aluminum matrix composites for green tribology, sustainability, and energy efficiency – a review. Int. J. Adv. Manuf. Technol. **83**, 325–346 (2016). https://doi.org/10.1007/s00170-015-7528-x
20. Omrani, E., Moghadam, A.D., Algazzar, M., Menezes, P.L., Rohatgi, P.K.: Effect of graphite particles on improving tribological properties Al-16Si-5Ni-5 graphite self-lubricating composite under fully flooded and starved lubrication conditions for transportation applications. Int. J. Adv. Manuf. Technol. **87**, 929–939 (2016). https://doi.org/10.1007/s00170-016-8531-6
21. Fusaro, R.L.: Effect of atmosphere and temperature on wear, friction, and transfer of polyimide films. ASLE Trans. **21**(2), 125–133 (1978)
22. Hoffman, J.D., Williams, G., Passaglia, E.: Analysis of the alpha, beta, and gamma relaxations in polychlorotrifiuorethylene and polyethylene: dielectric and mechanical properties. In: Boyer, R.F. (ed.) Transitions and Relaxations in Polymers. J. Polym. Sci: Pt. C, Polym. Symp. 14, 173–235 (1966)
23. Fusaro, R.L.: Friction transition in polymide films as related to molecular relaxations and structure. NASA TN D-7954 (1975)
24. Booser, R.E. (ed.): CRC Handbook of Lubrication. Theory and Design, vol. 2. CRC Press, Boca Raton (1984)
25. Fusaro, R.L.: Self-lubricating polymer composites and polymer transfer film lubrication for space application. NASA TM102492 (1990)
26. Pooley, C.M., Tabor, D.: Friction and molecular structure: the behavior of some thermoplastics. Proc. R. Soc. Lond. A. **A329**, 251–274 (1972)
27. Fusaro, R.L.: Evaluation of several polymer materials for use as solid lubricants in space. STLE Tribol. Trans. **31**(2), 174–181 (1988)
28. Brewe, D.E., Scibbe, H.N., Anderson, N.J.: Film-transfer studies of seven ball-bearing retainer materials in 60 °R (33 °K) hydrogen gas at 0.8 million DN value. NASA TN D-3730 (1966)
29. Kannel, J.W., Rolling, D.K.F.: Element Bearings in Space. The 20th Aerospace Mechanisms Symposium, NASA CP-2423, pp. 121–132. National Aeronautics and Space Administration, Washington, DC (1986)
30. Fusaro, R.L.: Effect of load, area of contact and contact stress on the wear mechanisms of a bonded solid lubricant film. Wear. **75**, 403–422 (1982)
31. Fusaro, R.L.: Mechanisms of lubrication and wear of a bonded solid-lubricant film. ASLE Trans. **24**(2), 191–204 (1981)
32. Fusaro, R.L.: Counterface effects on the tribological properties of polyimide composites. Lubr. Eng. **42**(11), 668–675 (1986)
33. Gillham, J.K.: Torsional braid analysis (TBA) of polymers. In: Dawkins, J.V. (ed.) Developments in Polymer Characterisation – 3. Springer, Dordrecht (1982). https://doi.org/10.1007/978-94-009-7346-6_5
34. Stevens, K.T.: The tribology of gears for satellite applications. In: Guyenne, T.D., Hunt, J.J. (eds.) First European Space Mechanisms and Tribology Symposium, ESA-SP-196, pp. 131–146. European Space Agency, Paris (1983)
35. Todd, M.J.: Solid lubrication of ball bearings for spacecraft mechanisms. Tribol. Int. **15**(6), 331–337 (1982)
36. Vest, C.E., Ward Jr., B.W.: Evaluation of space lubricants under oscillatory and slow speed rotary motion. Lubr. Eng. **24**(4), 163–172 (1968)

37. Briscoe, M., Todd, M.J.: Considerations on the lubrication of spacecraft mechanisms. In: The 17th Aerospace Mechanisms Symposium, NASA CP-2273. National Aeronautics and Space Administration, Washington, DC, pp. 19–37 (1983)
38. Roberts, W.H.: Some current trends in tribology in the UK and Europe. Tribol. Int. **19**(6), 295–311 (1986)
39. Gould, S.G., Roberts, E.W.: The in-vacuum torque performance of dry-lubricated ball bearings at cryogenic temperatures. In: The 23rd Aerospace Mechanisms Symposium, NASA CP-3032. National Aeronautics and Space Administration, Washington, DC, pp. 319–333 (1989)
40. Wisander, D.N., Maley, C.E., Johnson, R.L.: Near and friction of filled polytetrafluoroethylene compositions in liquid nitrogen. ASLE Trans. **2**(I), 58–66 (1959)
41. Wisander, D.N., Ludwig, L.P., Johnson, R.L.: Wear and friction of various polymer laminates in liquid nitrogen and in liquid hydrogen. NASA TN D-3706 (1966)
42. Scibbe, H.W., Anderson, W.J.: Evaluation of ball-bearing performance in liquid hydrogen at DN values to 1.6 million. ASLE Trans. **5**(I), 220–232 (1962)
43. Cunningham, R.E., Anderson, W.: Evaluation of 40-mm bore ball bearings operating in liquid oxygen at DN values to 1.2 million. NASA TN D-2637 (1967)
44. Zaretsky, E.V., Scibbe, H.N., Brewe D.E.: Studies of low and high temperature cage materials. NASA TM X-52262 (1967)
45. Scibbe, H.W., Brewe, D.E., Coe, H.H.: Lubrication and wear of ball bearings in cryogenic hydrogen. NASA TM X-52476 (1968)
46. Kannel, J.N., Dufrane, K.F., Barber, S.A., Gleeson, J.: Development of improved self-lubricating cages for SSME HPOTP Bearings. In: Richmond, R.J., Wu, S.T. (eds.) Advanced Earth-to-Orbit Propulsion Technology 1988, vol. l. NASA CP-3012-VOL-I. National Aeronautics and Space Administration, Washington, DC, pp. 175–189 (1988)
47. Poole, W.E., Bursey, R.M. Jr.: Pratt and Whitney cryogenic turbopump bearing experience. In: Richmond, R.J., Wu, S.T. (eds.) Advanced Earth-to-Orbit Propulsion Technology 1988, vol. l. NASA CP-3012-VOL-I. National Aeronautics and Space Administration, Washington, DC, pp. 190–199 (1988)
48. Zhu, J., Ma, L., Dwyer-Joyce, R.: Friction and wear behaviours of self-lubricating peek composites for articulating pin joints. Tribol. Int. (2019). https://doi.org/10.1016/j.triboint.2019.04.025
49. Zhu, J., Xie, F., Dwyer-Joyce, R.S.: PEEK composites as self-lubricating bush materials for articulating revolute pin joints. Polymers. **12**(3), 665 (2020). https://doi.org/10.3390/polym12030665

Tribology of Self-Lubricating Polymer Nanocomposites

5

Andrea Sorrentino

Contents

Abstract

In the last few years, polymeric materials filled with different kinds of nanomaterials have attracted particular attention as useful alternatives in structural components subjected to severe friction and wear loading conditions. The intention of this chapter is to give a comprehensive picture of these nanofillers and to

A. Sorrentino (✉)
Institute for Polymers, Composites and Biomaterials (IPCB), National Research Council (CNR), Lecco, Italy
e-mail: andrea.sorrentino@cnr.it

P. L. Menezes et al. (eds.), *Self-Lubricating Composites*,
https://doi.org/10.1007/978-3-662-64243-6_5

show their ability to improve friction and wear behavior of polymer composites. The aim is to organize the current state-of-the-art knowledge on these nanomaterials and point out on the key mechanisms governing their reinforcing effects. Despite the existing differences between literature results, there is a general agreement on the crucial role played by size, shape, concentration, and distribution of these fillers within the polymer matrix. The compatibility/interaction between filler and matrix is another important aspect in determining good filler dispersion and effective load transfer between the phases. As a consequence, the development of polymer nanocomposites showing high tribological features requires a deep selection of the nanofiller type and dimension along with its possible surface modification. Fortunately, modern technologies allow the design and the preparation of complex hybrid nanostructures able to put together the benefit of several structural factors. Although the state of the art demonstrates the potential of these materials, further researches are, however, necessary in order to definitely reach all possible improvements attainable for future high-demanding tribological applications.

5.1 Introduction

Nanotechnology promises breakthroughs in many areas such as materials and manufacturing, nanoelectronics, medicine and healthcare, energy, biotechnology, and food [1–3]. In the area of tribology, nanotechnology is expected to have a profound impact on design, friction reduction, wear resistance, and lubrication of moving/sliding surfaces [4–6]. The use of nanomaterials can offer a number of benefits for extending the systems lifetime, preventing their chemical and/or mechanical degradation and controlling temperature and moisture transmission [7, 8]. The key characteristic of nanomaterial is its enormous surface area-to-volume ratio, which in turn is the main responsible for the surprizing physical and chemical properties showed by these materials [9, 10]. When properly controlled, these features can be used to enhance efficiency and resistance of existing materials [11, 12]. Nanoparticles are already introduced in commercial liquid and semi-liquid lubricants for obtaining advanced capabilities and functionalities [13, 14]. Improved antiwear performances, thermal and chemical stability, as well as controlled fluidity and heat transfer, are some of the declared benefits [15, 16]. In several lubricant formulations, the aptitude of nanoparticles to carry a wide variety of additives, antioxidants, anticorrosion, and antifungal agents has been reported [17, 18].

Self-lubricant polymeric materials are normally used in applications where lightness, safety, versatility, and low cost are necessary [19]. Some examples of these applications include gears, bearing cages, artificial human joint bearing surfaces, food industry, aviation, or aerospace [20, 21]. Nanometric filler addition is a simple route to obtain a fine tuning of the mechanical and thermal properties of polymeric materials [7, 22]. In fact, a huge literature on the polymer/nanoparticles composites generally termed as “nanocomposites” reports excellent performance [23–25]. The

reinforcing effects of these fillers depend on their dimensions, shape, dispersion, distributions, and compatibility with the matrix [26, 24]. When all these factors are carefully controlled, materials with impressive properties are obtained [27, 28]. Among the other factors, the filler dimensions have attracted particular interest in recent years [10, 29, 30]. The growing commercial availability of materials with controlled nanometric dimensions open the possibility to develop a plethora of new polymer-based composites [20]. Nanomaterials are generally classified according to the number of dimensions outside the range from 1 to 100 nm. Accordingly, the 0D-materials are particles with all the three dimensions below 100 nm, the 1D-materials have two dimensions below 100 nm, and the 2D-materials have only one dimension in the nanometer scale. Among the 0D-materials there are carbon nanomaterials, Al_2O_3, $CaCO_3$, CuO, SiO_2, SiC, Si_3N_4, ZnO, ZrO_2, and TiO_2. Classical examples of 1D-materials are the carbon nanotubes and carbon nanofibers. 2D-materials include the wide class of the layered materials such as natural cationic clays, graphene, and molybdenum disulfide.

Despite the actual availability, up to now, only a limited number of these nanomaterials have been tested in polymeric materials for tribological applications [7]. When properly combined, these nanomaterials strengthen the polymer matrix and increase its load-bearing capacity [10, 29, 31]. Such improvements can expand the use of polymer materials to the applications where the control of the chemistry and morphology occurring within a few nanometers are a critical factor determining friction, wear, and stick-slip [4, 8, 32]. A correct choice of the filler-matrix pair is a complex task [33]. The filler size, shape, concentration, and, of course, the materials itself influence the lubrication performance of a specific system [34, 35]. Experimental results on the tribology characterization of nanoparticle-filled polymers have shown interesting but sometimes contradictory results. In some cases, filler contributes to enhanced wear resistance, while in other cases they have contributed to the properties deterioration of the composite [36]. Sometimes the same filler shows opposite trends when was reduced in size or when was chemically changed its affinity with the polymer matrix. In literature, particular attention was devoted to the effect of the nanofiller on the transfer film formation [4, 8]. Often, the presence of nanoparticles renders the transfer film more thin and tenacious [37]. Dispersion is another important factor in order to yield a good property profile. The natural tendency to agglomerate of the nanoparticles is considered to be a common problem, especially at higher filler contents. Some of the gains in wear resistance was also attributed to an increase in the thermal conductivity of the nanocomposite. High thermal conductivity facilitates the dissipation of the heat generated during friction and thus lowers the working temperature of the system [38].

In Fig. 5.1 the wear rates found in the literature for several polymer composites are reported [23]. In order to make a direct comparison between the different systems, results are normalized to that of the respective neat matrix. Obviously, better filler improvement is denoted by lower wear rate values at minimum filler additions [23]. It is quite evident from the plot that microcomposites require at least 10 wt% of loading for obtaining a reduction of 1 order of magnitude in the wear rate. Nanocomposites systems show a more complex behavior. In one case, filler

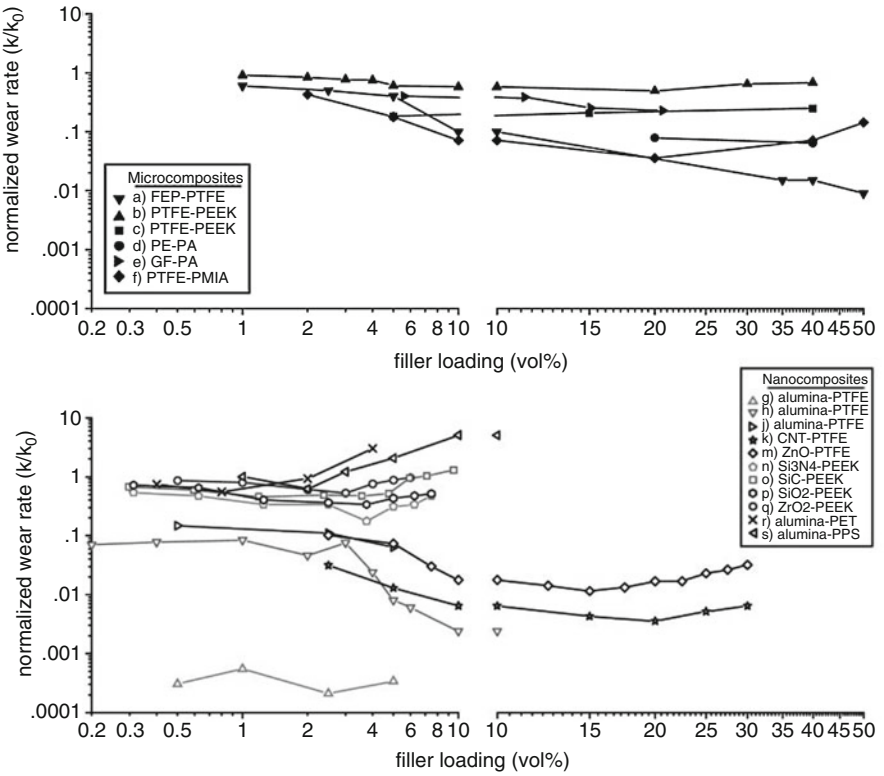

Fig. 5.1 Normalized wear rate plotted versus filler loading reported in the following references: (**a**) [39, 40]; (**b**) [41]; (**c**) [42]; (**d**) [43]; (**e**) [44]; (**f**) [45]; (**g**) [46]; (**h**) [47]; (**j**) [48]; (**k**) [49]; (**m**) [50]; (**n**) [51]; (**o**) [41]; (**p**) [52]; (**q**) [51]; (**r**) [53]; (**s**) [34]. (Reproduced from [23])

concentrations lower than 1 wt% is sufficient for obtaining reductions greater than 1000 times. Evidently, nanofillers have the potential to impart new and outstanding properties to the materials for tribological applications. However, there are several aspects of these systems that must be analyzed before to obtain a complete control of their improving mechanisms [8].

This chapter presents an overview of the principal nanometric fillers actually under investigations. They were grouped into filler dimensions and are analyzed with emphasis to their tribological behavior.

5.2 0-D Fillers

The well-known metallic, ceramic, or polymeric "nanoparticles" represent the broad class of zero dimensional fillers [54]. They can be hard or soft, composed of single or multichemical elements, and exhibit various shapes and forms [55]. Up to now, several types of such nanoparticles have been incorporated into polymer matrices to improve their wear performances. In general was found that they became effective in

change the matrix wear properties at very low concentrations. It generally means that the resulting composite can be improved while retaining other properties such as density or color. Probably, the most interesting and used of these nanoparticles are those inorganic and hard. The interest in this type of nanoparticles is related to their ability to improve the mechanical modulus and the impact resistance of the polymer matrix [1].

Soft polymeric nanoparticles are also used as filler for reducing the friction [18]. Even if, in this case, the composite material becomes somewhat less tough in comparison to the pristine polymer and thus more prone to wear, a proper optimization can avoid these problems.

Current technologies allow to synthesize nanoparticles with any type of shape or dimension, either immobilized or coated onto different surface types [7, 54]. A complete and updated list of all available nanoparticles is really hard to compile [8, 18]. In the following are reported, some of the most important along with exemplary experimental results found in the literature.

5.2.1 Alluminia Oxide

Probably the alumina nanoparticles are the class of nanofiller more investigated and utilized in tribological applications [47, 56]. Lower concentrations of nanometric Al_2O_3 in polyamide produce a significant reduction in wear rates [57]. Similar results were found in polyimide nanocomposites, where reduction in friction coefficient and wear volume is observed at very low filler concentrations. In both cases, the filler addition changes the rate in transfer film formation and modifies its morphology. The wear resistance has been found to increase also in other thermoplastic materials such as poly(ethylene terephthalate) (PET) and PTFE [53]. In both cases, filler content up to 5 vol% was found to enable the deposition of thin uniform transfer films on the counterface. Higher concentrations in Al_2O_3 generally results in filler agglomeration with a resulting degradation of the transfer film. The wear rate of polyphenylene sulphide (PPS) filled with Al_2O_3 nanoparticles was studied by Schwartz and Bahadur [34]. Also in this case, the formation of the transfer film and thus the steady state wear rate resulted strongly influenced by the concentration of the filler addition. However, the coefficient of friction results almost unaffected. The reduction in wear rate was related to the increase in bond strength between the transfer film and the counterface [34].

The roughness of the counterface has a strong effect on the wear resistance of the Al_2O_3/PPS nanocomposites [58]. For the counterface with the lower roughness, the addition of Al_2O_3 nanoparticles did not have an effect on the wear rate. A morphological investigation revealed that by decreasing the roughness of the counterface the transfer film becomes nonuniform with much of the metal surface exposed. As the percentage of uncovered metal is the main responsible for the wear rate, the filler resulted less active in the case of the smoothest counterface [58].

The effect of the filler size on PTFE wear resistance was studied by Mcelwain in his master thesis [59]. α phase alumina particles with different sizes were used as filler for the PTFE matrix. In Fig. 5.2 is reported the evolution of the wear volume

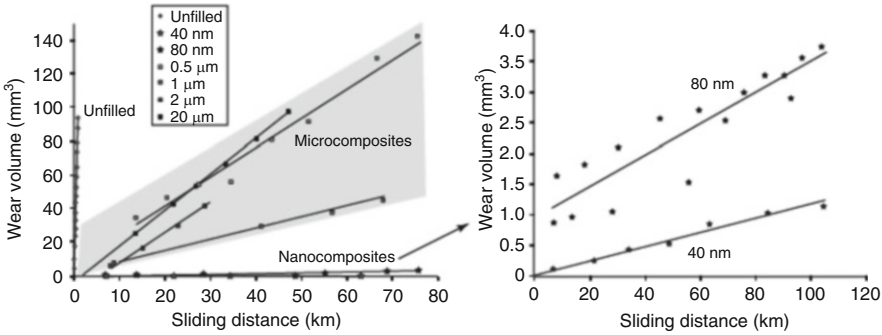

Fig. 5.2 Effect of the particle size on the wear volume of PTFE filled with 5 wt% of α phase alumina filler. (Reproduced from [59])

with the sliding increase obtained with a three-pin-on-disk tribometer (speed of 10 mm/s and contact pressure of 3.1 MPa). It is clear from the Fig. 5.2 that the wear resistance progressively increases with the reduction in the filler dimension.

The effects of Al_2O_3 nanoparticles on tribological properties of polyoxymethylene (POM) nanocomposites have been investigated under dry and oil lubricated sliding conditions [56]. Polymeric coatings containing Al_2O_3 nanoparticles showed enhanced abrasive and scratch resistance compared to that of the neat polymer [60]. The improvement was attributed to the hardening effect of Al_2O_3 nanoparticles on the polymer matrix.

For phenolic composites, an optimal Al_2O_3 filler content was found to be less than 3 wt% [61]. The detrimental effects of the agglomeration of Al_2O_3 nanoparticles in the transfer film of epoxy composites have been reported [35]. The same authors [62] report that the combination of nano- Al_2O_3 (13 nm) and micro-$CaSiO_3$ (4-15 μm) induced some kind of synergistic effect and improved both the wear resistance and the stiffness of epoxy.

In summary, the existence of an optimum filler concentration has been explained by the formation of abrasive agglomerates within the protective transfer films [63]. In all cases analyzed, the transfer film was reported to become discontinuous and poorly bonded to the counterface with increasing the filler concentration. It has been showed that the chemical grafting of the Al_2O_3 nanoparticles prevents agglomeration of the particles at the sliding interface and increase the abrasive wear resistance of the composite [35, 64].

5.2.2 Copper Nanoparticles

Copper-based particles in both micro- and nano sizes have been extensively investigated as polymer filler in tribological applications. CuO in micrometer size was added to high-density polyethylene [65, 66], polyamide [67], PEEK [68], polyphenylene sulfide (PPS) [69], and thermosetting polyester [70]. In all cases, a

good enhancement in the wear resistance was obtained. Similar results were obtained by adding micrometric CuS to PTFE [71], polyamide [72], PEEK [73], and PPS [74, 75] systems. Several investigations have pointed out that the same benefits of microsize Cu-based fillers can be obtained by using the same filler in nanometric dimensions. In this case, however, the best results are obtained at extremely smaller volume fractions [76]. The addition of 1–4 vol% of CuO nanoparticles to a PPS matrix leads to a strong reduction of the wear rate in the transient stage. The improvement is maintained also in the steady state where the wear volume per unit sliding distance reduces from 0.291 mm^3/km of the unfilled PPS to 0.047mm^3/km of the sample added with 2 vol% of CuO [76]. The reduction in wear rate was attributed to the development of a more uniform and better-bonded transfer film over the counterface [76].

5.2.3 Zinc Oxide

The addition of nanometric ZnO to polyurethane (PU) coatings has proven to decrease the friction coefficient and the wear rate of these materials [77]. Results showed that the presence of ZnO nanoparticles can help the adhesion of the transfer films to the counterface. In contrast, the addition of ZnO nanoparticles to a PPS matrix strongly decreases its wear resistance during sliding against a tool steel counterface [78]. In this case, a discontinuous and poorly bonded transfer film was produced during sliding. Li et al. [50] have shown that the addition of nanometric ZnO to a PTFE matrix lead to an increase in wear resistance. Probably, the contradictory results found with ZnO nanoparticles are due to their abrasive properties. Different filler sizes, as well as changes in the test conditions, are responsible for the different tribological behavior showed by these nanocomposites.

5.2.4 Titanium Dioxide

The addition of 1–5 wt% of TiO_2 nanoparticles in the range 30–50 nm to a PPS matrix was effective in reducing the composite wear rate [78]. Similarly to that found for other nanoparticles, lower filler additions ensure the formation of a uniform transfer film on the counterface. With the increase in TiO_2 concentrations, the transfer film became thick and lumpy, and it also did not cover the counterface completely. As a result, wear rate increased considerably up to exceed that of the unfilled PPS. The effects of the particle dimensions on the wear resistance of epoxy resin have been investigated [79]. TiO_2 particle in nanometric dimensions was found more effective in wear reduction than that in the micrometer dimensions [79]. Increasing the bond between the filler and the matrix has also been shown to have positive effects on the wear resistance. Chang et al. [80] showed that the addition of 5 vol% TiO_2 nanoparticles to poly(etherimide) (PEI) containing short carbon fibers and graphite flakes increased the wear resistance of the composite.

Also in the case of polyamide 66 (PA66) containing short carbon fibers and graphite flakes, the addition of TiO_2 nanoparticles produces a strong increase in the wear resistance [81, 82]. Similar synergisms were found with epoxy matrix filled with short carbon fibers, graphite flakes, and TiO_2 nanoparticles [79, 83].

5.2.5 Silica Nanoparticles

The use of SiO_2 nanoparticles as fillers in polymer matrices has shown mixed results on wear. The tribological characterization of PEEK filled with SiO_2 nanoparticles has shown a positive effect of this filler on the wear rate and friction coefficient of the composite [52]. Opposite effects were found for a poly(phthalazine ether sulfone ketone) (PPESK) matrix [84]. In that case, both micro- and nano SiO_2 particles induce a significant abrasive wear loss. For an epoxy matrix, SiO_2 nanoparticles were shown to increase the wear resistance with the increase of bond strength between the particles and the matrix [85]. Polycarbonate (PC) filled with nanometric SiO_2 showed high hardness and stiffness with respect to the polymer matrix [86]. Smaller scratch depth and lower frictional coefficient were found by tests carried out on the PC/SiO_2 nanocomposites. The wear mechanism of polyamide-1010 (PA-1010) filled with nanometric SiO_2 showed lower friction and better wear resistance with respect to the pure PA-1010 [87].

Also for the nanometric SiO_2, filler dimensions, as well as particles agglomeration, are the key factors for the nanocomposites improvement.

5.2.6 Carbon Nanomaterials

Carbon nanomaterials (CN) such as carbon black, fullerenes, and its derivate have been investigated as fillers for tribological applications. They have high surface area, are chemically and thermally stable, have relatively low cost, and generally are environmentally friendly. Melt compounding is generally sufficient to achieve a good distribution of carbon nanomaterials in the bulk of thermoplastics polymers [88–91]. However, the dispersion of these nanomaterials can be optimized by applying combined processes, such as chemical and mechanical pretreatments of the polymer and nanofiller [7, 92–94]. The addition of CN to a PTFE matrix results in a both compressive strength and hardness increase [95, 96]. The wear rate was found to decrease up to 150 times for PTFE containing 2 wt% of carbon nanomaterials [96]. Small quantities (<1 wt%) of C_{60} fullerene added to a natural rubber caused great variations in the friction coefficient [97]. Different types of fluorocopolymers added with 10–15 wt% of carbon nanomaterials increased resistance to abrasive surfaces.

Figure 5.3 shows the wear rate and the friction coefficient of nylon 1010 and its composites filled with MoS_2 (SL) microparticles and chopped carbon fiber

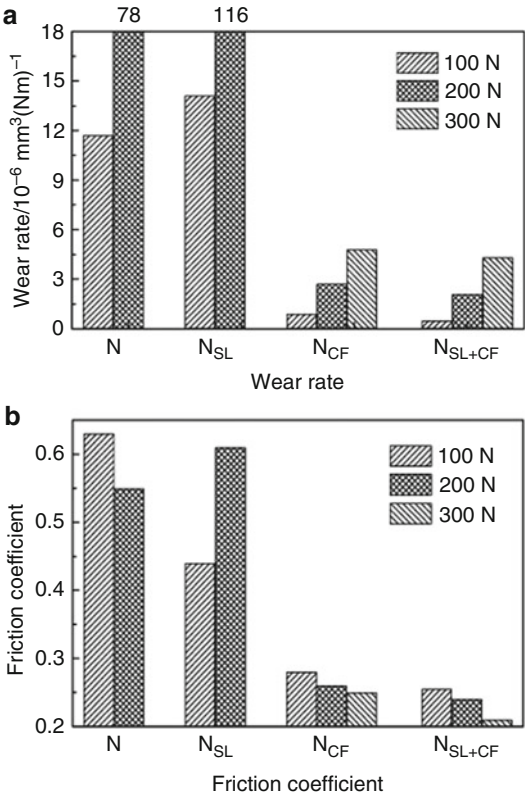

Fig. 5.3 Wear rate and Friction coefficient of Nylon 1010 and its composites filled with MoS_2 (SL) microparticles and chopped carbon fiber under various loads in dry sliding friction. (Reproduced from [98])

(CF) under various loads in dry sliding friction [98]. Unfilled nylon sample showed excessive wear probably due to the melting process taking place during the frictional process. Similar results were found by adding 10 wt% of MoS_2 microparticles. On the opposite, by adding 10 wt% of chopped carbon fiber, the wear rate was approximately reduced by a factor of 10. More interesting, the reduction in wear was greater when chopped carbon fiber and MoS_2 microparticles were combined. The authors found that the combination of the two fillers helps the formation of thin, uniform, and continuous transfer film [98].

The wear behavior of epoxy matrices in the presence of glass fibers and graphite was investigated by Suresha et al. [99]. The authors reported a pronounced reduction in wear rate as well as in frictional coefficient. A similar behavior was found for composites of PEI, carbon fibers, and graphite [80]. The incorporation of graphite particles (GPs) significantly reduces friction of polymer composites [100, 101]. It was proposed that the nanoparticles removed from the matrix debris act as third body elements in the contact region. Thus, they can reduce the shear stress in the contact region and accordingly enhance the matrix damage [102].

5.2.7 Other Nanoparticles

Schwartz and Bahadur [75] identified two opposite behaviors in polymeric composites filled with inorganic fillers. They found that AgS and CuS fillers contribute to increasing the wear resistance of a PPS matrix, whereas the same addition of ZnF_2 and SnS particles strongly reduced wear resistance. The authors suggested that this opposite behavior is due to the different mechanical properties of the filler [75]. In particular, the AgS and CuS particles are more prone to be deformed during flow with respect to the hard and abrasive ZnF_2 and SnS particles. Similar conclusions were reached using copper particles added to polyoxymethylene (POM) [103]. Also in this case, results have been explained by a predominantly plastic deformation mechanism of Cu particles [103]. However, the abrasive properties are strongly depended by the particle size used [15, 34, 53, 104, 105]. Wang et al. [51] investigated the influence of several ZrO_2 nanoparticles, varying from 10 to 100 nm, in reducing the wear of a PEEK matrix. Effective reduction of the wear rate was monitored only when the particles were less than 15 nm in size. Xing and Li [106] evaluated the wear properties of an epoxy matrix filled with spherical particle varying from 120 to 510 nm. They also found that the smaller the particles used as fillers, the better was the wear resistance of the composites.

Si_3N_4 and SiC nanoparticles grafted with polyacrylamide (PAAM) were used as filler for epoxy matrix [105]. Experimental results show that the compatibilization of the filler contributes to increased wear resistance of the epoxy composite. Inorganic nanoparticles such as $CaCO_3$ were added to several self-lubricating composites containing glass fibers with the aim to improve the adhesion between the reinforcing fibers and the matrix [107]. The resulting materials were able to operate under more severe sliding conditions than the composites with nanoparticles alone.

5.3 1-D Fillers

Filler with one dimension outside the nanometric range includes nanotubes, nanorods, nanofibers, and nanowires. They can be metallic, ceramic, or polymeric and can be amorphous or crystalline. The addition of these fillers to a polymer matrix has shown interesting results in terms of load-bearing capacity and toughness. These fillers can promote the formation of a tenacious and thin transfer film on the counterface and reduce the wear of the composites.

5.3.1 Carbon Nanotubes

Carbon nanotubes (CNT) are excellent filler for reinforcing polymers. They are exceptionally stiff and strong with a Young's modulus in the order of TPa and a tensile strength 100 times stronger than that of steel [29, 108]. Also, the nanometer size ensures extremely large interface and potentially excellent bonding [109, 110]. CNT-based nanocomposites are expected to have excellent tribological

properties [111, 112]. For that reason, several investigations have focused on the friction properties of thermoplastic and thermosetting composites filled with carbon nanotubes [113–115]. Results show that the experimental factors that are the main responsible for the tribological behavior of the CNT-nanocomposites are [116–118]:

(a) The preparation and purification method of the nanotubes
(b) The dispersion method
(c) The filler concentration in the nanocomposites
(d) Compatibilization with the polymer matrix

The effect of the addition of CNT on the wear life and load-bearing capacity of common polymers in tribological applications, such as polyethylene (HDPE and UHMWPE), has been analyzed by several authors [119–122]. The wear resistance of the composites is generally improved by the addition of low CNT concentrations [123]. It was explained by the reinforcement effect of CNT. However, CNTs are not easily dispersed in the polymer matrix and, especially at high concentrations (>5%), they tend to form large agglomerates. For this reason, poor mechanical and tribological properties are sometimes observed [119]. Low friction coefficient was obtained for nanocomposite reinforced with amino-functionalized CNT [124]. The conclusion was that a uniform distribution of CNTs in the matrix is a prerequisite for lowering friction.

A decrease in the wear rates of PTFE sliding over steel can be achieved by adding CNTs [49, 125]. The friction coefficient was observed to increase for the same CNT concentration [49]. The effect of the CNT on the friction coefficient on different polyamides (PA) was analyzed under dry and lubricated wear conditions [126–128]. In these cases, CNTs were able to reduce both the friction coefficients and the wear rates. The decrease in friction coefficients is ascribed to the improved strength properties of the polymer along with the lubricating action of CNT [49]. CNTs were also able to increase the wear resistance of epoxy resin [117, 129] and high resistant composites such as PEEK reinforced with carbon fibre [130]. In this case, the favorable effect of CNT was explained by the enhanced resistance of the matrix to the shear stresses [131].

5.3.2 Carbon Nanofibers

Carbon nanofibers (CNFs) are morphologically differentiated from carbon nanotubes by the orientation of the graphene planes [132]. They can be imagined as stacked graphitic discs, truncated cones, or planar layers along the filament length. These nanostructures have an outer diameter in the range 50–100 nm. However, commercial CNF fibers are slightly larger (100–200 nm) in diameters. This particular micrometric structure confers to the carbon nanofibers a semi-conducting behavior [133]. These fillers also have chemically active end planes on both the inner and outer surfaces [134]. CNFs are particularly suitable as reinforcing fillers in polymeric composites [135] and as an additive in carbon fiber reinforced plastics

[136, 137]. The addition of CNFs to a PEEK matrix strongly reduces unlubricated wear over alloy steel [138]. They result effective also when were added to a ternary composite such as PEEK reinforced with ordinary carbon fibers or PTFE. It was suggested that CNFs reduce to small graphitic debris particles during shear stress. These nanoparticles can anchor to the counterface and reduce its roughness [139, 140]. In addition, CNFs are able to reinforce the transfer film [107].

5.4 2-D Fillers

Two-dimensional nanomaterials such as clay, graphene, metal chalcogenides, and transition metal oxides are a broad range of materials that cover a variety of different properties. They have a layered structure with weak van der Waals interactions between them. Typically, the single layers of these materials are few nanometers thick with extraordinary electronic, magnetic, and thermal properties. The use of 2D nanomaterials for controlling friction and wear has received increased attention over the past few years [141, 142].

5.4.1 Clays

The most common clay materials are that identified as 2:1 phyllosilicates (montmorillonite, saponite). They are diffuse in nature as micron-size multilayered tactoids [143]. The individual layers having thicknesses of about 1 nm and surface lengths on the order of 100–1000 nm [144]. The layered structure of silicate makes it possess good solid lubrication [145]. Exfoliation and dispersion of natural clay in the polymer matrix are the necessary prerequisite for the nanocomposite formation [146, 147]. Several modification procedures were developed for expands the spacing between the individual clay layers and improves their compatibility with polymers [148, 149]. The effectiveness of these methods is found strongly dependent on the processing conditions as well as the polymer characteristics [26, 94, 150]. The clay sheets act like impermeable obstacles for gases or vapor diffusing through the matrix [30]. Good dispersion and surface interaction between filler and polymer are necessary for the mechanical and barrier improvements [24, 31, 144]. Dispersion is also responsible for the increase in wear resistance of several polymer nanocomposites [151, 152]. Yuan et al. [153] studied the scratch resistance of a polypropylene (PP) reinforced with an organo-modified montmorillonites. Figure 5.4 shows the surface deformation morphology of neat PP and PP modified with 4 wt% of nanoclay under identical scratch test conditions. Both samples showed periodic multiple ripple-type deformation tracks. However, nanoclay reinforcement decreases the susceptibility of the system to micro- and nanoscale deformation. It was attributed to the increased in modulus and yield strength of the composite [153].

Polyamide 6 (PA6) modified with neat or organically modified clay show different behaviors. Increased wear resistance was observed only for nanocomposites containing organically modified clays [151]. The authors suggest that the increase

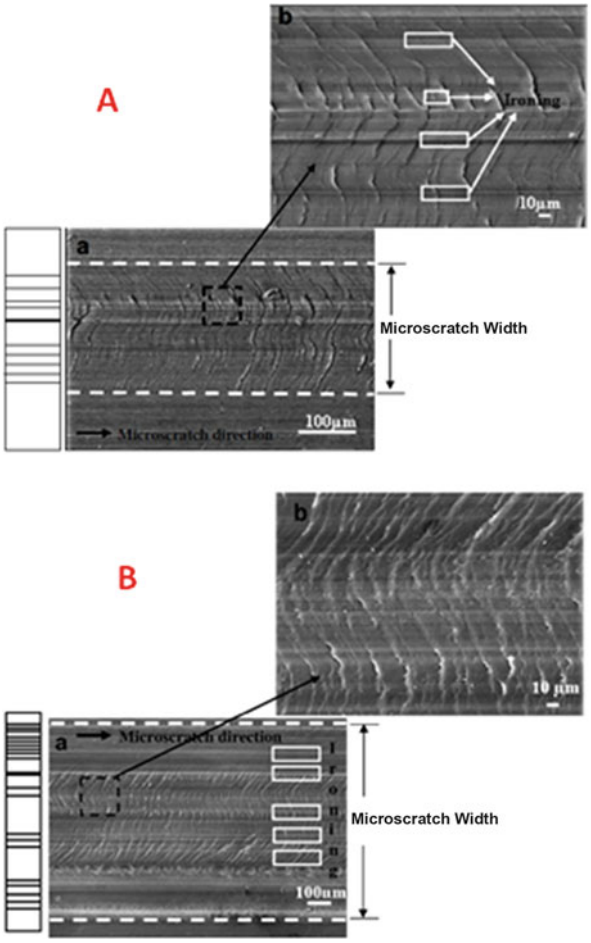

Fig. 5.4 Surface deformation morphology of microscratches: (**a**) Pure PP and (**b**) PP-4 wt% clay nanocomposite. (Reproduced from [153])

is achieved only if a good dispersion of the clay platelets in the polymer matrix is combined with a high level of compatibility between the clay and the polymer matrix. Similar results were found for PA nanocomposites systems filler with different types of organically modified clays [154, 155]. The addition of these nanomaterials also affects tribo-chemical processes taking place in friction contact zone. The dispersion of clay particles in a PI matrix was found to inhibit the degradation of macromolecules. As a result, wear resistance of the PI nanocomposite is enhanced. However, at higher clay concentrations the formation of large clay aggregates was observed on the counterface [92]. This was associated with high wear degradation rate. Nanoclay fillers were reported to increase the wear resistance of many thermoplastic polymers such as polycarbonate, polyester, polyamide, and polyvinylidenefluoride (PVDF) [156]. Tribological tests indicate that the addition of organo-modified montmorillonite enhanced wear resistance, antifriction property, and better fabric integrity of self-lubricating liners [157].

5.4.2 Graphene

Graphene sheets formally are two-dimensional layers of sp2-bonded carbon. The one-atom thick structure is expected to have a range of unusual properties [158]. High-quality graphene can be synthesized by chemical-vapor deposition [159]. It has been used in transparent conductors, flexible electronics, field-effect transistors, fuel cells, batteries, solar cells, biomaterials, biosensors, and water purifiers [160–162].

Graphene has been proposed as an alternative to conventional filler in the fields of transportation and electronics. Unfortunately, its cost and the difficulty to obtain as free single layers have limited its applications. Two derivates of graphene materials, namely, graphene oxide (GO) and reduced GO (rGO), have been proposed as substitutes [163, 164]. They are formally derived from low-cost graphite by chemical oxidation or electrochemical exfoliation and can be easily dispersed into polymeric materials [165–167]. The unique physical, mechanical, and chemical properties of graphene-like make it an attractive candidate for many tribological applications [168, 169].

Graphene oxide has been added to UHMWPE and characterized with a microhardness tester and high speed reciprocating tribometer [170]. Results show that the wear resistance and hardness of the composites are improved significantly, while the coefficient of friction increases rapidly. GO/polyimide (PI) nanocomposites were prepared by in situ polymerization techniques. The GO/PI exhibited better mechanical and thermal properties. Also the wear resistance of PI was found to increase [171]. Pan et al. [172] analyzed the tribological performance of graphene modified PI coatings. They found a sensible increase in the wear resistance of the coating. Better performances were found by increasing the interaction between the graphene filler and polyimide matrix [173]. PI/GO nanocomposites have demonstrated good tribological properties also under seawater-lubricated conditions [171]. Song et al. [174] prepared Cu nanoparticles decorated on polydopamine (PDA) functionalized graphene oxide (GO) nanosheets. Tests with sliding steel surfaces showed that the soybean oil with 0.1 wt% Cu/PDA/GO nanocomposites had the lowest friction coefficient under all of the sliding conditions. Kalin M et al. [175] investigated the effect of solid lubricant nanoparticles on poly-ether-ether-ketone (PEEK) composites. In the PEEK matrix, different types of nanoparticles were added, like graphene, WS_2 needle-like, WS_2 fullerene-like, and CNT. The results obtained under dry sliding conditions show that the morphology of the nanoparticles has an important effect on the friction coefficient and the wear behavior [175].

5.4.3 Molybdenum Disulfide

Molybdenum disulfide (MoS_2) is a naturally mined inorganic material that occurs as the mineral Molybdenite. Molybdenum disulfide has many unique properties, which makes it one of the most popular solid lubricants on the market [176, 177]. Similar to

graphite, these materials possess layered structures that can be exfoliated into small thicknesses containing mono- or multilayers [178, 179]. Among the 2D materials, molybdenum compounds are probably the most interesting for tribological applications. In particular, the interest for the molybdenum disulfide (MoS_2) in nanometric dimensions has increased exponentially due to their impressive chemical and physical properties [180, 181]. Nanometric MoS_2 have shown better lubrication performance than bulk MoS_2 [98]. Thus, considerable attention has been given to the preparation of MoS_2-based nanocomposites. Even if the MoS_2 can be easily dispersed and exfoliated in polymers [182–188], its tendency to re-organize in large agglomerate is still a big problem. Several synthetic routes were suggested to obtain 2D crystals of MoS_2 on a stable nanometric scale [189, 190]. Intercalation-exfoliation methods in common liquid solvents [191] and micromechanical exfoliation of natural molybdenite crystals were also proposed [192]. A simple and versatile method for the production of 2D nanosheet crystals of MoS_2 was proposed [5, 193, 194]. The nanosheets covered by a protective oleylamine coating were successfully tested as additives for high-performance liquid and solid lubricants [5]. Moreover, hybrid organic-inorganic oleylamine@MoS_2-CNT nanocomposites were obtained and successfully tested as nanoadditive for grease lubricant [195].

The introduction of MoS_2@oleylamine into a Polystyrene matrix was found to reduce its mechanical properties [196, 197]. A noticeable reduction of both the glass transition temperature and the elastic modulus was observed. The friction coefficient, as well as the wear resistance of PS nanocomposites, was found to decrease [196, 197].

Several polymeric matrices were proposed as a matrix for MoS_2 nanocomposites. They include polyoxymethylene (POM) [198, 199] and high-density polyethylene (HDPE) [200].

MoS_2 as micro- and nano-platelet and sphere were added to POM and HDPE matrices [200, 201]. Results show that the two structures exhibited a similar performance in friction reduction under dry friction. However, in the case of HDPE matrix, the nano-platelet MoS_2 showed lower friction coefficients than both microplatelets and nano-spheres. Chemical intercalation of MoS_2 can help its dispersion during the mechanical mixing [202]. However, the chemical intercalation can destroy the crystal structure of MoS_2 and negatively affect its lubrication performance [199].

Xin et al. [203] prepared a self-lubricating and antiwear polyimide composites by adding different percentages of graphene oxide/nano-MoS_2 hybrid. Figure 5.5a shows the friction coefficient of the various composites analyzed in the paper. The hybrid addition was found to reduce the friction coefficient. However, a fluctuation phenomenon appears in the curves when the filler concentration became higher than 0.5 wt%. The authors suggested [203] that at high concentrations the self-lubricating effect receded, due to the stacking of the nano-hybrid sheets. The effect of various additives on the friction coefficient is shown in Fig. 5.5b. A combination of the protective effect of graphene sheets, rolling friction effect of the detached nano-MoS_2 particles, and a transfer film composed of MoS_2 were proposed as a synergic mechanism for the enhancement of the tribological properties.

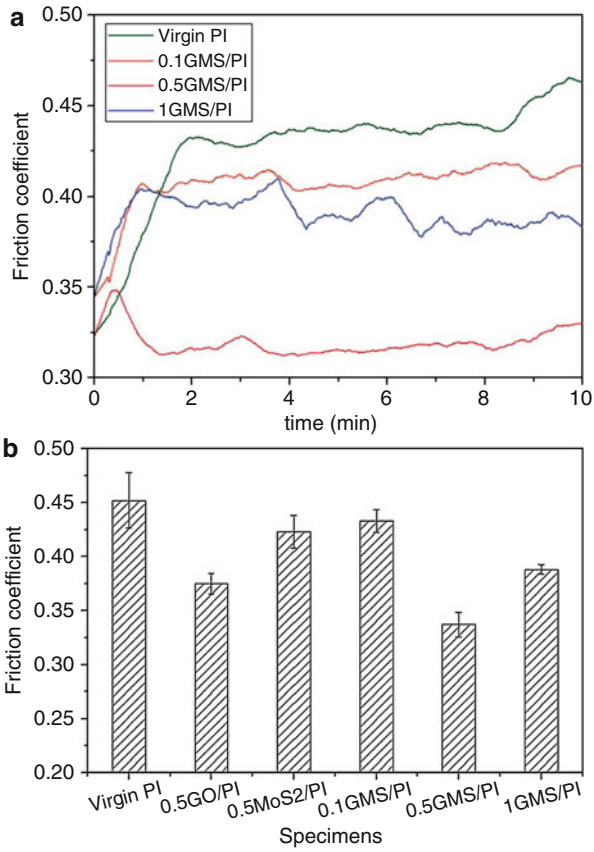

Fig. 5.5 (**a**) Friction coefficients of neat polyimide (PI), 0.1 wt% of graphene oxide/nano-MoS_2 in PI matrix (0.1GMS/PI), 0.5 wt% of graphene oxide/nano-MoS_2 in PI matrix (0.5GMS/PI), and 1 wt% of graphene oxide/nano-MoS_2 in PI matrix (1GMS/PI) specimens as a function of sliding time. (**b**) Friction coefficients of virgin PI, 0.5 wt% of graphene oxide in PI matrix (0.5GO/PI), 0.5 wt% of MoS_2 in PI matrix (0.5MoS_2/PI), 0.1 wt% of graphene oxide/nano-MoS_2 in PI matrix (0.1GMS/PI), 0.5 wt % of graphene oxide/nano-MoS_2 in PI matrix (0.5GMS/PI), and 1 wt% of graphene oxide/nano-MoS_2 in PI matrix (1GMS/PI) specimens. (Reproduced from [203])

5.5 Trends and Perspectives

The trend in the area of polymers composites for tribological applications is quickly moving towards multifunctional materials and coatings. Materials that can sustain high pressure and velocity with low wear rate are needed for the incoming high-tech applications. Nanomaterials offer new and intriguing possibility to design and develop innovative materials with these advanced properties. They will positively affect the quality, safety, and security of the polymer composites. The main advantage of these materials over traditional fillers is in its ability to improve mechanical, electrical and chemical properties at very low concentrations. As a matter, several examples of nanotechnology-based composites materials are already present on the market. The actual limitation to the definitive diffusion of these materials is the lack of information about their tribology performance. In fact, the tribological research on these systems is still at a relatively early stage. Additional experimental results and innovative research works are thus necessary. New chemical and physical approach

are necessary for improving the compatibility of the nanofillers with the matrix. Attention must be devoted to the development of new methods for achieving controlled in situ structuring of particles in three-dimensional structure. Researchers are called to further improve the performances of these materials and expand their use in newer tribological applications.

Acknowledgments The author acknowledges the financial support from the "VINMAC" (INNOVATIVO SISTEMA INTEGRATO DI VENTILAZIONE INDUSTRIALE IN MATERIALI COMPOSITI) project Regione Lombardia POR FESR 2014-2020 ASSE 1 – AZIONE I.1.B.1.3 BANDO LINEA R&S PER AGGREGAZIONI, ID 139455 CUP: E67H16000980009.

References

1. Gorrasi, G., Sorrentino, A.: Mechanical milling as a technology to produce structural and functional bio-nanocomposites. Green Chem. **17**, 2610–2625 (2015). https://doi.org/10.1039/C5GC00029G
2. Rogers, B., Adams, J., Pennathur, S.: Nanotechnology: Understanding Small Systems. CRC Press, Boca Raton (2014)
3. Reddy, B. (ed.): Advances in Diverse Industrial Applications of Nanocomposites. InTech (2011). https://doi.org/10.5772/1931
4. Briscoe, B.J., Sinha, S.K.: Tribological applications of polymers and their composites – past, present and future prospects. In: Tribology of Polymeric Nanocomposites, pp. 1–22. Elsevier, Amsterdam (2013). https://doi.org/10.1016/B978-0-444-59455-6.00001-5
5. Gnerre, C., Ciambelli, P., Altavilla, C., Sarno, M., Siraw, Y., Petrone, V., Senatore, A., Nobile, M.R., Somma, E.: Tribological and rheological properties of tungsten disulphide nanosheets as additive in lubricant mineral oil. In: Veneto Nanotech (ed.) International Conference Nanotechnology Nanomaterials, Venezia, pp. 177–178. (2010)
6. Menezes, P.L., Ingole, S.P., Nosonovsky, M., Kailas, S.V., Lovell, M.R.: Tribology for Scientists and Engineers. Springer, New York (2013)
7. Delogu, F., Gorrasi, G., Sorrentino, A.: Fabrication of polymer nanocomposites via ball milling: present status and future perspectives. Prog. Mater. Sci. **86**, 75–126 (2017). https://doi.org/10.1016/j.pmatsci.2017.01.003
8. Davim, J.P.: Tribology of Nanocomposites. Springer, Berlin (2013)
9. Caseri, W.: Nanocomposites of polymers and inorganic particles. In: Hybrid Materials, pp. 49–86. Wiley-VCH Verlag GmbH & Co. KGaA, Weinheim (2007). https://doi.org/10.1002/9783527610495.ch2
10. Sinha Ray, S., Okamoto, M.: Polymer/layered silicate nanocomposites: a review from preparation to processing. Prog. Polym. Sci. **28**, 1539–1641 (2003). https://doi.org/10.1016/j.progpolymsci.2003.08.002
11. Yin, Y., Talapin, D.: The chemistry of functional nanomaterials. Chem. Soc. Rev. **42**, 2484 (2013). https://doi.org/10.1039/c3cs90011h
12. Sorrentino, A.: Nanocoatings and ultra-thin films for packaging applications. In: Makhlouf, A. S.H., Tiginyanu, I. (eds.) Nanocoatings Ultra-Thin Film, pp. 203–234. Elsevier, Oxford (2011). https://doi.org/10.1533/9780857094902.2.203
13. Huang, H.D., Tu, J.P., Gan, L.P., Li, C.Z.: An investigation on tribological properties of graphite nanosheets as oil additive. Wear. **261**, 140–144 (2006)
14. Kim, D., Archer, L.A.: Nanoscale organic– inorganic hybrid lubricants. Langmuir. **27**, 3083–3094 (2011)
15. Stachowiak, G., Batchelor, A.W.: Engineering Tribology. Butterworth-Heinemann, Oxford (2013)

16. Czichos, H.: Chapter: 1 Introduction and background. In: Tribology a Systems Approach to the Science and Technology of Friction, Lubrication and Wear, pp. 1–13. Elsevier, Berlin (1978). https://doi.org/10.1016/S0167-8922(09)70004-5
17. Rudnick, L.R.: Lubricant Additives: Chemistry and Applications. CRC press, Boca Raton (2009)
18. Wang, Q., Chung, Y.: Encyclopedia of Tribology. Springer, New York (2013)
19. Menezes, P.L., Kailas, S.V., Lovell, M.R.: Fundamentals of engineering surfaces. In: Tribology for Scientists and Engineering, pp. 3–41. Springer, New York (2013). https://doi.org/10.1007/978-1-4614-1945-7_1
20. Friedrich, K., Schlarb, A.K., Bahadur, S., Schwartz, C.: Tribology of Polymeric Nanocomposites. Elsevier, Amsterdam (2013). https://doi.org/10.1016/B978-0-444-59455-6.00002-7
21. Guadagno, L., De Vivo, B., Di Bartolomeo, A., Lamberti, P., Sorrentino, A., Tucci, V., Vertuccio, L., Vittoria, V.: Effect of functionalization on the thermo-mechanical and electrical behavior of multi-wall carbon nanotube/epoxy composites. Carbon N. Y. **49**, 1919–1930 (2011)
22. Baillie, C.: Green Composites, Polymer Composites and the Environment. CRC Press, Cambridge (2004)
23. Burris, D.L., Boesl, B., Bourne, G.R., Sawyer, W.G.: Polymeric nanocomposites for tribological applications. Macromol. Mater. Eng. **292**, 387–402 (2007). https://doi.org/10.1002/mame.200600416
24. Sorrentino, A., Tortora, M., Vittoria, V.: Diffusion behavior in polymer-clay nanocomposites. J. Polym. Sci. Part B Polym. Phys. **44**, 265–274 (2006). https://doi.org/10.1002/polb.20684
25. Sorrentino, A., Vertuccio, L., Vittoria, V.: Influence of multi-walled carbon nanotubes on the β form crystallization of syndiotactic polystyrene at low temperature. Express Polym Lett. **4**, 339–345 (2010). https://doi.org/10.3144/expresspolymlett.2010.43
26. Pavlidou, S., Papaspyrides, C.D.: A review on polymer–layered silicate nanocomposites. Prog. Polym. Sci. **33**, 1119–1198 (2008). https://doi.org/10.1016/j.progpolymsci.2008.07.008
27. Gorrasi, G., Attanasio, G., Izzo, L., Sorrentino, A.: Controlled release mechanisms of sodium benzoate from a biodegradable polymer and halloysite nanotube composite. Polym. Int. **66**, 690–698 (2017). https://doi.org/10.1002/pi.5309
28. Liparoti, S., Landi, G., Sorrentino, A., Speranza, V., Cakmak, M., Neitzert, H.C.: Flexible poly (amide-imide)-carbon black based microheater with high-temperature capability and an extremely low temperature coefficient. Adv. Electron. Mater. **2**, 1600126 (2016). https://doi.org/10.1002/aelm.201600126
29. Gorrasi, G., Di Lieto, R., Patimo, G., De Pasquale, S., Sorrentino, A.: Structure–property relationships on uniaxially oriented carbon nanotube/polyethylene composites. Polymer (Guildf). **52**, 1124–1132 (2011). https://doi.org/10.1016/j.polymer.2011.01.008
30. Sorrentino, A., Gorrasi, G., Vittoria, V.: Environmental Silicate Nano-Biocomposites. Springer, London (2012). https://doi.org/10.1007/978-1-4471-4108-2
31. Ajayan, P.M., Schadler, L.S., Braun, P.V. (eds.): Nanocomposite Science and Technology. Wiley-VCH Verlag GmbH & Co. KGaA, Weinheim (2003). https://doi.org/10.1002/3527602127
32. Bhushan, B.: Micro/Nanotribology and Its Applications. Springer Netherlands, Dordrecht (1997). https://doi.org/10.1007/978-94-011-5646-2
33. Chand, N., Fahim, M.: Introduction to tribology of polymer composites. In: Tribology of Natural Fiber Polymer Composites, pp. 59–83. Elsevier, Cambridge (2008). https://doi.org/10.1533/9781845695057.59
34. Schwartz, C.J., Bahadur, S.: Studies on the tribological behavior and transfer film–counterface bond strength for polyphenylene sulfide filled with nanoscale alumina particles. Wear. **237**, 261–273 (2000)
35. Wetzel, B., Haupert, F., Qiu Zhang, M.: Epoxy nanocomposites with high mechanical and tribological performance. Compos. Sci. Technol. **63**, 2055–2067 (2003). https://doi.org/10.1016/S0266-3538(03)00115-5

36. Bhushan, B.: Fundamentals of Tribology and Bridging the Gap Between the Macro- and Micro/Nanoscales. Springer Netherlands, Dordrecht (2001). https://doi.org/10.1007/978-94-010-0736-8
37. Chang, L., Zhang, Z., Ye, L., Friedrich, K.: Tribological properties of epoxy nanocomposites: III. Characteristics of transfer films. Wear. **262**, 699–706 (2007)
38. Hutchings, I., Shipway, P.: Design and selection of materials for tribological applications. In: Tribology Friction and Wear of Engineering Materials, pp. 283–302. Elsevier, Oxford (2017). https://doi.org/10.1016/B978-0-08-100910-9.00008-8
39. Blanchet, T.A., Peng, Y.-L.: Wear resistant irradiated FEP/unirradiated PTFE composites. Wear. **214**, 186–191 (1998). https://doi.org/10.1016/S0043-1648(97)00254-8
40. Menzel, B., Blanchet, T.A.: Effect of particle size and volume fraction of irradiated FEP filler on the transfer wear of PTFE. Tribol. Lubr. Technol. **58**, 29 (2002)
41. Wang, Q.-H., Xue, Q.-J., Liu, W.-M., Chen, J.-M.: The friction and wear characteristics of nanometer SiC and polytetrafluoroethylene filled polyetheretherketone. Wear. **243**, 140–146 (2000)
42. Lu, Z.P., Friedrich, K.: On sliding friction and wear of PEEK and its composites. Wear. **181**, 624–631 (1995)
43. Palabiyik, M., Bahadur, S.: Mechanical and tribological properties of polyamide 6 and high density polyethylene polyblends with and without compatibilizer. Wear. **246**, 149–158 (2000)
44. Bahadur, S., Polineni, V.K.: Tribological studies of glass fabric-reinforced polyamide composites filled with CuO and PTFE. Wear. **200**, 95–104 (1996)
45. Liu, X., Li, T., Tian, N., Liu, W.: Tribological properties of PTFE-filled PMIA. J. Appl. Polym. Sci. **74**, 747–751 (1999)
46. Burris, D.L., Sawyer, W.G.: Tribological sensitivity of PTFE/alumina nanocomposites to a range of traditional surface finishes. Tribol. Trans. **48**, 147–153 (2005)
47. Sawyer, W.G., Freudenberg, K.D., Bhimaraj, P., Schadler, L.S.: A study on the friction and wear behavior of PTFE filled with alumina nanoparticles. Wear. **254**, 573–580 (2003)
48. Burris, D.L., Sawyer, W.G.: Improved wear resistance in alumina-PTFE nanocomposites with irregular shaped nanoparticles. Wear. **260**, 915–918 (2006)
49. Chen, W.X., Li, F., Han, G., Xia, J.B., Wang, L.Y., Tu, J.P., Xu, Z.D.: Tribological behavior of carbon-nanotube-filled PTFE composites. Tribol. Lett. **15**, 275–278 (2003)
50. Li, F., Hu, K., Li, J., Zhao, B.: The friction and wear characteristics of nanometer ZnO filled polytetrafluoroethylene. Wear. **249**, 877–882 (2001)
51. Wang, Q., Xue, Q., Liu, H., Shen, W., Xu, J.: The effect of particle size of nanometer ZrO_2 on the tribological behaviour of PEEK. Wear. **198**, 216–219 (1996)
52. Wang, Q., Xue, Q., Shen, W.: The friction and wear properties of nanometre SiO_2 filled polyetheretherketone. Tribol. Int. **30**, 193–197 (1997)
53. Bhimaraj, P., Burris, D.L., Action, J., Sawyer, W.G., Toney, C.G., Siegel, R.W., Schadler, L.S.: Effect of matrix morphology on the wear and friction behavior of alumina nanoparticle/poly (ethylene) terephthalate composites. Wear. **258**, 1437–1443 (2005)
54. Higgs, C.F., Marinack, M., Mpagazehe, J., Pudjoprawoto, R.: Particle tribology: granular, slurry, and powder tribosystems. In: Tribology for Scientists and Engineering, pp. 391–445. Springer, New York (2013). https://doi.org/10.1007/978-1-4614-1945-7_12
55. Schmid, G. (ed.) Nanoparticles: From Theory to Application, 2nd Completely Revised and Updated Edition. Wiley-VCH Verlag GmbH & Co. KGaA (2010)
56. Sun, L.-H., Yang, Z.-G., Li, X.-H.: Study on the friction and wear behavior of POM/Al_2O_3 nanocomposites. Wear. **264**, 693–700 (2008)
57. Zhao, L., Zheng, L., Zhao, S.: Tribological performance of nano-Al_2O_3 reinforced polyamide 6 composites. Mater. Lett. **60**, 2590–2593 (2006)
58. Zhang, G., Wetzel, B., Jim, B., Österle, W.: Impact of counterface topography on the formation mechanisms of nanostructured tribofilm of PEEK hybrid nanocomposites. Tribol. Int. **83**, 156–165 (2015)

59. Burris, D.L., Santos, K., Lewis, S.L., Liu, X., Perry, S.S., Blanchet, T.A., Schadler, L.S., Sawyer, W.G.: Polytetrafluoroethylene matrix nanocomposites for tribological applications. In: Developments of Nanocomposites/Coatings for Special Applications, pp. 403–438. Elsevier, Amsterdam (2008). https://doi.org/10.1016/S1572-3364(08)55017-8
60. Wang, Y., Lim, S., Luo, J.L., Xu, Z.H.: Tribological and corrosion behaviors of Al_2O_3/polymer nanocomposite coatings. Wear. **260**, 976–983 (2006)
61. Song, H.-J., Zhang, Z.-Z., Men, X.: Effect of nano-Al_2O_3 surface treatment on the tribological performance of phenolic composite coating. Surf. Coatings Technol. **201**, 3767–3774 (2006)
62. Wetzel, B., Haupert, F., Friedrich, K., Zhang, M.Q., Rong, M.Z.: Impact and wear resistance of polymer nanocomposites at low filler content. Polym. Eng. Sci. **42**, 1919–1927 (2002)
63. Luo, T., Wei, X., Zhao, H., Cai, G., Zheng, X.: Tribology properties of Al_2O_3/TiO_2 nanocomposites as lubricant additives. Ceram. Int. **40**, 10103–10109 (2014)
64. Shi, G., Zhang, M.Q., Rong, M.Z., Wetzel, B., Friedrich, K.: Sliding wear behavior of epoxy containing nano-Al_2O_3 particles with different pretreatments. Wear. **256**, 1072–1081 (2004)
65. Bahadur, S., Tabor, D.: Role of fillers in the friction and wear behavior of high-density polyethylene. In: Polymeric Wear and Its Control, pp. 253–268. ACS Publications, New York (1985). https://doi.org/10.1021/bk-1985-0287.ch017
66. Kato, K.: Wear in relation to friction – a review. Wear. **241**, 151–157 (2000)
67. Bahadur, S., Gong, D., Anderegg, J.W.: The role of copper compounds as fillers in transfer film formation and wear of nylon. Wear. **154**, 207–223 (1992)
68. Vande Voort, J., Bahadur, S.: Effect of PTFE Addition on the Transfer Film, Wear and Friction of PEEK-CuO Composite. American Society of Mechanical Engineers, New York (1995)
69. Yu, L., Yang, S., Liu, W., Xue, Q.: An investigation of the friction and wear behaviors of polyphenylene sulfide filled with solid lubricants. Polym. Eng. Sci. **40**, 1825–1832 (2000). https://doi.org/10.1002/pen.11314
70. Bahadur, S., Zhang, L., Anderegg, J.W.: The effect of zinc and copper oxides and other zinc compounds as fillers on the tribological behavior of thermosetting polyester. Wear. **203**, 464–473 (1997)
71. Bahadur, S., Tabor, D.: The wear of filled polytetrafluoroethylene. Wear. **98**, 1–13 (1984)
72. Kapoor, A., Bahadur, S.: Transfer film bonding and wear studies on CuS-nylon composite sliding against steel. Tribol. Int. **27**, 323–329 (1994)
73. Vande Voort, J., Bahadur, S.: The growth and bonding of transfer film and the role of CuS and PTFE in the tribological behavior of PEEK. Wear. **181**, 212–221 (1995)
74. Yu, L., Bahadur, S.: An investigation of the transfer film characteristics and the tribological behaviors of polyphenylene sulfide composites in sliding against tool steel. Wear. **214**, 245–251 (1998)
75. Schwartz, C.J., Bahadur, S.: The role of filler deformability, filler–polymer bonding, and counterface material on the tribological behavior of polyphenylene sulfide (PPS). Wear. **251**, 1532–1540 (2001)
76. Cho, M.H., Bahadur, S.: Study of the tribological synergistic effects in nano CuO-filled and fiber-reinforced polyphenylene sulfide composites. Wear. **258**, 835–845 (2005)
77. Song, H.-J., Zhang, Z.-Z., Men, X.-H., Luo, Z.-Z.: A study of the tribological behavior of nano-ZnO-filled polyurethane composite coatings. Wear. **269**, 79–85 (2010)
78. Bahadur, S., Sunkara, C.: Effect of transfer film structure, composition and bonding on the tribological behavior of polyphenylene sulfide filled with nano particles of TiO_2, ZnO, CuO and SiC. Wear. **258**, 1411–1421 (2005)
79. Zhang, Z., Breidt, C., Chang, L., Haupert, F., Friedrich, K.: Enhancement of the wear resistance of epoxy: short carbon fibre, graphite, PTFE and nano-TiO_2. Compos. Part A Appl. Sci. Manuf. **35**, 1385–1392 (2004)
80. Chang, L., Zhang, Z., Zhang, H., Friedrich, K.: Effect of nanoparticles on the tribological behaviour of short carbon fibre reinforced poly (etherimide) composites. Tribol. Int. **38**, 966–973 (2006)

81. Chang, L., Zhang, Z., Zhang, H., Schlarb, A.K.: On the sliding wear of nanoparticle filled polyamide 66 composites. Compos. Sci. Technol. **66**, 3188–3198 (2006)
82. You, Y.-L., Li, D.-X., Si, G.-J., Deng, X.: Investigation of the influence of solid lubricants on the tribological properties of polyamide 6 nanocomposite. Wear. **311**, 57–64 (2014)
83. Su, F., Zhang, Z., Liu, W.: Mechanical and tribological properties of carbon fabric composites filled with several nano-particulates. Wear. **260**, 861–868 (2006)
84. Shao, X., Tian, J., Liu, W., Xue, Q., Ma, C.: Tribological properties of SiO_2 nanoparticle filled–phthalazine ether sulfone/phthalazine ether ketone (50/50 mol%) copolymer composites. J. Appl. Polym. Sci. **85**, 2136–2144 (2002)
85. Zhang, M.Q., Rong, M.Z., Yu, S.L., Wetzel, B., Friedrich, K.: Effect of particle surface treatment on the tribological performance of epoxy based nanocomposites. Wear. **253**, 1086–1093 (2002)
86. Wang, Z.Z., Gu, P., Zhang, Z.: Indentation and scratch behavior of nano-SiO_2/polycarbonate composite coating at the micro/nano-scale. Wear. **269**, 21–25 (2010)
87. Li, Y., Ma, Y., Xie, B., Cao, S., Wu, Z.: Dry friction and wear behavior of flame-sprayed polyamide1010/n-SiO_2 composite coatings. Wear. **262**, 1232–1238 (2007)
88. Moniruzzaman, M., Winey, K.I.: Polymer nanocomposites containing carbon nanotubes. Macromolecules. **39**, 5194–5205 (2006)
89. Kumar, S., Doshi, H., Srinivasarao, M., Park, J.O., Schiraldi, D.A.: Fibers from polypropylene/nano carbon fiber composites. Polymer (Guildf). **43**, 1701–1703 (2002)
90. De Zhang, W., Shen, L., Phang, I.Y., Liu, T.: Carbon nanotubes reinforced nylon-6 composite prepared by simple melt-compounding. Macromolecules. **37**, 256–259 (2004)
91. Nobile, M.R., Valentino, O., Morcom, M., Simon, G.P., Landi, G., Neitzert, H.-C.: The effect of the nanotube oxidation on the rheological and electrical properties of CNT/HDPE nanocomposites. Polym. Eng. Sci. **57,** 665–673 (2017). https://doi.org/10.1002/pen.24572
92. Lai, S., Yue, L., Li, T., Liu, X., Lv, R.: An investigation of friction and wear behaviors of polyimide/attapulgite hybrid materials. Macromol. Mater. Eng. **290**, 195–201 (2005)
93. Ambrosio-Martin, J., Fabra, M.J., López-Rubio, A., Gorrasi, G., Sorrentino, A., Lagaron, J. M.: Assessment of ball milling as a compounding technique to develop nanocomposites of poly (3-Hydroxybutyrate-co-3-Hydroxyvalerate) and bacterial cellulose nanowhiskers. J. Polym. Environ. **24**, 241–254 (2016)
94. Vertuccio, L., Gorrasi, G., Sorrentino, A., Vittoria, V.: Nano clay reinforced PCL/starch blends obtained by high energy ball milling. Carbohydr. Polym. **75**, 172–179 (2009). https://doi.org/10.1016/j.carbpol.2008.07.020
95. Dolmatov, V.Y.: Detonation nanodiamonds in oils and lubricants. J. Superhard Mater. **32**, 14–20 (2010)
96. Dubkova, V.I., Korzhenevskii, A.P., Krut, N.P., Komarevich, V.G., Kul, L.V.: Detonation-synthesis nanodiamonds in compositions of ultrahigh-molecular-weight polyethylene. J. Eng. Phys. Thermophys. **89**, 1024–1033 (2016)
97. Jurkowska, B., Jurkowski, B., Kamrowski, P., Pesetskii, S.S., Koval, V.N., Pinchuk, L.S., Olkhov, Y.A.: Properties of fullerene-containing natural rubber. J. Appl. Polym. Sci. **100**, 390–398 (2006)
98. Wang, J., Gu, M., Songhao, B., Ge, S.: Investigation of the influence of MoS_2 filler on the tribological properties of carbon fiber reinforced nylon 1010 composites. Wear. **255**, 774–779 (2003). https://doi.org/10.1016/S0043-1648(03)00268-0
99. Suresha, B., Chandramohan, G., Renukappa, N.M.: Mechanical and tribological properties of glass–epoxy composites with and without graphite particulate filler. J. Appl. Polym. Sci. **103**, 2472–2480 (2007)
100. Khun, N.W., Zhang, H., Lim, L.H., Yue, C.Y., Hu, X., Yang, J.: Tribological properties of short carbon fibers reinforced epoxy composites. Friction. **2**, 226–239 (2014)
101. Quan, H., Zhang, B., Zhao, Q., Yuen, R.K.K., Li, R.K.Y.: Facile preparation and thermal degradation studies of graphite nanoplatelets (GNPs) filled thermoplastic polyurethane (TPU) nanocomposites. Compos. Part A Appl. Sci. Manuf. **40**, 1506–1513 (2009)

102. Song, F., Wang, Q., Wang, T.: High mechanical and tribological performance of polyimide nanocomposites reinforced by chopped carbon fibers in adverse operating conditions. Compos. Sci. Technol. **134**, 251–257 (2016)
103. Larsen, T.Ø., Andersen, T.L., Thorning, B., Horsewell, A., Vigild, M.E.: Changes in the tribological behavior of an epoxy resin by incorporating CuO nanoparticles and PTFE microparticles. Wear. **265**, 203–213 (2008)
104. Qian, F., Melhachat, B., Chen, C., Jiang, K., Zhao, Z., Yang, X.: A Mössbauer study of iron/polytetrafluoroethylene nanocomposites prepared by high-energy ball milling. Nucl. Sci. Tech. **17**, 139–142 (2006). https://doi.org/10.1016/S1001-8042(06)60027-4
105. Rong, M.Z., Zhang, M.Q., Shi, G., Ji, Q.L., Wetzel, B., Friedrich, K.: Graft polymerization onto inorganic nanoparticles and its effect on tribological performance improvement of polymer composites. Tribol. Int. **36**, 697–707 (2003)
106. Xing, X.S., Li, R.K.Y.: Wear behavior of epoxy matrix composites filled with uniform sized sub-micron spherical silica particles. Wear. **256**, 21–26 (2004)
107. Friedrich, K., Zhang, Z., Schlarb, A.: Effects of various fillers on the sliding wear of polymer composites. Compos. Sci. Technol. **65**, 2329–2343 (2005). https://doi.org/10.1016/j.compscitech.2005.05.028
108. Dai, H.: Carbon nanotubes: opportunities and challenges. Surf. Sci. **500**, 218–241 (2002). https://doi.org/10.1016/S0039-6028(01)01558-8
109. Gorrasi, G., Sorrentino, A.: Photo-oxidative stabilization of carbon nanotubes on polylactic acid. Polym. Degrad. Stab. **98**, 963–971 (2013). https://doi.org/10.1016/j.polymdegradstab.2013.02.012
110. De Vivo, B., Lamberti, P., Tucci, V., Guadagno, L., Vertuccio, L., Vittoria, V., Sorrentino, A.: Comparison of the physical properties of epoxy-based composites filled with different types of carbon nanotubes for aeronautic applications. Adv. Polym. Technol. **31**, 205–218 (2012). http://www.scopus.com/inward/record.url?eid=2-s2.0-84864683182&partnerID=40&md5=de0bac503009e539f5488443837fb5e5
111. Wang, C., Xue, T., Dong, B., Wang, Z., Li, H.-L.: Polystyrene–acrylonitrile–CNTs nanocomposites preparations and tribological behavior research. Wear. **265**, 1923–1926 (2008)
112. Al-Kawaz, A., Rubin, A., Badi, N., Blanck, C., Jacomine, L., Janowska, I., Pham-Huu, C., Gauthier, C.: Tribological and mechanical investigation of acrylic-based nanocomposite coatings reinforced with PMMA-grafted-MWCNT. Mater. Chem. Phys. **175**, 206–214 (2016)
113. Dasari, A., Yu, Z.-Z., Mai, Y.-W.: Fundamental aspects and recent progress on wear/scratch damage in polymer nanocomposites. Mater. Sci. Eng. R Reports. **63**, 31–80 (2009). https://doi.org/10.1016/j.mser.2008.10.001
114. Yang, Z., Dong, B., Huang, Y., Liu, L., Yan, F.-Y., Li, H.-L.: Enhanced wear resistance and micro-hardness of polystyrene nanocomposites by carbon nanotubes. Mater. Chem. Phys. **94**, 109–113 (2005)
115. Liu, S., Hsu, W., Chang, K., Yeh, J.: Enhancement of the surface and bulk mechanical properties of polystyrene through the incorporation of raw multiwalled nanotubes with the twin-screw mixing technique. J. Appl. Polym. Sci. **113**, 992–999 (2009)
116. Martínez-Hernández, A.L., Velasco-Santos, C., Castano, V.: Carbon nanotubes composites: processing, grafting and mechanical and thermal properties. Curr. Nanosci. **6**, 12–39 (2010)
117. Jacobs, O., Xu, W., Schädel, B., Wu, W.: Wear behaviour of carbon nanotube reinforced epoxy resin composites. Tribol. Lett. **23**, 65–75 (2006)
118. Chen, H., Jacobs, O., Wu, W., Rüdiger, G., Schädel, B.: Effect of dispersion method on tribological properties of carbon nanotube reinforced epoxy resin composites. Polym. Test. **26**, 351–360 (2007)
119. Zoo, Y.-S., An, J.-W., Lim, D.-P., Lim, D.-S.: Effect of carbon nanotube addition on tribological behavior of UHMWPE. Tribol. Lett. **16**, 305–309 (2004)
120. Kanagaraj, S., Varanda, F.R., Zhil'tsova, T.V., Oliveira, M.S.A., Simões, J.A.O.: Mechanical properties of high density polyethylene/carbon nanotube composites. Compos. Sci. Technol. **67**, 3071–3077 (2007). https://doi.org/10.1016/j.compscitech.2007.04.024

121. Lee, J., Kathi, J., Rhee, K.Y., Lee, J.H.: Wear properties of 3-aminopropyltriethoxysilane-functionalized carbon nanotubes reinforced ultra high molecular weight polyethylene nanocomposites. Polym. Eng. Sci. **50**, 1433–1439 (2010)
122. Bin Ali, A., Abdul Samad, M., Merah, N.: UHMWPE hybrid nanocomposites for improved tribological performance under dry and water-lubricated sliding conditions. Tribol. Lett. **65**, 102 (2017). https://doi.org/10.1007/s11249-017-0884-y
123. Samad, M.A., Sinha, S.K.: Effects of counterface material and UV radiation on the tribological performance of a UHMWPE/CNT nanocomposite coating on steel substrates. Wear. **271**, 2759–2765 (2011)
124. Kim, J., Im, H., Cho, M.H.: Tribological performance of fluorinated polyimide-based nanocomposite coatings reinforced with PMMA-grafted-MWCNT. Wear. **271**, 1029–1038 (2011)
125. Vail, J.R., Burris, D.L., Sawyer, W.G.: Multifunctionality of single-walled carbon nanotube–polytetrafluoroethylene nanocomposites. Wear. **267**, 619–624 (2009)
126. May, B., Hartwich, M.R., Stengler, R., Hu, X.G.: The influence of carbon nanotubes on the tribological behavior and wear resistance of a polyamide nanocomposite. In: Advance Tribology, pp. 515–515, Springer, Berlin/Heidelberg (2009). https://doi.org/10.1007/978-3-642-03653-8_163
127. Meng, H., Sui, G.X., Xie, G.Y., Yang, R.: Friction and wear behavior of carbon nanotubes reinforced polyamide 6 composites under dry sliding and water lubricated condition. Compos. Sci. Technol. **69**, 606–611 (2009)
128. Giraldo, L.F., López, B.L., Brostow, W.: Effect of the type of carbon nanotubes on tribological properties of polyamide 6. Polym. Eng. Sci. **49**, 896–902 (2009)
129. Armstrong, G., Ruether, M., Blighe, F., Blau, W.: Functionalised multi-walled carbon nanotubes for epoxy nanocomposites with improved performance. Polym. Int. **58**, 1002–1009 (2009)
130. Li, J., Zhang, L.Q.: The effects of adding carbon nanotubes to the mechanical and tribological properties of a carbon fibre reinforced polyether ether ketone composite. Proc. Inst. Mech. Eng. Part C J. Mech. Eng. Sci. **223**, 2501–2507 (2009)
131. Cai, H., Yan, F., Xue, Q.: Investigation of tribological properties of polyimide/carbon nanotube nanocomposites. Mater. Sci. Eng. A. **364**, 94–100 (2004)
132. Endo, M., Kim, Y.A., Hayashi, T., Fukai, Y., Oshida, K., Terrones, M., Yanagisawa, T., Higaki, S., Dresselhaus, M.S.: Structural characterization of cup-stacked-type nanofibers with an entirely hollow core. Appl. Phys. Lett. **80**, 1267–1269 (2002)
133. Liu, Q., Ren, W., Chen, Z.-G., Yin, L., Li, F., Cong, H., Cheng, H.-M.: Semiconducting properties of cup-stacked carbon nanotubes. Carbon N. Y. **47**, 731–736 (2009)
134. Endo, M., Kim, Y.A., Ezaka, M., Osada, K., Yanagisawa, T., Hayashi, T., Terrones, M., Dresselhaus, M.S.: Selective and efficient impregnation of metal nanoparticles on cup-stacked-type carbon nanofibers. Nano Lett. **3**, 723–726 (2003)
135. Choi, Y.-K., Gotoh, Y., Sugimoto, K., Song, S.-M., Yanagisawa, T., Endo, M.: Processing and characterization of epoxy nanocomposites reinforced by cup-stacked carbon nanotubes. Polymer (Guildf). **46**, 11489–11498 (2005)
136. Yokozeki, T., Iwahori, Y., Ishiwata, S.: Matrix cracking behaviors in carbon fiber/epoxy laminates filled with cup-stacked carbon nanotubes (CSCNTs). Compos. Part A Appl. Sci. Manuf. **38**, 917–924 (2007)
137. Yokozeki, T., Iwahori, Y., Ishiwata, S., Enomoto, K.: Mechanical properties of CFRP laminates manufactured from unidirectional prepregs using CSCNT-dispersed epoxy. Compos. Part A Appl. Sci. Manuf. **38**, 2121–2130 (2007)
138. Werner, P., Altstädt, V., Jaskulka, R., Jacobs, O., Sandler, J.K.W., Shaffer, M.S.P., Windle, A. H.: Tribological behaviour of carbon-nanofibre-reinforced poly (ether ether ketone). Wear. **257**, 1006–1014 (2004)
139. Zhang, L.C., Zarudi, I., Xiao, K.Q.: Novel behaviour of friction and wear of epoxy composites reinforced by carbon nanotubes. Wear. **261**, 806–811 (2006)

140. Yang, Z., Dong, B., Huang, Y., Liu, L., Yan, F.-Y., Li, H.-L.: A study on carbon nanotubes reinforced poly (methyl methacrylate) nanocomposites. Mater. Lett. **59**, 2128–2132 (2005)
141. Elinski, M.B., Liu, Z., Spear, J.C., Batteas, J.D.: 2D or not 2D? The impact of nanoscale roughness and substrate interactions on the tribological properties of graphene and MoS_2. J. Phys. D. Appl. Phys. **50**, 103003 (2017). http://stacks.iop.org/0022-3727/50/i=10/a=103003
142. Pan, B., Tan, J., Jia, H., Chen, J., Tai, Y., Liu, J., Zhang, Y., Niu, Q.: Tribological behavior of phenolic nanocomposites reinforced by 2D atomic crystal of boron nitride. J. Polym. Mater. **33**, 567 (2016)
143. Uddin, F.: Clays, nanoclays, and montmorillonite minerals. Metall. Mater. Trans. A. **39**, 2804–2814 (2008). https://doi.org/10.1007/s11661-008-9603-5
144. Alexandre, M., Dubois, P.: Polymer-layered silicate nanocomposites: preparation, properties and uses of a new class of materials. Mater. Sci. Eng. R Reports. **28**, 1–63 (2000). https://doi.org/10.1016/S0927-796X(00)00012-7
145. Yu, Y., Gu, J., Kang, F., Kong, X., Mo, W.: Surface restoration induced by lubricant additive of natural minerals. Appl. Surf. Sci. **253**, 7549–7553 (2007)
146. Lange, J., Wyser, Y.: Recent innovations in barrier technologies for plastic packaging? A review. Packag. Technol. Sci. **16**, 149–158 (2003). https://doi.org/10.1002/pts.621
147. Sorrentino, A., Pantani, R., Brucato, V.: Injection molding of syndiotactic polystyrene/clay nanocomposites. Polym. Eng. Sci. **46**, 1768–1777 (2006)
148. Gorrasi, G., Milone, C., Piperopoulos, E., Lanza, M., Sorrentino, A.: Hybrid clay mineral-carbon nanotube-PLA nanocomposite films. Preparation and photodegradation effect on their mechanical, thermal and electrical properties. Appl. Clay Sci. **71**, 49–54 (2013). https://doi.org/10.1016/j.clay.2012.11.004
149. Raka, L., Sorrentino, A., Bogoeva-Gaceva, G.: Isothermal crystallization kinetics of polypropylene latex-based nanocomposites with organo-modified clay. J. Polym. Sci. Part B Polym. Phys. **48**, 1927–1938 (2010). https://doi.org/10.1002/polb.22069
150. Hussain, F.: Review article: polymer-matrix nanocomposites, processing, manufacturing, and application: an overview. J. Compos. Mater. **40**, 1511–1575 (2006). https://doi.org/10.1177/0021998306067321
151. Dasari, A., Yu, Z.-Z., Mai, Y.-W., Hu, G.-H., Varlet, J.: Clay exfoliation and organic modification on wear of nylon 6 nanocomposites processed by different routes. Compos. Sci. Technol. **65**, 2314–2328 (2005)
152. Jawahar, P., Gnanamoorthy, R., Balasubramanian, M.: Tribological behaviour of clay–thermoset polyester nanocomposites. Wear. **261**, 835–840 (2006)
153. Yuan, Q., Ramisetti, N., Misra, R.D.K.: Nanoscale near-surface deformation in polymer nanocomposites. Acta Mater. **56**, 2089–2100 (2008). https://doi.org/10.1016/j.actamat.2007.12.051
154. Srinath, G., Gnanamoorthy, R.: Effect of nanoclay reinforcement on tensile and tribo behaviour of Nylon 6. J. Mater. Sci. **40**, 2897–2901 (2005)
155. Srinath, G., Gnanamoorthy, R.: Two-body abrasive wear characteristics of Nylon clay nanocomposites – effect of grit size, load, and sliding velocity. Mater. Sci. Eng. A. **435**, 181–186 (2006)
156. Peng, Q.-Y., Cong, P.-H., Liu, X.-J., Liu, T.-X., Huang, S., Li, T.-S.: The preparation of PVDF/clay nanocomposites and the investigation of their tribological properties. Wear. **266**, 713–720 (2009)
157. Fan, B., Yang, Y., Feng, C., Ma, J., Tang, Y., Dong, Y., Qi, X.: Tribological properties of fabric self-lubricating liner based on organic montmorillonite (OMMT) reinforced phenolic (PF) nanocomposites as hybrid matrices. Tribol. Lett. **57**, 22 (2015)
158. Landi, G., Sorrentino, A., Fedi, F., Neitzert, H.C., Iannace, S.: Cycle stability and dielectric properties of a new biodegradable energy storage material. Nano Energy. **17**, 348–355 (2015). https://doi.org/10.1016/j.nanoen.2015.09.006

159. Li, X., Cai, W., An, J., Kim, S., Nah, J., Yang, D., Piner, R., Velamakanni, A., Jung, I., Tutuc, E.: Large-area synthesis of high-quality and uniform graphene films on copper foils. Science (80). **324**, 1312–1314 (2009)
160. Choi, W., Lahiri, I., Seelaboyina, R., Kang, Y.S.: Synthesis of graphene and its applications: a review. Crit. Rev. Solid State Mater. Sci. **35**, 52–71 (2010)
161. Allen, M.J., Tung, V.C., Kaner, R.B.: Honeycomb carbon: a review of graphene. Chem. Rev. **110**, 132–145 (2009)
162. Landi, G., Fedi, F., Sorrentino, A., Neitzert, H.C., Iannace, S.: Gelatin/graphene systems for low cost energy storage. In: AIP Conference Proceedings, vol. 1599(1), pp. 202–205. AIP Publishing, Naples (2014). https://doi.org/10.1063/1.4876813
163. Dreyer, D.R., Park, S., Bielawski, C.W., Ruoff, R.S.: The chemistry of graphene oxide. Chem. Soc. Rev. **39**, 228–240 (2010)
164. Wei, D., Grande, L., Chundi, V., White, R., Bower, C., Andrew, P., Ryhänen, T.: Graphene from electrochemical exfoliation and its direct applications in enhanced energy storage devices. Chem. Commun. **48**, 1239–1241 (2012)
165. Shen, X.-J., Pei, X.-Q., Fu, S.-Y., Friedrich, K.: Significantly modified tribological performance of epoxy nanocomposites at very low graphene oxide content. Polymer (Guildf). **54**, 1234–1242 (2013)
166. Landi, G., Sorrentino, A., Iannace, S., Neitzert, H.C.: Differences between graphene and graphene oxide in gelatin based systems for transient biodegradable energy storage applications. Nanotechnology. **28**, 54005 (2016). https://doi.org/10.1088/1361-6528/28/5/054005
167. Furio, A., Landi, G., Altavilla, C., Sofia, D., Iannace, S., Sorrentino, A., Neitzert, H.C.: Light irradiation tuning of surface wettability, optical, and electric properties of graphene oxide thin films. Nanotechnology. **28**, 54003 (2016)
168. Berman, D., Erdemir, A., Sumant, A.V.: Graphene: a new emerging lubricant. Mater. Today. **17**, 31–42 (2014). https://doi.org/10.1016/j.mattod.2013.12.003
169. Pan, B., Peng, S., Song, S., Chen, J., Liu, J., Liu, H., Zhang, Y., Niu, Q.: The adaptive tribological investigation of polycaprolactam/graphene nanocomposites. Tribol. Lett. **65**, 9 (2017)
170. Tai, Z., Chen, Y., An, Y., Yan, X., Xue, Q.: Tribological behavior of UHMWPE reinforced with graphene oxide nanosheets. Tribol. Lett. **46**, 55–63 (2012)
171. Min, C., Nie, P., Song, H.-J., Zhang, Z., Zhao, K.: Study of tribological properties of polyimide/graphene oxide nanocomposite films under seawater-lubricated condition. Tribol. Int. **80**, 131–140 (2014)
172. Pan, B., Xu, G., Zhang, B., Ma, X., Li, H., Zhang, Y.: Preparation and tribological properties of polyamide 11/graphene coatings. Polym. Plast. Technol. Eng. **51**, 1163–1166 (2012)
173. Huang, T., Xin, Y., Li, T., Nutt, S., Su, C., Chen, H., Liu, P., Lai, Z.: Modified graphene/polyimide nanocomposites: reinforcing and tribological effects. ACS Appl. Mater. Interfaces. **5**, 4878–4891 (2013)
174. Song, H., Wang, Z., Yang, J., Jia, X., Zhang, Z.: Facile synthesis of copper/polydopamine functionalized graphene oxide nanocomposites with enhanced tribological performance. Chem. Eng. J. **324**, 51–62 (2017). https://doi.org/10.1016/j.cej.2017.05.016
175. Kalin, M., Zalaznik, M., Novak, S.: Wear and friction behaviour of poly-ether-ether-ketone (PEEK) filled with graphene, WS_2 and CNT nanoparticles. Wear. **332**, 855–862 (2015)
176. Landi, G., Altavilla, C., Ciambelli, P., Neitzert, H.C., Iannace, S., Sorrentino, A.: Preliminary investigation of polystyrene/MoS2-Oleylamine polymer composite for potential application as low-dielectric material in microelectronics. In: AIP Conference Proceedings, p. 20044. AIP Publishing, Naples (2015). https://doi.org/10.1063/1.4937322
177. Singer, I.L., Pollock, H.: Fundamentals of Friction: Macroscopic and Microscopic Processes. Springer Netherlands, Dordrecht (1992). https://doi.org/10.1007/978-94-011-2811-7

178. Balendhran, S., Deng, J., Ou, J.Z., Walia, S., Scott, J., Tang, J., Wang, K.L., Field, M.R., Russo, S., Zhuiykov, S.: Enhanced charge carrier mobility in two-dimensional high dielectric molybdenum oxide. Adv. Mater. **25**, 109–114 (2013)
179. Kalantar-Zadeh, K., Tang, J., Wang, M., Wang, K.L., Shailos, A., Galatsis, K., Kojima, R., Strong, V., Lech, A., Wlodarski, W.: Synthesis of nanometre-thick MoO_3 sheets. Nanoscale. **2**, 429–433 (2010)
180. Radisavljevic, B., Radenovic, A., Brivio, J., Giacometti, V., Kis, A.: Single-layer MoS_2 transistors. Nat. Nanotechnol. **6**, 147–150 (2011). https://doi.org/10.1038/nnano.2010.279
181. Kumar, A., Ahluwalia, P.K.: Electronic structure of transition metal dichalcogenides monolayers 1H-MX2 (M= Mo, W; X= S, Se, Te) from ab-initio theory: new direct band gap semiconductors. Eur. Phys. J. B. **85**, 186 (2012)
182. Bissessur, R., Gallant, D., Brüning, R.: Novel nanocomposite material consisting of poly [oxymethylene-(oxyethylene)] and molybdenum disulfide. Mater. Chem. Phys. **82**, 316–320 (2003). https://doi.org/10.1016/S0254-0584(03)00310-9
183. Bissessur, R., White, W.: Novel alkyl substituted polyanilines/molybdenum disulfide nanocomposites. Mater. Chem. Phys. **99**, 214–219 (2006). https://doi.org/10.1016/j.matchemphys.2005.10.012
184. Lin, B.-Z., Ding, C., Xu, B.-H., Chen, Z.-J., Chen, Y.-L.: Preparation and characterization of polythiophene/molybdenum disulfide intercalation material. Mater. Res. Bull. **44**, 719–723 (2009). https://doi.org/10.1016/j.materresbull.2008.09.031
185. Wang, T., Liu, W., Tian, J., Shao, X., Sun, D.: Structure characterization and conductive performance of polypyrrol-molybdenum disulfide intercalation materials. Polym. Compos. **25**, 111–117 (2004). https://doi.org/10.1002/pc.20009
186. Naffakh, M., Díez-Pascual, A.M., Remškar, M., Marco, C.: New inorganic nanotube polymer nanocomposites: improved thermal, mechanical and tribological properties in isotactic polypropylene incorporating INT-MoS_2. J. Mater. Chem. **22**, 17002 (2012). https://doi.org/10.1039/c2jm33422d
187. Basavaraj, E., Ramaraj, B.: Polycarbonate/molybdenum disulfide/carbon black composites: physicomechanical, thermal, wear, and morphological properties. Polym. Compos. **33**, 619–628 (2012). https://doi.org/10.1002/pc.22179
188. Basavaraj, E., Ramaraj, B.: A study on mechanical, thermal, and wear characteristics of nylon 66/molybdenum disulfide composites reinforced with glass fibers. Polym. Compos. **33**, 1570–1577 (2012). https://doi.org/10.1002/pc.22293
189. Benavente, E., González, G.: Microwave activated lithium intercalation in transition metal sulfides. Mater. Res. Bull. **32**, 709–717 (1997). https://doi.org/10.1016/S0025-5408(97)00037-8
190. Najmaei, S., Zou, X., Er, D., Li, J., Jin, Z., Gao, W., Zhang, Q., Park, S., Ge, L., Lei, S., Kono, J., Shenoy, V.B., Yakobson, B.I., George, A., Ajayan, P.M., Lou, J.: Tailoring the physical properties of molybdenum disulfide monolayers by control of interfacial chemistry. Nano Lett. **14**, 1354–1361 (2014). https://doi.org/10.1021/nl404396p
191. Divigalpitiya, W.M.R., Morrison, S.R., Frindt, R.F.: Thin oriented films of molybdenum disulphide. Thin Solid Films. **186**, 177–192 (1990). https://doi.org/10.1016/0040-6090(90)90511-B
192. Zhou, X., Wu, D., Shi, H., Fu, X., Hu, Z., Wang, X., Yan, F.: Study on the tribological properties of surfactant-modified MoS_2 micrometer spheres as an additive in liquid paraffin. Tribol. Int. **40**, 863–868 (2007). https://doi.org/10.1016/j.triboint.2006.09.002
193. Altavilla, C., Sarno, M., Ciambelli, P.: A novel wet chemistry approach for the synthesis of hybrid 2D free-floating single or multilayer nanosheets of MS_2 @oleylamine (M═Mo, W). Chem. Mater. **23**, 3879–3885 (2011). https://doi.org/10.1021/cm200837g
194. Altavilla, C., Ciambelli, P., Sarno, M.: "One-pot" synthesis of 2D, 1D, e 0D nano crystals of tungsten and molybdenum chalcogenides (WS_2,MoS_2) functionalized with long chain amine and/or carboxylic acid and/or thiol, WO/2012/042511. http://patentscope.wipo.int/search/en/detail.jsf?docId=WO2012042511&recNum=3&docAn=IB2011054334&queryString=NONOTUBE*or%22NANOTUBE*%22&maxRec=1363 (2012). Accessed 14 Oct 2014

195. Altavilla, C., Sarno, M., Ciambelli, P., Senatore, A., Petrone, V.: New "chimie douce" approach to the synthesis of hybrid nanosheets of MoS_2 on CNT and their anti-friction and anti-wear properties. Nanotechnology. **24**, 125601 (2013). https://doi.org/10.1088/0957-4484/24/12/125601
196. Sorrentino, A., Altavilla, C., Merola, M., Senatore, A., Ciambelli, P., Iannace, S.: Nanosheets of MoS_2-oleylamine as hybrid filler for self-lubricating polymer composites: thermal, tribological, and mechanical properties. Polym. Compos. **36**, 1124–1134 (2015)
197. Altavilla, C., Fedi, F., Sorrentino, A., Iannace, S., Ciambelli, P.: Polystyrene/MoS2@oleylamine nanocomposites. In: AIP Conference Proceedings, Naples, pp. 194–197 (2014). https://doi.org/10.1063/1.4876811
198. Hu, K.H., Wang, J., Schraube, S., Xu, Y.F., Hu, X.G., Stengler, R.: Tribological properties of MoS_2 nano-balls as filler in polyoxymethylene-based composite layer of three-layer self-lubrication bearing materials. Wear. **266**, 1198–1207 (2009)
199. Hu, K.H., Schraube, S., Xu, Y.F., Hu, X.G., Stengler, R.: Micro-tribological behavior of polyacetal-based self-lubrication composite materials modified with MoS_2. Tribology. **30**, 38–45 (2010)
200. Hu, K.H., Hu, X.G., Wang, J., Xu, Y.F., Han, C.L.: Tribological properties of MoS_2 with different morphologies in high-density polyethylene. Tribol. Lett. **47**, 79–90 (2012)
201. Wang, J., Hu, K.H., Xu, Y.F., Hu, X.G.: Structural, thermal, and tribological properties of intercalated polyoxymethylene/molybdenum disulfide nanocomposites. J. Appl. Polym. Sci. **110**, 91–96 (2008)
202. Yang, J.-F., Parakash, B., Hardell, J., Fang, Q.-F.: Tribological properties of transition metal dichalcogenide based lubricant coatings. Front. Mater. Sci. **6**, 116–127 (2012). https://doi.org/10.1007/s11706-012-0155-7
203. Xin, Y., Li, T., Gong, D., Xu, F., Wang, M.: Preparation and tribological properties of graphene oxide/nano-MoS_2 hybrid as multidimensional assembly used in the polyimide nanocomposites. RSC Adv. **7**, 6323–6335 (2017). https://doi.org/10.1039/C6RA27108A

Polymeric Solid Lubricant Transfer Films: Relating Quality to Wear Performance

6

Jiaxin Ye, Diana Haidar, and David Burris

Contents

Abstract

Polymers and polymer composites are often described as solid lubricants because they provide relatively low friction coefficients and wear rates in unlubricated and other extreme tribological conditions. However, few, if any, are inherently lubricious or wear resistant. These materials achieve useful tribological properties by depositing a layer of debris onto the mating counterface; this sacrificial layer is called a transfer film and it shields the polymer from damage by the harder counterface. The friction and wear performance of these systems depend as much on the formation, evolution, and stability of the transfer film as they do on the structure and composition of the solid lubricant itself. Although it is understood that transfer films are essential for high tribological performance of polymers and polymer composites, the causal relationship between transfer film

J. Ye
Institute of Tribology, Hefei University of Technology, Hefei, China

D. Haidar · D. Burris (✉)
Department of Mechanical Engineering, University of Delaware, Newark, DE, USA
e-mail: dlburris@udel.edu

P. L. Menezes et al. (eds.), *Self-Lubricating Composites*,
https://doi.org/10.1007/978-3-662-64243-6_6

qualities and wear resistance remains uncertain due largely to the difficulty in quantitatively measuring their properties. There have been increased efforts, particularly in the last 10 years, to develop quantitative methods to assess the topographical, adhesive, mechanical, and chemical properties of polymer transfer films. This chapter reviews the latest efforts to measure transfer film qualities and quantitatively relate them to the tribological performance of solid lubricant polymers.

6.1 Background

Certain polymer blends and composites achieve low friction coefficients ($\mu < 0.2$) and low wear rates ($k < 10^{-6}$ mm^3/Nm) without intentional external lubrication of the contact area [1–3]; as such, these materials are known as solid lubricants. Unfortunately, no general rules exist to guide the design of such materials, and solid lubricant materials discovery almost always involves substantial trial and error. Fillers, depending on their properties, can affect the tribology of polymers by preferentially supporting load [4], arresting subsurface cracks [5], and modifying interfacial shear strength [6] to name a few mechanisms. However, none of these functions explains the orders of magnitude effects some small changes in filler composition [2, 7], loading [2, 8], or environment [9, 10] are known to have on the wear rate of the system. Normally, the polymer produces wear debris during sliding against a hard metallic counterface, most commonly steel. These debris particles are dragged through the contact and are eventually ejected from the wear track in most cases. In special cases, the debris can adhere to the counterface to initiate the formation of a layer called the transfer film. Regardless of the materials used, low wear sliding of polymeric materials always leaves a thin and continuous transfer film on the steel counterpart. Likewise, high wear sliding of polymers always leaves a thick and patchy transfer film. The studies of polymer solid lubricants in the literature provide strong evidence that the properties of transfer films and the measured wear rates are related [11–20].

Briscoe [13] first recognized the relationship between transfer film properties and polymer wear rate and concluded that the primary role of the filler is to help adhere the debris to the counterface. He suggested that active fillers degrade the relatively inert polymer chains thereby creating new opportunities for bonding with the counterface. Bahadur and Gong [21] asserted that the role of a filler is to enhance counterface adhesion by having the active filler itself create the bond between the polymer debris and counterface. Both theories support the need for a tribochemically adhered transfer film that reduces wear by protecting the polymer from the hard and high energy counterface. Bahadur and Tabor [22] conducted a clever experiment to test this idea. They used low wear polymers to form high quality transfer films and then measured the wear rates of traditionally high wear polymers against presumably protective predeposited transfer films. Interestingly, these high quality predeposited films had no effect on the wear rate of the high wear polymers. On further inspection, they found that the predeposited transfer film was removed almost immediately

during sliding against the new polymer pin. Based on this observation, they concluded that the high-quality transfer films must be a consequence of the small debris generated during low wear sliding and not the cause of low wear. This is supported by evidence from Ricklin [23], Tanaka and Kawakami [24], Blanchet and Kennedy [5], and Burris and Sawyer [2], all of whom concluded that effective fillers reduced the wear of polytetrafluoroethylene (PTFE) by disrupting subsurface damage and thereby reducing debris size.

PTFE-based polymer systems have been the subject of numerous studies of the relationship between tribochemistry, transfer film adhesion, and tribological performance. Gong et al. [25] and Blanchet et al. [26] used XPS (X-ray photoelectron spectroscopy) to study the effects of tribochemistry on transfer film adhesion and wear reduction of PTFE-based materials. Although they observed clear evidence of tribochemistry in the form of metal fluorides, these reaction products occurred in both low and high wear systems. Furthermore, because fluorine is monovalent, metal-fluorides represent the transfer of fluorine from the polymer to the counterface and not a bond between them. Both studies concluded that tribochemically induced transfer film adhesion was not the primary means of wear reduction in the PTFE system.

Although much of the recent literature suggests that tribochemistry is simply a consequence of bond-breaking during tribological contact, other studies have shown clear evidence that it can play a critical role in wear reduction. During studies of a particularly low wear alumina-PTFE system in environments of variable humidity, Krick et al. [9] found that the wear rate increased by orders of magnitude as the availability of gaseous water was systematically removed. This observation provides strong evidence that tribochemistry plays an important role in the wear reduction of PTFE and, potentially, polymers in general [9, 10, 27]. To date, however, the link between tribochemistry, transfer film adhesion, and wear reduction remains uncertain.

The way in which transfer films develop may have equally important implications for elucidating causation between transfer film qualities, adhesion, and wear rate. Based on XPS studies, Gong et al. [28] concluded that PTFE-based transfer films grow over time. They interpreted their result as evidence of a thickening process in which new layers deposit onto old layers; the role of the filler, they proposed, is to strengthen the bond at these internal interfaces within the transfer film. Blanchet et al. [26] found similar evidence of growth but concluded that transfer film growth was the result of new debris adhering to remaining areas of exposed counterface. Ye et al. [29] used in situ optical microscopy to study the development of a transfer film in real time. Their results showed that the transfer film developed as new debris adhered to remaining areas of exposed counterface. The results also showed that existing transfer films thickened with increased sliding. More importantly, they showed that the transfer film of a low wear PTFE-based system was very stable; many of the debris particles deposited early in the test could be identified at the end of the test. The results demonstrated that the transfer films of this very wear resistant polymer are themselves very wear resistant. Ye et al. [6] studied the wear rate of this transfer film directly and found it to be exceedingly resistant to removal with an

effective wear rate orders of magnitude lower than that of the parent polymer. Interestingly, the wear rate increased by many orders of magnitude when the surface energy of the wear probe increased beyond a threshold value, thus demonstrating that a low wear condition simply reflects the presence of a single weak interface to accommodate sliding.

There is little doubt based on the literature that transfer films play one or more critical roles in governing the wear response of polymeric solid lubricants. Nonetheless, the specific way in which fillers, polymers, stresses, and environments govern the development and properties of the transfer films remain unclear. This chapter reviews the most recent advancements in this field that have helped to shape our understanding of the cause-effect relationships between materials design, transfer film properties, and tribological performance of these polymer systems.

6.2 Properties of Transfer Films

6.2.1 Topography

Transfer films and their properties are central to most hypothesized mechanisms of polymer wear reduction. The reason is well-illustrated by Fig. 6.1. Two 5 wt% alumina-PTFE nanocomposites were prepared identically and tested under the same tribological conditions (50 mm/s, 6.4 MPa). The only known differences were the size, morphology, and phase of the alumina filler particles. The Δ-Γ phase alumina-PTFE composite produced a moderate wear rate of 10^{-5} mm^3/Nm, while the α phase alumina-PTFE composite produced a low wear rate of 10^{-7} mm^3/Nm. There are marked visual differences between the transfer films produced by these materials. The transfer film of the moderate wear rate composite is thicker and patchier, while the transfer film of the low wear rate composite is thinner and more complete. It is logical to conclude that the 100X difference in wear rates is somehow related to the

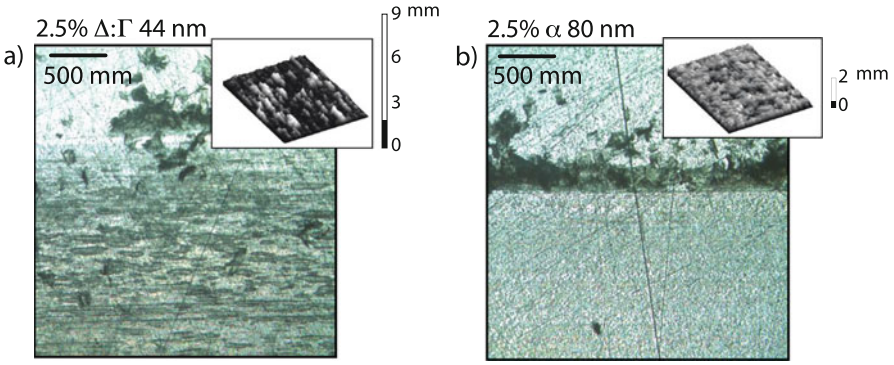

Fig. 6.1 Two types of transfer films of PTFE nanocomposites: (**a**) transfer film of a moderate wear system (K~ 10^{-5} mm^3/Nm, 44 nm Δ: Γ alumina) and (**b**) transfer film of an ultra-low-wear system (K~10^{-7} mm^3/Nm, 80 nm α alumina)

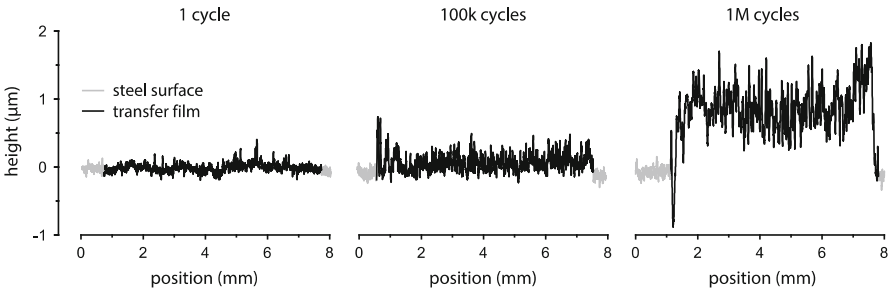

Fig. 6.2 Stylus profilometry measurements of transfer film thickness. (Image reprinted from [27] with permission)

obvious visual differences between the transfer films formed by these similar composite materials.

There are numerous examples in the literature for which improved wear resistance of a filled polymer is accompanied by comparable visual improvements in the appearance of the transfer film [5, 14–17, 21, 22, 30–33]. Wang et al. [7] found that nanoscale ZrO_2 significantly reduced the wear of polyetheretherketone (PEEK). Scanning electron microscopy revealed that the transfer film of unfilled PEEK was "thick, lumpy, and incoherent" while that of ZrO_2-PEEK nanocomposite was "thin, uniform, and coherent." They obtained similar results from a study of nanoscale SiC in PEEK [8] and described the transfer films as "thin, uniform, and tenacious" based on similar post-test visual observations of transfer films. The authors attributed the tribological benefits of nanofillers in PEEK to improvements in quality of the transfer films. Li et al. [9] found that the addition of nanoscale ZnO to polytetrafluoroethylene (PTFE) reduced its wear rate while improving the "uniformity and tenacity" of the transfer films. Sawyer et al. [10] described the transfer films of low wear nanoscale alumina reinforced PTFE as "well adhered, smooth, and continuous." Bhimaraj et al. [11] found that alumina filled polyethylene terephthalate (PET) nanocomposites produced more "coherent and uniform" transfer films with increasing nanoparticle loading. McCook et al. [12] noted that more "uniform" transfer films accompanied improved friction and wear performance of their epoxy nanocomposites.

Although there is clearly a ubiquitous relationship between wear rate and transfer film quality, it is difficult to assess the state of the art in general due to a lack of standard definitions for the terms used to describe these properties. "Thinness" can be quantified and is the obvious place to begin defining transfer film quality. A traditional 1-D thickness measurement is illustrated in Fig. 6.2. In these measurements, a sharp stylus is lightly loaded and dragged across the width of the transfer film, while a displacement transducer tracks the deflection of the tip. The height of the transfer film was determined here using the bare counterface as a baseline for subtraction. The average height of the transfer film was defined as the difference between the *average height* within the wear track and the average height outside the wear track [27]. Blanchet and Kennedy [5] were among the first to use this method to

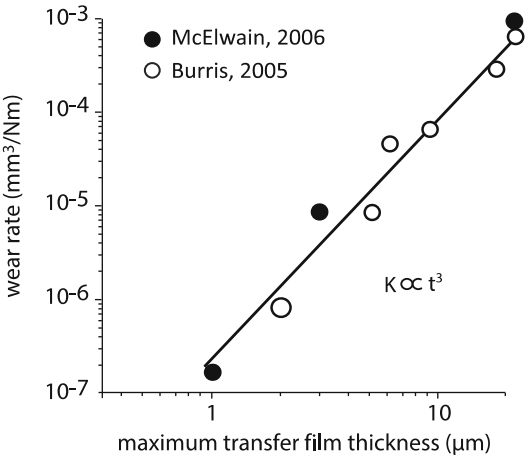

Fig. 6.3 Observed correlation between transfer film thickness and wear rates of various PTFE-based systems. (Image reprinted from [19, 34] with permission)

determine the thickness of unfilled PTFE transfer films, which they reported to be in the range from 4 to 20 μm. Pitenis et al. [27] used this method to show that the transfer films of alumina-PTFE nanocomposites thickened with increased sliding distance and approached ~1 μm at steady state (Fig. 6.2). When they removed environmental moisture, the transfer films thickened and wear rates increased [10].

Many transfer films are discontinuous or patchy. In these cases, the thickness from the method described above will depend on thickness and coverage (the output thickness will be half the transfer film thickness at 50% coverage). A different approach is necessary if the goal is to assess thickness directly. Burris and Sawyer [34] used optical profilometry to obtain the same type of surface profile information, but instead of quantifying the average thickness as described above, they quantified the maximum thickness, which depends only on heights of the transferred debris particles. McElwain [35] used mapping stylus profilometry to quantify maximum transfer film thickness for similar materials. Despite differences in the techniques used, their data suggest that the wear rate of this system is proportional to the cube of the maximum transfer film thickness (Fig. 6.3).

Laux and Schwartz [36] proposed a robust method to quantify average thickness that is independent of the coverage; their method is illustrated in Fig. 6.4. When the transfer film is statistically distinct from the roughness, two peaks will emerge in the probability density function of surface height; the lower elevation peak is associated with the counterface and the higher elevation peak is associated with the transfer film. Laux and Schwartz fit two Gaussian curves to the data set and used the distance between the fitted peaks to quantify the most probable thickness of the transfer film. Using this method, they found no strong correlation between wear and transfer films thickness for unfilled PEEK tested at varying conditions [36, 37]. The correlation between transfer film thickness and wear rate appears to be system specific.

Transfer film coverage is similarly intuitive as a potential driver of wear protection; many researchers have used adjectives like complete, uniform, and continuous to describe them [30, 31, 33, 38–40]. In theory, the film area fraction (X), which is

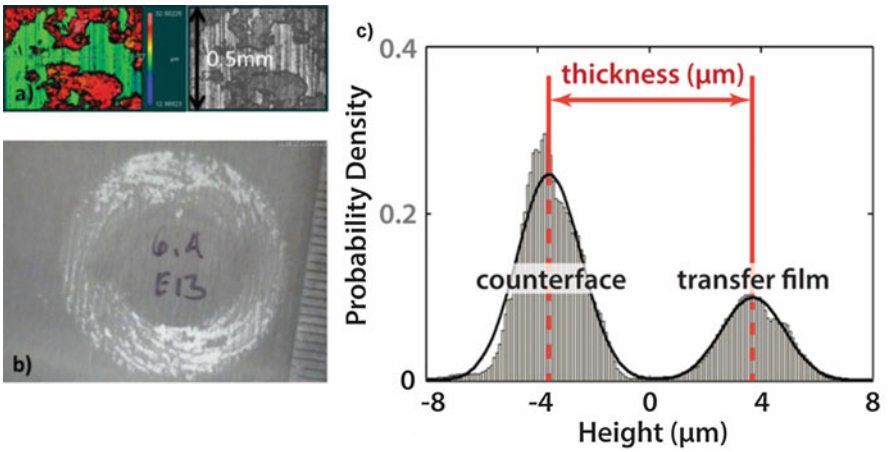

Fig. 6.4 Laux and Schwartz's method of measuring transfer film thickness using the counterface's surface height histogram: (**a**) scanning white light interferometry image of the wear track, (**b**) optical image of the wear track, and (**c**) probability density of the wear track height distribution. (Image reprinted from [36] with permission)

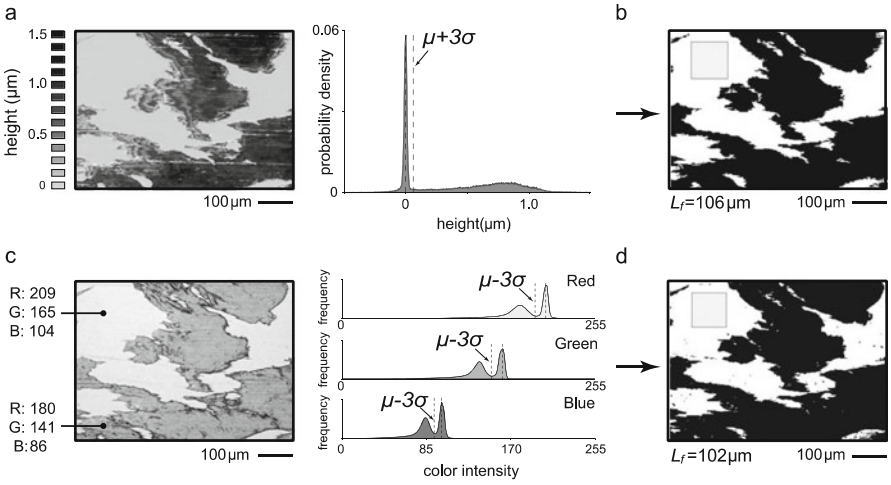

Fig. 6.5 Example of converting color images or height profiles to pixel representations of transfer film (black) and exposed counterface (white) to measure (**a**) area fraction and (**b**) free-space length. (Image reprinted from [41] with permission)

the ratio of film coverage area to total area, is easy to quantify using optical microscopy, electron microscopy, or profilometry images. In some cases, by simply applying a threshold pixel value, transfer film images can be converted into binary maps from which area fraction is readily calculated, as illustrated by Fig. 6.5. Images size is also critical to the differentiation between the film and the counterface as

shown by Ye et al. [41]. Bhimaraj et al. [42] studied the wear and transfer film coverage of polyethylene terephthalate (PET) nanocomposites with different filler loadings and although transfer film area fraction increased with increased filler loading, area fraction and wear were not well correlated. Laux and Schwartz [36] used the same method to quantify transfer film area fraction and studied the effect of sliding direction on the wear of PEEK. They found that the wear rate decreased by 60% with a 100% increase in the transfer film area fraction when the sliding direction changed from single direction to reciprocating. Similarly, Ye et al. [41] found that the transfer film area fraction of a PTFE nanocomposite increased with decreased wear rate throughout a single wear test.

Transfer film thickness and coverage likely play an important role in wear mitigation but neither factor alone appears to be a reliable predictor of wear rate. Laux and Schwartz [37] suggested that transfer film heterogeneity/discontinuity is likely to be more directly relatable to the wear rate. This effect of nonuniformity is consistent with observations from Blanchet et al. [26] that transfer films developed by gradually filling in remaining areas of exposed counterface.

Because covered areas are theoretically protected, future transfer and wear are more likely governed by the nature of the uncovered areas than by the nature of the covered areas; this is consistent with the transfer films in Fig. 6.1. The high quality transfer film is thinner and covers more area, but the visual impression of "uniformity" comes from the fact that the characteristic size of the "gaps"/transfer film-free space/areas of exposed counterface have been substantially reduced. Thus, we propose that heterogeneity should be defined by the characteristic size of the uncovered areas or the free-spaces and not by their total area or area fraction.

Ye et al. [41] proposed that the free-space length (L_f), or the size of the characteristic free-space, limits the size of the wear fragment and may therefore serve as a more reliable topographical predictor of wear rate. The method used to measure free-space length begins with a representative image of the surface, which is then converted into a black and white image; black represents transfer film and white free-space. Their custom Matlab script used Monte Carlo simulation to identify the smallest randomly placed square for which the most probable number of intersecting transfer film pixels is zero; this length is the free-space length. The method is illustrated in Fig. 6.5 using optical and stylus based measurements of the same region. In theory, decreased free-space lengths should produce smaller debris; smaller debris consume less volume while producing thinner and more stable transfer films. Ye et al. [41] studied the relationship between free-space length and wear rate using low wear alumina-PTFE during the transition from high wear during run-in to low wear at steady state. Optical observations showed that the free space decreased with sliding distance as new debris gradually filled in the gaps in the transfer film as described previously by Blanchet et al. [26]. Changes in the free-space length were accompanied by changes in the wear rate as shown in Fig. 6.6a. Wear rate is plotted versus free-space length in Fig. 6.6b; the results suggest that reduced free-space

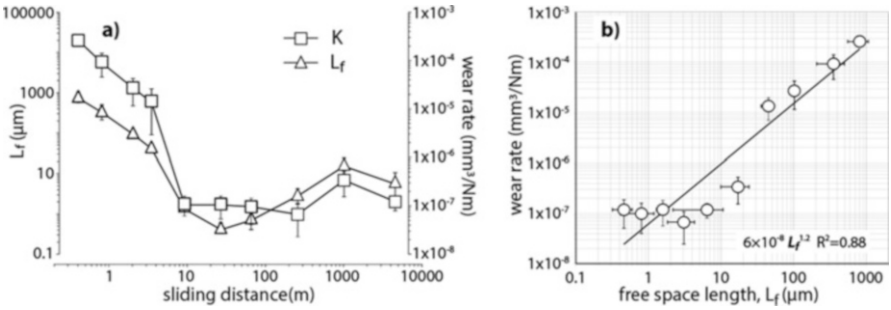

Fig. 6.6 (**a**) Transfer film free-space length and wear rate of an alpha-alumina PTFE nanocomposite during the course of a single wear test. (**b**) In-situ wear rate plotted against transfer film free-space length. (Image reprinted from [41] with permission)

length reduces wear down to a minimum value below which the wear rate remains constant at a value associated with the polymer on a perfect transfer film.

The relationship between free-space length and wear rate in Fig. 6.6a suggests that changes in free-space length ***caused*** changes in wear rate, particularly since increased wear rate at 1 km of sliding was preceded by an increase in free-space length. This fact combined with the ubiquitous observation that transfer films of all polymers become thinner and more continuous with reduced wear rates suggests that there may be some universal relationship between transfer film topography and polymer wear. Haidar et al. (manuscript under review by the journal *Wear*) tested the generality of the relationship between wear rate and transfer film topography using 10 different but representative polymers and polymer composites to determine the strength of correlation between wear rate and transfer film thickness, area fraction, and free-space length; the results are shown in Fig. 6.7. Although there is no reason to believe there should be a universal relationship between wear rate and transfer film properties, the data generally reflect the expected relationships; wear rate tended to decrease with increased coverage, decreased thickness, and decreased free-space length. The best fits to the data are shown as dashed lines. The variation between the data and the bet-fit model was used as an indicator of uncertainty when using the model fit to independently predict wear rate; the grey region represents the mean plus and minus one uncertainty. The uncertainty in the predicted wear rate is 8x based on the free-space length alone, 17x based on the area fraction alone, and 21x based on the thickness alone.

The existing studies show that transfer film topography has limited utility as an independent predictor of wear rate. Nonetheless, despite enormous variations in the material properties of the polymers, their wear properties, and the characteristics of their transfer films, there was a remarkably strong correlation between wear rate and free-space length. Future efforts by other investigators to quantify the topographical qualities of transfer films and relate them to wear rates of polymers will clarify

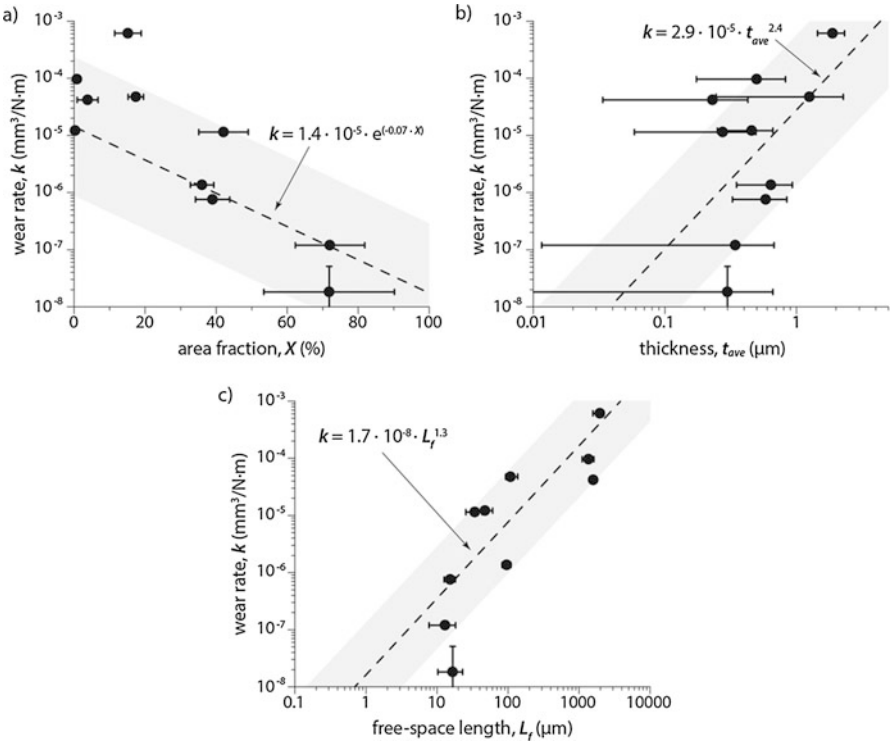

Fig. 6.7 A case study of correlation comparison between three transfer film quantifiers and the composite pin's wear rate. Materials studied by Haidar et al. (manuscript submitted to the journal *Wear*) include: PTFE, PEEK, PET, PPS, Epoxy, 5% wt. γ-Al_2O_3 + PTFE, 5% wt. α-Al_2O_3 + PTFE, 5% wt. γ-Al_2O_3 + PEEK, 5% wt. α-Al_2O_3 + PEEK and 32% wt. PEEK + PTFE

whether any general relationship exists between the topographical properties of transfer films and the wear of polymers.

6.2.2 Adhesion

Most hypotheses of polymer wear resistance are rooted in transfer film adhesion. Many have suggested the adhesion strength at the film-counterface interface determines the tenacity of the transfer film and the wear rate of the polymer. Bahadur and Tabor first showed evidence that transfer films are most likely adhered by mechanical engagement of the debris with the topographical features of the counterface [22]. While studying the effect of counterface finish on the transfer and wear of various PTFE composites, Burris and Sawyer [34] showed that while even extreme roughness and smoothness failed to affect transfer and wear of these materials at steady state, scratches oriented in the direction of sliding disrupted the formation of

the transfer film and increased wear rates by orders of magnitude. They concluded that debris was simply pushed from the contact because the surface lacked the features necessary to entrap the debris. Harris et al. [43] systematically studied the wear of the same material system against surfaces with a unidirectional finish. The lowest wear rates and best transfer films were observed when the surface roughness was aligned against the sliding direction. Wear resistance and transfer film quality degraded as the orientation approached the sliding direction. Laux and Schwartz studied the effect of roughness orientation on the transfer of polyetheretherketone (PEEK) using unidirectional surface finishes with a circular wear path. They found that the transfer films were thickest and patchiest when the sliding direction approached the roughness orientation [36]. TEM studies of the transfer films of a low wear epoxy nanocomposite [44] showed evidence that the transfer film initiated in the scratches. In sum, these results suggest strongly that polymer transfer films initiate by some form of mechanical engagement with topographical features of the counterface.

In cases of random surface finish, recent studies have shown that the low wear alumina-PTFE system can only achieve low wear and quality transfer films if there is sufficient water available to fuel a particular tribochemical pathway [9]. During sliding in humid environments, chain scission of the polymer backbone led to the formation of carboxylates, which directly linked degraded polymer chains to the counterface and filler particles. [27, 45]. Thus, both mechanical and chemical factors are necessary but neither sufficient for the formation of quality transfer films.

Transfer films only protect the polymer from contacting the counterface if they persist. Many have used the fact that transfer films are thin and continuous during low wear as evidence that they are also "tenacious," which implies persistence, longevity, and resistance to removal. However, Bahadur and Tabor showed that even high quality transfer films were quickly removed when the parent low wear polymer was replaced with a high wear polymer [22]. The preexisting transfer film had no wear reducing effect on the high wear polymer because the transfer film lacked tenacity. To date the relationship between wear rate, quality, persistence, and adhesive strength remains unresolved.

In 2013, Ye et al. [29] set out to determine the extent to which the transfer films of low wear alumina-PTFE persisted during sliding. Fig. 6.8 shows images of the transfer film after ~500 m of sliding. This point in the experiment is particularly interesting because it shows how the steady state transfer film initiates. At 485 m, the transfer film consists of a sparse collection of micron and even submicron debris fragments. After 20 m of additional sliding, it is clear that many of the fragments remain. As sliding continues, these debris fragments grow, merge, and homogenize into larger domains that can easily be identified after tens of thousands of additional sliding cycles. This study provides direct insight into the formation mechanisms of a specific transfer film and demonstrates, despite prior evidence to the contrary, that persistence is likely a necessary component of ultra-low-wear sliding of polymeric solid lubricants [40, 46, 47].

Persistence is almost certainly a function of the adhesive strength between the film or debris fragments and the counterface. Unfortunately, transfer film adhesion has proven difficult to quantify. The most common means to quantify coating adhesion is

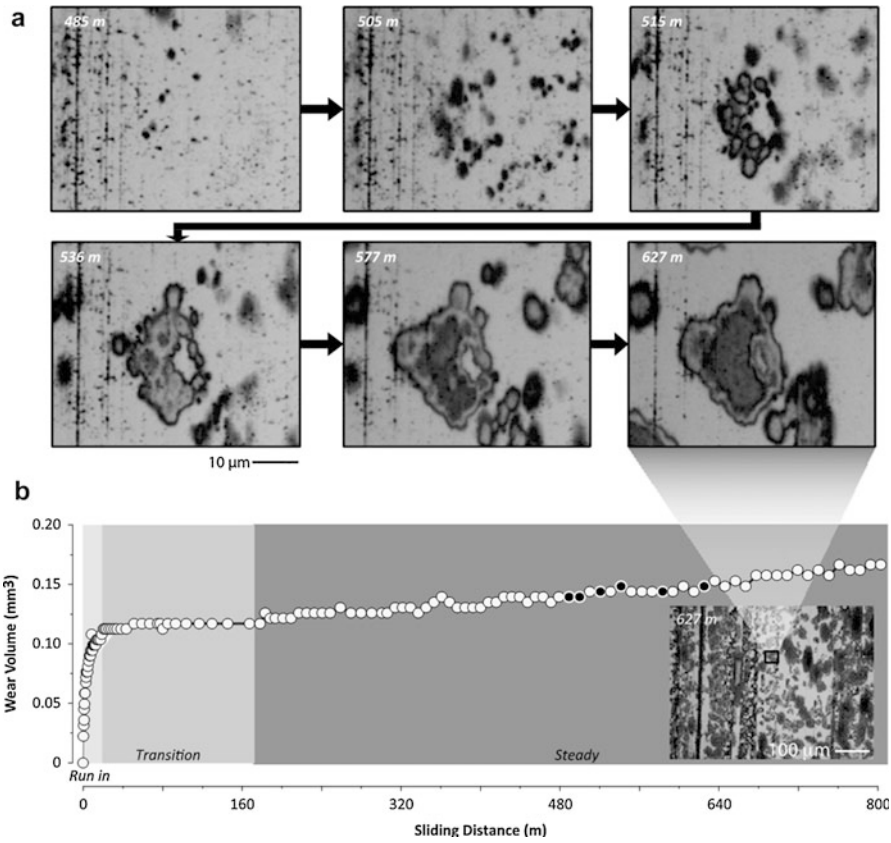

Fig. 6.8 Images of transfer film development in an ultra-low-wear alumina–PTFE nanocomposite: (**a**) images illustrating the evolution of the steady state transfer film as a function of distance slid; (**b**) wear volume as a function of distance slid. (Image reprinted from [29] with permission)

the scratch test. Typically, the normal force is ramped as an indenter slides across the coating surface; the load at which coating failure occurs provides an indirect measure of adhesion strength [48]. A more direct method is the peel test [49, 50]. Schwartz and Bahadur [33] bonded a copper tab to predeposited alumina-PPS nanocomposite transfer films and measured the peel strength as a function of alumina loading. They found that transfer film adhesion strength increased with increased filler loading (up to 2%) and counterface roughness. The results were consistent with debris size regulation and improved engagement of smaller debris fragments with the rough surface. In a subsequent paper, Bahadur and Sunkara [16] measured the wear rates and the transfer film adhesion strength of PPS nanocomposites of different filler types and loadings. Although the wear rates of the composites were both higher and lower than that of the unfilled polymer, their values correlated strongly with the adhesive strength of the transfer film (Fig. 6.9).

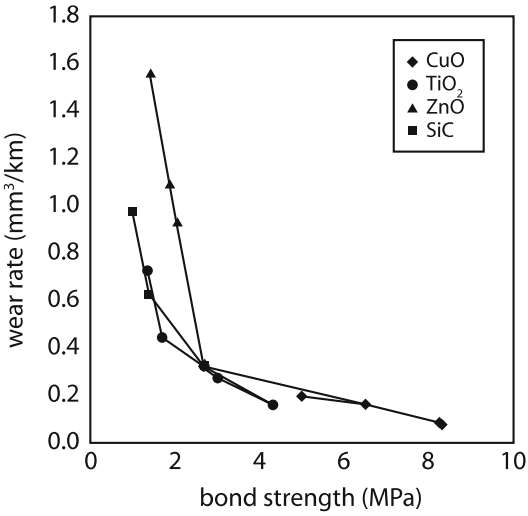

Fig. 6.9 Measured transfer film counterface bond strength versus composite's wear rates. (Image reprinted from [16] with permission)

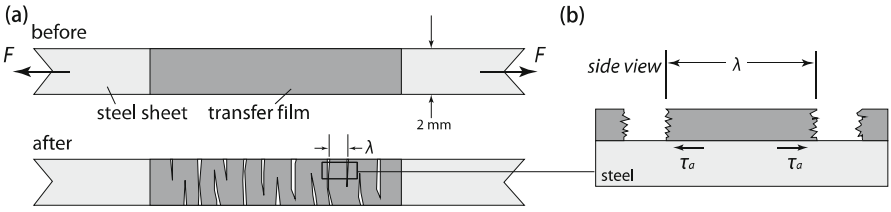

Fig. 6.10 Thin-film stretch method for measuring transfer film adhesion strength by (**a**) pulling a sample with a predeposited transfer film in tension along the sliding direction in the native wear tests until transverse cracks within the film initiated and (**b**) observing the transverse cracks, which have an average crack spacing of λ. This value was found to be inversely proportional to the adhesion shear strength at the film-substrate interface. (Image reprinted from [41] with permission)

The scratch and peel tests have important practical limitations. Neither test provides a useful measure of adhesion strength when the interfacial shear strength exceeds the shear strength of the film [48]. Furthermore, free-spaces from heterogeneity confound the measurements by providing direct bond sites between the adhesive and the counterface in peel tests and by nucleating failure in scratch tests. Lastly, the measurements are confounded by potential contributions from the addition of a second contact interface (adhesive-transfer film and indenter-transfer film). Agrawal and Raj [51, 52] solved these issues with the thin-film stretch test illustrated in Fig. 6.10. The film and counterface are loaded in tension until cracks form and stabilize or until the counterface fails. Mathematically, they showed that the ratio of the crack spacing to coating thickness is proportional to the *normalized* adhesive strength, which is defined as the ratio of adhesive shear strength to cohesive shear strength. This method requires no additional interface and provides spatial specificity for statistical evaluation. One potentially significant downside of the method is

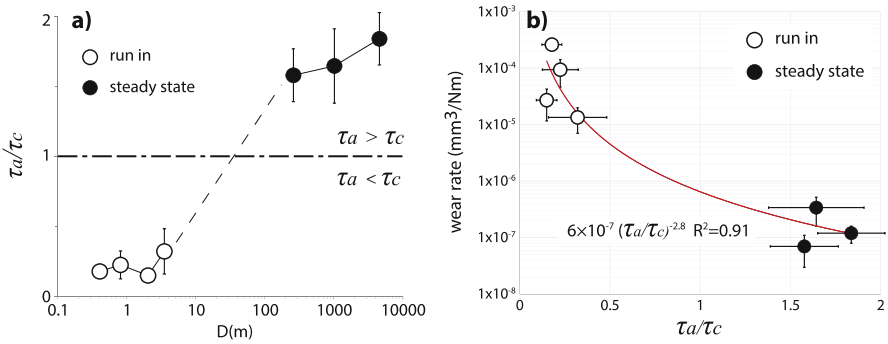

Fig. 6.11 (**a**) Normalized transfer film adhesion strength plotted against the sliding distance of an ultra-low wear PTFE nanocomposite. (**b**) Composite wear rate plotted against the normalized film adhesion strength. (Image reprinted from [6] with permission)

that it only measures the ratio of adhesive strength to cohesive strength; measurements of absolute adhesive strength require knowledge of the absolute cohesive strength of the transfer film. The other downside of the method is that the substrate must have a larger ultimate strain than the transfer film.

Although the normalized adhesive strength is often viewed as a limitation of the stretch method, it is likely a better predictor of transfer film persistence than adhesive strength alone. One could argue that delamination is favored if the cohesive strength significantly exceeds the adhesive strength. Delamination is an undesirable failure route because it leaves the surface completely unprotected. Cohesive failure would be expected when the adhesive strength exceeds the cohesive strength. Cohesive failure leaves the counterface protected and is therefore the preferred failure mode. For this reason, the normalized adhesive strength is likely a more valuable metric of coating adhesion than the adhesive strength.

Ye et al. [6] used the thin-film stretch method to study the evolution of the normalized adhesive strength of the low wear alumina-PTFE transfer film from run-in to steady state; the results are shown in Fig. 6.11a. In the beginning of the test, wear rates were high and the cohesive strength of the transfer film exceeded its adhesive strength, which suggests that delamination was the favored failure mode. In situ studies of the thick flaky transfer films of this material during run-in have shown that they were removed and replenished on each pass of the pin [29]; this fact implies that transfer films failed to protect the polymer during the run-in. This is supported by recent experiments, which showed that removing the transfer film by replacing the counterface with a fresh counterface had no detectable effect on the wear volume produced by the pin (Fig. 6.12) [53]. In this case, visual improvements in the transfer film during the run-in period were caused by reduced wear not the cause of reduced wear [22].

The transition to low wear was accompanied by the first observations of adherent debris (20 m of sliding in Fig. 6.8). Unfortunately, the fragments were too small

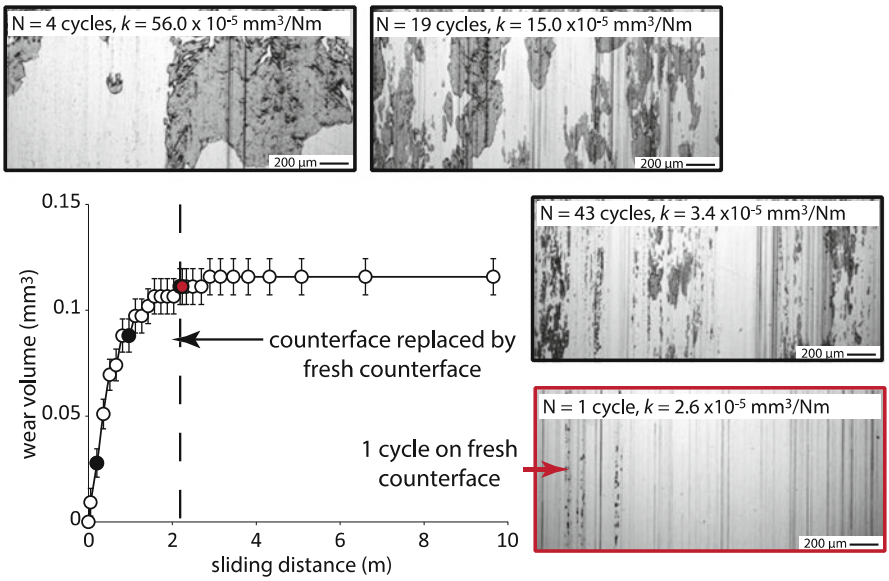

Fig. 6.12 Wear volume plotted against sliding distance for a test in which the developing transfer film was removed after cycle 43 and replaced with a fresh counterface. The results show that the transfer film and wear rate develop as they would in an uninterrupted test, which suggests that the transfer film develops in response to the developing surface properties of the pin. (Image reprinted from [53] with permission)

during this transition period to produce detectable cracking patterns [29]. However, as Fig. 6.8 demonstrates, these debris fragments merged and homogenized with increased sliding to create larger domains with detectable cracking patterns. The first possible measurement in the steady state sliding period revealed clear evidence that the bond between the transfer film and the counterface significantly exceeded the strength of the film itself, which suggests that cohesive failure was favored over delamination. This transition in normalized adhesive strength accompanies improved topographical quality of the transfer film (Fig. 6.6), the onset of transfer film persistence (Fig. 6.8), and dramatically reduce wear rate (Fig. 6.11), all of which is consistent with the expected transition from delamination to cohesive failure. The wear rate decreased as the normalized adhesive strength increased with sliding distance, which suggests that improved bonding of the transfer film contributes as a cause of wear reduction.

Another way to measure the transfer film persistence is through a direct transfer film wear rate measurement. From a simple control-volume analysis, this value represents the minimum possible wear rate of the solid lubricant system at steady state as noted by Blanchet and Kennedy [5]. Wang et al. [54–56] used bare steel spheres to quantify the wear resistance of predeposited transfer films. Standard gravimetric and volumetric wear measurements are difficult due to the fact that

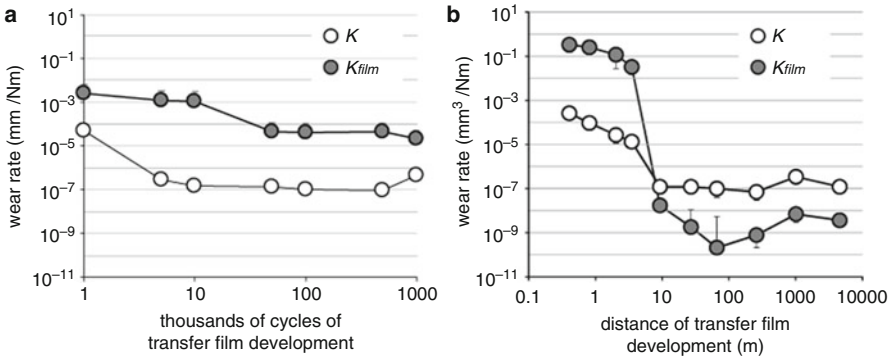

Fig. 6.13 Comparison of wear rates of an alumina-PTFE nanocomposite (K) and the corresponding transfer film (K_{film}) at predefined cycles of development in the native wear test: (**a**) Result from Urueña et al. [58] using a steel sphere to measure transfer film wear rates, (**b**) Result from Ye et al. [6] using a polyethylene sphere to measure transfer film wear rates. All error bars represent 95% confidence intervals. (Image reproduced from [6, 58] with permission)

transfer films are thin and discontinuous. Because increased friction is expected when metal first contacts metal, the friction coefficient provides a useful indicator of coating failure. Wang et al. [55, 56] used this friction coefficient transition method to show that PTFE composite transfer films persisted 10X longer distances than those of unfilled PTFE. Using similar methods, Li et al. [57] showed that the wear lives of their transfer films were sensitive to the load, speed, and the counterface roughness used in creating the transfer film. Urueña et al. [58] used the same friction-based steel ball-on-film configuration to study wear rates of the low-wear alumina–PTFE transfer films described previously as persistent and well adhered. They used mean film thickness measurements with reasonable geometric assumptions to estimate the worn volume and wear rate at failure. As expected, the wear rate of the transfer film decreased as the wear rate of the polymer decreased during the development of the transfer film (Fig. 6.13a). Surprisingly, however, the wear rates of the transfer films were orders of magnitude larger than the wear rate of the parent system. This result implies that the transfer film was worn immediately and played no role in wear reduction, which is unlikely based on the observations and reasoning discussed previously. The alternative is that the test itself had artificially increased the wear rate of the transfer film, which is more likely given the differences in the contacting materials and pressures.

Ye et al. [6] tested the wear rates of the same transfer films using a high-density polyethylene sphere to provide a better mechanical surrogate to the original polymer pin. The transfer film wear rate and the original solid lubricant pin wear rate are plotted against the accumulated sliding distance used to generate the transfer film in Fig. 6.13b. During running-in, the transfer film wear rate is much larger than the pin's wear rate; the transfer films were easily/immediately removed, which is

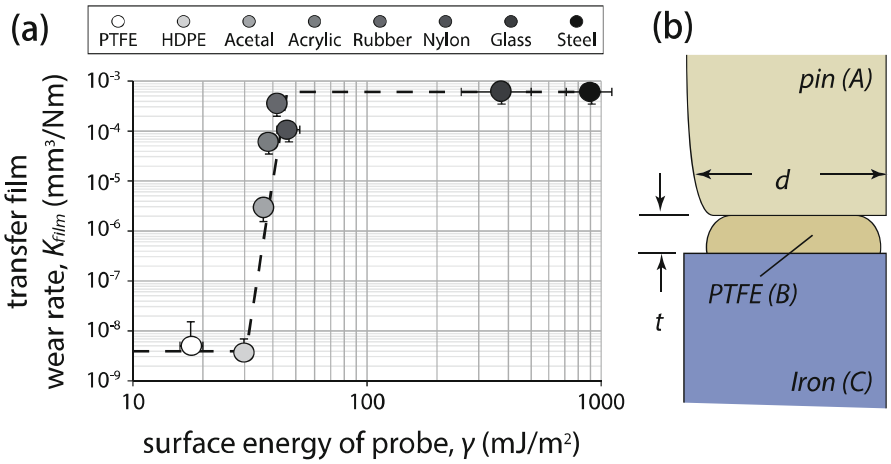

Fig. 6.14 (**a**) Surface energies of the probes versus ultra-low-wear Al_2O_3/PTFE transfer film wear rates in microtribometry experiments. Error bars represent the 95% confidence interval; and (**b**) three-body wear model involving a pin (A), transfer film (B), and counterface (C) (Reprinted with permission from [6])

consistent with the results of direct optical observations of the transfer film evolution [29]. After the transition (~7 m of accumulated sliding distance in this case), the transfer film wear rate decreased sharply and stayed well below the pin's wear rate; this is consistent with the persistence observed from direct optical observations [29] and the transition from weak to strong normalized adhesion strength (Fig. 6.11).

Despite significant potential for differences in the source materials, preparation procedures, and testing conditions between these independent studies, the steady state wear behaviors of the polymer nanocomposites were indistinguishable (Fig. 6.13a, b). Clearly, the wear behavior of this material is robust and insensitive to these differences. The strong agreement in polymer wear rates makes the orders of magnitude disagreements in transfer film wear rates that much more remarkable.

Ye et al. [6] repeated the measurements with spherical probes of varying material to clarify the cause of the enormous differences in the wear response of the same transfer film to different probes. Ultimately, the wear rate of the ultra-low wear transfer film did not vary systematically with contact pressure, friction coefficient, or shear stress during sliding. It did vary systematically as a function of probe surface energy as shown in Fig. 6.14a. Both PTFE and HDPE promoted ultra-low wear behavior of the transfer films. When tested against polymer probes of higher surface energy, the wear rate increased by orders of magnitude. They proposed that low surface energy probes reduced wear by 5 orders of magnitude by setting up a preferred slip system for which pure interfacial sliding becomes favorable over adhesive wear. For this system, interfacial sliding became favorable when the surface energy of the probe was less ~30 mJ/m^2, which is comparable to estimates of that of the film. These results reinforce the fact that the wear resistance of a material,

particularly a transfer film, can depend as strongly on the properties of the countersurface as it does on the properties of the wear surface.

6.2.3 Mechanical Properties

Mechanical properties are also believed to be important contributors to the stability of transfer films and the wear resistance of polymers. Gong et al. [28] first proposed that increased transfer film cohesive strength discourages transfer film failure at internal interfaces and thereby stabilizes the film. However, as illustrated previously, stronger transfer films may be more likely to delaminate without a corresponding increase in strength at the counterface. Mechanical properties can also provide useful information about filler accumulation and polymer degradation, both of which change mechanical properties like hardness, toughness, and modulus.

The primary challenge to measuring the mechanical properties of thin films is isolating the properties of the film from those of the much stiffer and harder substrate [59, 60]. Friedrich et al. [61] used micro-indentation and measured transfer film hardness of two fiber-reinforced PEEK composites with different fiber orientations (normal vs. parallel) relative to the sliding surface. They found that composites produced lower wear rates and harder transfer films when fibers were oriented normally to the sliding interface. Randall et al. [62, 63] studied the correlation between transfer film hardness and wear of several ceramic coatings. They found the most wear resistant coating had transfer films that were ~30% harder than either the sliding counterpart suggesting a possible metal alloying effect. Ye [64] measured transfer film hardness and modulus of the low-wear alumina-PTFE system using AFM-based nanoindentation and found that the transfer film hardens and stiffens during sliding. However, Chang et al. [65] showed that the indentation hardness of thin (200 nm) epoxy transfer films had been artificially increased by contributions from the substrate. When transfer films thin and harden, it becomes difficult to differentiate between hardening of the film material and the effect of the substrate [61–63].

The substrate effect may be avoided by indenting on the running film, which forms on the sliding surface of the bulk solid lubricant. McCook et al. [18] measured hardness and modulus for running films of low wear PTFE-epoxy composites and found that the hardness and modulus of the worn surface were uniformly reduced. The results suggested that the running film was PTFE rich, which likely contributed to the low measured values of friction coefficient and wear rate. Krick et al. [66] measured the mechanical properties of running films from a low wear alumina-PTFE nanocomposite as a function of sliding distance. The film hardened and stiffened with increased sliding distance and decreased wear rate (Fig. 6.15). They concluded that filler accumulation and PTFE degradation were both likely contributors. Their results indicate that the cohesive strength of the running film increased by >2X. If we assume the transfer film is identical to the mated running film, then the absolute adhesive strength of these transfer films increased by >10X from run-in to steady state based on the results from Fig. 6.11.

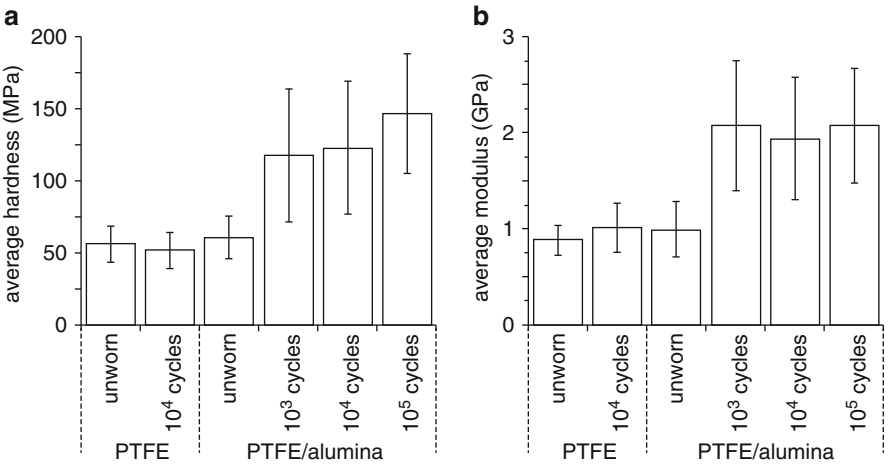

Fig. 6.15 Average (**a**) hardness and (**b**) reduced modulus of worn and unworn PTFE and PTFE–Al_2O_3 nanocomposites, for indentation contact depths in the range of 100–150 nm. Error bars represent ±1 standard deviation from the mean. (Image reprinted from [66] with permission)

6.2.4 Tribochemistry

Tribochemistry is an important factor governing the adhesion and mechanical properties of transfer films. Briscoe [13] first proposed that effective fillers reduce wear by promoting polymer degradation and thereby increasing the adhesive strength of the transfer film. Bahadur and Tabor [22] found that even high quality transfer films did not stick around long after the parent pin was replaced and concluded that transfer film adhesion must be primarily mechanical in nature. Studies on PTFE-based solid lubricants have shown that ultra-low wear sliding is consistently accompanied by small wear debris, thin transfer films, and brown discoloration of both sliding surfaces [7, 9, 10, 19, 27, 29, 45, 66, 67]. This discoloration indicates tribochemical degradation, which is particularly remarkable for PTFE given its unique resistance to chemical attack.

A recent study by Krick et al. [9] provided the most compelling evidence to date that a specific chemistry is required for ultra-low wear sliding of the low wear α phase alumina-PTFE nanocomposite system. As they removed water from the environment, the wear rate of the system increased by two orders of magnitude from 10^{-7} mm^3/Nm to 10^{-5} mm^3/Nm, the latter of which is more typical of PTFE composites. This increase in wear rate in dry environments was accompanied by the loss of the brown discoloration and a transition toward large flaky debris fragments. The inability of this low wear material to achieve low wear in dry environments has been reproduced independently by Pitenis et al. [10] and Khare et al. [53]. Since the environmental constituents have no obvious effects on the mechanical or structural properties of the composite, the most reasonable conclusion is that wear rates

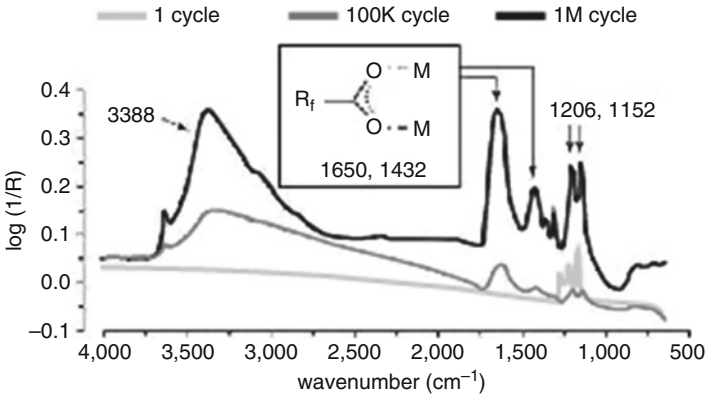

Fig. 6.16 Infrared reflectance results from the metal surface after one cycle of sliding (light grey line), 100 k (gray line) and 1 M (black line) cycles. (Reprinted with permission from [27, 45])

increased due to the loss of favorable tribochemistry at the sliding interface; thus, a specific tribochemistry appears necessary for ultra-low wear of this system.

XPS studies of the transfer films of this low wear alumina-PTFE system by Burris et al. [68] revealed an unexpected peak at 288 eV, which they attributed to a tribochemical degradation product. Computational modeling by Onodera et al. [69, 70] showed that end-chain carboxyl groups formed in humid environments and suggested that they help bond PTFE transfer films to metal counterfaces. Experimental infrared spectroscopic (IR) studies by Pitenis et al. [10] and Harris et al. [45] showed that the new tribochemical product was a metal chelate salt of perfluorinated carboxylic acid (Fig. 6.16). Harris et al. [45] proposed a realistic reaction route that involved mechanical rupture of PTFE chains and fibrils, reaction of chain ends with oxygen and then water to form carboxylic acid, and, finally, chelation of the acid at the chain end to metal atoms in the counterface and filler particles. The reaction products increase with sliding distance (Fig. 6.16), which helps explain why these transfer films become more persistent, better adhered, stronger, and more wear resistant with increased sliding distances.

6.3 Causes and Consequences: A Case Study with a Low Wear Composite

Despite the compelling evidence from Pitenis et al. [10] and Harris et al. [45] that tribochemistry is necessary to anchor transfer films, recent studies of the run-in period of this particular PTFE nanocomposite provides further insights into the timing of favorable tribochemistry and its role in low wear sliding of polymers. Ye et al. [29] showed that the transfer films were compositionally and mechanically

identical to the unworn composite and Pitenis et al. [10] found a comparable lack of carboxylates during run-in. Furthermore, Khare et al. [53] showed that, unlike at steady state, the run-in and transition behaviors of this material are completely independent of environment. Thus, the transition to low wear during run-in appears to occur without the benefit of favorable tribochemistry. Ye et al. [29] showed that the wear rate and the transfer film of these low wear alumina-PTFE composites were indistinguishable from those of unfilled PTFE initially, which suggests that the crack arresting role of the filler is negligible initially. With each pass, however, they observed reduced wear rate and thinner transfer films of characteristically smaller debris. Although the transfer films were immediately dislodged throughout run-in, Khare et al. [53] showed that the transfer film had no effect on the wear rate of the polymer during run-in; they did this by interrupting the test and replacing the transfer film with a fresh steel counterface. If anything, the wear rate of the pin was lower when the transfer film was removed from the contact, which demonstrates that the perceived improvements in transfer film quality during the run-in period are consequences of an increasingly wear resistant running surface and not the cause of progressively reduced wear rates. The result suggests that filler accumulation and mechanical conditioning of the running surface (e.g., filler accumulation, polymer orientation, polymer crazing) are responsible for the transition from large debris and high wear to small debris and low wear.

During the run-in phase, wear continues to decrease until effectively stopping at a critical point Ye et al. [29] defined as the transition. The system wear rate is well below 10^{-6} mm^3/Nm and Ye et al. [29] report the first compositional evidence of polymer degradation at this point. Interestingly, Khare et al. [53] observed indistinguishable run-in and transition features when they removed ambient moisture to preclude favorable tribochemistry. This is not entirely surprising given that the run-in is independent of tribochemistry [10, 29] and suggests that low wear of this system does not require favorable tribochemistry, at least initially. These results suggest that mechanical debris size regulation is the first step toward low wear in this particular system. These debris fragments can become so small that they automatically adhere to produce stable low energy surfaces. Mechanical stability must precede tribochemical stability because the products of improbable chemical events take time to accumulate [10]. As low wear sliding continues, adhered debris fragments grow by scavenging material from the pin (Fig. 6.8). As debris fragments grow, adhesion energy becomes less competitive with elastic energy until they destabilized at a critical thickness Ye et al. [6] estimates to be on the order of ~1 μm for PTFE. However, if the humidity is sufficient, tribochemical reactions begin to link the polymer chemically to the counterface, thus increasing the critical thickness for instability as the film grows. This, we propose, explains why run-in is independent of environment, why low wear was achievable but unstable in dry nitrogen [53], and why the system can sustain low wear indefinitely in humid environments [9]. The cross-linking effect of tribochemistry is consistent with the substantial increases in adhesion strength [6, 29, 58], hardness [64, 66], and modulus [64, 66] for this system from run-in to steady state.

6.4 Summary

This chapter reviews the latest methods to quantify the topographical, adhesive, mechanical, and chemical properties of polymeric transfer films. Topographical features of interest, including thickness, area fraction, and free-space length, have been quantified primarily with profilometry and microscopy. Both thickness and area fraction tend to correlate strongly with wear rate for specific systems but less so across systems. Based on limited studies, the free-space length appears to be the best of the three for predicting wear rates in general. It is interesting to note that the free-space length is most closely related to the visual cues that have motivated use of the terms "uniform," "coherent," and "continuous" [31, 38, 71–74]. Nonetheless, despite consistent evidence that transfer film properties correlate strongly with wear rate, no universal function is likely to emerge.

Although peel and scratch tests are typical for qualifying coating adhesion, such measurements are confounded by the discontinuous nature of transfer films. The tensile cracking test eliminates the need for a second interface and is not affected by discontinuity in the transfer film. Additionally, it provides a direct measure of adhesion strength per unit cohesion strength; since adhesive failure is far more detrimental to tribopolymer wear than cohesive failure, this property is perhaps the most direct measure of transfer film adhesion performance. Lastly, although a wear test appears to be the most direct measure of tenacity, we have shown that the measured wear rates of transfer films can vary by many orders of magnitude depending on the surface properties of the probe material used; caution is necessary when interpreting the results of transfer film wear tests in an absolute sense for this reason.

Hardness and modulus are the most common mechanical metrics of transfer film performance and both are typically quantified with micro and nano-indentation. Because transfer films are thin and soft, the results are confounded by effects from the counterface, which effectively converts an inherently quantitative measurement into a qualitative assessment. Some have quantified the mechanical properties of the running film on the soft polymer surface as a way to address this issue of transfer film characterization. However, caution must be exercised when using running films as surrogates for transfer films because there is some evidence that the films are compositionally distinct despite developing at the same tribological interface.

Finally, we have used a particularly well-studied alumina-PTFE system as a case study for wear reduction. Based on the methods described throughout, its transfer films are thin, well-covered, persistent, well-adhered, chemically distinct, and mechanically stronger than the unworn composite. These changes are strongly associated with a favorable tribochemical reaction; polymer chains break mechanically during sliding, react with gaseous oxygen and water from the environment to form carboxylic acid, then chelate to metal surfaces to strengthen the film and bond it to the counterface. The end result is a stable and protective film that minimizes the wear rate of the system.

The mechanisms of wear mitigation in this system, particularly the tribochemical aspects, are likely unique given that the four order of magnitude wear reducing effect of fillers appears to be limited to fluoropolymers [2, 67]. Nonetheless, it is interesting that transfer film uniformity, thickness, coverage, bond strengthening, chemical

degradation, and mechanical strengthening are recurring themes in the tribopolymer literature. Although the exact mechanisms are likely system-specific, the quantitative methods described here may be used broadly to expose common trends and elucidate general causation relationships. Ultimately, knowledge of these causation relationships will be critical to materials discovery by design rather than the more traditional trial and error-based approaches.

Acknowledgments The authors are very grateful for the financial support from the Air Force Office of Scientific Research (FA9550-10-1–0295), the National Science Foundation Graduate Research Fellowship (1247394), the National Natural Science Foundation of China (51505117), and the Anhui Provincial Natural Science Foundation (1608085QE98).

References

1. Burris, D.L., Sawyer, W.G.: A low friction and ultra low wear rate PEEK/PTFE composite. Wear. **261**(3–4), 410–418 (2006)
2. Burris, D.L., Sawyer, W.G.: Improved wear resistance in alumina-PTFE nanocomposites with irregular shaped nanoparticles. Wear. **260**(7–8), 915–918 (2006)
3. McCook, N.L., et al.: Epoxy, ZnO, and PTFE nanocomposite: friction and wear optimization. Tribol. Lett. **22**(3), 25–257 (2006)
4. Lancaster, J.K.: Polymer-based bearing materials: the role of fillers and fibre reinforcement. Tribology. **5**(6), 249–255 (1972)
5. Blanchet, T.A., Kennedy, F.E.: Sliding wear mechanism of polytetrafluoroethylene (PTFE) and PTFE composites. Wear. **153**(1), 229–243 (1992)
6. Ye, J., Moore, A.C., Burris, D.L.: Transfer film tenacity: a case study using ultra-low-wear alumina–PTFE. Tribol. Lett. **59**(3), 1–11 (2015)
7. Burris, D.L.: Wear-Resistance Mechanisms in Polytetrafluoroethylene (PTFE) Based Tribological Nanocomposites. University of Florida, Gainesville (2006)
8. Burris, D.L., et al.: A route to wear resistant PTFE via trace loadings of functionalized nanofillers. Wear. **267**(1–4), 653–660 (2009)
9. Krick, B.A., et al.: Environmental dependence of ultra-low wear behavior of polytetrafluoroethylene (PTFE) and alumina composites suggests tribochemical mechanisms. Tribol. Int. **51**(0), 42–46 (2012)
10. Pitenis, A.A., et al.: In Vacuo Tribological behavior of polytetrafluoroethylene (PTFE) and alumina nanocomposites: the importance of water for ultralow wear. Tribol. Lett. **53**, 1–9 (2014)
11. Lancaster, J.K.: Lubrication by transferred films of solid lubricants. A S L E Trans. **8**(2), 146–155 (1965)
12. Briscoe, B.J., Pogosian, A.K., Tabor, D.: The friction and wear of high density polythene: the action of lead oxide and copper oxide fillers. Wear. **27**(1), 19–34 (1974)
13. Briscoe, B.: Wear of polymers: an essay on fundamental aspects. Tribol. Int. **14**(4), 231–243 (1981)
14. Bahadur, S., Gong, D., Anderegg, J.W.: The role of copper compounds as fillers in transfer film formation and wear of nylon. Wear. **154**(2), 207–223 (1992)
15. Briscoe, B.J., Sinha, S.K.: Wear of polymers. Proc. Inst. Mech. Eng. J J. Eng. Tribol. **216**(6), 401–413 (2002)
16. Bahadur, S., Sunkara, C.: Effect of transfer film structure, composition and bonding on the tribological behavior of polyphenylene sulfide filled with nano particles of TiO2, ZnO, CuO and SiC. Wear. **258**(9), 1411–1421 (2005)
17. Friedrich, K., Zhang, Z., Schlarb, A.K.: Effects of various fillers on the sliding wear of polymer composites. Compos. Sci. Technol. **65**(15–16), 2329–2343 (2005)

18. McCook, N.L., et al.: Wear resistant solid lubricant coating made from PTFE and epoxy. Tribol. Lett. **18**(1), 119–124 (2005)
19. Burris, D.L., et al.: Polymeric nanocomposites for Tribological applications. Macromol. Mater. Eng. **292**(4), 387–402 (2007)
20. Ye, J., Burris, D.L., Xie, T.: A review of transfer films and their role in ultra-low-wear sliding of polymers. Lubricants. **4**(1), 4 (2016)
21. Bahadur, S., Gong, D.: The action of fillers in the modification of the tribological behavior of polymers. Wear. **158**(1–2), 41–59 (1992)
22. Bahadur, S., Tabor, D.: The wear of filled polytetrafluoroethylene. Wear. **98**(0), 1–13 (1984)
23. Ricklin, S.: Review of Design Parameters for Filled PTFE Bearing Materials. Lubrication Engineering. **33**(9), 487–490 (1977)
24. Tanaka, K., Kawakami, S.: Effect of various fillers on the friction and wear of polytetrafluoroethylene-based composites. Wear. **79**(2), 221–234 (1982)
25. Gong, D., Qunji, X., Hongli, W.: ESCA study on tribochemical characteristics of filled PTFE. Wear. **148**(1), 161–169 (1991)
26. Blanchet, T.A., Kennedy, F.E., Jayne, D.T.: XPS analysis of the effect of fillers on PTFE transfer film development in sliding contacts. Tribol. Trans. **36**(4), 535–544 (1993)
27. Pitenis, A.A., et al.: Ultralow wear PTFE and alumina composites: it is all about Tribochemistry. Tribol. Lett. **57**(2), 1 (2015)
28. Gong, D., Qunji, X., Hongli, W.: Physical models of adhesive wear of polytetrafluoroethylene and its composites. Wear. **147**(1), 9–24 (1991)
29. Ye, J., Khare, H.S., Burris, D.L.: Transfer film evolution and its role in promoting ultra-low wear of a Ptfe nanocomposite. Wear. **297**(1–2), 1095–1102 (2013)
30. Chen, W.X., et al.: Tribological behavior of carbon-nanotube-filled PTFE composites. Tribol. Lett. **15**(3), 275–278 (2003)
31. Sawyer, W.G., et al.: A study on the friction and wear behavior of PTFE filled with alumina nanoparticles. Wear. **254**(5–6), 573–580 (2003)
32. Bahadur, S.: The development of transfer layers and their role in polymer tribology. Wear. **245** (1–2), 92–99 (2000)
33. Schwartz, C.J., Bahadur, S.: Studies on the tribological behavior and transfer film–counterface bond strength for polyphenylene sulfide filled with nanoscale alumina particles. Wear. **237**(2), 261–273 (2000)
34. Burris, D.L., Sawyer, W.G.: Tribological sensitivity of PTFE/alumina nanocomposites to a range of traditional surface finishes. Tribol. Trans. **48**(2), 147–153 (2005)
35. McElwain, S.: Wear Resistant PTFE Composites Via Nano-scale Filler Particles. Rensselaer Polytechnic Institute, Troy/New York (2006)
36. Laux, K.A., Schwartz, C.J.: Influence of linear reciprocating and multi-directional sliding on PEEK wear performance and transfer film formation. Wear. **301**(1), 727–734 (2013)
37. Laux, K.A., Schwartz, C.J.: Effects of contact pressure, molecular weight, and supplier on the wear behavior and transfer film of polyetheretherketone (PEEK). Wear. **297**(1), 919–925 (2013)
38. Li, F., et al.: The friction and wear characteristics of nanometer ZnO filled polytetrafluoroethylene. Wear. **249**(10–11), 877–882 (2001)
39. Blanchet, T.A., Kandanur, S.S., Schadler, L.S.: Coupled effect of filler content and Countersurface roughness on PTFE nanocomposite wear resistance. Tribol. Lett. **40**(1), 11–21 (2009)
40. Zhang, G., et al.: Role of monodispersed nanoparticles on the tribological behavior of conventional epoxy composites filled with carbon fibers and graphite lubricants. Wear. **292**, 176–187 (2012)
41. Ye, J., Khare, H.S., Burris, D.L.: Quantitative characterization of solid lubricant transfer film quality. Wear. **316**(1–2), 133–143 (2014)
42. Bhimaraj, P., et al.: Tribological investigation of the effects of particle size, loading and crystallinity on poly (ethylene) terephthalate nanocomposites. Wear. **264**(7), 632–637 (2008)
43. Harris, K.L., et al.: Wear debris mobility, aligned surface roughness, and the low wear behavior of filled polytetrafluoroethylene. Tribol. Lett. **60**(1), 1–8 (2015)

44. Zhang, G., et al.: Formation and function mechanisms of nanostructured tribofilms of epoxy-based hybrid nanocomposites. Wear. **342–343**, 181–188 (2015)
45. Harris, K.L., et al.: PTFE tribology and the role of Mechanochemistry in the development of protective surface films. Macromolecules. **48**(11), 3739–3745 (2015)
46. Kandanur, S.S., et al.: Suppression of wear in graphene polymer composites. Carbon. **50**(9), 3178–3183 (2012)
47. Kandanur, S.S., et al.: Effect of activated carbon and various other nanoparticle fillers on PTFE wear. Tribol. Trans. **57**(5), 821–830 (2014)
48. Bull, S.J., Berasetegui, E.G.: An overview of the potential of quantitative coating adhesion measurement by scratch testing. Tribol. Int. **39**(2), 99–114 (2006)
49. Committee, D.: Test Method for Peel or Stripping Strength of Adhesive Bonds. ASTM International, West Conshohocken, PA (2010)
50. Committee, D.: Test Method for Strength Properties of Adhesives in Cleavage Peel by Tension Loading (Engineering Plastics-to-Engineering Plastics). ASTM International, West Conshohocken, PA (2012)
51. Agrawal, D.C., Raj, R.: Measurement of the ultimate shear strength of a metal-ceramic interface. Acta Metall. **37**(4), 1265–1270 (1989)
52. Agrawal, D.C., Raj, R.: Ultimate shear strengths of copper-silica and nickel-silica interfaces. Mater. Sci. Eng. A. **126**(1–2), 125–131 (1990)
53. Khare, H.S., et al.: Interrelated effects of temperature and environment on wear and Tribochemistry of an ultralow wear PTFE composite. J. Phys. Chem. C. **119**(29), 16518–16527 (2015)
54. Wang, Y., Yan, F.: Tribological properties of transfer films of PTFE-based composites. Wear. **261**(11–12), 1359–1366 (2006)
55. Wang, Y., Yan, F.: A study on tribological behaviour of transfer films of PTFE/bronze composites. Wear. **262**(7–8), 876–882 (2007)
56. Wang, Y., Wang, H., Yan, F.: Investigation of transfer film of PTFE/bronze composites on 2024Al surface. Surf. Interface Anal. **41**(9), 753–758 (2009)
57. Li, H., et al.: A study of the tribological behavior of transfer films of PTFE composites formed under different loads, speeds and morphologies of the counterface. Wear. **328–329**, 17–27 (2015)
58. Urueña, J.M., et al.: Evolution and wear of fluoropolymer transfer films. Tribol. Lett. **57**(2), 1–8 (2015)
59. Pharr, G.M., Oliver, W.C.: Measurement of thin film mechanical properties using nano-indentation. MRS Bull. **17**(07), 28–33 (1992)
60. Oliver, W.C., Pharr, G.M.: Measurement of hardness and elastic modulus by instrumented indentation: advances in understanding and refinements to methodology. J. Mater. Res. **19**(01), 3–20 (2004)
61. Friedrich, K., et al.: Experimental and numerical evaluation of the mechanical properties of compacted wear debris layers formed between composite and steel surfaces in sliding contact. Wear. **251**(1–12), 1202–1212 (2001)
62. Randall, N.X., Bozet, J.L.: Nanoindentation and scanning force microscopy as a novel method for the characterization of tribological transfer films. Wear. **212**(1), 18–24 (1997)
63. Randall, N.X., Harris, A.: Nanoindentation as a tool for characterising the mechanical properties of tribological transfer films. Wear. **245**(1–2), 196–203 (2000)
64. Ye, J.: Characterizing PTFE Transfer Film Properties to Elucidate Transfer Film's Role in Ultra-low Wear Sliding of Polymer Nanocomposites, p. 173. University of Delaware, Newark (2014)
65. Chang, L., et al.: Tribological properties of epoxy nanocomposites: III. Characteristics of transfer films. Wear. **262**(5–6), 699–706 (2007)
66. Krick, B.A., Ewin, J.J., McCumiskey, E.J.: Tribofilm formation and run-in behavior in ultra-low-wearing polytetrafluoroethylene (PTFE) and alumina nanocomposites. Tribol. Trans. **57**(6), 1058–1065 (2014)
67. Sidebottom, M.A., et al.: Ultralow wear Perfluoroalkoxy (PFA) and alumina composites. Wear. **362–363**, 179–185 (2016)

68. Burris, D.L., et al.: Polytetrafluoroethylene matrix nanocomposites for tribological applications. In: Tribology of Polymeric Nanocomposites. Elsevier, Amsterdam (2008)
69. Onodera, T., et al.: Chemical reaction mechanism of polytetrafluoroethylene on aluminum surface under friction condition. J. Phys. Chem. C. **118**(10), 5390–5396 (2014)
70. Onodera, T., et al.: Effect of Tribochemical reaction on transfer-film formation by poly (tetrafluoroethylene). J. Phys. Chem. C. **118**(22), 11820–11826 (2014)
71. Wang, Q., et al.: The effect of particle size of nanometer ZrO2 on the tribological behaviour of PEEK. Wear. **198**(1–2), 216–219 (1996)
72. Wang, Q., Xue, Q., Shen, W.: The friction and wear properties of nanometre SiO 2 filled polyetheretherketone. Tribol. Int. **30**(3), 193–197 (1997)
73. Wang, Q.-H., et al.: The effect of nanometer SiC filler on the tribological behavior of PEEK. Wear. **209**(1–2), 316–321 (1997)
74. Wang, Q.-H., et al.: The friction and wear characteristics of nanometer SiC and polytetrafluoroethylene filled polyetheretherketone. Wear. **243**(1), 140–146 (2000)

Self-Lubricating Alumina Matrix Composites

7

Ashish K. Kasar and Pradeep L. Menezes

Contents

Abstract

Alumina is a widely used ceramic for tribological applications such as gears, bushings, bearings, etc. due to its chemical and physical stability. However, the friction between alumina-alumina is high, which reduces its usage for tribological applications. To overcome the high friction, various solid lubricants can be added in the alumina matrix that makes self-lubricating alumina composites. In this chapter, mainly three categories of solid lubricants: soft material, lamellar solids, and other materials (oxides, sulfates, etc.) used in alumina matrix are discussed. Mostly, these solid lubricants form a tribo-layer at the interface between alumina composite and counterpart and reduce friction. The amount of solid lubricants needs to be optimized because the excessive amount can cause severe wear that can damage the dimensional stability of the component. While discussing the suitable solid lubricants for the alumina matrix, various synthesis techniques have also been highlighted because synthesis techniques are critical to disperse the solid lubricants uniformly.

A. K. Kasar
Mechanical Engineering Department, University of Nevada, Reno, NV, USA

P. L. Menezes (✉)
Department of Mechanical Engineering, University of Nevada, Reno, NV, USA
e-mail: pmenezes@unr.edu

P. L. Menezes et al. (eds.), *Self-Lubricating Composites*,
https://doi.org/10.1007/978-3-662-64243-6_7

7.1 Introduction

Ceramics are nonorganic solid material that consists of metal or nonmetal compounds with ionic or covalent bonds. Ceramic materials contain a combination of properties, including low density, resistance to chemicals, high wear resistance, and stability for a wide temperature range. Due to these properties, structural ceramic materials have the potential to be utilized in the tribological applications. These structural ceramic materials have a wide range of compounds including oxides, carbides, nitrides, and borides.

However, the major limitation of structural ceramics is the high coefficient of friction (COF) for tribological applications. Self-lubricating ceramic composites have suitable tribological properties, especially for high-temperature applications, where a lubricious layer of solid lubricant (SL) materials forms at the interface during sliding that can significantly reduce the energy loss due to friction. Interestingly, some oxide ceramics act as SL materials that can be added in the ceramics to form self-lubricating ceramic composites. These solid lubricating oxide materials are listed in Table 7.1.

The self-lubrication performance of ceramic composites depends on the formation of transfer film of SL at the interface. The transfer film formation is controlled by many factors including volume/weight fraction of SL (inclusion), mechanical properties of the SL, and operating conditions of tribo-contact. For example, the higher transfer film thickness is expected by increasing the volume fraction of SL or by choosing the softer solid particles as predicted by a mathematical model for 3 mol% yttria-doped zirconia (3Y-TZP) [1]. In this model, fair assumptions were taken by considering the elastic deformation of the matrix whereas graphite deforms plastically to de-bond with the matrix and form the transfer layer. The predicted transfer layer thickness by varying the volume fraction and considering the variation in yield strength of the SL phase (inclusions) are shown in Fig. 7.1. However, the SLs in the ceramic matrix can only be loaded up to a critical amount. The critical amount of the SL phase in the ceramic matrix can be evaluated by friction performance along with wear rate/volume, mechanical strength, and other required properties of the composites. Experimentally, Xue et al. [2] observed that 24.4 vol% graphite content in the ZrO_2 (Y_2O_3 mol%) reduced COF from 0.56 to 0.29 against GCr15 steel whereas the wear increased from 5.8×10^{-6} to 8×10^{-5} mm^3m^{-1}. Therefore, it is essential to optimize the SL amount in the matrix based on other required properties.

Table 7.1 Categories of SL materials

Soft materials	Lamellar solids	Organic polymers	Other compounds (oxides, sulfates, and phosphates)
Bi, Ag, Cu, Sn, In, Pb, CaF_2, BaF_2, PbS	MoS_2, WS_2, h-BN, graphite.	PTFE, nylon, waxes	TiB_2, B_2O_3, MoO_2, MoO_3, ZnO_2, Re_2O_7, TiO_2, Ag_2O, CuO, $BaSO_4$

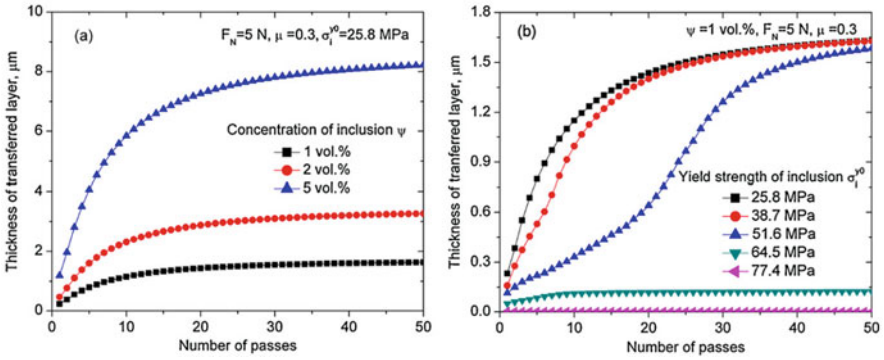

Fig. 7.1 Predicted transfer layer thickness for ceramic composite using a model [1]

Table 7.2 Properties of Al_2O_3 ceramic [9]

Properties	Value
Density	3.95 g/cm^3
Melting point	2050 °C
Yield strength	455 MPa
Elastic modulus	380 GPA
Thermal conductivity	40 W/m.K
Coefficient of thermal expansion	8.0×10^{-6}/°C

This chapter reviews the studies on tribological performance of Al_2O_3 matrix self-lubricating composites. Alumina is the most common ceramic materials which employed at high temperature for various applications due to its high-temperature stability, lower density, high hardness, and being chemically inert. The physical and mechanical properties of the alumina are listed in Table 7.2. However, the friction and wear performance of alumina is poor under the dry sliding condition that limits the applicability for tribological applications. To overcome the poor tribological performance of alumina, coatings of SLs materials have been provided, such as polytetrafluoroethylene (PTFE) [3], Ag [4, 5], TiB_2 [6–8], etc. Coating of these SL materials provides lower friction, whereas hard alumina base acts as a wear-resistance substrate to support the soft and shearing SL phases. This chapter is focused on understanding the tribological performance of alumina composite reinforced with SLs rather than the coating of SL materials.

In this chapter, the sections are divided based on the different categories of SLs described in Table 7.1 which are soft material, lamellar solids, and other compounds (oxides and sulfates). The organic polymers are excluded because these have not been used widely as a lubricating material in Al_2O_3 matrix. On the contrary, alumina has been used as a reinforcement material in polymers [10–13]. The feasibility of the various SLs from the rest three categories in Al_2O_3 matrix at different working conditions is evaluated by understanding the mechanism. Often, SLs, in combination

with different categories, are used for superior lubrication. Such studies have been assigned to subsections based on the most effective SL observed in the study.

7.2 Soft Materials

CaF_2 is the most common soft SL material, which is often used as SL in ceramic matrix composites. The Al_2O_3-CaF_2 composites can be synthesized by different methods. For example, the laser-cladded Al_2O_3-30 wt% CaF_2 coating on Al_2O_3 showed improved friction and wear properties compared to monolithic laser-cladded Al_2O_3 [14]. The Al_2O_3 showed a COF of 0.6, whereas the composite showed COF of 0.48 when tested against hardened steel on the pin-on-wheel test setup with a normal load of 98 N at room temperature. The composite showed 40 times lesser wear compared to monolithic laser-cladded Al_2O_3. The improved tribological performance was observed due to uniform distribution of the soft spherical CaF_2 phase in the plate-like framework of Al_2O_3 phase. The lower amount of CaF_2 (3 wt%) was also observed to improve tribological properties of Al_2O_3-ZrO_2 (15 wt%) composite prepared by the plasma spray method [15]. The COF was reduced upto 40%. Also, the observed wear rate was four times lower at 20 N as compared with those of composites without CaF_2. In this study, 3 mol% Y_2O_3-stabilized ZrO_2 was added in Al_2O_3 matrix, which forms eutectic ceramic composites, and it is well known to improve the mechanical properties of Al_2O_3 [16–18].

Similar to CaF_2, BaF_2 and SrF_2 are also considered a soft phase that can act as SLs. Murakami et al. [19] investigated the three different composites: Al_2O_3–31BaF_2–19CaF_2, Al_2O_3–50CaF_2, and Al_2O_3–50SrF_2 (mass %) that were synthesized by spark plasma sintering and tested at 600 °C against alumina ball with a normal load of 4.9 N. Among all the composites, Al_2O_3–31BaF_2–19CaF_2 showed the best tribological performance with 0.3–0.4 COF and wear rate of the composite was 0.8×10^{-5} mm^3/N.m. The Al_2O_3–31BaF_2–19CaF_2 composite also showed 4 GPa of microhardness that is two times higher than the hardness of other alumina composites. The SL phases provided lower friction and wear but also resulted in finer microstructure that improves hardness. This suggests that the combination of SL phases in the alumina matrix can outperform a single SL.

Secondary hard phases such as ZrO_2, TiC, SiC, and TiN, etc. have also been added in the alumina matrix along with SL materials. The purpose of secondary hard phases is to strengthen the composite by whisker, precipitate, and dispersion strengthening. For example, Al_2O_3/TiC composite with CaF_2 showed improved tribological and mechanical properties [20]. These composites were prepared by hot pressing at 36 MPa in N_2 atmosphere for 15 min at 1700 °C. The composition and properties of the composites are listed in Table 7.3. Table 7.3 indicates that the mechanical properties (flexure strength and hardness) deteriorated with the addition of SL CaF_2, whereas the COF and wear rate reduced till 10 vol% of CaF_2. Therefore, Al_2O_3/TiC/15%CaF_2 composite provides optimized mechanical and tribological properties. In this work, properties were not compared with respect to monolithic

Table 7.3 Mechanical and tribological properties of Al_2O_3/TiC/CaF_2 composites

Composition (vol%) Al_2O_3: TiC = 1:1	Flexure strength (MPa)	Hardness (GPa)	COF	Wear rate (10^{-5} mm^3/N.m)
Al_2O_3 + TiC	800	20	0.47	2.7
Al_2O_3 + TiC + 5% CaF_2	478	13.2	0.31	2.5
Al_2O_3 + TiC + 10% CaF_2	590	15.3	0.27	1.8
Al_2O_3 + TiC + 15% CaF_2	418	9.6	0.30	3.5

Al_2O_3. However, TiC is expected to enhance the mechanical properties of Al_2O_3, whereas CaF_2 provided self-lubrication.

7.3 Lamellar Solids

Carbonaceous material such as graphite, graphene, and carbon nanotubes (CNTs) have been extensively studied for tribological applications due to their lamellar structure [21–26]. These carbonaceous materials have also been utilized in the alumina matrix. Bagde et al. [27] studied Al_2O_3-13TiO_2-15% Ni-graphite coatings deposited by plasma spray. The tribological tests were carried out against 21 and 36 μm SiC papers. The observed friction and wear results are shown in Fig. 7.2a, b, respectively. It can be seen that the addition of Ni-graphite reduced the COF at all the loads against both the SiC papers. The effect of Ni-graphite is higher on the wear rate as it reduced by 1.5–2 times. A similar effect of Ni-graphite on the Al_2O_3-SiO_2 plasma sprayed coating was observed where graphitic lubricating layers reduced friction at the interface, and the ceramic matrix worked as a load-bearing element [28].

Similar to graphite, graphene has also been found to form tribo-layer during sliding in Al_2O_3-graphene composites [29, 30]. Al_2O_3-0.22 wt% graphene composites were prepared by spark plasma sintering at 80 MPa and 1500 °C [29]. The tribological tests against Al_2O_3 ball at 20 N showed ~10% and 50% decrease in COF and wear rate for graphene composite with respect to pure Al_2O_3 sample. The formation of a uniform tribo-layer of graphene was observed by Zhang et al. in Al_2O_3-graphene nanoplatelet composite synthesized by spark plasma sintering [30]. The authors observed optimum tribological performance with 0.5 vol% graphene nanoplatelet with 65 and 25% decrease in wear volume and friction coefficient, respectively, with respect to pure Al_2O_3. Graphene content higher than the optimum amount showed higher wear. Graphene oxide, which contains oxygen-carrying groups such as -OH, -COOH, etc., on the edges of graphene sheets [23], has also been found effective to improve the tribological performance of Al_2O_3. Al_2O_3-graphene oxide composite synthesized by spark plasma sintering resulted in five times lower wear compared to monolithic alumina tested against alumina ball at 10 N normal load [31]. However, a detailed study on graphene and graphene oxide-Al_2O_3 composite suggests that unoxidized graphene provides superior mechanical properties than the graphene oxide and reduced graphene oxide [32]. It is due to the

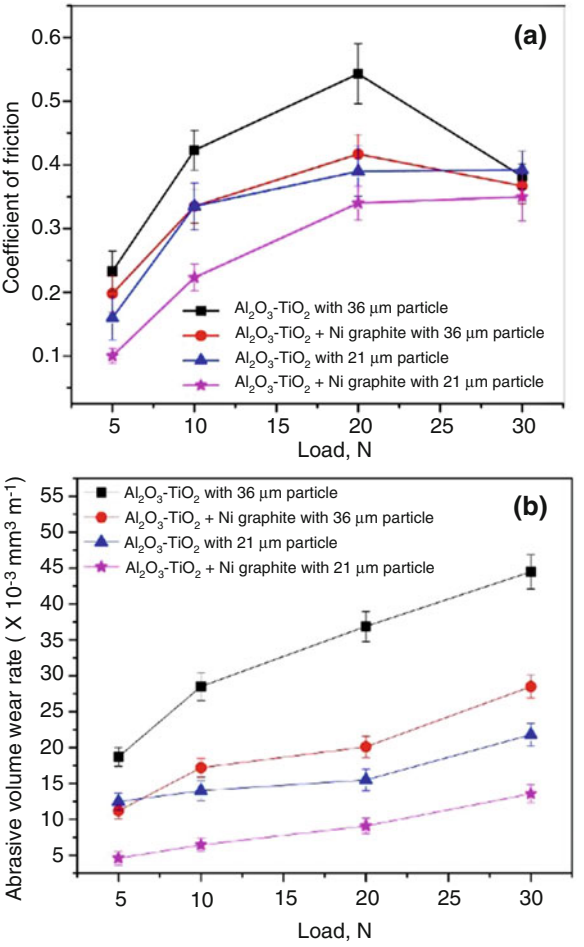

Fig. 7.2 (**a**) COF and (**b**) wear rate of Al_2O_3-13TiO_2 and Al_2O_3-13TiO_2 + Ni graphite composite against 21 and 36 μm SiC abrasive surfaces [27]

presence of structural defects in graphene oxide and reduced graphene oxide that can deteriorate the mechanical properties of the composite. The wear and friction data of Al_2O_3-unoxidized graphene is shown in Fig. 7.3, where unoxidized graphene is denoted by EG and LPS denotes liquid phase sintering. It can be seen that the wear rate of the graphene-containing composite reduced by one order of magnitude and friction was reduced by 15–20% compared to pure Al_2O_3. Other than the tribological properties, the addition of graphene in Al_2O_3 matrix led to the improvement in mechanical [33–35] and different functional properties [36, 37].

The other attractive carbonaceous material is carbon nanotubes (CNTs). CNTs have also been employed in the Al_2O_3 matrix. Al_2O_3-CNTs composite synthesized by hot pressing at 1800 °C under 40 MPa. The Al_2O_3-CNTs composite showed improved mechanical and tribological performance as compared to pure Al_2O_3

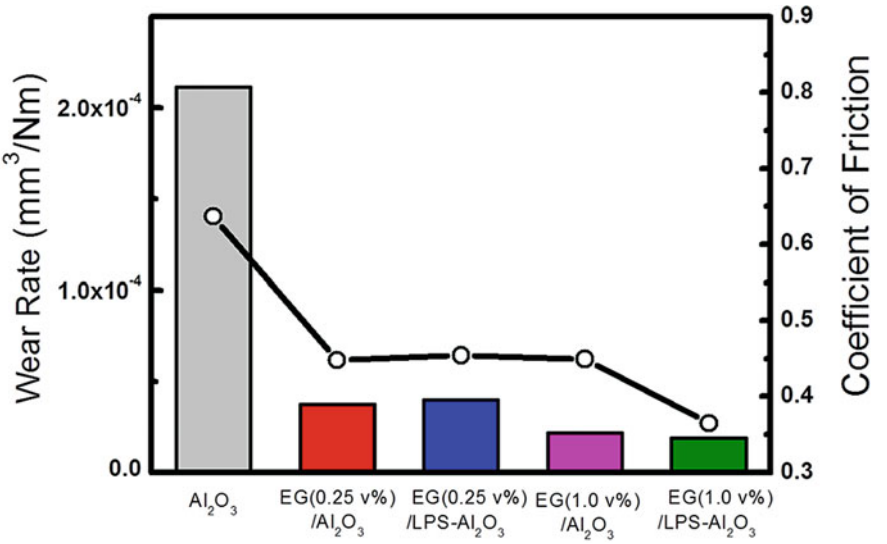

Fig. 7.3 Wear rate and COF for Al_2O_3-unoxidized graphene (EG) tested against WC ball at 25 N with 10 cm/s sliding speed for 2000 m [32]

[38]. The effect of CNTs concentration on the microhardness of the composites is shown in Fig. 7.4a. The highest microhardness was observed for 4 wt% CNTs in the alumina matrix. Any further addition of CNTs led to a reduction in hardness due to inhomogeneous dispersion of CNTs. The tribological tests were carried out using silicon nitride ball as a counterpart at 25 N and 10 mm/s sliding velocity. Figure 7.4b shows the variation in COF and wear with respect to CNTs content. It can be seen that the Al_2O_3-CNTs composite with 4 wt% yielded least wear loss with COF of 0.43. The composite with 12.5% CNTs provided the lowest COF of 0.3 but higher wear rate, which is more than two times of pure alumina. Similar behavior was also observed by Lim et al. who showed an increase in wear rate with CNTs content for hot-pressed Al_2O_3-CNTs composite (Fig. 7.5a) [39]. The authors also prepared the composite by tape casting other than hot pressing. In tape casting, the ceramic slurry was cast in thin layers followed by drying. These layers were laminated by hot pressing. The resulted composite showed a reduction in wear loss with the increase in CNTs content while maintaining the same friction coefficient (Fig. 7.5a, b). In this study, the tribological tests were performed against silicon nitride ball at 25 N load with 10 mm/s sliding speed. The tape casting method allowed to disperse higher amount of CNTs in alumina to achieve superior tribological and mechanical properties.

The other lamellar SLs are MoS_2, BN which have been used as reinforcements in various metallic and ceramic materials, including alumina. For example, Su et al. [40] prepared the Al_2O_3/MoS_2 composite by in situ syntheses of MoS_2 in the porous Al_2O_3 matrix. The porous Al_2O_3 matrix was developed by sintering the green body made of Al_2O_3 and graphite (10 vol%), the graphite oxidized during sintering in air

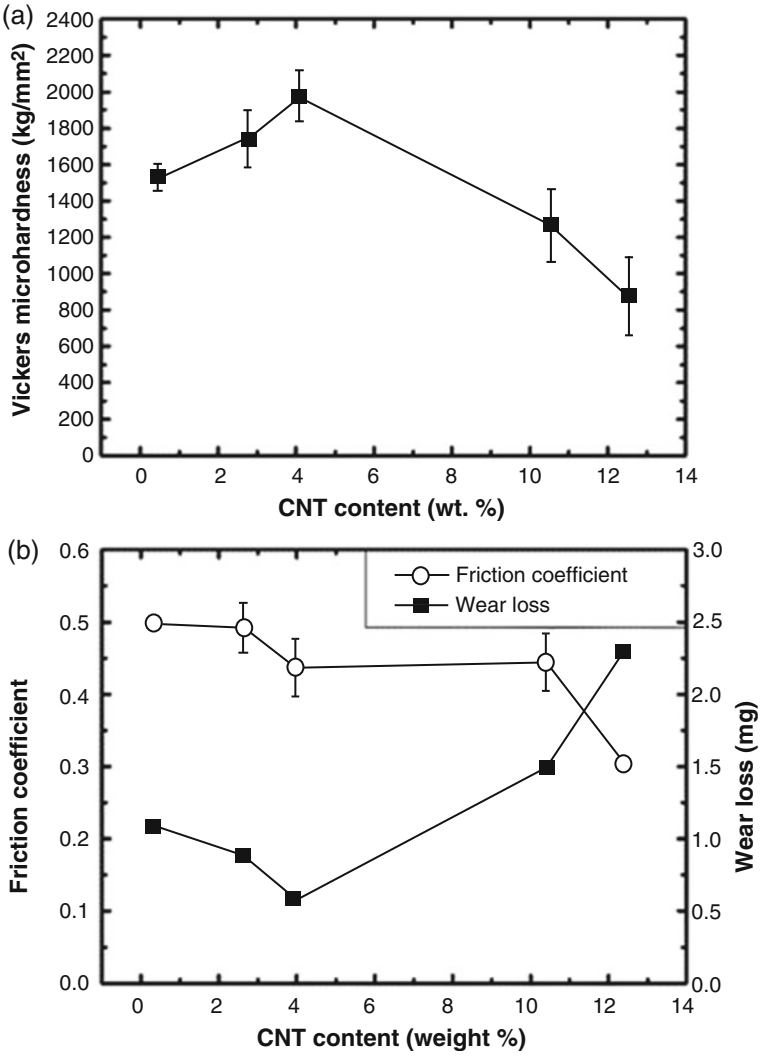

Fig. 7.4 (**a**) Microhardness, (**b**) COF and wear loss of the Al_2O_3-CNTs composite [38]

and led to formation of pores. After sintering, the porous sample was immersed in a solution that consists of sodium molybdate, thiourea, and deionized water under vacuum. After vacuum infusion, the porous samples immersed in solution were heated at 220 °C in stainless steel autoclave for 56 h. This hydrothermal process led to the formation of MoS_2 in the pores of the sintering Al_2O_3 matrix. The tribological property of resulted composite was tested against Si_3N_4 ball in a vacuum environment ($<5.0 \times 10^{-5}$ mbar) at 5 N normal load. The COF of the composite (0.2) was reduced significantly compared to sintered Al_2O_3 sample (0.75) as shown in Fig. 7.6a. At the same time, three orders of magnitude reduced wear rate due to the formation of MoS_2 film at the interface. EDS on wear track of Al_2O_3-MoS_2

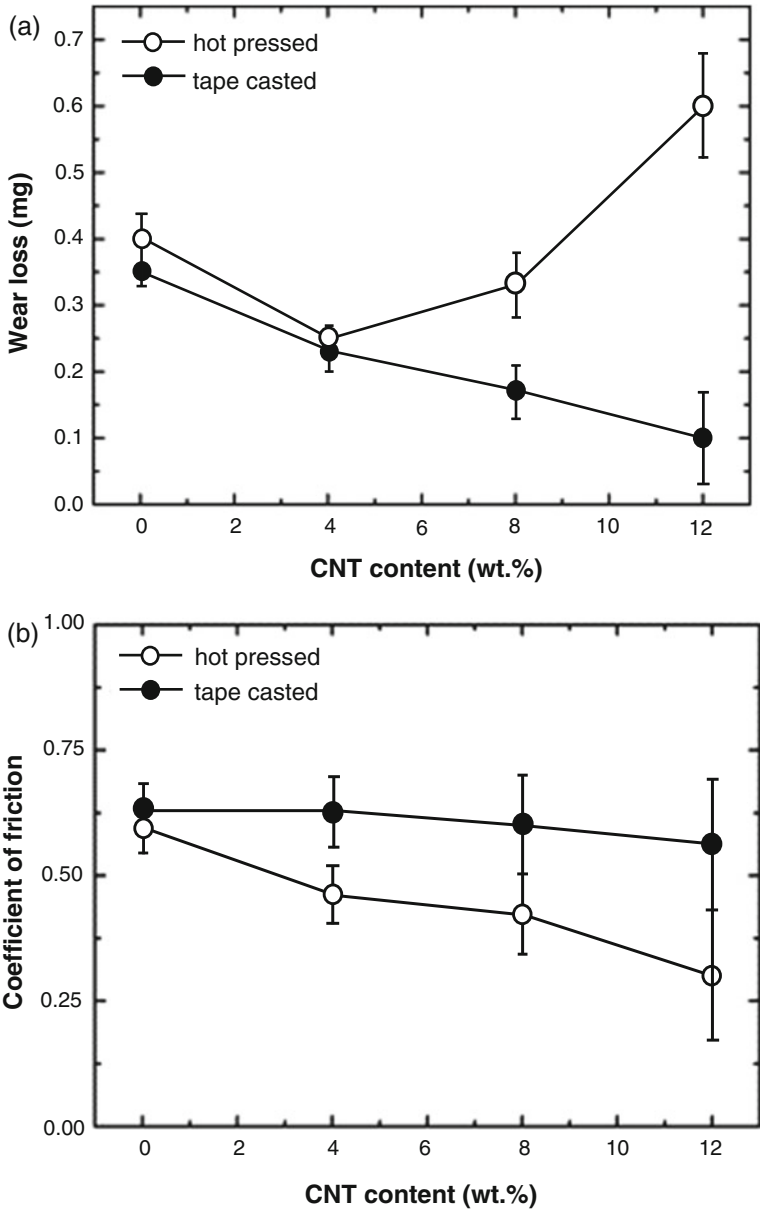

Fig. 7.5 The effect of CNTs content on (**a**) wear loss and (**b**) COF of Al_2O_3-CNTs composite synthesized by hot pressing and tape casting method [39]

composite (Fig. 7.6c) showed the presence of Mo and S, which were not present on the wear track of Al_2O_3 (Fig. 7.6a).

The combination of two lamellar SLs MoS_2, BN on mechanical properties was investigated by Deng et al. [41]. The composites were prepared using these lamellar

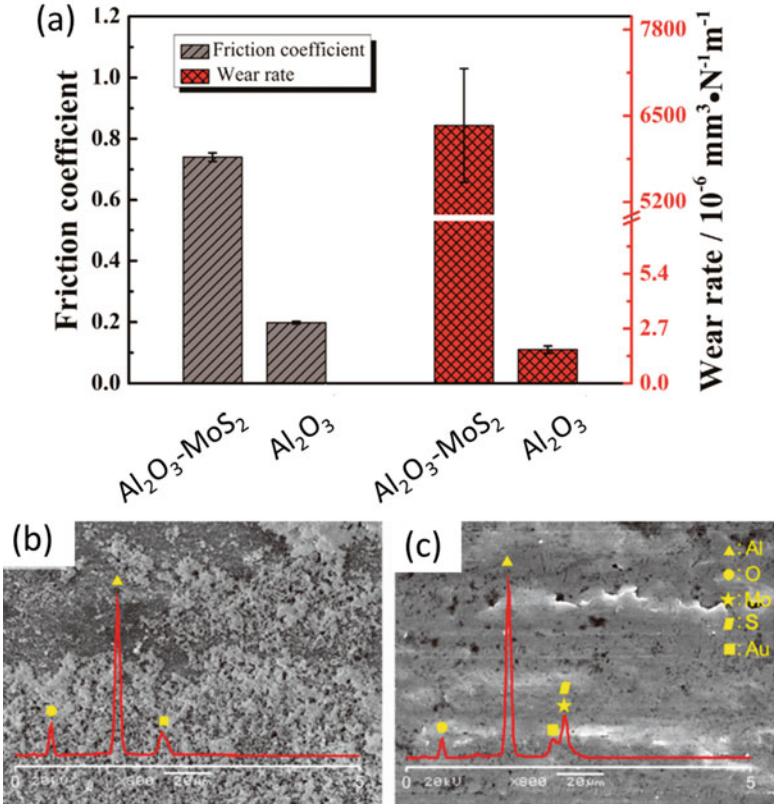

Fig. 7.6 (**a**) Friction and wear rate of Al_2O_3-MoS_2 composite, (**b**) and (**c**) are wear track of Al_2O_3 and Al_2O_3-MoS_2 composite, respectively [40]

solids (5, 10, and 15 vol%) in the Al_2O_3-TiC matrix (1:1 vol ratio) by hot pressing in an argon atmosphere for 15 min at 1700 °C. For all the composites, hardness and fracture toughness reduced with an increase in SL content. With 15 vol% of MoS_2, the hardness and fracture toughness were reduced by 2.1 and 1.73 times, respectively, whereas 15 vol% of BN reduced the same by 8.7 and 2.6 times with respect to the Al_2O_3-TiC matrix. These results support that the addition of SLs cause a reduction in mechanical properties. However, a hard phase such as TiC or SiC can be added in the alumina matrix to compensate for the loss in mechanical properties.

7.4 Other Compounds

In this section, other SL compounds such as sulfates and oxides are included. The most common SL sulfates are $BaSO_4$. Murkami et al. [42] studied the Al_2O_3 reinforced with $BaSO_4$ SL. The Al_2O_3-50% $BaSO_4$ composites were prepared by

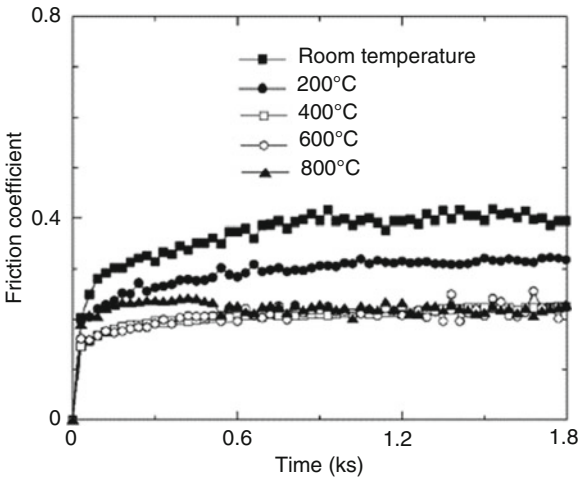

Fig. 7.7 Friction coefficient of Al_2O_3-50$BaSO_4$-20Ag against alumina ball at different temperatures [43]

spark plasma sintering. The tribological tests against Al_2O_3 ball were conducted at up to 800 °C. The composite was able to retain a COF between 0.2 and 0.4 over the temperature range. The lower friction was due to the formation of $BaSO_4$ film at the interface. An extension to this study, the same research group investigated the tribological performance of Al_2O_3-50$BaSO_4$-20Ag, Al_2O_3-50$BaSO_4$-10SiO_2, Al_2O_3-50$SrSO_4$, and Al_2O_3-50$PbSO_4$-5SiO_2. Among all the composites, Al_2O_3-50$BaSO_4$-20Ag showed the least COF. At the temperature range of 400–800 °C, the COF for Al_2O_3-50$BaSO_4$-20Ag was 0.2, as shown in Fig. 7.7. The micrographs of wear tracks are shown in Fig. 7.8. Ag tribo film was observed on the wear track of the samples tested at 400 °C and above that reduced the COF to 0.2. The authors also stated that the $BaSO_4$ has a barite-type structure that can be cleaved along (0 0 1), which results in lower COF. Also, the $BaSO_4$ becomes ductile above 400 °C that can further enhance the self-lubrication behavior.

The effect of different oxides on the tribological behavior of alumina composites was investigated by Kerkwijk et al. [44]. The different alumina composites with 5 wt% of MgO, CuO, MnO_2, and B_2O_3 reinforcement were synthesized by isostatic pressing at 400 MPa. The green pellets after isostatic pressing was sintered at 1500 °C for 2 h. The sliding tests were conducted against alumina ball at room temperature with a 10 N normal load. The composites with MnO_2, MgO, and B_2O_3 showed mean COF values of 0.48, which is lower than the other composites and pure alumina (0.55). For the composites with CuO and ZnO, the observed COF are 0.65 and 0.49, respectively. The addition of oxides other than CuO resulted in lowering the friction of alumina from 0.55 to ~0.48. These ceramic composites also showed low specific wear rates, in the range of 10^{-9} to 10^{-8} mm^3/Nm.

Al_2O_3 is also used as a cutting tool where friction and wear are important parameters for the tool's performance and life. These tools can be reinforced with

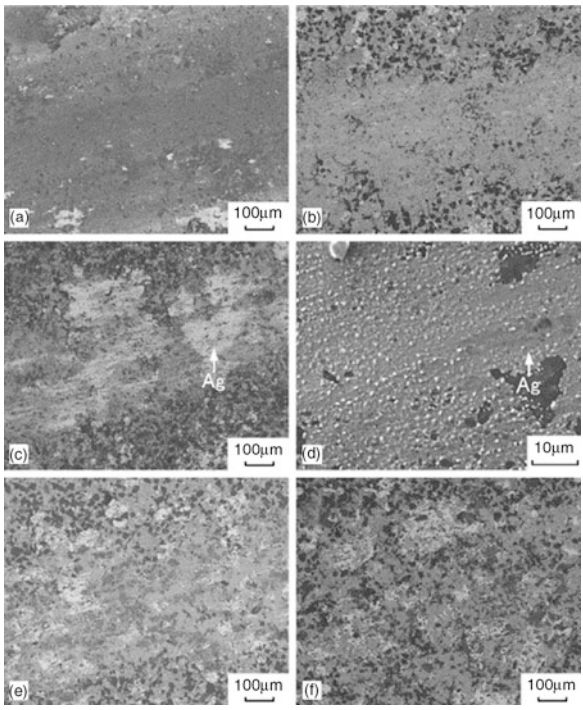

Fig. 7.8 Wear track of Al_2O_3-50$BaSO_4$-20Ag at (**a**) room temperature, (**b**) 200 °C, (**c**, **d**) 400 °C, (**e**) 600 °C, and (**f**) 800 °C [43]

SLs, for example, Al_2O_3-TiB_2 ceramic cutting tools were synthesized with different TiB_2 content (10–40 vol%) by hot pressing and tested through dry high-speed machining on hardened steel while measuring friction, wear, and cutting speed [8]. It was found that both wear and COF at the tool–chip interface were reduced with increase in sliding speed and TiB_2 content. The composite with 40 vol% resulted in a COF of 0.2, which was ~42% lower than the composite with 10 vol% TiB_2. The cutting speed during the experiment was 200 m/min. Flank wear was also reduced for Al_2O_3-40 vol% TiB_2 and it was 30–40% lesser than the Al_2O_3-10 vol% TiB_2 composite. The observed lower COF and wear was due to the formation of a self-lubricating oxide film (TiO_2) at the tool–chip interface because of the tribological chemical reaction at the elevated cutting temperature. The mechanism was confirmed by carrying out the same cutting process in a nitrogen atmosphere where no oxides were performed, and wear was significantly higher.

In addition to uniform reinforcement of SLs, laminated alumina composites have been studied to improve mechanical properties along with tribological properties. The laminated ceramic structure is inspired by structures available in nature, such as shells, lignum, or teeth that show improved failure behavior in comparison with monolithic ceramic material. Qi et al. [45] prepared the laminated structure of Al_2O_3/Mo by powder metallurgy route by stacking the alternate layers of ball-milled powders in a mold followed by hot pressing at 1550 °C and 25 MPa for 90 min in

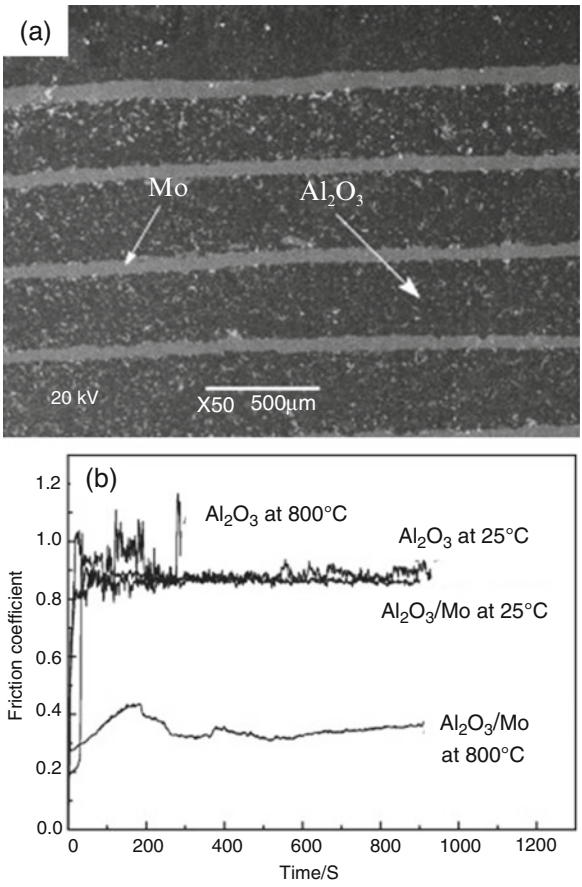

Fig. 7.9 (**a**) SEM micrograph of Al_2O_3/Mo-laminated composites and (**b**) friction coefficients of Al_2O_3/Mo-laminated composites and monolithic Al_2O_3 ceramics at 25 and 800 °C [45]

an inert atmosphere of Ar. The SEM micrograph of Al_2O_3/Mo-laminated composites is shown in Fig. 7.9a. The laminated structure showed improved fracture toughness of 9.14 MPa $m^{1/2}$ compared with fracture toughness of monolithic alumina that is 5.69 MPa $m^{1/2}$. The tribological performance of the structure was tested at 25 and 800 °C against the alumina pin at 70 N. The friction coefficient is shown in Fig. 7.9b. At room temperature, the laminated structure showed the same friction as the monolithic alumina. However, a drastic decrease in friction from 0.9–0.4 can be observed at 800 °C for the laminated structure. The reduction in COF was due to the formation of molybdenum oxides (MoO_2 and $MoO_{2.8}$) observed by XRD on the wear track. The plastic deformation ability of molybdenum oxides provided the laminated structure self-lubricating properties at high temperature.

A further change in design to improve the self-lubricity of the Al_2O_3-Mo-laminated structure was carried out by Zhang et al. [46], where laser surface texture was created on the laminated structure as shown in Fig. 7.10a. The SLs materials, MoS_2

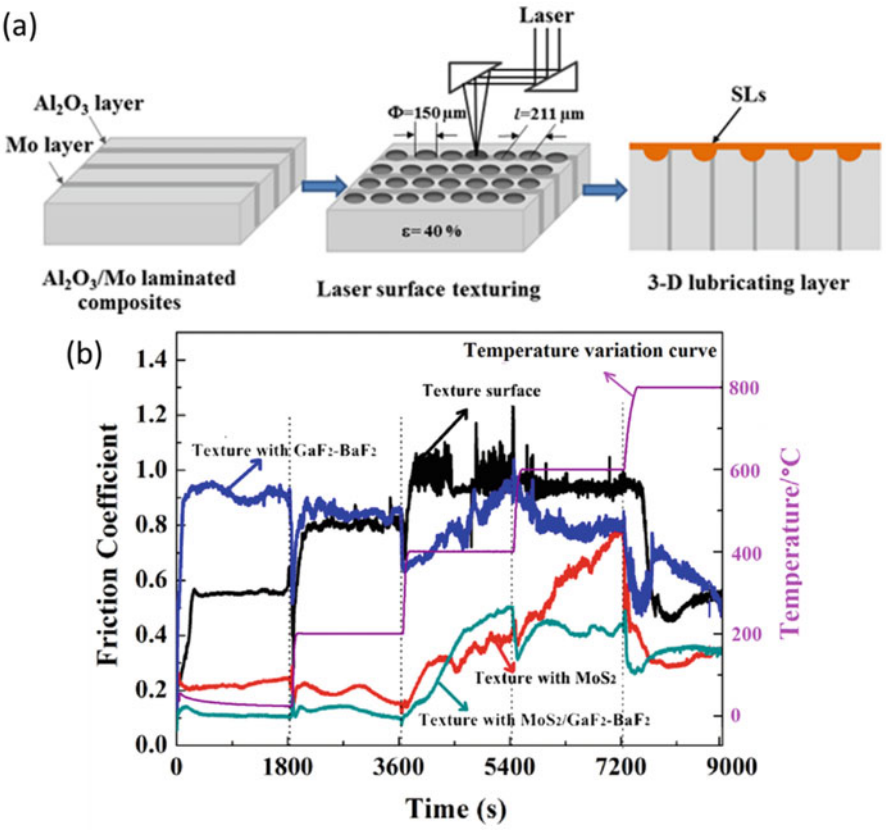

Fig. 7.10 (**a**) Schematic of fabricating Al_2O_3/Mo-laminated composite with laser texturing + SLs, and (**b**) COF of the laminated structure with burnished SLs at different temperatures [46]

and CaF_2–BaF_2, were burnished on the textured surface. The tribological performance of the prepared structure was tested against alumina pin from room temperature to 800 °C. The observed COF trends are shown in Fig. 7.10b. Figure 7.10b shows that the composite structure containing MoS_2 had lower friction coefficient of 0.1–0.2 from room temperature to 200 °C. Whereas, the composite with CaF_2-BaF_2 had higher friction at room temperature. At 600 °C, composite with MoS_2 showed higher friction compared to the composite with combination of MoS_2 and CaF_2-BaF_2. It suggests that MoS_2 reduces friction at lower temperatures, whereas CaF_2-BaF_2 helps to maintain lower friction at the higher temperature range. Therefore, the combination of these SLs is preferable. The lower friction is due to the transfer film of MoS_2 and in situ formed oxides. The formation of MoO_2 is explained in the previous paragraph. The MoO_2 was also reacted with CaF_2-BaF_2 to form $CaMoO_4$ and $BaMoO_4$ during sliding at the higher temperature and improve high-temperature lubrication.

7.5 Conclusions

In this chapter, SLs have been characterized based on their nature, such as soft material, which is easy to deform that can reduce friction at the interface. The SLs are discussed mainly for the alumina matrix for room temperature and high-temperature applications. It has also shown that the combination of SLs from different categories have been effective at different temperature range, such as CaF_2 is mainly suitable for high-temperature application whereas graphite and MoS_2 work well even at room temperature in the alumina matrix.

Self-lubrication nature of the alumina composites is governed by the formation of continuous tribo-layer at the interface that minimizes the contact between counter bodies and reduces friction. However, the addition of SLs in alumina is decided by two factors: (i) excessive amount can cause nonuniform dispersion and (ii) excessive amount can increase wear drastically. The nonuniform dispersion of SLs can be taken care of by suitable synthesis techniques or prior colloidal mixing. However, the severe wear can be controlled by optimizing the amount of SLs based on the application parameters, such as load, velocity, roughness, and properties of the counterpart.

Other than conventional reinforced alumina composites, laminated structures of alumina have also been developed with Mo, where the formation of MoO_2 provided lower friction. Further enhancement on this laminated structure has been carried out by the formation of small grooves using laser treatment. These grooves acted as a sink for SLs materials for the continuous formation of tribo-layer. Overall, it has been seen that alumina is compatible with all the SLs without the formation of any unwanted chemical compound. The inherent properties of alumina combined with SLs make the composite suitable for tribological applications at extreme environments.

Funding The authors appreciate the funding from NASA CAN, grant number NV-80NSSC20M0221.

References

1. Song, J., Valefi, M., de Rooij, M., Schipper, D.J.: A mechanical model for surface layer formation on self-lubricating ceramic composites. Wear. **268**(9), 1072–1079 (2010). https://doi.org/10.1016/j.wear.2010.01.012
2. Liu, H., Xue, Q.: The tribological properties of TZP-graphite self-lubricating ceramics. Wear. **198**(1), 143–149 (1996). https://doi.org/10.1016/0043-1648(96)06946-3
3. Wang, Z., Wu, L., Qi, Y., Cai, W., Jiang, Z.: Self-lubricating Al_2O_3/PTFE composite coating formation on surface of aluminium alloy. Surf. Coat. Technol. **204**(20), 3315–3318 (2010). https://doi.org/10.1016/j.surfcoat.2010.03.049
4. Putyra, P., Podsiadło, M., Smuk, B.: Alumina composites with solid lubricant content. J. Achiev. Mater. Manuf. Eng. **41**(1-2), 34–39 (2010)
5. Jin, Y., Kato, K., Umehara, N.: Effects of sintering aids and solid lubricants on tribological behaviours of CMC/Al_2O_3 pair at 650°C. Tribol. Lett. **6**(1), 15–21 (1999)
6. Masanta, M., Shariff, S.M., Choudhury, A.R.: Tribological behavior of TiB_2–TiC–Al_2O_3 composite coating synthesized by combined SHS and laser technology. Surf. Coat. Technol. **204**(16), 2527–2538 (2010). https://doi.org/10.1016/j.surfcoat.2010.01.027
7. Jianxin, D.: Friction and wear behaviour of Al_2O_3/TiB_2/SiCw ceramic composites at temperatures up to 800 C. Ceram. Int. **27**(2), 135–141 (2001)

8. Jianxin, D., Tongkun, C., Lili, L.: Self-lubricating behaviors of Al_2O_3/TiB_2 ceramic tools in dry high-speed machining of hardened steel. J. Eur. Ceram. Soc. **25**(7), 1073–1079 (2005)
9. Taylor, A.: Ceramics – Materials, Joining and Applications. https://www.twi-global.com/technical-knowledge/job-knowledge/ceramics-materials-joining-and-applications-054.aspx (2020). Accessed 10 July 2020
10. Burris, D.L., Sawyer, W.G.: Tribological sensitivity of PTFE/alumina nanocomposites to a range of traditional surface finishes. Tribol. Trans. **48**(2), 147–153 (2005)
11. Xiang, D., Li, K., Shu, W., Xu, Z.: On the tribological properties of PTFE filled with alumina nanoparticles and graphite. J. Reinf. Plast. Compos. **26**(3), 331–339 (2007)
12. Guglani, L., Gupta, T.: Wear and mechanical properties of nylon 66–Al_2O_3 microcomposite. J. Reinf. Plast. Compos. **36**(17), 1254–1262 (2017)
13. Saravanan, D., Palanisamy, C., Raajeshkrishna, C.: Tribological performance of multi walled carbon nanotubes–alumina hybrid/epoxy nanocomposites under dry sliding condition. Mater. Res. Express. **6**(10), 105067 (2019)
14. Wang, H.M., Yu, Y.L., Li, S.Q.: Microstructure and tribological properties of laser clad CaF_2/Al_2O_3 self-lubrication wear-resistant ceramic matrix composite coatings. Scr. Mater. **47**(1), 57–61 (2002). https://doi.org/10.1016/S1359-6462(02)00086-6
15. Kim, S.H., Hannula, S.P., Lee, S.W.: Effects of the sliding conditions on the tribological behavior of atmospheric plasma sprayed Al_2O_3–15wt.% ZrO_2–CaF_2 composite coating. Surf. Coat. Technol. **210**, 127–134 (2012). https://doi.org/10.1016/j.surfcoat.2012.09.003
16. Sarkar, D., Adak, S., Mitra, N.: Preparation and characterization of an Al_2O_3–ZrO_2 nanocomposite, part I: powder synthesis and transformation behavior during fracture. Compos. A: Appl. Sci. Manuf. **38**(1), 124–131 (2007)
17. Wang, C.-J., Huang, C.-Y., Wu, Y.-C.: Two-step sintering of fine alumina–zirconia ceramics. Ceram. Int. **35**(4), 1467–1472 (2009)
18. Niu, F., Wu, D., Ma, G., Wang, J., Guo, M., Zhang, B.: Nanosized microstructure of Al_2O_3–ZrO_2 (Y_2O_3) eutectics fabricated by laser engineered net shaping. Scr. Mater. **95**, 39–41 (2015)
19. Murakami, T., Ouyang, J.H., Sasaki, S., Umeda, K., Yoneyama, Y.: High-temperature tribological properties of Al_2O_3, Ni–20mass% Cr and NiAl spark-plasma-sintered composites containing BaF_2–CaF_2 phase. Wear. **259**(1), 626–633 (2005). https://doi.org/10.1016/j.wear.2004.12.019
20. Deng, J., Liu, L., Yang, X., Liu, J., Sun, J., Zhao, J.: Self-lubrication of $Al_2O_3/TiC/CaF_2$ ceramic composites in sliding wear tests and in machining processes. Mater. Des. **28**(3), 757–764 (2007)
21. Dorri Moghadam, A., Omrani, E., Menezes, P.L., Rohatgi, P.K.: Mechanical and tribological properties of self-lubricating metal matrix nanocomposites reinforced by carbon nanotubes (CNTs) and graphene – a review. Compos. Part B. **77**, 402–420 (2015). https://doi.org/10.1016/j.compositesb.2015.03.014
22. Kasar, A.K., Menezes, P.L.: Synthesis and recent advances in tribological applications of graphene. Int. J. Adv. Manuf. Technol. **97**(9-12), 3999–4019 (2018)
23. Kasar, A.K., Xiong, G., Menezes, P.L.: Graphene-reinforced metal and polymer matrix composites. JOM. **70**(6), 829–836 (2018)
24. Tan, H., Wang, S., Yu, Y., Cheng, J., Zhu, S., Qiao, Z., Yang, J.: Friction and wear properties of Al-20Si-5Fe-2Ni-graphite solid-lubricating composite at elevated temperatures. Tribol. Int. **122**, 228–235 (2018)
25. Omrani, E., Moghadam, A.D., Menezes, P.L., Rohatgi, P.K.: Influences of graphite reinforcement on the tribological properties of self-lubricating aluminum matrix composites for green tribology, sustainability, and energy efficiency—a review. Int. J. Adv. Manuf. Technol. **83**(1-4), 325–346 (2016)
26. Wu, S., Tian, S., Menezes, P.L., Xiong, G.: Carbon solid lubricants: role of different dimensions. Int. J. Adv. Manuf. Technol. (2020). https://doi.org/10.1007/s00170-020-05297-8
27. Bagde, P., Sapate, S.G., Khatirkar, R.K., Vashishtha, N.: Friction and abrasive wear behaviour of Al_2O_3-13TiO_2 and Al_2O_3-13TiO_2+Ni graphite coatings. Tribol. Int. **121**, 353–372 (2018). https://doi.org/10.1016/j.triboint.2018.01.067
28. Zhao, X., Li, S., Hou, G., An, Y., Zhou, H., Chen, J.: Influence of doping graphite on microstructure and tribological properties of plasma sprayed $3Al_2O_3$–$2SiO_2$ coating. Tribol. Int. **101**, 168–177 (2016). https://doi.org/10.1016/j.triboint.2016.04.028

29. Gutierrez-Gonzalez, C.F., Smirnov, A., Centeno, A., Fernández, A., Alonso, B., Rocha, V.G., Torrecillas, R., Zurutuza, A., Bartolome, J.F.: Wear behavior of graphene/alumina composite. Ceram. Int. **41**(6), 7434–7438 (2015). https://doi.org/10.1016/j.ceramint.2015.02.061
30. Zhang, C., Nieto, A., Agarwal, A.: Ultrathin graphene tribofilm formation during wear of Al_2O_3–graphene composites. Nanomater. Energy. **5**(1), 1–9 (2016)
31. Gutiérrez-Mora, F., Cano-Crespo, R., Rincón, A., Moreno, R., Domínguez-Rodríguez, A.: Friction and wear behavior of alumina-based graphene and CNFs composites. J. Eur. Ceram. Soc. **37**(12), 3805–3812 (2017). https://doi.org/10.1016/j.jeurceramsoc.2017.02.024
32. Kim, H.J., Lee, S.-M., Oh, Y.-S., Yang, Y.-H., Lim, Y.S., Yoon, D.H., Lee, C., Kim, J.-Y., Ruoff, R.S.: Unoxidized graphene/alumina nanocomposite: fracture-and wear-resistance effects of graphene on alumina matrix. Sci. Rep. **4**(1), 1–10 (2014)
33. Wang, K., Wang, Y., Fan, Z., Yan, J., Wei, T.: Preparation of graphene nanosheet/alumina composites by spark plasma sintering. Mater. Res. Bull. **46**(2), 315–318 (2011). https://doi.org/10.1016/j.materresbull.2010.11.005
34. Porwal, H., Tatarko, P., Grasso, S., Khaliq, J., Dlouhý, I., Reece, M.J.: Graphene reinforced alumina nano-composites. Carbon. **64**, 359–369 (2013). https://doi.org/10.1016/j.carbon.2013.07.086
35. Liu, J., Yan, H., Jiang, K.: Mechanical properties of graphene platelet-reinforced alumina ceramic composites. Ceram. Int. **39**(6), 6215–6221 (2013). https://doi.org/10.1016/j.ceramint.2013.01.041
36. Fan, Y., Jiang, W., Kawasaki, A.: Highly conductive few-layer graphene/Al_2O_3 nanocomposites with tunable charge carrier type. Adv. Funct. Mater. **22**(18), 3882–3889 (2012)
37. Centeno, A., Rocha, V.G., Alonso, B., Fernández, A., Gutierrez-Gonzalez, C.F., Torrecillas, R., Zurutuza, A.: Graphene for tough and electroconductive alumina ceramics. J. Eur. Ceram. Soc. **33**(15), 3201–3210 (2013). https://doi.org/10.1016/j.jeurceramsoc.2013.07.007
38. An, J.W., You, D.H., Lim, D.S.: Tribological properties of hot-pressed alumina–CNT composites. Wear. **255**(1), 677–681 (2003). https://doi.org/10.1016/S0043-1648(03)00216-3
39. Lim, D.S., You, D.H., Choi, H.J., Lim, S.H., Jang, H.: Effect of CNT distribution on tribological behavior of alumina–CNT composites. Wear. **259**(1), 539–544 (2005). https://doi.org/10.1016/j.wear.2005.02.031
40. Su, Y., Zhang, Y., Song, J., Hu, L.: Novel approach to the fabrication of an alumina-MoS_2 self-lubricating composite via the in situ synthesis of nanosized MoS_2. ACS Appl. Mater. Interfaces. **9**(36), 30263–30266 (2017)
41. Deng, J., Can, T., Sun, J.: Microstructure and mechanical properties of hot-pressed Al_2O_3/TiC ceramic composites with the additions of solid lubricants. Ceram. Int. **31**(2), 249–256 (2005). https://doi.org/10.1016/j.ceramint.2004.05.009
42. Murakami, T., Ouyang, J., Umeda, K., Sasaki, S., Yoneyama, Y.: High-temperature friction and wear properties of X-BaSO4 (X: Al_2O_3, NiAl) composites prepared by spark plasma sintering. Mater. Trans. **46**(2), 182–185 (2005)
43. Murakami, T., Ouyang, J.H., Sasaki, S., Umeda, K., Yoneyama, Y.: High-temperature tribological properties of spark-plasma-sintered Al_2O_3 composites containing barite-type structure sulfates. Tribol. Int. **40**(2), 246–253 (2007). https://doi.org/10.1016/j.triboint.2005.09.013
44. Kerkwijk, B., García, M., van Zyl, W.E., Winnubst, L., Mulder, E.J., Schipper, D.J., Verweij, H.: Friction behaviour of solid oxide lubricants as second phase in α-Al_2O_3 and stabilised ZrO_2 composites. Wear. **256**(1), 182–189 (2004). https://doi.org/10.1016/S0043-1648(03)00388-0
45. Qi, Y.-e., Zhang, Y.-S., Hu, L.-T.: High-temperature self-lubricated properties of Al_2O_3/Mo laminated composites. Wear. **280-281**, 1–4 (2012). https://doi.org/10.1016/j.wear.2012.01.010
46. Fang, Y., Fan, H., Song, J., Zhang, Y., Hu, L.: Surface engineering design of Al_2O_3/Mo self-lubricating structural ceramics-part II: continuous lubrication effects of a three-dimensional lubricating layer at temperatures from 25 to 800° C. Wear. **360**, 97–103 (2016)

Recent Progress in Self-Lubricating Ceramic Composites

8

Guangyong Wu, Chonghai Xu, Guangchun Xiao, and Mingdong Yi

Contents

Abstract

Structural ceramic composites have received increasing attention over the past few decades for their potential applications in various fields. Lubrication is usually required for moving ceramic parts because of their high coefficient of friction under dry sliding conditions. Self-lubricating ceramic composites have been applied in severe operating conditions where conventional lubrication method, such as liquid lubrication, is unavailable. The solid lubricants added in

G. Wu
School of Mechanical Engineering, Shandong University, Jinan, China
e-mail: gywu168@sina.com

C. Xu (✉)
School of Mechanical Engineering, Shandong University, Jinan, China

School of Mechanical and Automotive Engineering, Qilu University of Technology, Jinan, China

Key Laboratory of Advanced Manufacturing and Measurement and Control Technology for Light Industry in Universities of Shandong, Qilu University of Technology, Jinan, China
e-mail: xch@qlu.edu.cn

G. Xiao · M. Yi
School of Mechanical and Automotive Engineering, Qilu University of Technology, Jinan, China

Key Laboratory of Advanced Manufacturing and Measurement and Control Technology for Light Industry in Universities of Shandong, Qilu University of Technology, Jinan, China

P. L. Menezes et al. (eds.), *Self-Lubricating Composites*,
https://doi.org/10.1007/978-3-662-64243-6_8

self-lubricating ceramic composites can reduce the coefficient of friction. However, they decrease mechanical properties and then weaken antiwear property of the ceramic composites, which consequently restricts self-lubricating ceramic composites' application scope. Therefore, there is a contradiction between the antifriction and antiwear properties of self-lubricating ceramic composites and many efforts from researchers have been devoted to resolve it. In this chapter, two new types of self-lubricating ceramic composites were elaborated. Graded self-lubricating ceramic composites were developed by adopting the design concept of functionally graded materials (FGMs). Their characteristics are that the solid lubricant content decreases with a gradient from the surface to the center and thermal residual compressive stresses exist in the surface after the sintering process. The gradient distribution of solid lubricant and the thermal residual compressive stresses are used to improve the mechanical properties of the ceramic composites. Another new type of self-lubricating ceramic composites is those with the addition of coated solid lubricants. The solid lubricant powders are firstly coated by metal or metallic oxide, etc., to form core-shell structured composite powders and then mixed with the ceramic matrix powders to prepare self-lubricating ceramic composites by sintering. The shell substance is used to protect the solid lubricant core from reacting with the ceramic matrix during the sintering process and promote the relative density of the ceramic composites. The two new types of self-lubricating ceramic composites showed superior mechanical properties and tribological properties to the traditional self-lubricating ceramic composites.

8.1 Introduction

Nowadays, structural ceramic composites have been paid attention increasingly for their distinctive properties, such as high hardness, high wear resistance, high-temperature resistance, and good chemical inertness [1]. They have been widely used for many applications, for instance, cutting tools, bearing parts, valve seats, etc. However, the friction coefficient of moving ceramic parts, especially of those made of alumina based ceramic composites, is relatively high [2]. Higher friction coefficient causes more cost and energy waste. The traditional oil or grease lubrication not only leads to environmental pollution, but also loses efficacy under harsh conditions, such as elevated temperature. Besides, due to poor thermal shock resistance of ceramic composites, inappropriate cooling will cause hot cracks and breakage. Therefore, development and application of ceramic composites with self-lubricating function is an effective and eco-friendly solution to improve the antifriction properties.

So far there are three main methods to make ceramic composites possess self-lubricating function: (1) make use of tribochemical reaction under high working temperature to get in situ formed tribofilm with lubricating function on the surface of ceramic composites, (2) adopt coating, impregnation, or implantation technologies

to enable the surface of ceramic composites to have lubricating function, and (3) fabricate self-lubricating ceramic composites which contain solid lubricants. Compared with the other two methods, the third one can make ceramic composites possess self-lubricating function during their whole service life because there are always solid lubricants in the composites. Besides, it can make the self-lubricating function be available in a wide working temperature range.

The traditional self-lubricating ceramic composites are homogeneous materials with the addition of pristine solid lubricants. Many researches revealed that the added solid lubricants can produce both positive and negative effects on properties of ceramic composites [3, 4]. On the one hand, the solid lubricant can reduce the friction coefficient by forming a tribofilm in the working areas. However, on the other hand, the dispersed solid lubricants can cause a decline in mechanical properties of the ceramic matrix, especially the hardness and fracture toughness, and thus reduce the wear resistance of the ceramic composite [5]. Thus, the traditional self-lubricating ceramic composites are not available to possess rational combination of antifriction and antiwear properties, which consequently restricts their application scope. It is urgent and significant to develop new type of self-lubricating ceramic composites.

In the past few years, we proposed and developed two new types of self-lubricating ceramic composites by modifying the traditional self-lubricating ceramic composites at macroscopic and microscopic level, respectively. The first type is graded self-lubricating ceramic composites [6–8]. It is macrostructural modification to the traditional self-lubricating ceramic composites. The second type is self-lubricating ceramic composites with the addition of metal coated solid lubricants [9]. It is microstructural modification to the traditional self-lubricating ceramic composites.

This chapter introduced the two new types of self-lubricating ceramic composites. Their microstructures, mechanical properties, and tribological properties were studied in detail.

8.2 Graded Self-Lubricating Ceramic Composites

Graded self-lubricating ceramic composites were proposed in terms of macrostructural modification to the traditional self-lubricating ceramic composites. This new type of self-lubricating ceramic composite is characterized by gradually decreasing distribution of solid lubricants from the composite's working surface to its interior and the residual compressive stresses existing in the working surface. There are two design criteria for the graded self-lubricating ceramic composites. Firstly, the solid lubricants should be gradually reduced from the working surface to the interior. Secondly, the thermal expansion coefficient of the composite should gradually increase from the working surface to the inside in order to form residual compressive stresses in the working surface after the sintering process [10].

CaF_2 is well known as a high-temperature solid lubricant and Al_2O_3/(W,Ti)C ceramic is a kind of widely used ceramic material, thus Al_2O_3/(W,Ti)C and CaF_2 were chosen to be the matrix material and solid lubricant, respectively. The starting

Table 8.1 Physical properties of the starting powders

Starting powder	Density ρ ($g{\cdot}cm^{-3}$)	Young's modulus E (GPa)	Poisson's ratio ν	Thermal expansion coefficient α ($\times 10^{-6}\ K^{-1}$)	Thermal conductivity k ($W{\cdot}m^{-1}\ K^{-1}$)
α-Al_2O_3	3.99	380	0.26	8.5	40.37
(W,Ti)C	9.56	550	0.194	5.8	26.74
CaF_2	3.18	75.8	0.26	18.85	9.71

powders were commercial Al_2O_3, (W,Ti)C, and CaF_2 and their physical properties are listed in Table 8.1.

Al_2O_3/(W,Ti)C/CaF_2 graded self-lubricating ceramic composite was designed in disk shape with its compositional distribution changing along the thickness direction. In order that the top and bottom surfaces of the composite can be used as work surfaces with the same self-lubricating performance, a symmetrically laminated structure with seven layers was adopted. Because the graded self-lubricating ceramic composite consists of three components which are Al_2O_3, (W,Ti)C, and CaF_2, a multicomponent gradient distribution model was proposed [7, 8]. The distribution model uses symmetrical power-law functions containing two compositional distribution exponents n_1 and n_2 which are for CaF_2 and (W,Ti)C, respectively.

The geometry model of Al_2O_3/(W,Ti)C/CaF_2 graded self-lubricating ceramic composite is a cylinder in a Cartesian coordinate system. The cylinder's bottom surface is in the X-Y plane and its axis coincides with the Z axis. The diameter and height of the cylinder are D and H, respectively. Because of their very small amounts, pores and sintering additives are not taken into account in the multicomponent distribution model. By regarding α-Al_2O_3 and (W,Ti)C as a matrix component, the volume fraction of CaF_2 in Al_2O_3/(W,Ti)C/CaF_2 material along the thickness of the material is given as:

$$V_{CaF_2} = f_1(\xi) = \begin{cases} \left(f_1^{CF} - f_0^{CF}\right)\left[\frac{0.5-\xi}{0.5}\right]^{n_1} + f_0^{CF} & 0 \le \xi \le 0.5 \\ \left(f_1^{CF} - f_0^{CF}\right)\left[\frac{\xi-0.5}{0.5}\right]^{n_1} + f_0^{CF} & 0.5 \le \xi \le 1 \end{cases} \tag{8.1}$$

Where ξ is the ratio of arbitrary coordinate value along the thickness direction (z) to the total thickness of the Al_2O_3/(W,Ti)C/CaF_2 material (H), i.e., z/H, and the range of ξ is [0,1]; ${f_1}^{CF}$ and ${f_0}^{CF}$ are volume fractions of CaF_2 in the Al_2O_3/(W,Ti)C/CaF_2 material of the surface layers and the middle layer, respectively; n_1 is the compositional distribution exponent for CaF_2 distributing in the Al_2O_3/(W,Ti)C/CaF_2 material.

Then the composition profile of the Al_2O_3/(W,Ti)C matrix component is determined as $V_{Al_2O_3/(W,Ti)C} = 1 - V_{CaF_2}$.The volume fraction of (W,Ti)C in the matrix along the thickness of the Al_2O_3/(W,Ti)C/CaF_2 material is given as:

$$V^*_{(W,Ti)C} = f_2(\xi) = \begin{cases} \left(f_1^{WT} - f_0^{WT}\right)\left[\frac{0.5-\xi}{0.5}\right]^{n_2} + f_0^{WT} & 0 \le \xi \le 0.5 \\ \left(f_1^{WT} - f_0^{WT}\right)\left[\frac{\xi-0.5}{0.5}\right]^{n_2} + f_0^{WT} & 0.5 \le \xi \le 1 \end{cases} \tag{8.2}$$

Where ξ is the same as in Eq. (8.1); ${f_1}^{WT}$ and ${f_0}^{WT}$ are volume fractions of (W,Ti)C in the Al_2O_3/(W,Ti)C matrixes of the surface layers and the middle layer, respectively; n_2 is the compositional distribution exponent for (W,Ti)C distributing in the Al_2O_3/(W,Ti)C matrix.

The volume fraction of (W,Ti)C in Al_2O_3/(W,Ti)C/CaF_2 material along the thickness of the material should be given as:

$$V_{(W,Ti)C} = (1 - f_1(\xi))f_2(\xi) \tag{8.3}$$

And the volume fraction of Al_2O_3 in Al_2O_3/(W,Ti)C/CaF_2 material along the thickness of the material should be given as:

$$V_{Al_2O_3} = (1 - f_1(\xi))(1 - f_2(\xi)) = 1 - V_{CaF_2} - V_{(W,Ti)C} \tag{8.4}$$

The combinations of nonnegative values of n_1 and n_2 can determine the compositional distributions of Al_2O_3/(W,Ti)C/CaF_2 material and then its gradients of microstructure as well as properties. According to values of n_1 and n_2, Al_2O_3/(W,Ti)C/CaF_2 material can be categorized into five general types:

(a) $n_1 = n_2 = 0$. Volume fraction of CaF_2 in the whole material and volume fraction of (W,Ti)C in the matrix are constant to form homogeneous material.
(b) $n_1 = 0$, $n_2 \neq 0$. Volume fraction of CaF_2 in the whole material is constant and volume fraction of (W,Ti)C in the matrix is varying to form the first kind of graded material.
(c) $n_1 \neq 0$, $n_2 = 0$. Volume fraction of CaF_2 in the whole material is varying and volume fraction of (W,Ti)C in the matrix is constant to form the second kind of graded material.
(d) $n_1 = n_2 \neq 0$. Volume fraction of CaF_2 in the whole material and volume fraction of (W,Ti)C in the matrix are varying with the same rate to form the third kind of graded material.
(e) $n_1 \neq n_2 \neq 0$. Volume fraction of CaF_2 in the whole material and volume fraction of (W,Ti)C in the matrix are varying with different rates to form the fourth kind of graded material.

In order to conform the two design criteria and use a simpler structure, the compositional distribution exponents were chosen to be $n_1 = n_2 = 2.0$. The detailed design procedure was presented in [7]. Table 8.2 lists the compositions of each layer and their physical properties which were calculated by the formulae in [10].

The Al_2O_3/(W,Ti)C/CaF_2 graded self-lubricating ceramic composite was prepared using a layer stacking method and powder metallurgical process. The detailed preparation process and measurement method of mechanical properties were described in [7]. An Al_2O_3/(W,Ti)C/CaF_2 homogeneous self-lubricating ceramic composite was also made from the same ingredients with the surface layers of the graded composite. Phase identification was made by X-ray diffraction (XRD) using an X-ray diffractometer (Bruker D8 ADVANCE). XRD patterns were recorded from

Table 8.2 Compositions and physical properties of graded layers

Layer number	Content of CaF_2 (Vol. %)	Volume ratio of (W,Ti)C: α-Al_2O_3 in matrix (Vol %)	Young's modulus E (GPa)	Poisson's ratio ν	Thermal expansion coefficient α ($\times 10^{-6}$ K^{-1})	Thermal conductivity k ($W \cdot m^{-1}$ K^{-1})
4th	0	30:70	424.710	0.242	7.660	35.156
3rd;5th	3.3	40:60	420.602	0.235	7.516	32.275
2nd;6th	6.7	50:50	415.416	0.229	7.386	29.643
1st;7th	10	60:40	410.367	0.223	7.262	27.303

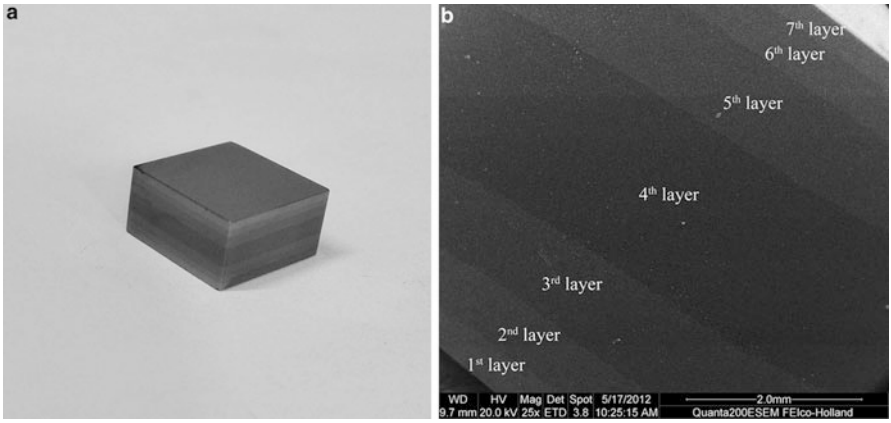

Fig. 8.1 (**a**) Optical photograph and (**b**) SEM micrograph of Al_2O_3/(W,Ti)C/CaF_2 graded composite

20° to 80° with a step of 0.02° under the condition of 40 kV and 20 mA. The componential distribution of Al_2O_3/(W,Ti)C/CaF_2 graded composite was analyzed by line scanning technique with energy dispersive spectrometer (EDS, Oxford INCAx-act). The microstructures were observed on polished cross section and fracture surfaces by environmental scanning electron microscope (ESEM, model FEI-quanta 200).

Optical photograph of Al_2O_3/(W,Ti)C/CaF_2 graded ceramic composite is shown in Fig. 8.1a. It can be seen that the layers are perpendicular to the thickness direction. SEM micrograph of the cross section surface is shown in Fig. 8.1b. A symmetrical seven-layer structure can be easily observed. The higher the (W,Ti)C content of a layer is, the brighter the layer looks like. The layer interfaces are straight and parallel to each other, which is in accord with the design objective.

The microstructural changes which agree with the gradient variation of the components are shown in Fig. 8.2. The darker phase in the micrographs is identified by EDS to be Al_2O_3 and the brighter phase is (W,Ti)C and CaF_2. From the first layer (surface layer) to the fourth layer (middle layer), because the content of Al_2O_3

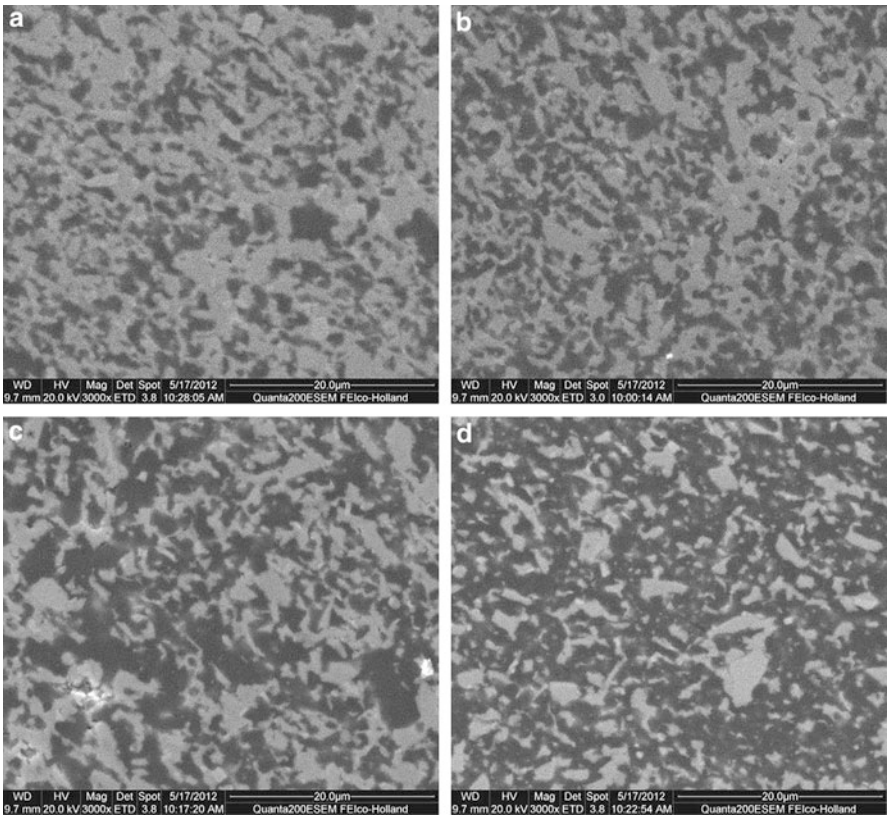

Fig. 8.2 SEM micrographs of the polished surface of Al_2O_3/(W,Ti)C/CaF_2 graded composite: (**a**) the 1st layer, (**b**) the 2nd layer, (**c**) the 3rd layer, and (**d**) the 4th layer

increases meanwhile the content of (W,Ti)C and CaF_2 decreases layer by layer, the proportion of darker areas in the micrographs increases and brighter areas follow the opposite variation trend. Furthermore, the phases in each layer are uniformly distributed and form relatively dense microstructures.

The SEM micrographs of the fractured surface of the Al_2O_3/(W,Ti)C/CaF_2 graded self-lubricating ceramic composite are shown in Fig. 8.3. It can be seen that each phase in the different layers has small and uniform grains. The cavities that are left after grains were pulled out can be observed. This sign indicates typical intergranularc fracture. The wavy or stepped features formed after grains were fractured can also be observed, which indicates typical transgranular fracture. Therefore, mixed intergranular fracture and transgranular fracture are fracture modes of the graded self-lubricating ceramic composite.

Figure 8.4 illustrates XRD pattern of surface layer of the Al_2O_3/(W,Ti)C/CaF_2 graded self-lubricating ceramic composite. It can be seen that Al_2O_3, (W,Ti)C, and CaF_2 phases well exist in the composite.

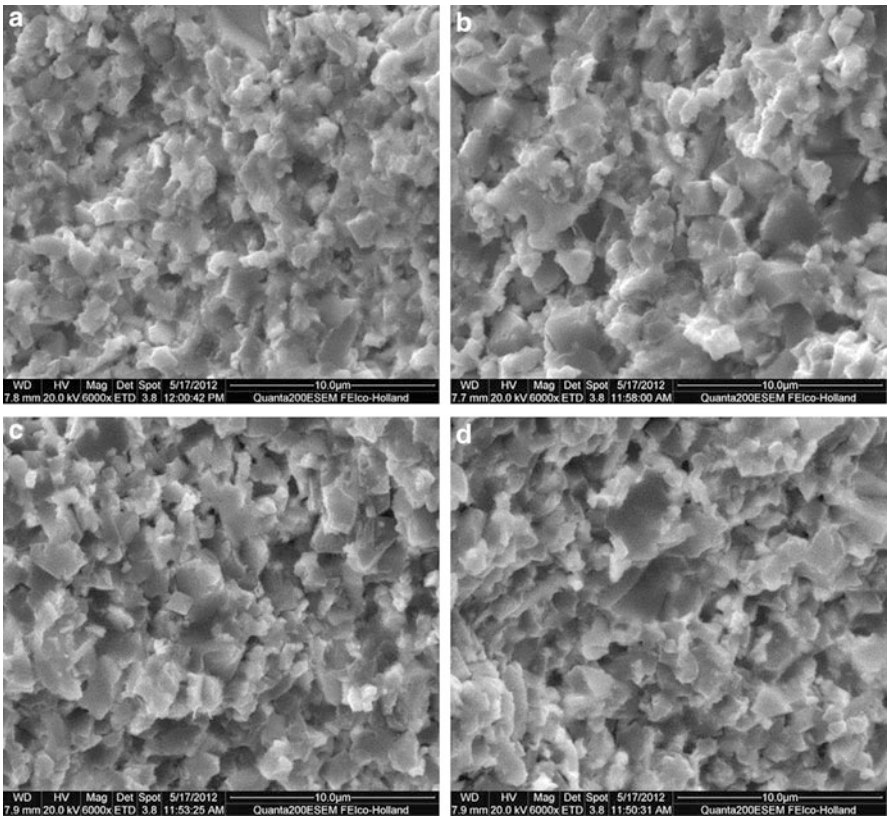

Fig. 8.3 SEM micrographs of the fractured surface of Al_2O_3/(W,Ti)C/CaF_2 graded composite: (**a**) the 1st layer, (**b**) the 2nd layer, (**c**) the 3rd layer, and (**d**) the 4th layer

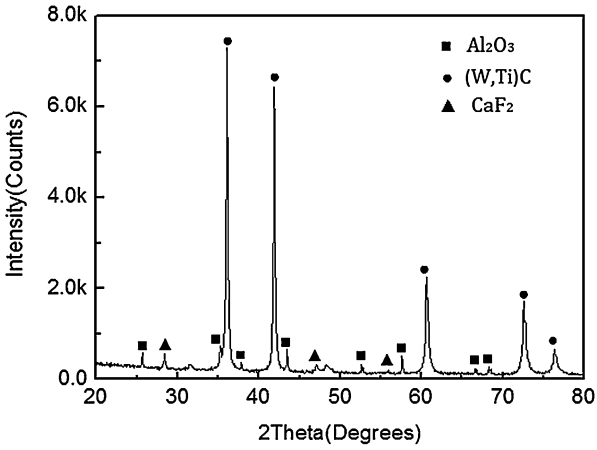

Fig. 8.4 XRD pattern of surface layer of Al_2O_3/(W,Ti)C/CaF_2 graded composite

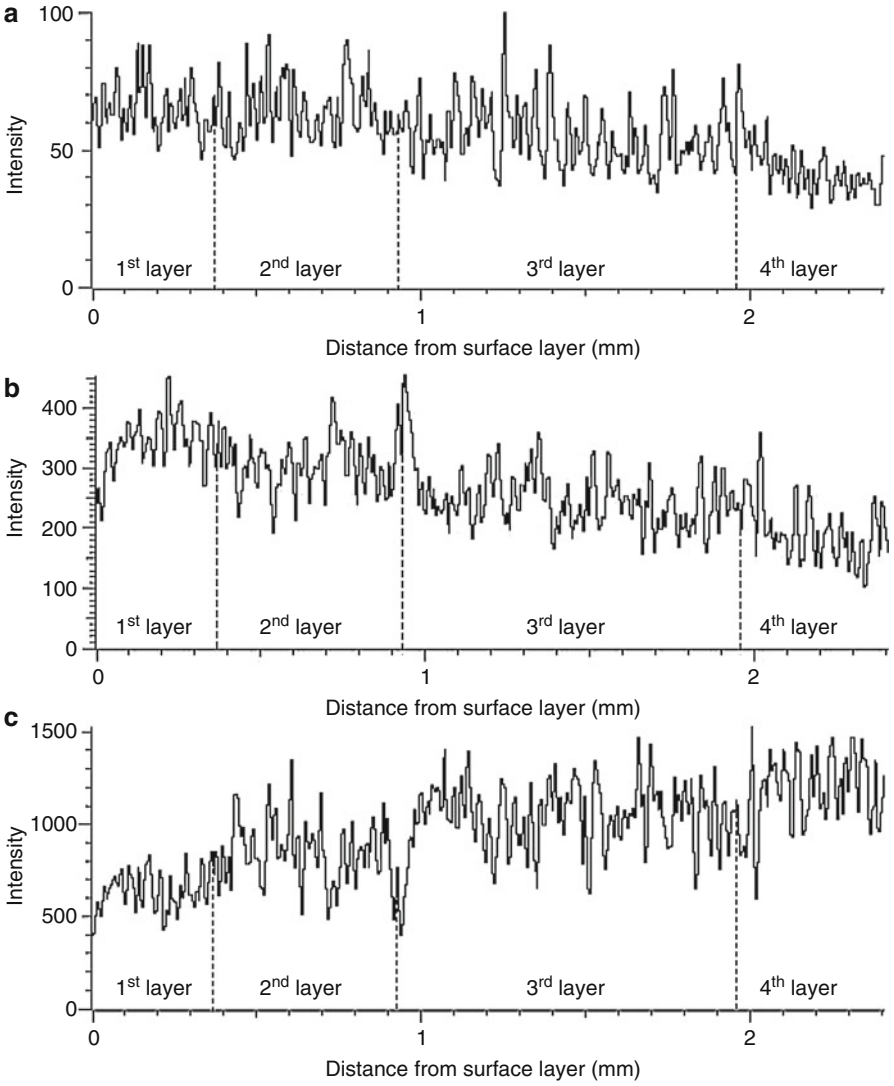

Fig. 8.5 Line scanning patterns for elemental distributions along the compositional gradient direction: (**a**) Ca element, (**b**) Ti element, and (**c**) Al element

Elemental gradient distributions from a surface layer (first layer) to the middle layer (fourth layer) are shown in Fig. 8.5. It can be seen that the concentrations of Ca and Ti elements decrease from the surface layer to the middle layer in the graded composite, whereas the Al concentration follows the opposite trend. It is indicated that the graded distributions of Al_2O_3, (W,Ti)C, and CaF_2 conform to the design scheme shown in Table 8.2. It should be noticed that a small amount of elemental Ca is detected in the middle layer of the material where no CaF_2 was added. The

Table 8.3 Mechanical properties of the self-lubricating ceramic composites

Specimen	Flexural strength (MPa)	Vickers hardness (GPa)	Fracture toughness ($MPa \cdot m^{1/2}$)
Graded composite	769±22[a]	15.36 ± 0.3[b]	4.02 ± 0.2[b]
Homogeneous composite	617 ± 31	12.89 ± 0.5	3.81 ± 0.3

[a]The testing forces were loaded perpendicularly with respect to the layers
[b]The data were from measurements taken on the surface layers

concentration of elemental Ca sharply decreases from the boundary of the fourth layer and the third layer to the interior of the fourth layer. This result could be attributed to the melting point of CaF_2, which is lower than the sintering temperature. Some CaF_2 may have melted during the sintering process and diffused into the middle layer from the adjacent layers.

The mechanical properties of Al_2O_3/(W,Ti)C/CaF_2 graded self-lubricating ceramic composite and the homogeneous composite are listed in Table 8.3. The flexural strength, Vickers hardness, and fracture toughness of the Al_2O_3/(W,Ti)C/CaF_2 graded composite are respectively 25%, 19%, and 6% higher than those of the Al_2O_3/(W,Ti)C/CaF_2 homogeneous composite. The significant improvement in the mechanical properties can be attributed to the two design criteria. Firstly, the decreasing gradient of the CaF_2 content from the surface layers to the middle layer of the graded composite can ensure excellent self-lubricating properties in the surface layers because of its relatively high CaF_2 content, and improve the flexural strength of the whole material due to substantially higher flexural strength of the middle layer where no CaF_2 had been added. Secondly, residual compressive stresses in the surface layers were caused by the mismatched thermal coefficients of expansion between adjacent layers. The presence of these stresses can effectively improve the mechanical properties of the surface layers, especially the fracture toughness and hardness [11].

The thermal residual stresses were calculated by the indentation method [12]. The indentation was produced by a Vickers indenter on central line of each layer of a cross section of the composite, using a load of 49 N. The indents were aligned in the way that their diagonals and possible radial cracks were parallel and perpendicular to the graded layers. As shown in Fig. 8.6a, the indentation cracks that are perpendicular to the layers are clearly shorter and narrower than those parallel to the layers, which indicates the presence of compressive stresses in the surface layers. It can be seen from Fig. 8.6b that the exterior layers are subjected to compressive stresses while tensile stresses are found in the interior layers. The profile of residual stresses satisfactorily conforms to the design objective.

The dry friction and wear test took pin-on-disk type and was carried out on a MMW-1A multipurpose friction and wear testing machine. The pin specimen (10 mm × 10 mm × 5 mm, Ra 0.1 μm) was made of the self-lubricating ceramic composites by cutting, grinding, and polishing. The disk was a hardened 45# carbon steel ring (Φ54mm × Φ38mm × 10 mm, HRC 45, Ra 0.08 μm). The pin and disk were ultrasonically cleaned for 10 min in acetone and then completely dried in a

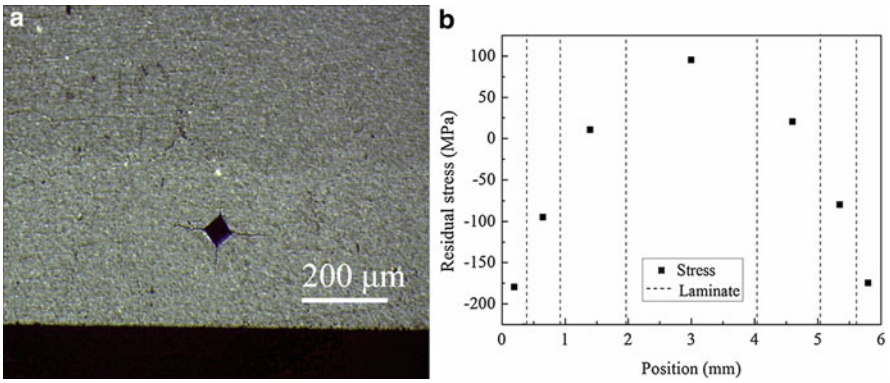

Fig. 8.6 (**a**) Optical micrograph of an indentation on the surface layer, and (**b**) profile of residual stresses measured by the indentation method

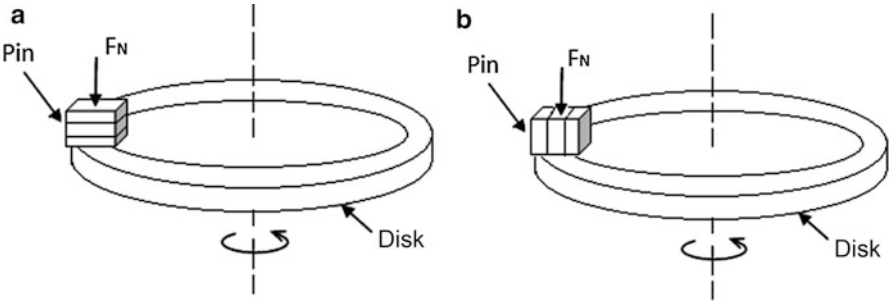

Fig. 8.7 Schematic diagrams of the testing device and clamping mode of pin specimen

vacuum drying oven. The schematic diagrams of the friction and wear testing device and clamping mode of pin specimen are shown in Fig. 8.7. During the dry friction and wear test, the pin specimen of Al_2O_3/(W,Ti)C/CaF_2 graded composite was clamped in the way shown as Fig. 8.7a and was sliding on the disk with a rotational speed of 100–300 r/min under a normal load of 100 N.

The friction coefficient μ of the ceramic composite was calculated by the formula:

$$\mu = F/P = M/(\mathrm{R} \cdot P) \tag{8.5}$$

where F is the fiction force (N); P is the normal load (N); M is the friction torque (N·m); R is intermediate radius of the steel ring (m). The friction coefficient was acquired directly from the friction and wear machine.

The wear rate W (mm^3/N·m) of the ceramic composite was calculated by the formula:

$$W = V/(L \cdot P) = m/(2\pi \cdot \mathrm{R} \cdot n \cdot t \cdot \rho \cdot P) \tag{8.6}$$

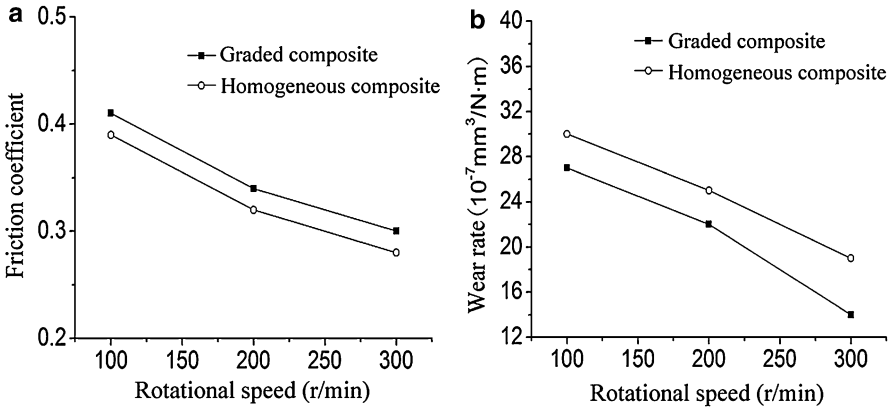

Fig. 8.8 Effect of rotational speed on (**a**) friction coefficient and (**b**) wear rate

where V is the volume loss (mm^3); L is the sliding distance (m); m is the mass loss (g); n is the rotational speed (r/min); t is the friction duration (min); ρ is the density (g/mm^3) and was measured by Archimedes method.

As shown in Fig. 8.8a, the friction coefficient of the two ceramic composites decreases with the increase of rotational speed from 100 r/min to 300 r/min. It is indicated that their antifriction property at relatively high speed is better than that at lower speed. It can also be seen that the fiction coefficient of Al_2O_3/(W,Ti)C/CaF_2 graded ceramic composite is slightly higher than that of the homogeneous one. The homogeneous ceramic composite and the surface layer of the graded ceramic composite were made from the same combined powders. They have the same CaF_2 content and other constituent content. Thus the antifriction property of Al_2O_3/(W,Ti)C/CaF_2 graded ceramic composite is comparable to that of the homogeneous one. As shown in Fig. 8.8b, the wear rate of the two ceramic composites decreases as the rotational speed increases from 100 r/min to 300 r/min. Besides, the wear rate of Al_2O_3/(W,Ti)C/CaF_2 graded ceramic composite is lower than that of Al_2O_3/(W,Ti)C/CaF_2 homogeneous composite. It means that the graded composite has better antiwear property than the homogeneous composite. According to the research of Evans et al. [5], the improvement in antiwear property should be attributed to the enhancement of mechanical properties of the graded ceramic composite, which was caused by the residual compressive stresses existing in the surface layer.

The pin specimen of the graded self-lubricating ceramic composite was clamped in the way shown as Fig. 8.7b. The cross section was used as the rubbing surface to make all layers sliding against the disk at the same time. The effect of CaF_2 content on the wear property of the ceramic composite was analyzed by observing the wear morphologies of graded layers with different composition. Figure 8.9 shows wear morphologies of graded layers with different composition under the normal load of 100 N and rotational speed of 200 r/min. It is shown that the worn surface of the fourth layer, where no CaF_2 was added, is rough and abounds with furrow-like

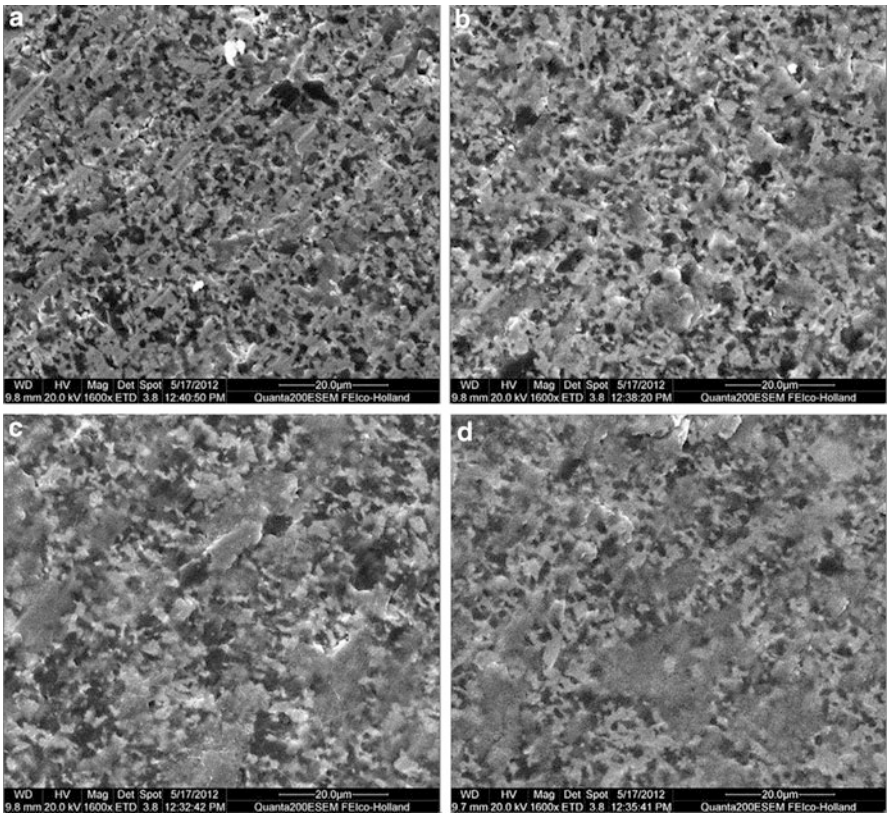

Fig. 8.9 SEM micrographs of wear morphologies of different layers: (**a**) 4th layer with 0 Vol.% CaF_2, (**b**) 3rd layer with 3.3 Vol.% CaF_2, (**c**) 2nd layer with 6.7 Vol.% CaF_2, (**d**) 1st layer with 10 Vol.% CaF_2

scratches, which is a typical sign of abrasive wear. With the increase of CaF_2 content, tribofilm with increasing coverage area was formed and abrasive wear was alleviated layer by layer. It indicates that the CaF_2 solid lubricant was released and smeared on the worn surfaces, because CaF_2 has planes of perfect crystal cleavage in its crystal structure suggesting low-shear strength [13]. Relatively complete tribofilm was formed on the wear surface of the surface layer containing 10Vol.% CaF_2. The tribofilm played a major role in antifriction and wear resistance.

8.3 Self-Lubricating Ceramic Composites with Metal Coated Solid Lubricants

Self-lubricating ceramic composites with the addition of metal coated solid lubricants were proposed in terms of microstructural modification to the traditional self-lubricating ceramic composites. Metal coated solid lubricants are composite

Table 8.4 Composition and parameters of the electroless nickel plating bath

Role in the bath	Chemical	Parameter
Main salt	Nickel sulfate ($NiSO_4 \cdot 6H_2O$)	25 g/L
Reducing agent	Sodium hypophosphite ($NaH_2PO_2 \cdot H_2O$)	25 g/L
Complexing agent	Tri-sodium citrate ($C_6H_5Na_3O_7 \cdot 2H_2O$)	50 g/L
Buffering agent	Ammonium chloride (NH_4Cl)	30 g/L
pH adjuster	Aqueous ammonia ($NH_3 \cdot H_2O$)	Proper amount
pH of solution		9.5–10.0
Plating temperature		45–50 °C
Loading ratio		2–10 g/L

powders with a solid lubricant core and metallic shell. There are many methods to synthesize core-shell composite powders with metallic shell, such as precipitation [14], chemical vapor deposition [15], electroplating [16], electroless plating [17], displacement plating [18], thermo-chemistry co-reduction [19], and gas suspension spray coating [20]. Among these methods, electroless plating has been recognized as one of the most convenient and effective techniques [21]. It is an autocatalytic chemical reduction process in which the reducing agent is oxidized and metallic ions are reduced and then deposited on the substrate surface.

In the study, metal coated solid lubricant powders were firstly prepared by ultrasonic assisted electroless plating process, and then the as-prepared coated powders were mixed with ceramic matrix powders to prepare self-lubricating ceramic composites by hot pressing.

Al_2O_3/(W,Ti)C, CaF_2, and Ni were chosen to be the matrix material, solid lubricant, and metal for coating, respectively. The starting powders were commercially available α-Al_2O_3, (W,Ti)C, and CaF_2 with average particle size of 0.5 μm, 2.5 μm, and 5 μm, respectively. Before electroless nickel plating process, the raw CaF_2 powders were cleaned, coarsened, sensitized, and activated [9]. After that, the CaF_2 powders were dispersed in distilled water and then poured into an electroless nickel plating bath with ultrasonic agitation. The composition and parameters of the plating bath are listed in Table 8.4 [9]. The overall reaction in the electroless plating can be expressed as follows [22]:

$$2Ni^{2+} + 8H_2PO_2^- + 2H_2O \rightarrow 6H_2PO_3^- + 2H^+ + 3H_2 \uparrow + 2P + 2Ni \qquad (8.7)$$

Because $NaH_2PO_2 \cdot H_2O$ was used as reductant in the plating bath, phosphorus element was electroless co-deposited with nickel atoms on CaF_2 powders to form core-shell structure. After electroless plating, the nickel coated CaF_2 powders (CaF_2@Ni) were rinsed with distilled water for several times and then dried in a vacuum oven at 100–110 °C for 8–10 h.

Figure 8.10 shows SEM micrographs of pristine CaF_2 powders and CaF_2@Ni powders with different CaF_2 loading ratios. It can be seen from Fig. 8.10a that the pristine CaF_2 powders have irregular and polyhedral shape with clean and smooth

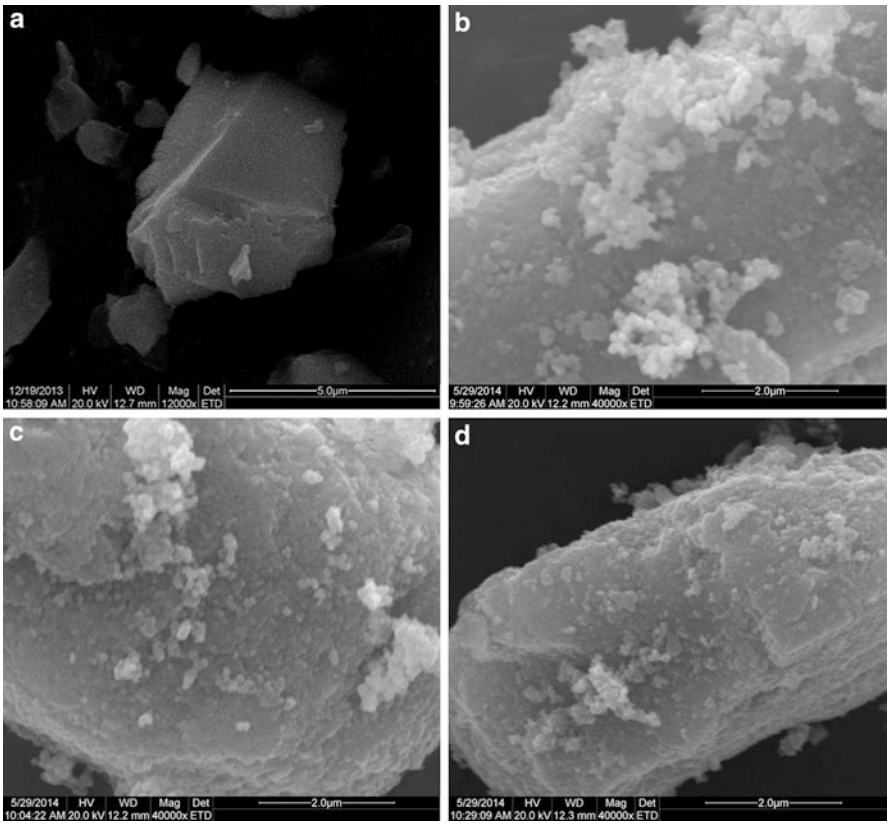

Fig. 8.10 SEM micrographs of (**a**) pristine CaF_2 powders and CaF_2@Ni powders with different CaF_2 loading ratios: (**b**) 2 g/L, (**c**) 5 g/L, (**d**) 10 g/L

surfaces. By contrast, the CaF_2@Ni powders exhibit coarse surfaces with regular nanometric spheres, as shown in Fig. 8.10b–d. When CaF_2 loading ratio is 2 g/L, the nickel coating is complete but has a lot of free Ni aggregates. When CaF_2 loading ratio is 10 g/L, the nickel coating is incompact and incomplete. The nickel coating with CaF_2 loading ratio of 5 g/L is uniform, compact, and complete. Therefore, CaF_2@Ni powders prepared when CaF_2 loading ratio was 5 g/L were used to prepare Al_2O_3/(W,Ti)C/CaF_2@Ni ceramic composite.

Figure 8.11 shows XRD pattern of CaF_2@Ni composite powders when CaF_2 loading ratio of electroless plating was 5 g/L. Besides sharp diffraction peaks belonging to CaF_2, noncrystalline background appears and there is a hillock-like peak (shown in dashed frame) near $2\theta = 45°$. EDS was used to further confirm the coating composition, as shown in Fig. 8.12. It is obviously seen that Ni and P peaks appear at the EDS spectrum besides Ca and F peaks. The XRD and EDS analysis evidently confirm that CaF_2 powders were covered by amorphous Ni-P alloy.

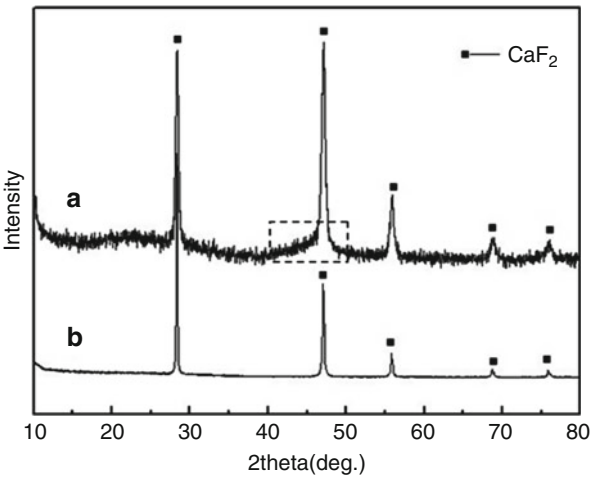

Fig. 8.11 XRD patterns of (**a**) CaF_2@Ni composite powders and (**b**) pristine CaF_2 powders

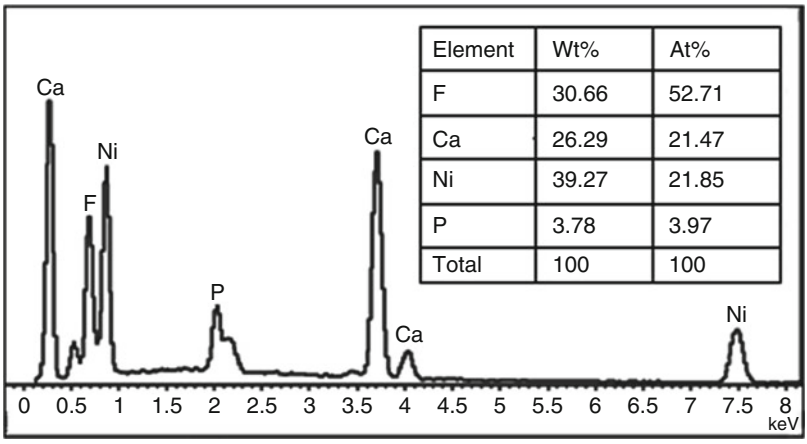

Element	Wt%	At%
F	30.66	52.71
Ca	26.29	21.47
Ni	39.27	21.85
P	3.78	3.97
Total	100	100

Fig. 8.12 EDS spectrum of CaF_2@Ni composite powders

The as-prepared CaF_2@Ni powders were mixed with the raw α-Al_2O_3 and (W,Ti)C powders (α-Al_2O_3:(W,Ti)C = 55:45, v/v) and hot pressed to produce Al_2O_3/(W,Ti)C/CaF_2@Ni ceramic composite containing 10 vol.% CaF_2@Ni powders. The detailed preparation process and measurement method of mechanical properties were described in [9]. An Al_2O_3/(W,Ti)C/CaF_2 ceramic composite with 10 vol.% uncoated CaF_2 was also prepared by using the same technical process.

Figure 8.13 shows SEM micrographs of the polished surfaces of the two ceramic composites. The light gray phase is identified by EDS to be (W,Ti)C and CaF_2, and the deep gray phase is Al_2O_3. It can be seen that the (W,Ti)C phase of Al_2O_3/(W,Ti)C/CaF_2@Ni composite is uniformly distributed in the Al_2O_3 matrix and has smoother grains than Al_2O_3/(W,Ti)C/CaF_2 composite. It is deduced that the

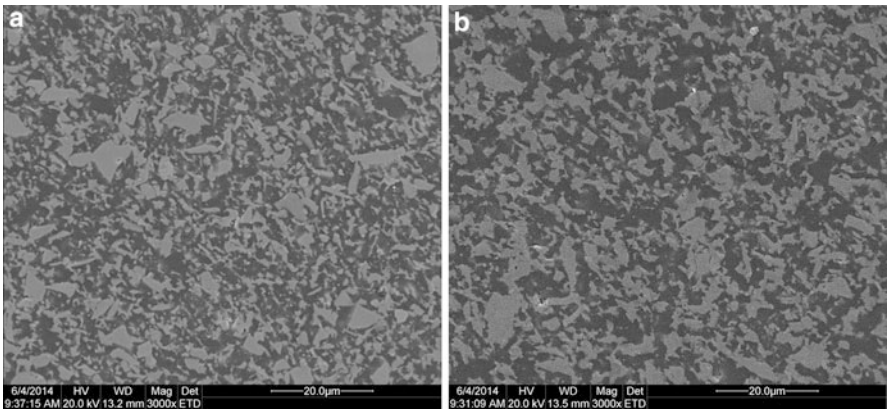

Fig. 8.13 SEM micrographs of polished surfaces: (**a**) Al_2O_3/(W,Ti)C/CaF_2 and (**b**) Al_2O_3/(W,Ti)C/CaF@Ni.

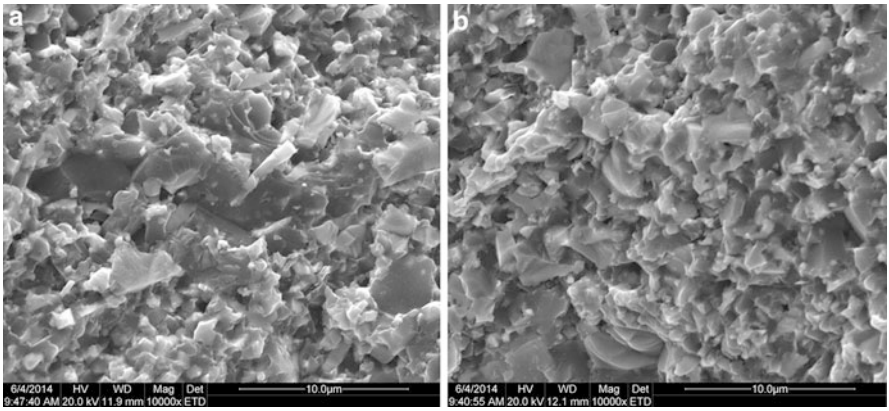

Fig. 8.14 SEM micrographs of fracture surfaces: (**a**) Al_2O_3/(W,Ti)C/CaF_2 and (**b**) Al_2O_3/(W,Ti)C/CaF_2@Ni

pointedness of (W,Ti)C in Al_2O_3/(W,Ti)C/CaF_2@Ni composite fused during the sintering process due to the addition of CaF_2@Ni powders.

Figure 8.14 presents SEM micrographs of the fracture surface of the two ceramic composites. The microstructure of Al_2O_3/(W,Ti)C/CaF_2 composite is not so homogeneous and some grains with abnormal growth can be seen. By contrast, the microstructure of Al_2O_3/(W,Ti)C/CaF_2@Ni composite is compact and the grain size of each phase is uniform. The addition of CaF_2@Ni powders leads to the improvement in microstructure. For one thing, adding the coated powders enhanced dispersity of the solid lubricants in the ceramic composite. For another, the nickel was in fluid phase at the sintering temperature and played a role in promoting densification and preventing grains from abnormally growing. Furthermore, fracture modes of the both ceramic composites are mixed transgranular fracture and intergranular fracture.

The measured flexural strength of the Al_2O_3/(W,Ti)C/CaF_2@Ni composite was 582 ± 27 MPa, which is 15% higher than that of the Al_2O_3/(W,Ti)C/CaF_2 composite (506 ± 21 MPa). The Vickers hardness of the Al_2O_3/(W,Ti)C/CaF_2@Ni composite was 14.1 ± 0.4 GPa, which was increased by 5% compared to that of the Al_2O_3/(W,Ti)C/CaF_2 composite (13.4 ± 0.3 GPa). The fracture toughness measured on the surface layers of the Al_2O_3/(W,Ti)C/CaF_2@Ni composite was 4.3 ± 0.3 MPa·$m^{1/2}$, which is 19% higher than that of the Al_2O_3/(W,Ti)C/CaF_2 composite (3.6 ± 0.2 MPa·$m^{1/2}$). The enhancement of the mechanical properties can be attributed to two reasons: firstly, the inhomogeneous distribution of a second phase and abnormally grown grains can act as the fracture origin and then do harm to mechanical properties [23], so the enhanced flexural strength and hardness of Al_2O_3/(W,Ti)C/CaF_2@Ni composite may be caused by its more homogeneous microstructure refined by adding CaF_2@Ni powders. Secondly, ceramic materials can be toughened by incorporating ductile metal particles in terms of sintering metal coated ceramic powders [24, 25]. The main toughening mechanisms are the bridging effect and the deflection of cracks by the metal particles. So the addition of CaF_2@Ni powders should account for the notable fracture toughness improvement of Al_2O_3/(W,Ti)C/CaF_2@Ni composite.

The dry friction and wear test took pin-on-disk type and was carried out on the MMW-1A multipurpose friction and wear testing machine. The pin specimen (10 mm × 10 mm × 5 mm, Ra 0.1 μm) was made of the self-lubricating ceramic composites by cutting, grinding, and polishing. The disk was a hardened 45# carbon steel ring (Φ54mm × Φ38mm × 10 mm, HRC 45, Ra 0.08 μm). The pin and disk were ultrasonically cleaned for 10 min in acetone and then completely dried in a vacuum drying oven. During the dry friction and wear test, the pin specimen was sliding on the disk with a rotational speed of 100–400 r/min under a normal load of 20 N.

The effect of the rotational speed on the friction coefficient is illustrated in Fig. 8.15a. It can be seen that with the increase of rotational speed from 100 r/min to 400 r/min, the friction coefficient of the two composites shows a downward trend. In addition, the friction coefficient of Al_2O_3/(W,Ti)C/CaF_2@Ni composite is smaller than that of Al_2O_3/(W,Ti)C/CaF_2 composite at each rotational speed. This phenomenon can be attributed to the different addition methods of CaF_2. For Al_2O_3/(W,Ti)C/CaF_2 composite, a chemical reaction between CaF_2 and Al_2O_3 may occur during the sintering process [26]:

$$3CaF_2(s) + Al_2O_3(s) \rightarrow 3CaO(s) + 2AlF_3(g) \tag{8.8}$$

The reaction results in loss of some CaF_2 and weakens the self-lubricating property of the ceramic composite. For Al_2O_3/(W,Ti)C/CaF_2@Ni composite, the metal shell of the CaF_2@Ni powders can prevent or reduce the reaction between CaF_2 and Al_2O_3. Thus Al_2O_3/(W,Ti)C/CaF_2@Ni composite exhibits better anti-friction property than Al_2O_3/(W,Ti)C/CaF_2 composite.

Figure 8.15b illustrates the effect of the rotational speed on the wear rate of the two composites. Firstly, the wear rate of the two composites decreases as the rotational speed increases from 100 r/min to 400 r/min. Secondly, the wear rate of Al_2O_3/(W,Ti)C/CaF_2@Ni composite is lower than that of Al_2O_3/(W,Ti)C/CaF_2 composite. It

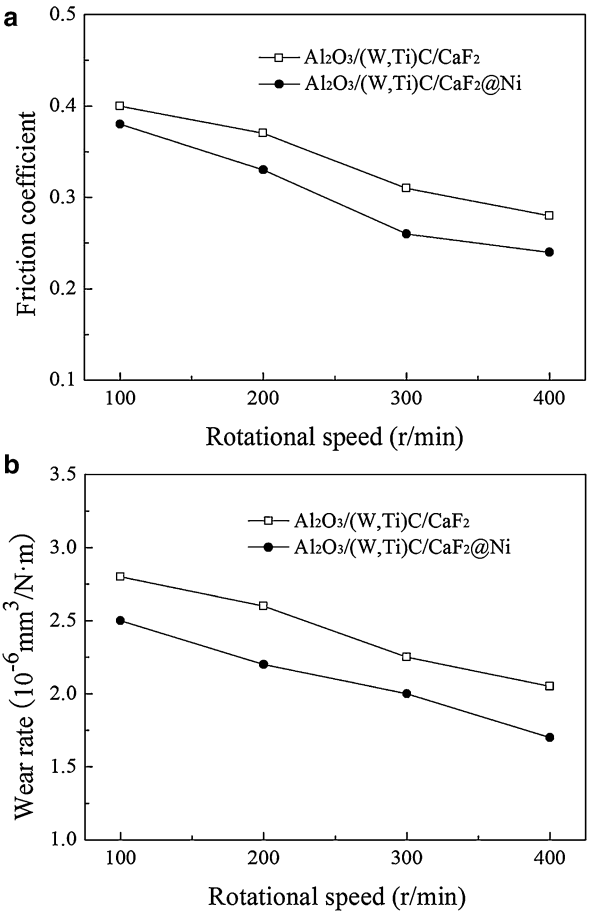

Fig. 8.15 Effect of rotational speed on (**a**) friction coefficient and (**b**) wear rate

indicates that the antiwear property of the composite with the addition of CaF_2@Ni powders is superior to that of the composite with the addition of pristine CaF_2 powders. Evans et al. reported that the wear rate of ceramic material is inversely proportional to the product of its fracture toughness and hardness, i.e., $K_{IC}^{3/4}H^{1/2}$ [5]. Therefore, the better antiwear property of Al_2O_3/(W,Ti)C/CaF_2@Ni composite can be ascribed to the higher mechanical properties especially the hardness and fracture toughness.

The worn surfaces of the two composites under the rotational speed of 200 r/min are presented in Fig. 8.16a and c, respectively. It can be seen that the worn surface of Al_2O_3/(W,Ti)C/CaF_2 composite is rougher than that of Al_2O_3/(W,Ti)C/CaF_2@Ni composite, which verifies the wear resistance of the latter is higher than the former. In addition, EDS analysis reveals that more Ca and less Fe exist on the worn surface of Al_2O_3/(W,Ti)C/CaF_2@Ni composite in comparison to Al_2O_3/(W,Ti)C/CaF_2 composite, as shown in Fig. 8.16b and d. It is indicated that the ceramic composite with

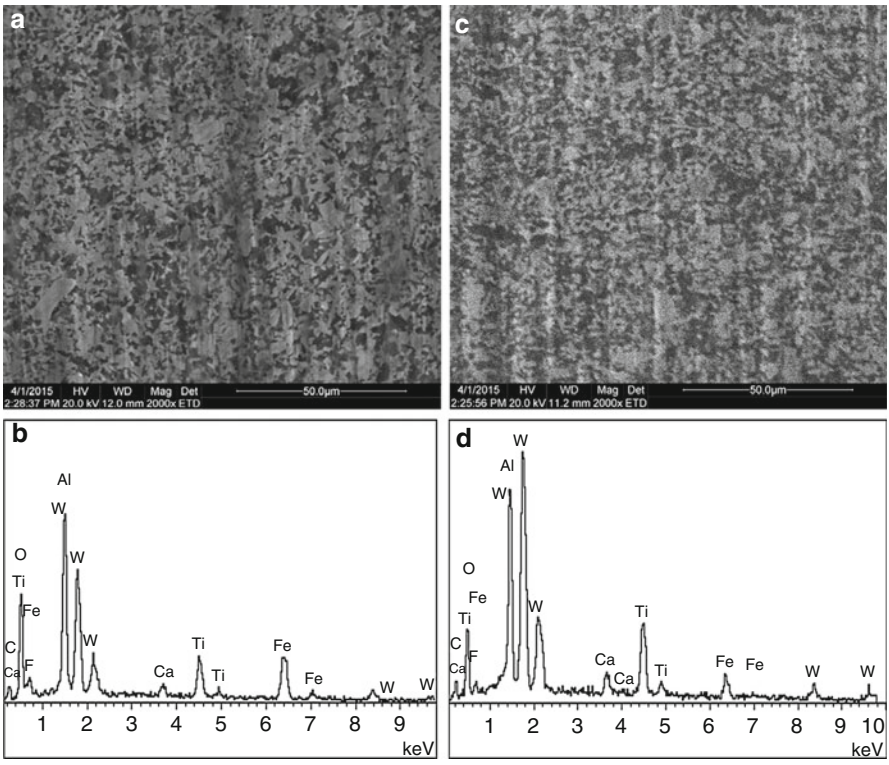

Fig. 8.16 (**a**) SEM micrograph and (**b**) EDS analysis of worn surface of Al_2O_3/(W,Ti)C/CaF_2; (**c**) SEM micrograph and (**d**) EDS analysis on worn surface of Al_2O_3/(W,Ti)C/CaF_2@Ni.

the addition of CaF_2@Ni powders has better antiadhesive property than the ceramic composite with the addition of pristine CaF_2 powders.

8.4 Summary

Aiming at the difficult problem that the traditional self-lubricating ceramic composites are not available to possess rational combination of antifriction and antiwear properties, two new types of self-lubricating ceramic composites were developed in recent years. They modified the traditional self-lubricating ceramic composites at macroscopic and microscopic levels, respectively.

Al_2O_3/(W,Ti)C/CaF_2 graded self-lubricating ceramic composite was developed in terms of macrostructural modification. The microstructures changed layer by layer, which agreed with the gradient variation of the components. The exterior layers were subjected to compressive stresses and the interior layers were subjected to tensile stresses. The flexural strength, Vickers hardness, and fracture toughness of the Al_2O_3/(W,Ti)C/CaF_2 graded composite were respectively 25%, 19% and 6% higher than those of the homogeneous Al_2O_3/(W,Ti)C/CaF_2 composite. The dry friction and

wear test showed that the graded self-lubricating ceramic composite had comparable antifriction properties and superior antiwear properties to the homogeneous composite. The evident improvement in the mechanical and tribological properties can be attributed to the fulfillment of the two design criteria. For one thing, the gradually decreasing distribution of CaF_2 from the composite's surface layers to middle layer ensured good self-lubricating property of the surface layers and enhanced the flexural strength of the graded composite. For another, the existing residual compressive stresses increased hardness, fracture toughness, and antiwear properties of the surface layers of the graded composite.

Al_2O_3/(W,Ti)C/CaF_2@Ni self-lubricating ceramic composite with the addition of metal coated solid lubricants was developed in terms of microstructural modification. As compared with the Al_2O_3/(W,Ti)C/CaF_2 composite, the microstructure of Al_2O_3/(W,Ti)C/CaF_2@Ni composite was more uniform. The flexural strength, Vickers hardness, and fracture toughness were increased by about 15%, 5%, and 19%, respectively. The dry friction and wear test showed that Al_2O_3/(W,Ti)C/CaF_2@Ni composite had obviously better antifriction and antiwear properties than Al_2O_3/(W,Ti)C/CaF_2 composite. The addition of CaF_2@Ni powders led to the improvement in the microstructure, mechanical properties, and tribological behaviors. Firstly, the nickel shell of CaF_2@Ni powders promoted dispersity of CaF_2 in the ceramic composite and protected CaF_2 from reacting with the Al_2O_3 matrix, which enhanced antifriction property. Secondly, the nickel shell promoted the ceramic composite's densification, prevented grains from abnormally growing, and toughened the ceramic composite, which improved the microstructure, mechanical properties, and antiwear property.

Acknowledgments This research work was supported by the National Natural Science Foundation of China, Grant No. 51075248 and Grant No. 51575285.

References

1. Reis, P., Filho, V., Davim, J.P., Xu, X., Ferreira, J.M.F.: Wear behavior on advanced structural ceramics: α-sialon matrix reinforced with b-sialon fibers. Mater. Design. **26**, 417–423 (2005)
2. Deng, J., Cao, T.: Self-lubricating mechanisms via the in situ formed tribofilm of sintered ceramics with CaF_2 additions when sliding against hardened steel. Int. J. Refract. Met. Hard Mater. **25**, 189–197 (2007)
3. Carrapichano, J.M., Gomes, J.R., Silva, R.F.: Tribological behaviour of Si_3N_4-BN ceramic materials for dry sliding applications. Wear. **253**, 1070–1076 (2002)
4. Deng, J., Cao, T., Ding, Z., Liu, J., Sun, J., Zhao, J.: Tribological behaviors of hot-pressed Al_2O_3/TiC ceramic composites with the additions of CaF_2 solid lubricants. J. Eur. Ceram. Soc. **26**, 1317–1323 (2006)
5. Evans, A.G., Wilshaw, T.R.: Quasi-static solid particle damage in brittle solids – I. Observations analysis and implications. Acta Metall. **24**, 939–956 (1976)
6. Wu, G., Xu, C., Zhang, Y., Yi, M.: State of the art of graded self-lubricating ceramic cutting tool materials. Appl. Mech. Mater. **66–68**, 1598–1604 (2011)
7. Xu, C.H., Wu, G.Y., Xiao, G.C., Fang, B.: Al_2O_3/(W,Ti)C/CaF_2 multi-component graded self-lubricating ceramic cutting tool material. Int. J. Refract. Met. Hard Mater. **45**, 125–129 (2014)
8. Xu, C., Wu, G., Zhang, Y., Yi, M., Xiao, G., Fang, B.: Development of multicomponent graded self-lubricating ceramic cutting tool materials. J. Mech. Eng. **50**(7), 94–101 (2014)

9. Wu, G., Xu, C., Xiao, G., Yi, M., Chen, Z., Xu, L.: Self-lubricating ceramic cutting tool material with the addition of nickel coated CaF_2 solid lubricant powders. Int. J. Refract. Met. Hard Mater. **56**, 51–58 (2016)
10. Ai, X., Zhao, J., Huang, C., Zhang, J.: Development of an advanced ceramic tool material – functionally gradient cutting ceramics. Mater. Sci. Eng. A. **248**(1–2), 125–131 (1998)
11. Mehrali, M., Wakily, H., Metselaar, I.H.S.C.: Residual stress and mechanical properties of Al_2O_3/ZrO_2 functionally graded material prepared by EPD from 2-butanone based suspension. Adv. Appl. Ceram. **110**, 35–40 (2011)
12. Hvizdoš, P., Jonsson, D., Anglada, M., Anné, G., Biest, O.V.D.: Mechanical properties and thermal shock behaviour of an alumina/zirconia functionally graded material prepared by electrophoretic deposition. J. Eur. Ceram. Soc. **27**, 1365–1371 (2007)
13. Shuaib, M., Davies, T.J.: Wear behaviour of a REFEL SiC containing fluorides up to 900 °C. Wear. **249**, 20–30 (2001)
14. Li, G., Huang, X., Guo, J.: Fabrication of Ni-coated Al_2O_3 powders by the heterogeneous precipitation method. Mater. Res. Bull. **36**, 1307–1315 (2001)
15. Chen, C.-C., Chen, S.-W.: Nickel and copper deposition on Al_2O_3 and SiC particulates by using the chemical vapour deposition-fluidized bed reactor technique. J. Mater. Sci. **32**, 4429–4435 (1997)
16. Chen, L., Yu, G., Chu, Y., Zhang, J., Hu, B., Zhang, X.: Effect of three types of surfactants on fabrication of Cu-coated graphite powders. Adv. Powder Technol. **24**, 281–287 (2013)
17. Amirjan, M., Zangeneh Madar, K., Parvin, N.: Evaluation of microstructure and contiguity of W/Cu composites prepared by coated tungsten powders. Int. J. Refract. Met. Hard Mater. **27**, 729–733 (2009)
18. Zhang, R., Gao, L., Guo, J.: Preparation and characterization of coated nanoscale Cu/SiCp composite particles. Ceram. Int. **30**, 401–404 (2004)
19. Li, J., Chen, W., Tao, W., Shao, F., Ding, B.: Nano-composite powder of tungsten coated copper produced by thermo-chemistry co-reduction. Rare Met. Mater. Eng. **41**, 2091–2094 (2012)
20. Choi, W.C., Byun, D., Lee, J.K., Cho, B.W.: Electrochemical characteristics of silver- and nickel-coated synthetic graphite prepared by a gas suspension spray coating method for the anode of lithium secondary batteries. Electrochim. Acta. **50**, 523–529 (2004)
21. Xu, X., Cui, Z.D., Zhu, S.L., Liang, Y.Q., Yang, X.J.: Preparation of nickel-coated graphite by electroless plating under mechanical or ultrasonic agitation. Surf. Coating Technol. **240**, 425–431 (2014)
22. Hu, B., Sun, R., Yu, G., Liu, L., Xie, Z., He, X., et al.: Effect of bath pH and stabilizer on electroless nickel plating of magnesium alloys. Surf. Coating Technol. **228**, 84–91 (2013)
23. Oh, S.-T., Sando, M., Niihara, K.: Mechanical and magnetic properties of Ni-Co dispersed Al_2O_3 nanocomposites. J. Mater. Sci. **36**, 1817–1821 (2001)
24. Mao, D.S., Liu, X.H., Li, J., Guo, S.Y., Zhang, X.B., Mao, Z.Y.: A fine cobalt-toughened Al_2O_3-TiC ceramic and its wear resistance. J. Mater. Sci. **33**, 5677–5682 (1998)
25. Zhu, L., Luo, L., Li, J., Wu, Y.: The influence of powder characteristics on mechanical properties of Al_2O_3-TiC-Co ceramic materials prepared by Co-coated Al_2O_3/TiC powders. Int. J. Refract. Met. Hard Mater. **34**, 61–65 (2012)
26. Wang, Q., Ge, Y., Cui, W., Chen, K., Ferreira, J.M.F., Xie, Z.: Carbothermal synthesis of micro-scale spherical AlN granules with CaF_2 additive. J. Alloy Compd. **663**, 823–828 (2016)

Surface Engineering Design of Alumina-Matrix Composites

9

Yongsheng Zhang, Hengzhong Fan, Litian Hu, Yuan Fang, and Junjie Song

Contents

Abstract

The three-dimensional lubricating layer on a ceramic surface realizes the integration of the structure and lubricating function in ceramic materials, which can achieve outstanding lubricating properties and maintain the excellent mechanical properties of ceramics, solving the special lubrication and wear failure in mechanical systems under extreme conditions (e.g., corrosive environment and wide-temperature range condition). In this chapter, two kinds of surface-lubricating structural-laminated ceramics with high reliability were designed and prepared based on experiment research and theoretical simulation. These ceramics can achieve stable and effective lubrication in a water environment and wide-temperature range condition. These materials are Al_2O_3/Ni- and

Y. Zhang (✉) · L. Hu · Y. Fang
State Key Laboratory of Solid Lubrication, Lanzhou Institute of Chemical Physics, Chinese Academy of Sciences, Lanzhou, China

H. Fan · J. Song
State Key Laboratory of Solid Lubrication, Lanzhou Institute of Chemical Physics, Chinese Academy of Sciences, Lanzhou, China

University of Chinese Academy of Sciences, Beijing, China

P. L. Menezes et al. (eds.), *Self-Lubricating Composites*,
https://doi.org/10.1007/978-3-662-64243-6_9

Al_2O_3/Mo-laminated composites suitable for use in a water environment and in wide-temperature range conditions, respectively. The relation between the surface microstructure of the prepared materials and their properties (mechanical and tribological) was investigated. Results indicated that the integration of the structure and lubricating function of the ceramic composites is realized through the bionic, surface microstructure, and three-dimensional self-lubricating design of the materials, further improving their lubricating and practical properties. Factors that can influence the tribological behavior and wear failure of the above materials were proposed through the systematic study of the tribological behavior under different environments and test conditions, as well as the relation among the structure, composition, and properties of these two kinds of materials. In addition, theoretical models of the relation between the structural parameters and performance of the materials were built. These methods provided theories and technologies for the preparation and application of high performance lubricating materials that can be used in corrosive and wide-temperature range environments.

9.1 Introduction

Lubrication in extreme environment is a key factor that affects the security, high efficiency, and stable operation of a mechanical system. This factor also restricts the development of high-end equipment. During the past decades, various self-lubricating materials have been developed for different machineries. These developments were geared toward improving the properties of materials, allowing them to surmount severe challenges under extreme conditions. The lubricating materials for different fields must be capable of working in corrosive environments or other extreme conditions (e.g., wide-temperature range condition requires continuous and complex multienvironment lubrications) for a long time. In the current science and technology development context, high-performance ceramic lubricating materials are the most promising candidates for the harsh environment application of wear-resistant components because of their excellent mechanical properties, such as high strength, resistance to corrosion, and oxidation stability under extreme conditions, and insensitivity to defects. Moreover, ceramic lubricating composites are the only material that can work above 1000 °C and in complex harsh environments [1–6]. Nevertheless, the high friction coefficient of this kind of material under dry sliding, boundary lubrication conditions, and brittleness of the ceramic matrix itself limit their practical application in tribological and high-end equipment areas. Therefore, the design and fabrication of high-performance lubricating materials must be geared toward improving both the mechanical and lubricating properties. This can also solve the limited application of ceramic lubricating materials.

Laminating composites is one of the new strategies. The method integrates strong or weak interfaces with ceramics inspired by bionic multilayer structures, such as shells, lignum, and teeth. It has attracted significant research attention because of the excellent mechanical properties of structured ceramics. These materials possess

noncatastrophic fracture behavior and damage tolerance that exhibit much higher fracture toughness and work of fracture than monolithic ceramics [7–9]. The pioneering work of Clegg et al. successfully fabricated SiC/graphite-laminated composites using SiC as the strong layers and graphite as the weak interface. These materials exhibited great mechanical properties with a fracture toughness and work of fracture of 15 MPa · $m^{1/2}$ and 4625 J · m^{-2}, respectively. Moreover, the laminated composites also showed excellent lubricating property and wear resistance because of their special weak interfacial graphite layer [10]. According to previous studies, Al_2O_3/Ni and Al_2O_3/Mo are typical laminated composites. Al_2O_3/Ni and Al_2O_3/Mo are promising candidates in corrosive environment and high temperature condition applications, respectively. The two typical laminated composites exhibit excellent mechanical properties that can achieve security, high efficiency, and stable operation for mechanical systems as structural materials [11, 12]. Nevertheless, the friction coefficient and wear rate of Al_2O_3/Ni-laminated composites are high and unstable under boundary lubricating conditions. The room and medium-temperature friction coefficients of Al_2O_3/Mo-laminated composites are high under dry sliding conditions. Thus, these factors limit the application of these two laminated composites in lubricating areas.

Laser surface texturing (LST), which forms regular micro-patterns on the sliding surface, is generally recognized as an effective means to improve the tribological property of moving part surfaces. Previous studies showed that the introduction of specific texturing on sliding surfaces can effectively alleviate the friction and wear of materials, increase the lifetime of the sliding contacts by trapping wear debris, or promote the retention of a lubricant film between mating surfaces [13–18]. This method combined with laser surface texture and solid lubricant films can significantly improve the tribological performance of materials. The mechanism of such composition-lubrication structure involves the use of textured microdimples on the material surface to store lubricants. Lubricants are squeezed on the friction surface to form a lubricating film during friction. This method improves the contact states between the friction pair. This process leads to reduced frictional wear and increased service life of materials. The method of forming a composite lubricating layer on a textured surface mainly includes burnishing, sputtering, and hot press sintering. Lubricants stored in textured micropatterns can supply the friction surface continuously, prolonging the service life of materials [19–24]. Therefore, the integration of LST and lubricants on the surface of materials is an effective means to achieve outstanding lubricating properties for the materials. However, few in-depth and systematic studies are available on the combination of laser surface texturing and bionic-laminated ceramics. These studies are necessary to investigate and improve the application limits of these laminated ceramic composites systematically.

On the basis of this background, two kinds of surface-lubricating structural-laminated ceramics with high reliability were designed and prepared. The three-dimensional lubricating layer fabricated on the ceramic surface realizes the integration of structure and lubricating function in laminated ceramic materials. This method can achieve outstanding lubricating properties and maintain the excellent mechanical properties of the ceramic. This process can also address the special

lubrication and wear failure in mechanical system under corrosive environment and wide-temperature range conditions, respectively. These materials are surface textured integrated with diamond-like carbon (DLC) film, LaF_3-doped MoS_2 composite coating of alumina/nickel-laminated composites, and surface textured integrated with solid lubricants of alumina/molybdenum-laminated composites. These are suitable for use in a water environment and wide-temperature range conditions, respectively. The relation between the surface microstructure of the prepared materials and their properties (mechanical and tribological) was investigated.

9.2 Laser Surface Texturing and Tribological Properties of Ceramic Composites

Zirconia toughened alumina (ZTA) ceramic nanocomposites are potential candidates for the application of wear-resistant components because of their excellent properties, such as superior strength and fracture toughness, high wearability and hardness, low specific density, and antioxidation effect. Nevertheless, the friction coefficient and wear rate of ZTA nanocomposites are high under dry sliding conditions, which limit the application of these nanocomposites in tribological areas. LST is the basis for the integration of structured and lubricating functions in ceramics. The friction reduction mechanisms of surface texturing with different shapes and dimensions were investigated in several research works. The mechanisms mainly contain preventing stiction during start-up in magnetic storage industry, trapping wear debris in the texture micropatterns to reduce friction and wear, improving load capacity by enhancing hydrodynamic and hydrostatic lubrications, and acting as reservoirs to enhance lubricant retention and provide continuous lubrication to sliding surfaces [15, 25, 26]. The method is simple and effective in achieving antifriction and reduces the coefficient friction on the surface of ceramics by laser surface texturing. This part aims to reveal the microtexture mechanism that affects the tribological properties of ZTA nanocomposites and provide guidance for the optimum design of a composition-lubrication structure on the surface of laminated ceramic materials.

By controlling the sintering temperature properly, ZTA nanocomposites with excellent mechanical properties were prepared by hot pressing. The microhardness and bending strength of the sintered nanocomposites were approximately 17.01 GPa and 470 MPa, respectively. A commercial pulsed Nd:YAG laser was employed to produce the texture on the surface of the ZTA nanocomposites [27].

The scanning electron microscopy (SEM) photographs of the surface morphology of the ZTA nanocomposites with laser textures are presented in Fig. 9.1a. The 3D characteristic profiles of the textured surface for the nanocomposites are exhibited in Fig. 9.1b. A size-controlled microdimpled texture with a regular pattern was successfully fabricated on the surface of the ZTA nanocomposites by a pulsed Q-switch Nd:YAG solid-state laser. Through the optimized design of the laser texturing parameters, the tribological performance of the ZTA nanocomposites was significantly improved [27]. Figure 9.2 shows the curves of the friction coefficients of the

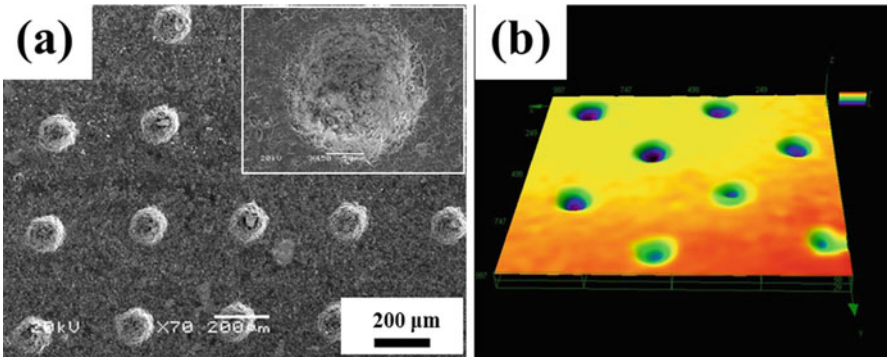

Fig. 9.1 SEM photographs (**a**) and 3D characteristic profiles (**b**) of the textured surface for the nanocomposites

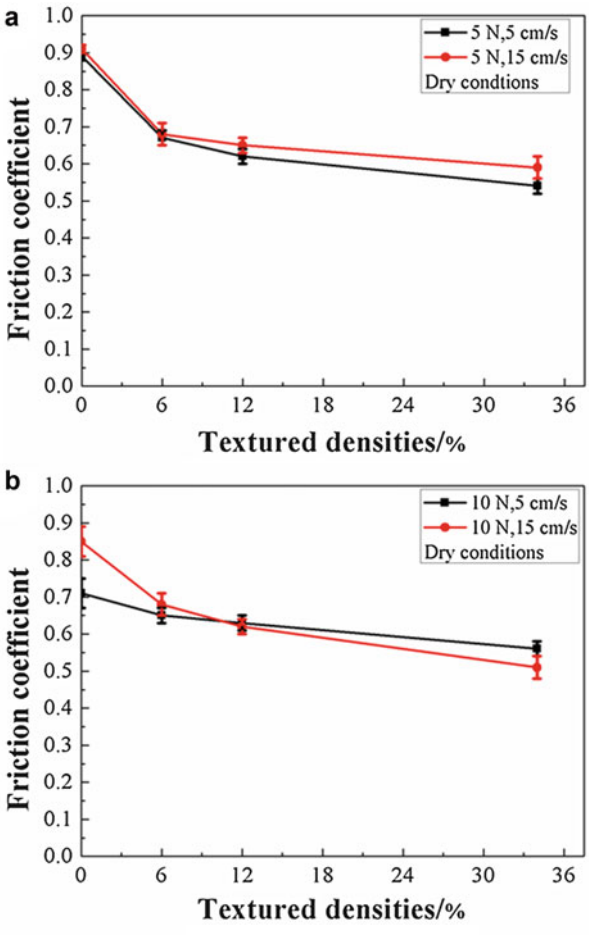

Fig. 9.2 Friction coefficient under dry contact for untextured and textured surfaces with different densities [27]

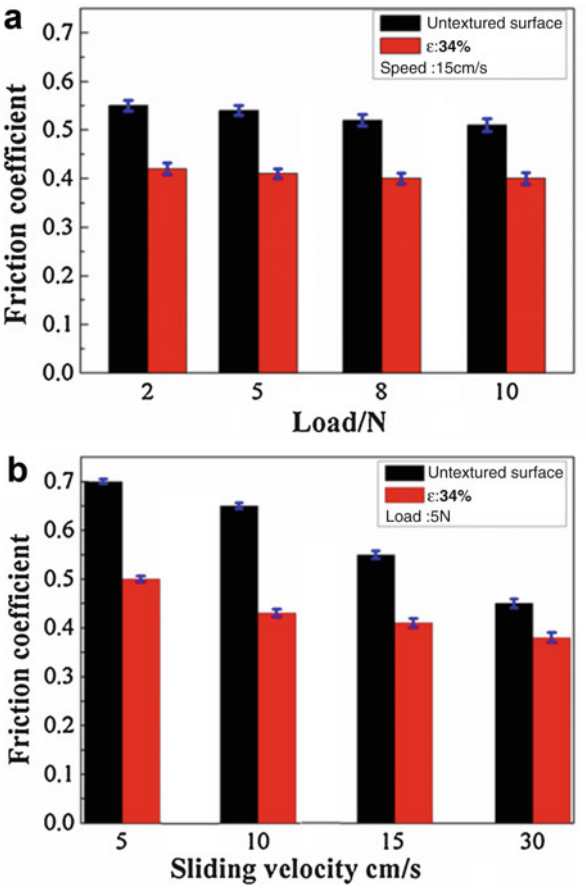

Fig. 9.3 Average values of friction coefficient for the untextured and textured surfaces under different loads (**a**) and sliding velocities (**b**) under water lubrication [27]

untextured and textured surfaces of the ZTA nanocomposites under dry contact. The results indicated that the textured ZTA nanocomposite surface exhibited a low coefficient under dry friction conditions, especially under a relatively high load and sliding speed. Moreover, the texture density has an important effect on the property of the materials. The dense micro-dimples were advantageous in improving the tribological properties of the material. When the texture density is 34%, the friction coefficient of the textured ZTA nanocomposites can be reduced to 0.5. This value was approximately 44% lower than that of the untextured ZTA nanocomposite surface.

Figure 9.3 shows the average values of the friction coefficients of the untextured and textured ZTA nanocomposite surfaces at different loads and sliding speeds in a water environment. The increase in texture density resulted in an increase in water storage capacity. Thus, the reduction of the friction coefficient was primarily

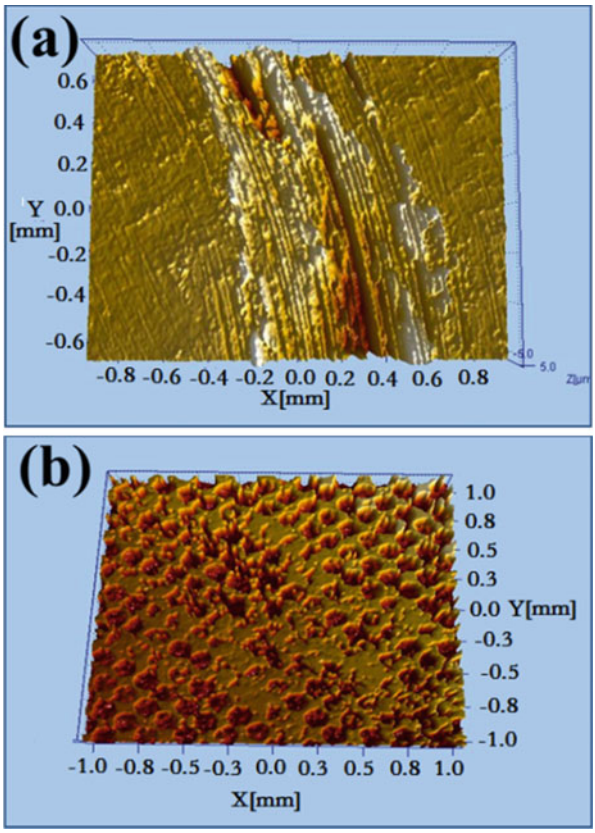

Fig. 9.4 3D topographical of the wear scars of the untextured (**a**) and textured $\varepsilon = 34\%$ (**b**) surfaces

attributed to the secondary lubricating effect produced by the lubricant (water) stored in the microdimples of the ZTA nanocomposite surfaces.

Figure 9.4 shows the typical 3D topographical structure of the worn surfaces of the untextured (Fig. 9.4a) and textured (Fig. 9.4b) samples. As shown in Fig. 9.4a, the untextured surfaces exhibited serious plough and adhesion wear under dry condition. By contrast, the textured surfaces exhibited excellent antiwear ability. The wear debris was effectively trapped and stored by the produced microdimples. This phenomenon can prevent abrasive wear and reduce plowing of the friction surfaces.

The understanding of such mechanisms provides guidance for the optimized design of a composition-lubrication structure on the ceramic surface. The process also provides theoretical guidance and technology support for the application of new ceramic materials in the high-technology fields. Therefore, the following laser surface texturing technology is used to design the surface composition-lubrication structure of alumina-matrix-laminated composites.

9.3 Surface Lubricating Design, Fabrication, and Tribological Properties in a Water Environment of Al_2O_3/Ni-Laminated Composites

The chemical resistance of lubricating ceramics is the ability of a material to resist the destructive effect of an aggressive environment. In addition to the properties of the corrosive medium, this ability depends also on the microstructure of the lubricating ceramic material and conditions of the corrosion process, especially in medium-material contact [28–30]. High-performance alumina-matrix lubricating ceramics are potential candidates for the application of wear-resistant components because of their high wearability and hardness, low specific density, and anti-oxidation effect. However, the ability to resist the corrosive environment, such as liquids (solution of acid, alkaline, salts, molten salts, glasses, slags and metals, water, and so on), is one of the most limited properties of materials in many industrial applications. Therefore, designing and fabricating alumina-matrix-laminated composites with excellent mechanical and tribological properties that are adapted to the corrosive environment is significant. The combination of the bionic design with corrosion-resistant weak interface and surface lubricating design suitable for corrosive environment of ceramic-matrix-laminated composites is a promising way to achieve the optimal integration of mechanical and tribological properties. In this section, a surface lubricating structural Al_2O_3/Ni-laminated ceramics was designed and fabricated with high reliability and suitable for use in a water environment; the material can achieve stable and effective lubrication under water-based corrosive environments [31, 32].

First, Al_2O_3/Ni-laminated composites with excellent mechanical properties were successfully fabricated through layer-by-layer pressing and hot-press sintering method. Their bending strength, fracture toughness, and work of fracture can reach up to 470 MPa, 9.6 $MPa \cdot m^{1/2}$, and 1952 $J \cdot m^{-2}$, respectively [31]. On the basis of the Al_2O_3/Ni-laminated composites, two types of surface composition-lubrication structures were fabricated through the laser texturing and deposition/spraying technologies [31, 32]. These methods improved the surface tribological performance of the Al_2O_3/Ni-laminated composites under water environment remarkably. The regularity of the internal relationships between the surface texture micropattern and the microstructure, chemical composition, and properties of the lubricating films was systematically investigated. This process provided an important theoretical and experimental basis for the design of materials for water-based corrosive environments. The schematic and design concept of the surface composition-lubrication structure on the surface of Al_2O_3/Ni-laminated composites is shown in Fig. 9.5.

The microstructures of typical Al_2O_3/Ni-laminated composites are illustrated in Fig. 9.6, where the dark layer is the Al_2O_3 layer and the light layer is the Ni, which is markedly thinner than the Al_2O_3 layer. The laminated composites present a relatively straight obvious multilayer structure. The boundary between the strong/weak layer was sharp and without clear delamination (Figs. 9.6a, b). Moreover, the Al_2O_3 and Ni layers in the composites were all fully densified because of their good sinterability. Thus, Ni and Al_2O_3 presented compact-crystallized structures with no obvious

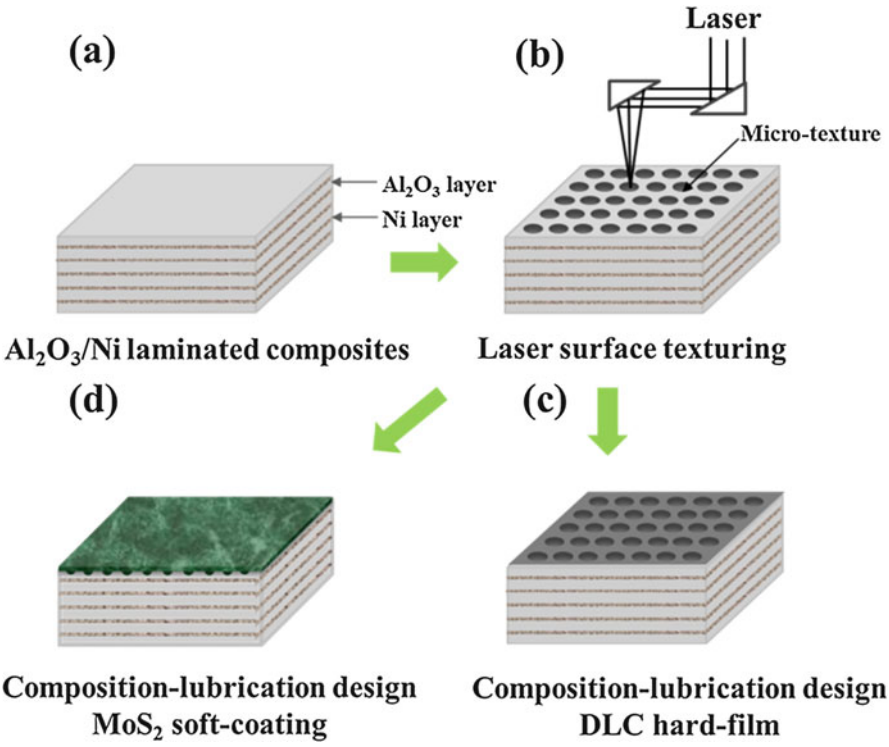

Fig. 9.5 The schematic and surface lubricating design concept of Al_2O_3/Ni-laminated composites

flaws (Fig. 9.6c). These special weak interfacial layers played an important role in improving the mechanical and tribological properties of the laminated composites.

The SEM microtexture photographs of DLC films and LaF_3-doped MoS_2 composite coatings of the Al_2O_3/Ni-laminated composites are presented in Fig. 9.7a and b, respectively. As seen from Fig. 9.7a, the microdimples of DLC films are uniform. The surface around the microdimples is smooth, indicating the absence of notable cracks or other morphological discontinuities. As seen from Fig. 9.7b, the LaF_3-doped MoS_2 composite coatings on the textured surfaces are composed of closely packed powder particles. No obvious microcracks, holes, or other defects can be observed on the textured LaF_3-doped MoS_2 composite coatings. The LaF_3-doped MoS_2 composite coatings on the textured surface exhibit a relatively rough surface morphology.

Fig. 9.8a shows the different surface types of friction behaviors of Al_2O_3/Ni-laminated composites. The textured DLC films with different microdimple area densities are illustrated in Fig. 9.8b. The synergistic effect of a surface texture and DLC film in a water environment is a dominant cause of the decrease of the surface friction coefficient of the material. When friction against a stainless steel pin occurs in a water environment, the friction coefficient of the composition-lubrication structure can decrease to 0.06. This value is nearly one order of magnitude lower

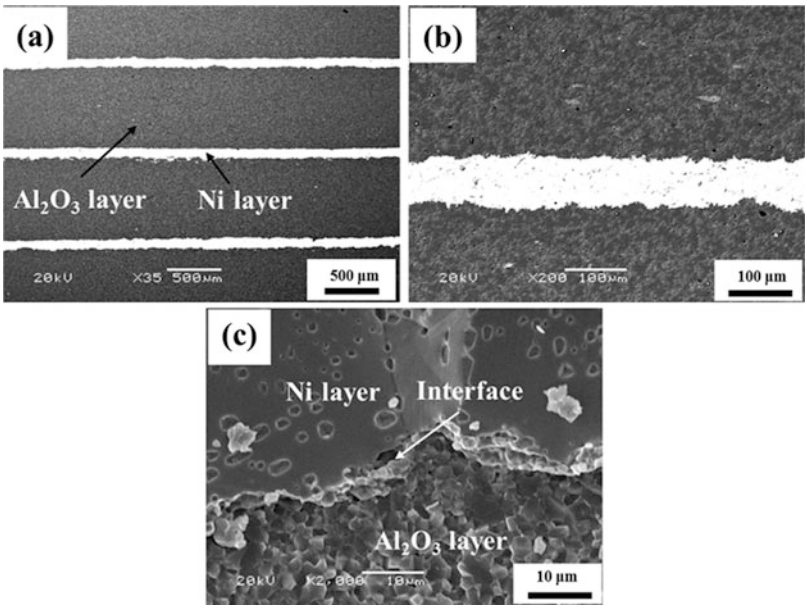

Fig. 9.6 Multilayer and cross-section microstructure of the Al_2O_3/Ni-laminated composites

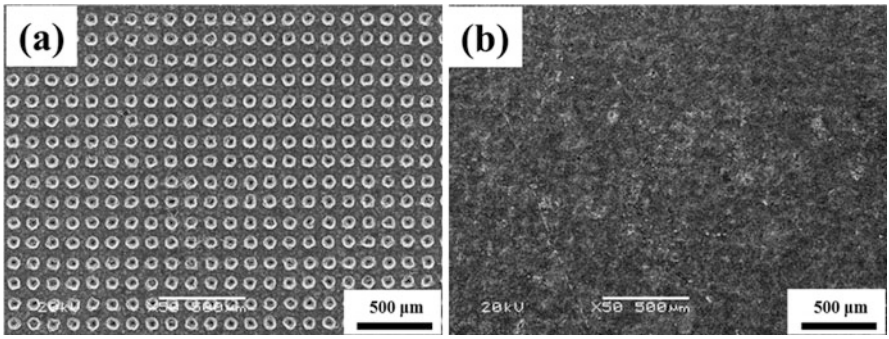

Fig. 9.7 Textured surface lubricating structure with (**a**) DLC films and (**b**) LaF_3-doped MoS_2 composite coating of the Al_2O_3/Ni-laminated composites

than that of the uncoated smooth ceramic surface (0.51). Moreover, the microdimple density of the texture with DLC film plays a key role in improving the tribological properties. When the texture density is low, the tribological properties of the composition-lubrication structure primarily depend on the synergistic lubrication of the surface texture and the DLC thin film because of the low storage of lubricant in the microdimples and the low viscosity feature of water. For high-density textured surfaces, the increase of texture density decreases with DLC content on the surface. This phenomenon indicates that the lubrication effect of DLC decreases. Meanwhile,

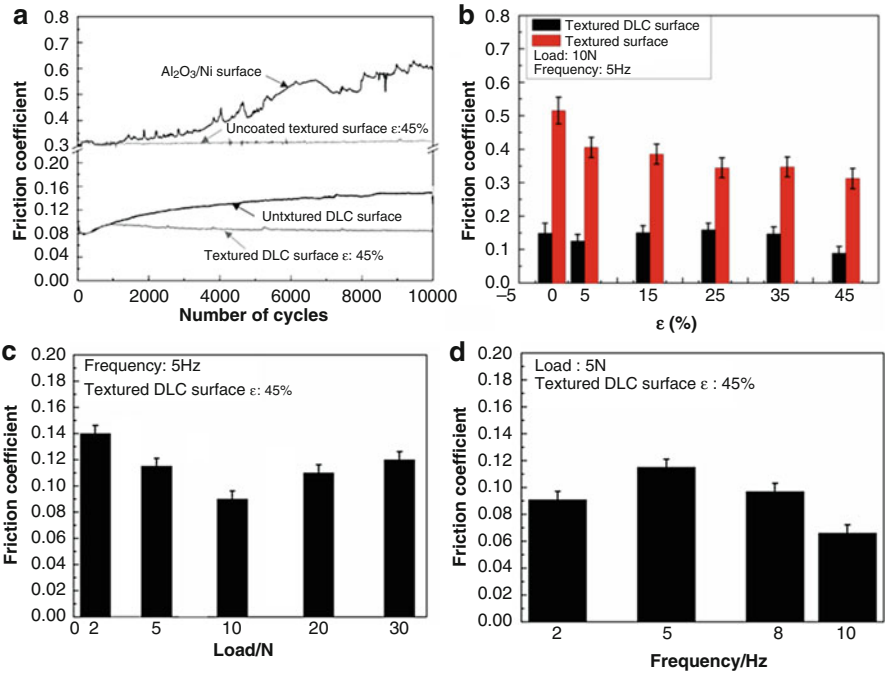

Fig. 9.8 Friction coefficient curves (**a**) and the average values friction coefficients (**b**, **c**, **d**) of samples [31]

the increase of the texture density increases the storage volume of the lubricant that facilitates the formation of lubricating films on the friction surface. When the texture density is 5% or 45%, the composition-lubrication structure exhibits optimal tribological properties and adequate environmental adaptability. Figure 9.8c and d shows the average evolution values of the friction coefficients of the high-density (45%) textured DLC films at different loads and sliding frequencies under water lubrication. As shown in the figure, the textured DLC surface with a microdimple density of 45% exhibits excellent tribological properties in these working conditions. The friction coefficient of the textured surfaces is in the range of 0.06–0.14. The test conditions exhibited a significant effect on the tribological properties of the materials. The effect of sliding frequency on the friction coefficients was larger than the effect of the load.

Figure 9.9 shows the typical SEM micrographs of the worn surfaces of the untextured surface of DLC films (Fig. 9.9a) and textured surface of DLC films (Fig. 9.9b). As shown in Fig. 9.9a, the DLC films on the untextured substrate are severely worn out and flaked off, whereas the textured DLC films are intact and merely exhibit a very small abrasion at the edge of the microdimples (Fig. 9.9b). Therefore, the textured surfaces effectively prevented the peeling of DLC films and exhibited excellent antiwear ability. The performance of the Al_2O_3/Ni-laminated composites can be improved significantly by introducing a regular texture and DLC

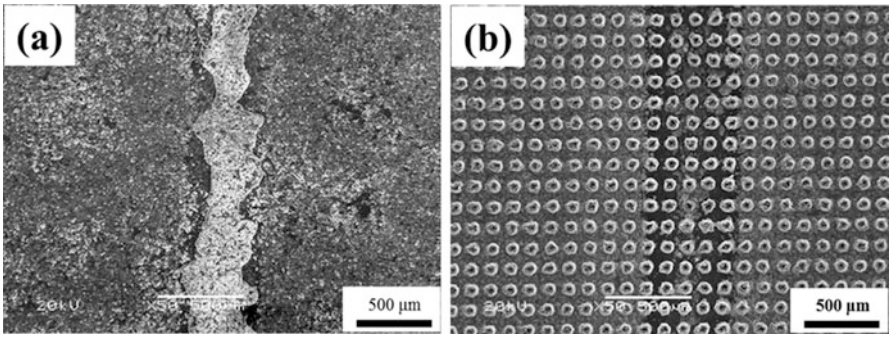

Fig. 9.9 SEM morphologies of the wear tracks of untextured (**a**) and textured DLC films

films on the surface of the materials. Thus, low and stable friction coefficients can be obtained on the sliding surface.

For the soft composition-lubrication layers of LaF_3-doped MoS_2 composite coatings on the surface of Al_2O_3/Ni-laminated composites, the following results were can be determined through the systematic investigation of the tribological behavior and fatigue failure mechanism in a water environment. Surface texture can significantly reduce the contact angle between the surfaces of Al_2O_3/Ni-laminated composites. The lubricant of water promoting the formation of water film and reducing the friction coefficient of the friction pair surfaces effectively. The friction coefficient of the soft composite lubrication surface can be reduced to 0.08, which is less than one-sixth of that of the smooth surface. The sliding lifetime of the lubricating coating can be increased by a factor of more than 10^5 cycles because of the self-locking function of the surface microtexture on the adhesive coating and its secondary lubrication effect, as shown in Fig. 9.10.

The typical SEM morphologies of the wear tracks of untextured and textured LaF_3-doped MoS_2 composite coatings are shown in Fig. 9.11. The untextured LaF_3-doped MoS_2 composite coating surface has flaked off completely resulting in severe wear off. However, for the sample with textured LaF_3-doped MoS_2 composite coating surface, some LaF_3-doped MoS_2 composite lubricants still exist in the sliding area and in microdimples though the coating has flaked off of local region. The LaF_3-doped MoS_2 lubricants in microdimples can be continually replenished into the sliding surface when the coating on the wear scar is quickly worn off. This phenomenon will provide further lubrication.

9.4 Surface Lubricating Design, Fabrication, and Tribological Properties Under a Wide-Range Temperature of Al_2O_3/Mo-Laminated Composites

The rapid development in aerospace, military industry, and other high-tech fields has resulted in the increasing demands for high-temperature wear-resistant materials and high-temperature self-lubricating technology. Self-lubricating composites with

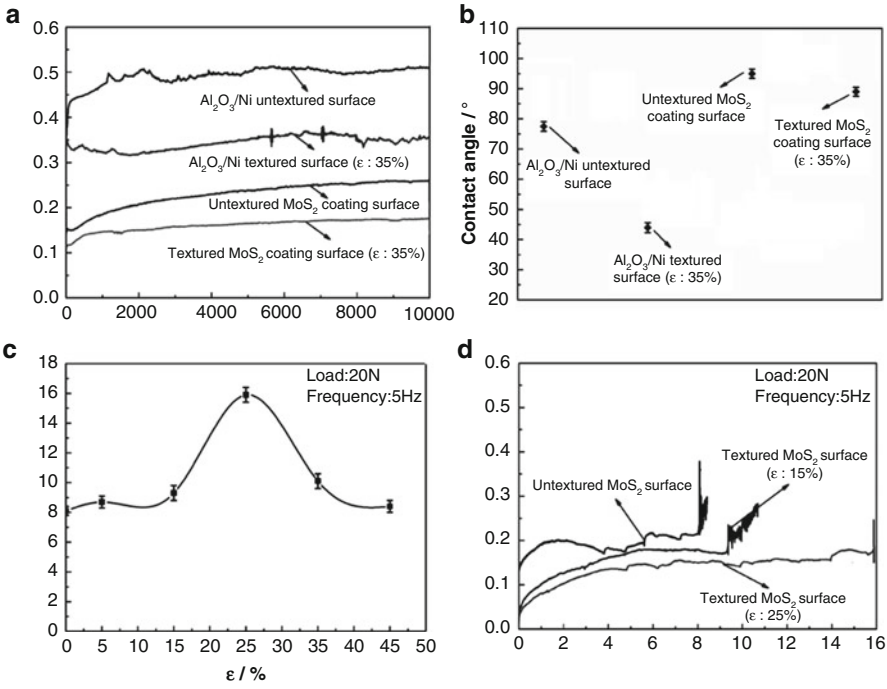

Fig. 9.10 The friction curves (**a**) and the contact angles of water droplets (**b**) on material surface at a normal load of 10 N and the sliding frequency of 5 Hz; the wear life (**c**) and typical friction curves (**d**) of LaF_3-doped MoS_2 composite coatings with different microdimpled densities at a normal load of 20 N and the sliding frequency of 5 Hz [32]

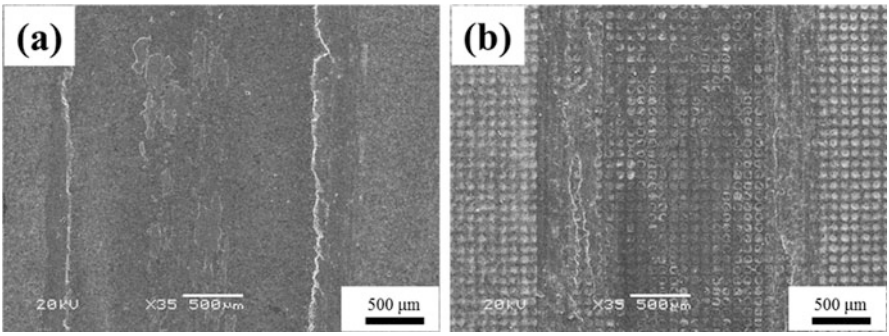

Fig. 9.11 The typical SEM morphologies of the wear tracks of LaF_3-doped MoS_2 composite coatings for untextured surface (**a**) and textured surface (**b**) after worn-out

excellent tribological performance in a wide-temperature range are urgently needed. However, lubricating materials are highly sensitive to temperature. The preparation of self-lubricating composites with wide-temperature range lubrication is very challenging and meaningful. Mechanical lubrication at temperatures above 400 °C

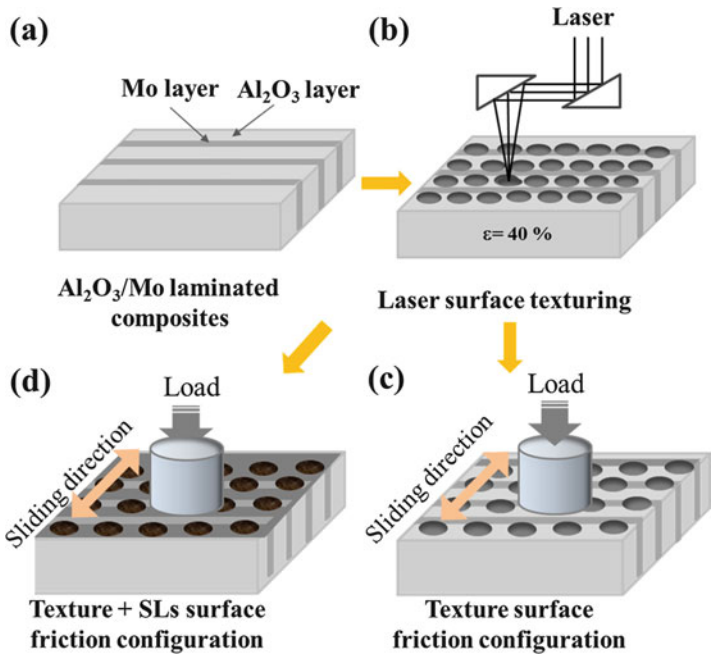

Fig. 9.12 The schematic and surface lubricating design concept of Al_2O_3/Mo-laminated composites

can only depend on solid lubricants (SLs). Thus, two or three SLs are usually combined. Moreover, their synergy lubrication effect is fully utilized to achieve materials with wide-temperature range lubrication. In this part, we developed a three-dimensional lubricating layer by combining the optimized surface textures and SLs. Texture patterns were used as storage carrier of SLs. This structure can realize continuous lubrication from room temperature to 800 °C by fully utilizing the synergy effect and antifriction of the surface texture and SLs stored in the micro-dimples. Two types of different textured density surfaces and the three-dimensional lubricating layer with combined laser surface texture and solid film lubricant of Al_2O_3/Mo-laminated composites were fabricated. The synergy lubrication effect and mechanism of different lubricants from room temperature to 800 °C were discussed [33, 34]. The schematic and surface wide range lubricating design concept of Al_2O_3/Mo-laminated composites are shown in Fig. 9.12.

Using the LST technology, different microdimple densities and microgroove textures were fabricated on the surface of the Al_2O_3/Mo-laminated composites. Figure 9.13 shows the surface morphology of Al_2O_3/Mo-laminated composites with two types of microtextures and composite SLs. Clear and uniform micro-dimples and microgrooves with smooth edges are observed. The shape of the

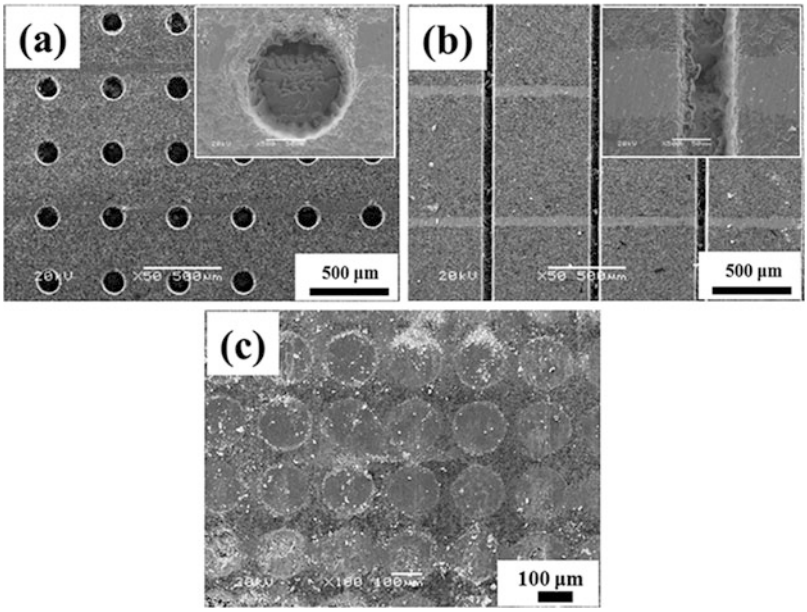

Fig. 9.13 The surface morphology with microdimples (**a**), microgrooves (**b**), and burnished composite SLs (**c**) of Al_2O_3/Mo-laminated composites

microdimples is not influenced by the metal Mo layer (Figs. 9.13a, b). As shown in Fig. 9.13c, the textured microdimples are all filled with SLs after repeated wiping.

Figure 9.14 shows the friction coefficients of laser textured surfaces with different microdimple densities (a) and different microgroove densities (b) at room temperature and 800 °C. Considering the following advantages of the microtexture that increases the contact pressure of the friction surface, traps wear debris, and promotes the formation of lubricating film at high temperatures, the friction coefficients of Al_2O_3/Mo-laminated composites at 800 °C and at room temperature can be further reduced. Meanwhile, the friction coefficient of the material decreases with the increase in the texture surface density. At room temperature, the surface texture trapped wear debris. The friction coefficient of the surface texture can be decreased to as low as 0.5, which is 39% less than that of the untextured surface. Furthermore, the surface with a microdimpled texture exhibited a lower friction coefficient than that with a microgrooved texture. The surface texture facilitated an increase in the contact pressure of the friction pair and the contact area of the material surface with air at 800 °C. Thus, the formation and transfer of the lubricating film of MoO_3 are facilitated. The friction coefficient can be reduced to as low as 0.22. This value is 55% less than that of the untextured surface.

Then, applying composite lubricants on the surface of optimized textured Al_2O_3/Mo-laminated composites and forming a surface three-dimensional lubricating layer can achieve the continuous lubrication of the material from room temperature to

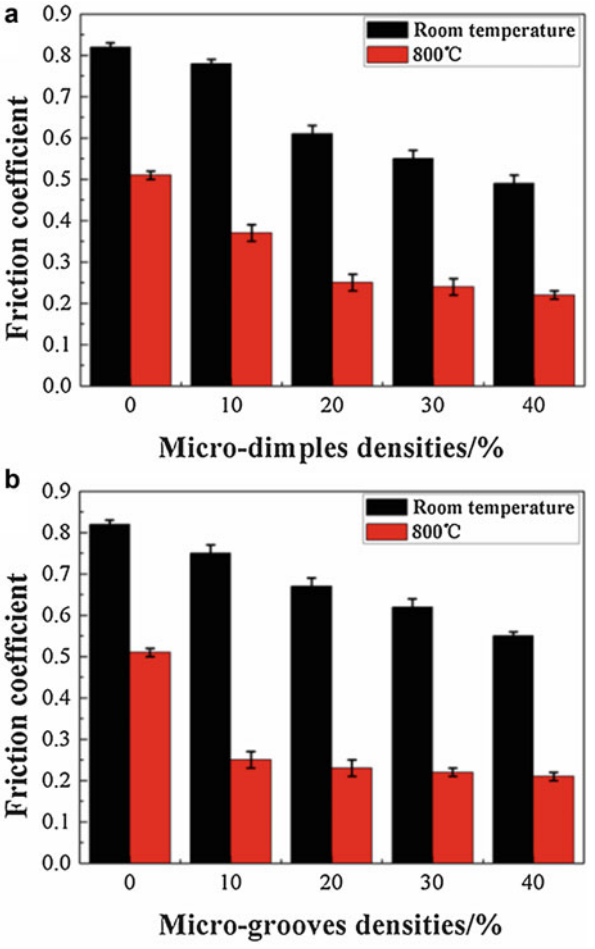

Fig. 9.14 Friction coefficients of laser textured surfaces with different microdimples densities (**a**) and different microgrooves densities (**b**) at room temperature and 800 °C [33]

800 °C. Surface texture plays a key role in storing lubricants that can" constantly lubricate the sliding surface during the friction process to form a continuous, uniform lubricating film. Therefore, the friction coefficient and wear of the sliding surface can be decreased, and the lifetime of the material can be effectively increased.

Herein, the three-dimensional structure combined with excellent antifriction and antiwear properties of solid lubricants with unique structural characteristics of microtexture effectively improved the tribological performance of materials at room temperature and up to increased temperatures. Therefore, the continuous lubrication of materials in a wide-temperature range can be sufficiently realized. For the surface of the MoS_2/CaF_2-BaF_2 composite lubricants, the friction coefficients were below 0.50 throughout the entire temperature range. The lubrication effect was provided by MoS_2 at a temperature range from room temperature to 600 °C. From 600 °C to 800 °C, the synergetic effects of CaF_2-BaF_2 eutectic,

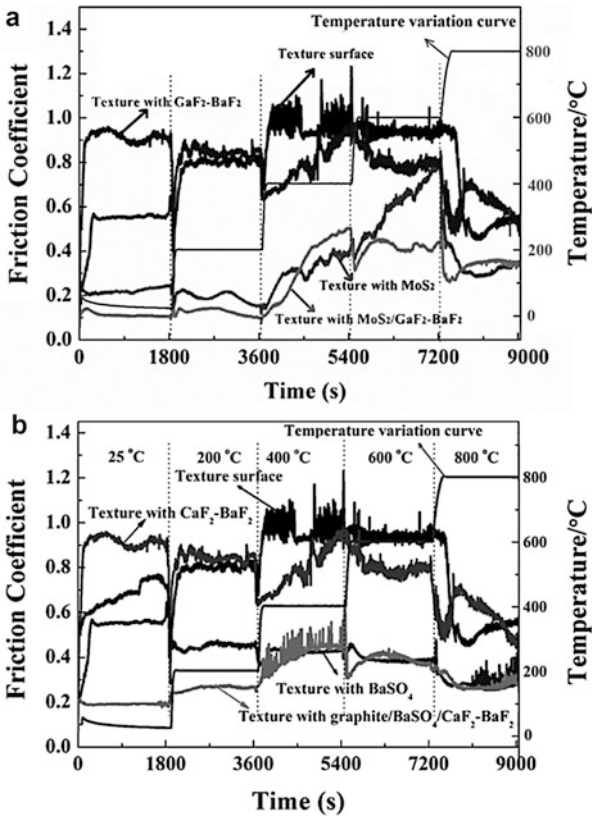

Fig. 9.15 Friction coefficients of surface burnished with different solid lubricants from room temperature to 800 °C [34, 35]

$CaMoO_4$, and $BaMoO_4$ effectively provided the lubrication effect. Composite graphite/$BaSO_4$/CaF_2-BaF_2 lubricants maintained the friction coefficient of materials below 0.45 in the entire tested temperature range from room temperature to 800 °C. The lubrication effect was provided by graphite, $BaSO_4$, and the synergy effect of $BaMoO_4$ and $CaMoO_4$ at room, medium and high temperatures, respectively (Fig. 9.15).

Figure 9.16 shows the typical wear tracks of the untextured surface (Fig. 9.16a), textured without burnishing SLs (Figs. 9.16b, c), and textured surface with burnishing SLs at 800 °C under the same conditions. The untextured surface exhibited serious wear and plastic deformation mainly because of the temperature increase in the friction experiment. However, for the textured surface without burnishing SLs, trapping wear debris in the microgrooves and microdimples can be clearly observed. The texture also maintained relatively intact morphology. For the textured surface burnished with SLs, microdimples maintained relatively intact morphology. A mild wear surface was also produced after a long friction experiment. The SLs stored in microdimples were squeezed to the friction surface during friction process forming a continuous lubricating film.

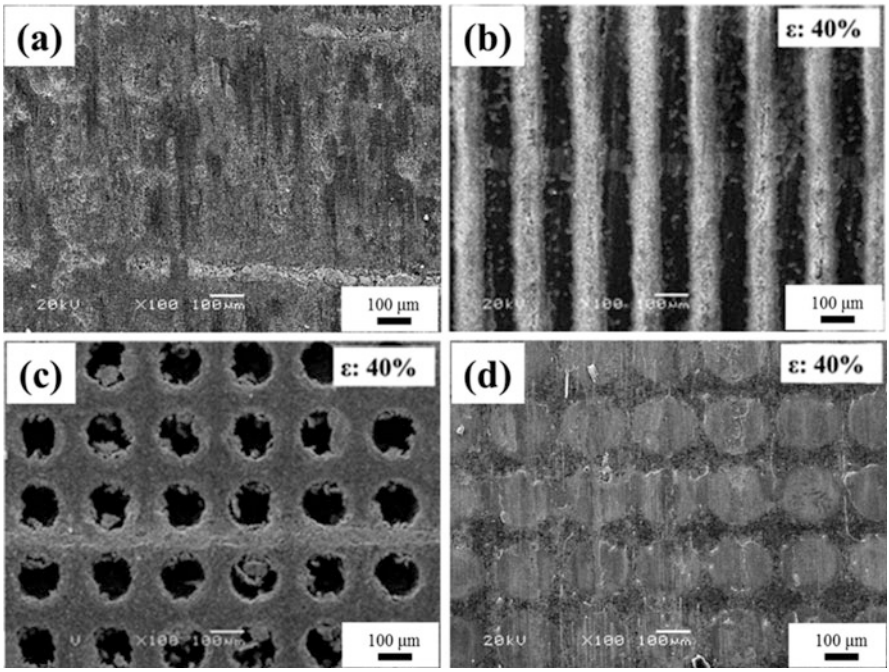

Fig. 9.16 Worn surfaces of untextured surface (**a**), textured surfaces with microgrooves (**b**), microdimples (**c**) and textured surface with burnished SLs (**d**) at 800 °C

In summary, Al_2O_3/Ni and Al_2O_3/Mo-laminated composites with surface composition-lubrication structure realize the integration of mechanical and lubricating properties. The performance of the surface composition-lubrication layers can be facility controlled by the design of the texture micropattern, film/coating characteristics and compound of solid lubricants. The excellent mechanical and tribological properties of the optimal laminated and surface composition-lubrication structure enable them to be used in a wide range of applications. These methods also provided theories and technologies for the preparation and application of high performance lubricating materials that can be used in corrosive and wide-temperature range environments.

Acknowledgment This work was supported by the National Natural Science Foundation of China (51775534) and the Youth Innovation Promotion Association CAS (2013272).

References

1. Zhang, Y.S., Hu, L.T., Chen, J.M., Liu, W.M.: Lubrication behavior of Y-TZP/Al_2O_3/Mo nanocomposites at high temperature. Wear. **268**(9–10), 1091–1094 (2010)
2. Hu, T.C., Zhang, Y.S., Hu, L.T.: Mechanical and wear characteristic of Y-TZP/Al_2O_3 nanocomposites. Ind. Lubr. Tribol. **66**(2), 209–214 (2014)

3. Qi, Y.E., Zhang, Y.S., Hu, L.T.: High-temperature self-lubricated properties of Al_2O_3/Mo laminated composites. Wear. **280–281**, 1–4 (2012)
4. Fang, Y., Zhang, Y.S., Song, J.J., Fan, H.Z., Hu, L.T.: Design and fabrication of laminated-graded zirconia self-lubricating composites. Mater. Des. **49**, 421–425 (2013)
5. Qi, Y.E., Zhang, Y.S., Fang, Y., Hu, L.T.: Design and preparation of high-performance alumina functional graded self-lubricated ceramic composites. Compos. Part B Eng. **47**, 145–149 (2013)
6. Fang, Y., Zhang, Y.S., Song, J.J., Fan, H.Z., Hu, L.T.: Influence of structural parameters on the tribological properties of Al_2O_3/Mo laminated nanocomposites. Wear. **320**, 152–160 (2014)
7. Wang, C.A., Huang, Y., Zan, Q.F., Zou, L.H., Cai, S.Y.: Control of composition and structure in laminated silicon nitride/boron nitride composites. J. Am. Ceram. Soc. **85**(10), 2457–2461 (2002)
8. Hwu, K.L., Derby, B.: Fracture of metal/ceramic laminates-II. Crack growth resistance and toughness. Acta Mater. **47**(2), 545–563 (1999)
9. Wang, C.A., Huang, Y., Zan, Q.F., Guo, H., Cai, S.Y.: Biomimetic structure design-a possible approach to change the brittleness of ceramics in nature. Mater. Sci. Eng. C. **11**(1), 9–12 (2000)
10. Clegg, W.J., Kendall, K., Alford, N.M., Button, T.W., Birchall, J.D.: A simple way to make tough ceramics. Nature. **347**(6292), 455–457 (1990)
11. Zuo, K.H., Jiang, D.L., Lin, Q.L.: Mechanical properties of Al_2O_3/Ni laminated composites. Mater. Lett. **60**(9–10), 1265–1268 (2006)
12. Song, J.J., Zhang, Y.S., Fang, Y., Fan, H.Z., Hu, L.T., Qu, J.M.: Influence of structure parameters and transition interface on the fracture property of Al_2O_3/Mo laminated composite. J. Eur. Ceram. Soc. **35**, 1581–1591 (2015)
13. Ryk, G., Kligerman, Y., Etsion, I.: Experimental investigation of laser surface texturing for reciprocating automotive components. Tribol. Trans. **45**(4), 444–449 (2002)
14. Yu, X.Q., He, S., Cai, R.L.: Frictional characteristics of mechanical seals with a laser-textured seal face. J. Mater. Process. Technol. **129**(1–3), 463–466 (2002)
15. Etsion, I., Halperin, G., Brizmer, V., Kligerman, Y.: Experimental investigation of laser surface textured parallel thrust bearings. Tribol. Lett. **17**(2), 295–300 (2004)
16. Kawasegi, N., Sugimori, H., Morimoto, H., Morita, N., Hori, I.: Development of cutting tools with microscale and nanoscale textures to improve frictional behavior. Precis. Eng. J. Int. Soc. Precis. Eng. Nanotechnol. **33**(3), 248–254 (2009)
17. Baumgart, P., Krajnovich, D.J., Nguyen, T.A., Tam, A.C.: A new laser texturing technique for high-performance magnetic disk drives. IEEE Trans. Magn. **31**(6), 2946–2951 (1995)
18. Varenberg, M., Halperin, G., Etsion, I.: Different aspects of the role of wear debris in fretting wear. Wear. **252**(11–12), 902–910 (2002)
19. Etsion, I., Halperin, G.: A laser surface textured hydrostatic mechanical seal. Tribol. Trans. **45**(3), 430–434 (2002)
20. Kovalchenko, A., Ajayi, O., Erdemir, A., Fenske, G., Etsion, I.: The effect of laser surface texturing on transitions in lubrication regimes during unidirectional sliding contact. Tribol. Int. **38**(3), 219–225 (2005)
21. Hu, T.C., Zhang, Y.S., Hu, L.T.: Tribological investigation of MoS_2 coatings deposited on the laser textured surface. Wear. **278–279**, 77–82 (2012)
22. Uehara, Y., Wakuda, M., Yamauchi, Y., Kanzaki, S., Sakaguchi, S.: Tribological properties of dimpled silicon nitride under oil lubrication. J. Eur. Ceram. Soc. **24**(2), 369–373 (2004)
23. Wang, X., Adachi, K., Otsuka, K., Kato, K.: Optimization of the surface texture for silicon carbide sliding in water. Appl. Surf. Sci. **253**(3), 1282–1286 (2006)
24. Schreck, S., Zum Gahr, K.H.: Laser-assisted structuring of ceramic and steel surfaces for improving tribological properties. Appl. Surf. Sci. **247**(1–4), 616–622 (2005)
25. Etsion, I., Kligerman, Y., Halperin, G.: Analytical and experimental investigation of laser-textured mechanical seal faces. Tribol. Trans. **42**(3), 511–516 (1999)
26. Etsion, I., Sher, E.: Improving fuel efficiency with laser surface textured piston rings. Tribol. Int. **42**(4), 542–547 (2009)

27. Fan, H.Z., Hu, T.C., Zhang, Y.S., Fang, Y., Song, J.J., Hu, L.T.: Tribological properties of micro-textured surfaces of ZTA ceramic nanocomposites under the combined effect of test conditions and environments. Tribol. Int. **78**, 134–141 (2014)
28. Hnatko, M., Galusek, D., Šajgalík, P.: Low cost preparation of Si_3N_4-SiC micro/nano composites by in-situ carbothermal reduction of silica in silicon nitride matrix. J. Eur. Ceram. Soc. **24**(2), 189–196 (2004)
29. Křesťan, J., Šajgalík, P., Pánek, Z.: Carbothermal reduction and nitridation of powder pyrophyllite raw material. J. Eur. Ceram. Soc. **24**(5), 791–796 (2004)
30. Balog, M., Šajgalík, P., Lenčéš, Z., Kečkéš, J., Huang, J.T.: Liquid phase sintering of SiC with AlN and rare-earth oxide additives, silicon-based structural ceramics for the new millennium. Brito ME, Lin HT, Plucknett K (Eds.) Ceram. Trans. **142**, 191–202 (2003)
31. Fan, H.Z., Zhang, Y.S., Hu, T.C., Song, J.J., Ding, Q., Hu, L.T.: Surface composition-lubrication design of Al_2O_3/Ni laminated composites–Part I: tribological synergy effect of micro-dimpled texture and diamond-like carbon filmsin a water environment. Tribol. Int. **84**, 142–151 (2015)
32. Fan, H.Z., Hu, T.C., Wan, H.Q., Zhang, Y.S., Song, J.J., Hu, L.T.: Surface composition-lubrication design of Al_2O_3/Ni laminated composites – Part II: tribological behavior of LaF_3-doped MoS_2 composite coating in a water environment. Tribol. Int. **96**, 258–268 (2016)
33. Fang, Y., Zhang, Y.S., Fan, H.Z., Hu, T.C., Song, J.J., Hu, L.T.: Surface composition-lubrication design of Al_2O_3/Mo laminated composites – Part I: influence of laser surface texturing on the tribological behavior at 25 and 800 °C. Wear. **334–335**, 23–34 (2015)
34. Fang, Y., Fan, H.Z., Song, J.J., Zhang, Y.S., Hu, L.T.: Surface engineering design of Al_2O_3/Mo laminated composites – Part II: continuous lubrication effects of a three-dimensional lubricating layer at temperatures from 25 to 800 °C. Wear. **360–361**, 97–103 (2016)
35. Fang, Y., Fan, H.Z., Zhang, Y.S., Song J.J., Hu, L.T.: Preparation and tribological performance of three-dimensional lubricating layer on the surface of Al_2O_3/Mo self-lubricating structural ceramics. Tribol. **37**(3), 395–401 (2017 in Chinese)

Environmental Analysis of Self-Lubricating Composites: A Review

10

Mohammad Hasan Balali, Narjes Nouri, and Wilkistar Otieno

Contents

Abstract

Human activities have affected the balance in the eco-system and put the habitant surrounding us in a catastrophic danger. Most of these wrecking effects which had been strengthened or emerged recently would also last for a long period of time. Taking immediate thoughtful actions are necessary to prevent high risk human activities. Based on the data collected for global surface mean temperature and CO_2 emission, it has been shown that a huge discrepancy in climate is already occurring. There are various reasons which are causing climate change, specifically global warming, which most of those would be discussed in this study. The

M. H. Balali (✉)
Department of Industrial and Manufacturing Engineering, College of Engineering & Applied Science, University of Wisconsin-Milwaukee, Milwaukee, WI, USA
e-mail: mbalali@uwm.edu

N. Nouri
Lubar School of Business, University of Wisconsin-Milwaukee, Milwaukee, WI, USA

W. Otieno
Industrial and Manufacturing Engineering Department, University of Wisconsin-Milwaukee, Milwaukee, WI, USA

P. L. Menezes et al. (eds.), *Self-Lubricating Composites*,
https://doi.org/10.1007/978-3-662-64243-6_10

negative effects of different materials on the eco-system have one of the biggest shares in environmental concerns. Emerging Eco-tribology science helped design products and processes for the environment. The design of products has been significantly modified to be more environmental friendly and sustainable. A brief review of tribology and different definitions, which had been changed during the time, will be discussed in this study. Furthermore, eco-tribology has a positive effect in reducing energy consumption and increasing the lifetime of the products. Lubricant is an example of the materials which produce environment destructive waste. In the recent decades, researchers improved the lubricant materials to be less destructive for the environment. Self-lubricant composites, for instance, significantly reduced the drawbacks of lubricant materials. The advantage is not only improving wear resistance and reduced COF, but also the elimination of the need for external lubricants. Aluminum/graphite (Al/Gr) composites have been used as self-lubricating materials due to the superior lubricating effect of graphite during sliding process. This study reviews the environmental concerns and advances of eco-tribological, lubricant and self-lubricant composites.

10.1 Introduction

Environmental effects of different materials that are used in human activities are one of the most concerning issues for scientists, environmental researchers, and policy makers. Global warming, climate change, and environmental pollutions are getting more tangible for everyone in every corner of the world [1]. Finding a better substitute for hazardous materials would improve the life's quality for the next generations. "Fig. 10.1" shows the progress in global mean surface temperature of earth since 1880. Some actions should be taken to stop or slow down this increasing trend of temperature. Carbon emission is always an important factor in environmental analysis since the negative effects of carbon on environment are usually irreparable. "Fig. 10.2" shows the global carbon emission from fossil fuels since 1900. The growing trend of global carbon emission from fossil fuels is as concerning as increasing trend of global mean surface temperature.

Derek Markham [4] summarized the top 10 causes and effects for global warming as follow:

Causes:

- Carbon dioxide emissions from burning fossil fuel in power plants
- Carbon dioxide emissions from burning gasoline for transportation purposes
- Methane emissions from animals, agriculture such as rice paddies, and from Arctic seabed
- Deforestation, especially tropical forests for wood, pulp, and farmland
- Increase in usage of chemical fertilizers on croplands

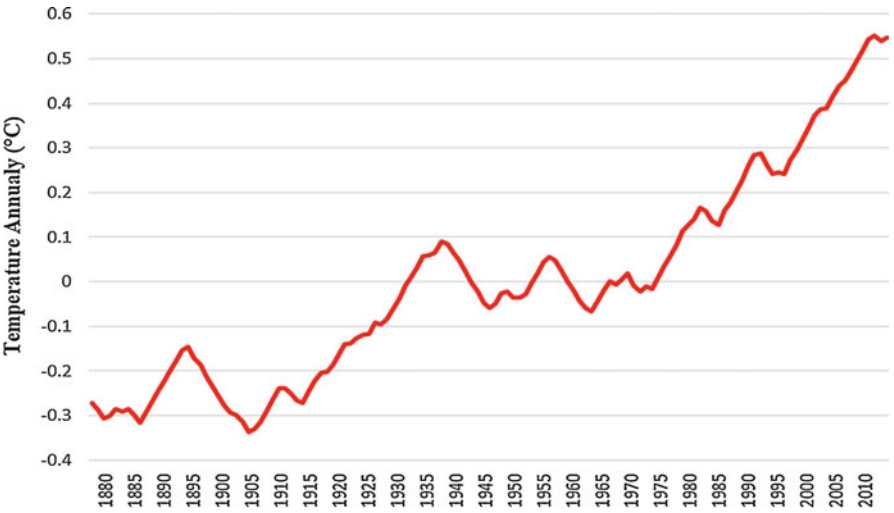

Fig. 10.1 Global mean surface temperature, 5-year annual running mean Earth Observatory, NASA [2]

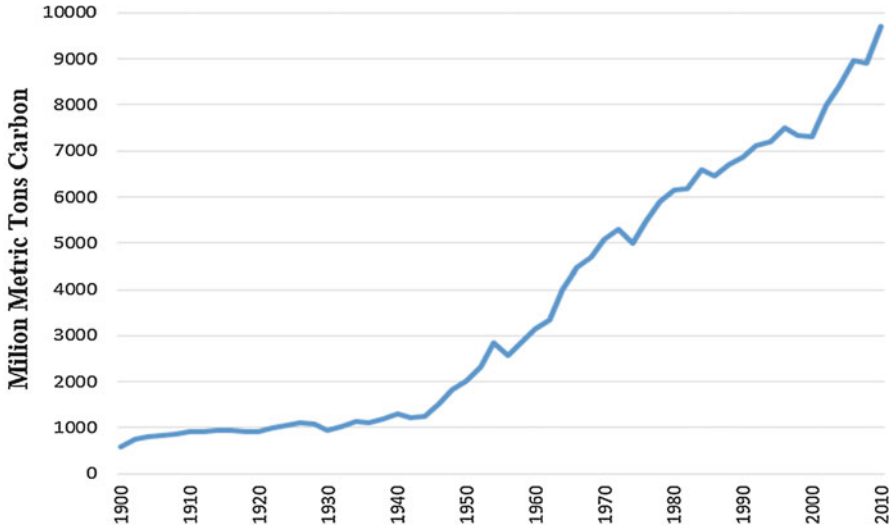

Fig. 10.2 Global Carbon emission from fossil fuels, United States Environmental Protection Agency [3]

Effects:

- Rise in sea levels in worldwide scale
- More killer storms all around the world
- Massive crop failures

- Widespread extinction of species of animals, plants and other creatures
- Disappearance of coral reefs

Based on IPCC Fourth Assessment Report 2007 [5], most of the climate scientists agree that the main cause of the current level of temperature which leads to global warming has been done by human activities. "Fig. 10.3" shows a schematic view of a layer of greenhouse gases around earth. Water vapor (H_20), nitrous oxide (N_2O), carbon dioxide (CO_2), and methane (CH_4) have the largest shares in green-house gases [6].

Based on NASA report [7], the possible consequences following climate change are as follows:

- Change will continue in this century and after that
- Global temperature will continue to rise
- Frost-free season will be lengthening
- Precipitation patterns will be changed
- More droughts and heat waves
- Hurricanes will become stronger and more intense
- Sea level will be raised 1–4 feet by 2100
- Arctic likely to become ice-free

Human activities should be modified to minimize their negative effects on the environment. Tribology is playing an important role in this cycle to help the environment deal with all those problems and reduce the negative effects of some materials on it. But how tribology works to benefit the environment is a question that

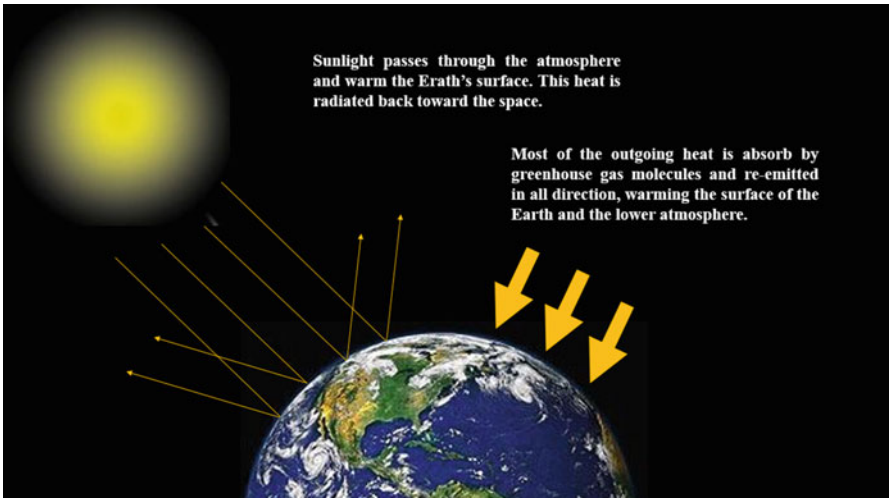

Fig. 10.3 A layer of greenhouse gases, primarily water vapor, including small amounts of carbon dioxide, methane, and nitrous oxide [5]

is being frequently asked. Tribology can help various technologies such as energy efficiency and durability of vehicles, household appliances, industrial machines, and plants to become more mature and productive. Tribology also supports the societal ideas to decrease substances from products that would be a menace to the environment, which has included abolishing asbestos from vehicle brake systems, replacing refrigerants with CFC-substitutes, and controlling the lead used in bearings [8, 9]. Therefore, reducing the usage of some destroying materials and substituting them with less wrecking materials would significantly help the environment.

Although, from an economic standpoint, enforcing law to fix or reduce environmental issues is not profitable for policy makers at this point but, these matters usually create huge costs in the long term that will justify its expenditure. Moreover, most of the damages caused by human activities are irrecoverable or it takes a long time to be mended in the environment. It means that using more sustainable and environmental friendly materials is an economically justified plan in the long term. A good design of sustainable materials would have positive impact on both economic and environment at the same time.

This study is a review of the development of the tribology and lubricating materials starting with a brief review of environmental problems associated with lubricating materials and their effects on eco-system and energy sector. This chapter places extra emphasis on the role of advanced lubricating materials on energy sector since energy became the most concerning issues of societies in recent decades. Different definition and applications of tribology have been presented. In addition to the tribology aspects of environmental friendly materials, some economic benefits have been mentioned as well. Using the advanced tribological materials could save millions of dollar in global scale. For instance, car industries could reduce the fuel consumption of the produced car which leads to saving both money and energy. Different advantages of using self-lubricating composites have been reported in this study. Applying more advanced self-lubricating composites can improve the environmental issues while have positive impacts on economics.

10.2 Eco-Tribology

Tribology is assisting societies to be more sustainable and productive and it is not only human but all the living creatures can benefit from tribology since it can reduce negative effects of some materials and make their habitat more sustainable. Although global economic is still an important matter in eco-tribology, environmental effects are more crucial to decide about the value of a product [8].

Through time, objectives of the tribology have been expanded gradually, tribology for energy conservation (1997), environmental friendly tribology (2000), ecological tribology or eco-tribology (2000), green tribology (2003), and lifecycle tribology (2004) [10]. Controlling friction, reducing wear, and improving lubrication have extended to save energy and materials, reducing emissions, shock absorption, decreasing noise pollution, developing bio- and eco-lubrication, and improving

quality of life and to become the basics of the tribology in the recent decades [10, 11].

Green tribology should be able to provide the full technical support for the preservation of energy, resources, environmental protection, and improvement of quality of life and to decrease the natural disasters. Certainly, it is an important way forward to be a more sustainable society [10, 12]. Green tribology has been emerged to keep both sides of the sustainable developments and society and it meant as a new way of thinking which shows views on ecological balance and environmental protection and so embodies the ideology of the sustainable developments of nature and society perfectly at a same time. The main objectives of green tribology can be summarized into 3L + 1H, namely, respectively, low energy consumption, low discharge (CO_2), low environmental cost, and high quality of life [12].

As it has been mentioned above, saving energy resources and reducing the destructive environmental impact of the sources are the most important goals of eco-tribology. Using environmental friendly lubricant materials in energy sector can significantly reduce the negative environmental impacts. Using renewable energy resources coupled with energy storage systems has been more developed during recent years [13, 14]. Eco-friendly materials which are used in energy storage systems can significantly reduce environmental effects. Therefore, eco-tribology plays an important role in energy consumption saving sector and affect societies and quality of life [15].

Useful lifetime of products can be extended by using materials with less wear and friction, better design, and advanced lubrication. The main results of using the useful lifetime of products are the reduction in energy consumption, required energy for replacing the worn or failed components, and the time and resources for machinery.

From the economic point of view, using renewable and recycled materials has direct and indirect savings of raw materials and sources and saving the energy since less energy is needed for the extraction and production of raw materials [16].

Wilfried J. Bartz [16] classified the tribologically appropriate selection of materials as follow:

- Materials with easy machinability and deformability consume less energy and less man power needed for components production.
- For longer lifetime of products, low wear materials should be used to save man power, energy and raw materials.
- Tribological contacts with low friction resulting in reduced wear which leads to more usable lifetime.

Designers should attempt to create a balance between desire usage of energy sources and the adverse environmental effects which can last forever. A main goal of this is decreasing the inefficient systemic losses through the wear and friction. Durability and sustainability are the main characteristics of a mechanical system. It is necessary to control the frictional and wear losses to achieve durability and sustainability [17].

S. Zhang [18] stated that the main objectives of tribology are mostly controlling friction, reducing wear, and improving lubrication. Tribology should be able to meet

the demands of a sustainable society. The ecological balance and environmental impact at that time owing to the restrictions of the times did not consider as it was expected. Thereupon, green tribology has been emerged to keep abreast of the sustainable developments of societies. Green is a new concept that represents the views on ecological balance and environmental effects and so embodies the ideology of the sustainable developments of nature and society perfectly.

10.3 Lubricants

All waste lubricants can easily destroy soil's microflora and make it infertile in the long term. Even very low doping in water makes it unsuitable for drinking because of the smell, taste, and health hazards. Millions of tons of waste lubricants are released in the world every year. Consequently, more severe regulations and rules are needed to protect the environment and decrease the harmful effects of these products. Saving nonrenewable resources and reducing the harmful environmental effects of lubricants are the two main missions of these regulations [19].

M. Stojilković et al. [19] concluded that lubricants can be considered environmentally acceptable if they meet some requirements which rapid biodegradability, nontoxicity to humans, marines, or even bacteria are the most important ones.

Biodegradability means the tendency of lubricants to be decomposed by microorganisms. Eco-toxicity implies a toxic effect on plants and animals and not on the human health. Substances with a Lethal Dose LD 50 $>$ 1000 ppm/kg are barely considered toxic. [19].

W.J. Bartz [16] determined the important aspects for a reduced impairment of environment by lubricants as follow:

- Less outflows to reduce the pollution
- Extended lubricant change periods or even fill for life lubrication
- avoiding lubricant consumption side effects to save energy
- Treatments, recycling and disposal

L.A. Bronshteyna and J.H. Kreiner [20] estimated that approximately 11% of the total energy annually consumed in the USA in the four sections of transportation, turbomachinery, power generation, and industrial processes can be saved through new developments in lubrication and tribology.

In 1994, 500 million vehicles were registered for use globally with an additional 40 to 50 million cars produced in the world every year [16] (International Organization of Motor Vehicle Manufacturers. See: http://www.worldometers.info/cars/). About 10% reduction in the mechanical losses due to effective tribology leads to a 1.5% drop in the fuel consumption equating to about 340 liter of petrol during car's lifetime (about 125.000 miles) apart from the environmental gains due to reduced emissions and durability [15] (Taylor CM. Automobile engine tribology – design considerations for efficiency). Thus, it becomes clear that if you integrate these small

savings ($350) per car to the vast number of cars currently in use, the economic savings and environmental benefits are huge.

Based on the 2016 data from http://www.worldometers.info/cars/ and International Organization of Motor Vehicle Manufacturers (OICA), it is estimated that for the first time in 2010 the number of passenger cars traveling the streets and roads of the world was reached to 1 billion-unit mark. In this scale, the effects of tribology in fuel consumption reduction are completely tangible. "Fig. 10.3" shows that motor vehicles mileage (miles per vehicles) had been significantly increased from 1949 to 2010 while the vehicles fuel consumption (gallon per vehicle) had been decreased. Although Tribology is not the only reason and there are different substitutions for fuel, positive effects of tribology are undeniable (Fig. 10.4).

G. Howarth and M. Hadfield [22] have generated a model assessing the sustainable development aspects of a product from a design perspective depicting the environmental, social, and economic impact.

Kenneth Holmberg and Ali Erdemir [23] reported the followings in their studies. One-fifth of all energy produced worldwide that is about 100 million terajoule is used annually to overcome friction. The largest quantities of energy are used by industry (29%) and transportation (27%) sections. Based on our recent studies on energy use in passenger cars, trucks, and buses, it has been concluded that it is possible to save as much as 17.5% of the energy use in road transports in a short period of time, about 5–9 years by effective implementation of new tribological solutions. This equals to annual energy savings of 11.6 oxyjoules, fuel savings of 330 billion liters, and 860 million tons reduction in CO_2 emissions. In a paper mill, 15–25% of the energy used is spent to overcome friction. The electrical energy used by a paper machine is distributed as 32% to overcome friction, 36% for the paper

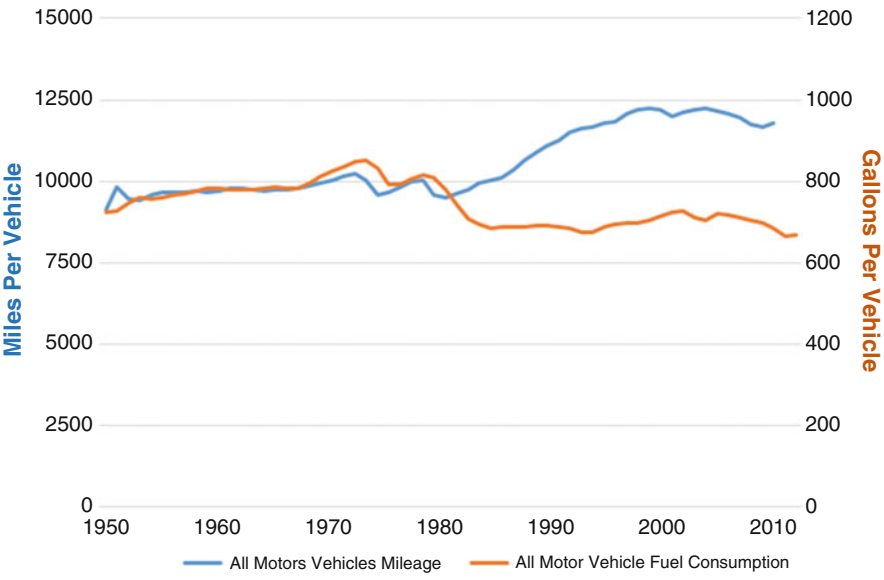

Fig. 10.4 Motor Vehicle Mileage, Fuel Consumption, and Fuel Economy, 1949–2010 [21]

production and mass transportation, and 32% is lost in other sectors. In paper machines, 11% of the total energy used to overcome friction can be saved by the implementation of new tribological technologies.

Energy is a key resource in a lot of sectors today and will be crucial for the sustainability of our society in the future. As it was stated above, considerable amount of energy is consumed to overcome friction, especially in the transportation, industrial, and power-generation sectors, and major economic losses are also due to wear of products and components and their replacement [23].

It is necessary to take actions, if possible, using machine element types processing higher efficiencies, e.g., spur gears instead of worm gears, roller bearings, instead of mixed film lubricated journal bearings and the result is less consumption of energy.

Reduced consumption of lubricants can be realized by:

- Optimum-design seals which reduces leakage
- Lubricants with higher stability against oxidation and thermal degradation and contamination by liquid and solid matters

A reduction of energy consumption can be achieved by different types of savings, as defined below:

- Direct savings: Primary savings reduction of mechanical friction losses such as operating cost
- Secondary savings: less frequent replacement of worn and failed parts and less necessity to reproduce them such as metal working and maintenance cost
- Tertiary savings: less expenditure for extraction and reproduction of raw materials required for the production of parts which have to be replaced such as cost of energy content of materials
- Indirect savings: reduction of investment cost by extended useful lifetime of machines and machine elements and selecting smaller machines
- Short-term savings: characterized by the fact that no additional cost for research and development is needed and only the consequent application of available knowledge is enough
- Medium-term savings: research and development cost for, e.g., 5 years have to be spent in order to transform basic and scientific knowledge into practical usable forms.
- Long-term savings: using solutions which at present are not yet conceivable.

I. Tzanakisa, M. Hadfield, et al. [17] reported that lubricants greatly contribute to decreasing frictional losses in mechanical systems. It is expected that low-viscosity, long life oils will be developed with advanced additives such as friction modifiers and antiwear and antioxidation agents. Research on decreasing the detrimental impacts of lubricants on the environment now encompasses such topics as halogen-free and biodegradable oils, carbon-neutral vegetable oils, the minimum quantity of lubrication (MQL) [24], and process fluid lubrication such as water lubrication [25, 8] (Fig. 10.5).

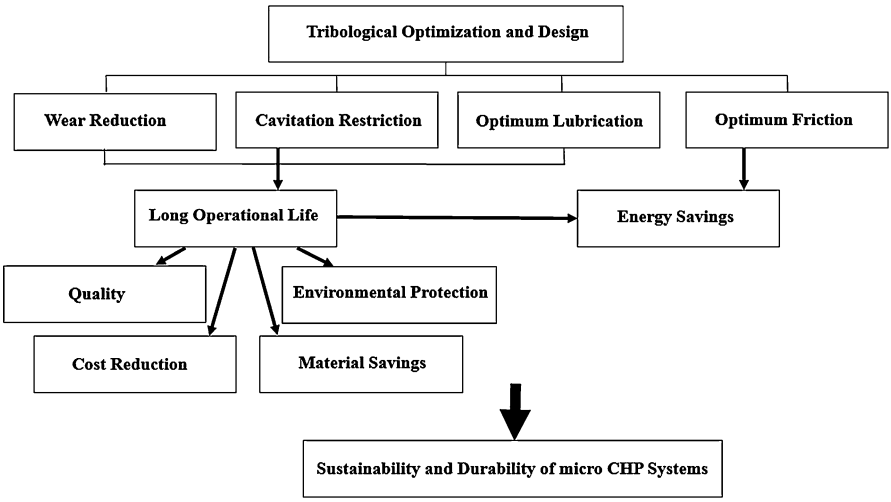

Fig. 10.5 Schematic representation of the tribological optimization of the scroll expander [17]

I. Tzanakisa, M. Hadfield, et al. [17] indicated that frictional losses, sliding wear, cavitation, and oil degradation are the critical damage mechanisms of the scroll expander which can seriously affect the performance and the lifespan of the scroll and the micro-CHP unit. A number of recommendations provided to industry after the completion of the research project in order for the durability and sustainability of the scroll to be improved. These were successfully adapted by industry and applied to their new generation scroll expander systems alleviating any undesirable effects (Fig. 10.6).

A novel fullerene-like hydrogenated carbon film was prepared by pulse bias-assisted plasma enhanced chemical vapor deposition, and its mechanical and tribological properties were investigated. This film displayed super-low friction and wear in both dry inert and humid ambient atmospheres and less sensitivity to H_2O and O_2 molecules in air [18, 26].

V. Rodriguez et al. [27] reported that graphite, molybdenum disulfide (MoS_2), and polytetrafluoroethylene (PTFE) are a few examples of predominant materials which used as solid lubricants. Other examples of lubricants include boron nitrite, talc, calcium fluoride, cerium fluoride, and tungsten disulfide. These lubricants are less common but in some cases can outperform graphite and MoS_2.

V. Rodriguez et al. [27] and Rudnick [28] concluded that applications involving high-temperature and high load carrying requirements have their highest efficiency using Graphite. In contrast, PTFE does not have layered structure. It has an exceptionally low coefficient of friction. Both static and dynamic coefficients are smaller than that of any other solid lubricant and the lubrication properties are at least partially the result of its high softening point [27, 28].

The most recent iridologists result investigating the lubricant behavior of unexplored or even of new materials proved that PEEK with fiber reinforcement

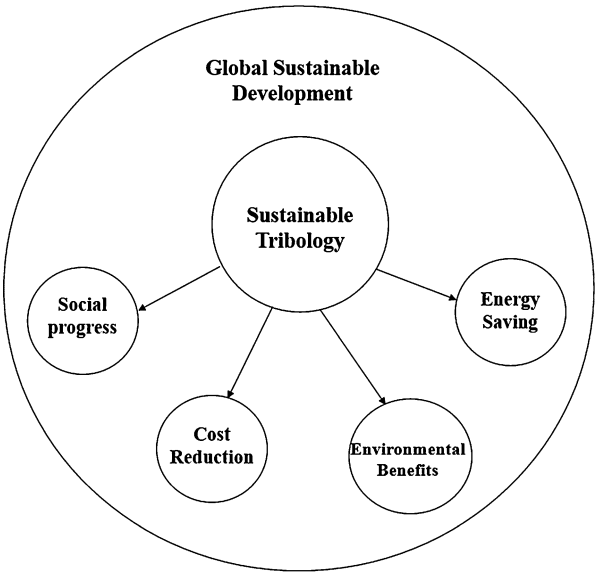

Fig. 10.6 The impact of sustainable tribology to sustainable development [17]

and lubricant additives are very efficient. As an example, Briscoe et al. [29] investigated the friction and wear properties of 10% PTFE in a PEEK matrix. A significant reduction in the coefficient of friction and an improved wear resistance was the outcome of this experiment. Other investigations also showed an optimum of increase in wear resistance and minimum frictional coefficient [27, 30].

According to a study by A.D. Moghadam et al. [31], development of advanced metal matrix nanocomposites for structural engineering and functional devices could be consequence of rapid innovation in nanotechnology in past few years. Carbonous materials, such as graphite, carbon nanotubes (CNTs), have attracted the attention of researchers to synthesize lightweight self-lubricating metal matrix nanocomposites with superior tribological properties for various applications in automotive and aerospace industries based on their unique properties and lubricious nature. Adding CNT and graphene to metals decreases both coefficient of friction and wear rate while increases the tensile strength.

The results of A.D. Moghadam et al. [32] show that reducing energy consumption and improving heat dissipation between two moving solids can be reached through designing advanced tribological materials. Self-lubricating MMCs have advantages of improving wear resistance, reducing COF, and eliminating the need for external lubricants to avoid seizing. Bidaki and Akhlaghi [33] concluded that self-lubricating materials are characterized by their capability for transferring microscopic amounts of lubricant material, which creates a film that shows the lubrication and reduces friction over the contact surface. MMCs reinforced with graphite particles are self-lubricating and have superior wear resistance and reduced COF since the graphite particles work as a solid lubricant between contact surfaces.

E. Omrani et al. [34] stated that aluminum/graphite (Al/Gr) composites are examples of self-lubricating materials which have been used because of their superior lubricating effects of graphite during sliding process. The effects of different parameters such as (a) material properties, graphite size, and volume fraction and (b) mechanical factors, applied load, and sliding speed on the tribological properties of self-lubricating aluminum composites are important. To reduce the external use of petroleum-based lubricants in sliding contacts, self-lubricating composites can be used into different operating systems is a solution in a way to help the environment and reduce energy dissipation in industrial components in order to increase sustainability and energy efficiency. Self-lubrication is one of the capabilities of materials to transfer embedded solid lubricants, such as graphite to the contact surface to decrease wear rate and COF while there is not any external lubricant. Solid self-lubricating composites are usually solid carbon (carbon fibers graphite particles, CNTs, graphene), molybdenum disulfide, and hexagonal boron nitride [34, 35].

10.4 Conclusion

Recently, human activities changed the balance in the eco-system and caused several environment dangers which last for centuries. Environmental hazards are effecting the human, animal wildlife, plants, and our planet as a whole. Immediate thoughtful actions are necessary more than ever to help decreasing destructive human activities. Climate change is occurring right now, and there is no more time to waste for taking actions. Some materials have negative impact on the eco-system which should be redesigned and modified. Currently there are lots of products which design has been significantly modified to be more environmental friendly and sustainable. For instance, lubricant materials have been improved based on latest science to reduce their discharging wastes. The positive effects of eco-tribological materials in reducing energy consumption and increasing the lifetime of the products have been also discussed. Self-lubricant composites such as aluminum/graphite (Al/Gr) composites which have been mentioned in this study have significantly less drawbacks than some common lubricants. This study was a comprehensive review of the environmental concerns and advances of eco-tribological, lubricant, and self-lubricant composites.

References

1. Balali, M.H., Nouri, N., Rashidi, M., Nasiri, A., Otieno, W.: A multi-predictor model to estimate solar and wind energy generations. Int. J. Energy Res. (2017). https://doi.org/10.1002/er.3853
2. N. Earth Observatory, (2015)
3. United States Environmental Protection Agency. (2011)
4. Markham, D.: Global Warming Effects and Causes: A Top 10 List. planetsave.com. (2009)
5. Report, IPCC Fourth Assessment, (2007)
6. N. Report, A blanket around the Earth
7. NASA, Vital Signs of Planet Blobal Climate Change

8. Sasaki, S.: Environmentally friendly tribology (Eco-tribology). J. Mech. Sci. Technol. **24**, 67–71 (2010)
9. Zarandi, M.A.F., Pillai, K.M.: "Spontaneous imbibition of liquid in glass fiber wicks, Part II: Validation of a diffuse-front model," Transport Phenomena and Fluid Mechanics. AlChe. (2017). https://doi.org/10.1002/aic.15856
10. Zhang, S.-W.: Green tribology: fundamentals and future development. Short Commun. **1**, 186–194 (2013)
11. Shafiee, S., McCay, M.H.: A Hybrid energy storage system based on metal hydrides for solar thermal power and energy systems. In: Proceedings of ASME 2016 10th International Conference on Energy Sustainability, Charlotte (2016)
12. Zhang, S.W.: Current industrial activities of tribology in China. In: Plenary Lecture to the 5th China International Symposium. Beijing, China (2008)
13. Balali, M.H., Nouri, N., Nasiri, A., Seifoddini, H.: Development of an economical model for a hybrid system of grid, PV and energy storage systems. In: International Conference on Renewable Energy Research and Applications (ICRERA), Palermo, pp. 1108–1113 (2015) https://doi.org/10.1109/ICRERA.2015.7418582
14. Balali, M.H.: An Economical Model Development for a Hybrid System of Grid Connected Solar PV and Electrical Storage System. Theses and Dissertations, University of Wisconsin Milwaukee UWM Digital Commons (2015)
15. Balali, M.H., Pichka, K., Nouri, N., Seifoddini, H., Yue, X.: Classifying US states for facility location decisions using clustering algorithm. Int. Res. J. Appl. Basic Sci. **10**(2), 166–172 (2016)
16. Bartz, W.J.: Ecotribology: environmentally acceptable tribological practices. Tribol. Int. **39**, 728–733 (2006)
17. Tzanakisa, I., Hadfield, M., Thomas, B., Noya, S., Henshaw, I., Austen, S.: Future perspectives on sustainable tribology. Renew. Sust. Energ. Rev. **16**, 4126–4140 (2012)
18. Zhang, S.-W.: Green tribology: fundamentals and future development. Friction. **1**(2), 186–194 (2013)
19. Stojilković, M., Golubović, D., Ješić, D.: Ecotribology aspects in the lubricants application. 6th International Symposium on Exploitation of Renewable Energy Sources. EXPRES (2014)
20. Bronshteyna, L., Kreiner, J.: Energy efficiency of industrial oils. Tribol. Trans. **771–776**(4), 42 (1999)
21. U. E. I. A. EIA. http://www.eia.gov/totalenergy/data/annual/showtext.cfm?t=ptb0208
22. Howarth, G., Hadfield, M.: A sustainable product design model. Mater. Des. **27**, 1128–1133 (2006)
23. Holmberg, K., Erdemir, A.: Global impact of friction on energy consumption, economy and environment. FME Trans. **43**, 181–185 (2015)
24. Suda, S.: Developments in cutting fluids for MQL cutting. Tribologist. **47**(7), 550–556 (2002)
25. Sassaki, S.: The effects of surrounding atmosphere on the friction and wear of alumina, zirconia, silicon carbide and silicon nitride. Wear. **134**, 134–185 (1989)
26. Ji, L., Li, H., Zhou, F., Quan, W., Chen, J., Zhou, H.: Fullerene-like hydrogenated carbon films with super-low friction and wear, and low sensitivity to environment. J. Phy. D Appl. Phys. **43**, 015404 (2010)
27. Rodriguez, V., Sukumaran, J., Schlarb, A.K., DeBaets, P.: Influence of solid lubricants on tribological properties of polyetheretherketone (PEEK). Tribol. Int. **103**, 45–57 (2016)
28. Rudnick, L.: Lubricant Additives in Chemistry and Applications. CRC Press, Boca Raton (2009)
29. Briscoe, B., Lin Heng Yao, J., Stolarski, T.A.: The friction and wear of poly (tetrafluoroethylene)-poly (etheretherketone) composites: An initial appraisal of the optimum composition. Wear. **108**(4), 357–374 (1986)
30. Schroeder, R.: Failure mode in sliding wear of PEEK based composites. Wear. **301**, 717 (2013)
31. Moghadam, A.D., Schultz, B.F., Ferguson, J.B., Omrani, E., Rohatgi, P.K., Gupta, N.: Functional metal matrix composites: self-lubricating, self-healing, and nanocomposites-an outlook. JOM. **66**, 872 (2014)

32. Moghadam, A.D., Omrani, E., Menezes, P.L., Rohatgi, P.K.: Mechanical and tribological properties of self-lubricating metal matrix nanocomposites reinforced by carbon nanotubes (CNTs) and graphene – a review. Compos. Part B. **77**, 402–420 (2015)
33. Akhlaghi, F., Zare-Bidaki, A.: Influence of graphite content on the dry sliding and oil impregnated sliding wear behavior of Al 2024–graphite composites produced by in situ powder metallurgy method. Wear. **266**(1–2), 37–45 (2009)
34. Omrani, E., Moghadam, A.D., Menezes, P.L., Rohatgi, P.K.: Influences of graphite reinforcement on the tribological properties of self-lubricating aluminum matrix composites for green tribology, sustainability, and energy efficiency – a review. Int. J. Adv. Manuf. Technol. **85**, 325–346 (2016)
35. Balali, M.H., Nouri, N., Omrani, E., Nasiri, A., Otieno, W.: An overview of the environmental, economic, and material developments of the solar and wind sources coupled with the energy storage systems. Int. J. Energy Res. (2017). https://doi.org/10.1002/er.3755

Molecular Dynamics Simulation of Friction in Self-Lubricating Materials: An Overview of Theories and Available Models

11

Ali Bakhshinejad, Marjan Nezafati, Chang-Soo Kim, and Roshan M D'Souza

Contents

Abstract

In this chapter, an overview of theories and investigated computational models is presented. Among all available theoretical models, Quantum Mechanics (QM), Molecular Mechanics (MM), Monte Carlo (MC), and Molecular Dynamics (MD) are the most used models. MD was selected as the focus of this chapter, because of its high accuracy in predicting the molecular level motions while keeping the computational costs relatively low as well as availability of well-established modeling softwares (i.e., LAMMPS). MD models have been used to investigate mechanical and chemical behaviors of different phenomena, including friction and self-lubrication. The authors further reviewed available MD models in previous literatures with focus on self-lubricating materials. These models direct the contribution of different self-lubricating agents including graphite,

A. Bakhshinejad (✉) · M. Nezafati · C.-S. Kim · R. M. D'Souza
University of Wisconsin-Milwaukee, Milwaukee, WI, USA
e-mail: Bakhshi3@uwm.edu; nezafati@uwm.edu; kimcs@uwm.edu; dsouza@uwm.edu

P. L. Menezes et al. (eds.), *Self-Lubricating Composites*,
https://doi.org/10.1007/978-3-662-64243-6_11

graphene, MoS_2, and poly tetra-fluoro ethylene (PTFE) on the friction behavior of different composites. This review was conducted in order to show the power of computational modeling to predict the molecular level behaviors of different physical models.

11.1 Introduction

Friction, the force resisting relative motion between contacting surfaces and generating heat by converting kinetic energy, can be formulated as a function of normal load and coefficient of friction (COF).

$$F = \mu P \tag{11.1}$$

COF (expressed by μ) is a dimensionless scalar which is directly related to the material property and P is the normal load pressing the surfaces together. This theory was first formulated by Amontons (1699) and advanced by Coulomb (1785), and the equation is well known as Amontons-Columb law.

Wear is another phenomenon that happens in case of contact. In this process, one or both in-contact surfaces will lose material under mechanical and/or chemical processes [1]. The wear rate of the materials can be evaluated using two commonly used methods: (1) weight loss and (2) volume loss [2].

In most of the applications, liquid- or greased-based lubricants are used to reduce the effects of friction and wear. Lubricants are made of materials with lower shear strength compare to sliding surfaces [1]. Therefore, this layer of material between two sliding surfaces reduces friction during relative motion. Under extreme conditions, such as vacuum, extreme temperatures (low or high), and pressure contact and radiation, using the liquid lubricants becomes challenging. Under these circumstances, solid lubricants are the alternatives. These lubricants are made of low shear strength materials and functions same as liquid-based lubricants [3–5].

As opposed to the liquid-lubricants, a constant supply of solid-lubricants can be challenging. The most avant-garde solution to this challenge was the introduction of self-lubricating materials. A self-lubricating material is a composite with its matrix reinforced using solid lubricants such as graphite, MoS_2, (Fig. 11.1). These materials facilitate the relative motion by incorporating a self-dispensed and self-regulated

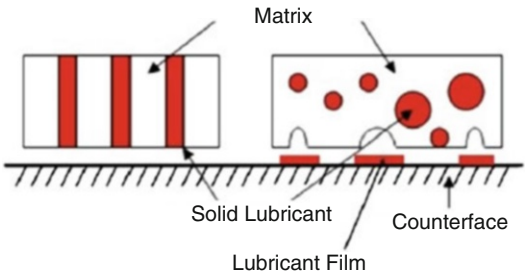

Fig. 11.1 Schematic of self-lubricating composites and its mechanism [15]. (With permission of Springer)

solid-lubricant delivery system. Since the initial development of self-lubricating materials, different groups researched and developed a variety of self-lubricating materials [3–11].

As shown in the Fig. 11.1, the solid-lubricant particles continuously will be exposed to the surface due to wear against the contact surface. These solid-lubricant particles then form a thin layer of lubricants which reduces the friction and wear effect of sliding. These layers are not present initially and form as results of worn surface and subsurface deformation [2, 12]. Different industries can benefit from self-lubricating effect, from atomistic scale (i.e., atomic force microscopy [13]) up to macro scale (i.e., bearing [14]).

As mentioned earlier, Amontons-Columb law can estimate the COF as a function of friction and applied normal forces. Despite the great success of this theory in bulk models, the Amontons-Columb law fails to predict the micro−/nanoscale behavior of the friction. The micro−/nanoscale behavior can be well described as a many-body system. In order to simulate a many-body system, a suitable molecular model of the system is formulated and the molecular trajectories are calculated using different numerical schemes.

These trajectories then are used to calculate the properties of the system. Different methods have been developed over the years. Quantum Mechanical (QM), Molecular Mechanics (MM), Monte Carlo (MC), and Molecular Dynamics (MD) are the most commonly used models. Each of these methods has their own advantages and disadvantages. Based on the application and the requirements of the problem, one can select the most appropriate approach.

In the next section, the most used theoretical models are introduced briefly and MD is described in more details. After that, a summary of investigated MD simulation of dry friction and a few self-lubricating materials are presented.

11.2 Methods

The Quantum Mechanical (QM) method solves a simplified Schrodinger's equation for a many-particle system where particles are treated as wave functions. The equations describe the spatial probability distributions corresponding to the energy states and are solved to obtain saddle points or minima on the potential energy surface. The Schrodinger wave equation describing the motions of electrons and nuclei in a molecular system is:

$$H\psi = E\psi \tag{11.2}$$

where H is the Hamiltonian and calculates as:

$$H = E_k \ + E_p \tag{11.3}$$

Here E_k is the kinetic energy and E_p represents the potential energy. For a *3D* system, the wave function ψ depends on the 3N coordinates of all the particles and

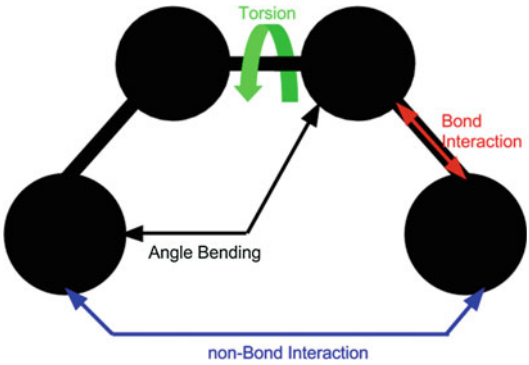

Fig. 11.2 Schematic representation of applied forces

therefore even for a relatively small number of particles, it is extremely difficult to solve the equation without simplifications or approximations. Despite the accuracy of the model which calculations match experimental data or a theoretical prediction, the exponential increment of computation time with the number of particles makes this method un-practical for more complicated models.

The Molecular Mechanics (MM) method is based on classical mechanics where atoms in the molecules are treated as particles with mass, which interact in a force field. The force field functions are obtained from quantum mechanics calculations. The bonds between the atoms are treated as springs and spring deformation is used to characterize bond stretching (E_{bond}), bending (E_{angle}), and torsion (E_{tor}) (Fig. 11.2). To mimic nonbonded atoms, van der Waals and electrostatic interaction are used ($E_{\text{non - bond}}$) (Fig. 11.2). Again, the aim is to find saddle points or minima on the potential energy surface using appropriate mathematical algorithms. The potential energy is typically the sum of all the energies associated with bonded and nonbonded interactions. A typical functional form of the potential energy function is:

$$E = E_{\text{bond}} + E_{\text{angle}} + E_{\text{tor}} + E_{LJ} + E_{\text{coul}} \tag{11.4}$$

$$E_{\text{bond}} = \sum_{\text{bonds}} \frac{1}{2} k_b (b - b_0)^2 \tag{11.5}$$

$$E_{\text{angle}} = \sum_{\text{angles}} \frac{1}{2} k_{\varnothing} (\varnothing - \varnothing_0)^2 \tag{11.6}$$

$$E_{\text{tor}} = \sum_{\text{tor}} \frac{1}{2} \tau [1 \pm \cos(n\alpha - \beta)] \tag{11.7}$$

$$E_{\text{non-bond}} = \sum_{\text{atomic pairs}} 4\varepsilon_{ij} \left[\left(\frac{\sigma_{ij}}{r_{ij}} \right)^{12} - \left(\frac{\sigma_{ij}}{r_{ij}} \right)^{6} \right] + k \frac{q_i q_j}{r_{ij}} \tag{11.8}$$

The bond stretching equation (Eq. 11.5) and bending energy equation (Eq. 11.6) are based on Hook's law. Here k_b represents the stiffness of the bond, b_0 stands for

the equilibrium length which both are depends on type of the bond (e.g., C–C, O–C, etc.), and b is the length of bond. Same as the bond stretching equation, in bending equation (Eq. 11.6), $k_{\varnothing}$ represents the stiffness of the angle, $\varnothing_0$ is the equilibrium angle, and $\varnothing$ stands for the angle of the bond. In order to correct the calculated energy (bond stretching energy + bending energy + non-bonded energy) and make it to agree with experimental measurements, the torsion energy (Eq. 11.7) was added to the energy equation as a periodic function. In this function (Eq. 11.7), τ controls the amplitude of the function and β shifts the function along the rotation angle axis (α). All parameters from torsion equation are assigned based on bond type (e.g., C-C-C-C, C-O-C-N). As mentioned before, van der Waals attraction, repulsion, and electrostatic interactions are taken into account as nonbonded energy (Eq. 11.8). The repulsion/attraction effect is modeled using Lennard–Jones potential where r_{ij} is the distance between two atoms and σ_{ij} and ε_{ij} are Lennard-Jones parameters depending on interacting atoms (e.g., C-O, C-H). The second term of Eq. 11.8 is Coulomb electrostatic potential where q is the partial charge of each atom and k is Coulomb's constant.

The Monte Carlo (MC) method is used to simulate systems with fixed N number of particles in a fixed volume V, at absolute temperature T. For such a system, MC as an iterative method tries to minimize the system's potential by randomly moving atoms into a new position. As the number of random numbers increases to infinity, the solutions get closer to the correct solution. In order to decrease the randomness and consequentially decreasing the computational time, since the Boltzmann factor causes the possible configurations to make non-uniform contributions, a sampling method can be implemented in the Metropolis method. Despite the MC's simplicity of implementation, it cannot be used to study time-dependent properties and is applicable only for configurations near equilibrium systems.

11.2.1 Molecular Dynamics

The Molecular Dynamics (MD) models can be categorized into two groups based on their formulation as classical and first-principles. In the classical approach, molecules are modeled as classical objects, something like "ball and stick" model. In this model, atoms are considered as soft balls and bonds model as elastic sticks, and the laws of classical mechanics define the dynamics of the system. The first-principles or quantum MD simulations take the quantum nature of chemical bonds into account explicitly. Despite its important improvement over the classical model, the computational cost of this model makes it impractical to implement. Therefore, in this section the classical MD model will be described and referred to as MD.

In MD simulation, the time evolution of a set of interacting particles is solved based on Newton's second law or the equation of motion for a many-body system as

$$F_i = m_i \frac{d^2 r_i(t)}{dt^2} \tag{11.9}$$

where F_i is the force acting on ith particle at time t and m_i is the mass of the particle. And $r_i(t)$ represents the position vector of ith particle at time t as $r_i(t) = (x_i(t),y_i(t),z_i(t))$. In MD, "Particles" usually refer to atoms, although they may represent any district entities that can be conveniently described in terms of a certain interaction law. To integrate the second-order differential equation of the equation of motion, the forces acting on each particle at each time step as well as their initial position and velocities need to be specified. Then the integration of the equations yields a trajectory that describes the position, velocities, and accelerations of the particles as they marching forward in time. As the particles move, their trajectories may be analyzed in order to calculate their average properties. Once the positions and velocities of each atom are known, the state of the system can be predicted at any time.

Interaction between particles can be calculated using force field or quantum chemical models, or via mixing force fields and quantum chemical models. The atomic force field model describes physical system as collection of atoms kept together by interatomic forces. The interaction law is specified by the potential $E(r_1,\ldots,r_N)$ (Eq. 11.4), which represents the potential energy of N interacting atoms as a function of their positions $r_i = (x_i,y_i,z_i)$. Given the potential, the force acting upon ith atom is determined by the gradient with respect to atomic displacements as:

$$F_i = -\nabla_{r_i} E(r_1,\ldots,r_N) = -\left(\frac{\partial E}{\partial x_i}, \frac{\partial E}{\partial y_i}, \frac{\partial E}{\partial z_i}\right) \tag{11.10}$$

Having the force fields as a function of particles location, one can calculate each particles position ($r_i(t + \Delta t)$) at time $t + \Delta t$ by integrating the Newton's equation of motion in time by knowing the positions at time t. Numerous numerical algorithms have been developed for integration. Some of the most used ones are: Verlet algorithm, Leap-frog algorithm, Velocity Verlet, and Beeman's algorithm. All the integration algorithms assume the position can be approximated by a Taylor series expansions. The basic formula for the Verlet algorithm can be expressed by writing two third-order Taylor expansion of the position $r(t)$, one forward and one backward in time:

$$r_i(t+\Delta t) = r_i(t) + v_i(t)\Delta t + \frac{1}{2}\frac{F_i(t)}{m_i}\Delta t^2 + \frac{1}{6} b_i(t)\Delta t^3 + O\left(\Delta t^4\right) \tag{11.11}$$

$$r_i(t-\Delta t) = r_i(t) - v_i(t)\Delta t + \frac{1}{2}\frac{F_i(t)}{m_i}\Delta t^2 - \frac{1}{6} b_i(t)\Delta t^3 + O\left(\Delta t^4\right) \tag{11.12}$$

where $v_i(t)$ represents the velocity and $b_i(t)$ the third derivative of position of the ith particle with respect to time. Adding the two expressions gives:

$$r_i(t+\Delta t) \cong 2r_i(t) - r_i(t-\Delta t) + \frac{F_i(t)}{m_i}\Delta t^2 \tag{11.13}$$

The truncation error of the algorithm when evolving the system by Δt is of the order of Δt^4. A problem with this version of the Verlet algorithm is that velocities are not directly calculated. While they are not needed for time evolution, their comprehension is sometimes necessary. Moreover, they are required to compute the kinetic energy K, whose evaluation is necessary to test the conservation of the total energy $E = K + V$. One simple way to calculate the velocity is by using the position as:

$$v_i(t) = \frac{r_i(t + \Delta t) - r_i(t + \Delta t)}{2\Delta t} \tag{11.14}$$

As one can immediately see, the error is not an order of Δt^4 anymore but Δt^2. To overcome this problem, different variations of the Verlet algorithm have been developed. The *leap-frog* and *velocity* Verlet scheme are two of many [16]. One cloud calculates the velocity using the *velocity* Verlet scheme as following:

$$r_i(t + \Delta t) = r_i(t) + v_i(t)\Delta t + \frac{1}{2}\, a_i(t)\Delta t^2 \tag{11.15}$$

$$v_i\left(t + \frac{\Delta t}{2}\right) = v_i(t) + \frac{1}{2}a_i(t)\Delta t \tag{11.16}$$

$$a_i(t + \Delta t) = -\frac{1}{m_i}\nabla_{r_i} E_i(r(t + \Delta t)) \tag{11.17}$$

$$v(t + \Delta t) = v\left(t + \frac{\Delta t}{2}\right) + \frac{1}{2}a(t + \Delta t)\Delta t \tag{11.18}$$

These equations can be solved in an iterative fashion. By setting the initial values of positions and velocities, one can numerically solve the above equations to obtain the new position and velocities. Once all the trajectories are obtained, they can be used to calculate other static and dynamic properties as well as system temperature.

As it can be observed, MM and MD are both based on classical mechanics and have some fundamental similarities. Both methods are computationally fast, can handle large number of atoms, and are using potentials obtained by QM. However, the advantage of MD compare to MM is that this method is capable of capturing the dynamic of the system and therefore ease of calculating non-equilibrium state of the system.

11.3 Simulating Friction Using Molecular Dynamics

Different research groups were trying to develop an equipment to measure the friction phenomena in the atomic level and validate the theory. The first atomic friction measurements were reported by Mate et al. [17]. Development of the atomic force microscope (AFM) enabled researchers to quantitatively measure friction forces. Since the first measurement, the AFM experiment setup has not changed a

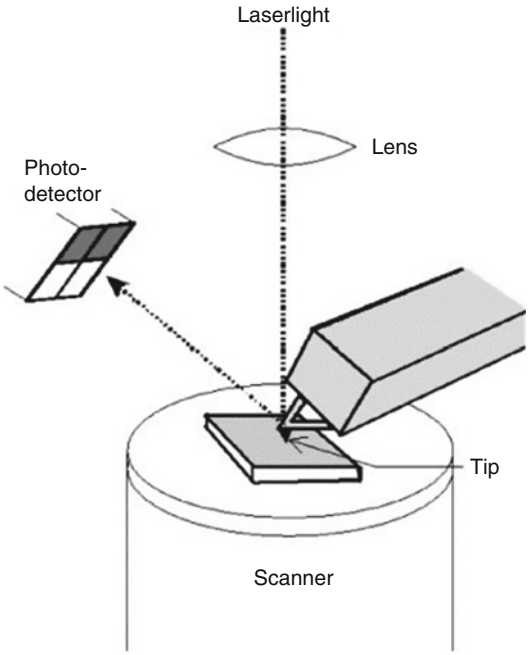

Fig. 11.3 Schematic of an atomic force microscope (AFM). (Reprinted from [18], Copyright 2005, with permission from Elsevier)

lot. An AFM setup consists of a nanoscale tip mounted on a microscale cantilever as well as a fixed substrate as schematically shown in Fig. 11.3. Moving the tip against the substrate under a small normal load of a few nano-Newton causes a torsion twisting in the cantilever. The torsional twisting is caused by the lateral force recorded by an optical technique. Moving the tip back and forth generates a force contrast pattern called a lateral force image (friction image), or a lateral trace (friction trace) which shows the resistance of the substrate to sliding tip. The variation of the friction trace is often not smooth due to the atomic discreteness of the surface, but it is more like a saw-tooth pattern refer to as stick-slip friction. It is called stick-slip since the tip sticks at some position for a while and then slips forward in the direction of the lateral forces. The stick-slip pattern can be used for friction-related quantities such as frictional resistance of the surface.

It has been shown that in dry surface contact, only a small number of micro- and nano size asperities come into contact. The friction between each asperity and the substrate called atomic friction. The process of how these asperities come into contact has a significant influence on the frictional characterization of the sliding surfaces. Taking advantage of computer experiment, one can predict the friction forces using different available models such as MD by calculating atom trajectories by computing Newton's Second law. Since predicting and modeling this level of complexity requires a large amount of computational power and effort, many researchers simplified their study by focusing on the sliding of single micro−/nanoscale asperity surface. This fundamental understanding becomes even more

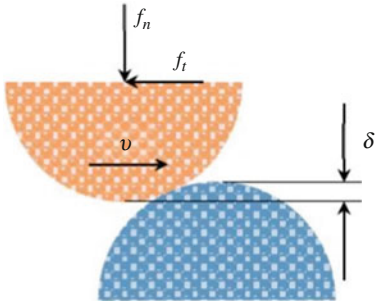

Fig. 11.4 Schematic asperity-asperity interaction [20]

relevant when we are looking at small-scale applications like Micro-electromechanical systems (MEMS) and Nanoelectromechanical systems (NEMS).

For better understanding, a single asperity-asperity interaction is described here (Fig. 11.4). In this model, an asperity on a moving base slides past on a stationary-based asperity under controlled velocity and normal load. The atoms on these asperities are initially at equilibrium where the attraction and repulsive forces from other atoms are balanced. As soon as the interaction starts, atoms in contact are no longer in balance. Under the influence of the interaction and the amount of forces applied on atoms, these atoms are moving away from their original position and may or may not return. Depending on the movement distance, if it is smaller than the bond length, by removing the forces atoms are able to get back to their original position. Otherwise, the atoms are displaced to the new positions. This model is the basis of different phenomena such as adhesion, plastic deformation, wear, and energy dissipation. As Gao et al. [19] showed, the number of atomic or molecular bonds that are broken or formed are directly proportional to the adhesion. Therefore, better understanding of this interaction can help with advancing the understanding of the other phenomena.

Bhavin et al. [21] developed a three dimensional geometrical model consists of two asperities each connected to a base in order to investigate the effect of different variables on friction coefficient. With moving one of the bases, the asperity-asperity interaction was modeled. Copper was chosen as the material in a lattice with the size of $3.615A^{\circ}$ with different orientation angles. The effect of different velocities was investigated as 10 *m/s* and 100 *m/s*. The time-step size was chosen as 0.002 ps. And the boundary condition was set to periodic at x and z-direction and shrink-wrapped in y-direction. In periodic directions, atoms can interact across the boundary, and they can exit from one end and enter from another end of the domain. As the shrink wrapping direction, the position of the face is set so as to encompass the atoms, no matter how far they move. As the result of the sliding (Fig. 11.5), they have studied effects of changing dimensions (radius of asperities (R) and interference (δ) as shown in Fig. 11.4), forces, sliding velocity, and lattice size for asperity-asperity interaction.

Using MD simulation other researchers were able to investigate different friction models. The atomic-scale friction of two diamond surfaces was modeled by Harrison et al. [22]. In this study as one of the early MD studies, they analyzed the friction as a

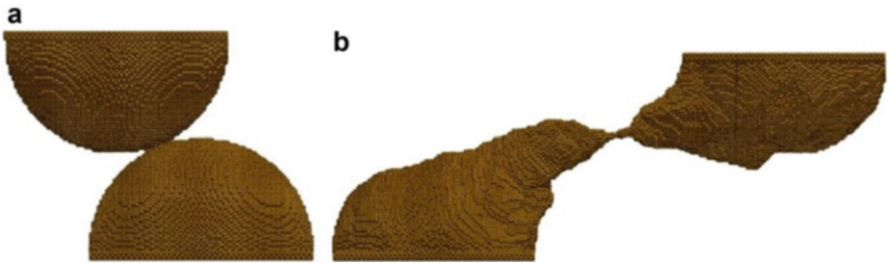

Fig. 11.5 Copper asperities before (**a**) and after (**b**) sliding process for $R = 7.5\ nm$, $v = 10\ m/s$ and $\delta/R = 0.1$ [20]

function of applied load, temperature, and sliding velocity. Zhang and Tanaka [23] showed four different deformation regimes as no-wear, adhering, plowing, and cutting of the surface by sliding a diamond tip on a flat copper. Song and Srolovitz [24] studied the effect of loading and unloading of forces between a single asperity surface and a flat surface. During repetitive contact, they observed the transformation from face-centered cubic into hexagonal close packed structure. Liu et al. [25] studied the effect of scratch direction on the friction coefficient. Zhang et al. [26] used MD to investigate the effect of stiffness of graphene on its friction behavior. The nanoscale friction between diamond-structure silicon (Si) and diamond was investigated by Bai et al. [27]. They have divided the friction into two stages: the static friction and the kinetic friction. The effective friction coefficient in a granular material was studied by Hurley and Andrade [28]. Hu et al. [29] studied the effect of adding Cu nanoparticles to the solid contact between friction surfaces. They have found that the friction forces are decreasing by increasing the sliding velocity. The atomic-scale friction of diamond (111) surface with boron doped diamond (111) surface was modeled by Wang et al. [30]. The effect of temperature and its relationship with roughness in dry sliding was studied by Spijker et al. [31]. Yang et al. [32] studied the nanoscale friction forces between hemisphere sphere sliding on rectangular solid plane. They have shown that with increasing the depth of the contact, the atoms close-packed accumulation increases.

11.4 Molecular Dynamics Simulation for Self-Lubricant Materials

MD simulations [13] have shown that the self-lubrication mechanism in two sliding surfaces is due to stabilization of the atomic cluster adsorbed from one surface to the other and the ability of the cluster structure adjustment. The self-lubricating ability of the material can be achieved by modifying the composition of the matrix with graphite [2, 9], graphene [33, 34], carbon nanotubes [35, 36], or inert polymeric molecules such as poly tetra-fluoro ethylene (PTFE) [10, 13]. Although the general influences of these components are similar, they each obey specific mechanism to result in self-lubricating effect.

11.4.1 Graphite and Graphene

The layered structure of graphite is a result of strong electronic σ-bonds between carbon atoms within a layer and weak electronic π-bonds between carbon atoms in adjacent layers. In this atomic structure, π-electrons play a dominant role in the intercalation among the carbon atoms and interactional atoms and facilitate the sliding process and reduce the friction between layers [9]. Yin et al. [37] modeled the sliding process and self-lubricating mechanism in alumina-graphite composite coating using MD simulation. Their model presents the preferred orientation for the hexagonal structure of graphite under shear forces during sliding of friction pairs. Figure 11.6 demonstrates the MD model, as two alumina surface glide under shear forces and the graphite shows significant stratification in the Z-direction. Over the simulation time the layers of graphite are adsorbed to the surfaces of the friction pair and decrease the chemical affinity between the contacting surfaces. Formation of layered structure of graphite with weak forces in c-direction and low adhesion explains the self-lubricating mechanism in the alumina-graphite composite.

As a two-dimensional material of sp2 carbon network, graphene has been introduced as an efficient solid lubricant [33]. Xu et al. [34] applied MD models to describe the "stick-slip" mechanism in few-layer (3–8) graphene (FLG). They divided the process to three stages including the initial stage, the developing stage, and the stable sliding stage to develop stable sliding interfaces. Their model contained 3–8 AB stacked graphene layers while each layer was composed of 3200 carbon. The top view of their system has been demonstrated in Fig. 11.7. The bottom layer shown in white has been fixed, and a constant velocity was applied to the two top layers in the shear direction, while they had constraints in other two orthogonal directions.

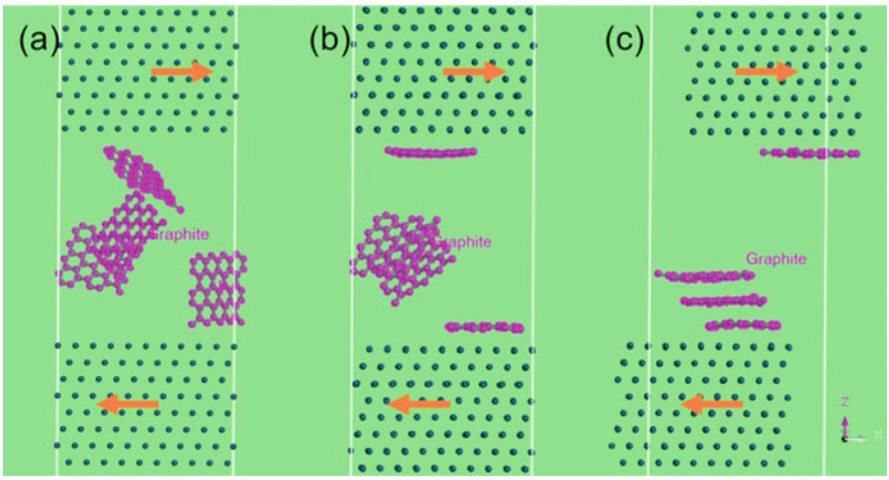

Fig. 11.6 MD model of sliding pair interface containing random graphite sheets after (**a**) 0 ps, (**b**) 30 ps, (**c**) 90 ps. (Reprinted from [37], Copyright 2016, with permission from Elsevier)

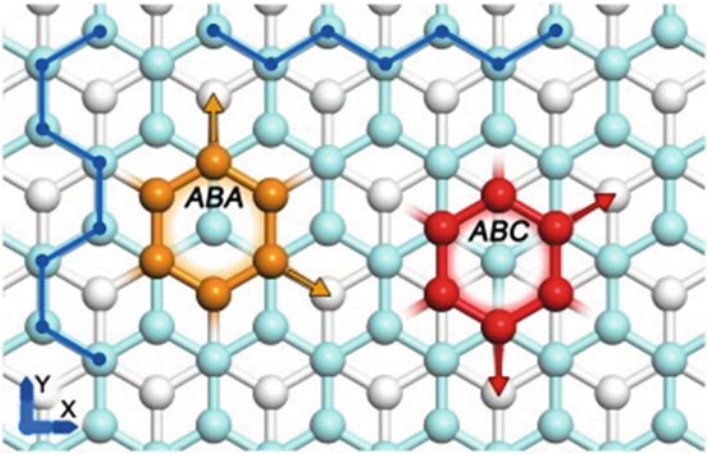

Fig. 11.7 Possible slip directions for the top layer in a three-layer graphene. The bottom layer and middle layer atoms are demonstrated in white and cyan, respectively, while the atoms of top layer with ABA and ABC stacking configurations have been presented in orange and red, respectively. (Reprinted from [34], Copyright 2012, with permission from Elsevier)

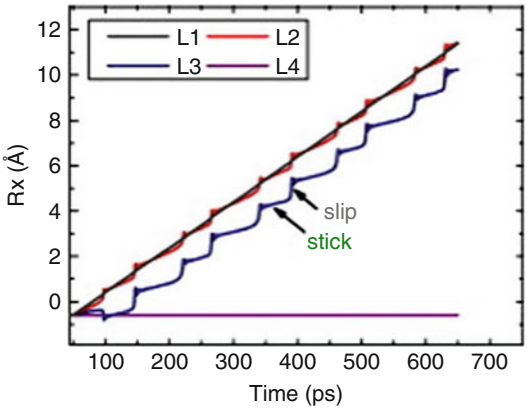

Fig. 11.8 Slip and stick during the motion of four graphene layers sliding in x-direction. (Reprinted from [34], Copyright 2012, with permission from Elsevier)

A sudden slip is observed after stick period in Fig. 11.8. The lateral stiffness of sliding body, which is greatly reduced by the existence of multiple weak interlayer interfaces, is always smaller than the lateral contact stiffness at the sliding interface, resulting in stick-slip system according to PT model (Prandtl-Tomlinson model) [38]. PT model suggests that the stick-slip feature is inevitable for systems containing more than three layers of graphene. This model confirms that the friction forces drop dramatically with decreasing the number of graphene layers, and they vanish as the number of layers decreases to three or two layers. Nanolubrication and self-lubricating materials can benefit from this mechanism of sliding in layers of graphene.

Graphene is also known to potentially control the nanowear on some substrates. The MD model by Zhang et al. [39] proves that during C_{60} intrusion, graphene can control nanowear. This MD Model consists of one lower and one upper substrates of Si (100) containing 4145 and 716 atoms, respectively. Depending on the position of the graphene layer covering each of these substrates, four different cases were compared as demonstrated in Fig. 11.9. In all the cases, the two surfaces made an angle (α) where the lower substrate was horizontal and a C_{60} intruding through the sliding substrates. The nanowear for the contact surface was evaluated by the number of dropped atoms (Si atoms that displaced more than the cutoff distance of 0.27 nm from the substrate). Figure 11.9 displays four different conditions for the nanowear test. In Fig. 11.9a the highest amount of wear is observed during intrusion of C_{60} between Si surfaces. Figure 11.9b shows the system when the upper substrate is layered by graphene. In this case the interactions among the C_{60} and two substrates are smaller than the first case. The upper substrate still bends during sliding and some of the Si atoms were pulled off from the bottom of the upper substrate. The third case is when only the lower substrate is layered by graphene as demonstrated in Fig. 11.9c. The MD calculations showed that in this case and also in a system including two graphene layers on both upper and lower substrates (Fig. 11.9d), no Si atom is pulled off from either of the substrates and only a slight bending is observed on the upper substrate. This MD model showed that through layering graphene on the substrate surfaces nanowear can be controlled in the system and no-wear of the sliding substrates can be realized.

11.4.2 Carbon Nanotubes (CNT)

Carbon nanotubes (CNTs) can be described as a rolled sheet/s of carbon atoms. Depending on the number of sheets, it can be single-walled carbon nanotubes (SWCNTs) with diameter of 1–2 nm or double- and multiwalled carbon nanotubes with diameter ranging from 4 to 20 nm (Fig. 11.10) [35].

Yao and Lordi [40] measured the SWCNTs stiffness using MD simulation as 1 TPa. Despite better mechanical property of SWCNTs compared to multiwalled carbon nanotubes (MWNTs), due to their higher production expenses, SWCNTs are less employed as a reinforcement. One of the limitations of MWNTs is telescoping effect where inner tubes can be pulled out from outer tubes due to tensile stresses. Interfacial friction and sliding of SWCNTs and MWCNTs embedded in an amorphous carbon matrix were modeled using MD by Li et al. [36]. Pavia and Curtin [41] also studied the interfacial sliding effect in ceramic composites using MD.

The mechanical behavior of individual single and multiwalled carbon nanotubes has been exclusively modeled and studied by different groups using MD. Zhao et al. [42] estimated the binding energy of two parallel SWCNTs as well as two cross MWCNTs using MD. The self-assembly process of edge-unpassivated graphene nanoribbons with defects using SWNCT was modeled by Zhang and Chen [43]. The vibration characterization of single and double carbon nanotubes was studied using MD models by Ansari et al. [44]. Ghosh and Padmanabhan [45] modeled the effect

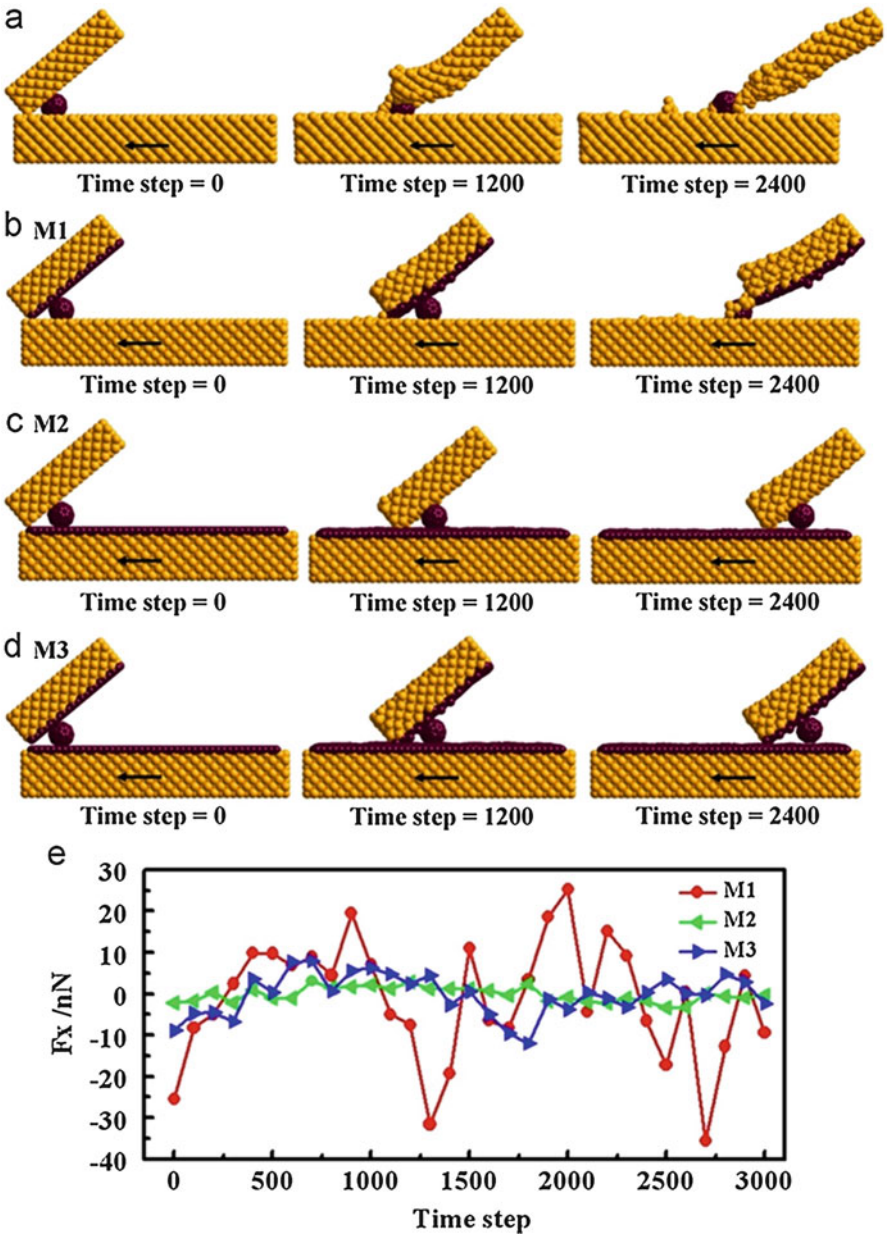

Fig. 11.9 MD model snapshots during *C*60 ball intrusion (**a**) for two sliding Si substrates, (**b**) upper substrate layered by grapheme, (**c**) lower substrate layered by graphene, (**d**) both upper and lower substrates layered by graphene. (Reprinted from [39], Copyright 2012, with permission from Elsevier)

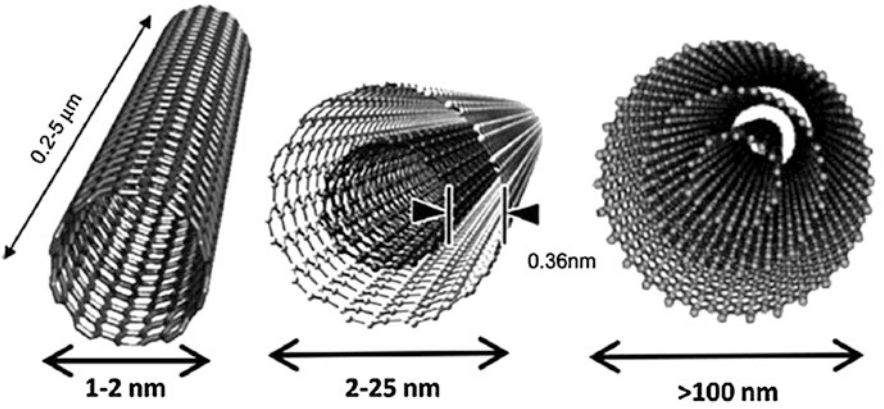

Fig. 11.10 Single-, double-, and multiwalled carbon nanotubes (CNTs). (Reprinted from [35], Copyright 2015, with permission from Elsevier)

of different types of defection on SWCNTs capacity of hydrogen adsorption using both MD and density functional theory (DFT). These publications are just a few of so many of available studies in the literature on the behavior of carbon nanotubes.

Despite exclusive studies using MD simulation of individual SWCNTs and MWCNTs in the literature, to the best of authors' knowledge, there is no specific MD study, addressing the lubricating behavior of composites using carbon nanotubes as reinforcement.

11.4.3 MoS_2-Based Nanostructures

D-transition metal dichalcogenides (TmS_2, Tm = Mo, W, Nb, and Ta) not only reduce the friction coefficient as lubricant materials, but also they maintain their lubricating capability at higher loads compared to the traditional lubricants. The tribological properties of these materials can even enhance if they are applied in the form of spherical or cylindrical nanostructures. The "bearing effect" is known to be responsible for this enhancement. Due to this effect the nanoparticles enter the intersurface area and act as a ball bearing during the sliding of the two surfaces against each other [46]. Among this group of materials, MoS_2 has been the center of attention in recent studies. Dallavalle et al. [47] introduced an MD model to describe the lubrication effect of MoS_2 nanotubes. They simulated the sliding of the top layers by keeping the velocities of the top sulfur atoms constant in the a-direction and unrestricted in the b- and c-directions. The sliding direction was kept constant during the simulation, while a normal load was applied on the top surface as demonstrated in Fig. 11.11. The model studies the sliding process in both a- and b-directions for an armchair double-wall nanotube, indices pairs such as (29,29)@(36,36). Constant number, volume, and temperature (NVT) ensemble at 298 K was used for all the calculations with sliding velocity of 100 m/s. The sliding of the double walled

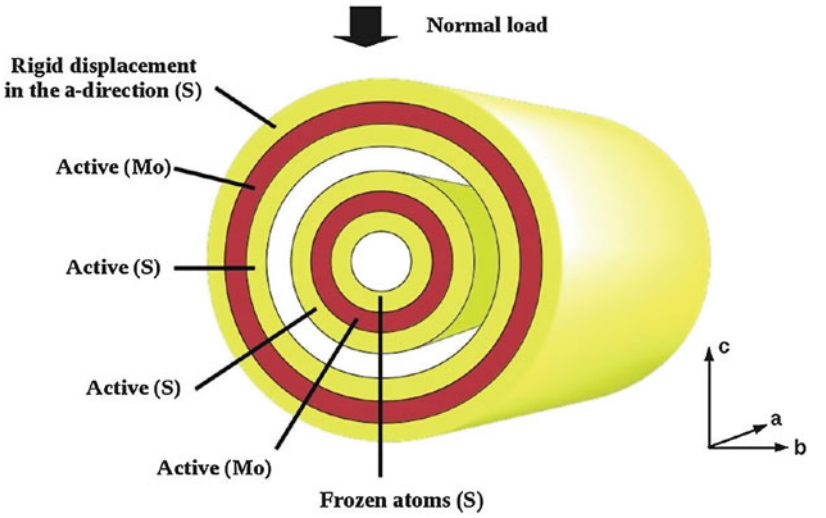

Fig. 11.11 Schematic of DWNT during the sliding modeled with MD simulation. A normal load is applied in the c-direction and the motion of the DWNT is rigid in a-direction. (Reprinted with permission from [47]. Copyright 2012 American Chemical Society)

nanotube (DWNT) in a-direction showed that the top layer slides along a sinusoidal, zigzag rout, because the sulfur atoms avoid each other and try to stay close to molybdenum atoms. For sliding in b-direction, the top layer has a random motion with an occasional large diagonal movement.

This model averages the frictional coefficient over the forces of the sulfur atoms, from auto-correlation function (ACF) of the forces using Green-Kubo equation (Eq. 11.19) and the friction coefficient from classical physics Amonton's laws (Eq. 11.20).

$$K = c \int_0^{\infty} < A(t)d(t) > \tag{11.19}$$

where K is the friction coefficient, A are the forces experienced by the system in the friction process, and in Eq. 11.20, F is the lateral friction force and L is the normal, externally applied load.

$$\mu = \frac{F}{L} \tag{11.20}$$

They showed that the friction differs for sliding in a- and b-direction because of the smaller oscillations observed during the dynamics and sudden diagonal displacement of MoS_2 layer in b-direction. The microscopic model based on the Green-Kubo equation demonstrates a high lubricating performance of MoS_2 in optimal conditions. They also showed a reverse relationship between the friction coefficient and

force, which can be explained by increase in repulsive contribution of the Lennard-Jones potential at higher loads. This contribution results in better sliding and lower friction coefficient in MoS_2 DWNTs.

11.4.4 Poly Tetra-Fluoro Ethylene (PTFE) (Polymeric Agents)

Poly tetra-fluoro ethylene (PTFE) can be applied in metal-, ceramic-, and carbon-based composites to improve the mechanical and thermal properties and more importantly to decrease the friction [6–8]. This resin has excellent antiwear performance. It is chemically stable and naturally softer than conventional metals, so; it can reduce the friction if applied as sliding parts between sliding metallic surfaces. It has been suggested that the formation of transfer films is responsible for the friction reduction [48]. Although the thickness of this film is only few nanometers, its presence between sliding PTFE and metallic surface reduces the friction and results in self-lubricating effect in the composite. Here we will go over some atomistic models covering both formation of the nanoscale transfer film and also the self-lubrication mechanism in corresponding composites.

Onodera et al. [10] evaluated the friction behavior of aluminum surface considering the chemical reaction with Polytetrafluoroethylene. Their model benefited from quantum chemical molecular dynamics (QCMD) method and considered aluminum oxide to represent a typical surface of aluminum alloy. α-Al_2O_3 and three layers of PTFE chains aligned parallel to the α-Al_2O_3 surface form the geometry of the model. The topmost surface of α-Al_2O_3 was fully terminated by the OH groups to represent the chemisorption of water vapor from the atmosphere in contact with the aluminum surface. Mechanical forces on the α-Al_2O_3 layer consist of vertical pressure of 500 MPa forcing the oxide toward the polymeric layers and the shear velocity of 100 m/s resulting in the sliding of the α-Al_2O_3 over the polymer. One bottom layer of the crystalline PTFE was fixed to represent the bulk material. This model suggested that the formation of the transfer film is conditional to elimination of the interfacial electrostatic repulsion between two sliding surfaces. Such repulsive forces are the result of formation of aluminum fluoride due to reaction of the aluminum atom from the surface oxide with the fluorine from the PTFE chain during the sliding. In another model [11], they showed that the tribological performance of the surface can be enhanced by the chemical reaction of the aluminum surface with water vapor in the atmosphere. The carboxyl group that forms as a product of such reaction results in increasing the amount of transfer film on aluminum surface and consequently improving the self-lubrication behavior of the surface. They used classical MD method to study the sliding of the PTFE/aluminum interface with three different structures as demonstrated in Fig. 11.12. The first configuration in Fig. 11.12a represents the interface between OH-terminated α-Al_2O_3 and genuine PTFE prior to their tribochemical reaction, Fig. 11.12b shows the tribochemical reaction on the α-Al_2O_3/*PTFE* interface and the F-terminated α-Al_2O_3/*genuine* PTFE interface. Figure 11.12c also models the F-terminated α-Al_2O_3/*genuine* PTFE interface where the top layer of PTFE contains

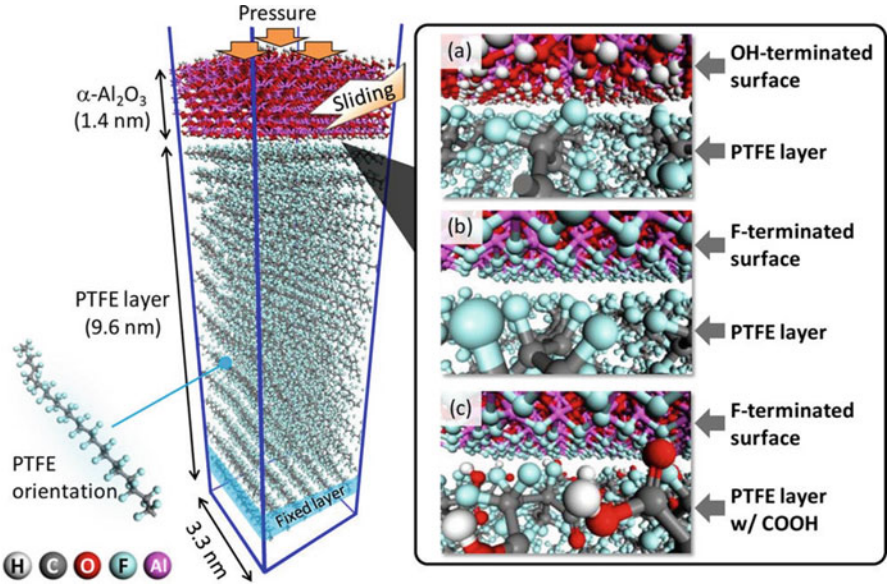

Fig. 11.12 Transfer film formation on PTFE α-Al_2O_3 (**a**) PTFE/OH-terminated α-Al_2O_3 (**b**) PTFE/F-terminated α-Al_2O_3 and (**c**) PTFE with carboxyl group/F-terminated α-Al_2O_3. (Reprinted with permission from [11]. Copyright 2014 American Chemical Society)

several carboxyl groups as a product of chemical reaction between PTFE and water vapor. A periodic boundary condition was applied to the system for the MD model at temperature of 300 K. The topmost layer of α-Al_2O_3 was under vertical pressure in such way that on a real contact area of PTFE/Al system, the pressure was set to a few hundred mega-pascals (500 MPa) in the molecular-level because on a real contact area of PTFE/Al system, the pressure is much higher than a macroscopic contact pressure which is typically in the mega-pascal order. The bottom layer of the PTFE was fixed and sliding parallel to PTFE chains with velocity of 10 m/s was applied to the α-Al_2O_3 as demonstrated in Fig. 11.13. In the first model in Fig. 11.13a, the PTFE transfer film was generated on the OH-terminated surface and the sliding interface appeared between the PTFE layers and not in the *PTFE*/α-Al_2O_3 interface. The second model in Fig. 11.13b, which represents an F-terminated α-Al_2O_3 surface only two of the PTFE layers form the transfer film. The chemical reaction between PTFE and α-Al_2O_3 is responsible for the difference between these two models. When the hydroxyl group stays on the α-Al_2O_3 surface, the electrostatic attraction between the hydrogen atoms and fluorine atoms in PTFE facilitates the transfer of PTFE. On the other hand when the α-Al_2O_3 is terminated by fluorine atoms, the electrostatic repulsion between PTFE and the F-terminated α-Al_2O_3 inhibits the transfer of PTFE layer. The third model is when the carboxyl group forms as a product of interaction with water vapor. In such case as shown in Fig. 11.13c although the surface was terminated by fluorine atoms, three or four layers of PTFE were transferred.

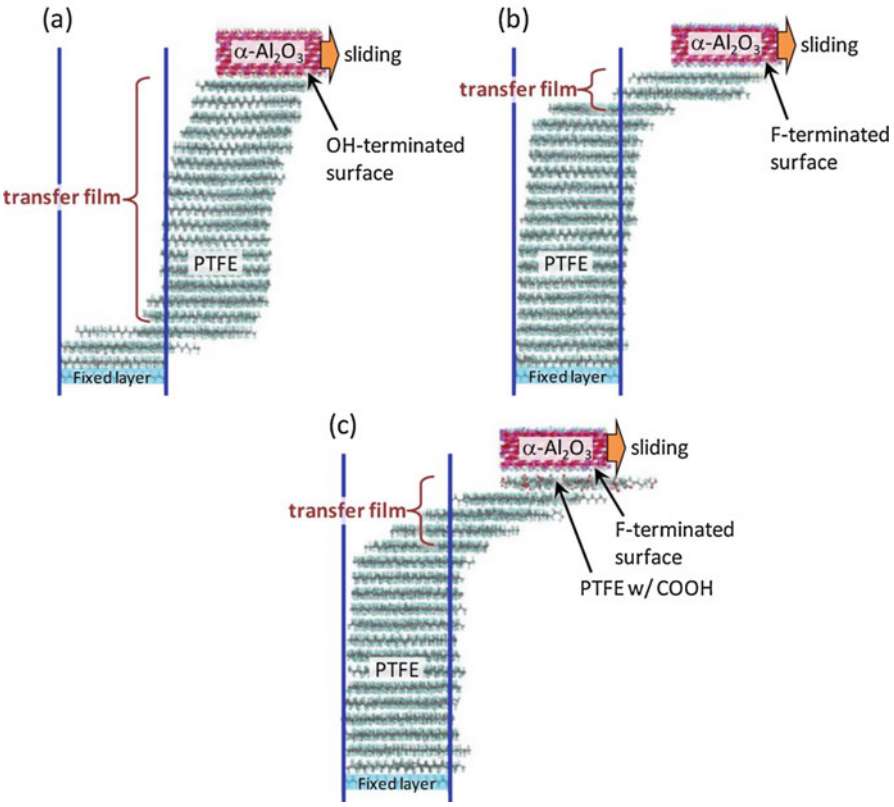

Fig. 11.13 Final structure of the three different PTFE/α-Al_2O_3 interface of Fig. 11.12 from MD simulation with sliding distance of 5 *nm* for all the models. (Reprinted with permission from [11]. Copyright 2014 American Chemical Society)

11.5 Conclusion

In this chapter, the commonly used theoretical and MD models describing the friction behavior of self-lubricating materials have been discussed. Different mechanisms have been reported to be responsible for friction reduction in such materials including the bearing effect in MoS_2 and carbon nanotubes, and the anisotropic forces between carbon atoms facilitating the sliding of graphite sheets.

These mechanisms were studied using MD models over the last three decades. It has been shown and validated by different groups that computational models are accurate methods to enhance the understanding of such phenomena. Despite the exclusive number of MD researches on different materials, there are only a few studies with focus on self-lubricant materials. The main reason is the complexity of self-lubricating systems which is a drawback for researchers to develop such models. Another limiting factor is the computational expense of these studies which growth

exponentially with increase in the number of modeled atoms. Therefore, the computational models of self-lubricating materials require more research in MD model implementation.

References

1. Menezes, P.L., Reeves, C.J., Lovell, M.R.: Fundamentals of Lubrication, pp. 295–340. Springer, New York (2013). https://doi.org/10.1007/9781-4614-1945-7-10
2. Omrani, E., Moghadam, A.D., Menezes, P.L., Rohatgi, P.K.: Influences of graphite reinforcement on the tribological properties of self-lubricating aluminum matrix composites for green tribology, sustainability, and energy efficiencya review. Int. J. Adv. Manuf. Technol. **83**(1–4), 325–346 (2016)
3. Dorri Moghadam, A., Schultz, B.F., Ferguson, J.B., Omrani, E., Rohatgi, P.K., Gupta, N.: Functional metal matrix composites: self-lubricating, self-healing, and nanocomposites-an outlook. JOM. **66**(6), 872–881 (2014.) http://link.springer.com/10.1007/s11837-014-0948-5
4. Shankara, A., Menezes, P.L., Simha, K.R.Y., Kailas, S.V.: Study of solid lubrication with MoS_2 coating in the presence of additives using reciprocating ball-on-flat scratch tester. Sadhana. **33** (3), 207–220 (2008.) http://link.springer.com/10.1007/s12046-008-0014-5
5. Omrani, E., Dorri Moghadam, A., Menezes, P.L., Rohatgi, P.K.: New Emerging Self-lubricating Metal Matrix Composites for Tribological Applications, pp. 63–103. Springer, Cham (2016). https://doi.org/10.1007/9783-319-24007-7-3
6. Chen, W.X., Li, F., Han, G., Xia, J.B., Wang, L.Y., Tu, J.P., Xu, Z.D.: Tribological behavior of carbon-nanotube-filled PTFE composites. Tribol. Lett. **15**(3), 275–278 (2003)
7. Krick, B.A., Ewin, J.J., Blackman, G.S., Junk, C.P., Gregory Sawyer, W.: Environmental dependence of ultra-low wear behavior of polytetrafluoroethylene (PTFE) and alumina composites suggests tribochemical mechanisms. Tribol. Int. **51**, 42–46 (2012). https://doi.org/10.1016/j.triboint.2012.02.015
8. Ye, J., Khare, H.S., Burris, D.L.: Transfer film evolution and its role in promoting ultralow wear of a PTFE nanocomposite. Wear. **297**(1–2), 1095–1102 (2013)
9. Chung, D.D.L.: Review: graphite. J. Mater. Sci. **37**(8), 1475–1489 (2002)
10. Onodera, T., Kawasaki, K., Nakakawaji, T., Higuchi, Y., Ozawa, N., Kurihara, K., Kubo, M.: Chemical reaction mechanism of polytetrafluoroethylene on aluminum surface under friction condition. J. Phys. Chem. C. **118**(10), 5390–5396 (2014)
11. Onodera, T., Kawasaki, K., Nakakawaji, T., Higuchi, Y., Ozawa, N., Kurihara, K., Kubo, M.: Effect of Tribochemical reaction on transfer-film formation by poly(tetrafluoroethylene). J. Phys. Chem. C. **118**(22), 11820–11826 (2014). https://doi.org/10.1021/jp503331e
12. Rohatgi, P.K., Ray, S., Liu, Y.: Tribological properties of metal matrix-graphite particle composites. Int. Mater. Rev. **37**(1), 129–152 (1992). https://doi.org/10.1179/imr.1992.37.1.129
13. Livshits, A.I., Shluger, A.L.: Self-lubrication in scanning-force-microscope image formation on ionic surfaces. Phys. Rev. B. **56**(19), 12482 (1997)
14. Orkin, S., Hudacko, V.: Self-lubricating bearing. US Patent 3,428,374, 18 Feb 1969. [Online]. Available: https://www.google.com/patents/US3428374
15. MacKerell, J.A.D., Bashford, D., Bellott, M., Dunbrack, J.R.L., Evanseck, J.D., Field, M.J., Fischer, S., Gao, J., Guo, H., Ha, S., Joseph-McCarthy, D., Kuchnir, L., Kuczera, K., Lau, F.T. K., Mattos, C., Michnick, S., Ngo, T., Nguyen, D.T., Prodhom, B., Reiher, W.E., Roux, B., Schlenkrich, M., Smith, J.C., Stote, R., Straub, J., Watanabe, M., Wiorkiewicz-Kuczera, J., Yin, D., Karplus, M.: All-atom empirical potential for molecular modeling and dynamics studies of proteins. J. Phys. Chem. B. **102**(18), 3586–3616 (1998). https://doi.org/10.1021/jp973084f
16. Allison, T.C., Coskuner, O., Gonzalez, C.A.: Metallic Systems: A Quantum Chemist's Perspective. CRC Press, Boca Raton (2011)

17. Mate, C.M., McClelland, G.M., Erlandsson, R., Chiang, S.: Atomic-scale friction of a tungsten tip on a graphite surface. Phys. Rev. Lett. **59**(17), 1942–1945 (1987). https://doi.org/10.1103/PhysRevLett.59.1942
18. Butt, H.-J., Cappella, B., Kappl, M.: Force measurements with the atomic force microscope: technique, interpretation and applications. Surf. Sci. Rep. **59**(1), 1–152 (2005)
19. Jianping Gao, Luedtke, W.D., Gourdon, D., Ruths, M., Israelachvili, J.N., Landman, U.: Frictional forces and Amontons' law: from the molecular to the macroscopic scale. J. Phys. Chem. B. **108**(11), 3410–3425 (2004). https://doi.org/10.1021/jp036362l
20. Vadgama, B.N.: Molecular Dynamics Simulations of Dry Sliding Asperities to Study Friction and Frictional Energy Dissipation. Ph.D. dissertation, Auburn University (2014)
21. Vadgama, B.N., Jackson, R.L., Harris, D.K.: Molecular scale analysis of dry sliding copper asperities. Appl. Nanosci. **5**(4), 469–480 (2015.) http://link.springer.com/10.1007/s13204-014-0339-9
22. Harrison, J.A., White, C.T., Colton, R.J., Brenner, D.W.: Molecular-dynamics simulations of atomic-scale friction of diamond surfaces. Phys. Rev. B. **46**(15), 9700–9708 (1992). https://doi.org/10.1103/PhysRevB.46.9700
23. Zhang, L., Tanaka, H.: Towards a deeper understanding of wear and friction on the atomic scalea molecular dynamics analysis. Wear. **211**(1), 44–53 (1997.) http://linkinghub.elsevier.com/retrieve/pii/S0043164897000732
24. Song, J., Srolovitz, D.J.: Atomistic simulation of multicycle asperity contact. Acta Mater. **55** (14), 4759–4768 (2007)
25. Liu, X., Liu, Z., Wei, Y.: Ploughing friction and nanohardness dependent on the tip tilt in nano-scratch test for single crystal gold. Comput. Mater. Sci. **110**, 54–61 (2015)
26. Zhang, H., Guo, Z., Gao, H., Chang, T.: Stiffness-dependent interlayer friction of graphene. Carbon. **94**, 60–66 (2015)
27. Bai, L., Sha, Z.-D., Srikanth, N., Pei, Q.-X., Wang, X., Srolovitz, D.J., Zhou, K.: Friction between silicon and diamond at the nanoscale. J. Phys. D Appl. Phys. **48**(25), 255303 (2015)
28. Hurley, R.C., Andrade, J.E.: Friction in inertial granular flows: competition between dilation and grain-scale dissipation rates. Granul. Matter. **17**(3), 287–295 (2015). https://doi.org/10.1007/s10035-015-0564-2
29. Hu, C., Bai, M., Lv, J., Liu, H., Li, X.: Molecular dynamics investigation of the effect of copper nanoparticle on the solid contact between friction surfaces. Appl. Surf. Sci. **321**, 302–309 (2014)
30. Wang, L., Shen, B., Sun, F.: Investigation of the atomic-scale friction of boron doped diamond using molecular dynamics. J. Comput. Theor. Nanosci. **11**, 1550 (2014)
31. Spijker, P., Anciaux, G., Molinari, J.-F.: Relations between roughness, temperature and dry sliding friction at the atomic scale. Tribol. Int. **59**, 222–229 (2013)
32. Yang, X.J., Zhan, S.P., Chi, Y.L.: Molecular dynamics simulation of nanoscale sliding friction process between sphere and plane. Appl. Mech. Mater. **268–270**, 1134–1142 (2012.) http://www.scientific.net/AMM.268-270.1134
33. Lee, C., Li, Q., Kalb, W., Liu, X.-Z., Berger, H., Carpick, R.W., Hone, J.: Frictional characteristics of atomically thin sheets. Science. **328**(October 2016), 76–80 (2010)
34. Xu, L., Ma, T.B., Hu, Y.Z., Wang, H.: Molecular dynamics simulation of the interlayer sliding behavior in few-layer graphene. Carbon. **50**(3), 1025–1032 (2012)
35. Dorri Moghadam, A., Omrani, E., Menezes, P.L., Rohatgi, P.K.: Mechanical and tribological properties of self-lubricating metal matrix nanocomposites reinforced by carbon nanotubes (CNTs) and graphene – a review. Compos. Part B. **77**(July 2016), 402–420 (2015)
36. Li, L., Niu, J.B., Xia, Z.H., Yang, Y.Q., Liang, J.Y.: Nanotube/matrix interfacial friction and sliding in composites with an amorphous carbon matrix. Scr. Mater. **65**(11), 1014–1017 (2011)
37. Yin, B., Peng, Z., Liang, J., Jin, K., Zhu, S., Yang, J., Qiao, Z.: Tribological behavior and mechanism of self-lubricating wear-resistant composite coatings fabricated by one-step plasma electrolytic oxidation. Tribol. Int. **97**, 97–107 (2016). https://doi.org/10.1016/j.triboint.2016.01.020

38. Xu, L., Ma, T.-B., Hu, Y.-Z., Wang, H.: Vanishing stick-slip friction in few-layer graphenes: the thickness effect. Nanotechnology. **22**(28), 285708 (2011)
39. Zhang, Q., Diao, D.: Potential of graphene layer controlling nano-wear during C60 intrusion by molecular dynamics simulation. Wear. **306**(1–2), 248–253 (2012). https://doi.org/10.1016/j.wear.2012.09.003
40. Yao, N., Lordi, V.: Young's modulus of single-walled carbon nanotubes. J. Appl. Phys. **84**(i), 1939 (1998.) http://scitation.aip.org/content/aip/journal/jap/84/4/10.1063/1.368323
41. Pavia, F., Curtin, W.: Interfacial sliding in carbon nanotube/diamond matrix composites. Acta Mater. **59**(17), 6700–6709 (2011)
42. Zhao, J., Jia, Y., Wei, N., Rabczuk, T.: Binding energy and mechanical stability of two parallel and crossing carbon nanotubes. Proc. R. Soc. Lond. A. **471**(2180), 20150229 (2015)
43. Zhang, C., Chen, S.: Defect- and dopant-controlled carbon nanotubes fabricated by self-assembly of graphene nanoribbons. Nano Res. **8**(9), 2988–2997 (2015.) http://link.springer.com/10.1007/s12274-015-0804-0
44. Ansari, R., Ajori, S., Ameri, A.: On the vibrational characteristics of singleand double-walled carbon nanotubes containing ice nanotube in aqueous environment. Appl. Phys. A. **121**(1), 223–232 (2015.) http://link.springer.com/10.1007/s00339-015-9413-8
45. Ghosh, S., Padmanabhan, V.: Adsorption of hydrogen on single-walled carbon nanotubes with defects. Diam. Relat. Mater. **59**, 47–53 (2015)
46. Stefanov, M., Enyashin, A.N., Heine, T., Seifert, G.: Nanolubrication: how do MoS_2-based nanostructures lubricate? J. Phys. Chem. C. **112**(46), 17764–17767 (2008)
47. Dallavalle, M., Sandig, N., Zerbetto, F.: Stability, dynamics, and lubrication of MoS_2 platelets and nanotubes. Langmuir ACS J. Surf. Colloid. **28**(19), 7393–7400 (2012.) http://www.ncbi.nlm.nih.gov/pubmed/22530739
48. Wang, Y., Yan, F.: Tribological properties of transfer films of PTFE-based composites. Wear. **261**(11–12), 1359–1366 (2006)